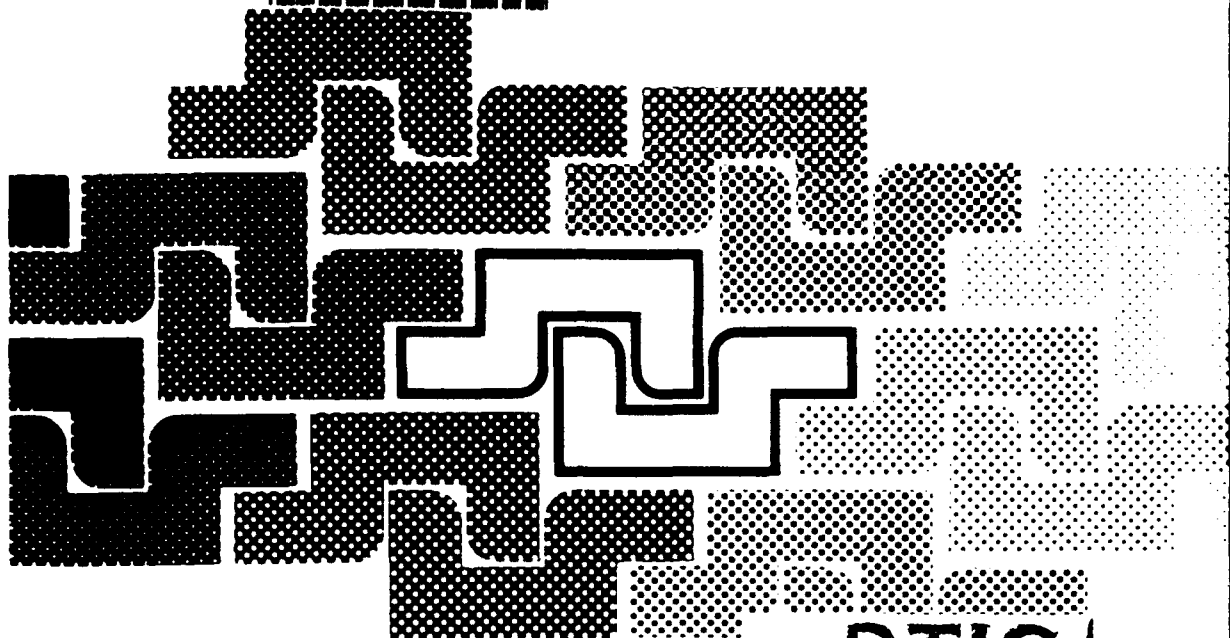


AD-A278 115



DISTRIBUTION STATEMENT A

**Approved for public release
Distribution Unlimited**

DTIC
ELECTE
APR 14 1994
S B D

Future Directions of Nonlinear Dynamics in Physical and Biological Systems

Edited by

P. L. Christiansen

J. C. Eilbeck and

R. D. Parmentier

NATO ASI Series

Series B: Physics Vol. 312

94-11254



94 4 12 176

Future Directions of Nonlinear Dynamics in Physical and Biological Systems

Accession For	
NTIS GRA&I	<input checked="" type="checkbox"/>
DTIC TAB	<input type="checkbox"/>
Unannounced	<input type="checkbox"/>
Justification	
By	
Distribution	
Availability Codes	
Dist	Avail and/or Special
A-1	

NATO ASI Series

Advanced Science Institutes Series

A series presenting the results of activities sponsored by the NATO Science Committee, which aims at the dissemination of advanced scientific and technological knowledge, with a view to strengthening links between scientific communities.

The series is published by an international board of publishers in conjunction with the NATO Scientific Affairs Division

A Life Sciences	Plenum Publishing Corporation
B Physics	New York and London
C Mathematical and Physical Sciences	Kluwer Academic Publishers
D Behavioral and Social Sciences	Dordrecht, Boston, and London
E Applied Sciences	
F Computer and Systems Sciences	Springer-Verlag
G Ecological Sciences	Berlin, Heidelberg, New York, London,
H Cell Biology	Paris, Tokyo, Hong Kong, and Barcelona
I Global Environmental Change	

Recent Volumes in this Series

- Volume 307** — Negative Differential Resistance and Instabilities in 2-D Semiconductors
edited by N. Balkan, B. K. Ridley, and A. J. Vickers
- Volume 308** — Photonic Band Gaps and Localization
edited by C. M. Soukoulis
- Volume 309** — Magnetism and Structure in Systems of Reduced Dimension
edited by Robin F. C. Farrow, Bernard Dieny, Markus Donath, Albert Fert, and B. D. Hermsmeier
- Volume 310** — Integrable Quantum Field Theories
edited by L. Bonora, G. Mussardo, A. Schwimmer, L. Girardello, and M. Martellini
- Volume 311** — Quantitative Particle Physics: *Cargèse 1992*
edited by Maurice Lévy, Jean-Louis Basdevant, Maurice Jacob, Jean Iliopoulos, Raymond Gastmans, and Jean-Marc Gérard
- Volume 312** — Future Directions of Nonlinear Dynamics in Physical and Biological Systems
edited by P. L. Christiansen, J. C. Eilbeck, and R. D. Parmentier
- Volume 313** — Dissociative Recombination: Theory, Experiment, and Applications
edited by Bertrand R. Rowe, J. Brian A. Mitchell, and André Canosa



Series B: Physics

Future Directions of Nonlinear Dynamics in Physical and Biological Systems

Edited by

P. L. Christiansen

The Technical University of Denmark
Lyngby, Denmark

J. C. Eilbeck

Heriot-Watt University
Edinburgh, United Kingdom

and

R. D. Parmentier

University of Salerno
Baronissi, Italy

DTIC QUALITY INSPECTED 3

Plenum Press

New York and London

Published in cooperation with NATO Scientific Affairs Division

Proceedings of a NATO Advanced Study Institute on
Future Directions of Nonlinear Dynamics in Physical and Biological Systems,
held July 23-August 1, 1992 (in honor of Alwyn Scott's sixtieth birthday),
in Lyngby, Denmark

NATO-PCO-DATA BASE

The electronic index to the NATO ASI Series provides full bibliographical references (with keywords and/or abstracts) to more than 30,000 contributions from international scientists published in all sections of the NATO ASI Series. Access to the NATO-PCO-DATA BASE is possible in two ways:

—via online FILE 128 (NATO-PCO-DATA BASE) hosted by ESRIN, Via Galileo Galilei, I-00044 Frascati, Italy

—via CD-ROM "NATO-PCO-DATA BASE" with user-friendly retrieval software in English, French, and German (©WTV GmbH and DATAWARE Technologies, Inc. 1989)

The CD-ROM can be ordered through any member of the Board of Publishers or through NATO-PCO, Overijse, Belgium.

Library of Congress Cataloging-in-Publication Data

Future directions of nonlinear dynamics in physical and biological systems / edited by P.L. Christiansen, J.C. Eilbeck, and R.D. Parmentier.

p. cm. -- (NATO ASI series. Series B, Physics ; v. 312)
"Published in cooperation with NATO Scientific Affairs Division."
"Proceedings of a NATO Advanced Study Institute on Future Directions of Nonlinear Dynamics in Physical and Biological Systems, held July 23-August 1, 1992 (in honor of Alwyn Scott's sixtieth birthday) in Lyngby, Denmark"--T.p. verso.

Includes bibliographical references and index.

ISBN 0-306-44562-X

1. Dynamics--Congresses. 2. Nonlinear theories--Congresses.
3. Scott, Alwyn, 1931- I. Christiansen, Peter L., 1937-
II. Eilbeck, J. C. III. Parmentier, Robert D. IV. North Atlantic Treaty Organization. Scientific Affairs Division. V. NATO Advanced Study Institute on Future Directions of Nonlinear Dynamics in Physical and Biological Systems (1992 : Lyngby, Denmark)
VI. Series.

QC133.F88 1993

531'.11'01175--dc20

93-11313

CIP

ISBN 0-306-44562-X

©1993 Plenum Press, New York
A Division of Plenum Publishing Corporation
233 Spring Street, New York, N.Y. 10013

All rights reserved

No part of this book may be reproduced, stored in retrieval system, or transmitted in any form or by any means, electronic, mechanical, photocopying, microfilming, recording, or otherwise, without written permission from the Publisher

Printed in the United States of America

SPECIAL PROGRAM ON CHAOS, ORDER, AND PATTERNS

This book contains the proceedings of a NATO Advanced Research Workshop held within the program of activities of the NATO Special Program on Chaos, Order, and Patterns.

- Volume 208 — MEASURES OF COMPLEXITY AND CHAOS
edited by Neal B. Abraham, Alfonso M. Albano,
Anthony Passamante, and Paul E. Rapp
- Volume 225 — NONLINEAR EVOLUTION OF SPATIO-TEMPORAL STRUCTURES
IN DISSIPATIVE CONTINUOUS SYSTEMS
edited by F. H. Busse and L. Kramer
- Volume 235 — DISORDER AND FRACTURE
edited by J. C. Charmet, S. Roux, and E. Guyon
- Volume 236 — MICROSCOPIC SIMULATIONS OF COMPLEX FLOWS
edited by Michel Mareschal
- Volume 240 — GLOBAL CLIMATE AND ECOSYSTEM CHANGE
edited by Gordon J. MacDonald and Luigi Sertorio
- Volume 243 — DAVYDOV'S SOLITON REVISITED: Self-Trapping of Vibrational
Energy in Protein
edited by Peter L. Christiansen and Alwyn C. Scott
- Volume 244 — NONLINEAR WAVE PROCESSES IN EXCITABLE MEDIA
edited by Arun V. Holden, Mario Markus, and Hans G. Othmer
- Volume 245 — DIFFERENTIAL GEOMETRIC METHODS IN THEORETICAL
PHYSICS: Physics and Geometry
edited by Ling-Lie Chau and Werner Nahm
- Volume 256 — INFORMATION DYNAMICS
edited by Harald Atmanspacher and Herbert Scheingraber
- Volume 260 — SELF-ORGANIZATION, EMERGING PROPERTIES, AND
LEARNING
edited by Agnessa Babloyantz
- Volume 263 — BIOLOGICALLY INSPIRED PHYSICS
edited by L. Peliti
- Volume 264 — MICROSCOPIC ASPECTS OF NONLINEARITY IN CONDENSED
MATTER
edited by A. R. Bishop, V. L. Pokrovsky, and V. Tognetti
- Volume 268 — THE GLOBAL GEOMETRY OF TURBULENCE: Impact of Nonlinear
Dynamics
edited by Javier Jiménez
- Volume 270 — COMPLEXITY, CHAOS, AND BIOLOGICAL EVOLUTION
edited by Erik Mosekilde and Lis Mosekilde

SPECIAL PROGRAM ON CHAOS, ORDER, AND PATTERNS

Volume 272 — PREDICTABILITY, STABILITY, AND CHAOS IN N-BODY
DYNAMICAL SYSTEMS
edited by Archie E. Roy

Volume 276 — GROWTH AND FORM: Nonlinear Aspects
edited by M. Ben Amar, P. Pelcé, and P. Tabeling

Volume 278 — PAINLEVÉ TRANSCENDENTS: Their Asymptotics and Physical
Applications
edited by Decio Levi and Pavel Winternitz

Volume 280 — CHAOS, ORDER, AND PATTERNS
edited by Roberto Artuso, Predrag Cvitanović, and Giulio Casati

Volume 284 — ASYMPTOTICS BEYOND ALL ORDERS
edited by Harvey Segur, Saleh Tanveer, and Herbert Levine

Volume 291 — PROTEIN TRANSFER IN HYDROGEN-BONDED SYSTEMS
edited by T. Bountis

Volume 292 — MICROSCOPIC SIMULATIONS OF COMPLEX HYDRODYNAMIC
PHENOMENA
edited by Michel Mareschal and Brad Lee Holian

Volume 298 — CHAOTIC DYNAMICS: Theory and Practice
edited by T. Bountis

Volume 312 — FUTURE DIRECTIONS OF NONLINEAR DYNAMICS IN PHYSICAL
AND BIOLOGICAL SYSTEMS
edited by P. L. Christiansen, J. C. Eilbeck, and R. D. Parmentier

PREFACE

Early in 1990 a scientific committee was formed for the purpose of organizing a high-level scientific meeting on Future Directions of Nonlinear Dynamics in Physical and Biological Systems, in honor of Alwyn Scott's 60th birthday (December 25, 1991). As preparations for the meeting proceeded, they were met with an unusually broad-scale and high level of enthusiasm on the part of the international nonlinear science community, resulting in a participation by 168 scientists from 23 different countries in the conference, which was held July 23 to August 1 1992 at the Laboratory of Applied Mathematical Physics and the Center for Modelling, Nonlinear Dynamics and Irreversible Thermodynamics (MIDIT) of the Technical University of Denmark. During the meeting about 50 lectures and 100 posters were presented in 9 working days.

The contributions to this present volume have been grouped into the following chapters:

1. Integrability, Solitons, and Coherent Structures
2. Nonlinear Evolution Equations and Diffusive Systems
3. Chaotic and Stochastic Dynamics
4. Classical and Quantum Lattices and Fields
5. Superconductivity and Superconducting Devices
6. Nonlinear Optics
7. Davydov Solitons and Biomolecular Dynamics
8. Biological Systems and Neurophysics.

Al Scott has made early and fundamental contributions to many of these different areas of nonlinear science. They form an important subset of the total number of the papers and posters presented at the meeting. Other papers from the meeting are being published in a special issue of *Physica D Nonlinear Phenomena*.

People who have worked with Al know that he insists that everyone should do what he or she likes to do; this is certainly true, but it is also true that from the very early days he has demonstrated a unique ability to stimulate research in new directions. Moreover, his ability to interact with people and to transmit his optimism and enthusiasm to those around him has furnished a solid launching pad for these new lines of research. Many

friends and colleagues around the world are thankful to Al for having received such a stimulus. This was the essential motivation for our meeting and for the publication of these Proceedings. It is a small way of saying "Thank you, Al, and many happy returns".

It is our pleasure to acknowledge financial support from the NATO Scientific and Environmental Affairs Division (grant SA.9-15-03), the Army Research Office of the United States Army Laboratory Command (grant 29333 MA-CF), the United States Army European Research Office (grant RD 6891-MA-02), the National Science Foundation (grant ASI 910728), the Danish Technical Research Council (grant 16-4932-1 OS), NORDITA, the COWI foundation (grant A-51.77/TJ/IJO), and The Technical University of Denmark (basic research grant to MIDIT).

The Scientific Committee, consisting of D.K. Campbell, Los Alamos, G. Careri, Rome, P.L. Christiansen, Lyngby, A.S. Davydov, Kiev, J.C. Eilbeck, Edinburgh, A. Luther, Copenhagen, D.W. McLaughlin, Princeton, A.C. Newell, Tucson, and R.D. Parmentier, Salerno, was particularly helpful in the organization of the scientific program.

We warmly thank K. Fisker, L. Fønss, L. Gudmandsen, L. MacNeil, M.P. Sørensen, E. Yde and many students at MIDIT for their generous assistance during the meeting and the preparation of these Proceedings.

Peter Christiansen
Chris Eilbeck
Bob Parmentier

CONTENTS

1. INTEGRABILITY, SOLITONS AND COHERENT STRUCTURES

Perturbative Painlevé Analysis	1
R. Conte, A. Fordy, and A. Pickering	
Difference Scheme of Soliton Equations	7
R. Hirota, S. Tsujimoto, and T. Imai	
Solitons in Crossed-Field Devices	17
D.J. Kaup	
The Numerical Inverse Scattering Transform: Nonlinear Fourier Analysis for Laboratory and Oceanic Wave Data	27
A.R. Osborne	
Solitons in Discrete Systems	37
M. Toda	
Low-Dimensional Behaviour in the Rotating Driven Cavity Problem	45
E.A. Christensen, J.N. Sørensen, M. Brøns, and P.L. Christiansen	
Vortex Dipoles Colliding with Curved Walls	51
E.A. Coutsias, J.P. Lynov, A.H. Nielsen, M. Nielsen, J. Juul Rasmussen, and B. Stenum	
The Use of Generalized Zakharov Systems in Elastic Surface Waves	55
H. Hadouaj and G.A. Maugin	
Vortex Dynamics in 2-Dimensional Flows	59
J.S. Hesthaven, J.P. Lynov, J. Juul Rasmussen and G.G. Sutyrin	
Self-Supporting Gap Solitons in Nonlinear Lattices	63
Yuri S. Kivshar	
Dynamics of Solitons in Polyacetylene in the Step-Potential Model	67
Christoph Kuhn	

Soliton-Like Structure in (2+1) Dimensions	73
B. Piette and W.J. Zakrzewski	

Solitons on a Nonlinear Klein-Gordon Equation	77
B.N. Prasanna	

2. NONLINEAR EVOLUTION EQUATIONS AND DIFFUSIVE SYSTEMS

A Collective Coordinate Approach to the One-Dimensional Nonlinear Schrödinger Equation with Spatial Periodic Potentials	85
A.R. Bishop and R. Scharf	

Length Scales in Solutions of Dissipative Partial Differential Equations	97
M.V. Bartuccelli, C.D. Doering, J.D. Gibbon, and S.J.A. Malham	

Hamilton Structure of Unstable Nonlinear Schrödinger Equation	101
S.A. Darmany and V.I. Rupasov	

On the Forced Eckhaus Equation	105
S. De Lillo	

New Aspects of Chaotic Dynamics in Nonlinear Schrödinger Systems	109
Th. Eickermann, R. Grauer, and K.H. Spatschek	

Resonance Phenomena in Soliton-Impurity Interactions	113
Z. Fei, Yu.S. Kivshar and L. Vázquez	

Two and Many Impurity Effects in Soliton Dynamics	117
Yu.S. Kivshar, A. Sánchez, and L. Vázquez	

Self-Focussing of Coupled Guided Acoustic Waves at a Nonlinear Resonance	121
A.P. Mayer	

Some Exact Wave Solutions in Terms of the Weierstrass Functions for Nonlinear Hyperbolic Equations	125
A.M. Samsonov	

3. CHAOTIC AND STOCHASTIC DYNAMICS

Controlling Chaos in Hamiltonian Systems	129
Y.-C. Lai, M. Ding, and C. Grebogi	

Deterministic Disorder in Two-Dimensional Media	139
M.I. Rabinovich and A.L. Fabrikant	

Phase Shifts and Nonlinear Effects in Stochastic Resonance	153
M.I. Dykman, R. Manella, P.V.E. McClintock, and N.G. Stocks	
Controlling Dependence on Initial Conditions in Chaotic Systems	157
T. Kapitaniak	
Dynamical Systems Analysis of an Aerodynamic Decelerator: Bifurcation to Divergence and Flutter	161
L.J. Piscitelle	
Chaos in a Model of a Railway Wheelset	165
E. Slivsgaard and C. Knudsen	
Nonlinear Modelling of Shimmying Wheels	169
G. Stépán	
Chaotic Solitons and Vacuum	173
P.J. Werbos and P.A. Hansson	

4. CLASSICAL AND QUANTUM LATTICES AND FIELDS

Q-Hermitian Conjugation, Quantum Groups and Squeezing	177
E. Celeghini, M. Rasetti, and G. Vitiello	
Large-Amplitude Narrow Solitons in Lattices	185
K.A. Gorshkov, O.A. Druzhinin, and L.A. Ostrovsky	
Dynamical Structures in 2D Lattices	195
M. Remoissenet, J. Pouget, and J.M. Tamga	
Model Hamiltonian, Coherent State and Anharmonic Localized Modes as Dynamical Self-Trapping in Nonlinear Systems and Biological Macromolecules	203
S. Takeno	
Quantum Holstein Polaron Model and Classical Charged Gas on a Ring	213
X. Wang	
The Quantum Ablowitz-Ladik Equation as a Q-Boson System	217
R.K. Bullough, N.M. Bogoliubov, and G.D. Pang	
Moving Localized Modes in Nonlinear Lattices	223
Ch. Claude, Yu.S. Kivshar, O. Kluth, and K.H. Spatschek	
Quantum Solitons in the DNLS and Hubbard Models	227
H. Gilhøj, J.C. Eilbeck, and A.C. Scott	

Stationary Solitons in Discrete Lattices of Different Dimensionality	231
V.A. Kuprievich	
Numerical and Experimental Studies on the AC-Driven Damped Toda Lattice	235
T. Kuusela and J. Hietarinta	
Quantum Effects in the Nonlinear Nonadiabatic Dimer	239
R. Mannella, D. Vitali, L. Bonci, and P. Grigolini	
On the Discrete and Continuum Integrable Heisenberg Spin Chain Models . .	243
K. Porsezian	
Dynamics and Instability of Nonlinear Patterns in Phase Transformation Problems	249
J. Pouget	
Discrete Modulated Waves	257
M. Rose	
Toda Solitons and the Mössbauer Effect	261
M.V. Sataric, R.B. Žakula, S. Zeković, and J.A. Tuszyński	

5. SUPERCONDUCTIVITY AND SUPERCONDUCTING DEVICES

Bipolaronic Charge Density Waves, Polaronic Spin Density Waves and High T _c Superconductivity	265
S. Aubry	
Inductively Coupled Long Josephson Junctions: Collective Coordinate Analysis and I-V Characteristics	267
T. Bountis and T. Skiniotis	
The Sine-Gordon Equation and Superconducting Soliton Oscillators	283
S. Pnevmatikos and N.F. Pedersen	
Static Solutions of a Two Dimensional Josephson Window Junction	333
J.G. Caputo, M. Devoret, and N. Flytzanis	
Fluxon Oscillations in a Parallel Biased Array of Small Josephson Junctions	339
G. Costabile and P. Sabatino	
Linewidth of Josephson Oscillations in YBa ₂ Cu ₃ O _{7-x} Step Edge Grain Boundary Junctions	243
Yu.Ya. Divin, A.V. Andreev, A.I. Braginski, G.M. Fischer, K. Herrmann, J. Mygind, N.F. Pedersen, and M. Siegel	

Fluxon Dynamics in Discrete Sine Gordon System	347
G. Filatrella, S. Matarazzo, and S. Pagano	
Nonlinear Interaction of Fluxon and Plasma Waves in a Finite Josephson Junction	351
M. Jaworski	
Observation of Multiple Particle Tunneling in High Quality Superconducting Tunnel Junctions	355
A. Oliva and R. Monaco	
Nonlinearity in BCS Models of High-Tc Superconductors	359
T. Pavlopoulos, N. Lazarides, P.L. Christiansen, M.P. Sørensen, and P.N. Spathis	
Statics and Dynamics of Flux Vortices in Discrete Systems	363
G. Rotoli	
Soliton Type Propagation in HTcS Materials	367
J.A. Zagrodzinski	

6. NONLINEAR OPTICS

Dynamics of Solitary Waves in Nematic Liquid Crystals	371
F.Kh. Abdullaev, A.A. Abdumalikov, and E.N. Tsoi	
Quantum Capture in LB Monolayers and the Role of Thermal Fluctuations ..	381
J.A. Tuszynski, E.A. Bartnik, and K.J. Blinowska	
Soliton Mechanism of Optical Anisotropy Photoinduction in Two-Dimensional Molecular Systems	391
Yu.B. Gaididei	
Optical Second Harmonic Generation in a Langmuir-Blodgett Films	395
T. Geisler	
Nonlinear Envelope Waves in Inhomogeneous Media	399
B.A. Malomed	
Lyapunov Stability of Vector Solitons in Optical Fibres	405
V. Mezentsev and S. Turitsyn	
Chaos in Semiconductor Lasers with Optical Feedback	409
J. Mørk, B. Tromborg, J. Mark, and V. Velichansky	
Pulse Collisions in Bimodal Waveguides	413
D.F. Parker and C. Sophocleous	

Dynamic Response of Semiconductor Nonlinear Optical Waveguides	417
P.S. Spencer and K.A. Shore	

Dynamics of a Fibre Laser Coupled to a Nonlinear Fibre Cavity	421
M.P. Sørensen, T. Geisler, K.A. Shore, P.L. Christiansen, J. Mørk, and J. Mark	

7. DAVYDOV SOLITONS AND BIOMOLECULAR DYNAMICS

The Lifetime of Molecular (Davydov's) Solitons	425
A.S. Davydov	

Energy Transduction and Deterministic Protein Motions	435
R.J. Dwayne Miller, J. Deak, S. Palese, M. Pereira, L. Richard, and L. Schilling	

Soliton States in a Chain with Two Atoms in a Unit Cell	445
L. S. Brizhik	

Proton Transport in Hydrogen-Bonded Chains: A Two-Component Soliton Model Including Dipole Interactions	449
I. Chochliouros and J. Pouget	

The Ultrasonic Charge-Density-Waves and Integrable Many Particle Hénon-Heiles System	455
P.L. Christiansen, Yu.B. Gaididei, V.Z. Enol'skii, and D.V. Leykin	

The Frölich Charge-Density-Wave as a Lattice of Davydov's Solitons	461
A.A. Eremko	

Inelastic Neutron Scattering Study of the Quantum Sine-Gordon Breather in 4-Methyl-Pyridine	465
F. Fillaux, C.J. Carlile, and G.J. Kearley	

Modelling DNA Denaturation	469
V. Muto, F. Vadillo, and M. Lezaun	

A Proton Pathway with Large Proton Polarizability in Bacteriorhodopsin	473
J. Olejnik, B. Brzezinski, and G. Zundel	

Evaluation of the Strength of Coupling Between a Vibrational Exciton and a Specific Low Frequency Mode	477
P. Pumilia, R. Tubino, D.R. Ferro, G. Baldini, and S. Abbate	

Hierarchy of Nonlinear Dynamic Models of DNA	485
L. Yakushevich	

8. BIOLOGICAL SYSTEMS AND NEUROPHYSICS

Evolution and Co-Evolution in a Rugged Fitness Landscape	489
P. Bak, H. Flyvbjerg, and B. Lautrup	
Chaos in a Model of HIV Infection of the Immune System	499
O. Lund, E. Mosekilde, and J. Hansen	
Phase Locking of the Bonhoeffer-Van Der Pol Model	509
H. Friedman, S. Goshen, A. Rabinovitch, and R. Thieberger	
Continuous or Discrete State Dynamical Systems as Models for Computat in Neural Systems	13
A.V. Holden	
Turing Structures in <i>Drosophila</i> Morphogenesis	517
A. Hunding	
Nonlinear Forecasting of RR-Intervals of Human Electrocardiograms	523
B.L. Jørgensen, A. Junker, H. Mickley, M. Møller, E. Christiansen, and L.F. Olsen	
The Ultradian Clock Interacts with the Mitotic Oscillator to Give Dispersed and Quantized Cell Cycle Times. Noisy or Chaotic Trajectories?	527
D. Lloyd, A.L. Lloyd, L.F. Olsen, M.N. Stolyarov, and E.I. Volkov	
A Solitonic Model for the "Information Strings"	533
M.V. Sataříć, J.A. Tuszyński, and R.B. Žakula	
Rotating Vortices Initiation in Cardiac Muscle: Pulse Chemistry Control	539
C.F. Starmer, V.I. Krinsky, D.N. Romashko, and R.R. Aliev	
Participants	543
Index	555

PERTURBATIVE PAINLEVÉ ANALYSIS †

Robert Conte¹, Allan Fordy² and Andrew Pickering²

¹Service de physique de l'état condensé
Centre d'études de Saclay
F-91191 Gif-sur-Yvette Cedex, France

²Department of Applied Mathematical Studies and
Centre for Nonlinear Studies
University of Leeds, LS2 9JT, United Kingdom

0. Preface

We present an improved Painlevé test, which enables us to treat negative resonances. Since the method is explained in a recent paper [5] and in proceedings elsewhere, the present version is very short. We give a brief description of the method and outline three examples.

1. Introduction

An ODE is said to have the Painlevé property (PP) if its general solution is single valued (except, perhaps, at fixed critical points). Whilst most examples in the literature possess the stronger property: "The only movable singularities of the general solution are poles," the general PP allows, for instance, movable essential singularities and natural boundaries, provided no branching takes place at them. Many people use the quoted stronger property as their definition of the PP, but this is too restrictive and dismisses some interesting equations which do have the weaker property. There are several tests of the PP, devised by Kowalewskaya, Painlevé, Gambier, Bureau, Ablowitz, Ramani and Segur (ARS) and others (see [1] for references). Whilst these tests are distinct and sometimes test different properties, they are collectively known as "the Painlevé test". There are many papers and reviews, most of which can be found in the references of [1].

As was discovered by Ablowitz and Segur [2], the similarity (and other special) solutions of PDEs solvable by the inverse spectral transform (IST) satisfy ODEs with the P-type. This lead Weiss, Tabor and Carnevale [8] (WTC) to devise a direct test (based on that of ARS for ODEs) of the PP of PDEs. The WTC method has the advantage of giving a direct correspondence with IST, Bäcklund transformations, etc., even for ODEs.

The ARS and WTC tests (with various modifications) have been the most used in recent times (the 'soliton period') and have been extremely successful in isolating classes of 'integrable' equations. These methods construct a series expansion (about a pole) for the solution of a nonlinear equation (analogous to the Frobenius expansion

† This is an outline of the lecture given by Allan Fordy and is dedicated to Alwyn Scott for his 60th birthday.

for linear equations). For this to be a local representation of the general solution requires an adequate number of arbitrary constants (for ODEs) to be present. This, in turn, requires an adequate number of *non-negative integer* "resonances" or indices, which we show to be *equivalent* to the roots of the indicial equation in Frobenius' method for linear ODEs. Since these integer indices *a fortiori* differ by integers, compatibility conditions arise in order that logarithmic branching is avoided.

Any indices which are non-integer immediately indicate the presence of branching (algebraic or transcendental) so must be excluded. However, there are interesting and important equations which have some *negative* integer indices which do *not* give rise to corresponding arbitrary constants and which can *not* be tested for compatibility, using the above tests, thus leaving the question of logarithms undetermined.

In [6] we introduced a method of testing negative integer indices. By considering the Painlevé property of a nonlinear equation and its linearisation, the negative integer "Painlevé resonances" are converted into *positive* integer "Fuchs indices", which can thus be tested for compatibility. This method has been generalised in [5,7], where we consider a general perturbation series, including the results of [6] as the *first* order perturbation. The general method is described below.

2. The Perturbative Painlevé Method

In this paper, for simplicity, we consider a single ODE for a single function $u(x)$:

$$E \equiv K[u, x] = 0, \quad (2.1)$$

polynomial in u and its derivatives, analytic in x .

First, we perform a usual Painlevé analysis of this nonlinear ODE. About any family of movable pole-like singularities of u the standard Painlevé expansion takes the form:

$$u = u^{(0)} \equiv \sum_{j=0}^{+\infty} u_j^{(0)} \chi^{j+p}, \quad E = E^{(0)} \equiv \sum_{j=0}^{+\infty} E_j^{(0)} \chi^{j+q}, \quad (2.2)$$

in which negative integers p and q are the respective singularity orders of u and E . For this paper χ may be taken as $x - x_0$. In this expansion the arbitrary constants (apart from x_0) arise at non-negative integer indices (usually called "resonances"). Let \mathcal{R} be the set of indices. As mentioned above, these indices should be integer, but we do *not* insist on a "principal branch" having (apart from -1) a full complement of non-negative (integer) indices (usually required so that the general solution is locally represented by (2.2)). Let $\rho \in \mathcal{R}$ be the minimum index ($\rho \leq -1$). Assuming that no *branching* occurred in this 'standard' Painlevé expansion and that it does *not* represent the general solution (meaning the presence of negative indices other than -1), then we need to introduce the 'missing' coefficients.

We now seek a Laurent expansion for any solution which is *near* to the solution (2.2) obtained by the standard Painlevé method. We do this by considering a perturbation expansion, representing a nearby solution by an infinite perturbation series in a small parameter ϵ :

$$u = \sum_{n=0}^{+\infty} \epsilon^n u^{(n)}, \quad K[u, x] = 0, \quad (2.3a)$$

$$E = \sum_{n=0}^{+\infty} \epsilon^n E^{(n)} = 0. \quad (2.3b)$$

The condition that this expansion still be a solution generates the infinite sequence of successive differential equations

$$n = 0 : E^{(0)} \equiv K[u^{(0)}, x] = 0, \quad (2.4a)$$

$$n \geq 1 : E^{(n)} \equiv \hat{K}'[u^{(0)}, x]u^{(n)} - R^{(n)}(u^{(0)}, \dots, u^{(n-1)}) = 0, \quad (2.4b)$$

in which the expression $R^{(n)}$ represents the contribution of previous terms of the expansion; $R^{(1)}$ is identically zero. Each higher order equation (2.4b) is a linear inhomogeneous differential equation whose left hand side is the Fréchet operator $\hat{K}'[u^{(0)}, x]$ (independent of n) acting on $u^{(n)}$.

We carry out a Painlevé analysis of *each* of the equations (2.4). For $n \geq 1$ the equation for $u^{(n)}$ is *linear*, so the analysis is effectively that of Fuchs-Frobenius. The indices are (up to a shift) the roots of the indicial equation. For $n \geq 2$ the dominant behaviour of $u^{(n)}$ is determined by $R^{(n)}$ as $\chi^{n\rho}$, where ρ is the minimum index mentioned above. At each level of perturbation, compatibility conditions (sometimes *new*) arise at each integer index. Thus we derive (potentially) *more* necessary conditions for the equation to have the PP. At each level of perturbation we construct a *pole* expansion, but the order of the pole increases with the order of the perturbation. The resulting *infinite* perturbation expansion is a *doubly infinite* Laurent expansion:

$$u^{(n)} = \sum_{j=n\rho}^{+\infty} u_j^{(n)} \chi^{j+p}, \quad (2.5a)$$

$$E^{(n)} = \sum_{j=n\rho}^{+\infty} E_j^{(n)} \chi^{j+q}, \quad (2.5b)$$

$$u = \sum_{n=0}^{+\infty} \varepsilon^n \left[\sum_{j=n\rho}^{+\infty} u_j^{(n)} \chi^{j+p} \right] = \sum_{j=-\infty}^{+\infty} u_j \chi^{j+p}. \quad (2.5c)$$

This is not, generally, an essential singularity. For further explanation we refer the reader to [5].

3. Examples

In this section we present three equations and indicate the order of the perturbation needed to draw some conclusions.

Chazy's equation of class IV

This equation has the form [4]:

$$E \equiv -u''' - 3uu'' - 3u'^2 - 3u^2u' + 2d_3uu' + c_0u' + d_3u^3 + d_2u^2 + d_1u + d_0 = 0, \quad (3.1)$$

with c_0, d_i arbitrary analytic functions of x . This equation has two families:

$$p = -1, u_0^{(0)} = 1, \text{ indices } (-1, 1, 3), \hat{K} = -u''' - 3uu'' - 3u'^2 - 3u^2u', \quad (3.2a)$$

$$p = -1, u_0^{(0)} = 2, \text{ indices } (-2, -1, 3), \hat{K} = -u''' - 3uu'' - 3u'^2 - 3u^2u'. \quad (3.2b)$$

The *first family* is principal, so we do not expect higher orders to generate more compatibility conditions than the pure Painlevé test. The latter gives:

$$d_3 = 0, \quad d_2 = 0, \quad d_1 = c'_0. \quad (3.3)$$

These conditions were shown by Chazy to be both necessary and sufficient.

The *second family* is more interesting for, at the zeroth order, two compatibility conditions are still missing. We obtain at order ϵ^0 that $u_3^{(0)}$ is arbitrary, together with the condition:

$$d_1 - c'_0 + c_0 d_3 - 2d_2 d_3 + 2d'_2 = 0. \quad (3.4)$$

Whilst this is implied by (3.3), the two conditions are not equivalent. We need to use a first order perturbation to achieve equivalence.

Chazy's equation of class V

This has the form [4]:

$$E \equiv -u''' - 2uu'' - 4au'^2 - 2u^2u' + a_1u'' + c_0u' + d_2u^2 + d_1u + d_0 = 0, \quad (3.5)$$

with a_1, c_0, d_i arbitrary analytic functions of x .

The equation has two families:

$$p = -1, u_0^{(0)} = 1, \text{ indices } (-1, 1, 4), \hat{K} = -u''' - 2uu'' - 4u'^2 - 2u^2u', \quad (3.6a)$$

$$p = -1, u_0^{(0)} = 3, \text{ indices } (-3, -1, 4), \hat{K} = -u''' - 2uu'' - 4u'^2 - 2u^2u'. \quad (3.6b)$$

An analysis of the first family provides four conditions, equivalent to:

$$a_1 = 0, \quad d_2 = 0, \quad d_1 = \frac{c'_0}{2}, \quad d_0 = 0. \quad (3.7)$$

These necessary conditions are known to be also sufficient for the equation to have the PP [3,4].

Since the *second family* is nonprincipal, it is necessary to consider at least order $n = 1$. In fact, for this example it is necessary to consider a perturbation of order 2 in order to prove equivalence of the two families.

An example needing a seventh order perturbation

In his discussion of fourth order ODEs for which u'''' is linear in u''' , Bureau ([3] page 79) encountered the simplified equation:

$$u'''' + 3uu'' - 4u'^2 = 0. \quad (3.8)$$

The two families are

$$p = -2, u_0^{(0)} = -60, \text{ indices } (-3, -2, -1, 20), \hat{K} = u'''' + 3uu'' - 4u'^2, \quad (3.9a)$$

$$p = -3, u_0^{(0)} \text{ arb, indices } (-1, 0), \hat{K} = 3uu'' - 4u'^2. \quad (3.9b)$$

The *first family* provides, at zeroth order, only a two-parameter expansion. In carrying out a perturbation it is not until *seventh* order that any problems arise. At this order we find that both indices -1 and 20 are incompatible, so that the solution has a movable logarithmic singularity.

This example illustrates that it is not (with our current knowledge) possible to predict the order at which to stop !

4. Conclusions

The present method, which is based on perturbation theory, provides necessary conditions for a differential equation to have the PP. It proves the identity of Painlevé "resonances" with the Fuchs indices of a *linear* equation. In case some Painlevé indices are negative integers (apart from the ever present -1), these necessary conditions are new and the information they contain can be decisive.

If one takes account of the necessary conditions generated by the very first stages of the α -method of Painlevé, the present method provides infinitely many *necessary and sufficient* conditions for the absence of movable critical points of algebraic and logarithmic types. We do not yet know an upper bound, if one exists, on the perturbation order n , required to find *all* possible compatibility conditions, so our process is not finite, as would be required to define an algorithm. As explained by Painlevé, there are unfortunately no methods to determine when an essential singular point is not critical.

In [5] we present many examples which illustrate important features of our method.

Acknowledgements

Andrew Pickering was funded by an SERC "Earmarked" Studentship.

References

- [1] M.J.Ablowitz and P.A.Clarkson, "Solitons, Nonlinear Evolution Equations and Inverse Scattering", LMS Lecture Notes **149**, CUP, Cambridge, 1991.
- [2] M.J.Ablowitz and H. Segur, Exact linearization of a Painlevé transcendent, Phys. Rev. Lett. **38**, 1103-1106 (1977);
- [3] F.J.Bureau, Differential equations with fixed critical points, Annali di Matematica pura ed applicata **LXVI**, 1-116 (1964).
- [4] J.Chazy, Sur les équations différentielles du troisième ordre et d'ordre supérieur dont l'intégrale générale a ses points critiques fixes, Thèse, Paris (1910); Acta Math. **34** (1911), 317-385.
- [5] R.Conte, A.P.Fordy and A.Pickering, A perturbative Painlevé approach to nonlinear differential equations, preprint (1992).
- [6] A.P.Fordy and A.Pickering, Analysing negative resonances in the Painlevé test, Phys. Lett. A **160**, 347-354 (1991).
- [7] A.Pickering, Testing nonlinear evolution equations for complete integrability, Ph.D. Thesis, University of Leeds (1992).
- [8] J.Weiss, M.Tabor and G.Carnevale, The Painlevé property for partial differential equations, J. Math. Phys. **24**, 522-526 (1983).

DIFFERENCE SCHEME OF SOLITON EQUATIONS

Ryogo Hirota,¹ Satoshi Tsujimoto,² and Tatsuya Imai²

¹Department of Information and Computer Science

²Department of Electronics and Communication Engineering
School of Science and Engineering
Waseda University, Tokyo 169

INTRODUCTION

The study of discrete-time integrable systems is currently the focus of an intense activity^{1, 2, 3, 4}.

It is interesting to note that many of the well-known features of continuous-time integrable system such as Lax-pair, Bäcklund transformation, Painlevé property, etc., carry over to the case of discrete-time integrable system. As is noted in ref 4, intelligent space-time discretization of integrable systems is a notoriously difficult problem and versions of integrability are different depending on the way of discretization.

In a series of papers^{5, 6, 7} one of the authors has proposed a method of constructing nonlinear partial difference equations that exhibit solitons. The method uses the bilinear formalism and follows 3 steps. First, a given nonlinear partial differential equation is transformed into the bilinear form by the dependent variable transformation. Secondly the bilinear differential equation is discretized. Thirdly the bilinear difference equation is transformed back into the nonlinear difference equation by the associated dependent variable transformation.

In this paper we explain why it is relatively easy in the bilinear formalism to go from a continuous system to a discrete one without destroying integrability. Then we construct discrete-time Toda equations and a discretized 2-wave interaction.

N-SOLITON SOLUTION OF THE BILINEAR EQUATIONS

Recent development of the bilinear formalism reveals that the bilinear equations have an extremely simple structure (the Plücker relation or the Jacobi formula) if the soliton solutions are expressed by the determinants.

Take the Kadomtsev-Petviashvili(KP) equation for example

$$(4u_t - 6uu_x - u_{xx})_x - 3u_{yy} = 0, \quad (1)$$

which is transformed into the bilinear form

$$(D_x^4 - 4D_x D_t + 3D_y^2)\tau \cdot \tau = 0 \quad (2)$$

through the dependent variable transformation

$$u = 2(\log \tau)_{xx} \quad (3)$$

where integration constants are chosen to be zero. The wronskian form of the N-soliton solution to the KP equation is expressed by

$$\tau_{KP} = \det \left| \frac{\partial^{j-1} \phi_i}{\partial x^{j-1}} \right|_{1 \leq i, j \leq N} \quad (4)$$

where all ϕ_i satisfy the following linear differential equations for $n = 1, 2, \dots, \infty$

$$\frac{\partial \phi_i}{\partial x_n} = \frac{\partial^n \phi_i}{\partial x^n}, \quad (5)$$

where $x_1 = x, x_2 = y, x_3 = t, \dots$

Here we note that the Plücker relation are algebraic identities of determinants among which the simplest one is the following

$$\begin{vmatrix} a_0 & a_1 \\ b_0 & b_1 \end{vmatrix} \cdot \begin{vmatrix} a_2 & a_3 \\ b_2 & b_3 \end{vmatrix} - \begin{vmatrix} a_0 & a_2 \\ b_0 & b_2 \end{vmatrix} \cdot \begin{vmatrix} a_1 & a_3 \\ b_1 & b_3 \end{vmatrix} + \begin{vmatrix} a_0 & a_3 \\ b_0 & b_3 \end{vmatrix} \cdot \begin{vmatrix} a_1 & a_2 \\ b_1 & b_2 \end{vmatrix} = 0. \quad (6)$$

Recently Nakamura⁸ has shown that the bilinear KP equation reduces to the Jacobi formula of determinants provided that the solutions are expressed by the gramian type determinant

$$\tau_{KP} = \det |M_{ij}|_{1 \leq i, j \leq N}, \quad (7)$$

where

$$M_{ij} = c_{ij} + \int^x f_i g_j dx, \quad (8)$$

f_i and g_j satisfy the linear differential equations

$$\frac{\partial f_i}{\partial x_n} = \frac{\partial^n f_i}{\partial x^n}, \quad \frac{\partial g_j}{\partial x_n} = (-1)^{n-1} \frac{\partial^n g_j}{\partial x^n}. \quad (9)$$

In ref 7, a discrete bilinear equation was obtained:

$$[Z_1 \exp(D_1) + Z_2 \exp(D_2) + Z_3 \exp(D_3)]f \cdot f = 0 \quad (10)$$

where Z_i and D_i for $i = 1, 2, 3$ are arbitrary parameters and linear combinations of the bilinear operators D_t, D_x, D_y and D_n respectively. The equation generates various types of soliton equations including the KdV equation, the KP equation, the modified KdV equation, the sine-Gordon equation, etc. A Bäcklund Transformation and a Lax-pair for eq.(10) are also obtained.

As a special case of eq.(10) Miwa proposed the following bilinear difference equation:

$$\begin{aligned} & a(b-c)\tau(l-1, m, n)\tau(l, m-1, n-1) \\ & + b(c-a)\tau(l, m-1, n)\tau(l-1, m, n-1) \\ & + c(a-b)\tau(l, m, n-1)\tau(l-1, m-1, n) = 0 \end{aligned} \quad (11)$$

noindent where a, b, c are constants related to the intervals of the discrete space-time,⁹ which is called the discrete KP(d-KP) equation. The N-soliton solution of the d-KP equation τ_{disc} is expressed by a Casorati determinant (a discrete analogue of a wronskian):

$$\tau_{disc} = \det[\varphi_i(l, m, n, s + j - 1)]_{1 \leq i, j \leq N} \quad (12)$$

where $\varphi_i (i = 1, 2, \dots, N)$ satisfies the linear difference equation

$$\begin{aligned} \Delta_{-l}\varphi_i(l, m, n, s) &= \Delta_{-m}\varphi_i(l, m, n, s) = \Delta_{-n}\varphi_i(l, m, n, s) \\ &= \varphi_i(l, m, n, s + 1) \end{aligned} \quad (13)$$

where $\Delta_{-l}, \Delta_{-m}, \Delta_{-n}$ are the backward difference operators defined by

$$\Delta_{-l}\varphi_i \equiv [\varphi_i(l) - \varphi_i(l - 1)]/a, \quad (14)$$

$$\Delta_{-m}\varphi_i \equiv [\varphi_i(m) - \varphi_i(m - 1)]/b, \quad (15)$$

$$\Delta_{-n}\varphi_i \equiv [\varphi_i(n) - \varphi_i(n - 1)]/c. \quad (16)$$

On the other hand the N-soliton solution τ_{cont} of the continuous KP equation is expressed by

$$\tau_{cont} = \det \left[\frac{\partial^{j-1}}{\partial x_1^{j-1}} \varphi_i \right]_{1 \leq i, j \leq N}. \quad (17)$$

We show in the following that

$$\tau_{disc} = \tau_{cont} \quad (18)$$

up to a trivial factor. A general solution φ_{cont} to linear differential equation(5) is expressed by

$$\varphi_{cont} = \sum_p C_p \exp \left[\sum_{k=1}^{\infty} p^k x_k \right] \cdot p^s \quad (19)$$

while a general solution φ_{disc} to the linear difference equation(13) is expressed by

$$\varphi_{disc} = \sum_p C_p (1 - ap)^{-l} (1 - bp)^{-m} (1 - cp)^{-n} \dots p^s. \quad (20)$$

According to Miwa, we introduce an infinite number of coordinates $x_k (k = 1, 2, \dots)$ by

$$x_k = l \frac{a^k}{k} + m \frac{b^k}{k} + n \frac{c^k}{k} + \dots \quad (21)$$

Then we have

$$\begin{aligned} (1 - ap)^{-l} (1 - bp)^{-m} (1 - cp)^{-n} \dots \\ = \exp[-l \log(1 - ap) - m \log(1 - bp) - n \log(1 - cp) \dots] \\ = \exp \left[\sum_{k=1}^{\infty} p^k x_k \right], \end{aligned} \quad (22)$$

which gives

$$\varphi_{disc} = \varphi_{cont}. \quad (23)$$

Using a relation

$$\frac{\partial}{\partial x_1} \varphi_{cont}(s) = \varphi_{cont}(s + 1) \quad (24)$$

we find

$$\begin{aligned}
\tau_{disc} &= \det |\varphi_{disc,i}(l, m, n, s + j - 1)|_{1 \leq i, j \leq N} \\
&= \det \left| \frac{\partial^{j-1}}{\partial x_1^{j-1}} \varphi_{cont,i}(x_1, x_2, \dots, s) \right|_{1 \leq i, j \leq N} \\
&= \tau_{cont}.
\end{aligned} \tag{25}$$

Furthermore it can be shown that the bilinear d-KP eq. is reduced to the Plücker relation if τ_{disc} is expressed by the Casorati determinant and to the Jacobi formula of determinant provided that τ_{disc} is expressed by the discrete analogue of the gramian type determinant. The invariance of N-soliton solution of the bilinear equation under the transformation of the continuous coordinates x_1, x_2, \dots , into the discrete ones l, m, n, \dots , is a guiding principle of constructing discrete integrable systems.

DISCRETIZATION OF 2-D TODA MOLECULE EQUATION

We have the Toda lattice with free ends:

$$\frac{\partial^2}{\partial x \partial y} Q_n = V_{n+1} - 2V_n + V_{n-1}, \tag{26}$$

$$V_n = \exp(Q_n), \tag{27}$$

which has another expression:

$$\frac{\partial}{\partial x} V_n = V_n (J_n - J_{n+1}), \tag{28}$$

$$\frac{\partial}{\partial y} J_n = V_{n-1} - V_n, \tag{29}$$

for $n = 1, 2, 3, \dots, N-1$ with the boundary condition

$$V_0 = V_N = 0, \tag{30}$$

which is called the two-dimensional (2-D) Toda molecule equation. Let

$$V_n = \frac{\partial^2}{\partial x \partial y} \log(\tau_n). \tag{31}$$

Then eq.(26) is integrated with respect to x and y to give the bilinear form

$$\tau_n \frac{\partial^2 \tau_n}{\partial x \partial y} - \frac{\partial \tau_n}{\partial x} \frac{\partial \tau_n}{\partial y} = \tau_{n+1} \tau_{n-1} \tag{32}$$

where the integration constants are chosen to be zero. The boundary conditions eq.(30) are satisfied with $\tau_0 = 1$ and $\tau_N = \Phi(x)\chi(y)$, $\Phi(x)$ and $\chi(y)$ being arbitrary functions of x and y respectively.

Let a solution $\tau_n(x, y)$ to the bilinear eq.(32) be expressed by a two-directional wronskian of order n ,

$$\tau_n(x, y) = \det \left| \left(\frac{\partial}{\partial x} \right)^{i-1} \left(\frac{\partial}{\partial y} \right)^{j-1} \psi(x, y) \right|_{1 \leq i, j \leq n} \tag{33}$$

where $\psi(x, y)$ is an arbitrary function of x and y . Then eq.(32) becomes the Jacobi formula of determinants.

We conjecture that a difference analogue of the bilinear eq.(32) is the Jacobi formula which is expressed by a Casorati determinant

$$\hat{\tau}_n(l, m) = \det[\psi(l + i - 1, m + j - 1)]_{1 \leq i, j \leq n} \quad (34)$$

as follows

$$\hat{\tau}_n(l + 1, m + 1)\hat{\tau}_n(l, m) - \hat{\tau}_n(l + 1, m)\hat{\tau}_n(l, m + 1) = \hat{\tau}_{n+1}(l, m)\hat{\tau}_{n-1}(l + 1, m + 1). \quad (35)$$

The boundary conditions eq.(30) are satisfied with the following $\psi(l, m)$:

$$\psi(l, m) = \sum_{j=1}^{n+1} \hat{u}_j(l)\hat{v}_j(m). \quad (36)$$

Let $x = l\delta, y = m\epsilon$ where δ and ϵ are parameters specifying the intervals and $\hat{\tau}_n(l, m) = (\delta\epsilon)^{n(n-1)/2}\tau_n(x, y)$. Then eq.(35) is transformed into

$$\tau_n(x + \delta, y + \epsilon)\tau_n(x, y) - \tau_n(x + \delta, y)\tau_n(x, y + \epsilon) = \delta\epsilon\tau_{n+1}(x, y)\tau_{n-1}(x + \delta, y + \epsilon), \quad (37)$$

which is transformed back into a discretized 2-D Toda molecule equation:

$$\begin{cases} I_{n+1}(x, y)V_n(x, y) = I_n(x, y + \epsilon)V_n(x + \delta, y) \\ I_n(x, y) + \delta\epsilon V_n(x, y) = I_n(x, y + \epsilon) + \delta\epsilon V_{n-1}(x + \delta, y) \end{cases} \quad (38)$$

through the dependent variable transformation

$$I_n(x, y) = \frac{\tau_{n-1}(x, y)\tau_n(x + \delta, y)}{\tau_{n-1}(x + \delta, y)\tau_n(x, y)}, \quad (39)$$

$$V_n(x, y) = \frac{\tau_{n+1}(x, y)\tau_{n-1}(x, y + \epsilon)}{\tau_n(x, y)\tau_n(x, y + \epsilon)}. \quad (40)$$

Let $I_n(x, y) = 1 - \delta J_n(x, y)$. Then eq.(38) is transformed into

$$\begin{cases} \delta^{-1}[V_n(x + \delta, y) - V_n(x, y)] = V_n(x + \delta, y)J_n(x, y + \epsilon) - V_n(x, y)J_{n+1}(x, y), \\ \epsilon^{-1}[J_n(x, y + \epsilon) - J_n(x, y)] = V_{n-1}(x + \delta, y) - V_n(x, y), \end{cases} \quad (41)$$

which clearly shows that it becomes the 2-D Toda molecule equation in the small limit of δ and ϵ .

THE BÄCKLUND TRANSFORMATION

We have the discrete Toda molecule equation in the bilinear form

$$\tau_n(x + \delta, y + \epsilon)\tau_n(x, y) - \tau_n(x + \delta, y)\tau_n(x, y + \epsilon) = \delta\epsilon\tau_{n+1}(x, y)\tau_{n-1}(x + \delta, y + \epsilon). \quad (42)$$

Following the standard procedure we obtain a Bäcklund transformation for eq.(42):

$$\begin{cases} \tau_n(x, y + \epsilon)\tau'_n(x, y) - \tau_n(x, y)\tau'_n(x, y + \epsilon) \\ \quad = \epsilon\{\lambda\tau_{n+1}(x, y)\tau'_{n-1}(x, y + \epsilon) - \nu\tau_n(x, y + \epsilon)\tau'_n(x, y)\}, \\ \tau_n(x + \delta, y)\tau'_{n-1}(x, y) - \tau_n(x, y)\tau'_{n-1}(x + \delta, y) \\ \quad = \delta\{-\lambda^{-1}\tau_{n-1}(x + \delta, y)\tau'_n(x, y) + \mu\tau_n(x, y)\tau'_{n-1}(x + \delta, y)\}. \end{cases} \quad (43)$$

Let

$$\tau'_n(x, y) = \Psi_{n+1}(x, y)\tau_n(x, y). \quad (44)$$

Then eq.(43) is expressed, using eqs.(39),(40) and (44), by

$$\begin{cases} \psi_n(x, y) = \psi_n(x, y + \epsilon) + \epsilon V_{n-1}(x, y)\psi_{n-1}(x, y + \epsilon), \\ \psi_n(x + \delta, y) = I_n(x, y)\psi_n(x, y) + \delta\psi_{n+1}(x, y), \end{cases} \quad (45)$$

for $n = 0, 1, 2, \dots, N-1$ where we have chosen $\lambda = 1, \nu = \mu = 0$ for simplicity.

Let $\tilde{\psi}(x, y)$ be a N -dimensional vector:

$$\tilde{\psi}(x, y) = [\psi_1(x, y), \psi_2(x, y), \dots, \psi_N(x, y)]^T, \quad (46)$$

where T denotes the transposed matrix, and $L(x, y)$ and $R(x, y)$ be $N \times N$ matrices:

$$L(x, y) = \begin{pmatrix} 1 & & & & 0 \\ \delta V_1(x, y) & 1 & & & \\ & \delta V_2(x, y) & 1 & & \\ 0 & & \ddots & \ddots & \\ & & & \delta V_{N-1}(x, y) & 1 \end{pmatrix},$$

$$R(x, y) = \begin{pmatrix} I_1(x, y) & \epsilon & & & 0 \\ & I_2(x, y) & \epsilon & & \\ & & I_3(x, y) & \ddots & \\ 0 & & & \ddots & \epsilon \\ & & & & I_N(x, y) \end{pmatrix}.$$

Then eq.(45) is expressed with the matrices:

$$\begin{cases} \tilde{\psi}(x, y) = L(x, y)\tilde{\psi}(x + \delta, y), \\ \tilde{\psi}(x, y + \epsilon) = R(x, y)\tilde{\psi}(x, y), \end{cases} \quad (47)$$

and the compatibility condition of eq.(47) becomes a matrix equation:

$$R(x, y)L(x, y) = L(x + \delta, y)R(x, y + \epsilon), \quad (48)$$

which gives the discrete 2-D Toda molecule eq.

$$\begin{cases} I_n(x, y + \epsilon) - I_n(x, y) = \delta\epsilon[V_n(x, y) - V_{n-1}(x + \delta, y)], \\ I_n(x, y + \epsilon)V_n(x + \delta, y) = I_{n+1}(x, y)V_n(x, y). \end{cases} \quad (49)$$

LR FACTORIZATION METHOD

It is known¹⁰ that a discrete 2-D Toda molecule equation is reduced to a discrete 1-D Toda molecule equation by introducing a symmetric variable t with respect to x and y : $t = x + y, \delta = \epsilon$ and assuming that all dependent variables are functions of t only, namely $V_n(x, y) = V_n(t), I_n(x, y) = I_n(t), L(x, y) = L(t), R(x, y) = R(t)$, etc.

Accordingly we obtain a discrete 1-D Toda molecule equation:

$$\begin{cases} I_n(t + \delta) - I_n(t) = \delta^2[V_n(t) - V_{n-1}(t + \delta)], \\ I_n(t + \delta)V_n(t + \delta) = I_{n+1}(t)V_n(t), \end{cases} \quad (50)$$

which is expressed by a matrix equation:

$$R(t)L(t) = L(t + \delta)R(t + \delta). \quad (51)$$

Let us introduce a matrix $A(t)$ by

$$A(t) = L(t)R(t). \quad (52)$$

Then eq.(51) implies

$$A(t + \delta) = R(t)L(t). \quad (53)$$

Eqs.(52) and (53) for $\delta = 1$ are nothing but the LR factorization method of calculating eigenvalues of a matrix A . Hence we obtain eigenvalues of a matrix A by investigating the time-development of the Toda molecule equation¹². Details of the method will be published elsewhere.

Eqs.(52) and (53) show that

$$A(t + \delta) = L^{-1}(t)A(t + \delta)L(t). \quad (54)$$

Hence we have

$$Tr[A(t + \delta)]^m = Tr[A(t)]^m, \quad (55)$$

which implies that the trace of the m -th power of $A(t)$ is the m -th conserved quantity of the discrete 1-D Toda molecule equation. We note that the discrete 1-D Toda lattice equation with the periodic boundary conditions, $V_1(t) = V_{N+1}(t)$, $I_1(t) = I_{N+1}(t)$ is expressed by the same matrix equation as eq.(51) by introducing the periodicity of $V_n(t)$ and $I_n(t)$ into the matrices $L(t)$ and $R(t)$.

2-WAVE INTERACTION

We consider an discrete analogue of a system of coupled nonlinear partial differential equations describing interaction of two waves with constant velocities c_1 and $c_2 (\neq c_1)$

$$\begin{cases} \left(\frac{\partial}{\partial \tau} + c_1 \frac{\partial}{\partial \xi} \right) u = uv, \\ \left(\frac{\partial}{\partial \tau} + c_2 \frac{\partial}{\partial \xi} \right) v = -uv, \end{cases} \quad (56)$$

which is rewritten in the following form by the coordinates transformation

$$\begin{cases} \frac{\partial u}{\partial x} = uv, \\ \frac{\partial v}{\partial y} = -uv. \end{cases} \quad (57)$$

One of the authors has shown that eq.(57) is obtained by the Bäcklund transformation of the Toda molecule equation¹¹.

We show that the Bäcklund transformation of the discrete Toda molecule equation gives a discrete form of the 2-wave interaction. Let us introduce a couple of dependent variables $u_n(x, y)$ and $v_n(x, y)$ by

$$u_n \equiv \frac{\epsilon^{-1} [\tau_n(x, y + \epsilon) \tau'_n(x, y) - \tau_n(x, y) \tau'_n(x, y + \epsilon)]}{\tau_n(x, y + \epsilon) \tau'_n(x, y)} \quad (58)$$

$$= \lambda \frac{\tau_{n+1}(x, y) \tau'_{n-1}(x, y + \epsilon)}{\tau_n(x, y + \epsilon) \tau'_n(x, y)} - \nu \quad (59)$$

and

$$v_n \equiv - \frac{\delta^{-1} [\tau_n(x + \delta, y) \tau'_{n-1}(x, y) - \tau_n(x, y) \tau'_{n-1}(x + \delta, y)]}{\tau_n(x, y) \tau'_{n-1}(x + \delta, y)} \quad (60)$$

$$= \lambda^{-1} \frac{\tau_{n-1}(x + \delta, y) \tau'_n(x, y)}{\tau_n(x, y) \tau'_{n-1}(x + \delta, y)} - \mu, \quad (61)$$

where we have used eq.(43) in rewriting $u_n(x, y)$ and $v_n(x, y)$. Then we find that $u_n(x, y)$ and $v_n(x, y)$ satisfy a coupled difference equations.

$$\begin{cases} u_n(x + \delta, y) - u_n(x, y) &= \delta \{ [\nu + u_n(x + \delta, y)] v_n(x, y + \epsilon) - [\nu + u_n(x, y)] v_{n+1}(x, y) \}, \\ v_n(x, y + \epsilon) - v_n(x, y) &= \epsilon \{ [\mu + v_n(x, y + \epsilon)] u_{n-1}(x + \delta, y) - [\mu + v_n(x, y)] u_n(x, y) \}, \end{cases} \quad (62)$$

for $n = 1, 2, \dots, N$ which is a discrete analogue of 2N-wave interaction. As a very special case, let us take $N = 1, \mu = \nu = 0, v_2 = u_0 = 0$. Then eq.(62) is reduced to

$$\begin{cases} u_1(x + \delta, y) - u_1(x, y) &= \delta u_1(x + \delta, y) v_1(x, y + \epsilon), \\ v_1(x, y + \epsilon) - v_1(x, y) &= -\epsilon v_1(x, y) u_1(x, y), \end{cases} \quad (63)$$

which is a discrete form of 2-wave interaction.

It is also possible, by using the bilinear formalism, to construct the following nonlinear difference equation.

$$u_n(t + \delta) - u_n(t) = \delta [u_{n-1}(t + \delta) u_n(t) - u_n(t + \delta) u_{n+1}(t)], \quad (64)$$

which is reduced in the small limit of δ to a system of Lotka-Volterra prey-predator equations

$$\frac{d}{dt} u_n = u_n (u_{n-1} - u_{n+1}), \quad \text{for } n = -\infty, \dots, -1, 0, 1, \dots, \infty. \quad (65)$$

Details of derivation of eq.(64) will be published elsewhere.

References

1. B.Grammaticos, A.Ramani and V.Papageorgiou, Phys.Rev.Letters **67**(1991)1825.
2. A.Ramani, B.Grammaticos and J.Hietarinta, Phys.Rev.Letters **67**(1991)1829.
3. J.Gibbons and B.Kupershmidt, Phys.Letters A **165**(1992)105.
4. R.S.Ward, Phys.Letters A **165**(1992)325.
5. R.Hirota, J.Phys.Soc.Jpn. **43**(1977)1424.
6. R.Hirota, J.Phys.Soc.Jpn. **45**(1978)321.
7. R.Hirota, J.Phys.Soc.Jpn. **50**(1981)3785.
8. A.Nakamura, J.Phys.Soc.Jpn. **58**(1989)412.
9. T.Miwa, Proc.Jpn.Acad. **58**(1982)9.

10. R.Hirota, M.Ito and F.Kako, Progr.Theor.Phys.Suppl. 94(1988)42.
11. R.Hirota, J.Phys.Soc.Jpn. 57(1988)436.
12. W.W.Symes, Physica 4D(1982)275.

SOLITONS IN CROSSED-FIELD DEVICES

D.J. Kaup

Institute for Nonlinear Studies
Clarkson University
Potsdam, NY 13699

Abstract

A new application for soliton theory is the nonlinear evolution of an electromagnetic wave in a crossed-field device such as a magnetron or a crossed-field amplifier. With a singular perturbation analysis, we are able to more accurately predict the operating range of such devices. Important new insights into the physics of how these devices operate are also found.

1 Introduction

Crossed-field devices such as magnetrons and crossed-field amplifiers (CFA's) are very important as generators and amplifiers of high frequency (GHz) electromagnetic radiation. They are found in radar devices, telecommunication systems as well as in the now very common microwave ovens. Obviously, engineers know how to build them. But how do they operate and what are the exact physical principles on which they do operate? If such were fully understood, then one should be able to predict, from first principles, their operating characteristics such as the voltage operating range, power output, gain and etc. Unfortunately such cannot be done. The engineers have found some very good rules and design criteria for building these devices but the classical theories^{1,2} are not able to explain many of the important details of these criteria. In particular, the classical theories predict a much larger voltage operating range than is experimentally observed. What we will describe here is a nonlinear theory³ based on the nonlinear Schrodinger equation which will successfully predict an operating range much more in agreement with experiment.

In the next section, we will describe the geometry and the physical arrangement in a simple planar CFA. (Although actual devices are usually cylindrical, most CFA's do have a sufficiently small aspect ratio such that they can be approximated by a planar model.) The main points of this section will be to describe the structure of the electron

sheath about the cathode which is a key feature of these devices. In particular, we will delineate how the shear flow in the sheath and its height is related to the applied voltage. These are very important points since they determine whether or not an interaction between an *rf* electromagnetic wave near the anode will occur with the sheath through a very simple wave-particle interaction, $\omega = kv_0$. This interaction is the basis of the classical theory.

In Section III we will briefly describe the nonlinear analysis whereby we can obtain a nonlinear Schrodinger description of a propagating electromagnetic pulse and discuss its consequences. Here we will delineate our considerations which lead us to the NLS model. Our guiding principle will be the experimental operation of these devices, using this as a criteria for the validity of a theory. Since the theoretical calculations are given elsewhere, we shall avoid giving those here and instead simply give a concise verbal description of their results and consequences. Finally, in order to find a more accurate description of the experimental operating range, we are lead to consider a Vlasov-Poisson model which is currently being investigated. Already this model has provided physical justification as to why the classical and cold-fluid theories fail. The reason for this is quite simple and will be discussed at the end.

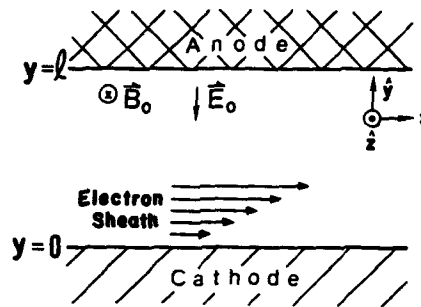


FIGURE 1 - Geometry and shear flow in a planar crossed-field device.

Finally I wish to acknowledge my collaborator in this work, Gary E. Thomas who is the group leader of the Advanced Technology Division of Varian Beverly. Gary has had considerable experience with these devices and has worked hard at keeping me "honest" in relation to the experimental situation through all my theoretical calculations. He originally studied solitons under Flora Chu (who was a student of A. C. Scott) at MIT, which explains in part his strong interest in this NLS approach.

2 Geometry and Simple Theory

The geometry of a planar magnetron is shown in Fig. 1. There is a large positive voltage on the anode relative to the cathode which pulls electrons out of the cathode and into the vacuum region between the cathode and anode. As the electrons

are accelerated toward the anode, a large magnetic field (perpendicular to the figure and into the paper) turns the electrons around, preventing them from reaching the anode. Eventually a stable sheath of electrons is formed about the cathode with the magnetic field producing a magnetic insulation between the cathode and anode. We shall always assume translational invariance parallel to the magnetic field.

There is an equilibrium configuration where the sheath is stationary and translationally invariant in the x-direction (parallel to the electrodes). One may easily solve for this configuration from the cold-fluid plasma equations coupled to Poisson's equation. There equations are

$$\partial_t \vec{v} + (\vec{v} \cdot \vec{\nabla}) \vec{v} = \vec{\nabla} \phi - \Omega \hat{k} \times \vec{v} \quad (1)$$

$$\nabla^2 \phi = \omega_p^2 \quad (2)$$

where $\phi = (e/m)$ times the electrostatic potential, $\Omega = (eB/mc)$ is the electron cyclotron frequency where B is the (static) magnetic field and ω_p^2 is the electron plasma frequency, $4\pi e^2 n_0/m$, where n_0 is the electron number density. These are the basic equations that we will use here. Everything will follow from this simple set of two equations.

The equilibrium configuration follows upon taking $\partial_t = 0 = \partial_x$ and $v_y = 0$. One then has

$$v_x = v_0 = \partial_y \phi / \Omega \quad (3)$$

$$\partial_y^2 \phi = \omega_p^2 \quad (4)$$

The boundary conditions on (4) are $\phi(0) = 0$ (simply choosing the cathode to be grounded) and $\partial_y \phi(0) = 0$ (space charge limited current condition - if this was nonzero then more electrons would be pulled out of the cathode causing it to decrease until it vanished anyway). Integrating (4) from the cathode to anode must then give the applied cathode-anode voltage. This gives only one condition on the electron density profile. However from these equations, there are no other conditions on the equilibrium density profile, $n_0(y)$. It is arbitrary except that (4) must integrate to give the correct applied interelectrode voltage.

From (3) and (4) it follows that

$$\partial_y v_0 = \omega_p^2 / \Omega \quad (5)$$

showing that the electrons will undergo a shear flow. This shear flow is an $E \times B$ drift, vanishing at the cathode and rising to some maximum value at the top of the electron sheath. Typical density profiles are shown in Fig. 2. The classical density profile², called a Brillouin flow, is shown in Fig. 2a. (The other profiles will be discussed later.) Here one assumes that the electron density takes on the maximum possible value (consistent with single-particle stability - to be discussed later) of $\omega_p^2 = \Omega^2$. The height of the profile, b , is then determined by the applied voltage. Integrating (4), we have

$$\phi = \frac{1}{2} \Omega^2 y^2 \quad (0 < y < b) \quad (6a)$$

$$\phi = b \Omega^2 (y - \frac{1}{2} b) \quad (b < y < \ell) \quad (6b)$$

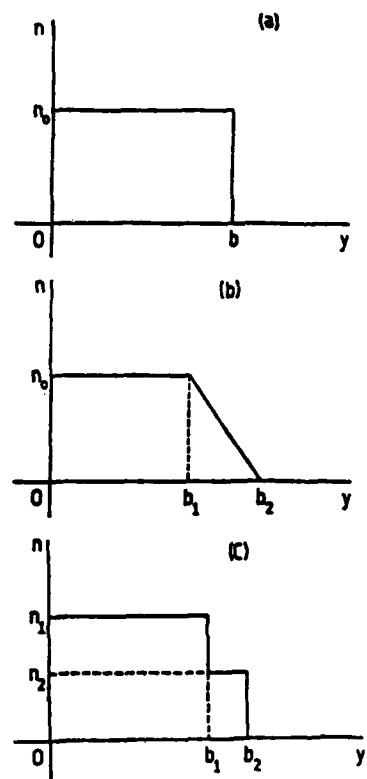


FIGURE 2a - The classical Brillouin (box) profile, b) The same with a ramp added, and c) The same with a plateau on the edge (double box).

where ℓ is the cathode-anode spacing. Requiring (6b) to give the correct applied voltage, V , gives

$$b(\ell - \frac{1}{2}b) = \frac{eV}{m\Omega^2} \quad (7)$$

which determines b . (Only one root is physical.) Note that from (3) and (6), the drift velocity

$$v_0 = \Omega y \quad (0 < y < b) \quad (8a)$$

$$v_0 = \Omega b \quad (b < y < \ell) \quad (8b)$$

increases linearly from zero at the cathode up to the value of Ωb at the top of the sheath ($y = b$).

The behavior of the equilibrium sheath as a function of applied voltage follows from these equations. As one increases the applied voltage from zero, the height of the profile, b [determined by (7)] also increases from zero monotonically up until $b = \ell$. At this voltage,

$$V_{cutoff} = \frac{1}{2} \frac{m}{e} \ell^2 \Omega^2 \quad (9)$$

the device will become conducting because the sheath has reached the anode. At this point, one no longer has magnetic insulation. This voltage is called the Hull cutoff voltage, V_{cutoff} . Also note that as the voltage increases from zero, the maximum drift velocity, $b\Omega$, also increases in a like manner since it is exactly proportional to b .

Now consider what happens when a small rf signal is injected at the left end and travels to the right in the same direction as the drift velocity, v_0 . (Such a signal is always localized near the anode due to the presence of a "slow wave structure" built into the anode. This structure does not directly interact with the sheath and serves only to slow the electromagnetic rf wave to a phase velocity much less than the speed of light. Given any frequency, it forces the rf wave to have a definite value for k where $\omega/k \ll c$.) If the voltage is so low such that the maximum drift velocity, $b\Omega$, is less than the phase velocity, ω/k , of the rf wave, then nothing happens. The drift velocity of all the electrons are too slow to stay in phase with the rf wave. Thus they see only an oscillating electric field which time averages to zero. If one now raises the applied voltage, one will reach a voltage at which the drift velocity of the electrons at the top of the sheath will exactly match the phase velocity of the rf signal. The voltage at which these velocities become equal is called the "Hartree voltage", V_H , and its value follows from $b\Omega = \omega/k$ and (7). This is

$$V_H = \frac{m\omega}{e k} (\Omega \ell - \frac{1}{2} \omega/k) \quad (10)$$

The significance of the Hartree voltage is that for voltages above the Hartree voltage, there is always a layer of electrons in the sheath whose drift velocity exactly matches the phase velocity of the rf wave on the anode structure ($v_0 = \omega/k$). Now this layer of electrons can strongly interact with the rf wave since they travel exactly in phase with it. Exactly what happens next is not fully understood, but what seems to happen is that the electrons in this layer are induced to move across the vacuum region onto the anode, depositing the electrostatic potential energy that they have gained (from the DC field) in phase with the rf wave, thereby amplifying it.

3 Nonlinear Analysis

Such are the basics of the classical theory. But it needs refinements. For example, one of the major differences between predictions of classical crossed-field device theory and actual operating performance of crossed-field amplifiers is the voltage range over which microwaves are generated. Classical theory^{1,2} predicts that operation should occur from the Hartree voltage to the Hull cutoff voltage. Experimental data⁴ obtained on crossed-field amplifiers shows that operation only occurs for ratios of applied voltage to Hartree voltage of up to 1.3. For typical operating magnetic field values, $1.3 V_{Hartree}$ is much less than the Hull cutoff voltage. For a theory to be considered valid for predicting crossed-field amplifier performance, that theory must predict the operating voltage range and provide an understanding of the physics responsible for this observed behavior.

Using this observed performance as a major check of our theoretical work, we have pursued an approach based on a nonlinear Schrodinger equation and a modulational instability. The motivation behind using an approach based on the nonlinear Schrodinger (NLS) equation was that an NLS equation is known to describe a large number of weakly nonlinear systems and it is widely accepted that crossed-field devices are at least weakly nonlinear if not strongly nonlinear systems. Furthermore, one can argue that the conditions in a crossed-field device are the same generic conditions which occurs whenever the NLS is applicable^{5,6,7}. Namely the motion is 1) essentially one-dimensional, 2) the wave is almost monochromatic, 3) the dispersion is weak, and 4) the nonlinearity (at least in the initial stages) is weak.

The key to understanding the operation of a crossed-field device lies in the plasma density profile shape. The classical profile shape, Brillouin flow² (see Fig. 2a), has been extensively analyzed^{8,9,10} in the literature. It does have an internal eigenmode which has wave-particle resonance ($v_0 = \omega/k$), but this resonance is well below the top of the sheath. This mode is almost never seen in particle simulations and also violates the engineering design criteria¹¹ where the resonance has to occur at the top of the sheath. Thus it does not predict the correct operating eigenfrequencies of such devices. This all indicates that the assumed classical profile may well be in error. Consequently, we have searched for other possible realistic profile shapes that could give the correct eigenfrequencies. One of our approaches has been to investigate how the higher order nonlinearities could eventually distort the original Brillouin density profile into some other shape. We had found that second-order (in amplitude) effects would introduce a density gradient¹². Consequently, one could expect the classical Brillouin profile rather quickly to adjust itself into a "box plus ramp" profile as shown in Fig. 2b. After this was realized, considerable theoretical and numerical effort¹³ went into trying to find an eigenfrequency when the resonance ($\omega = kv_0$) was located along the negative density gradient at the edge. This effort was a general failure for finding such an eigenfrequency. However it did reveal that the eigenfrequencies absolutely would not ever occur along a negative density gradient. In fact, they could only be found to exist when the resonance occurred in a constant density region (zero density profile). (Any density profile with a region of a positive density profile was always strongly linearly unstable¹⁴.)

After this, it was realized that any density profile in the form of either a box or a box plus ramp would never have a correct operational eigenfrequency. So the main question now became what would be the linear evolution of such an initial profile. To answer this, it was essential to study the general initial value problem and to study the evolution of the continuous spectrum. It was found that the continuous spectrum could always introduce plateaus at the resonances¹⁵. This then suggested the double-box profile shown in Fig. 2c. From our previous extensive numerical studies, it was recognized that such a profile could indeed have a second eigenfrequency on the outer

plateau. Numerical calculations quickly verified such, as well as the fact that this eigenfrequency was indeed in the correct operating range. Further exploration of this revealed that the parameter region of interest was when the thickness (in y) of the second box is very small. In this case, we could actually obtain analytical solution by using the thickness of this second box as a small parameter for expansion.

This result had given us a workable linear theory on which to base a nonlinear analysis. The general nonlinear theory was presented in 1989^{16,17} and was independent of the density profile shape. The only condition for the validity of this nonlinear analysis is the absence of any linear instabilities. The general results of this nonlinear analysis are quite generic. The analysis is based on a singular perturbation expansion¹⁸. In first order, one has the linear theory. If one has no linear instabilities, then one proceeds to second-order. Here one finds that the envelope will move with the group velocity, strong density gradients will tend to diffuse away¹², and the background shear flow will undergo a nonlinear shift^{12,16}. In third-order, the nonlinear shift in the background shear flow is the source of the nonlinearity which drives the nonlinear Schrodinger equation (NLS), which is

$$i\partial_\tau\Psi + \frac{1}{2}\omega_{kk}\partial_x^2\Psi + \Gamma\Psi^*\Psi^2 = 0 \quad (11)$$

In the above, τ is the (slow) time, $\omega(k)$ is the linear eigenfrequency, $\omega_{kk}(=\frac{d^2\omega}{dk^2})$ is the dispersion, $\chi = x - v_g t$ is the comoving coordinate where $v_g(=\frac{d\omega}{dk})$ is the group velocity, Γ is the nonlinear coefficient (complex in general), and Ψ is the normalized rf electric field amplitude inside the crossed-field device. Fundamental formulas for calculating the above coefficients in the general case have been give in References 16 and 17. These can be easily specialized to the case when the profile is the double-box profile in Fig. 2c.

In the limit of a small outer box on the profile, we can determine the frequency spectrum, the group velocity, the dispersion and the nonlinear coefficient. The general results³ are that the dispersion is always positive and the real part of the nonlinear coefficient, Γ , is always positive. Whence these modes are always MODULATIONALLY UNSTABLE and soliton formation is possible. Furthermore, the imaginary part of the nonlinear coefficient is always very much smaller than the real part. Thus damping can be neglected and the nonlinear evolution of this eigenmode will be described by the NLS, eq. (11).

Using this analytical solution to evaluate the coefficients we can predict the operating voltage range for the S-band crossed-field amplifier and compare these predictions to available experimental data³. This comparison, is shown in Fig. 3. The upper and lower curves of Fig. 3 are the cutoff and Hartree voltages respectively. According to classical theory, the device should operate anywhere between these voltages. The dots are experimental values delineating the lower and upper ranges of the actual operating voltage as a function of the (normalized) magnetic field, Ω/ω . Clearly, in reality, operation only occurs over a very small fraction of the region predicted by the classical theory. The middle curve is our prediction based on the NLS model. At low values of magnetic field it appears that there is close agreement between the predictions of the theory and the experimental data. Unfortunately, the theory does not correctly predict the behavior at high values of magnetic field. However, at least the maximum voltage curve from the nonlinear theory is less than the Hull cutoff curve.

The fact that the nonlinear theory does not correctly predict the high magnetic field behavior indicates that a simplifying assumption used may be incorrect. One possibility is that the cold-fluid assumption is incorrect and that finite temperature and pressure effects should be included. One can also show from a scaling analysis of the

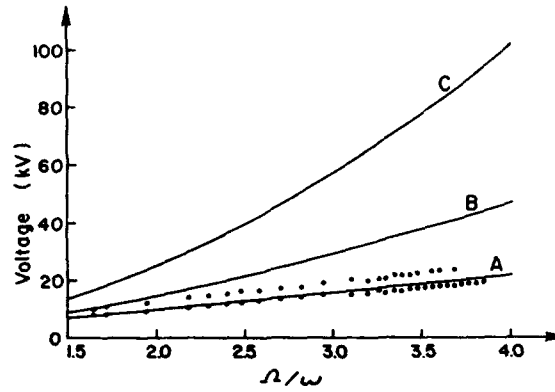


FIGURE 3 - Operating voltage vs. magnetic field for experiment (dots) and theory (solid lines). The dots indicate the maximum and minimum operating voltages for an experimental device. The curve labeled A is the Hartree voltage which is the minimum voltage at which the device should operate. The upper curve labeled C is the cutoff voltage which is the maximum operating voltage according to classical theory. The curve labeled B is the maximum operating voltage per our criteria.

cold fluid equations that the theoretical operating range must always increase as $\Omega^{\frac{1}{2}}$ for large magnetic fields. On the other hand, the experimental data indicates an operating range almost independent of the magnetic field. This further indicates that additional parameters (such as temperature) must be included.

This might seem strange at first that one would consider including temperature effects since typical operating voltages involved are on the order of kilovolts whereas thermal effects would be only on the order of volts (typical of the metallic work functions). However recent results on the Vlasov-Poisson system¹⁹ for a planar crossed-field device shows that thermal effects can be much more important than has been previously suspected. This is because electrons in a dense nonneutral plasma will not oscillate at the cyclotron frequency Ω . Rather they will oscillate²⁰ at the reduced hybrid frequency of Δ , where

$$\Delta^2 = \Omega^2 - \omega_p^2 \quad (12)$$

and their Larmor radius will typically be

$$r_L = v_T / \Delta \quad (13)$$

where v_T is a typical thermal velocity. For a Brillouin flow where $\omega_p^2 = \Omega^2$, one has $\Delta^2 = 0$ and therefore $r_L = \infty$! Thus in the interior of the sheath, where ω_p^2 is probably just less than Ω^2 , very small thermal velocities can now give rise to extremely large orbital variations¹⁹. In other words, the interior of the sheath is probably very far from being a cold laminar flow. Rather it is most likely closer to a hot turbulent flow where any cold-fluid mode deep in the sheath would be rapidly damped out due to the thermal noise. Thus we also have a very reasonable and physical explanation as to why any interior cold-fluid modes are not observed. They are simply heavily damped. Only for the modes near of on the edge of the top of the sheath, where the density of the sheath is dropping off toward zero, can the thermal damping be small. Only such modes could resonant with the rf wave along the anode.

Thus the inclusion of thermal and pressure effects may well be physically reasonable and is now being currently explored. We hope to eventually be able to calculate the thermal effects on the NLS coefficients and expect that this would be able to give us much better agreement between theory and experiment.

ACKNOWLEDGEMENT

This work has been supported in part by the Air Force Office of Scientific Research through Grant No. AFOSR-89-0510 and by NWSC, Crane, Indiana.

REFERENCES

- [1] John C. Slater, Microwave Electronics, Chapter 13 (D. Van Nostrand Co., Princeton, NJ 1959).
- [2] O. Buneman, R.H. Levy and L.M. Linson, Journal of Applied Physics 37, 8 (1966).
- [3] D.J. Kaup and Gary E. Thomas, J. Appl. Phys. 71, 5752 (1992).
- [4] Gary E. Thomas, IEEE Trans. on Electron Devices, ED-29, 1210, 1982; S.W. Shpock, MSEE Thesis entitled "Experimental Verification of Soliton Theory Using a Microwave Crossed-Field Amplifier", Univ. of Utah, 1984.
- [5] D.J. Benney and A.C. Newell, J. Math. and Phys. 46, 133 (1967).
- [6] V.E. Zakharov and A.B. Shabat, Zh. Eksper. Theoret. Fiz. 61, 118 (1971); Soviet Phys. JETP 34, 62 (1972).
- [7] A.K. Liu and D.J. Benney, Stud. Appl. Math. 64, 247 (1981).
- [8] R.V. Loveland and E. Ott, Phys. Fluids 17, 1263 (1974).
- [9] John Swegle, Phys. Fluids 26, 1670 (1983).
- [10] D. Chernin and Y.Y. Lau, Phys. Fluids 27, 2319 (1984).
- [11] Hunter McDowell, "Equations for Crossed-Field Tubes- Linear Case", Unpublished SFD Laboratories, Inc. Report; also see reference number 1.
- [12] D.J. Kaup, S. Roy Choudhury, and Gary E. Thomas, Phys. Rev. A 38, 1402-1409 (1988).
- [13] D.J. Kaup (Unpublished).
- [14] R.C. Davidson and K.T. Tang, Phys. Fluids 28, 1169 (1985).
- [15] D.J. Kaup, Phys. Fluids B2, 2253 (1990).
- [16] D.J. Kaup and Gary E. Thomas, Stud. Appl. Math 81, 37-78 (1989).
- [17] Errata for Reference 15 above. Stud. Appl. Math 83, 271 (1990).
- [18] A.H. Nayfeh, Introduction to Perturbation Techniques, (Wiley, New York, 1981).
- [19] D.J. Kaup and Gary E. Thomas, Phys. Fluids B4, 2640-2644 (1992).
- [20] S.A. Prasad, G.J. Morales, and B.D. Fried, Phys. Fluids 30, 3093-3105 (1987).

THE NUMERICAL INVERSE SCATTERING TRANSFORM: NONLINEAR FOURIER ANALYSIS FOR LABORATORY AND OCEANIC WAVE DATA

A.R. Osborne

Instituto di Fisica Generale dell'Università
Via Pietro Giuria 1
10125 Torino, Italy

INTRODUCTION

This paper summarizes a new numerical approach for the *nonlinear Fourier analysis of space and time series* of complex, nonlinear wave trains. The method, based upon the periodic/quasi-periodic *inverse scattering transform* (IST), is a kind of nonlinear generalization of the ordinary, linear Fourier transform. I focus on nonlinear wave motion for shallow water waves as governed by the Korteweg-deVries (KdV) equation. IST may be exploited to determine the *numerical inverse scattering transform* (NIST) spectrum of a measured or computed wave train which is assumed to be periodic (or quasi-periodic) in space or in time. The approach may also be applied to *numerically construct complex solutions* to the KdV equation. I build on previous successes in the application of the periodic scattering transform to the analysis of computer generated or experimentally measured data [Bishop, et al., 1986; Bishop and Lomdahl, 1986] [Osborne and Bergamasco, 1985, 1986] [Osborne and Segre, 1990] [Flesch, et al., 1991] [Osborne, et al., 1991] [Osborne, 1991a, 1991b] [Osborne, 1992]. In particular I analyze examples of computer generated wave trains and of measured wave data obtained in the Adriatic Sea, near Venice, Italy.

THE KdV EQUATION AND PERIODIC INVERSE SCATTERING THEORY

The Korteweg-deVries equation describes (among many physical applications) the motion of small, finite-amplitude nonlinear wave trains in shallow water. KdV was the first of many nonlinear wave equations to be completely integrated by what is now called the *inverse scattering transform* [Zakharov et al., 1980; Ablowitz and Segur, 1981; Dodd et al., 1982; Newell, 1985; Degasperis, 1991].

The dimensional form for the (space-like) KdV equation is given by:

$$\eta_t + c_0 \eta_x + \alpha \eta \eta_x + \beta \eta_{xxx} = 0 \quad (1)$$

$\eta(x, t)$ is the wave amplitude as a function of space x and time t . For shallow water wave motion the constant coefficients of KdV are given by $c_0 = (gh)^{1/2}$, $\alpha = 3c_0/2h$ and $\beta = c_0 h^2/6$. Eq. (1) has the linearized dispersion relation $\omega = c_0 k - \beta k^3$; g is the acceleration of gravity, c_0 is the linear phase speed and h is the water depth. Subscripts with respect to x and t refer to partial derivatives. KdV solves the *Cauchy problem*: given the spatial behavior of the wave train at $t = 0$, $\eta(x, 0)$, (1) determines the motion for all space and time thereafter, $\eta(x, t)$. Here we use periodic boundary conditions so that $\eta(x, t) = \eta(x+L, t)$, L the period.

The most common experimental situation is to record data as a function of time at a single spatial location; this implies the need to determine the scattering transform of a *time series*, $\eta(0, t)$. To this end one may apply the *time-like* KdV equation (TKdV) [Karpman, 1976; Ablowitz and Segur, 1981]:

$$\eta_x + c_0' \eta_t + \alpha' \eta \eta_t + \beta' \eta_{ttt} = 0 \quad (2)$$

where $c_0' = 1/c_0$, $\alpha' = -\alpha/c_0^2$ and $\beta' = -\beta/c_0^4$; (2) has the linearized dispersion relation $k = \omega/c_0 + (\beta/c_0^4)\omega^3$. TKdV solves a *boundary value problem*: given the temporal evolution $\eta(0, t)$ at a fixed spatial location $x = 0$, (2) determines the wave motion over all space as a function of time, $\eta(x, t)$. Either periodic ($\eta(x, t) = \eta(x, t+T)$) or quasi-periodic boundary conditions (there exists a $T(\epsilon)$ such that $|\eta(x, t+T) - \eta(x, t)| < \epsilon$ for all t) are assumed herein. TKdV is now routinely applied to the time series analysis of experimental data [Osborne 1991a; Osborne et al., 1991].

The solution to the periodic KdV equation (1) may be written as a *linear superposition of nonlinearly interacting, nonlinear waves* called hyperelliptic functions, $\mu_j(x; x_0, 0)$:

$$\lambda \eta(x, t) = -E_1 + \sum_{j=1}^N [2\mu_j(x; x_0, t) - E_{2j} - E_{2j+1}] \quad (3)$$

The constant parameter $\lambda = \alpha/6\beta$. This is the first of the trace formulae for the KdV equation [Dubrovin and Novikov, 1975; Flaschka and McLaughlin, 1976] and may be interpreted as a kind of *nonlinear Fourier series*. The constant parameters E_{2j} , E_{2j+1} are eigenvalues of the "main spectrum" of periodic theory as discussed in the next section; x_0 is an arbitrary base point in the interval $0 \leq x \leq L$. The μ_j are the *nonlinear oscillation modes* of periodic KdV. The μ_j spatially evolve according to the following system of coupled, nonlinear, ordinary differential equations:

$$\frac{d\mu_j}{dx} = \frac{2i\sigma_j R^{1/2}(\mu_j)}{\prod_{\substack{k=1 \\ j \neq k}}^N (\mu_j - \mu_k)} \quad (4)$$

where

$$R(\mu_j) = \prod_{k=1}^{2N+1} (\mu_j - E_k) \quad (5)$$

The $\sigma_j = \pm 1$ are the signs of the square root of $R(\mu_j)$. The μ_j dynamically evolve on two-sheeted Riemann surfaces; the branch points connecting the surfaces are referred to as "band edges" and are denoted by E_{2j} and E_{2j+1} . The μ_j lie inside an "open band," e.g. in the interval

$E_{2j} \leq \mu_j \leq E_{2j+1}$, and oscillate between these limits as a function of x . When a μ_j reaches a band edge (either E_{2j} or E_{2j+1}) the sign σ_j changes and the motion leaps to the other Riemann sheet. This fact, together with the strong nonlinear coupling occurring among the μ_j , presented considerable difficulties for Osborne and Segre [1990] in numerical integrations of (4).

The temporal evolution of the μ_j is given by:

$$\frac{d\mu_j}{dt} = -2[\lambda\eta(x, t) - 2\mu_j]\frac{d\mu_j}{dx} \quad (6)$$

where $\lambda\eta(x, t)$ is given by (3). The space (4) and time (6) ODEs evolve the $\mu_j(x, t)$ and the *nonlinear Fourier series* (3) allows one to construct general solutions to the KdV equation. In what follows I describe methods for numerically computing the oscillation modes $\mu_j(x, 0)$ at a particular instant of time, $t = 0$. The requisite numerical methods are then christened *space or time series nonlinear Fourier analysis procedures* [Osborne, 1991a].

Generally speaking I refer to the numerical determination of the *main spectrum* (E_i ; $1 \leq i \leq 2N+1$) and the *auxiliary spectrum* ($\mu_j(x_0)$, $\sigma_j = \pm 1$; $1 \leq j \leq N$) as the *direct scattering transform* (see details in the Section below). The computation of the hyperelliptic functions $\mu_j(x; x_0, t)$ as solutions of the nonlinear ODEs (4)-(6) and the construction of solutions of the KdV equation by the trace formula (3) constitutes the *inverse scattering transform*. Herein I (a) discuss new numerical procedures for obtaining the direct scattering transform and (b) show that the inverse scattering transform as obtained by numerical integration of (4)-(6) (e.g. as considered by Osborne and Segre [1990]) can be replaced by a much simpler, more precise and faster algorithm.

THE PERIODIC INVERSE SCATTERING TRANSFORM

The spectral problem (the direct scattering transform) for KdV is the Schroedinger eigenvalue problem:

$$\psi_{xx} + [\lambda\eta(x) + k^2] \psi = 0 \quad (k^2 = E) \quad (7)$$

where $\eta(x) = \eta(x, 0)$ is the solution to the KdV equation (1) at an arbitrary time $t = 0$; k is the spectral wavenumber. Periodic boundary conditions are assumed so that $\eta(x, t) = \eta(x + L, t)$ for L the period.

Details of the inverse scattering theory will not be given here, but may be found elsewhere [Dubrovin and Novikov, 1974; Dubrovin, Matveev and Novikov 1976]. For numerical purposes it is appropriate to consider a basis of solutions (c, s) such that [Flaschka and McLaughlin, 1976]:

$$\begin{pmatrix} c(x_0) & c'(x_0) \\ s(x_0) & s'(x_0) \end{pmatrix} = \begin{pmatrix} 1 & 0 \\ 0 & 1 \end{pmatrix} \quad (8)$$

The wronskian $W(c, s) = 1$ so that (c, s) is a basis set. The matrix α carries the solution matrix from point x to $x + L$:

$$\begin{pmatrix} c(x+L) & c'(x+L) \\ s(x+L) & s'(x+L) \end{pmatrix} = \begin{pmatrix} \alpha_{11} & \alpha_{12} \\ \alpha_{21} & \alpha_{22} \end{pmatrix} \begin{pmatrix} c(x) & c'(x) \\ s(x) & s'(x) \end{pmatrix} \quad (9)$$

α is often referred to as the *monodromy matrix*.

The so called *main spectrum* consists of eigenvalues E_i that correspond to the Bloch eigenfunctions for a particular period L . The *auxiliary spectrum* is defined as the eigenvalues for which the eigenfunction $s(x)$ have the fixed boundary conditions $s(x_0+L) = s(x_0) = 0$. To this end one has the specific spectral definitions:

$$\begin{aligned} \text{Main Spectrum } \{E_i; 1 \leq i \leq 2N+1\}: & \quad \frac{1}{2}(\alpha_{11} + \alpha_{22})(E) = \pm 1 \\ \text{Auxiliary spectrum } \{\mu_j; 1 \leq j \leq N\}: & \quad \alpha_{21}(\mu) = 0 \\ \{\sigma_j\} = \{\text{sgn} [\alpha_{11}(E) - \alpha_{22}(E)]_{E=\mu_j}; 1 \leq j \leq N\} \end{aligned} \quad (10)$$

The eigenvalues $\{E_i; \mu_j; \sigma_j\}$ constitute the *direct scattering transform* of a wave train of N degrees of freedom. The *inverse scattering transform*, (3)-(6), then allows for the construction of complex wave train solutions of the KdV equation.

THE NUMERICAL ALGORITHM

The numerical search for the scattering eigenvalues $\{E_i; \mu_j; \sigma_j\}$ suggests the need for the derivatives of the matrix α_{ij} with respect to the energy E . This is because one normally uses a Newtonian numerical root-finding algorithm to determine the eigenvalues. Such a procedure is always more precise when analytical expressions are available for the derivatives. To achieve this goal, a matrix method for obtaining the evolution of the eigenfunction ψ as a function of x and E for a particular wave train $\eta(x, 0)$ has been developed. Key to this approach is the analytical estimation of derivatives of the matrix elements with respect to E .

To this end the scattering equations are:

$$\begin{aligned} \psi_{xx} &= -q \psi \\ \psi_{xEx} &= -q \psi_E - \psi \end{aligned} \quad (11)$$

where the subscripts refer to differentiation with respect to x and E ; $q(x) = \lambda \eta(x) + E$. Writing (11) in four-vector notation and using a Taylor series expansion for the solution to the scattering equations (11) one obtains:

$$\begin{pmatrix} \psi(x+\Delta x) \\ \psi_x(x+\Delta x) \\ \psi_E(x+\Delta x) \\ \psi_{xE}(x+\Delta x) \end{pmatrix} = H \begin{pmatrix} \psi(x) \\ \psi_x(x) \\ \psi_E(x) \\ \psi_{xE}(x) \end{pmatrix} \quad (12)$$

where

$$H = \begin{pmatrix} T & 0 \\ T_E & T \end{pmatrix} \quad (13)$$

Each element of H is a two-by-two matrix. The matrix 0 has zero for all its elements and the other matrices are given by

$$T = \begin{pmatrix} \cos(\kappa\Delta x) & \frac{\sin(\kappa\Delta x)}{\kappa} \\ -\kappa \sin(\kappa\Delta x) & \cos(\kappa\Delta x) \end{pmatrix} \quad (14)$$

and

$$T_E = \frac{\partial T}{\partial E} = \begin{pmatrix} -\frac{\Delta x \sin(\kappa\Delta x)}{2\kappa} & \frac{\Delta x \cos(\kappa\Delta x)}{2\kappa^2} - \frac{\sin(\kappa\Delta x)}{2\kappa^3} \\ -\frac{\Delta x \cos(\kappa\Delta x)}{2} + \frac{\sin(\kappa\Delta x)}{2\kappa} & -\frac{\Delta x \sin(\kappa\Delta x)}{2\kappa} \end{pmatrix} \quad (15)$$

for $\kappa = (q)^{1/2} = (\lambda\eta(x) + E)^{1/2}$. While κ may be either real or imaginary, the matrix T_E is always real with determinant 1. This property is exploited in the numerical algorithm below.

As in previous numerical problems of this type I assume the wave train $\eta(x)$ has the form of a *piecewise constant function* with $2M$ partitions on the periodic interval $(0, L)$, where the discretization interval is $\Delta x = L/2M$ [Osborne, 1991a]. Each partition has wave amplitude η_n ($1 \leq n \leq 2M$) which is associated with a discrete value of the spatial variable $x_n = n\Delta x$. The four-by-four scattering matrix M can then be defined:

$$M = \prod_{n=M-1}^{-M} H(\eta_n, \Delta x) \quad (16)$$

The initial conditions of the basis (c, s) at the base point x_0 are given by:

$$\begin{pmatrix} c(x_0) \\ c'(x_0) \\ c_E(x_0) \\ c'_E(x_0) \end{pmatrix} = \begin{pmatrix} 1 \\ 0 \\ 0 \\ 0 \end{pmatrix} \quad \begin{pmatrix} s(x_0) \\ s'(x_0) \\ s_E(x_0) \\ s'_E(x_0) \end{pmatrix} = \begin{pmatrix} 0 \\ 1 \\ 0 \\ 0 \end{pmatrix} \quad (17)$$

From the definition of the matrix α_{ij} one has:

$$\{\alpha_{ij}\} = \begin{pmatrix} c(x+L) & c'(x+L) \\ s(x+L) & s'(x+L) \end{pmatrix} \begin{pmatrix} c(x) & c'(x) \\ s(x) & s'(x) \end{pmatrix}^{-1} \quad (18)$$

Thus at x_0 one finds

$$\frac{1}{2}(\alpha_{11} + \alpha_{22}) = \frac{1}{2}(M_{11} + M_{22}) \quad (19)$$

$$\alpha_{21} = M_{12} \quad (20)$$

while the derivatives are given by

$$\frac{\partial}{\partial E} \frac{1}{2}(\alpha_{11} + \alpha_{22}) = \frac{1}{2}(M_{31} + M_{42}) \quad (21)$$

$$\frac{\partial \alpha_{21}}{\partial E} = M_{32} \quad (22)$$

Implementation of the Numerical Algorithm

Because $\kappa = (\lambda\eta(x,0) + k^2)^{1/2}$ can be either real or imaginary, but not complex, the matrix H is always real. This result allows implementation of an algorithm which is entirely real. The following relations have been used in the computer code:

$$T_{11} = T_{22} = \begin{cases} \cos(\kappa' \Delta x) & \text{if } \kappa^2 \geq 0 \\ \cosh(\kappa' \Delta x) & \text{if } \kappa^2 < 0 \end{cases} \quad (23)$$

$$T_{12} = \begin{cases} \frac{\sin(\kappa' \Delta x)}{\kappa'} & \text{if } \kappa^2 \geq 0 \\ \frac{\sinh(\kappa' \Delta x)}{p'} & \text{if } \kappa^2 < 0 \end{cases} \quad (24)$$

$$T_{21} = \begin{cases} -\kappa' \sin(\kappa' \Delta x) & \text{if } \kappa^2 \geq 0 \\ \kappa' \sinh(\kappa' \Delta x) & \text{if } \kappa^2 < 0 \end{cases} \quad (25)$$

where

$$\kappa' = \sqrt{|\lambda \eta + k^2|} = \sqrt{|\kappa^2|} \quad (26)$$

and analogously for the matrix T_E .

The construction of complex solutions of the KdV equation by (3) is carried out by computing the auxiliary spectra $\mu_j(x_0 = x_n)$ for the $2M$ different base points $x_0 = x_{-M}, x_1, x_2, \dots, x_{M-1}$. This is done by computing $2M$ different monodromy matrices (16) which differ from each other by a horizontal shift Δx in the wave train η_n . This procedure arises from the following similarity transformation which is easily seen from (16):

$$M(x_{n+1}, E) = H(\eta_n, E) M(x_n, E) H(\eta_n, E)^{-1} \quad (27)$$

The latter expression relates the matrix $M(x_{n+1}, E)$ at a point x_{n+1} to the previously computed matrix $M(x_n, E)$ at x_n for a particular value of $E = k^2$. Values of the auxiliary spectra $\{\mu_j(x_n)\}$ for each x_n are computed from the matrices $M(x_n, E)$. Knowledge of the auxiliary spectra at every point x_n allows reconstruction of the wave train $\eta(x_n)$ via a discrete version of (3):

$$\lambda \eta(x_n) = -E_1 + \sum_{j=1}^N [2\mu_j(x_n) - E_{2j} - E_{2j+1}] \quad (28)$$

for $n = -M, \dots, 1, 2, \dots, M-1$. These are finite-term nonlinear generalizations of Fourier series for the discrete wave train $\eta(x_n)$. As indicated by the notation each nonlinear oscillation mode $\{\mu_j\}$ implicitly depends upon the associated wavenumber k_j of the mode. The k_j are theoretically given by the simple relation $k_j = j\Delta k$, $\Delta k = 2\pi/L$; surprisingly these are exactly the same as for the linear Fourier transform. The IST spectrum then consists of the widths of the open bands of the Floquet discriminant, $a_j = (E_{2j+1} - E_{2j})/2$, graphed as a function of k_j .

EXAMPLES OF NONLINEAR FOURIER ANALYSIS

I give three examples indicating how the algorithms discussed herein can be used. The first example shows how to construct solutions to the KdV equation using the numerical scattering transform (Fig. 1). The second example shows how the numerical IST can be used to analyze a computer generated wave train (Fig. 2). The last example shows how to analyze a typical time series recorded from the ocean (Fig. 3).

Fig. 1 illustrates the numerical construction of a three degree-of-freedom wave train. In panel (a) are the hyperelliptic functions μ_j , $j = 6, 9, 11$; in the present case the μ_j are constructed from a rather arbitrary selection of the eigenvalues E_{2j} , E_{2j+1} . The linear superposition of the three oscillation modes gives the solution to KdV as shown in the upper part of panel (a). Note that the hyperelliptic oscillation modes are highly non-sinusoidal in appearance due to nonlinear effects. In panel (b) are shown the amplitudes of the linear Fourier modes (solid line) and of the three hyperelliptic modes (vertical lines). Comparing these results one concludes that only three nonlinear oscillation modes (three $\mu_j(x)$) are required to describe the motion, while instead the number of linear Fourier modes is quite large (~ 50).

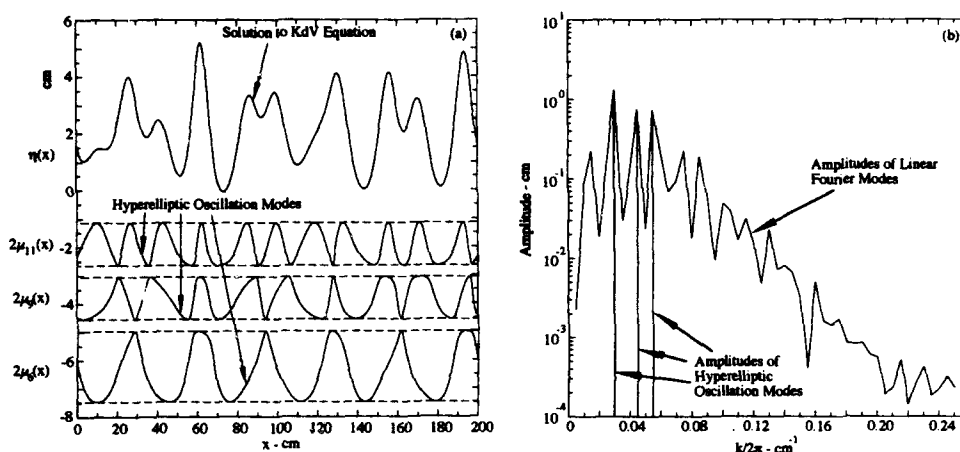


Figure 1. Synthesis of a wave train solution to the KdV equation. In (a) three hyperelliptic function oscillation modes are linearly superposed to give the solution to KdV. In (b) are graphed the linear Fourier transform of the wave train (solid line) and the three nonlinear Fourier amplitudes (the $\mu_j(x)$, vertical lines).

In Fig. 2 I consider a computer generated wave train, a negative gaussian pulse as shown in panel (a). The pulse is analyzed by the numerical IST algorithm. The Floquet discriminant is shown in (b), the first six hyperelliptic oscillation modes are graphed as a function of x in (c) and in panel (d) the amplitudes of the oscillation modes are graphed as a function of wavenumber. Physically, a fully negative wave train on the infinite line has only radiation modes in the infinite-line IST spectrum for KdV. The six hyperelliptic functions shown in Fig. 2(c) are the dominant modes in the *periodic* radiation spectrum.

As the final example I consider results recently published by Osborne et al. [1991] with regard to the analysis of nonlinear wave data obtained in a measurement program in the Adriatic Sea about 10 km from Venice, Italy. The data were recorded in 16.5 m of water on the research tower of the Italian National Research Council (Consiglio Nazionale delle Ricerche). A typical measured wave train, a 500 point time series, is shown in Fig. 3(a). A data set was selected for which most of the wave energy was in the dominant direction of propagation; only 2% of the wave energy was perpendicular to this direction. This insured that the waves were essentially unidirectional. The significant wave height (average of the highest one third waves) is $H_s = 3.0$ m and the dominant period $T_d = 9.1$ sec.

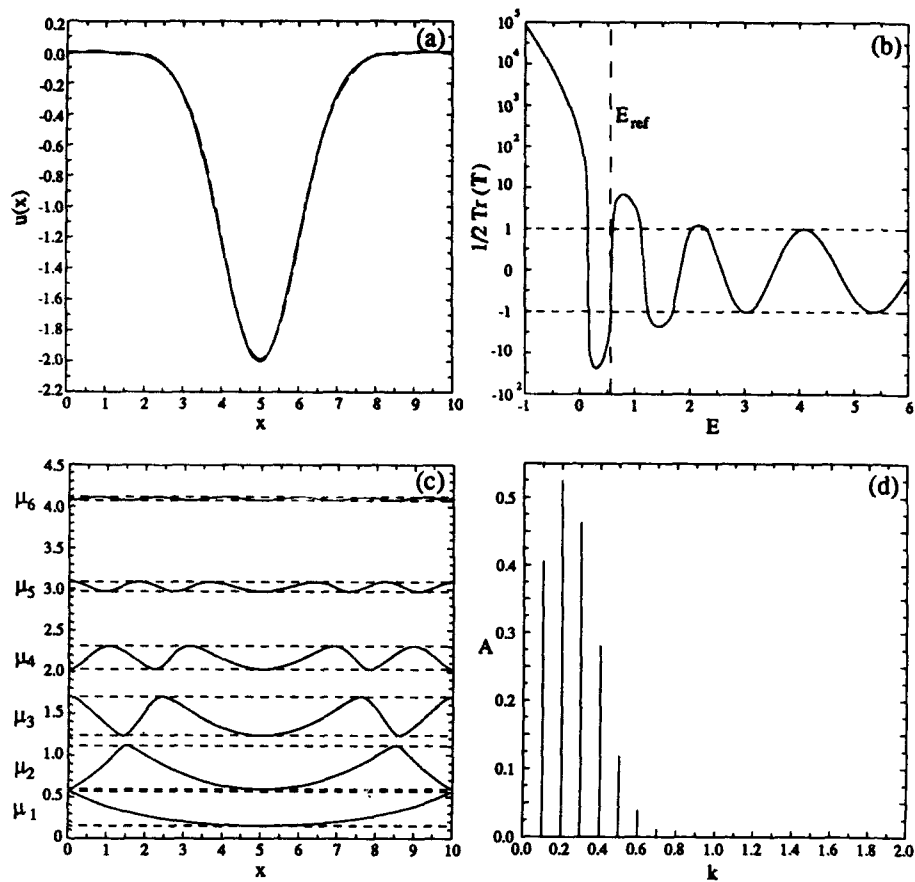


Figure 2. A negative gaussian pulse, assumed to propagate according to the nonlinear dynamics of the KdV equation, is shown in (a). The Floquet diagram is shown in (b) and the six most energetic hyperelliptic oscillation modes are graphed as a function of the spatial variable x in (c). The amplitudes of the oscillation modes (widths of the open bands in the Floquet spectrum) are graphed in (d).

On the basis of the Ursell number, $Ur = 2gH_s T_d^2 / 4h^2 \sim 8$, the Adriatic Sea waves may be judged to be mildly nonlinear. The linear Fourier spectrum is shown in Fig. 3(b); the result is quite typical of measured ocean wave spectra. The Floquet discriminant is shown in Fig. 3(c). The spectrum divides itself into two widely separated regions of activity corresponding to solitons (on the left) and radiation components (on the right). The IST spectrum is given in Fig. 2(d) where the spectral components are graphed as a function of frequency. The radiation spectrum is shown as a solid curve on the right, while the solitons are displayed on the left as vertical arrows. About 10% of the wave energy lies in the soliton part of the spectrum. In the originally measured wave train, the soliton components are obscured by the radiation modes, e.g. solitons reside in the spectrum, but they are not directly visible due to the presence of the energetic radiation components. The soliton dynamics are physically significant, but *not directly visible by an observer of the measured wave train*. Nevertheless, using the numerical methods described herein, we are able to locate the solitons and to explore their dynamics. This is done by a kind of *nonlinear filtering*. Returning to the spectrum in Fig. 3(d) one can think of each component (as a function of frequency) as contributing to the nonlinear Fourier series (28). By deleting the terms corresponding to the radiation modes, and then summing the remaining terms for the soliton part of the spectrum, we obtain *only* the contribution that the solitons make to the measured nonlinear wave train. The result of this numerical

calculation is given in Fig. 3(a) at the same scale as the measured time series. We see a long, low amplitude train, consisting of nine nonlinearly interacting solitons. We have therefore, using the numerical inverse scattering transform as a data analysis tool, found the solitons hidden in a sea of background radiation. An important physical result is that the solitons tend to be *phase locked* beneath the maxima of the wave packets. I am personally convinced that this fact provides an important clue to the eventual understanding of the behavior of nonlinear wave dynamics in the Ursell number regime under investigation. Theoretical understanding of these results is, however, still lacking.

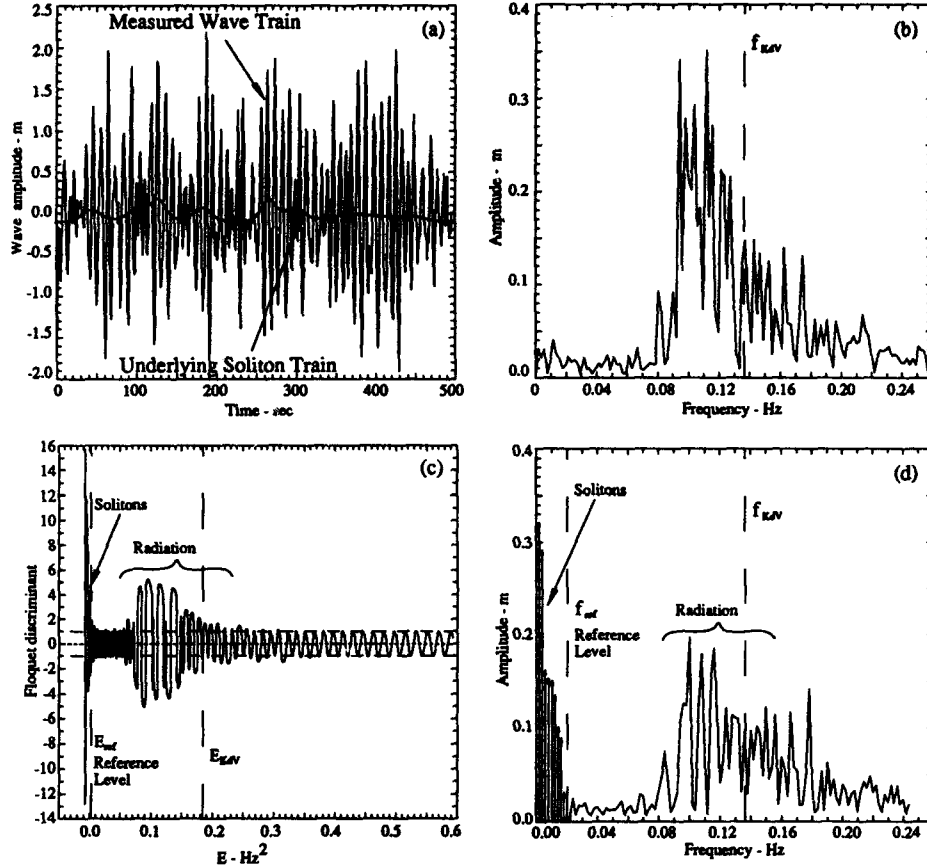


Figure 3. Numerical IST analysis of an experimentally measured wave train in 16.5 m water depth in the Adriatic Sea, about 10 km offshore Venice, Italy (a). The linear Fourier amplitudes are graphed in (b). In (c) the Floquet discriminant clearly shows well-separated regions dominated by solitons and radiation. The nonlinear Fourier (IST) spectrum is shown in (d), where nine solitons are present in the spectrum together with a strong radiation component. The radiation has been filtered from the measured signal and the resultant soliton train is then graphed beneath the measured wave train in (a). Osborne, et al., 1991, Phys. Rev. Lett. 64, No. 15:1733.

CONCLUSIONS

The periodic scattering transform for the KdV equation is exploited to analyze computer generated and experimentally measured data. The method gives rise to new physical understanding for the propagation of complex wave trains governed by KdV. I expect that

many surprises await further application of the approach to a wide variety of physical situations.

Acknowledgements

L. Bergamasco, G. Boffetta, G. Cavaleri, M. Petti and E. Segre are thanked for their collaboration on various aspects of this project. This work was supported in part by the Office of Naval Research of the United States of America (Grant N00014-92-J-1330) and by the Progetto Salvaguardia di Venezia del Consiglio Nazionale delle Ricerche, Italy.

REFERENCES

- Ablowitz, M. J. and Segur, H., 1981, "Solitons and the Inverse Scattering Transform," SIAM, Philadelphia.
- Bishop, A. R., Forest, M. G., McLaughlin, D. W., and Overman II, E. A., 1986, *Physica D* 18:293.
- Bishop, A. R., and Lomdahl, P. S., 1986, *Physica D* 18:54.
- Degasperis, A., 1991, "Nonlinear Wave Equations Solvable by the Spectral Transform," in: "Nonlinear Topics in Ocean Physics," A. R. Osborne ed., Elsevier, Amsterdam.
- Dodd, R. K., Eilbeck, J. C., Gibbon, J. D. and Morris, H. C., 1982, "Solitons and Nonlinear Wave Equations," Academic Press, London.
- Dubrovinn, B. A., and Novikov, S. P., 1974, *Sov. Phys. JETP* 40:1058.
- Dubrovinn, B. A., Matveev, V. B. and Novikov, S. P., 1976, *Russian Math. Surv.* 31:59.
- Flaschka, H. and McLaughlin, D. W., 1976, *Prog. Theoret. Phys.* 55:438.
- Flesch, R., Forest, M. G., and Sinha, A., 1991, *Physica D* 48:169.
- Karpman, V. I., 1975, "Non-Linear Waves in Dispersive Media," Pergamon, Oxford.
- Newell, A. C., 1985, "Solitons in Mathematics and Physics," SIAM, Philadelphia.
- Osborne, A. R. and Bergamasco, L., 1985, *Nuovo Cimento B* 85:2293.
- Osborne, A. R. and Bergamasco, L., 1986, *Physica D* 18:26.
- Osborne, A. R. and Segre, E., 1990, *Physica D* 44:575.
- Osborne, A. R., Segre, E., Boffetta, G., and Cavaleri, L., 1991, *Phys. Rev. Lett.* 64, No. 15:1733.
- Osborne, A. R., 1991a, in: "Nonlinear Topics in Ocean Physics," A. R. Osborne ed., North-Holland, Amsterdam.
- Osborne, A. R., 1991b, *J. Comp. Phys.* 94, No. 2:284.
- Osborne, A. R., 1992, in preparation.
- Zakharov, V. E., Manakov, S. V., Novikov, S. P. and Pitayevsky, M. P., 1980, "Theory of solitons. The Method of the Inverse Scattering Problem," Nauka, Moscow (in Russian).

SOLITONS IN DISCRETE SYSTEMS

Morikazu Toda

5-29-8-108 Yoyogi, Shibuya-ku
Tokyo 151, Japan

INTRODUCTION

Since nonlinear dynamics has been developed so widely that it is nearly impossible for me to choose appropriate topics in a reasonably impartial way avoiding dogma and prejudice even limited to the theories related to solitons in discrete systems.

This time, though it looks a little out of scope of the present title, let me begin with some historical stories how I happened to find the integrable lattice, the exponential lattice or the Toda lattice, and its lattice solitons. This is because I think that the story of discovery may be of some help to those who are searching some way of breakthrough in their researches. After that, explanation of other topics will also be given.

Then, in the latter half of my talk, I will present my comparatively recent finding that the motion in an exponential lattice looks as if it is composed of independent excitations, which are different from ordinary solitons. This seems asymptotically exact in the limit of very long lattice, and these excitations are definitely classified into two modes; harmonic or phonon mode and nonlinear or so to say pseudo-soliton mode. I found these modes by looking at the partition function of the exponential lattice. But the existence of such excitations, especially the pseudo-solitons is still an open question.

EXPONENTIAL LATTICE

I remember that it was around 1957 when we begun to have a group, called the lattice group, of physicists in Japan, who are particularly interested in exact solutions. We were stimulated by the computer experiments just started, which revealed that conventional perturbation method sometimes failed in grasping the specific feature of phenomena such as the localized modes around impurities, (Dean 1955), enhancement of heat flow due to nonlinearity of the interaction between lattice particles (Payton et al., 1967), and so on.

My study of nonlinear systems was put forward when I found papers by Ford (1961, 1964). He numerically studied nonlinear lattice with a few particles, and clarified that certain one-dimensional nonlinear lattices marvellously sustained the character of linear modes. (His study was initiated by the famous computer experiments

by Fermi et al. (1955). But I could not see these paper at that time). From his results, I thought that there would be a lattice model with some particular interaction between particles which would admit exact periodic wave solutions and possibly other solutions.

My strategy was as follows (Toda 1967). Firstly, we consider the equations of motion of an infinite lattice

$$m\ddot{x}_n = -\phi'(x_n - x_{n-1}) + \phi'(x_{n+1} - x_n), \quad (1)$$

and linearize the interaction terms by rewriting Eq.(1) as

$$m\dot{r}_n = 2s_n - s_{n-1} - s_{n+1}, \quad \dot{s}_n = -\partial\phi(r_n)/\partial r_n, \quad (2)$$

($r_n = x_n - x_{n-1}$). We assume that the last equation affords single valued solution

$$r_n = -\chi(\dot{s}_n)/m, \quad (3)$$

to have

$$\frac{d}{dt}\chi(\dot{s}_n) = -2s_n + s_{n-1} + s_{n+1} \quad (4)$$

which are called the dual equations of motion.

Secondly, the interaction $\phi(r)$ is expected to be something like the interatomic potential, which is harmonic for small oscillation, and $\phi(r)$ must not include parameters such as the amplitude, frequency, or wave-length which characterize particular solutions.

Lastly, I expected simple analytic solutions. Several candidate functions were examined. Finally I noticed some similarity between Eq.(4) and the equation

$$2\frac{\partial}{\partial u} \frac{\text{sn} u \text{ cn} u \text{ dn} u \text{ sn}^2 v}{1 - k^2 \text{sn}^2 u \text{ sn}^2 v} = \text{sn}^2(u+v) - \text{sn}^2(u-v). \quad (5)$$

Here sn, cn, dn are Jacobi's elliptic functions of the same modulus k . We put

$$s_n(u) = c \left\{ \int_0^u \text{dn}^2 u \, du - \frac{E}{K} u \right\}, \\ u = (\nu t \pm \frac{n}{\lambda}) 2K, \quad v = \frac{2K}{\lambda}, \quad (6)$$

(c, ν, λ are constants, $E = E(k)$ and $K = K(k)$ are the complete elliptic integrals of the 1st and 2nd kind), to find that the periodic function $s_n(u)$ (with the period $2K$) satisfies

$$\frac{c}{2K\nu} \frac{d}{dt} \log \left[1 + \frac{\dot{s}_n}{c2K\nu \left(\frac{1}{\text{sn}^2(2K/\lambda)} - 1 + \frac{E}{K} \right)} \right] = s_{n-1} + s_{n+1} - 2s_n. \quad (7)$$

Therefore Eq.(4) is satisfied when we assume that

$$c2K\nu \left(\frac{1}{\text{sn}^2(2K/\lambda)} - 1 + \frac{E}{K} \right) = a, \\ \frac{c}{2K\nu} = \frac{m}{b}, \\ \chi(\dot{s}_n) = -r = \frac{m}{b} \log \left(1 + \frac{\dot{s}_n}{a} \right) + m\sigma,$$

where a, b and σ are constants independent of λ and k .

The inverse function of $\chi(\dot{s}_n)$ gave the interaction potential of the nice form,

$$\phi(r) = \frac{a}{b} e^{-b(r-\sigma)} + a(r-\sigma) + \text{const.}, \quad (8)$$

which led to the equations of motion conveniently written as

$$m\ddot{x}_n = a \left\{ e^{-b(s_n - s_{n-1})} - e^{-b(s_{n+1} - s_n)} \right\}, \quad (9)$$

or

$$\frac{\ddot{s}_n}{a + \dot{s}_n} = \frac{b}{m} (s_{n-1} + s_{n+1} - 2s_n), \quad (10)$$

and the periodic solution (lattice cnoidal wave)

$$e^{-bs_n} - 1 = \frac{(2K\nu)^2}{ab/m} \left\{ \text{dn}^2 \left[2 \left(\nu t \pm \frac{n}{\lambda} \right) K \right] - \frac{E}{K} \right\}, \quad (11)$$

with the dispersion relation

$$2K\nu = \sqrt{\frac{ab}{m}} / \sqrt{\frac{1}{\text{sn}^2(2K/\lambda)} - 1 + \frac{E}{K}}. \quad (12)$$

Thus the lattice and the periodic solution were obtained at once.

Taking the long wavelength limit $\lambda \rightarrow \infty$, keeping $\alpha = 2K/\lambda$ finite ($k \rightarrow 1$), I derived the soliton solution (Toda 1967)

$$e^{-bs_n} - 1 = \frac{m}{ab} \beta^2 \text{sech}^2(\alpha n \pm \beta t), \quad \beta = \sqrt{\frac{ab}{m}} \sinh \alpha. \quad (13)$$

I immediately recognized that the soliton solution could be written in terms of

$$\text{sech}^2 u = \frac{\partial^2}{\partial u^2} \log \cosh u,$$

and was led to see that two-soliton solution were obtained as a second derivative of simple certain functions ψ (Toda, 1969) in such a way that

$$e^{-bs_n} - 1 = \frac{m}{ab} \frac{\partial^2}{\partial t^2} \log \psi. \quad (14)$$

Later it was found that multi-soliton solutions in general could be written in this form.

The integrable character of the exponential lattice was numerically demonstrated by Ford (1973) and Saito (1973), and it was analytically shown (Henon, 1974; Flaschka, 1974) that the exponential lattice of N particles had N independent constants of motion, which are in convolution (Manakov 1975). Therefore the lattice is integrable in Liouville's sense. The method of integration for the infinite exponential lattice was shown by Flaschka (1974) by using the inverse scattering transform, and by Hirota (1976) by his direct method. The method of solving the cyclic lattice was clarified by Date and Tanaka (1976), and Kac (1975).

The development of the theory of exponential lattice is well-known (Toda, 1989). We may refer to other ways of integration, Bäcklund transformation, generalized lattices including two-dimensional lattice, relation to integrable continuous systems

such as the KdV equation, study of nearly integrable systems, the Bethe ansatz, quantum lattice, and so on.

Fermi et al. (1955) discovered recurrence to initial state of some nonlinear lattices. Their model systems were not exponential lattice: they had cubic, quartic or broken linear nonlinearity. For these systems, it has been shown later (Saito et al., 1970) that when the parameter responsible for nonlinearity (or the initial energy) is increased beyond a certain threshold, stochastization of motion suddenly takes place, just like breakdown.

If the interaction force between particles vanishes when the separation gets too large, the lattice may be broken to pieces (chopping phenomena) by reflection of solitons at free boundaries (Toda et al., 1976).

Though the problem of thermal conductivity is very old, it is not yet fully clarified (Toda, 1979). There are at least four factors to be examined. They are effects of (1)impurities or defects, (2)nonlinearity, (3)dimensionality, and (4)the enormous number of atoms in real materials.

PARTITION FUNCTION

It is several years since I found a very strange but interesting formula related to the exponential lattice. It is that the motion in the lattice can be asymptotically decomposed into harmonic and nonlinear excitations. That is, the configurational part of the partition function $Q(\beta)$ per particle,

$$Q(\beta) = \int_{-\infty}^{\infty} \exp\{-\beta(e^{-r} - 1 + r)\} dr. \quad (15)$$

(in dimensionless form) can be written as (see APPENDIX)

$$Q(\beta) = \lim_{n \rightarrow \infty} \sqrt{\frac{2\pi}{\beta}} \prod_{j=1}^{n-1} \left\{ 1 - \exp\left(-\beta 2\pi \tan \frac{j\pi}{2n}\right) \right\}^{-1/2n}. \quad (16)$$

For a lattice of N particles, the partition function is $Q_N(\beta) = \{Q(\beta)\}^N$. Writing $N = 2n$, we see that the partition function for large N can be written asymptotically as

$$\begin{aligned} Q_N(\beta) &= \left(\sqrt{\frac{2\pi}{\beta}}\right)^N \prod_{j=1}^{N/2} \left\{ 1 - \exp\left(-\beta 2\pi \frac{j\pi}{N}\right) \right\}^{-1} \\ &= \left(\sqrt{\frac{2\pi}{\beta}}\right)^N \prod_{j=1}^{N/2} \sum_{n_j=0}^{\infty} e^{-\beta n_j \epsilon_j} \end{aligned} \quad (17)$$

where

$$\epsilon_j = 2\pi \tan \frac{j\pi}{N} \quad (j = 1, 2, \dots, N/2). \quad (18)$$

In the r.h.s. of Eq.(17), the factor $\sqrt{2\pi/\beta}$ is the partition function of a harmonic oscillator. The second factor, namely

$$e^{N\eta(\beta)} = \prod_{j=1}^{N/2} \left(1 - e^{-\beta \epsilon_j} \right)^{-1} \quad (19)$$

should be responsible for the nonlinearity of the interaction.

As a matter of fact, for low temperatures $\beta = 1/kT \rightarrow \infty$, where nonlinearity is not important, we have

$$e^{N\eta(\beta)} \simeq 1.$$

And, for high temperatures $\beta = 1/kT \rightarrow 0$, we have

$$e^{N\eta(\beta)} \simeq \prod_{j=1}^{N/2} \frac{1}{\beta \epsilon_j} = \left(\frac{1}{2\pi\beta} \right)^{N/2},$$

so that $Q(\beta) \simeq 1/\beta$, which coincides, as it should, with the hard sphere limit

$$\int_0^\infty e^{-\beta r} dr = \frac{1}{\beta}.$$

Thus Eq.(15) indicates that the motion in the lattice consists of harmonic oscillations and nonlinear excitations ϵ_j , which is quite different from the ordinary solitons. If such nonlinear excitations really exist, they may be called pseudo-solitons, or nonlinear modes.

When the one-dimensional lattice is under an external pressure P , we can make use of the effective potential $\phi_P(r)$ (we return to original units)

$$\begin{aligned} \phi_P(r) &= \frac{a}{b}(e^{-br} - 1 + r) + Pr \\ &= \phi_0 + \frac{a}{b}e^{-br_0} \left\{ e^{-b(r-r_0)} - 1 + b(r-r_0) \right\}, \end{aligned} \quad (20)$$

where

$$\begin{aligned} e^{-br_0} &= 1 + \frac{P}{a}, \\ \phi_0 &= \frac{P}{a} - \frac{a}{b} \left(1 + \frac{P}{a} \right) \log \left(1 + \frac{P}{a} \right). \end{aligned} \quad (21)$$

With these modifications, we have the partition function $Q_N(z) = \{Q(z)\}^N$,

$$Q(z) = \frac{1}{b} e^{-\beta\phi_0} \sqrt{\frac{2\pi}{z}} e^{\eta(z)}, \quad (22)$$

where

$$\eta(z) = -\frac{1}{N} \sum_{j=1}^{N/2} \log(1 - e^{-z\epsilon_j}) \quad (23)$$

with ϵ_j given by Eq.(18) and

$$z = \beta \frac{a}{b} \left(1 + \frac{P}{a} \right). \quad (24)$$

The factor $\sqrt{2\pi/z}$ on the r.h.s. of Eq.(22) is responsible for the harmonic part of the potential

$$\phi_P(r) \simeq (a + P)b(r - r_0)^2,$$

and $\eta(z)$ for the nonlinear part, or for the pseudo-solitons.

The lattice expands with increasing temperature. The change in the average distance between particles is calculated as

$$\begin{aligned}\bar{r} - r_0 &= \frac{\int_{-\infty}^{\infty} (r - r_0) \exp\{-\beta\phi_P(r)\} dr}{\int_{-\infty}^{\infty} \exp\{-\beta\phi_P(r)\} dr} \\ &= \frac{1}{2(a+P)} \left(kT + \frac{\tilde{E}}{N} \right),\end{aligned}\quad (25)$$

where the first term $kT/2(a+P)$ is due to the dependence of the harmonic part of the potential on the pressure P , and the second term is due to the energy \tilde{E} due to the pseudo-solitons, which is given as

$$\tilde{E} = \sum_{j=0}^{N/2} \frac{a}{b} \left(1 + \frac{P}{a} \right) \epsilon_j = -N \frac{a}{b} \left(1 + \frac{P}{a} \right) \frac{\partial \eta(z)}{\partial z}. \quad (26)$$

The limiting values of \tilde{E} are

$$\tilde{E} \rightarrow \begin{cases} N/2\beta & (T \rightarrow \infty) \\ 0 & (T \rightarrow 0) \end{cases}$$

Thermodynamic quantities, such as entropy, the Gibbs free energy and so on, can be written in terms of $\eta(z)$ and \tilde{E} .

APPENDIX

This appendix is to derive Eq.(16). Firstly, we notice that $Q(z)$ satisfies

$$Q(z) = e^{-1} \left(\frac{z+1}{z} \right)^{z+1} Q(z+1).$$

Taking the logarithm and summing up, we obtain

$$\begin{aligned}\log Q(z) - \log Q(z') &= -(z' - z) - z \log z \\ &\quad - \{\log z + \log(z+1) + \cdots + \log(z' - 1)\} + z' \log z' \\ &= \int_z^{z'} \log x dx - \{\log z + \log(z+1) + \cdots + \log(z' - 1)\}.\end{aligned}$$

Using the fact that

$$\log Q(z') \rightarrow \frac{1}{2} \log \left(\frac{2\pi}{z'} \right) \quad (z' \rightarrow \infty)$$

we get ($z' \rightarrow \infty$)

$$\log \left\{ \sqrt{\frac{z}{2\pi}} Q(z) \right\} = \int_z^{z'} \log x dx - \left\{ \frac{1}{2} \log z + \log(z+1) + \cdots + \log(z' - 1) + \frac{1}{2} \log z' \right\}.$$

Now, noticing the fact that $e^{\pm 2\pi i \zeta} - 1$ vanishes at $\zeta = \text{integer}$ in the complex ζ plane, we integrate $f(\zeta)/(e^{-2\pi i \zeta} - 1)$ in the upper half plane and $f(\zeta)/(e^{2\pi i \zeta} - 1)$ in the lower half plane, along indented rectangle whose corners are $n_1, n_2, n_2 \pm \infty i$, and $n_1 \pm \infty i$

(n_1 and n_2 are integers). Assuming $f(\zeta)$ to be analytic in the whole ζ -plane, we thus obtain the formula (Plana's expansion)

$$\frac{1}{2}f(n_1) + f(n_1 + 1) + \cdots + f(n_2 - 1) + \frac{1}{2}f(n_2) = \int_{n_1}^{n_2} f(x)dx \\ + \frac{1}{i} \int_0^\infty \frac{dy}{e^{2\pi y} - 1} \{f(n_2 + iy) - f(n_1 + iy) - f(n_2 - iy) + f(n_1 - iy)\}.$$

We put

$$f(n) = \log(z + n), \quad n_1 = 0, \quad z + n_2 = z'$$

to have

$$\int_z^{z'} \log x \, dx - \left\{ \frac{1}{2} \log z + \log(z + 1) + \cdots + \frac{1}{2} \log z' \right\} \\ = 2 \int_0^\infty \frac{\arctan(y/z)}{e^{2\pi y} - 1} dy \quad (z' \rightarrow \infty).$$

Therefore, we obtain

$$\log \left\{ \sqrt{\frac{z}{2\pi}} Q(z) \right\} = 2 \int_0^\infty \frac{\arctan(y/z)}{e^{2\pi y} - 1} dy, \\ = -\frac{1}{\pi} \int_0^{\pi/2} \log \{1 - \exp(-2\pi z \tan \theta)\} d\theta$$

which can be transformed to Eq.(16).

REFERENCES

- Dean, P., 1960, *Proc. Roy. Soc.* 254:507; 1961, *ibid.* 260:263.
 Date, E. and Tanaka, S., 1976, *Prog. Theor. Phys.* 55:457.
 Fermi, E., Pasta, J. and Ulam, S., 1955, *Los Alamos Rpt.* LA-1940.
 Flaschka, H., 1974, *Phys. Rev.* B9:1924; *Prog. Theor. Phys.* 51:703.
 Ford, J., 1961, *J. Math. Phys.* 2:387; Ford, J. and Waters, J., 1964, *ibid.* 4:1293.
 Ford, J., Stoddard, S.D., Turner, J.S., 1973, *Prog. Theor. Phys.* 50:1547.
 Henon, M., 1974, *Phys. Rev.* B9:1921.
 Hirota, R., and Satsuma, J., 1976, *Prog. Theor., Phys. Suppl.* 59:64.
 Kac, M. and van Moerbeke, P., 1975, *Proc. Nat. Acad. Sci. USA* 72:1627, 2879.
 Manakov, S.V., 1975, *Sov. Phys. JETP* 40:269.
 Payton, D.N., Rich, R. and Visscher, W.M., 1967, *Phys. Rev.* 160:129.
 Saito, N., Ooyama, N. and Aisawa, Y., 1973, *RIMS Rpt. Kyoto Univ.* 171:191.
 Saito, N., Ooyama, N., Aisawa, Y. and Hirooka, H., 1970, *Prog. Theor. Phys. Suppl.* 45:209.
 Toda, M., 1967, *J. Phys. Soc. Jpn.* 22:431; 23:501.
 Toda, M., 1968, *J. Phys. Soc. Jpn. Suppl.* 26:235.
 Toda, M., 1989, "Theory of Nonlinear Lattices", Springer-Verlag.
 Toda, M., Hirota, R. and Satsuma, J., 1976, *Prog. Theor. Phys. Suppl.* 59:148.
 Toda, M., 1979, *Phys. Scripta* 20:424.

LOW-DIMENSIONAL BEHAVIOUR IN THE ROTATING DRIVEN CAVITY PROBLEM

E.A. Christiansen¹, J.N. Sørensen², M. Brøns³, and P.L. Christiansen¹

¹Laboratory of Applied Mathematical Physics, Building 303

²Department of Fluid Mechanics, Building 404

³Mathematical Institute, Building 303

The Technical University of Denmark, DK-2800 Lyngby, Denmark

ABSTRACT

In searching for low-dimensional structures in the rotating driven cavity problem we use a Galerkin approximation to project the infinite Navier-Stokes equations into a finite dimensional subspace spanned by a number of basic modes. The resulting system of ODE's, where the variables are the amplitudes of the basic modes, is analysed using bifurcation theory. By this technique we established, with only 25 modes, the early transition to an oscillatory motion as a supercritical Hopf-bifurcation, and in particular we estimated the critical Reynolds number within 0.2% of the Reynolds number due to the full numerical system in 40000 degrees of freedom. Finally, we present the spectrum of the full numerical system in the range from stationary to chaotic fluid flow. This spectrum diagram will serve as the basic reference system through out all investigations.

INTRODUCTION

In the rotating driven cavity problem the fluid flow is created by letting one end cover of a closed, fixed cylinder with height, H , and radius, R , rotate with a constant angular velocity, Ω . With scaling time Ω^{-1} and length R , and denoting the cylindrical coordinates as (x,y) , $x \in [0, \lambda=H/R]$, $y \in [0,1]$, and the corresponding velocity components as (u,v) , we obtain in the circulation, Γ , vorticity, ω , and streamfunction, ψ , formulation of the axisymmetric Navier-Stokes equations, see Daube & Sørensen (1989),

$$\frac{\partial \Gamma}{\partial t} = \frac{1}{\text{Re}} \left(\frac{\partial^2 \Gamma}{\partial x^2} + \frac{\partial^2 \Gamma}{\partial y^2} - \frac{1}{y} \frac{\partial \Gamma}{\partial y} \right) - \left(\frac{\partial(u\Gamma)}{\partial x} + \frac{\partial(v\Gamma)}{\partial y} - \frac{v\Gamma}{y} \right), \quad (1)$$

$$\frac{\partial \omega}{\partial t} = \frac{1}{Re} \left(\frac{\partial^2 \omega}{\partial x^2} + \frac{\partial^2 \omega}{\partial y^2} + \frac{1}{y} \frac{\partial \omega}{\partial y} - \frac{\omega}{y^2} \right) - \left(\frac{\partial(u\omega)}{\partial x} + \frac{\partial(v\omega)}{\partial y} - \frac{\partial}{\partial x} \left(\frac{\Gamma^2}{y^2} \right) \right), \quad (2)$$

$$\frac{\partial \psi}{\partial y} = -uy, \quad \frac{\partial \psi}{\partial x} = vy, \quad \frac{\partial^2 \psi}{\partial x^2} + \frac{\partial^2 \psi}{\partial y^2} - \frac{1}{y} \frac{\partial \psi}{\partial y} = \omega y. \quad (3-4)$$

Eqs. (1-4) are seen to depend on the Reynolds number, $Re = R^2 \Omega / \nu$ (ν the kinematic viscosity). The boundary conditions, no slip, depend on the aspect ratio, $\lambda = H/R$.

The first comprehensive, experimental results were performed by Escudier (1984). By changing Re and λ he found up to three stationary vortex breakdowns. Lugt & Hausling (1982), Lopez & Perry (1992) and Daube & Sørensen (1989) confirmed some of these results numerically, and increasing the Reynolds number even further, Sørensen & Christensen (1992) clarified that transition to turbulentlike motion in the axisymmetric, numerical system is associated with various bifurcations. Recently, Christensen et al. (1992) used a Proper Orthogonal Decomposition technique (POD), Sirovich & Sirovich (1989), to identify the early transition as a supercritical Hopf-bifurcation. In the present study only the Reynolds number, Re , is to be varied, the aspect ratio, λ , is fixed to 2.

THE DYNAMICAL SYSTEM

Time series analysis of stable solutions to the full numerical system has given the following dependence between basic frequencies, ω , and the Reynolds number, Re . See figure 1.

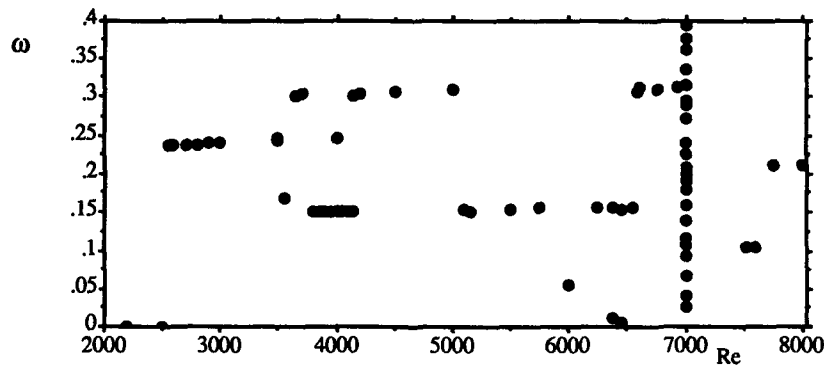


Figure 1. Spectrum diagram with basic frequencies.

The system is unlocked, because it is not driven by an external force, thus the frequencies change continuously between bifurcations. These bifurcations are seen as discontinuities, for example at $Re = 2544$, appearance or disappearance of basic frequencies, see $Re = 6300$ and $Re = 6550$, respectively, figure 1. Following we give a first description of the transition from stationary to turbulentlike motion based on the spectrum diagram.

Stationary solutions, $x = x(Re)$: $0 < Re < 2544$.

- Re: 1500, 1750 Stationary bifurcations, vortex breakdowns, Escudier (1984).
- Re: 2544 Supercritical Hopf bifurcation.

Periodic solutions, $x = x(Re, \omega, x_0)$: $2544 < Re < 6300$.

- Re: 3500 - 4200 Hysteresis.
- Re: 5100 - 6250 Period doubling (5100), change of solution (5150),
period tripling (5750-6000), period back-tripling (6000-6250).
- Re: 6300 Naimark-Sacker bifurcation to a torus.

Quasi-periodic solutions, $x = x(Re, \omega_1, \omega_2, x_0)$: $6300 < Re < 6550$.

- Re: 6375 - 6450 Period doubling torus-to-torus bifurcation.
- Re: 6550 Naimark-Sacker bifurcation to a periodic solution.

Through a chaotic region: $6550 < Re < 8000$.

- Re: 6550 - 6580 Period back-doubling.
- Re: 6930 - 6935 Naimark-Sacker bifurcation to a torus.
- Re: 6935 - 6940 Torus-to-chaotic transition through an unstable attractor.
- Re: 7500 - 7520 Chaotic to periodic transition.
- Re: 7600 - 7750 Period back-doubling.

THE PROJECTION METHOD

A simple spatial discretization of second order in equations (1-2) is used to obtain a first formulation in ODE's in order two times the number of nodes in the numerical grid, that is order 40000. Thus, denoting X as (Γ, ω) , utilizing the linearity between (Γ, ω) and u, v, ψ through a discretization of the definition and the Poisson equation (3-4) we have

$$\dot{X} = F(Re, X), \quad X \in \mathbb{R}^{40000}. \quad (5)$$

Now the POD technique is applied to obtain an orthogonal base system used in the Galerkin approximation. The technique has been generalized in order to operate with known solutions in the bifurcation theory. Then letting for example n_1 basevectors, $\varphi_{-(n_1-1)}, \dots, \varphi_0$, span some stationary solution space S_1, \dots, S_{n_1} , and letting m principal basevectors, $\varphi_1, \dots, \varphi_m$, represent the n_2 snapshots, X_1, \dots, X_{n_2} , of the full numerical system the m 'th most describing Galerkin approximation is written,

$$X(t) = X_S + \sum_{i=-(n_1-1)}^m a_i(t) \varphi_i, \quad (6)$$

where $m \leq n_2$, $X_S = S_1$, and $a = 0$ for $Re = Re_S$. Substituting (6) into (5) and dotting with the orthogonal basevectors, φ_i , $i = -(n_1-1), \dots, m$, we finally have in the system of ODE's,

$$\dot{a} = b_0 + \frac{1}{Re} b_1 + A_0 a + \frac{1}{Re} A_1 a + B(a, a), \quad a \in \mathbb{R}^{n_1+m}, \quad (7)$$

$$a(Re = Re_S) = 0, \text{ stationary solution.} \quad (7a)$$

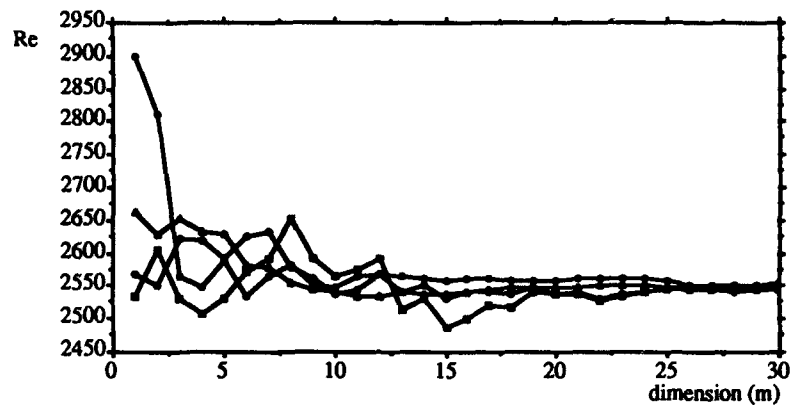


Figure 2. Determination of critical Reynolds number by different models.

b_0, b_1 are constant, A_0, A_1 linear and B is a bilinear vectorfunction. Following we present the determination of the critical Re as a function of the dimension m for different models, Christensen et al. (1992). From $m = 25$ the system of ODE's gives excellent results.

CONCLUSION

With the present projection method it has been possible to reduce dramatically the dimension of the non-trivial rotating driven cavity problem, and to identify the first transition from a stationary to an oscillatory motion. This is done as a supercritical Hopf-bifurcation at a critical Reynolds number, $Re = 2544$, and with a frequency, $\omega = 0.24$, which are in excellent agreement compared to the full numerical system (see Christensen et al., 1992). The projection method is by no means confined to a local description of a simple phenomenon in dynamical sense. In fact, Sirovich & Rodriguez (1987) were able to follow the Ginzburg-Landau equation through a chaotic region with only six modes. However, considering the complexity of the given problem and the present results, one must expect a need for a somewhat larger number of modes. Thus, a projection method to describe the next transitions is in preparation.

ACKNOWLEDGEMENT

(EAC) acknowledges financial support from the Danish Research Academy (Grant S910171), the Danish Technical Research Council (Grant 16-4967-2 OS), the Louis Dreyer Myhrwold's Fund and the Fisker & Nielsens Fund.

REFERENCES

- Aubry, N. (1991), On the hidden beauty of the POD, *Theoretical. Comput. Fluid Dynamics*, 2, 339-352.
- Christensen, E.A., Sørensen, J.N., Brøns, M. and Christiansen, P.L. (1992), Low-dimensional representation of early transition in rotating fluid flow, (In preparation).
- Daube, O. and Sørensen, J.N. (1989), Simulation numérique de l'écoulement périodique axisymétrique dans une cavité cylindrique, *C.R. Aca Sci Paris*, 308, 2, 443-469.

- Escudier,M.P. (1984), Observations of the flow produced in a cylindrical container by a rotating endwall, Experiments in Fluids, 2, 189-196.
- Lopez,J.M. and Perry,A.D. (1992), Axisymmetric vortex breakdown. Part 3. Onset of periodic flow and chaotic advection. J. of Fluid Mech., vol. 234, 449-471.
- Lugt,H.J. and Haussling,H.J. (1982), Axisymmetric vortex breakdown in rotating fluid within a container. Trans. ASME. J. Appl. Mech., vol. 49, 921-923.
- Petersen,C.K. (1988), Path user's guide, Dept of Appl Math and Nonlinear Studies, Univ of Leeds.
- Sirovich,L. and Rodrigues,J. (1987), Coherent structures and chaos: a model problem, Physics Lett A 120.
- Sirovich,L. and Sirovich,C.H. (1989), Low-dimensional description of complicated phenomena, in "The Connection between Infinite Dimensional Dynamical Systems", Nicolaenko,B., Foias,C. and Temam,R. eds., Contemporary Mathematics, 99, 277-305.
- Sørensen,J.N. and Christensen,E.A. (1992), Experimental and numerical studies of transition of rotating fluid in closed cylinder, (In preparation).
- Sørensen,J.N. and Ta Phuoc Loc (1989), High-order axisymmetric Navier-Stokes code description and evaluation of boundary conditions, Int. J. for Num. Meth. in Fluids, 9, 1517-1537.
- Wiggins,S. (1990), Introd. to Applied Nonlinear Dynamical Systems and Chaos, Springer-Verlag, TAM, 2.

VORTEX DIPOLES COLLIDING WITH CURVED WALLS

E.A. Coutias¹, J.P. Lynov, A.H. Nielsen, M. Nielsen,
J. Juul Rasmussen and B. Stenum

Association EURATOM - Risø National Laboratory
Optics and Fluid Dynamics Department
DK-4000 Roskilde, Denmark

¹Department of Mathematics and Statistics
University of New Mexico, Albuquerque, NM 87131, USA

INTRODUCTION

Incompressible, inviscid two-dimensional flows away from boundaries possess special stationary solutions in the form of coherent, isolated vortical structures. These solutions can be classified in terms of the spatial moments of the vorticity distribution about their centers. Flows involving several such structures can be seen in nature and in the laboratory. In case the structures remain well-separated, they can be described in terms of a few collective variables (strength and location for symmetric monopoles, plus eccentricity and orientation for elliptical ones, and similarly for dipolar structures). The vorticity, distributed among these structures, acts as a source for a collective velocity field, which away from the structures is harmonic. A small viscosity does not change the dynamics of these free-space structures substantially. The resulting dynamical system has been studied extensively both analytically and numerically.

Close encounters between structures cannot be fit into the narrow confines of the low dimensional theory. However, the theory seems adequate for the asymptotic behavior, away from close interactions. Thus, well defined isolated structures collide, and after a period of rapid readjustment new structures emerge that can again be described in terms of a few collective variables. Such phenomena have been studied extensively by numerical simulations in the last two decades, but an analytical theory for the scattering problem is still lacking.

In real flows one always must deal with boundaries, and although the vorticity field can be initially confined away from walls, momentum carrying structures such as dipoles will eventually approach walls and interact strongly with them. Since vorticity in unforced flows can only be created at solid walls, no-slip boundaries offer interesting possibilities for enhancement of the vorticity field and the introduction of novel structures and phenomena into the flow. In this paper we shall attempt to characterize some of the basic properties of this interaction by studying dipole collisions with walls both numerically and experimentally.

NUMERICAL RESULTS

The flow field is described by the Navier-Stokes equation

$$\frac{\partial \omega}{\partial t} + J(\omega, \psi) = \nu \nabla^2 \omega, \quad (1)$$

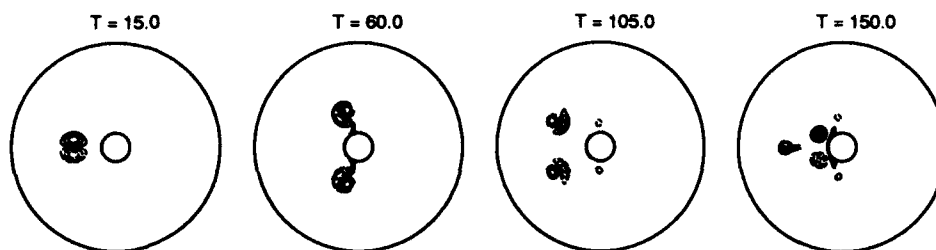


Figure 1. Numerical results showing contour plots of the vorticity field for a dipole with initial Reynolds number $Re = 2400$ interacting with a convex wall. Dashed lines indicate negative values.

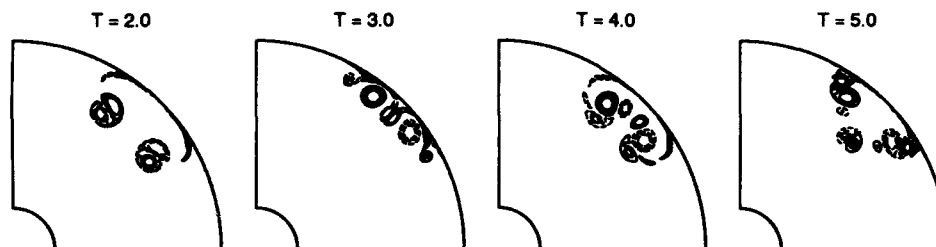


Figure 2. Same as figure 1 for a dipole with $Re = 4000$ interacting with a concave wall. At $T = 2$ the rebounded dipoles are already formed.

combined with the Poisson equation

$$\nabla^2 \psi = -\omega, \quad (2)$$

where

$$\nabla \times \vec{u} = \vec{\omega} = \omega \hat{z}, \quad \vec{u} = \nabla \psi \times \hat{z}, \quad J(f, g) \equiv \frac{\partial f}{\partial x} \frac{\partial g}{\partial y} - \frac{\partial g}{\partial x} \frac{\partial f}{\partial y}. \quad (3)$$

Here, \vec{u} is the velocity, ω the scalar vorticity, ψ the stream function and ν the viscosity.

The flow field is subject to no-slip conditions, so that it matches the wall velocity at the boundaries. This leads to both Dirichlet and Neumann conditions for the stream function ψ , so the Poisson equation is overdetermined. This implies that the vorticity field cannot be arbitrary, but must satisfy certain integral constraints so that it is compatible with the no-slip boundary conditions.

The Navier-Stokes equations are solved numerically in annular geometry employing a fully dealiased, spectral scheme based on Fourier-Chebyshev expansions. These allow very high resolution of boundary layers. Precomputed solvability constraints are enforced on each Fourier mode of ω . A more detailed description of how these solvability constraints are implemented in the numerical scheme is given by Coutsias and Lynov¹. Various global accuracy checks are implemented to diagnose the performance of the scheme: the conservation of total circulation is monitored, while comparisons are performed between the computed and theoretically predicted viscous evolutions for the total energy and total enstrophy (or squared vorticity). In all the simulations reported here, these were found to be in close agreement.

In our numerical studies, a Lamb dipole was made to collide with both concave and convex curved walls. Examples of the numerical results are presented in figs. 1 and 2. Qualitatively, the picture is not too different from that seen in collisions with flat walls, as it has previously been reported by several authors¹⁻³. We summarize here the main aspects of this interaction: As the dipole approaches the wall, it induces opposite-signed wall vorticity layers. These thicken due to viscosity. At minimum approach, these wall layers roll tightly into secondary



Figure 3. Results from the rotating tank experiment showing dye traces for a dipole with $Re \approx 2500$ interacting with a concave wall.

vortices and couple with opposing primary lobes. Wall vorticity production continues, feeding the secondary vortices through vortex sheets, as the former are being advected by the primaries. At a critical instant, detachment of the combined structures occurs. We believe this is connected to the accumulation of sufficient circulation in the secondaries, so that the new structures are close to the 'minimally interacting configuration' (rolling dipoles, see below) with primary to secondary circulation ratios close to 2.5.

As the Reynolds number (defined as $Re = ud_0/\nu$ with u and d_0 the dipole speed and diameter, respectively) increases, the secondary vortices become tighter and the circulation ratio of the detached dipoles decreases. The tighter, stronger secondary vortex devours part of the primary into an accretion ring, which is dissipated quickly. The rebounding dipoles circle around towards a second, double collision with the wall, initiating a complex interaction phase that may eventually lead to the ejection of a new ('baby') dipole, composed entirely of wall vorticity. The topology of this process (e.g. ejected dipole is composed of wall vorticity from the first or second detachment etc) is influenced quite sensitively by the presence of distant boundaries (e.g. the opposite channel wall), and by wall concavity. Asymmetric or angle dipole-wall collisions introduce further complications, e.g. angle collisions appear to enhance enstrophy production. These results will be reported elsewhere.

In all cases investigated, and in all stages of the process, vorticity was distributed primarily among a few isolated vortical structures, while ribbon-like forms (vortex sheets) appeared but dissipated quickly or rolled into tight vortices.

EXPERIMENTAL RESULTS

The experimental setup consists of a square tank with a flat bottom and side walls of length 1 m. Into this tank various cylindrical wall structures can be placed. The tank is filled with water to a level of 15 cm and brought into solid body rotation with an angular frequency of 0.63 s^{-1} . A dipole is created by injecting a jet of dyed water into the mid-plane of the water for a period of 5 s. Our setup is similar to that described by Flierl et al.⁴, who, however, did not investigate dipole-wall interactions. After a short transient period following the jet injection, the solid body rotation causes the flow to be very nearly two-dimensional as described by the Taylor-Proudman theorem.

In figure 3, the propagation of the dyed water inside and trailing a dipole colliding with a concave wall is shown. We see that the experimental results show the same topological flow evolution that was found in the numerical simulations.

DISCUSSION

A generic outcome of our numerical and experimental studies was the apparent evolution of the initially complex interaction process into a simpler state in which most of the remaining vorticity is concentrated near the wall, seemingly trapped in what can be called 'surface states'. These appear to be long lived, robust structures in which the original vortex couple is separated

by halos of oppositely signed, wall generated vorticity. For the time intervals studied, of order 3-4 rebound times, the halos still contain several small vortices rotating about the primaries which are only slowly evolving. These surface states can act as enstrophy sources, pumping wall vorticity away from the wall. This process is apparently enhanced by the presence of even distant no-slip walls quite dramatically⁵. Although our present simulations have not been advanced sufficiently in time, we feel it is fair to say that ultimately advective effects will decay, leaving quasi-stationary structures that evolve only through dissipation. These structures, being long lived, play an important role in subsequent flow events, as they can alter and enhance the domain of influence of a no-slip wall. A full understanding of these structures requires a careful formulation of the initial-boundary value problem of a vorticity concentration near a wall, and with the added complication that one is really considering a state that is decaying in time, even if this decay is very slow. Indeed, it seems that the ultimate evolution of these structures is a quasi-stationary state where all time evolution is dissipative, with no advection present.

Another special class of wall-bound structures appear to play an important role in the process of vortex rebound. Clearly a structure compatible with a line or circle of zero velocity could coexist with a rigid boundary and produce no strong boundary layers. As good candidates that fulfill this property approximately we consider dipoles with special vorticity balance to create a velocity field with a stagnation point on their perimeter. Such structures rotate but the point of contact with the circle circumscribed on their trajectory corresponds to zero fluid motion. Thus, in a setting where they move near a wall at such distance that they simply touch the wall tangentially, there should be minimal disturbance of their field due to the no-slip condition and, consequently, minimal generation of boundary layers. Since the velocity field about a dipole decays like $1/r^2$, the disturbance caused further away should also be fairly small. A special dipole in this category is the unbalanced Lamb dipole, with vorticity given by

$$\omega(r, \theta) = c^0 \left(1 - \frac{J_0(\gamma_{11}r/r_0)}{J_0(\gamma_{11})} \right) - \frac{2u\gamma_{11}}{r_0 J_0(\gamma_{11})} J_1(\gamma_{11}r/r_0) \cos \theta$$

inside the circle $r < r_0$ and zero outside. This dipole gyrates about a point at distance $R = 2u/c^0$ from its center with angular velocity $u/R = c^0/2$. In the special case $R = r_0$ we obtain the 'rolling dipole' which rotates about a point on its perimeter, and has zero velocity on the antipodal point. For this dipole the ratio of circulations is 2.65 and we believe it constitutes a fair approximation for the secondary dipoles emerging from dipole-wall collisions at moderate Re (≈ 2000) and small wall curvatures.

ACKNOWLEDGMENTS

The helpful assistance of Paul Barratt with the rotating tank experiments and of Lars Bækmark in running our computer systems is gratefully acknowledged.

REFERENCES

1. E.A. Coutias and J.P. Lynov, *Physica D.*, 51 (1991) 482-497.
2. P. Orlandi, *Phys. Fluids, A* 2 (1990) 1429-1436.
3. G.J.F. van Heijst and J.B. Flor, in: J.C.J. Nihoul and B.M. Jamart (Ed.), *Meso-scale/Synoptic Coherent Structures in Geophysical Turbulence*, Elsevier, Amsterdam, 1989, pp. 591-608.
4. G.R. Flierl, M.E. Stern and J.A. Whitehead, *Dyn. Atmos. Oceans*, 7, (1983) 233-263.
5. E.A. Coutias and J.P. Lynov, in preparation.

THE USE OF GENERALIZED ZAKHAROV SYSTEMS IN ELASTIC SURFACE WAVES

H. Hadoua and G.A. Maugin
 Laboratoire de Modélisation en Mécanique
 Université Pierre et Marie Curie, Tour 66, 4 Place Jussieu
 Boîte postale 162, 75252 Paris CEDEX 05

1. INTRODUCTION

In recent works^{1,2} the possible propagation of envelope solitons having the nature of shear-horizontal (SH) elastic surface waves was unequivocally proved mathematically for an elastic structure likely to be experimentally tested. This phenomenon may occur along a composite structure made of a nonlinear elastic isotropic substrate coated with a thin "slow" linear elastic film. Couples of materials for which this is indeed realizable were also determined. However, a strong decoupling hypothesis layed dormant in that approach. Namely, it was assumed that the SH wave in question remains decoupled from the so-called Rayleigh component, i.e., that vectorial elastic component that is polarized parallel to the sagittal plane (plane spanned by the direction of propagation X_1 and the normal to the limiting surface \underline{N}). This was considered in order to simplify the analysis, but it does not hold true in all rigor. A simple way to realize this fact is to recall what happens for *bulk* waves in nonlinear isotropic (a fortiori anisotropic) elasticity (See Ref.3, pp. 36-37). In that theory a *longitudinal* motion necessarily accompanies a transverse motion; e.g., one can write

$$\left. \begin{aligned} \square_T v &= 0 \\ \square_L u &= \gamma v_x v_{xx} \end{aligned} \right\} \quad (1.1)$$

where \square_T and \square_L are linear "transverse" and "longitudinal" (d'Alembertian) wave operators along x , v is the transverse component, u is the longitudinal component, a subscript x denotes partial differentiation with respect to x , and γ is a third-order elasticity coefficient. In an asymptotic analysis where $v = O(\varepsilon)$ as ε goes to zero, $u = O(\varepsilon^2) = O(v^2)$ makes the system (1.1) fully consistent. In particular, there is no feedback of u in the v equation, while the longitudinal component u is excited through the second harmonic of v . If this is true for bulk waves,

then the situation should be worst for surface waves as boundary conditions to be applied at the limiting surface-although free of tractions-usually couple both the longitudinal component u and the remaining transverse component w (so-called shear-vertical (SV) component) to produce what is commonly referred to as a *Rayleigh* surface wave⁴, in the *linear* approximation. But then, according to (1.1), the SH component should couple with the full Rayleigh one in nonlinear elasticity. This establishes the frame of mind in which the present paper develops. From (1.1), however, we shall still keep the idea that the SH component is *primary*, for instance, being preferably entered in the system through a transducer designed to that effect, while the Rayleigh component is only *secondary*, being essentially generated by the former. Furthermore, only the SH component a priori carries a *dispersion* effect due to the built-in vertical layering; but a straightforward generalization so as to include dispersion due, e.g., to discreteness, in the longitudinal component can be proposed heuristically.

In all, the main result of the present analysis which is essentially asymptotic in the manner of Whitham and Newell⁵⁻⁷, is that the complex amplitude a of the slowly varying envelope of the SH component and the real amplitude gradients (in the propagation direction) $n_1 = u_x$ and $n_2 = w_x$ of the Rayleigh components are in general governed by the following system (in the absence of dispersion in the Rayleigh subsystem) after normalization :

$$\left. \begin{aligned} i a_t + a_{xx} + 2 \lambda |a|^2 a + (\alpha_L n_1 + \alpha_T n_2) a &= 0 \\ (n_1)_{tt} - C_L^2 (n_1)_{xx} &= -\mu_L (|a|^2)_{xx} \\ (n_2)_{tt} - C_T^2 (n_2)_{xx} &= -\mu_T (|a|^2)_{xx} \end{aligned} \right\} \quad (1.2)$$

where λ is the real coefficient of self nonlinearity (of the SH mode) and α_L , α_T , μ_L and μ_T are real coupling coefficients. For $\lambda = \alpha_T = \mu_T = 0$, this system is none other than Zakharov's^{8,9} system for Langmuir-ion acoustic waves in plasmas, but with different physical interpretations. We coined the naming "generalized Zakharov's systems" for systems such as (1.2) and their associates. Two recent papers^{10,11} are devoted to the analytical and numerical study of system (1.2).

2. DISSIPATION-INDUCED EVOLUTION OF SOLITONS

We consider first the evolution of envelope solitary waves in the SH-dispersive a -system of (1.2) under the influence of dissipation (viscosities η_L and η_T) in the nondispersive (n_1 , n_2) Rayleigh subsystem. The two are coupled through the coupling coefficients μ_L and μ_T . In spite of its appearance, system (1.2) still conserve the number of (SH) surface phonons (or wave action)

$$N = \int_{-\infty}^{+\infty} |a|^2 dx \quad (2.1)$$

In the analytical treatment¹⁰ which applies the balance-equation

analysis⁹ to the slow dissipation-induced evolution of the exact one-soliton solution of the Zakharov system (for the sake of simplicity $\omega = 0$, $\mu_r = 0$ in (1.2), but this is justified¹²) although this system is not exactly integrable, three different scenarios of evolution are shown to be possible: (i) adiabatic (slow) transformation of a moving *subsonic* soliton into the stable quiescent one, (ii) complete adiabatic decay of a *transsonic* soliton with a small amplitude, and (iii) coming of the *transsonic* soliton with a large amplitude into a critical state, from which further adiabatic evolution is not possible. In the latter case a numerical investigation of the further evolution of the soliton is particularly enlightening. In a general case, it is shown that it abruptly splits into the stable quiescent soliton, the slowly decaying small-amplitude transsonic one, and a pair of left- and right-running acoustic pulses slowly fading under the action of the weak dissipation. The abrupt splitting seems to be a new type of inelastic process for a soliton, induced by small perturbations.

3. SOLITON-SOLITON COLLISION IN THE GENERALIZED ZAKHAROV SYSTEM

The generalized Zakharov system (1.2), in the absence of viscosity in the Rayleigh subsystem, admits both *subsonic* and *transsonic* one-soliton solutions. The question naturally arises of the interaction (collision) of such solitons (i.e., whether they are *indeed* solitons), for instance in symmetric soliton-soliton collisions. It was shown that the acoustic losses are exponentially small unless the velocities are much larger than the characteristic sound velocity (c_L) in the Rayleigh subsystem. The numerical simulation of the head-on soliton-soliton collision brings up two basic phenomena: (i) the collision of subsonic solitons always leads to their fusion into a breather, provided the system is sufficiently far from the integrable limit (i.e., the NLS case), and (ii) the collision between transsonic solitons gives rise to a multiple production of solitons (both subsonic and transsonic) and the quasi-elastic character of the collision is recovered in the limit of large velocities. This is illustrated in Figures 1 and 2.

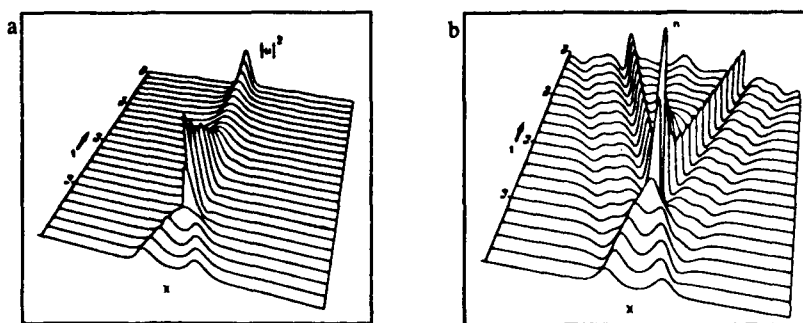


Figure 1 - Collision-induced fusion of subsonic solitons into a breather with acoustic emission in the Rayleigh subsystem: (a) $|u|^2$, (b) n .

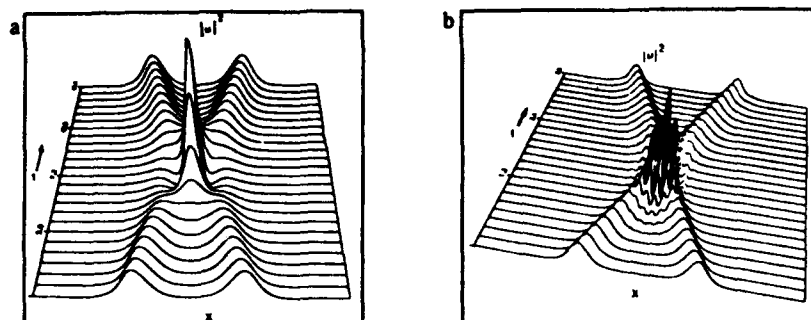


Figure 2 - Comparison between the soliton-soliton collision for system (1.2) close to the NLS limit (a), and the collision of two transsonic solitons at high velocities in the generalized Zakharov system (b).

4. CONCLUSION

Our surface-wave problem is governed by a so-called generalized Zakharov system at the thin film (interface).

It appears that the initial, purely mechanical, surface-wave problem considered yields, a very interesting physical application which may be of interest in signal processing (we have a mechanical analog of light solitons guided by optical fibers).

REFERENCES

1. H. Hadouaj and G.A. Maugin, C. R. Acad. Sci. II 309, 1877 (1989).
2. G.A. Maugin and H. Hadouaj, Solitary surface transverse waves on an elastic substrate coated with a thin film, Phys. Rev. B44, 1266(1991).
3. G.A. Maugin, "Nonlinear Electromechanical Effects and Applications", A Serie of Lectures, World Scientific, Singapore (1985).
4. J.D. Achenbach, "Wave Propagation in Elastic Solids", North-Holland, Amsterdam (1975).
5. G.B. Whitham, "Linear and Nonlinear Waves", Wiley, New York (1974).
6. D.J. Benney and A.C. Newell, The propagation of nonlinear wave envelopes, J. Math. Phys. (now Stud. Appl. Math.) 46, 133 (1967).
7. A.C. Newell, "Solitons in Mathematics and Physics", SIAM, Philadelphia (1985).
8. V.E. Zakharov, Collapse of Langmuir waves, Zh. Eksp. Teor. Fiz. 62, 1745 (1972). [Sov. Phys. JETP 35, 908 (1972)].
9. Yu. S. Kivshar and B.A. Malomed, Rev. Mod. Phys. 61, 763 (1989).
10. H. Hadouaj, B.A. Malomed and G.A. Maugin, Dynamics of a soliton in the generalized Zakharov's system, Phys. Rev. A 44, 3925 (1991).
11. H. Hadouaj, B.A. Malomed and G.A. Maugin, Soliton-soliton collisions in the generalized Zakharov's system, Phys. Rev. A 44, 3932 (1991).
12. G.A. Maugin, H. Hadouaj and B.A. Malomed, Nonlinear coupling between SH surface solitons and Rayleigh modes on elastic structures, Phys. Rev. B 45, 9688 (1992).

VORTEX DYNAMICS IN 2-DIMENSIONAL FLOWS

J.S. Hesthaven, J.P. Lynov, J. Juul Rasmussen and G.G. Sutyrin[†]

Association EURATOM - Risø National Laboratory
Optics and Fluid Dynamics Department
P.O. Box 49
DK-4000 Roskilde, Denmark

[†]P.P. Shirshov Institute of Oceanology
Russian Academy of Sciences
23 Krasikova Street
Moscow 117218, Russia

INTRODUCTION

A fundamental property of two-dimensional flows is the ability to support the existence of longlived, isolated vortical structures. Vortices in the form of monopoles, dipoles and tripoles are often encountered, e.g. in the atmosphere and oceans of large planets as well as in laboratory experiments. Such propagating structures may trap particles and convect them over distances much larger than their scale size. The understanding of their dynamical behaviour is therefore of great importance for comprehending transport mechanisms.

The monopolar vortex is stationary in isotropic flows. The dipolar vortex may propagate in any direction depending on the relative strength of the two vortices¹, while tripolar vortices are observed to be non-propagating, but rotating around their center². For anisotropic two-dimensional flows - i.e. on a rotating planet, where the anisotropy is brought about by the variation of the Coriolis parameter with latitude (the ' β -effect') - monopolar vortices are non-stationary and couple to linear Rossby waves³. Strong monopolar vortices may, however, survive for many turnaround times. Dipoles of permanent form exist only when propagating perpendicular to the gradient of the Coriolis parameter, i.e. zonally^{4,5}.

We have performed a detailed numerical study of the longtime evolution of monopolar and dipolar vortices in the 'equivalent barotropic vorticity equation', which can be used to model the evolution of two-dimensional flows in the mid-latitudes of large rotating planets⁶. A similar equation, the Hasegawa-Mima equation⁷, describes the nonlinear evolution of drift-waves in a magnetically confined, low-pressure plasma, where the density gradient causes the anisotropy.

THEORY

We consider the equivalent barotropic vorticity equation describing the Lagrangian invariance of the potential vorticity, Γ ,

$$\frac{d}{dt}\Gamma = 0, \quad \Gamma = q + \beta y = \nabla^2\phi - \phi + \beta y, \quad (1)$$

where d/dt is the material derivative, ϕ is the streamfunction and β is proportional to the gradient of the Coriolis parameter. We adopt local Cartesian coordinates (x, y) with positive

x eastward and positive y northward. The local fluid velocity \vec{v} is given as $\vec{v} = \hat{z} \times \nabla \phi$. The dispersion relation for the linear Rossby waves is $\omega = -k_x \beta / (1 + k^2)$, i.e. the waves only propagate westward with phase velocities $-\beta < \omega/k_x < 0$.

We use a pseudospectral method in double periodic geometry with an explicit 3rd order Adam-Bashforth Predictor-Corrector time integration scheme and zero-padding for de-aliasing. A hyperviscosity term proportional to $\nabla^6 \Gamma$ is added to Eq.(1) to ensure numerical stability. This is implemented implicitly. The simulations have been done on an Amdahl VP1100 with typically 15 cpu-sec/T for 256^2 modes and 100 timesteps per timeunit (T).

MONOPOLE EVOLUTION

When considering monopolar vortices, we only study the evolution of cyclones, e.g. ϕ is negative in the core region. The dynamics of anticyclones can be derived by using the symmetry relation $\phi(x, y, t) = -\phi(x, -y, t)$ of Eq.(1).

The initial condition for the simulation of the monopole dynamics is a Gaussian streamfunction, $\phi = -\phi_m \exp(-r^2/2)$, which gives rise to an annulus of negative potential vorticity around the positive vorticity core;

$$q_{\text{init}} = \phi_m(r^2 - 1) \exp(-r^2/2) \quad (2)$$

Here ϕ_m is the amplitude of the vortex. A strong monopole on the β -plane will have closed isolines of potential vorticity; a criteria for this is that $d\Gamma/dy|_{x=\text{const}} < 0$ somewhere along y . The strength of the monopole, ϕ_m , is measured in terms of β .

On the f -plane (i.e. $\beta = 0$) such vortices do not propagate, but they are known to be unstable with respect to azimuthal $l = 2$ perturbations⁸. As this instability evolves it deforms the core into an ellipse and causes the negative vorticity in the annulus to coalesce into two satellites, forming a tripole; intensively studied both numerically and experimentally^{2,9,10,11}.

On the β -plane an azimuthal $l = 1$ mode is introduced by the β -effect, setting up a secondary flow of dipolar nature. This gives rise to a propagation in the north-west direction^{13,14}. This north-west propagation may be understood from the Lagrangian conservation of Γ inside the closed vorticity lines. An estimate of the maximum excursion to the north, y_m , may be derived by employing this conservation^{13,14} to obtain $y_m = 2 \int_0^{r_c} q_{\text{init}} r dr / r_c^2$, where r_c is the radius of the vortex core.

We have considered several cases, i.e. several amplitudes ϕ_m . A localized, nearly linear perturbation ($\phi_m = .25\beta$) decays due to dispersion with an e -folding time $T_d \approx 8/\beta$ in agreement with linear calculations¹⁵.

By increasing the vortex intensity a core consisting of closed isolines of Γ appears and the vortex evolution becomes essentially nonlinear. For $\phi_m = 2\beta$ the radius of the core for a shielded vortex, Eq.(1), is $r_c \approx 1.2$ and the maximum meridional drift is $y_m \approx 3$. The numerical calculations show a decay of the vortex with near linear rate in agreement with previous simulations³. However, the vortex core maintains its identity essentially longer than T_d and drifts north-westward providing meridional displacement until the core finally disappears. Thus, even a weak monopole provides essential meridional transport of trapped particles due to nonlinear advection of the potential vorticity.

For $\phi_m \gg \beta$ an estimation of the meridional drift for a shielded cyclone gives $y_m \approx \phi_m/2\beta$. Thus, a strong vortex is able to provide long-distance meridional transport up to the limit latitude $y_m \gg 1$. The decay rate of the stream function amplitude is essentially smaller than for the previous case in agreement with previous calculations³. Comparison of trajectories for $\phi_m = 10\beta$ with those calculated by Sutyrin^{12,13} using an azimuthal $l = 1$ perturbation theory shows good agreement during the initial time (Fig.1). At longer times the flow field becomes strongly asymmetric (Fig. 2). The shape of the central part becomes elliptic and a tripolar structure appears in the vorticity field. This tripolar vortex rotates around its centre as it propagates and seems to be stable. Behind the vortex core we see a strongly nonlinear wave pattern. The formation of the tripolar structure is ascribed to the instability of the azimuthal $l = 2$ mode as discussed for the f -plane case¹⁰. The $l = 2$ is excited by the nonlinear interaction of the initial $l = 1$ mode perturbation and the β -effect. The evolution of the

strong monopole is similar to the evolution recently observed¹⁶ for the case of a topographic β -effect and essentially infinite Rossby radius. However, clear formation of a tripolar structure was not observed¹⁶.

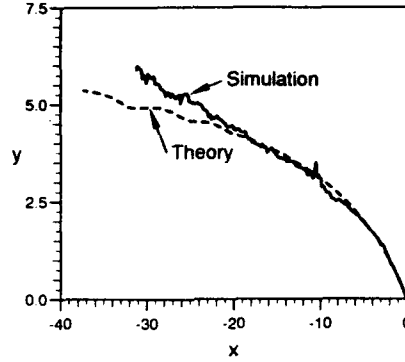


Figure 1: Trajectory of strong shielded monopole compared with azimuthal $l = 1$ mode theory.

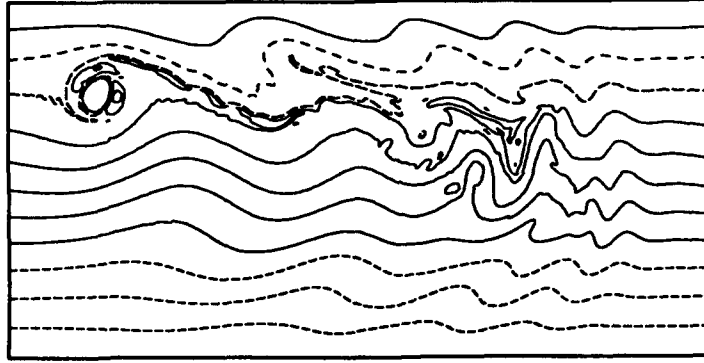


Figure 2: Contour plot of potential vorticity, Γ , at $T=400$ showing the tripole. Dashed lines indicate negative values.

DIPOLE EVOLUTION

Equation (1) has the exact stationary solution¹⁷;

$$q = \left(-(1 + \kappa^2)U \frac{\rho^2}{\kappa^2} \left(a \frac{J_1(\kappa r)}{J_1(\kappa a)} - r \left(\frac{\kappa^2}{\rho^2} + 1 \right) \right) - (U(1 + \kappa^2) + \beta)r \right) \sin \theta \quad r < R \quad (3)$$

$$q = \left(-(\rho^2 + 1)Ua \frac{K_1(\rho r)}{K_1(\rho a)} - (U(1 - \rho^2) + \beta)r \right) \sin \theta \quad r > R,$$

where $\rho^2 = (U + \beta)/U$. $\rho^2 > 0$ is necessary to ensure that the dipole solution is localized, i.e. $U > 0$ or $U < -\beta$ implying that the linear waves and the dipole cover complementary parts of the velocity space. a is the radius of the separatrix and U the horizontal propagation velocity. κ is found as the first solution to the equation

$$\frac{K_2(\rho a)}{\rho a K_1(\rho a)} = - \frac{J_2(\kappa a)}{\kappa a J_1(\kappa a)},$$

ensuring continuity of $\nabla \phi$ at $r = R$. As the initial condition for the simulation of the dipole dynamics we use an f -plane dipole obtained from the above for $\beta = 0$, and launched in various directions. All simulations have $a = 1$.

First we consider weak dipoles propagating in the linear Rossby wave regime ($U = .25\beta$). For eastward direction of propagation our calculations show that on the β -plane such a dipole almost does not propagate. In this case the drift velocity induced in the centre of each vortex by its partner is nearly compensated by the Rossby wave drift. Thus, such a dipolar configuration can be nearly stationary for quite long time, displaying a particular example of coherent structure. Ultimately, the slow meridional separation of the partners becomes so large that they stop interacting and start propagating as isolated monopoles; the cyclonic part propagates north-westward, the anticyclonic part south-westward. For initial westward propagation the strong coupling with linear waves and fast decay due to radiation is characteristic. In this case the meridional drift of the individual partners bring them closer together while propagating westward. For poleward direction of propagation the calculations show a disintegration of the dipole into two structures decaying with nearly linear rate.

For strong dipoles we choose $U = \beta$. For eastward direction of propagation the strong dipole decelerates while its partners slightly separate. The dipole adjusts to the steadily propagating solution of the form given by Eq.(3). For westward direction of propagation the strong dipole accelerates while its partners become closer. After the short period of adjustment the westward dipole propagates about twice as fast as the eastward one. In both cases the steadily propagating dipole, Eq.(3), on the β -plane is observed to be an attractor for initial f -plane dipoles. For northward direction of propagation the strong dipole oscillates propagating predominantly eastward. This calculation shows that even for $U = \beta$ the evolution of the f -plane dipole corresponds well with the theory of tilted intensive dipoles; described and developed assuming $U \gg \beta$ ⁴. Studies of tilted dipoles⁵ show that only eastward propagating dipoles are stable to angular perturbations.

CONCLUSIONS

It has been shown that dynamical properties of localized monopolar and dipolar vortices on the β -plane differ strongly from their properties on the f -plane without the β -effect. A strong monopolar vortex, being stationary on the f -plane, provides effective meridional transport on the β -plane due to self-propelling by the azimuthal $l = 1$ perturbation. Strong dipolar vortices, being most effective for transport on the f -plane, oscillate and propagate predominantly zonally without essential meridional transport.

An important new feature of the evolution of a strong monopolar vortex on the β -plane is the appearance of a tripolar structure due to a weak instability caused by meridional displacement of the vortex centre. Rotation and oscillation of the tripole leads to increasing mixing near the boundary of the vortex core and loss of some trapped particles. This intrinsically inviscid physical mechanism may play an important role in the evolution of coherent vortices providing an exchange between the vortex core and the surrounding flow.

References

- [1] Flierl, G.R., Stern, M.E., and Whitehead, J.A., 1983, *Dyn. Atmos. Oceans*, **7**, 233.
- [2] Van Heijst, G.J.F., and Klosterziel, R.C., 1989, *Nature*, **338**, 569.
- [3] McWilliams, J.C., and Flierl, G.R., 1979, *J. Phys. Oceanogr.*, **9**, 1155.
- [4] Nycander, J., and Isichenko, M.B., 1990, *Phys. Fluids B*, **2**, 2042.
- [5] Hesthaven, J.S., Lynov, J.P. and Nycander, J., 1992, *Phys. Fluids A* (in press).
- [6] Flierl, G.R., 1987, *Ann. Rev. Fluid Mech.*, **19**, 493.
- [7] Hasegawa, A., and Mima, K., 1977, *Phys. Fluids*, **21**, 87.
- [8] Gent, P.R., and McWilliams, J.C., 1986, *Geophys. Astrophys. Fluid Dyn.*, **35**, 209.
- [9] Legras, B., Santangelo, P., and Benzi, R., 1988, *Europhys. Lett.*, **5**, 37.
- [10] Carton, X.J., Flierl, G.R., and Polvani, L.M., 1989, *Europhys. Lett.*, **9**, 339.
- [11] Orlandi, P., and van Heijst, G.F.J., 1992, *Fluid Dyn. Res.*, **9**, 179.
- [12] Sutyrin, G.G., 1987, *Sov. Phys. Dokl.*, **32**, 791.
- [13] Sutyrin, G.G., 1988, *Fluid Dyn.*, **23**, 215.
- [14] Hesthaven, J.S., Lynov, J.P., Rasmussen, J.J. and Sutyrin, G.G., (to be published).
- [15] Flierl, G.R., 1977, *J. Phys. Oceanogr.*, **7**, 365.
- [16] Carnevale, G.F., Klosterziel, R.C., and van Heijst, G.F.J., 1991, *J. Mech.*, **233**, 119.
- [17] Larichev, V.D., and Reznik, G.M., 1976, *Dokl. Akad. Nauk. SSSR*, **231**, 1077.

SELF-SUPPORTING GAP SOLITONS IN NONLINEAR LATTICES

Yuri S. Kivshar ^{1,2}

¹Institut für Theoretische Physik I, Heinrich-Heine-Universität Düsseldorf, D-4000 Düsseldorf 1, Germany

²Institute for Low Temperature Physics and Engineering, 310164 Kharkov, Ukraine

One of the well-known effects of nonlinearity is to support stable propagation of localized structures in the frequency and velocity domains where propagation of linear waves is impossible. These localized structures may appear as a result of interplay between dispersion and nonlinearity. Many models describing microscopic phenomena in solid state physics are inherently discrete, with the lattice spacing between the atomic (or molecular) sites being a fundamental physical parameter. Due to specific properties of discrete systems, one may expect existence of the localized structures which have no direct analog in continuum models. In the present paper, taking the discrete Klein-Gordon model as a particular but rather general example, I show analytically that a new type of localized structures in nonlinear lattices may exist as a result of nonlinearity-induced symmetry breaking between two equivalent linear eigenmodes of the chain. These localized structures exist independently on the type of nonlinearity (self- or defocusing) and they are likely fundamental nonlinear excitations of discrete systems. I point out that the nonlinear structures described here have been already observed experimentally by Denardo *et al.*¹ in a damped and parametrically driven lattice of coupled pendulums as the so-called "noncutoff kinks".

The physical idea and the properties of the solutions obtained do not depend drastically on the type of a nonlinear chain, but, for definiteness, I consider the discrete Klein-Gordon model as a particular but rather general example, i.e. a one-dimensional chain made of particles (atoms) with unit mass, harmonically coupled with their nearest neighbors, and subjected to a nonlinear symmetric on-site potential. The same model has been analysed recently to modulational instability². Denoting by $u_n(t)$ the displacement of atom n , its equation of motion may be written in the form,

$$\ddot{u}_n + K(2u_n - u_{n+1} - u_{n-1}) + \omega_0^2 u_n - \beta u_n^3 = 0, \quad (1)$$

where K is the coupling constant, ω_0 is the frequency of small-amplitude on-site vibrations in the substrate potential, and β is the anharmonicity parameter of the

potential. The model given by Eq. (1) may be also considered as a small-amplitude expansion of the well-known sine-Gordon model, and numerous physical applications of both these models have been widely discussed in the literature (see, e.g., Ref. 3 and references therein).

Linear oscillations of the frequency ω and wavenumber q are described by the dispersion law,

$$\omega^2 = \omega_0^2 + 4K \sin^2(qa/2),$$

a being the lattice spacing. The linear spectrum has a ("natural") gap ω_0 , and it is limited by the cut-off frequency $\omega_{max}^2 = \omega_0^2 + 4K$ due to discreteness. The most interesting point of the discrete model spectrum is the point $q = \pi/2a$, which corresponds to the wavelength-four linear mode. In *any discrete* lattice there are two equivalent modes of such a type: at $q = \pi/2a$ all even particles are at rest and the odd ones oscillate with the opposite phases at the frequency $\omega_1^2 = \omega_0^2 + 2K$, or, vice versa, all odd particles are at rest but the even ones oscillate with the opposite phases at the same frequency. However, in a *diatomic* linear chain these modes exhibit a ("internal") gap in the linear spectrum and this gap is naturally proportional to the mass difference⁴. The physical problem I would like to discuss here is: Can nonlinearity itself induce a gap in the cw spectrum of a nonlinear chain and what is a physical consequence of this effect?

To answer this question I will introduce the new variables for the displacements of the atoms at different sites, i.e. $u_n = v_n$, for $n = 2k$, and $u_n = w_n$, for $n = 2k + 1$, to present Eq.(1) for odd and even numbers separately. Then, looking for solutions in the vicinity of the point $q = \pi/2a$, I use the following ansatz,

$$v_{2k} = (-1)^k [V(2k, t)e^{i\omega_1 t} + V^*(2k, t)e^{-i\omega_1 t}], \quad (2)$$

$$w_{2k+1} = (-1)^k [W(2k + 1, t)e^{i\omega_1 t} + W^*(2k + 1, t)e^{-i\omega_1 t}]. \quad (3)$$

where $\omega_1^2 = \omega_0^2 + 2K$ is the frequency of the wavelength-four linear mode, assuming that the functions $V(2k, t)$ and $W(2k + 1, t)$ are slowly varying in space and time. Substituting Eqs.(2),(3) into Eq.(1) and making the so-called "rotating-wave" approximation, i.e. keeping only the terms proportional to the first harmonic, I finally get the system of two coupled equations,

$$i\omega_1 \frac{\partial V}{\partial t} - aK \frac{\partial W}{\partial x} - \frac{3}{2}\beta |V|^2 V = 0, \quad (4)$$

$$i\omega_1 \frac{\partial W}{\partial t} + aK \frac{\partial V}{\partial x} - \frac{3}{2}\beta |W|^2 W = 0, \quad (5)$$

where the variable $x = 2ak$ is treated as continuous one.

Looking for the continuous-wave spectrum of this system, I find the result:

$$(\omega_1 \omega' - \frac{3}{2}\beta V_0^2)(\omega_1 \omega' - \frac{3}{2}\beta W_0^2) = a^2 K^2 q'^2, \quad (6)$$

where ω' and q' are the frequency and wavenumber of the odd and even solutions with the amplitudes W_0 and V_0 , respectively. The dispersion relation (6) exhibits a *nonlinearity-induced gap* in the cw spectrum and this gap is proportional to the difference in the amplitudes of odd and even particles oscillations,

$$\Delta\omega' = \frac{3\beta}{2\omega_1} |V_0^2 - W_0^2|. \quad (7)$$

Appearance of the gap in the cw spectrum may be a factor of the wave localization at the frequency ω_1 provided the nonlinearity will be large enough. However, this kind of localized structures has to differ drastically from the standard localized excitations of nonlinear (continuous or discrete) models. Indeed, both of the wavefield components, the odd and even ones, cannot be vanishing in the same direction because there is no gap in the linear spectrum and small-amplitude oscillations will be delocalized.

Analysing the localized structures related to the effective gap, I look for stationary solutions of Eq.(4),(5) in the form

$$(V, W) \propto (f_1, f_2)e^{-i\Omega t}, \quad (8)$$

assuming, for simplicity, the function f_1 and f_2 to be real. As a matter of fact, the system (4), (5) may display more complicated solutions, e.g., those with a spatially dependent phase. Then, the stationary solutions of Eqs. (4) and (5) may be found as those of the system of two ordinary differential equations of the first order,

$$\frac{df_1}{dz} = -\omega_1 \Omega f_2 + \lambda f_2^3, \quad (9)$$

$$\frac{df_2}{dz} = \omega_1 \Omega f_1 - \lambda f_1^3, \quad (10)$$

where $z = x/aK$ and $\lambda = 3\beta/2$. Equations (9), (10) describe the dynamics of a Hamiltonian system with one degree of freedom and the conserved energy,

$$E = -\frac{1}{2}\omega_1 \Omega (f_1^2 + f_2^2) + \frac{1}{4}\lambda (f_1^4 + f_2^4), \quad (11)$$

and they may be easily integrated. Different kinds of the solutions are characterized by different values of the energy E . On the phase plane (f_1, f_2) soliton solutions correspond to the separatrix curves connecting a pair of the neighboring saddle points $(0, f_0)$, $(0, -f_0)$, $(f_0, 0)$, or $(-f_0, 0)$, where $f_0^2 = \omega_1 \Omega / \lambda$. Calculating the value of E for these separatrix solutions, $E = -\omega_1^2 \Omega^2 / 4\lambda$, it is possible to obtain the soliton solutions in elementary functions,

$$f_2 = \frac{\omega_1 \Omega e^{\mp \sqrt{2}\omega_1 \Omega z} [2 \cosh(\sqrt{2}\omega_1 \Omega z) \pm \sqrt{2}]}{2\lambda \cosh(2\sqrt{2}\omega_1 \Omega z)}, \quad f_1 = f_2 \exp(\pm \sqrt{2}\omega_1 \Omega z). \quad (12)$$

The solutions (12), but for negative Ω , exist also for defocusing nonlinearity when $\lambda < 0$.

The results (12), together with (2),(3) and (8), give the shapes of the localized structures in the discrete nonlinear lattice. Because of all combinations of the signs are possible in Eq.(12), there are *four* solutions of this type. Let us fix the sign in Eq.(12), say minus, to analyse the structures of the odd and even particle oscillations. When $z \rightarrow +\infty$, the amplitude of the even particle oscillations, f_1 , goes to its limit value $f_0 = \sqrt{\omega_1 \Omega / \lambda}$. In the same time the amplitude of the odd particle oscillations vanishes (see Fig.1). However, when $z \rightarrow -\infty$, the asymptotic behaviour of the even and odd components is just reverse: $f_1 \rightarrow 0$ and $f_2 \rightarrow f_0$. Therefore, the whole localized structure represents two kinks in the odd and even oscillating modes which are composed to have opposite polarities, so that both of them cannot be localized in one direction (Fig.1). This result is the direct consequence of the nonlinearity-induced gap (7) in the cw spectrum (6), the gap being disappearing in the linear limit.

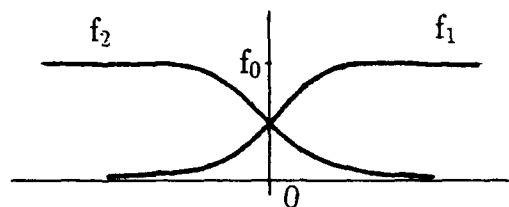


Fig.1 Structure of the localized mode given by Eq. (12).

It is important to note that the described localized structures have been recently observed experimentally as "noncutoff kinks" in a damped and parametrically driven experimental lattice of coupled pendulums and numerically in a simplified model¹. A parametric drive allows to compensate the dissipation-induced decay of the structures supporting steady-state regimes.

It is interesting to compare the localized structures described in this paper with the so-called gap solitons discovered in 1987 by Chen and Mills⁵. As is well known, the gap solitons may exist in nonlinear (continuous) periodic media as localized excitations when the nonlinear frequency is shifted into the gap of the linear spectrum induced by *periodicity* of the system parameters, e.g. by periodical change of the linear refractive index. From the viewpoint of the theory of gap solitons, the nonlinear localized structures described here may be called *self-supporting gap solitons*. Indeed, the linear spectrum has no gap, but the latter may appear due to nonlinearity. Thus, one group of the particles (e.g., at the even sites) of the chain creates asymptotically an *effective periodic potential* for the other group of the particles (e.g., at the odd sites), and vice versa, forming finally two parts of the structure which is similar in parts to spatially localized gap solitons.

I would like to thank Prof. A.M. Kosevich for stimulating discussions. The work was supported by the Alexander von Humboldt-Stiftung through a research fellowship.

REFERENCES

1. B. Denardo, B. Galvin, A. Greenfield, A. Larraza, S. Putterman, and W. Wright, Observation of localized structures in nonlinear lattices, *Phys. Rev. Lett.* 68: 1730 (1992).
2. Yu. S. Kivshar and M. Peyrard, Modulational instabilities in nonlinear lattices, *Phys. Rev. A* (1992).
3. Yu. S. Kivshar and B. A. Malomed, Dynamics of solitons in nearly integrable systems. *Rev. Mod. Phys.* 61: 763 (1989).
4. Yu. S. Kivshar and N. Flytzanis, Gap solitons in diatomic lattices, *Phys. Rev. A* (1992).
5. W. Chen and D. L. Mills, Gap solitons and the nonlinear optical response of superlattices. *Phys. Rev. Lett.* 58: 160 (1987).

DYNAMICS OF SOLITONS IN POLYACETYLENE IN THE STEP-POTENTIAL MODEL

Christoph Kuhn

Physikalische Chemie
Eidgenössische Technische Hochschule Zürich
CH-8092 Zürich
Switzerland

INTRODUCTION

The problem of transmitting a signal through a π -electron system has been widely discussed^{1,2}. Transport of solitons through a polyene chain was subject of a number of papers with (Klein-Gordon) models³⁻⁵, and the (Su-Schrieffer-Heeger)-model⁶⁻⁸. The lattice dynamics is treated in standard adiabatic approximation using Newton's equation of motion³⁻¹⁰. The force required to integrate Newton's equation is obtained as the negative gradient of a potential energy surface. The equation of motion is integrated numerically using finite time steps. The result of the integration depends on the accuracy and stability of the algorithm used¹¹.

We have recently shown¹², that the statics of solitonic excitations can be treated by a simple step-potential model of a nearly free π -electron (NFE) coupled to the lattice distortion leading essentially to the same results as the (SSH)-model¹³, in which an extended Hückel, tight-binding Hamiltonian is used. The effective potential of the (NFE)-model takes care of electron correlation effects implicitly and thus has been used successfully to calculate the linear and nonlinear polarizabilities of π -electron systems in an applied electric field^{14,15}. It has been extended to include electron correlation explicitly¹⁶. In the step potential model of a hydrocarbon chain of M bonds with unknown bond lengths d_1, d_2, \dots, d_M , the Schrödinger equation with a potential composed of bond

potentials V_1, V_2, \dots, V_M is solved ($V_i = \beta \frac{\hbar^2}{2m_e a^2} \left(\frac{d_i}{a} - 1 \right)$), where $\frac{\hbar^2}{2m_e a^2} = 1.944 \text{ eV}$.

$\beta = 19.4$ and $a = 1.40 \text{ \AA}$). The wave functions are obtained as outlined in¹². The lowest states are filled with the π -electrons present in the system and the π -electron density in the middle of each bond $\rho_i(V_1, V_2, \dots, V_M)$ is obtained. The electron-phonon coupling (i.e. the π -electron charge in the bond attracts the σ -bonded nuclei by Coulomb forces and thus reduces the carbon-carbon distance, while the Coulomb repulsion of the carbon ions, diminished by shielding of the σ -electrons, counteracts this) is described by

$$V_i = \alpha (1 - \rho_i a) \frac{\hbar^2}{2m_e a^2}, \quad \alpha = 1.95 \quad (1)$$

Applying (1) and solving the Schrödinger equation for the new configuration of bond potentials initiates in return a cycle of an iteration, which converges to selfconsistency between ρ_i and V_i and thus finds the equilibrium charge density $\tilde{\rho}_i (\tilde{V}_1, \tilde{V}_2, \dots, \tilde{V}_M)$ and bond lengths $\tilde{d}_1, \tilde{d}_2, \dots, \tilde{d}_M$. The bond lengths of polyenes and annulenes and the statics of solitonic excitations in polyacetylene are well described by this simple model. It is of interest to extend the step potential model to a description of soliton dynamics¹⁷.

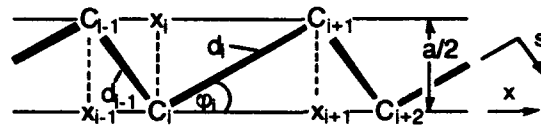


Figure 1. Zig-zag structure of polyacetylene along s . Coordinate x_i of CH group i moving on track along x . Bond length $d_i = (x_{i+1} - x_i) / \cos \varphi_i = a / (2 \sin \varphi_i)$ of bond i .

THE FORCE FIELD

Treating dynamics of the vibronic coupling in standard adiabatic approximation Newton's equation $M_{CH} \ddot{x}_i = F_i$ for each site i (Fig. 1) is applied. The force acting on adjacent sites is obtained from the strain within the bond, which is proportional to the deviation $\tilde{\rho}_i - \rho_i$ of the actual π -electron density ρ_i from its equilibrium density $\tilde{\rho}_i$.

$$F_i = \left[(\tilde{\rho}_i - \rho_i) \cos \varphi_i - (\tilde{\rho}_{i-1} - \rho_{i-1}) \cos \varphi_{i-1} \right] k a^2 \quad (2)$$

For small deviations of the actual density ρ_i from its equilibrium it is assumed that the equilibrium density $\tilde{\rho}_i$ is obtained by applying (1) once and solving the Schrödinger equation for the new configuration of bond potentials. Newton's equation with force (2) is approximated by a difference equation (Verlet algorithm) and is further simplified to an equation describing the time evolution of the bond potentials. Starting with an initial condition and proceeding with time step Δt

$$\begin{aligned} V_i^{t+\Delta t} &= 2V_i^t - V_i^{t-\Delta t} + (\Delta t \omega)^2 x_i^t \cdot \frac{\hbar^2}{2m_e a^2} \\ x_i^t &= \left[(\tilde{\rho}_{i+1} - \rho_{i+1}) - 2(\tilde{\rho}_i - \rho_i) + (\tilde{\rho}_{i-1} - \rho_{i-1}) \right] a \end{aligned} \quad (3)$$

With $\Delta t \omega = 0.5$ we have chosen a time step Δt sufficiently small to reach good accuracy and stability¹¹. The value of the time scale Δt is obtained by solving equation (3) to calculate the frequency ν_{\max} of the in-phase-stretching-mode of the polyene lattice and by fitting it with $\nu_{\max} = c \cdot 1400 \text{ cm}^{-1}$ obtained from the vibronic structure of the absorption band of polyenes. We find $\nu_{\max} = \frac{1}{19.1 \Delta t}$, thus $\Delta t = 1.25 \cdot 10^{-15} \text{ sec}$,

$k = \frac{M_{CH}}{\beta} \omega^2 = 11.2 \text{ eV/\AA}^2$. The velocity of sound is $v_s = \pi a \nu_{\max} = 1.85 \cdot 10^4 \text{ m sec}^{-1}$.

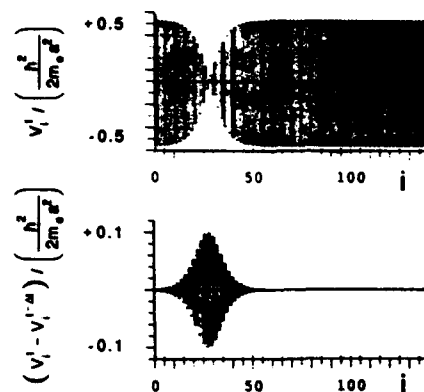


Figure 2. Initial bond potential V_i^1 (above), $V_i^1 - V_i^{1-\Delta t}$ (below) to dynamics in Fig. 3.

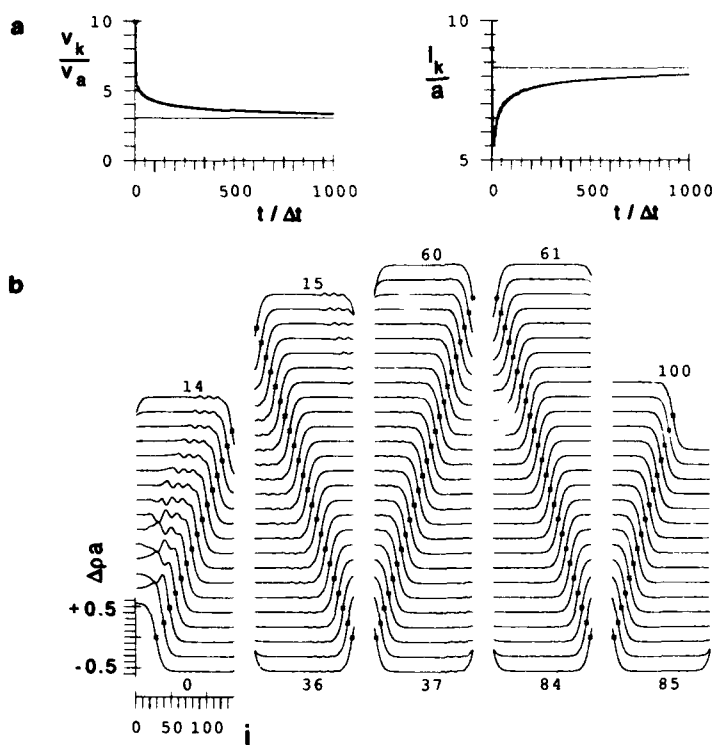


Figure 3. Dynamics of a neutral kink along a ring of 139 sites with initial kink velocity $v_k = 10 v_a$. Time evolution during 1000 time steps of $\Delta t = 1.25 \cdot 10^{-15}$ sec: a) v_k and kink width l_k . b) charge density alternation $\Delta \rho_i = (-1) (\rho_{i+1} - \rho_i)$, $\Delta \rho = 0$ indicated by star. Spot-light every $10\Delta t$ indicated by numbers 0-100. To avoid kink phonon collision, phonons evolving behind the kink are relaxed by removing kinetic energy.

In the following the time evolution of defects in the charge density alternation $\Delta\rho_i = (-1)^i (\rho_{i+1} - \rho_i)$ along the lattice is investigated.

SOLITON DYNAMICS

The time evolution of a neutral kink embedded in a ring with 139 sites initially at rest with velocity boosts (Fig. 2) of $v_k = 1.0 v_a$ is investigated (Fig. 3). Immediately after the boost the velocity of the kink v_k drops down to $v_k = 0.5 v_a$ as well as its width l_k , from initially $l_k = 9 a$ to $l_k = 6.5 a$ (Fig. 3a), while the rise of a huge hump behind the soliton takes over the excess kinetic energy. The hump starts to oscillate and smaller wiggles with frequency $0.94 v_{max}$ and wave length $13 a$ develop behind the kink, slowing it down further and increasing its width again (Fig. 3b). With progressive time evolution the amplitude of these wiggles fades away and the soliton reaches a constant width of $l_\infty = 8.3 a$ and a constant velocity of $v_\infty = 3.05 v_a$ without energy dissipation into the lattice. For this long time study the phonons behind the soliton are suspended at some distance from the soliton to avoid soliton-phonon collision. The total energy is not conserved during this procedure until steady state is reached. (Conservation of total energy is proved by demonstrating constant velocity of a kink moving with low speed). Bishop et al.⁷ and Guinea⁸ obtain within the SSH-model v_∞ values between $v_\infty = 0.9 v_a$ and $v_\infty = 4.0 v_a$ by using different values of adjustable parameters.

KINK SCATTERING

Figures 4 and 5 show computer simulations of two neutral kinks K^0 and R^0 embedded in a ring of 160 sites and approaching each other with velocities $v_K = +v_a$ and $v_R = -v_a$ respectively. For the well separated neutral kinks the spectrum has two nearly degenerate intergap states. These states are occupied with two electrons.

In the case of A_g -scattering (Fig. 4) this degeneracy is removed as the two kinks collide and annihilate, the lower, doubly occupied intergap state digs into the valence band, while the upper, empty intergap state digs into the conduction band. The kinks are trapped in "bounce resonances", an oscillation between the annihilated state of a defect free, but overshooted bond alternation with empty gap and the bound kink-antikink pair with two intergap states. The energy dissipates slowly into the lattice. This finding seems to be independent of the initial kink velocities.

In the case of B_u -scattering (Fig. 5) this degeneracy is removed slightly as the two kinks approach each other, the lower, singly occupied intergap state loses a small amount of energy, while the upper, singly occupied intergap state gains a small amount of energy. The kinks do not annihilate, but they stop before collision, and turn backwards. The degeneracy of states and the final kink velocities are restored. This finding seems to be independent of the initial kink velocities.

Guinea⁸ does not distinguish occupation configurations, but reports within the SSH-model scattering of neutral kinks with different initial velocities: the kinks "are trapped in bounce resonances" for small initial velocities and above a certain threshold "bounce twice and separate to infinity with velocities significantly lower than the initial ones". Similarly Campbell et. al.³⁻⁵ report within the Klein-Gordon models of kinks "trapped in bounce resonances" for small initial velocities and above a certain threshold of "n bounce collisions and separation to infinity" and of "narrow windows in which kinks are trapped in bounce resonances".

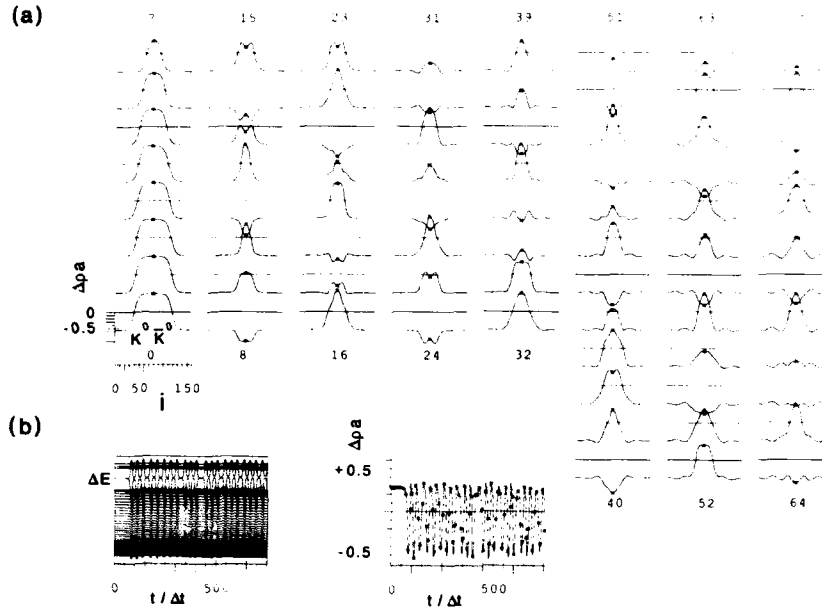


Figure 4. $A_g - K^0 R^0$ scattering. Two intergap states, lower state doubly occupied, upper state empty. Initial velocities $v_K = +v_a$ and $v_K = -v_a$. Time evolution during 750 time steps of a) charge density alternation $\Delta\rho$ ($\Delta\rho = 0$ indicated by line. Spotlight every 10 Δt indicated by numbers 0-75), b) eigenvalues (gap $\Delta E = 1.34$ eV), $\Delta\rho$ of central bonds.

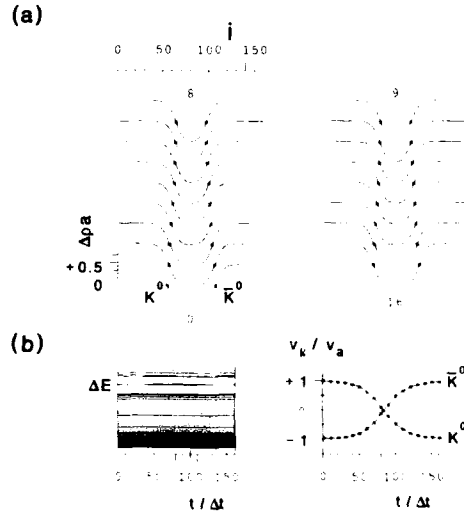


Figure 5. $B_u - K^0 R^0$ scattering. Two intergap states, both states singly occupied. Initial velocities $v_K = +v_a$ and $v_K = -v_a$. Time evolution during 160 time steps of a) charge density alternation $\Delta\rho$ ($\Delta\rho = 0$ indicated by line. Spotlight every 10 Δt indicated by numbers 0-16) b) eigenvalues (gap $\Delta E = 1.34$ eV), velocities v_K and v_K .

ACKNOWLEDGEMENTS

The author is grateful to Professor W. F. van Gunsteren for his continuous interest and encouragements and to Professors I. Kuščer and S. Roth for valuable discussions. The use of the computer facilities at the ETH is acknowledged.

REFERENCES

- 1 F.L. Carter, A. Schulz, D. Duckworth, Soliton switching and its implication for molecular electronics in "Molecular Electronic Devices II", F.L. Carter ed., M. Dekker, New York (1987)
- 2 S. Roth, H. Bleier, Can polyacetylene-solitons be used in molecular electronics? in "Molecular Electronics-Science and Technology", ed. A. Aviram, Engineering Foundation Conferences, New York (1989)
- 3 D.K. Campbell, J.F. Schonfeld, C.A. Windgate, Resonance structure in kink-antikink interactions in ϕ^4 theory, *Physica* 9D:1 (1983)
- 4 M. Peyrard, D.K. Campbell, Kink-antikink interactions in a modified Sine-Gordon model, *Physica* 9D:33 (1983)
- 5 D.K. Campbell, M. Peyrard, P. Sodano, Kink-antikink interactions in the double Sine-Gordon model, *Physica* 19D:165 (1986)
- 6 W.P. Su, J.R. Schrieffer, Soliton dynamics in polyacetylene, *Proc. Natl. Acad. Sci. USA* 77:5626 (1980)
- 7 A.R. Bishop, D.K. Campbell, P.S. Lomdahl, B. Horovitz, S.R. Philpot, Breathers and photoinduced absorption in polyacetylene, *Phys. Rev. Lett* 52:71 (1984)
- 8 F. Guinea, Dynamics of polyacetylene chains, *Phys. Rev. B* 30:1884 (1984)
- 9 C. Tric, Planar vibrations of carbon skeleton of polyenes, *J. Chem. Phys.* 51:4778 (1969)
- 10 T. Kakitani, Theoretical study of optical absorption curves of molecules III, force constant and bond interaction in conjugated molecules, *Prog. Theor. Phys.* 51:656 (1974)
- 11 H.J.C. Berendsen, W.F. van Gunsteren, Practical algorithms for dynamic simulations, in "Molecular-Dynamics Simulation of Statistical-Mechanical Systems", G. Ciccotti, W.G. Hoover eds., North-Holland, Amsterdam (1986)
- 12 C. Kuhn, Solitons, polarons, and excitons in polyacetylene: step-potential model for electron phonon coupling in π -electron systems, *Phys. Rev. B* 40:7776 (1989)
- 13 W.P. Su, J.R. Schrieffer, A.J. Heeger, Soliton excitation in polyacetylene, *Phys. Rev. B* 22:2099 (1980)
- 14 C. Kuhn, Step potential model for non-linear optical properties of polyenes, push-pull polyenes and cyanines and the motion of solitons in long-chain cyanines, *Synth. Met.* 43:3681 (1991)
- 15 C. Kuhn, Step potential model for nonlinear optical properties of polyenes, in "Electronic Properties of Polymers", Eds. H. Kuzmany, M. Mehring, S. Roth, Springer, Berlin (1992)
- 16 C. Kuhn, 2^1A_g below 1^1B_u in polyenes: correlation of nearly free π -electrons, *Synth. Met.* in press
- 17 C. Kuhn, Dynamics of solitons in polyacetylene in the step-potential model, *Synth. Met.* in press

SOLITON-LIKE STRUCTURE IN (2+1) DIMENSIONS

Bernard Piette and Wojciech J. Zakrzewski

Department of Mathematical Sciences
University of Durham
Durham DH1 3LE, England

Abstract: We study lump-like solutions of the S^2 sigma model and of the corresponding Skyrme models in (2+1) dimensions. We show that the pure S^2 model possesses conserved quantities that makes it quasi-integrable in the geodesic approximation. We also show that for some choices of the potential the Skyrme models have stable lump-like solutions that in the head-on collisions scatter at 90° to the direction of their approach while for some other ones form bound states of such lumps.

INTRODUCTION

Over the past few years classical field theories in (2+1) dimensions have become an increasingly important area of research. These models can be considered as low dimensional toy models describing various properties of lump-like structures which in (3+1) dimensions are thought to provide a good description of many physical objects such as nucleons or monopoles.

One of these models is the (2+1) dimensional Skyrme S^2 model which possess stable lump-like solutions that can be characterised by a topological quantity^[1]. This model is described by a three component vector field $\vec{\phi}$ lying on a sphere of radius 1, ie $\vec{\phi}$ satisfies $\vec{\phi} \cdot \vec{\phi} = 1$. The Lagrangian of the model is given by

$$\mathcal{L}_1 = (\partial^\mu \vec{\phi}) \cdot (\partial_\mu \vec{\phi}) - \theta_1 ((\partial^\mu \vec{\phi} \cdot \partial_\mu \vec{\phi})^2 - (\partial^\mu \vec{\phi} \cdot \partial^\nu \vec{\phi})(\partial_\mu \vec{\phi} \cdot \partial_\nu \vec{\phi})) - \theta_2 V(\phi^1, \phi^2, \phi^3), \quad (1)$$

where μ is the Lorentz index running from 0 to 2 for, respectively, t, x and y . The first term in (1) is the Lagrangian for the pure S^2 sigma model, the second one describes the additional Skyrme term and V is an arbitrary positive potential that goes to 0 as $\vec{\phi}$ goes to the north pole of the sphere ie to $\vec{\phi} = (0, 0, 1)$.

THE S^2 SIGMA MODEL

When we set $\theta_1 = \theta_2 = 0$, (1) becomes the Lagrangian for the S^2 sigma model which is invariant under spatial (x and y) conformal transformations. The model

possesses several conserved quantities. The finite energy static configurations of the model correspond to the mappings of the 2 dimensional sphere into itself and so these field configurations are characterised by an integer-valued topological charge describing such mappings. As the time evolution corresponds to a continuous transformation, the topological charge remains constant and so is conserved. The Lorentz invariance of the model generates four conserved quantities: the energy-momentum three-vector and the angular momentum. Moreover, as the model is invariant under the $O(3)$ group acting on S^2 , the three Noether charges

$$C_i = \epsilon_{ijk} \int dx dy (\phi_j \partial_i \phi_k - \phi_k \partial_i \phi_j), \quad i = 1, 2, 3 \quad (2)$$

are also conserved.

All static solutions of this model can be presented in an explicit form^[2]. They correspond to a number of lump-like configurations where the number of lumps is determined by the value of the topological charge. The existence of the multi-lump solutions is due to the fact that the lumps do not interact with each other. Moreover, as a consequence of the conformal symmetry, the lumps can have any size and be placed at an arbitrary distance from each other.

To see how the lumps evolve in time we have to perform numerical simulations. Unfortunately, the conformal symmetry of the S^2 model makes the lumps unstable, as they can shrink or spread out without any change in their potential energy, and indeed, this is what is seen in numerical simulations^[1].

In particular, when a single lump at rest is slightly perturbed it shrinks or spreads out very rapidly becoming infinitely broad or infinitely spiky. When two lumps are sent towards each other at a zero impact parameter, they collide, form a ring and then scatter at 90° . After the collision, the two lumps that emerge from the ring shrink or spread out as they move away from each other, thus exhibiting their instability.

Another technique, which has been widely used to study many models, is the geodesic approximation. If the lumps are given a very small amount of kinetic energy, one can assume that they will stay in a configuration very close to a static configuration. The idea of the approximation is to take the most general expression for a static configuration of a given number of lumps (say two) and assume that, for low velocities, the parameters of the static configuration become time dependent. This is not correct for the full field evolution, but can be correct "on average", ie after the integration over x and y . Thus substituting this ansatz into the Lagrangian, integrating over the spatial coordinates x and y , the field theoretical system reduces to a dynamical system with a finite number of degrees of freedom (five in this case). In fact, the resultant system of the ordinary differential equations has also to be solved numerically, but the calculations are much simpler to perform. The results obtained in this approximation are in a very close agreement with those obtained by integrating numerically the full equations of motion.

The conserved quantities described above, in particular C_i , do not translate trivially into the conserved quantities of the differential equations governing the geodesic approximation, but are nevertheless also nearly conserved. This we think may be a clue which may help us to formulate more precisely the concept of quasi-integrability of the model.

THE SKYRME MODEL

To cure the instability problem we have added a Skyrme and a potential term to the S^2 Lagrangian. The first term makes the lumps shrink and the second one forces them to spread out. Combined together the two terms stabilise the lumps. The Skyrme and the potential terms break, respectively, the spatial dilation and the

$O(3)$ symmetry of the S^2 model. For many specific choices of the potential term the model still possesses as its solution one extended structure solution of the pure S^2 model but with its overall size fixed by θ_1 and θ_2 . Other solutions also exist but some of them are unstable due to the forces which now act between the lumps.

Choosing $V = (1 + \phi_3)^4$, the basic solution corresponds to a single lump and its topological charge is one^[3]. The lump is stable under perturbations but its scattering properties are more complicated. Two lumps, initially placed some distance from each other, repel and so move away from each other. When two lumps are sent towards each other at a zero impact parameter, they progressively slow down, and if their speed is large enough, they collide, form a ring and scatter at 90° . After the scattering the two lumps emerge with their initial sizes. If the speed is too small, the two lumps slow down, stop and then move back to back. The critical speed that differentiates between the back to back and the 90° scattering increases with θ_1 and θ_2 . We have also observed that the scattering time is longer when the speed is close to this critical velocity. When the speed is very close to its critical value the total energy density has the form of a nearly perfect ring, whereas the kinetic energy density exhibits an oscillatory motion. This motion generates a ring structure from which two peaks emerge at 90° , come back to form a new ring, scatter along the original direction and emerge again at 90° etc for a few oscillations after which the two lumps eventually scatter either back to back or at 90° . This behaviour is very similar to the formation of a resonance seen in some dynamical systems.

For the scattering with non zero impact parameters, the results were very similar. Each time the two lumps scattered at an angle dependent on the incoming speed. At small speeds the lumps scattered at a small angle, whereas at large speeds, the scattering angle was larger than 90° , the larger the impact parameter the larger the angle.

Another interesting feature of the Skyrme models is that most of the scatterings of lumps have been almost perfectly elastic. By this, we mean that although during the scattering, a circular wave is emitted which carries away some energy, the energy of this wave is quite small. Even though it is very small, it is nonzero and so the kinetic energy (speed) of the two lumps after the interaction is always smaller than before it.

A similar behaviour is exhibited by a single lump. As we have said, the size of a lump is fixed in this model, but if a lump with an incorrect size is taken as an initial configuration its size changes to the correct value, and the excess of energy is got rid of by emitting a circular wave. This proves the stability of a single lump in this model.

The fact that the scattering of the lumps in this model is not purely elastic is an indication that the model is not completely integrable. Nevertheless, the behaviour of the lumps looks perfectly regular and resembles the behaviour seen in integrable models. In particular, all the extra radiation effects, though nonzero, are very small. This leads us to believe that between the integrable and strictly nonintegrable models there is an intermediate class of models which we will call quasi-integrable and that these models are quite similar to the integrable models, without having all their properties. We also believe that they may be quite relevant when we try to describe real phenomena in physics as, for example, small inelasticity is often observed in nature.

We have also studied the Skyrme with the following type of the potential^[4]:

$$V = \frac{1}{\lambda} [(\phi_1 + \lambda a^2(1 + \phi_3))^2 + \phi_2^2(1 + \phi_3)^2], \quad (3)$$

where λ and a are two arbitrary parameters. The static solutions for this model can be constructed analytically. They have a topological charge equal to two, and so

correspond to two lumps at rest. The parameter a in the potential is equal to half the distance between the two lumps. If a is 0, the two lumps are on top of each other, but as its value increases, the lumps are located further apart. The shape of the potential between the two lumps resembles the Morse potential but with a finite value at the origin.

This static solution thus corresponds to a bound state of two lumps. Moreover, it is also stable under small perturbations. If the lumps are given a small momentum, they oscillate around their equilibrium position, radiating this excess of energy until they stabilise at their position of equilibrium. If they are sent away from each other with enough energy, the two lumps split and escape to infinity. When sent towards each other with enough energy to overcome the potential barrier that separates them, the two lumps collide, form a ring and then emerge at 90° .

We have not been able to find the analytical form of the one lump solution of this model, but we have been able to determine it numerically in our simulations. Its energy is larger than half the energy of the pair, explaining why the pair is bound.

We have also been able to construct numerically static solutions for three, four and five lumps put together (for the same potential). In each case the lumps are situated on a circle with a radius which increases with the number of lumps. The energy per lump also increases with the number of the lumps, the most bound being the pair.

As the bound states of lumps are the most stable objects in this model, it is interesting to see how they behave when scattered against each other. In this case, the scattering depends crucially on the impact parameter, on the relative speed and also on the relative orientation of both pairs making it much more difficult to describe. Our observations can be summarised as follows. When the scattering takes place with a small kinetic energy, the two pairs hit each other and emerge in an excited state (the lumps oscillate around their equilibrium position). Higher energy scatterings depend on the relative orientation of the pairs. The pairs sometimes scatter back to back, sometimes at 90° , but we have also observed that for some very specific values and orientations, the pairs split and produce four isolated lumps that can move away from each other.

We conclude that the Skyrme model with the potential given by (3) is a good toy model to study various properties of bound states of lump-like field configurations and that these scattering properties are very complicated. Moreover, we hope it is telling us also what to expect in physically more relevant (3+1) dimensions.

REFERENCES

1. R.A. Leese, M. Peyrard and W.J. Zakrzewski, - Soliton stability in the $O(3)$ σ -model in (2+1) dimensions, *Nonlinearity* **3**, 773 (1990)
2. A. D'Adda, P. Di Vecchia and M. Luscher - A $\frac{1}{N}$ Expandable Series of Non-Linear σ Models With Instantons - *Nucl. Phys. B* **146**, 63 (1978)
3. M. Peyrard, B. Piette and W. Zakrzewski - Solitons Scattering in the Skyrme model in (2+1) Dimensions: 1. Soliton-Soliton Case. (to be published in *Nonlinearity*).
4. B. Piette and W. Zakrzewski - Skyrmion Model in (2+1) Dimensions with Soliton Bound States. Durham Preprint DTP-91/67.

SOLITONS ON A NONLINEAR KLEIN-GORDON EQUATION

B.N. Prasanna
33 Second Main Road
Vyalikaval
Bangalore - 560 003
India

INTRODUCTION

The nonlinear Klein-Gordon equation under investigation is

$$-\Phi_{xx} + (f(\Phi)\Phi_t)_t + \Phi = 0 \quad (1)$$

where $\Phi = \Phi(x, t)$ is a real-valued function and $f(\Phi)$ is a positive function of Φ for $|\Phi| < \infty$ with $f(0) = 1$. Eq. (1) is a conservative system since it can be derived from the Lagrangian density

$$\mathcal{L}(\Phi, \Phi_x, \Phi_t) = -\frac{1}{2}\Phi_x^2 + \frac{1}{2}f(\Phi)\Phi_t^2 - \frac{1}{2}\int_{-\infty}^{\Phi} f(\alpha)\alpha_t^2 d\alpha - \frac{1}{2}\Phi^2. \quad (2)$$

We consider two specific cases for $f(\Phi)$: (i) Linear: $f(\Phi) = 1 + h\Phi$, $|h\Phi| < 1$, (ii) Quadratic: $f(\Phi) = 1 + k\Phi^2$, $|k\Phi^2| < 1$. These two choices of $f(\Phi)$ take Eq.(1) respectively into

$$-\Phi_{xx} + \Phi_{tt} + \Phi = -(\Phi^2)_t \quad (3)$$

$$-\Phi_{xx} + \Phi_{tt} + \Phi = -(\Phi^3)_t, \quad (4)$$

where Φ is the normalised dependent variable ϕ . In each of the above equations the l.h.s. is the linear Klein-Gordon equation and the r.h.s. represents the nonlinear term.

SOLITARY WAVE SOLUTION

Since existence of solitary wave solution is a necessary (though by no means sufficient) condition for the existence of soliton solution for a nonlinear evolution equation, the solitary wave solution is investigated by introducing as in Scott et al¹ the transformation $\xi = x - ut$ where $u > 0$, so that $\partial x / \partial t = -\partial / (u \partial t) = d/d\xi$. The condition that a solitary wave is localised in space and time so that $d\bar{\Phi}/d\xi$ and $d^2\bar{\Phi}/d\xi^2$ must vanish as $|\xi| \rightarrow \infty$ implies that solitary wave solutions can exist only for $0 < u^2 < 1$. Eqs. (3) and (4) go over respectively into the normalised linear ODEs (5) and (6) as shown in Table 1.

Table 1. Normalization of Eqs.(3) and (4) into nonlinear ODEs.

	Ξ	$\bar{\Phi}$	Normalised NODE	
Eq.(3)	$\frac{\xi}{\sqrt{1-u^2}}$	$\frac{2u^2}{1-u^2} \bar{\Phi}$	$\frac{d^2}{d\Xi^2} (\bar{\Phi} - \frac{\bar{\Phi}^2}{2}) - \bar{\Phi} = 0$	(5)
Eq.(4)	$\frac{\xi}{\sqrt{1-u^2}}$	$\sqrt{\frac{3u^2}{1-u^2}} \bar{\Phi}$	$\frac{d^2}{d\Xi^2} (\bar{\Phi} - \frac{\bar{\Phi}^3}{3}) - \bar{\Phi} = 0$	(6)

Eqs. (5) and (6) have the respective solitary wave solutions

$$\bar{\Phi}(\Xi) = \frac{3}{2} \operatorname{sech}^2 \left(\frac{3}{2} \sqrt{1 - \frac{2}{3} \bar{\Phi}(\Xi)} + \frac{|\Xi|}{2} \operatorname{sgn}(|\Xi| - \Xi_1^*) - \Xi_1^* \theta(|\Xi| - \Xi_1^*) \right) \quad (7)$$

$$\bar{\Phi}(\Xi) = \sqrt{2} \operatorname{sech} \left(2 \sqrt{1 - \frac{1}{2} \bar{\Phi}(\Xi)} + |\Xi| \operatorname{sgn}(|\Xi| - \Xi_2^*) - 2\Xi_2^* \theta(|\Xi| - \Xi_2^*) \right) \quad (8)$$

where

$$\Xi_1^* = \sqrt{3} - 2 \tanh^{-1} \frac{1}{\sqrt{3}} \text{ and } \Xi_2^* = \sqrt{2} - \tanh^{-1} \frac{1}{\sqrt{2}}$$

are the points at which $d\bar{\Phi}/d\Xi$ has an algebraic singularity and $\theta(\Xi)$ is the unit step function. Eqs. (7) and (8) are sketched in Fig. 1. Both Eqs. (7) and (8) exhibit the salient feature of velocity dependent amplitude which is characteristic of the soliton.

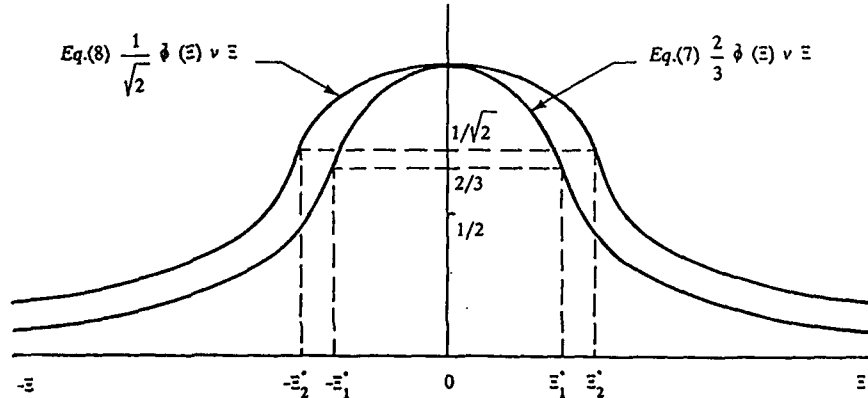


Figure 1. Solitary wave Profiles.

Table 2. Choices of q and r to derive Eqs. (3) and (4).

To Derive	From Eq. (9a) $a_1(t) = 0, a_2(t) = i$	From Eq. (9b) $a_1(t) = 0, a_2(t) = i$
Eq. (3)	q	q
	$(\Phi + \Phi^2)_t$	$(\Phi + \Phi^2)_t$
Eq. (4)	r	r
	-2Φ	2Φ
Eq. (4)	q	q
	$(\Phi + \Phi^3)_t$	$(\Phi + \Phi^3)_t$
Eq. (4)	r	r
	-2Φ	2Φ

In the research now in progress, confirmation of whether these solitary wave solutions are indeed solitons is being attempted via analytic and computational techniques.

ANALYTICAL: INVERSE SCATTERING METHOD

The general inverse scattering framework of Ablowitz et al² is sought to be applied by showing that Eqs. (3) and (4) can be derived from the Schrödinger potentials of the two-component linear system $Lv = \zeta v$ and $idv/dt = Bv$ where operators L and B are as in Eqs. (V.6) and (V.7) of Scott et al¹. Using the procedure outlined in Lamb one can obtain the nonlinear evolution equations for the Schrödinger potentials q and r :

$$iq_t + \left(\frac{1}{2} q_{xx} - q^2 r \right) a_2(t) - iq_x a_1(t) = 0 \quad (9a)$$

$$ir_t + \left(r^2 q - \frac{1}{2} r_{xx} \right) a_2(t) - ir_x a_1(t) = 0 \quad (9b)$$

Eqs. (3) and (4) can be derived from Eqs. (9a) and (9b) for various choices of q and r as shown in Table 2.

We envisage identification of the reflection coefficients $R_R(k)$ and $R_L(k)$ with their Fourier transforms and impose the restriction in order that the time dependence of the reflection coefficients be of simple exponential form. The knowledge of the reflection coefficients and their time dependence can then be used to determine the functions $A_R(x,ct)$ and $A_L(x,ct)$ of Lamb³ which describe the scattering for incidence from the right and the left respectively, by solving the Marchenko equations both when bound states are absent and when they are present. Determination of Φ then follows from

$$\Phi(x,t) = -2 \frac{\partial}{\partial x} A_R(x,x;t) = + 2 \frac{\partial}{\partial x} A_L(x,x;t) \quad .$$

COMPUTATIONAL: DISCRETIZATION OF THE INITIAL VALUE PROBLEM FOR EQ. (1)

The head-on collision of two solitary waves is sought to be simulated on a computer to determine whether they retain their shapes and velocities after collision. To begin with, Eq.(1) is rewritten as a matrix equation of the quasilinear hyperbolic type

$$U_t + A(U) U_x + D(U) = \underline{0}, \quad (10)$$

where

$$U(x,t) = \begin{bmatrix} \Phi_1 \\ \Phi \\ \Phi_2 \end{bmatrix}, A(U) = \begin{bmatrix} 0 & 1 & 0 \\ \frac{1}{f(\Phi)} & 0 & 0 \\ 0 & 0 & 0 \end{bmatrix}, D(U) = \begin{bmatrix} 0 \\ \frac{\phi_2}{f(\Phi)} \\ -\phi \end{bmatrix}.$$

(Φ_1 and Φ_2 are two new independent variables introduced to convert Eq. (1) into a system of three first-order PDEs.) Matrix $A(U)$ has eigenvalues $\lambda_i(U)$ and associated (left) eigenvectors $\eta_i(U)$, ($i = 1,2,3$), given by

$$\begin{bmatrix} \lambda_1 \\ \lambda_2 \\ \lambda_3 \end{bmatrix} = \begin{bmatrix} 0 \\ 1 \\ \frac{-1}{\sqrt{f(\Phi)}} \end{bmatrix}, \begin{bmatrix} \eta_1 \\ \eta_2 \\ \eta_3 \end{bmatrix} = \begin{bmatrix} 0 & 0 & 1 \\ 1 & \sqrt{f(\Phi)} & 0 \\ 1 & -\sqrt{f(\Phi)} & 0 \end{bmatrix}.$$

Next Eq. (10) is cast into its characteristic normal form

$$\eta_i(U) U_{,i} + \eta_i(U) D(U) = 0 \quad (i = 1,2,3) \quad (11)$$

where $U_{,i} = (\partial/\partial t + \lambda_i(U) \partial/\partial x) U$. In Fig. 2 suppose we know the value of vector U at the points $P(x - \Delta x, t)$, $Q(x, t)$ and $R(x + \Delta x, t)$, and want to advance the solution by Δt in time to $Q'(x, t + \Delta t)$. Let $Q'S_i$ be the characteristics of Q' associated with eigenvalues $\lambda_i(Q')$, $i = 1,2,3$. With this construction the finite-difference approximation to Eq.(11) is

$$\eta_i(U(Q')) \frac{U(Q') - U(S_i)}{QQ'} + \eta_i(U(Q')) D(U(Q')) = 0 \quad (i=1,2,3). \quad (12)$$

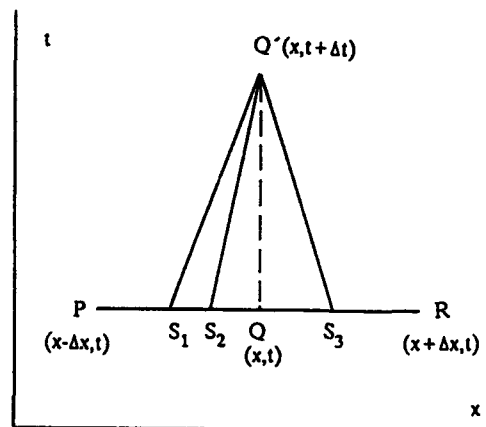


Figure 2. Scheme for discretizing $U_{,i}$.

Since points S_i do not in general coincide with netpoints P, Q and R only at which U is known, $U(S_i)$ is approximated by linear interpolation between values of U at adjacent netpoints. Plugging in the values of $D(U)$, $\lambda_i(U)$ and $\eta_i(U)$ one can write for the unknown vector $U(Q')$ the matrix equation

$$\begin{aligned}
 \begin{bmatrix} \phi_1(Q') \\ \phi(Q') \\ \phi_2(Q') \end{bmatrix} &= \begin{bmatrix} \frac{\Delta t}{2\Delta x \sqrt{f(\phi(Q))}} & \frac{\Delta t}{2\Delta x} & 0 \\ \frac{\Delta t}{2\Delta x f(\phi(Q))} & \frac{\Delta t}{2\Delta x \sqrt{f(\phi(Q))}} & 0 \\ 0 & 0 & 0 \end{bmatrix} \begin{bmatrix} \phi_1(P) \\ \phi(P) \\ \phi_2(P) \end{bmatrix} + \\
 &+ \begin{bmatrix} 1 - \frac{\Delta t}{\Delta x \sqrt{f(\phi(Q))}} & 0 & 0 \\ 0 & 1 - \frac{\Delta t}{\Delta x \sqrt{f(\phi(Q))}} & \frac{-\Delta t}{f(\phi(Q))} \\ 0 & \Delta t & 1 \end{bmatrix} \begin{bmatrix} \phi_1(Q) \\ \phi(Q) \\ \phi_2(Q) \end{bmatrix} + \\
 &+ \begin{bmatrix} \frac{\Delta t}{2\Delta x \sqrt{f(\phi(Q))}} & \frac{-\Delta t}{2\Delta x} & 0 \\ \frac{-\Delta t}{2\Delta x f(\phi(Q))} & \frac{\Delta t}{2\Delta x \sqrt{f(\phi(Q))}} & 0 \\ 0 & 0 & 0 \end{bmatrix} \begin{bmatrix} \phi_1(R) \\ \phi(R) \\ \phi_2(R) \end{bmatrix} \quad (13)
 \end{aligned}$$

Eq. (13) is the Courant-Isaacson-Rees algorithm for discretizing the initial value problem for Eq. (1).

For computer simulation, the upper half of the (x,t) -plane is divided into a grid of uniform with Δx a long the x -axis and Δt along the t -axis and grid numbered as shown in Fig. 3. (In Fig. 3 only the right quadrant is shown; the left quadrant is the mirror image of the right quadrant.) The grid points $(\pm K, L)$ has the co-ordinates $(\pm K\Delta^2, L\Delta t)$ where K and L are integers. We write two sets of Eq. (13), one set for pulse propagating from $x = -\infty$ to $+\infty$, and the other for pulse propagating from $x = +\infty$ to $-\infty$. In either case the solitary wave of Eq. (7) or (8) as appropriate is assigned as initial values. A computer can be programmed to solve Eq. (13) for $U(K, L+1)$ and $U(-K, L+1)$. The progress of the pulses and the aftermath of their collision can thus be studied.

t						
$0, L+1$	$1, L+1$	$2, L+1$		$K-1, L+1$	$K, L+1$	$K+1, L+1$
$0, L$	$1, L$	$2, L$		$K-1, L$	K, L	$K+1, L$
$0, 2$	$1, 2$	$2, 2$		$K-1, 2$	$K, 2$	$K+1, 2$
$0, 1$	$1, 1$	$2, 1$		$K-1, 1$	$K, 1$	$K+1, 1$
$0, 0$	$1, 0$	$2, 0$		$K-1, 0$	$K, 0$	$K+1, 0$
						x

Figure 3. Grid for Computer Simulation.

ACKNOWLEDGMENT

The author is indebted to Professor Alwyn C. Scott for suggesting the problem reported in this research.

REFERENCES

1. A.C.Scott, F.Y.F.Chu and D.W.McLaughlin, 'The Soliton: A New Concept in Applied Science', Proc. IEEE, 61: 1443 (1973).
2. M.J.Ablowitz, D.J.Kaup, A.C.Newell and H.Segur, 'Nonlinear Evolution Equations of Physical Significance', Phys. Rev. Lett., 31: 125 (1973).
3. G.L.Lamb, Elements of Soliton Theory, John Wiley and Sons, New York (1980).
4. R.Courant, W.Isaacson and M.Rees, 'On the Solution of Nonlinear Hyperbolic Equations by Finite Differences', Comm. Pure Appl. Math., 5: 243 (1952).

A COLLECTIVE COORDINATE APPROACH TO THE ONE-DIMENSIONAL NONLINEAR SCHRÖDINGER EQUATION WITH SPATIAL PERIODIC POTENTIALS

A. R. Bishop¹ and Rainer Scharf^{1,2}

¹Theoretical Division and Center for Nonlinear Studies
Los Alamos National Laboratory
Los Alamos, New Mexico 87545, USA

²Present address: Institut für Theoretische Physik
Universität Hannover, D-3000 Hannover 1, Germany

INTRODUCTION

This article is motivated by two very important considerations in nonlinear science: (i) that the *combination* of nonlinearity with disorder and/or noise is an essential direction for research; and (ii) that nonlinear mode reductions to low-dimensional systems via the use of "collective coordinate" descriptions of coherent space-time structures is one of the very few robust techniques for general nonlinear equations supporting such "soliton-like" or "particle-like" solutions.

First, consider the combination of nonlinearity and disorder. Recent years have seen an enormous progress in understanding the effects of disorder in linear systems like Anderson localization and the transition from insulating to conducting behavior in $d = 3$ dimensions at zero temperature upon decreasing the disorder. Completely ordered, integrable nonlinear systems in $d = 1$ are also fairly well understood by now. The understanding of the interplay between disorder and nonlinearity, on the other hand, is still in its infancy.¹ Both, nonlinearity and disorder, may give rise to self-localized excitations (solitons or Anderson localized wave packets, respectively). Therefore it is natural to ask how these effects might reinforce, complement, or frustrate each other. Transport properties in disordered, nonlinear materials for example strongly depend on whether solitons behave as "particles" in the presence of disorder or interact very strongly with other degrees of freedom. Does the nonlinearity lead to adaptive behavior of excitations in disordered materials which preserves coherence? How do nonlinear excitations interact with each other in the presence of disorder? Does initially distributed energy self-focus as in modulationally unstable nonlinear equations? These and other issues are of great experimental concern in fields from nonlinear optics, to polaron formation in solid state materials,

to vibron localization in natural and synthetic biomolecules, etc., all of which are central to the concerns of this Conference.

Turning now to the use of collective coordinate reduction techniques, it is clear that these are only valuable for the above problems to the extent that "particle" solutions of the underlying nonlinear equations remain valid—other degrees of freedom may be excited or the "particles" may be destroyed by certain perturbations. However, we have found² in the model problem described here that quite primitive collective coordinates can indeed provide a quantitative description of much of the phase space of competing nonlinearity and disorder driving forces. We should emphasize, however, that this report should be viewed only as a component of a much larger study of disorder combined with nonlinearity, particularly the questions of (a) transport and (b) energy focusing in disordered, nonlinear systems. In addition, we also mention that we are successfully extending collective coordinate approaches to higher dimensional systems, in particular to vortex and domain wall excitations in $(2 + 1)$ -dimensional magnet and Josephson junction array contexts.³

In view of space limitations, we specifically restrict ourselves here to the $(1 + 1)$ -dimensional nonlinear Schrödinger (NLS) equation in a periodic (*parametric*) perturbing potential, and we focus on a central phenomenon of "*length-scale*" competition.² The competition here refers to that between the *period* of the perturbing potential and two characteristic lengthscales related to the soliton (breather) solution of the unperturbed NLS equation—the two lengthscales are related to the width (or amplitude) and internal phase of the soliton. Collective coordinate, effective particle descriptions are found to be very efficient if there is not direct competition of those lengthscales with the perturbation's period. However, if this competition occurs, solitons are easily destroyed and then energy refocussing may occur elsewhere in the system—for this reason, the single color periodic perturbation is quite fundamental to the problem of soliton formation and propagation in a perturbing field of *general* color (randomness).

Our strategy here is to compare our collective coordinate results with explicit numerical solutions of the full perturbed NLS equations. All numerical results were obtained upon numerically integrating the integrable spatial discretization of the NLS equation, given by Ablowitz and Ladik⁴ (see also [5]), in the continuum limit using a Runge Kutta-Verner fifth and sixth order method. To damp away unwanted excitations and radiation, the spatial domain was divided into a central half supporting the soliton (being at rest or moving) and two quarters at the boundary where the system was damped with a damping constant increasing smoothly from zero towards the boundaries. Although not described here, we have also used the same collective coordinate approach to the perturbed $(1 + 1)$ -dimensional NLS and sine-Gordon equations under a variety of other parametric perturbations: local impurities;⁶ a uniform ramp;⁵ quasi-periodic;² random;⁶ as well as an external periodic "kicking,"⁶ interesting for the quantized systems. We have also successfully employed collective coordinate reductions to describe chaotic interactions of two solitons in a periodic potential.⁷ For the sine-Gordon case, the additional phenomenon of breather break-up to kink-antikink pairs in a periodic potential has been observed and understood.^{8,9}

THE PERTURBED NLS EQUATION

The $(1 + 1)$ -dimensional NLS equation and the behavior of its solutions under a variety of perturbations is well investigated.¹⁰ This body of work can be

characterized by the kind of perturbation added to the NLS equation: (i) driving, periodic in space and time, with inclusion of damping; (ii) isolated impurities; (iii) spatially periodic stationary potentials; (iv) spatially random stationary potentials. The initial conditions chosen depend on the application in question. One can either look for modulational instability starting from a homogeneous initial state, investigate transmission properties using a plane wave solutions entering the nonlinear disordered region from a linear region without disorder, or start with soliton solutions of the unperturbed NLS equation and monitor their behavior under the perturbation.

We are interested in the behavior of coherent excitations under stationary, spatially periodic perturbations. This is the simplest model of disorder in nonlinear materials having a wide range of applications. Away from the perturbative regime knowledge about exact solutions is very limited. Therefore the usual strategy is to start with exact solutions of the unperturbed NLS equation and observe numerically whether and how they adjust to the perturbation. After different scenarios are identified, perturbation expansions starting from nontrivial perturbed solutions might give insight into the mechanisms underlying the different scenarios.

Here we investigate a perturbed NLS equation of the following form:

$$i\psi_t + \psi_{xx} + 2\psi|\psi|^2 = \epsilon\psi \cos(kx). \quad (1)$$

The perturbation introduces a lengthscale $\lambda = 2\pi/k$ which breaks the lengthscale invariance of the unperturbed ($\epsilon = 0$) NLS equation. Rescaling spatial and temporal coordinates and the amplitude of the field allows us to choose the wavelength of the potential as the unit of length. Therefore only lengthscale ratios involving the period of the potential will be relevant variables.

For vanishing perturbation ($\epsilon = 0$) the traveling nonlinear wave solutions of Eq. (1) are proportional to the elliptic functions $\text{cn}u$ or $\text{dn}u$ with $u = \alpha(x - vt - x_0)$. In addition to these extended wavelike solutions, localized solutions are possible:

$$\psi(x, t) = 2i\eta \frac{e^{i\dot{q}x/2 - i\Phi}}{\cosh(2\eta(x - q))}, \quad (2)$$

with the soliton position $q(t) = -4\xi t + q_0$ and its phase $\Phi(t) = 4(\xi^2 - \eta^2)t + \Phi_0$, where $\xi = i\eta$ is the complex pole of the analytically continued reflection coefficient corresponding to a single soliton (see for example [11]).

THE "EFFECTIVE PARTICLE" LIMIT

If the width of the soliton is much smaller than the period of the perturbing potential ($\eta \gg k$) then the soliton is only influenced by local properties of the potential, e.g., its gradient, its curvature, and so on. If we take into account only the gradient of the perturbing potential $V(x)$, then the resulting NLS equation is still completely integrable.¹²

$$i\psi_t + \psi_{xx} + 2\psi|\psi|^2 = \epsilon\psi(V_0 + V_1x). \quad (3)$$

In particular (3) allows for soliton solutions of the form given in Eq. (2) with the position q and the phase Φ fulfilling the following equations of motion:

$$\begin{aligned}\ddot{q} &= -2\epsilon V_1, \\ \dot{\Phi} &= \frac{1}{4}\dot{q}^2 - 4\eta^2 + \epsilon V_0.\end{aligned}\quad (4)$$

If the potential is nonlinear, then we make a Taylor expansion around the instantaneous position of the soliton. We keep only terms linear in $(x - q)$, as higher order terms will be proportional to higher powers of the lengthscale ratio k/η , which we assumed to be a small quantity in this section. This leads to:

$$\begin{aligned}\ddot{q} &= -2\epsilon V'(q), \\ \dot{\Phi} &= \frac{1}{4}\dot{q}^2 - 4\eta^2 + \epsilon(V(q) - qV'(q)).\end{aligned}\quad (5)$$

Obviously the position of the soliton does not depend on its phase. Therefore we will drop the phase $\Phi(t)$.

For a general perturbing potential, the NLS equation will no longer be completely integrable. Nevertheless, the dynamics still possesses two integrals of motion, namely the energy E and the "norm" N :

$$\begin{aligned}N &= \int_{-\infty}^{+\infty} |\psi|^2 dx, \\ E &= \int_{-\infty}^{+\infty} (|\psi_2|^2 - |\psi|^4 + \epsilon|\psi|^2 V(x)) dx.\end{aligned}\quad (6)$$

We can refine our previous considerations, which led to an equation of motion for the soliton position q , by using the collective coordinate ansatz (2) for the solution and demanding the constancy of energy and norm:

$$\begin{aligned}N &= 4\eta, \\ E &= \eta \left(\dot{q}^2 - \frac{16}{3}\eta^2 \right) + V_{\text{eff}}(q),\end{aligned}\quad (7)$$

where the effective potential is given by

$$V_{\text{eff}}(q) = 4\eta^2 \epsilon \int_{-\infty}^{+\infty} \text{sech}^2(2\eta(x - q)) V(x) dx. \quad (8)$$

This leads directly to the following conditions

$$\begin{aligned}\dot{\eta} &= 0, \\ \ddot{q} &= -\frac{1}{2\eta} V'_{\text{eff}}(q).\end{aligned}\quad (9)$$

In particular we find for $V(x) = \cos(kx)$:

$$V_{\text{eff}}(q) = \frac{\epsilon k \pi}{\sinh(k\pi/4\eta)} \cos(kq). \quad (10)$$

From this we derive the equation of motion for the soliton position:

$$\ddot{q} = \frac{\epsilon k^2 \pi}{2\eta \sinh(k\pi/4\eta)} \sin(kq). \quad (11)$$

Comparing expression (11) with the equation of motion for q derived earlier (see Eq. (5)), we observe the influence of the lengthscale ratio k/η . If the soliton is very narrow compared to the wavelength of the potential ($k/\eta \ll 1$), then we recover the previous result. Numerical evidence shows that Eq. (11) is still useful even for $k/\eta \approx 1/2$, when the approximation (5) is no longer sufficient. Figure 1 gives an example for a soliton moving in a long-wavelength cosine potential and compares its motion with the prediction of the effective particle dynamics. Note the excellent agreement.

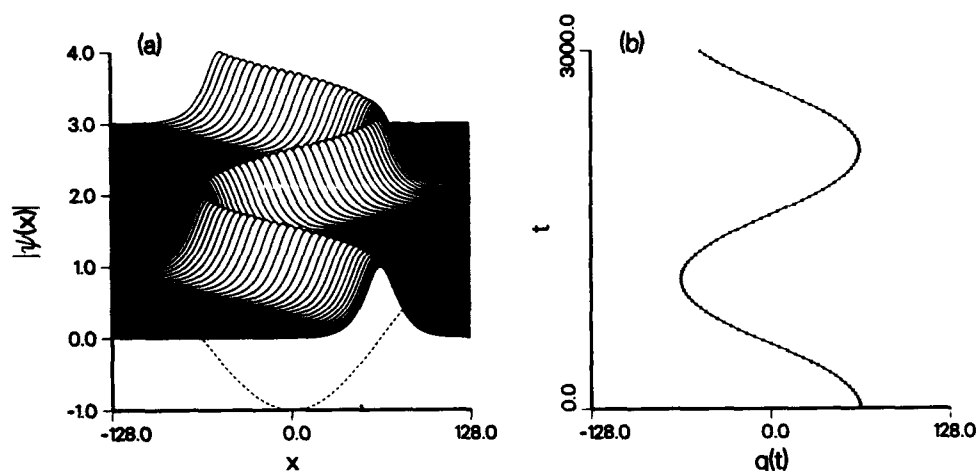


Fig. 1. The particle limit. Parameters: $\epsilon = 0.01$, $\lambda = 256$. Initial values: $\dot{q} = 0$, $\eta = 0.05$. Integration time: $T = 3000$. (a) The behavior of the full NLS equation (1) (dashed line: perturbing cosine potential). (b) The position of the NLS soliton (full line) compared with the position of the effective particle dynamics (10) (crosses).

The opposite limit ($k/\eta \gg 1$) is also notable. Although the soliton ansatz (2) is no longer justified, the effective potential $V_{\text{eff}}(q)$ given in (10) is exponentially small in the lengthscale ratio. Indeed, as we will see in the next section, when the coherent excitation covers many periods of the perturbing potential, the influence of the potential on the center of mass motion of the excitation is exponentially small in the lengthscale ratio.

So far we have neglected changes of the soliton shape and radiative effects completely. Two cases are accessible to analytical treatment: when the soliton emits radiation without interacting with it or when the soliton traps the radiation in the form of a shape modulation of sufficiently simple form. We address the second case in the next two sections.

THE "RENORMALIZED PARTICLE" LIMIT

Now we turn to the opposite limit ($\eta \ll k$) where the width of the soliton is much larger than the period or the characteristic lengthscale of the perturbing potential. Taking the soliton given in Eq. (2) as initial condition, we observe that

the effective potential it experiences initially in the presence of a perturbation $\cos(kx)$ is given by Eq. (10). This effective potential is exponentially small for $k/n \gg 1$. The initial energy of the soliton depends only very weakly on the perturbing potential because the soliton "smoothes over" the short wavelength perturbation. Nevertheless the potential will affect the coherent excitation locally and change its shape in the course of time. Numerically evidence shows that the soliton is influenced by the perturbation on two different time scales. An initial adjustment occurs nearly instantaneously leading to a burst of radiation emitted by the soliton. An immediate effect of this is that the soliton shape shows a modulation with the wavelength of the perturbation. Then, on a much longer timescale, the soliton continues to radiate but with much smaller power compared to the initial burst.

As the two lengthscales involved are very different, the dynamical equations can be solved approximately using a separation of lengthscales. We separate the "dressed soliton" solution of Eq. (1) into two parts:

$$\psi(x, t) = \Psi(x, t)(1 + \chi(kx)) . \quad (12)$$

The first ("slow") part, Ψ turns out to be the unperturbed soliton (2) fulfilling the homogeneous NLS equation ($\epsilon = 0$). The second ("fast") part gives the effect of the perturbation $\epsilon \cos(kx)$ on the short lengthscales.

If we put the ansatz (12) into Eq. (1) and average over the fast variables we find for the slow part of the dynamics, up to $O(\epsilon)$,

$$i\Psi_t + \Psi_{xx} + 2\Psi|\Psi|^2 = 0 , \quad (13)$$

which is the unperturbed NLS equation with the soliton solution given in Eq. (2). The fast part of the dynamics fulfills, up to $O(\epsilon)$,

$$\chi_{xx}\Psi + 2\chi_x\Psi_x + 2(\chi + \bar{\chi})\Psi|\Psi|^2 = \Psi \cos(kx) , \quad (14)$$

where $\bar{\chi}$ denotes the complex conjugate of χ . In this equation we treat $\Psi(x, t)$ as an adiabatic perturbation in the spatial variable leading to χ of the form (upon neglecting terms of $O(k^{-4})$):

$$\chi = -\frac{\cos(kx)}{k^2 - \dot{q}^2} + \frac{i\dot{q} \sin(kx)}{k(k^2 - \dot{q}^2)} . \quad (15)$$

This gives (up to $O(\epsilon)$):

$$|\psi(x, t)|^2 = 4n^2 \text{sech}^2(2\eta(x - q)) \left(1 - \frac{2\epsilon \cos(kx)}{k^2 - \dot{q}^2} \right) . \quad (16)$$

The result (16) shows that for slow solitons ($|\dot{q}| < k$) the spatial modulations of $|\psi|$ are *out of phase* by π with the perturbing cosine potential: local maxima of the shape modulations of the soliton fall into minima of the potential. This is what one would expect for the case of a soliton at rest. Equation (16) predicts that a similar result holds for sufficiently slow solitons as well. Figure 2 gives examples

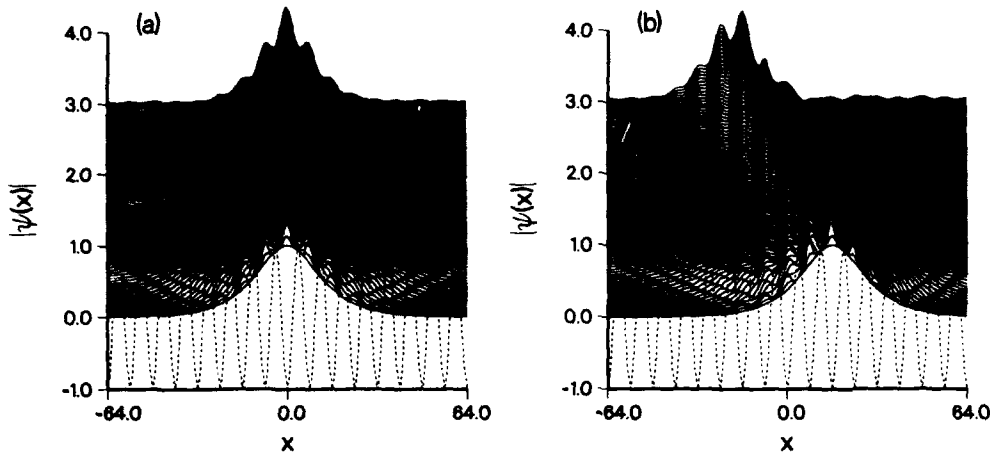


Fig. 2. The renormalized particle limit. Parameters: $\epsilon = -0.1$, $\lambda = 8$. Initial values: $\eta = 0.05$. Integration time: $T = 200$. (a) Soliton at rest: $\dot{q} = 0$. (b) Slowly moving soliton: $\dot{q} = -0.2$.

for soliton-like excitations at rest or slowly moving in a cosine-potential, which are in agreement with our theoretical prediction. Note that $|\dot{q}| < k$ is fulfilled in both cases.

Later, we will also address the large velocity case and the transition region between small and large velocity, giving rise to an additional lengthscale competition which destabilizes coherent excitations.

The shape modulation of the dressed solitons can be analyzed in terms of radiation with wavelength $\lambda = 2\pi/k$ being trapped on the soliton. To understand why this excitation is trapped, assume it would be able to propagate away from it. If the amplitude of the radiation is small, then we can neglect the nonlinear term in the perturbed NLS equation. The radiation has a wavelength coinciding with the wavelength of the potential. In this case only standing wave solutions exist for the linear Schrödinger equation and free propagation is not possible. Excitations of this wavelength, which occur naturally as shape modes of solitons in spatially periodic potentials, are therefore trapped on the solitons and are forced to move with them.

THE PHASE-LENGTHSCALE COMPETITION

Above, where we discussed the renormalized particle limit, we restricted the velocity of the soliton to sufficiently small values. Now we make more precise what "sufficiently small" means. Equation (15), giving the shape modulation of the soliton in the presence of a short wavelength perturbation, is valid not only for $|\dot{q}| \ll k$ but as long as $|\dot{q}^2 - k^2| \gg \eta$. Now we turn to the case $|\dot{q}| > k$ and find from Eq. (16) that the spatial modulation of $|\psi|$ is *in phase* with the perturbing potential.

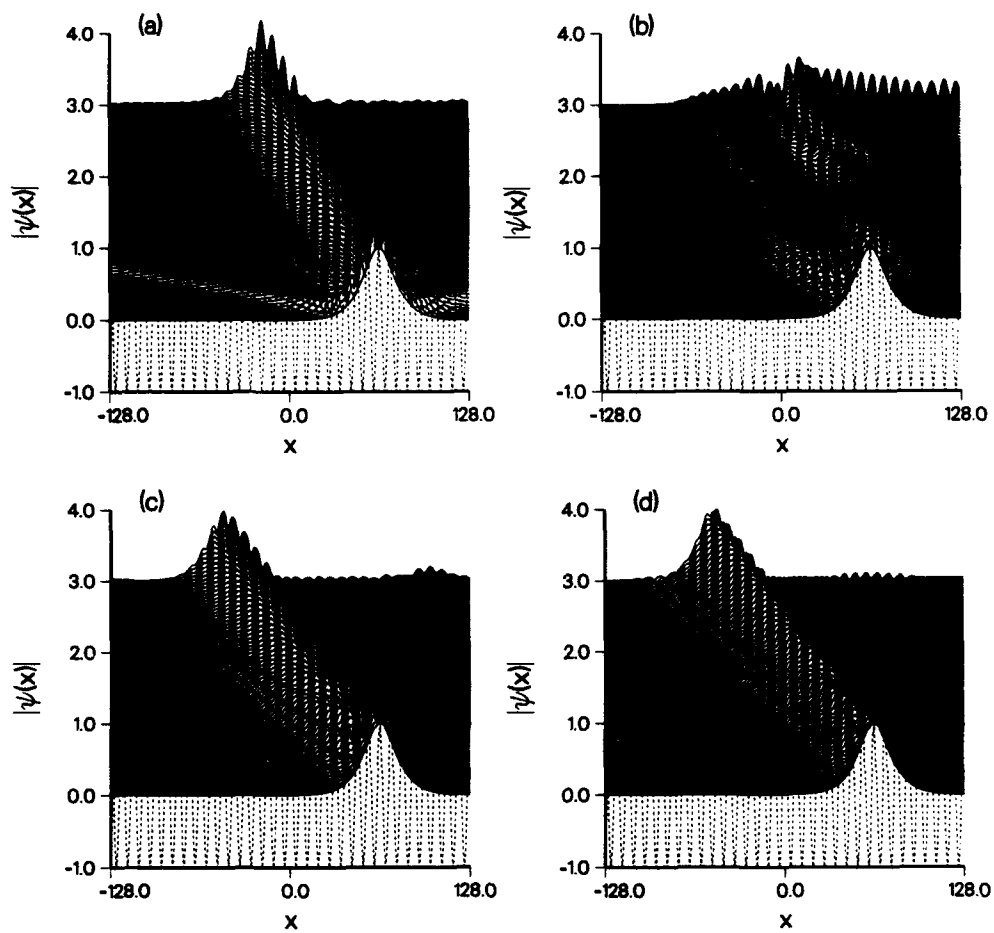


Fig. 3. The phase resonance $|\dot{q}| \approx k$. Parameters: $\epsilon = 0.1$, $\lambda = 8$ (or $k \approx 0.785$), $\eta = 0.05$.
 (a) $\dot{q} = -0.2$, $T = 500$. (b) $\dot{q} = -0.8$ (or $|\dot{q}| \approx k$), $T = 125$. (c) $\dot{q} = -1.2$, $T = 100$. (d) $\dot{q} = -1.6$ (or $|\dot{q}| \approx 2k$), $T = 80$.

Equations (15,16) already indicated where the crossover to the large velocity behavior occurs, namely at $|\dot{q}| = k$. Here the sign of the shape modulation changes. In addition at this point the perturbative result suffers from a singularity which wavelength of the perturbation and the wavelength of the phase modulation leads to a resonance which breaks up coherent excitations even for very small amplitude of the perturbation. This is illustrated in Fig. 3 together with the small and large velocity dressed soliton cases. Exactly at the resonance ($|\dot{q}| = k$) the soliton breaks up into a standing wavetrain with $\lambda = k$ which switches back and forth between being in phase and out of phase with the potential.

Staying well away from this resonance, either above ($|\dot{q}| > k$) or below ($|\dot{q}| < k$), guarantees stable propagation of coherent excitation. These dressed solitons are quite robust and behave like bare solitons in many respects, for example upon collision.²

We collect our results in Fig. 4 for fixed k and variable soliton velocity $v = \dot{q}$ showing the norm N of the excitation after 10,000 timesteps and the exponential decay rate κ of the norm (after damping away radiation and other excitations traveling with velocities different from the soliton velocity), both giving information about the stability of the excitation. As can be seen from Fig. 4, the solitons are most unstable for $|\dot{q}| \approx k$ and $|\dot{q}| \approx 2k$; but only in the former case is a resonance observed as described in Eq. (15). The difference between these two cases is also illustrated in Fig. 3. For $|\dot{q}| \approx 2k$ the soliton decays by spreading very slowly without apparent resonant behavior.

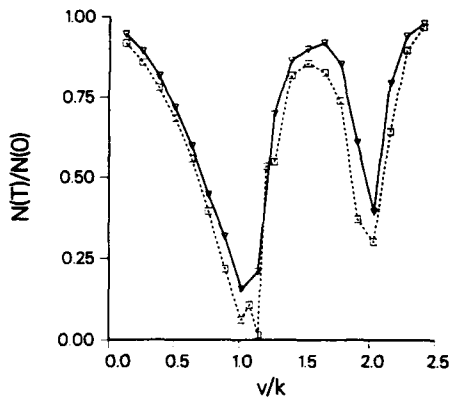


Fig. 4. Phase resonance and soliton stability. Parameters: $\epsilon = -0.1$, $\lambda = 8$, $\eta = 0.05$ (dashed line and squares); $\epsilon = -0.025$, $\lambda = 16$, $\eta = 0.025$ (full line and triangles). Integration time $T = 10000$. Norm ratio $N(T)/N(0)$.

THE AMPLITUDE-LENGTHSCALE COMPETITION

If the width of the coherent excitation is comparable to the period of the perturbing potential ($\eta \approx k$), then neither the particle picture nor the renormalized particle picture can describe the outcome appropriately. That both approximation schemes fail has a deeper reason. The competition of length scales leads to complicated behavior in space and time which involves many degrees of freedom. There no longer exists a small number of collective degrees of freedom which can adequately describe the essential features of the dynamics. As all approximation techniques fail badly, we have to resort to numerical techniques to determine the parameter range in which lengthscale competition leads to breakup of coherent excitations.

In Fig. 5 we illustrate the lengthscale competition in question for a soliton with initial velocity $|\dot{q}|$ well below the resonance at k for potentials with widely different k -values but fixed amplitudes. Upon varying the wavelength of the potential from

$\lambda \ll 1/\eta$ through $\lambda \approx 1/\eta$ to $\lambda \gg 1/\eta$, we observe smoothing over the potential, break-up of the soliton and trapping in the potential, and particle-like motion in the long-wavelength potential, respectively. For the long-wavelength case see Fig. 1 where the potential has the same amplitude as in Fig. 5. As our numerical studies indicate for stronger perturbations, the most robust excitation is the dressed soliton ($\lambda \ll 1/\eta$), whereas the effective particle soliton ($\lambda \gg 1/\eta$) very quickly begins to show dispersion induced by the curvature of the potential for the relatively large perturbation amplitude used in this case.

We collect our numerical results for solitons with initial velocity $|q|$ well above the resonance at k in Fig. 6. This shows the effect of cosine-potentials with a wide range of wavelengths on a fast moving soliton for large times. As long as the initial condition is well separated from the parameter region of competing lengthscales ($\eta \approx k$), the soliton can propagate in particle-like fashion for relatively large perturbations.

DISCUSSION

We have seen that the perturbed NLS equation can support soliton-like excitations as long as their two characteristic lengthscales are very different from the typical lengthscale of the perturbing potential. These excitations have either the shape of unperturbed solitons and move like particles in a long wavelength effective potential, or their shape is strongly modulated by a short wavelength potential and they move like renormalized particles.

We identified two different situations of competing lengthscales when the simple picture leading to a collective variable description fails: phase-lengthscale competition and amplitude-lengthscale competition. In both cases a large number of degrees of freedom is involved in the dynamics, and a simple collective variable description is no longer feasible. In these cases a small perturbation already can lead to a breakup of the coherent excitation, generating radiation as well as trapped smaller excitations.

Multicolor perturbing potentials of sufficiently small amplitude and with small or vanishing Fourier components at the wavelengths leading to lengthscale competition allow for long-lived soliton-like coherent excitations. The dynamics of these dressed solitons can be described by a collective variable approach similar to the one given above.

The nearly elastic collision of two dressed solitons² shows that, apart from situations of competing lengthscales, those features of the NLS equation, which are usually connected to its complete integrability, are relatively stable under a large class of spatially periodic or quasi-periodic perturbations which break the complete integrability. This "structural stability" of the NLS equation explains its relevance for many physical systems (e.g., optical fibers, plasmas) where perturbation of the completely integrable NLS equation are not necessarily small. It is *not* the complete integrability of the NLS equation which seems to be important for this structural stability. We have, for example, demonstrated⁷ that already a cosine-perturbation like in Eq. (1) can lead to soliton chaos in the *two-soliton* long-wavelength case, emphasizing the nonintegrability under this perturbation. Nevertheless a successful collective variable description is still possible in this case.

Our results indicate that, for a given correlation length of the disorder present in a nonlinear system, spatially extended coherent excitations are much more stable than excitations with a width comparable to the correlation length. Correspondingly, in the case of a lattice we expect that nonlinear excitations extending over many lattice spacings are more stable than excitations extending only over a few lattice

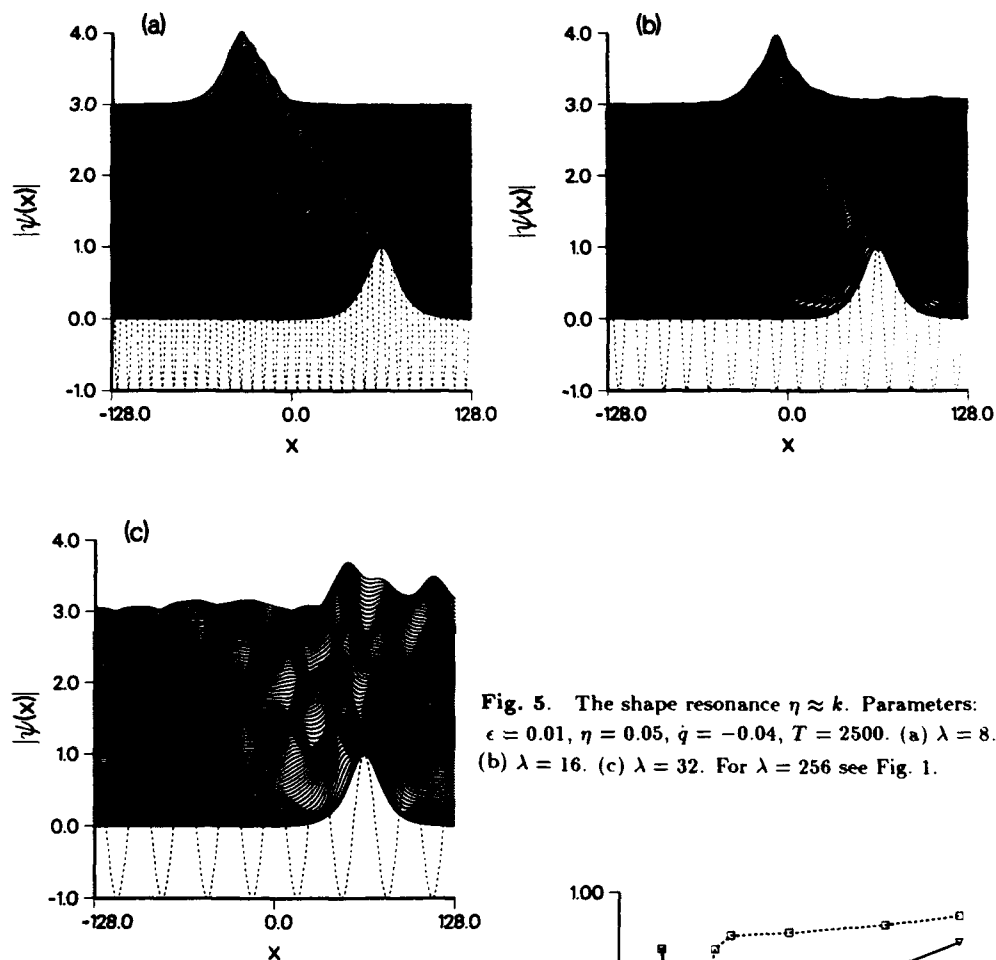
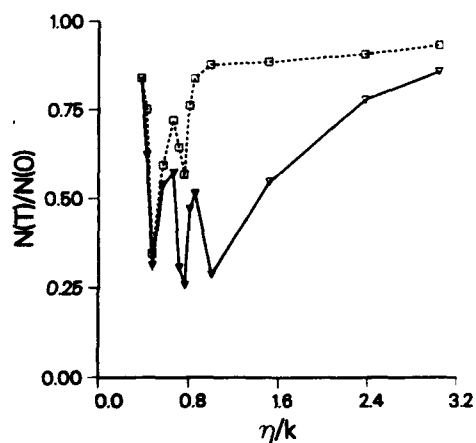


Fig. 5. The shape resonance $\eta \approx k$. Parameters: $\epsilon = 0.01$, $\eta = 0.05$, $\dot{q} = -0.04$, $T = 2500$. (a) $\lambda = 8$. (b) $\lambda = 16$. (c) $\lambda = 32$. For $\lambda = 256$ see Fig. 1.

Fig. 6. Shape resonance and soliton stability. Parameters: $\dot{q} = 1.2$, $\eta = 0.05$, $T = 10000$. $\epsilon = 0.1$ (dashed line and squares); $\epsilon = 0.2$ (full line and triangles). Norm ratio $N(T)/N(0)$.



sites. The former can more effectively average-out impurities and modulations on the scale of a few lattice spacings than the latter.

In the case of polarons the charge of an electron added to an ionic crystal leads to a lattice distortion giving rise to an effective (nonlinear) self-interaction of the excess charge. Polarons (and bipolarons for pairs of electrons) are the resulting coherent nonlinear excitations. They can extend over a few lattice spacings distorting the lattice strongly (small polaron) or over many lattice spacings with a milder lattice distortion (large polaron). In disordered ionic lattices large polarons are therefore expected to smooth-out the disorder and propagate long distances before they are scattered. In contrast, small polarons are much more strongly affected by disorder. They are expected to be scattered more often and to be trapped even by local impurities.

Finally, we mention two directions of our research on the NLS system. First, we are extending the class of perturbations to spatially random disorder. A collective variable approach combined with *inverse scattering* perturbation theory¹⁰ is giving information about the radiation generated in these potentials, as well as our other cases. Second, the collective variable approach is being extended to higher-dimensional, perturbed field equations. The behavior of single excitations is, of course, expected to be much richer in two and more spatial dimensions. For example, numerical studies³ on layered magnets and two-dimensional Josephson junction arrays suggest that both "vortex" and "wall" elementary excitations, and their vortex-vortex, wall-wall, vortex-wall interactions, are crucial elementary processes controlling the bridge between microscopic descriptions and macroscopic responses.

ACKNOWLEDGMENTS

We acknowledge support for this work by the U.S. Department of Energy. We would like to thank Ed Overman for making his IST code available to us and Yuri Kivshar and Angel Sanchez for help and advice.

REFERENCES

1. *Disorder and Nonlinearity*, Springer Proceedings in *Physics*, Vol. 39, edited by A. R. Bishop, D. K. Campbell, and St. Pnevmatikos (Springer-Verlag, Berlin, 1989); *Nonlinearity with Disorder*, Springer Proceedings in *Physics*, edited by F. Kh. Abdullaev, A. R. Bishop, and St. Pnevmatikos (Springer-Verlag, Berlin, 1992).
2. R. Scharf and A. R. Bishop, *Phys. Rev. A* (submitted 1992).
3. F. G. Mertens *et al.*, in preparation; N. Grønbech-Jensen *et al.*, in preparation.
4. M. J. Ablowitz and J. F. Ladik, *J. Math. Phys.* **17**, 1011 (1976).
5. R. Scharf and A. R. Bishop, *Phys. Rev. A* **43**, 6535 (1991).
6. R. Scharf and A. R. Bishop, in Ref. [1].
7. R. Scharf and A. R. Bishop, *Phys. Rev. A* (September 1992).
8. R. Scharf, Y. S. Kivshar, A. Sánchez, A. R. Bishop, *Phys. Rev. A* **45**, 5369 (1992).
9. A. Sánchez, R. Scharf, L. Vázquez, A. R. Bishop, *Phys. Rev. A* **45**, 6031 (1992).
10. Yu. S. Kivshar and B. A. Malomed, *Rev. Mod. Phys.* **61**, 763 (1989).
11. R. K. Dodd, J. C. Eilbeck, J. D. Gibbon, and H. C. Morris, *Solitons and Nonlinear Waves* (Academic Press, New York, 1982).
12. H.-H. Chen and C.-S. Liu, *Phys. Rev. Lett.* **37**, 693 (1976).

LENGTH SCALES IN SOLUTIONS OF DISSIPATIVE PARTIAL DIFFERENTIAL EQUATIONS

M.V. Bartuccelli,¹C.D. Doering,²J.D. Gibbon,¹ and S.J.A. Malham¹

¹Department of Mathematics
Imperial College
London SW7 2BZ, England

²Department of Physics
Clarkson University
Potsdam, NY 13676, USA

An interesting and important question in the study of the behaviour of solutions of dissipative partial differential equations, is whether it can be shown that large fluctuations or excursions away from temporal and spatial averages can occur. If it can be demonstrated that the solutions of these equations can allow such fluctuations away from averages, then these must have narrow spatial and temporal bandwidths and the width of these will give information about the smallest scale in the flow. Any numerical scheme must 'resolve' these spikes to get an accurate representation of the flow. The question of the smallest length scale is the topic of this paper.

In the theory of attractors in PDEs^{1,2,3,4,5,6} it has become conventional to measure the smallest scale using upper bounds on the Lyapunov dimension of the universal attractor. This upper bound \mathcal{N} , is usually interpreted as the number of degrees of freedom in the PDE under investigation. On a domain $[0, L]^d$ of volume L^d (d spatial dimensions), \mathcal{N} is related to the minimum scale l by $\mathcal{N} = (L/l)^d$. In other words, \mathcal{N} represents the number of eddies of volume l^d which are contained in the box of volume L^d . The only problem that exists with this approach is whether computing a lower bound on l from an upper bound of the Lyapunov dimension is always correct. In general this identification is not quite so simple as one might hope. In fact, for the complex Ginzburg-Landau (CGL) equation on periodic boundary conditions,

$$A_t = RA + (1 + i\nu)\Delta A - (1 + i\mu)|A|^2 A$$

it was shown analytically⁷ that when $d = 2$ (but not when $d = 1$), very spiky fluctuations (interpreted as strong turbulence) can occur in certain regions of the (μ, ν) plane but not in the rest of this plane. The spiky fluctuations occur on scales $l \geq R^{-|\nu|}$, whereas in the rest of the plane, where only weak turbulence can occur, $l \geq R^{-1/2}$. The Lyapunov dimension of the attractor in both regions was found to be uniform giving $l \geq R^{-1/2}$. In some sense this result is not surprising as the method of computing the evolution of volume elements of the universal attractor through which one finds an upper bound on the Lyapunov dimension, requires a time average on low norms of the velocity field. It contains no information on higher norms, in which the energy may be appreciable during the interval of the spike. This average takes account only of dynamics on scales larger than the spikes. In this sense, this method is certainly good for weak turbulence but is less sure for strong turbulence. It therefore seems necessary to find an alternative definition of a length scale which takes account of the possibility of large spikes or fluctuations.

In what follows we concentrate on one of the most important systems of dissipative partial differential equations, namely the Navier-Stokes equations, even though the argument can be applied to other parabolic equations.

The conventional scale in 3d turbulence is the Kolmogorov scale which is usually defined as

$$l \equiv \lambda_{KG} = (\nu^3/\epsilon)^{1/4}$$

where ν is the viscosity of the fluid and

$$\epsilon = 2\nu L^{-3} \int_{\Omega} (D\underline{u})^2 dx$$

is the energy dissipation rate per unit mass and time. This scale can be found via the Lyapunov dimension of the 3d Navier-Stokes attractor. Below we show how to obtain a set of length scales which give the Kolmogorov scale for flows which represent homogeneous decaying turbulence. For more general flows we show that the length scales are much smaller than Kolmogorov.

We take the Navier-Stokes equations on a periodic domain $\Omega = [0, L]^d$ in d spatial dimensions, with ν as viscosity and a C^∞ time-independent forcing function \mathbf{f} . In the velocity form they are

$$u_t + (u \cdot \nabla)u = \nu \Delta u - \nabla P + \mathbf{f} \quad \text{div } u = 0$$

In the vorticity notation these assume the following form

$$\omega_t + (u \cdot \nabla)\omega = \nu \Delta \omega + (\omega \cdot \nabla)u + F$$

$$\omega = \text{curl}(u), \quad F = \text{curl}(\mathbf{f}).$$

The vortex stretching term $(\omega \cdot \nabla)u$ vanishes for $d = 2$, but not for $d = 3$. In this latter case it has a strong influence on the evolution of the flow. Now we define a set of quantities in d spatial dimensions^{8,9}

$$F_N = \sum_{i=1}^d \sum_{|n|=N} \left(\int (D^n u_i)^2 dx + \tau_0^2 \int (D^n f_i)^2 dx \right) \equiv H_N + f_N$$

where $\tau_0 = \nu^{-1} L^2$, $D^N = \frac{\partial^{n_1+\dots+n_d}}{\partial x_1^{n_1} \dots \partial x_d^{n_d}}$ and $n_1 + \dots + n_d = N$.

From the Navier-Stokes equations, we can prove⁸ that the F_N satisfy for $N \geq 1$ and $d = 2, 3$ the differential inequality (ladder inequality)

$$\frac{1}{2} \dot{F}_N \leq -\nu \frac{F_N^{1+1/s}}{F_N^{1/s}} + (c_{N,s} \|Du\|_\infty + \nu \lambda_0^{-2}) F_N$$

where the $c_{N,s}$ are constants, $1 \leq s \leq N$, $\lambda_0^{-2} = L^{-2} + \lambda_f^{-2}$, λ_f is the cut-off in the spectrum of the forcing, and $\|Du\|_\infty = \sup_{x \in \Omega} |Du(x)|$. Then we can prove⁸ the following in $3d$

$$\begin{aligned} \overline{\|Du\|_\infty} &\leq c \nu^{-3} [\overline{\|Du\|_2^4} + \|Du_f\|_2^4] + L^{-3/2} \overline{\|Du\|_2} + c_2 \nu \lambda_0^{-2} \\ &< \|Du\|_\infty > \leq c \nu^{-3} [<\|Du\|_2^4> + \|Du_f\|_2^4] + L^{-3/2} <\|Du\|_2^2> + c_2 \nu \lambda_0^{-2}. \end{aligned}$$

In the vorticity form they assume the following expression

$$\begin{aligned} \overline{\|\omega\|_\infty} &\leq c_1 \nu^{-3} [\overline{\|\omega\|_2^4} + \|\omega_f\|_2^4] + L^{-3/2} \overline{\|\omega\|_2} + c_2 \nu \lambda_0^{-2} \\ <\|\omega\|_\infty> &\leq c_1 \nu^{-3} [<\|\omega\|_2^4> + \|\omega_f\|_2^4] + L^{-3/2} <\|\omega\|_2> + c_2 \nu \lambda_0^{-2}. \end{aligned}$$

The overbar means limsup over all smooth initial conditions as $t \rightarrow \infty$, the $<\cdot>$ means time average, the c 's are constants, and $\|g\|_p^p := \int_\Omega |g(x)|^p dx < +\infty$, $p \geq 1$.

Now we define our dynamic length scales as follows:

$$(length)^{-1} \equiv l^{-1} \sim \left(\frac{F_N}{F_r} \right)^{\frac{1}{2(N-r)}}.$$

If we time average the square of these length scales we get

$$< l^{-2} > = \left\langle \left(\frac{F_N}{F_r} \right)^{\frac{1}{N-r}} \right\rangle.$$

Then we can show that the following is true⁸

$$< l^{-2} > \leq c \nu^{-1} <\|Du\|_\infty> + \lambda_0^{-2}.$$

For homogeneous decaying turbulence, when $\|Du\|_\infty \approx \|Du\|_2 L^{-3/2}$ we get that, up to a non-dimensional constant, l is bounded below by the Kolmogorov length scale, that is

$$l \geq c \lambda_{KG}.$$

This result was also obtained by Henshaw, Kreiss and Reyna¹⁰.

More generally⁸ inserting the $<\|Du\|_\infty>$ estimate found above we get:

$$< l^{-2} > \leq \lambda_K^{-2} + \lambda_0^{-2} + \lambda_f^{-2} + \nu^{-4} [<\|Du\|_2^4> + \|Du_f\|_2^4].$$

The two extra terms with the ν^{-4} coefficient in the inequality above, reveal the mechanism of how deeper scales than the Kolmogorov scale λ_K are potentially possible. In fact, if $<\|Du\|_2^4>$ remains finite, the ν^{-4} coefficient is significant as it allows these terms to become large for high Reynolds numbers.

If, instead of taking the time average, we consider the limsup over all smooth initial conditions as $t \rightarrow \infty$ then for $d = 3$ we get the following result⁸

$$\overline{l^{-2}} \leq c \frac{[\overline{\|Du\|_2^4} + \|Du_f\|_2^4]}{\nu^4}.$$

Again, if $\overline{\|Du\|_2^4}$ remains finite one can see that these length scales are even smaller than those computed via the time average operation, and, we believe, they are the smallest.

REFERENCES

- [1] C. Foias and G. Prodi, *Sur le Comportement Global des Solutions Non-Stationnaires des Equations de Navier-Stokes en Dimension 2*, Rend. Sem. Mat. Padova, 39: 1-39 (1967).
- [2] R. Temam. "Infinite Dimensional Dynamical Systems in Mechanics and Physics", Springer Applied Mathematics Series, VOLUME 68, Springer, Berlin, 1988.
- [3] P. Constantin and C. Foias, "The Navier-Stokes Equations," Chicago University Press, 1989.
- [4] P. Constantin, C. Foias, R. Temam, *Attractors Representing Turbulent Flows*, Memoirs of AMS, (1985).
- [5] P. Constantin, C. Foias, O. P. Manley, R. Temam, *Determining Modes and Fractal Dimension of Turbulent Flows*, Journal of Fluid Mechanics, 9D: 157-188, (1985).
- [6] P. Constantin, C. Foias, R. Temam, *On the Dimension of the Attractors in Two-Dimensional Turbulence*, Physica, 30D: 284-296, (1988).
- [7] M. V. Bartuccelli, P. Constantin, C. R. Doering, J. D. Gibbon and M. Gisselält, *On the Possibility of Soft and Hard Turbulence in the Complex Ginzburg-Landau Equation*, Physica D44: 421-444 (1990).
- [8] M. V. Bartuccelli, C. R. Doering, J. D. Gibbon and S. J. A. Malham, *Length scales in solutions of the Navier-Stokes Equations*, preprint.
- [9] M. V. Bartuccelli, C. R. Doering, J. D. Gibbon, *Ladder Theorems for the 2d and 3d Navier-Stokes Equations on a Finite Periodic Domain*, Nonlinearity, 4: 531-542, (1991).
- [10] W. D. Henshaw, H. O. Kreiss and L. G. Reyna, *On Smallest Scale Estimates for the Incompressible Navier-Stokes Equations*, Theoret. Comput. Fluid Dynamics, 1:65-95 (1989).

HAMILTON STRUCTURE OF UNSTABLE NONLINEAR SCHRÖDINGER EQUATION

Sergei A. Darmanyany¹ and Valery I. Rupasov²

¹Thermal Physics Department
Uzbek Academy of Sciences
700135 Tashkent, Uzbekistan

²Institute for Spectroscopy
Russian Academy of Sciences
142092 Troitsk, Moscow Reg., Russia

INTRODUCTION

It is well known the dynamics of short pulses in optical fibers is described by the following equation¹

$$iu_z + u_{tt} + 2\gamma(\bar{u}u)u = 0 \quad (1)$$

where u, z, t are dimensionless amplitude of the electromagnetic field, propagation distance and time respectively. The nonlinear modulation of a high frequency mode in electron beam plasma² is also described by the equation (1), which is different from conventional nonlinear Schrödinger equation by the permutation of time and space variables. The Eq. (1) has been named by authors of paper² as the unstable nonlinear Schrödinger equation (UNSE). The inverse scattering method for Eq. (1) has been developed in the paper³.

Here we construct the Hamilton structure of UNS equation that plays the very important role for the correct quantization of UNS model. The quantization method proposed by Lai and Haus⁴ is valid only in quasi-classical limit.

HAMILTON STRUCTURE

The unstable nonlinear Schrödinger equation can be derived from the variational principle for action

$$S = \int dt L$$

where the Lagrange function of the field is given by

$$L = \int dx [\bar{u}_t u_t + \frac{i}{2}(\bar{u}_z u - \bar{u} u_z) - \gamma(\bar{u}u)^2] \quad (2)$$

The canonically conjugated momenta $\pi(t, x)$ and $\bar{\pi}(t, x)$ to the fields (coordinates) $u(t, x)$ and $\bar{u}(t, x)$ are determined by the following expressions

$$\begin{aligned}\pi(t, x) &\equiv \frac{\delta L}{\delta u_t} = \bar{u}_t \\ \bar{\pi}(t, x) &\equiv \frac{\delta L}{\delta \bar{u}_t} = u_t\end{aligned}\quad (3)$$

Using the conventional definition for the Poisson brackets of any field functionals

$$\{f, g\} = \int dx \left[\left(\frac{\delta f}{\delta \pi} \frac{\delta g}{\delta u} - \frac{\delta g}{\delta \pi} \frac{\delta f}{\delta u} \right) + \left(\frac{\delta f}{\delta \bar{\pi}} \frac{\delta g}{\delta \bar{u}} - \frac{\delta g}{\delta \bar{\pi}} \frac{\delta f}{\delta \bar{u}} \right) \right]$$

we find the nonvanish canonical Poisson brackets for the fields and momenta

$$\begin{aligned}\{\pi(x), u(y)\} &= \delta(x - y) \\ \{\bar{\pi}(x), \bar{u}(y)\} &= \delta(x - y)\end{aligned}\quad (4)$$

The model Hamilton function has the following form

$$H \equiv \int dx (\pi u_t + \bar{\pi} \bar{u}_t) - L = \int dx [\bar{\pi} \pi + i \bar{u} u_x + \gamma (\bar{u} u)^2] \quad (5)$$

It is easy to see the Hamilton equations of motion for the dynamical variables

$$\begin{aligned}u_t &= \{H, u\} = \frac{\delta H}{\delta \pi} = \bar{\pi} \\ \bar{\pi}_t &= \{H, \bar{\pi}\} = -\frac{\delta H}{\delta \bar{u}} = -i u_x - 2\gamma (\bar{u} u) u\end{aligned}\quad (6)$$

are equivalent to UNSE.

The model Hamilton function is determined by T_{00} component

$$H = \int dx T_{00}$$

of the momentum-energy tensor

$$T_{\mu\nu} = \frac{\delta L}{\delta u_{,\nu}} u_{,\mu} + \frac{\delta L}{\delta \bar{u}_{,\nu}} \bar{u}_{,\mu} - L \delta_{\mu\nu}$$

(where $u_{,\nu} = \partial u / \partial x^\nu$, $x^\nu = (t, x)$) and the momentum of the system by T_{10} component

$$P = \int dx T_{10} = \int dx (\bar{u}_t u_x + u_t \bar{u}_x) = \int dx (\pi u_x + \bar{\pi} \bar{u}_x) \quad (7)$$

We also can determine the charge and the current in the system. Multiplying Eq. (1) by \bar{u} and conjugated equation by u and subtracting the second expression from the first one we obtain the following continuity equation

$$\frac{\partial}{\partial t} (u_t \bar{u} - \bar{u}_t u) + \frac{\partial}{\partial x} (i \bar{u} u) = 0$$

Hence, the expression

$$Q = i \int dx (u_t \bar{u} - \bar{u}_t u) = i \int dx (\bar{u} \pi - \pi u) \quad (8)$$

one can consider as the charge, and

$$J = \int dx \bar{u} u \quad (9)$$

as the current in the system.

POISSON BRACKETS FOR MONODROMY MATRIX ELEMENTS

The auxiliary spectral problem

$$\Phi_x = U \Phi,$$

where

$$U = 2\lambda i[\lambda \sigma^z + \sqrt{\gamma}(\bar{u} \sigma^+ + u \sigma^-)] + \sqrt{\gamma}(\bar{u}_t \sigma^+ - u_t \sigma^-) - i\gamma(\bar{u} u) \sigma^z$$

and σ^i are ordinary Pauli matrices, has been investigated in paper³. Here we present the expression for the Poisson brackets for monodromy matrix elements. First of all note that the Poisson brackets for U-matrix elements are

$$\begin{aligned} \{U(x, \lambda) \otimes U(y, \mu)\} &= i\gamma^{3/2} \bar{u} \delta(x-y) [\sigma^z \otimes \sigma^+ - \sigma^+ \otimes \sigma^z] \\ &\quad - i\gamma^{3/2} u \delta(x-y) [\sigma^z \otimes \sigma^- - \sigma^- \otimes \sigma^z] \\ &\quad + 2i\gamma(\lambda + \mu) \delta(x-y) [\sigma^+ \otimes \sigma^- - \sigma^- \otimes \sigma^+] \end{aligned} \quad (10)$$

Then, following to Takhtajan and Faddeev⁵ we easily obtain the following expression for the monodromy matrix $T(x, y, \lambda)$ on finite interval (x, y)

$$\{T(x, y, \lambda) \otimes T(x, y, \mu)\} = [r(\lambda, \mu), T(x, y, \lambda) \otimes T(x, y, \mu)] \quad (11)$$

where $[,]$ denotes the commutator, \otimes -tensor multiplication and

$$r(\lambda, \mu) = \frac{\gamma}{2(\lambda - \mu)} \begin{pmatrix} 0 & 0 & 0 & 0 \\ 0 & 1 & -1 & 0 \\ 0 & -1 & 1 & 0 \\ 0 & 0 & 0 & 0 \end{pmatrix}$$

It is interesting to note that in our case r -matrix coincides with r -matrix for conventional nonlinear Schrödinger equation.

CANONICAL QUANTIZATION

Using the canonical quantization rules we should define the quantum unstable Schrödinger (QUS) model as the model with the Hamiltonian

$$H = \int dx [\pi^+ \pi + i u^+ u_x + \gamma u^+ u^+ u u] \quad (12)$$

and the commutation relations for the operators of the fields and momenta

$$[u(x), \pi(y)] = i\delta(x-y), \quad [u^+(x), \pi^+(y)] = i\delta(x-y) \quad (13)$$

In the absence of interaction ($\gamma = 0$) the model eigenstates are plane waves ($\propto \exp[i(\omega t - kx)]$), where $\omega^2 = k$, and hence our model contains both particles ($\omega = +\sqrt{k}$) and antiparticles ($\omega = -\sqrt{k}$). Restricting our consideration by the sector

$k > 0$ we can represent the field operators as a superposition of the plane waves corresponding to particles and antiparticles

$$u(t, z) = \int_0^\infty \frac{dk}{2\pi} \frac{1}{\sqrt{2\omega}} \{a_k \exp[i(\omega t - kz)] + b_k^\dagger \exp[-i(\omega t + kz)]\} \quad (14)$$

$$\pi(t, z) = \int_0^\infty \frac{dk}{2\pi} i\sqrt{\frac{\omega}{2}} \{a_k^\dagger \exp[-i(\omega t - kz)] - b_k \exp[i(\omega t + kz)]\}$$

where $\omega(k) = +\sqrt{k}$. In the terms of creation (annihilation) operators of particles a^\dagger (a) and anti-particles b^\dagger (b) the free field Hamiltonian and the operators of momentum, charge and current takes the following form

$$H_0 = \int \frac{dk}{2\pi} \omega(k) (a_k^\dagger a_k + b_k^\dagger b_k) \quad (15)$$

$$P = \int \frac{dk}{2\pi} k (a_k^\dagger a_k - b_k^\dagger b_k) \quad (16)$$

$$Q = \int \frac{dk}{2\pi} (a_k^\dagger a_k - b_k^\dagger b_k) \quad (17)$$

CONCLUSIONS

Thus, we have shown the consistent application of the canonical quantisation rules to the classical UNS model leads to quantum model containing both particles and antiparticles. It is easy to see that our quantum version of UNSE is substantially different from the conventional quantum nonlinear Schrödinger model⁶. So, at present the exact diagonalisation problem of quantum UNS model is open one.

REFERENCES

1. A. Hasegawa and F. Tappert, Transmission of stationary nonlinear optical pulses in dispersive dielectric fibers, *Appl. Phys. Lett.* 23:142 (1973).
2. T. Yajima and M. Wadati, The unstable nonlinear Schrödinger equation, in: "Integrable and Superintegrable Systems" B.A. Kupershmidt, ed., World Scientific, (1990).
3. T. Yajima and M. Wadati, Solitons in electron beam plasma, *J. Phys. Soc. Jpn.* 59:3237(1990).
4. Y. Lai and H.A. Haus, Quantum theory of solitons in optical fibers. II. Exact solution, *Phys. Rev. A* 40:854(1989).
5. L.A. Takhtajan and L.D. Faddeev. "Hamilton Approach in Soliton Theory," (in Russian), Nauka, Moscow (1986).
6. H.B. Thacker, Exact integrability in quantum field theory and statistical systems, *Rev. Mod. Phys.* 53:258(1984).

ON THE FORCED ECKHAUS EQUATION

Silvana De Lillo

Dipartimento di Fisica

Università di Perugia

INFN Sezione di Perugia

Perugia, Italy

Parametrically forced nonlinear Schroedinger type equations have recently been investigated¹ in connection with the existence of nonlinear bound state solutions and of their stability. In this note we review some recent results², concerning the Eckhaus equation in an external potential $V(x)$ and the properties of its bound state solutions. Some new results, related to the time asymptotic behavior of the solutions, will also be reported.

We consider the parametrically forced Eckhaus equation²

$$i\Psi_t + \Psi_{xx} + 2(|\Psi|^2)_x \Psi + |\Psi|^4 \Psi - V(x)\Psi = 0 \quad (1)$$

where $\Psi \equiv \Psi(x,t)$ and the parametric forcing $V(x)$ acts as an external potential.

We introduce the linearizing transformation

$$\phi(x,t) = C\Psi(x,t) \exp\left[\int_{-\infty}^x dx' |\Psi(x',t)|^2\right], \quad (2.a)$$

Let us now consider a harmonic oscillator potential

$$V(x) = x^2. \quad (7)$$

The general solution of the Schroedinger equation (3) has the (well known) form

$$\varphi(x,t) = \sum_{n=0}^{\infty} c_n H_n(x) \exp\left[-\frac{1}{2}x^2 - i(2n+1)t\right] \quad (8)$$

where $H_n(x)$ are the Hermite polynomials.

The corresponding general solution of the Eckhaus equation (1) is given by (2.b) with (8). The special case $c_n = \delta_{nm}$ corresponds to the time independence of $|\varphi(x,t)|^2$

$$|\varphi(x,t)|^2 = c_m^2 H_m^2(x) \exp(-x^2) \quad (9)$$

The same property still holds for $\Psi(x,t)$, namely

$$|\Psi(x,t)|^2 = c_m^2 H_m^2(x) \exp(-x^2) \left[C^2 + c_m^2 \int_{-\infty}^x dy H_m^2(y) \exp(-y^2) \right]^{-1} \quad (10)$$

is also time independent. We note however that $|\varphi(x,t)|$ is symmetric in x , while the symmetry is lost for $|\Psi(x,t)|$.

We finally note that for the harmonic oscillator potential (7) the mean value $\bar{x}(t)$ of the position x with respect to the solution $\varphi(x,t)$ of the linear Schroedinger equation (3)

$$\bar{x}(t) = \int_{-\infty}^{+\infty} dx x |\varphi(x,t)|^2 \quad (11)$$

oscillates harmonically

$$\bar{x}(t) = \bar{x}(0) \cos 2t + \frac{1}{2} \dot{\bar{x}}(0) \sin 2t \quad (12)$$

No analogous results holds for the mean value $\tilde{x}(t)$ of x , taken with respect to $\Psi(x,t)$:

$$\tilde{x}(t) = \int_{-\infty}^{+\infty} dx x |\Psi(x,t)|^2 \quad (13)$$

This is of course a consequence of the nonlinear correction that appears in (6.b).

$$\Psi(x,t) = \varphi(x,t) / \left[|C|^2 + 2 \int_{-\infty}^x dx' |\varphi(x',t)|^2 \right]^{1/2}, \quad (2.b)$$

with C a constant. We also restrict our attention to the case in which $\Psi(x,t)$ and $\varphi(x,t)$ vanish (sufficiently fast) as $x \rightarrow -\infty$.

It is immediate to see that (2) maps equation (1) into the linear Schroedinger equation

$$i\phi_t + \phi_{xx} - V(x)\phi = 0 \quad (3)$$

Note that the above result is independent of the external potential $V(x)$, moreover it would hold without modification even if the external potential were time dependent.

Bound state solutions can be normalized by setting

$$\int_{-\infty}^{+\infty} dx |\phi(x, t)|^2 = \int_{-\infty}^{+\infty} dx |\Psi(x, t)|^2 = 1 \quad (4.a)$$

with the constraint on the constant C

$$|C|^2 = 2/(e^2 - 1) \quad (4.b)$$

For this class of solutions of the linear Schroedinger equation there hold the classical Ehrenfest theorems

$$(d/dt) \int_{-\infty}^{+\infty} dx x |\phi(x, t)|^2 = i \int_{-\infty}^{+\infty} dx \{ \phi(x, t) [\phi_x(x, t)]^* - [\phi(x, t)]^* \phi_x(x, t) \} \quad (5.a)$$

$$(d/dt)^2 \int_{-\infty}^{+\infty} dx x |\phi(x, t)|^2 = -2 \int_{-\infty}^{+\infty} dx V_x(x) |\phi(x, t)|^2 \quad (5.b)$$

For the solutions $\Psi(x, t)$ of the Eckhaus equation (1), the corresponding results are

$$(d/dt) \int_{-\infty}^{+\infty} dx x |\Psi(x, t)|^2 = i \int_{-\infty}^{+\infty} dx \{ \Psi(x, t) [\Psi_x(x, t)]^* - \Psi(x, t) [\Psi_x(x, t)]^* \} \quad (6.a)$$

$$(d/dt)^2 \int_{-\infty}^{+\infty} dx x |\Psi(x, t)|^2 = -2 \int_{-\infty}^{+\infty} dx V_x(x) |\Psi(x, t)|^2 + \\ -2 \int_{-\infty}^{+\infty} dx [(|\Psi(x, t)|^2)_2]^2 \quad (6.b)$$

Let us now turn our attention to the time asymptotic behavior of the solutions of the Eckhaus equation (1). Without loss of generality we put $C=1$ in (2) and consider the initial value problem for equation (1), characterized by the initial datum

$$\Psi(x, 0) = \Psi_0(x) \quad (14)$$

asymptotically vanishing as $|x| \rightarrow \infty$.

Via (2.a) we obtain the (asymptotically vanishing) initial datum for equation (3)

$$\varphi(x,0)=\varphi_0(x)=\Psi_0(x)\exp\left[\int_{-\infty}^x dx' |\Psi_0(x')|^2\right]. \quad (15)$$

The initial value problem for equation (1) is then solved by solving the analogous problem for equation (3) and then by recovering the solution $\Psi(x,t)$ via (2.b), once $\varphi(x,t)$ is known.

The long time behavior of the solution $\varphi(x,t)$ of the linear Schroedinger equation (3), corresponding to the initial datum (15), can be analyzed with standard scattering techniques.

For potentials $V(x)$ belonging to the class L_2^1 where

$$L_2^1 = \left\{ V(x): \int_{-\infty}^{+\infty} (1+|x|^2) V(x) dx < \infty \right\}. \quad (16)$$

The only nondecaying contributions to the solution $\varphi(x,t)$ are due to the bound states of the potential³. The transformation (2.b) then implies that an analogous result holds also for the solution $\Psi(x,t)$ of the forced Eckhaus equation. Localized solutions of the nonlinear equation (1) are then obtained as a nonlinear combination of the bound states of the potential of the linear Schroedinger equation (3).

REFERENCES

1. A. Soffer and M.I. Weinstein, "Multichannel nonlinear scattering for nonintegrable equations", *Commun. Math. Phys.*, 133: 119 (1990).
2. F. Calogero and S. De Lillo, "The Eckhaus equation in an external potential", *J. Phys. A*, 25: L287 (1992).
3. M.J. Ablowitz and S. De Lillo, unpublished (1992).

NEW ASPECTS OF CHAOTIC DYNAMICS IN NONLINEAR SCHRÖDINGER SYSTEMS

Th. Eickermann, R. Grauer, and K.H. Spatschek

Institut für Theoretische Physik I, Heinrich-Heine-
Universität Düsseldorf, D-4000 Düsseldorf 1, Germany

INTRODUCTION

A generic model equation for the envelope of weakly nonlinear, weakly dispersive waves is the nonlinear Schrödinger (NLS) equation. Collisionally damped Langmuir-waves in a plasma driven by an external rf-capacitor field for example are described by the driven and damped NLS

$$iq_t + q_{xx} + 2|q|^2 q - \omega q = -i\epsilon - i\gamma q. \quad (1)$$

Although this equation is integrable only for $\gamma = 0, \epsilon = 0$, it is well known¹ that solitons still play an important role for the dynamics in the general case. Nozaki and Beeki¹ have observed, that a phase locked soliton like solution of (1) exists as long as the damping rate γ is not too large. Increasing the driving ϵ , the system undergoes a Hopf-bifurcation and the soliton starts to oscillate periodically in time. In the nearly infinite line case further increase of ϵ leads to a sequence of period doubling bifurcations and finally to a chaotic time evolution. An example of such a chaotic motion is shown in fig. 1.a). A more detailed numerical investigation³ shows, that the system obeys the Feigenbaum-scaling.

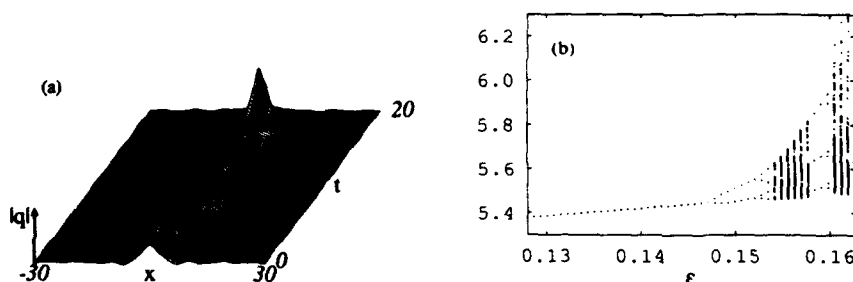


Fig. 1 a) chaotic time evolution of a soliton with $\epsilon = 0.15, \gamma = 0.11, \omega = 1$. b) period-doubling for $\gamma = 0.11, \omega = 1$, length of system $l = 80$.

Fig. 1.b) shows a characteristic parameter at Poincaré times plotted versus ϵ , which is used as a bifurcation parameter here. In the present contribution we show (by numerical simulation), that besides the period doubling route to chaos also other phenomena which are typical for dynamical systems can be observed. One of them is intermittency, which is expected and found close to the regular windows in the chaotic regime. In addition, choosing the parameters of (1) in analogy to Grauer and Birnir², who investigated breather dynamics in the NLS regime of a driven and damped sine Gordon equation, we can find quasiperiodicity here too.

Our second task is to compare two methods for deriving low degree of freedom models for the dynamics of the PDE. We can make use of the fact, that (1) is near integrable and expand the solution of the equation in the (nonlinear) base of solitons and radiation. The second way is fully numerically. The Karhunen Loève expansion allows us to find the optimum base functions for a linear expansion. Those can be used in a Galerkin method.

NUMERICAL RESULTS

From the theory of nonlinear maps it is known, that a saddle node bifurcation is typically accompanied by intermittency. Asymptotically the number of regular iterates n_r is connected with the distance from the bifurcation point by:

$$n_r \sim (\epsilon - \epsilon_0)^{-1/2}. \quad (2)$$

Such bifurcations take place at the limits of the regular windows in the chaotic regime. Therefore we investigated the large period 3 window, which can be seen in fig. 1.b). Fig. 2.a) shows the real part of the solution at Poincaré times for $\epsilon = 0.158349$, $\gamma = 0.11$. The interchange of regular and chaotic behaviour can clearly be seen. In fig. 4 $1/n_r^2$ is plotted as a function of ϵ . As predicted, this function is linear, with the bifurcation point $\epsilon_0 = 0.158351$.

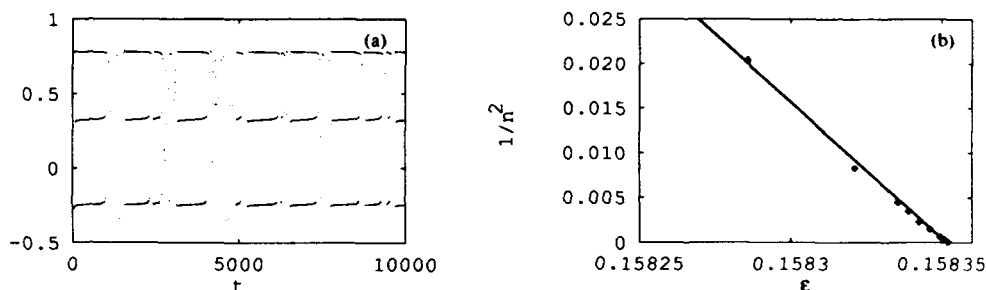


Fig. 2 intermittency for $\gamma = 0.11$, $\omega = 1$, $L = 80$. a) $\epsilon = 0.158349$, real part of solution at Poincaré-times. b) scaling of regular times: $1/n_r^2$ is plotted as a function of ϵ .

Taki et al.⁵ have given formulas, which connect the parameters of a driven damped sine Gordon equation and (1). Using them for the set of parameters in which Grauer and Birnir² found quasiperiodicity, we get to weakly damped ($\gamma = 0.035$) short length ($l = 24$) Schrödinger systems with periodic boundary conditions. As fig. 3 shows, we can find a narrow interval of quasiperiodic behaviour between period 1 and period 3 states.

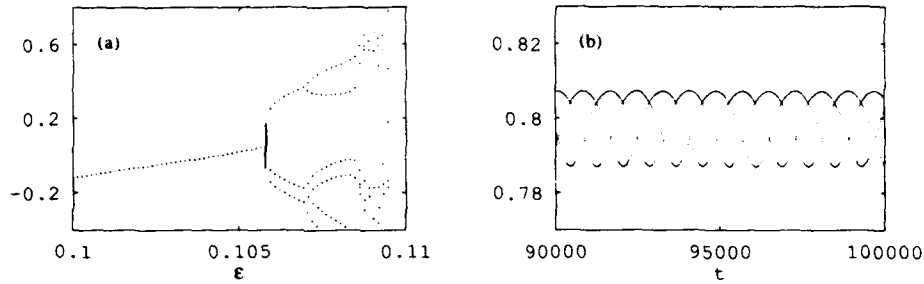


Fig. 3 quasiperiodicity for $\gamma = 0.035, \omega = 1, L = 12$, a) qp. and period 3 phaselocking. b) real part of solution at Poincaré times for $\epsilon = 0.1066$.

IST DIAGNOSTIC AND VARIATION OF ACTION METHOD

In the following we discuss two different collective coordinate descriptions. The first of them has been discussed in great detail elsewhere^{3,4} and is therefore described only briefly. Making use of the fact, that for $\gamma, \epsilon \ll 1$ the system is near-integrable, we solved the Zakharov-Shabat scattering problem numerically (for both infinite and periodic boundary conditions) for data like those shown in fig. 1.a). The result was, that a soliton and radiation modes about $k = 0$ dominate the dynamics. Based on this, we chose a soliton and $k = 0$ -radiation with time dependent amplitude and phase as ansatz-functions in the Lagrange density for (1):

$$l = \left\{ \frac{i}{2} (q_t q^* - q_t^* q) + |q|^4 - |q_x|^2 - \omega |q|^2 \right\} e^{2\gamma i}. \quad (3)$$

The resulting set of 4 real Euler-Lagrange equations shows a good qualitative and quantitative agreement with the PDE.

KARHUNEN-LOÈVE EXPANSION AND GALERKIN APPROXIMATION

A disadvantage of the method stated above is that it is restricted to near-integrable systems. A more general approach is based upon the Karhunen-Loève expansion^{6,7}. Given a time series $q(x, t_i), i = 1..N$ and the two-point correlation function

$$K(x, x') = \langle q(x) q^*(x') \rangle \quad (4)$$

with

$$\langle f \rangle = \frac{1}{N} \sum_{i=1}^N f(t_i) \quad (5)$$

the following eigenvalue problem

$$\int K(x, x') \phi_i(x') dx = \lambda_i \phi_i(x) \quad (6)$$

is defined. Its solutions are called empirical eigenfunctions. Among others they have the property, that for each N , they build an optimal set of base functions for an approximation of q in the sense, that the approximation error

$$\left\langle \left\| q(x) - \sum_{i=1}^N a_i \phi_i(x) \right\| \right\rangle \quad (7)$$

is minimal. The eigenvalues are a measure for the average mass contained in the modes. From a time-series with 5000 samples taken from a run in the time-chaotic parameter-regime, we achieved the modes and eigenvalues shown in fig. 4. As one can see 2 modes already contain 97 % of the mass and 3 modes even 99 %. Using these modes in a Galerkin-approximation, it's a simple task to construct sets of ODE's with an arbitrary number of modes.

Fig. 5 shows a bifurcation-diagram based on a 2-mode-model. The 3-mode-model is not plotted here, since its results are not different from the former. Since for fig. 1.b) the Poincaré-map was defined in the same manner as for fig. 5, using the projection of the PDE-solution to the first empirical eigenfunction, those pictures can be compared directly. Finally it is interesting to compare the modes, found by the KL-expansion with the soliton or radiation-modes, which had been used in the variation of action method. By a numerical fit the 1. mode is clearly identified as a soliton (1.4 % deviation in mass). The 2. mode is essentially (up to a 10 % error) the derivation of the soliton with respect to it's amplitude.

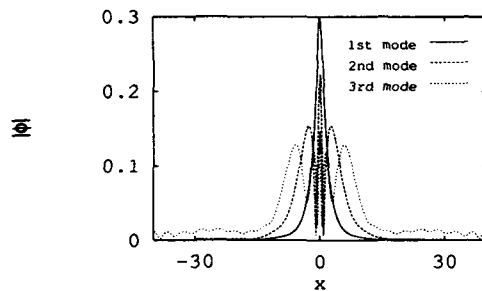


Fig. 4 First 3 empirical eigenfunctions with probabilities of 82 %, 15 % and 2 %.

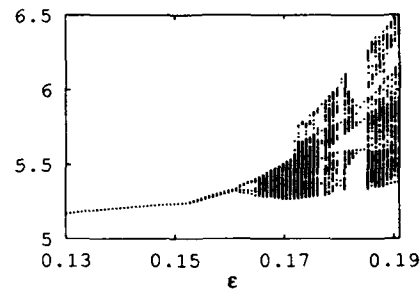


Fig. 5 period-doubling in 2-mode Galerkin-approximation, real part of amplitude of 1st mode at Poincaré-times is plotted versus ϵ .

REFERENCES

1. K. Nozaki, and N. Bekki, *Physica* **21D**, 381 (1986)
2. R. Grauer, and B. Birnir, *Physica* **56D**, 165 (1992)
3. K.H. Spatschek, H. Pietsch, E.W. Leadke, and Th. Eickermann, In **Singular behaviour and Nonlinear Dynamics**, eds. St. Pnevmatikos, T. Bountis, and Sp. Pnevmatikos, World Scientific Singapore 1989
4. Th. Eickermann, and K.H. Spatschek, In: **Inverse Methods in Action**, ed. P.C. Sabatier, 511-518, Springer (1990)
5. M. Taki, K.H. Spatschek, J.C. Fernandez, R. Grauer, and G. Physica **40D**, 65 (1989)
6. J.L. Lumley, In: **Atmospheric Turbulence and Radio Wave Propagation** eds. A.M. Yaglom and V.I. Tatarski, 166-178, Moscow: Nauka, (1967)
7. L. Sirovich, In: **New Perspectives in Turbulence**, ed. L. Sirovich, 139-163, Springer (1990)

RESONANCE PHENOMENA IN SOLITON-IMPURITY INTERACTIONS

Zhang Fei,¹ Yuri S. Kivshar,² and Luis Vázquez¹

¹Departamento de Física Teórica I, Facultad de Ciencias Físicas
Universidad Complutense, E-28040 Madrid, Spain

²Institut für Theoretische Physik
Universität Düsseldorf, D-4000 Düsseldorf 1, Germany

We consider the sine-Gordon (SG) system including a local inhomogeneity

$$u_{tt} - u_{xx} + [1 - \epsilon \delta(x)] \sin u = 0, \quad (1)$$

where $\delta(x)$ is the Dirac δ -function. When the perturbation is absent ($\epsilon = 0$), the SG model (1) supports topological solitons (kinks). For $\epsilon > 0$ the system admits a localized impurity mode: $u = a(t)e^{-\epsilon|x|/2}$, where $a(t) = a_0 \cos(\Omega t + \theta)$, $\Omega = \sqrt{1 - \epsilon^2/4}$.

We have studied the kink-impurity interactions by direct numerical simulations with Eq.(1). The initial conditions are taken as a kink centered at $X = -6$, moving toward the impurity with a given velocity $V_i > 0$. The main results are summarized as follows

- There are three different regions of initial kink velocity, namely, region of pass, of capture and of reflection (see Fig.1). A critical velocity $V_c(\epsilon)$ exists, such that if $V_i > V_c$, the kink will pass the impurity inelastically and escape to the positive infinity, losing part of its kinetic energy through radiation and excitation of an impurity mode.
- If $V_i < V_c$, the kink cannot escape to infinity after the first interaction, but it will stop, and then return to interact with the impurity again. For most velocities, the kink will lose energy again in the second interaction and finally get trapped by the impurity. However, for some special incoming velocities, the kink may escape to the negative infinity after the second interaction, i.e., the kink may be totally reflected by the impurity (see Fig. 1)
- In quantitative analysis, we find that the time interval between the first and the second interaction can be estimated by

$$T_{12}(V_i) = \frac{a}{\sqrt{V_c^2 - V_i^2}} + b \quad (2)$$

where V_i is the kink initial velocity, a and b are two parameters, e.g., at $\epsilon = 0.7$, we have $a = 3.31893$ and $b = 1.93$.

- We have observed that the reflection of the kink is carried out in two steps, the first interaction excites the impurity mode and traps the kink, while the second interaction is just a reverse process, it will extinguish the impurity mode, retransferring enough energy back to the kink, and thus allowing it to escape. In this case, a resonance condition is satisfied

$$T_{12}(V) = nT_{im} + \tau. \quad (3)$$

where T_{im} is the period of the impurity mode oscillation, τ is an offset phase, and n is an integer.

- Combining Eqs.(2) and (3), we may obtain a formula to predict the centers of the resonance windows,

$$V_n^2 = V_c^2 - \frac{a^2}{(nT_{im} + \tau - b)^2}, \quad n = 2, 3, \dots \quad (4)$$

This formula can give very accurate predictions comparing with the numerical results.

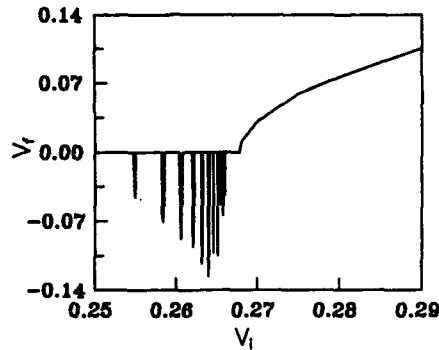


Figure 1. The final (SG) kink velocity as a function of the initial velocity at $\epsilon = 0.7$. Zero final velocity means that the kink is captured by the impurity.

Now let us consider the kink-impurity interactions in the ϕ^4 model

$$\phi_{tt} - \phi_{xx} + [1 - \epsilon\delta(x)](-\phi + \phi^3) = 0 \quad (5)$$

In the absence of perturbations, the ϕ^4 model also admits kinks, which have an internal oscillating mode with frequency $\omega_1 = \sqrt{3}/2$. It is well known that the existence of the kink internal mode is very important for the resonance phenomena in the kink-antikink collisions [3]. In the presence of the impurity, the ϕ^4 equation also has an impurity mode: $u(x, t) = a_0 \cos(\Omega t + \theta)e^{-\epsilon|x|}$, where Ω and ϵ are connected by the dispersion relation $\Omega^2 = 2 - \epsilon^2$.

By numerical simulations we also observe a set of resonance windows in which the kink can be reflected by an attractive impurity (Fig.2). We find that both the kink internal mode and the impurity mode are excited during the scattering, and the resonance phenomena observed are due to an energy exchange between the kink translational mode, kink internal mode, and the impurity mode. Moreover, we observe a new interesting feature in the resonant interactions: some intermediate windows disappear showing quasi resonance effects (see Fig.2). Although a much smaller velocity step ($\Delta V = 10^{-5}$) has been used to scan these windows, we have not found real kink reflection. Instead we have only observed quasi-resonances, i.e., if the kink initial velocity is close to some values, the second interaction will reflect the kink at a larger distance from the impurity, but the kink cannot escape to infinity. Therefore, the resonance structures observed here are quite different from those for the SG model in which the resonance windows come out one by one and they can be easily predicted by a simple formula (4). Furthermore, here we have observed a "three-bounce" resonance window in which the kink can escape after colliding with the impurity for three times.

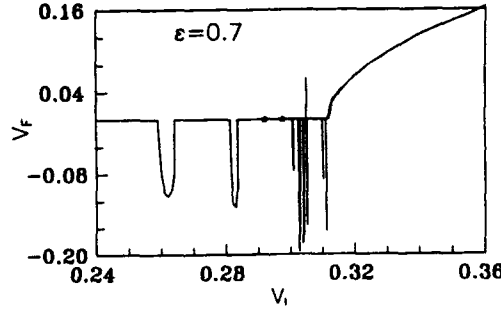


Figure 2. The same as in Fig.1 but for the ϕ^4 model (5) with $\epsilon = 0.7$. The two stars indicate the disappeared windows.

To study analytically the kink-impurity interactions in the SG model, we use a collective-coordinate method taking into account two dynamical variables, namely the kink coordinate $X(t)$ and the amplitude of the impurity mode oscillation $a(t)$ (for the ϕ^4 model the kink internal mode amplitude must also be used, see Ref [4]). By substituting the ansatz

$$u = 4 \tan^{-1} \exp[x - X(t)] + a(t)e^{-\epsilon|x|/2} \quad (6)$$

into the Lagrangian of the system,

$$L = \int_{-\infty}^{\infty} dx \left[\frac{1}{2} u_t^2 - \frac{1}{2} u_x^2 - (1 - \epsilon \delta(x))(1 - \cos u) \right], \quad (7)$$

we may derive the following (reduced) effective Lagrangian

$$L_{eff} = 4\dot{X}^2 + \frac{1}{\epsilon}(\dot{a}^2 - \Omega^2 a^2) - U(X) - aF(X), \quad (8)$$

where $U(X) = -2\epsilon/\cosh^2 X$, and $F(X) = -2\epsilon \tanh X/\cosh X$. The equations of motion for the two dynamical variables are the following

$$\begin{cases} 8\ddot{X} + U'(X) + aF'(X) = 0, \\ \ddot{a} + \Omega^2 a + (\epsilon/2)F(X) = 0. \end{cases} \quad (9)$$

The system (9) describes a particle (kink) with coordinate $X(t)$ and mass 8 scattered by an attractive potential $U(X)$ ($\epsilon > 0$), and "weakly" coupled with a harmonic oscillator $a(t)$ (the impurity mode). Here we say "weakly" because the coupling term $aF(X)$ is of order $O(\epsilon)$ and it decays exponentially. In Fig.3 we present a schematic picture for the system (9). It has been shown that this dynamical model (9) can describe the main features of the kink-impurity interactions. In particular, it can be used to estimate the critical velocity and to predict the resonance phenomena [1,2].

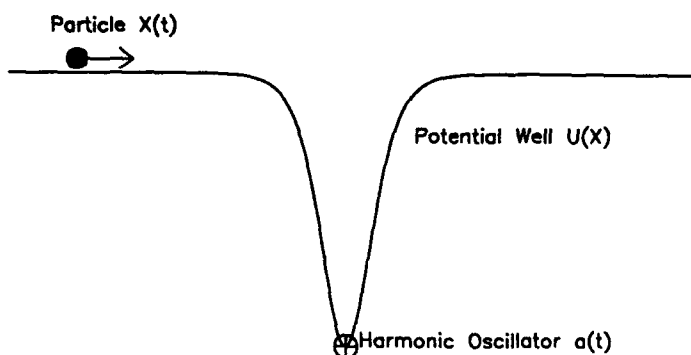


Figure 3. A particle moving in a potential well and weakly coupled with an oscillator. The schematic drawing of the system (9).

ACKNOWLEDGEMENT

This work is partially supported by the Comision Interministerial de Ciencia y Tecnologia (Spain) under Grant No.TIC 73/89.

REFERENCES

- [1] Yu.S. Kivshar, Zhang Fei, and L. Vázquez, Phys. Rev. Lett. **67**, 1177 (1991).
- [2] Zhang Fei, Yu.S. Kivshar, and L. Vázquez, Phys. Rev. A **45**, 6019 (1992).
- [3] D.K. Campbell, J.F.Schonfeld, and C.A. Wingate, Physica D **9**, 1 (1983).
- [4] Zhang Fei, Yu.S. Kivshar, and L. Vázquez, Phys. Rev. A, (1992) (submitted).

TWO AND MANY IMPURITY EFFECTS IN SOLITON DYNAMICS

Yuri S. Kivshar,^{1,2} Angel Sánchez,¹ and Luis Vázquez¹

¹Dpto. de Física Teórica I, Facultad de Ciencias Físicas
Universidad Complutense, E-28040 Madrid, Spain

²Institut für Theoretische Physik I, Heinrich-Heine-
Universität Düsseldorf, D-4000 Düsseldorf 1, Germany

INTRODUCTION

Since perfect systems are an idealization never found in nature, the study of the effects of disorder on them is of paramount importance. In particular, nonlinear models, which have been very much fruitful in many fields of physics,¹ have been the subject of an intense effort in this direction.² A complete description of this problem can only be achieved through a step-by-step analysis, in which the influence of one, two, and many impurities are addressed separately, one after the other. In this fashion, the knowledge acquired on the one-impurity problem helps understand the new features arising when two impurities are present, and this can be later used to account for the unavoidable cooperative effects which appear in a system with many impurities present. This work is a part of such a project, devoted to the study of nonlinear excitation dynamics in Nonlinear Klein-Gordon models. The one impurity problem is discussed in another contribution in this volume,³ and here we deal with the remaining stages of the work.

THE TWO IMPURITY PROBLEM

The model we work with here is that of an inhomogeneous sG system which, in dimensionless units, is given by

$$u_{tt} - u_{xx} + [1 + \epsilon(\delta(x) + \delta(x - D))] \sin u = 0. \quad (1)$$

Physically, this equation is associated, for instance, to the presence of pointlike inhomogeneities in a Josephson Junction, where u stands for the normalized flux.⁴

A complete analysis of this problem, which includes also the Korteweg-de Vries and the Nonlinear Schrödinger equations, has been carried out in Ref. 5. Here we briefly summarize the results for the sine-Gordon model (1). The problem (1) can be dealt with analytically in an approximate fashion. Using the perturbation theory based on

the Inverse Spectral Transform,^{5,6} it is possible to compute, following the standard procedure, the spectral energy density emitted by the kink upon collision with the two impurities. Integrating over the wavenumbers directed backwards gives the energy reflected by the impurities, and hence the reflection coefficient, defined as the ratio of the reflected energy to the unperturbed soliton energy. The best way to present the results is to compare them to the reflection coefficient for one impurity, and this yields

$$\frac{R_2}{2R_1} \simeq 1 + \frac{1}{(1 + D^2/\pi^2)^{1/4}} \cos \left[\frac{D}{v} - \frac{1}{4} \tan^{-1} \left(\frac{D}{\pi} \right) \right], \text{ when } v^2 \ll 1, \quad (2)$$

$$\frac{R_2}{2R_1} \simeq 1 + 3 \left(\frac{d}{\sinh d} + \frac{2 \cosh d}{\sinh^2 d} - \frac{2d \cosh^2 d}{\sinh^3 d} \right), \text{ when } (1 - v^2) \ll 1. \quad (3)$$

In (3), $d \equiv 2D/\sqrt{1 - v^2}$, v is the kink speed, and R_i is the reflection coefficient for i impurities. Notice that in both cases, when the distance between impurities $D \rightarrow 0$, $R_2/2R_1 = 2$ (the soliton is scattered by a single impurity of twice the strength), whereas if $D \rightarrow \infty$ $R_2/2R_1 \rightarrow 1$ (the scattering is independent and no interference between backscattered waves arises).

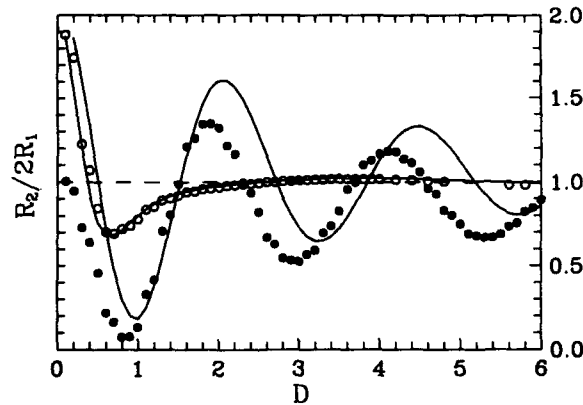


Figure 1. The ratio of the reflection coefficient of two impurities to that of one impurity. Lines are the theoretical prediction given by Eqs. (2) and (3). Circles are numerical results; empty for $v = 0.9$ kinks, and full for $v = 0.4$ kinks.

The results (2), (3) are shown in Figure 1, plotted as solid lines. It is evident that fast solitons do not show any signature of interference effects, whereas slow ones (not so slow as to be pinned by the impurity) exhibit oscillations in their reflection coefficient as a function of the distance between impurities. The results have been confirmed numerically, as can be seen also from Figure 1. The small discrepancy for

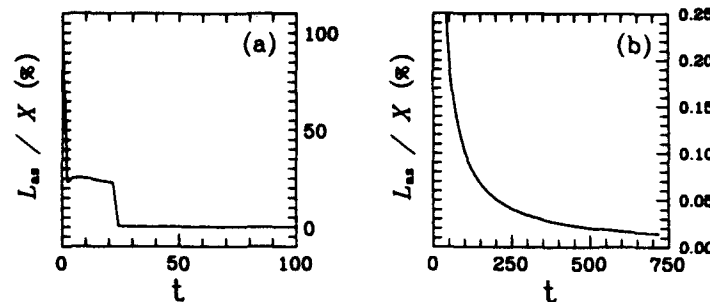


Figure 2. (a) Asymptotic difference L_{as} as a percentage of the position $X(t)$ vs time, when $\epsilon = 0.1$, $v_0 = 0.3$ ($t_0 = 24.1$), and $\tau_0 = 3t_0$. (b) Long time behavior for the same parameters.

slow solitons is due to the fact that they slow down a little while travelling between the impurities, as a consequence of the energy loss after the first collision. This effect, which is not accounted for in our perturbation theory, can be proven⁵ to be responsible for the differences appearing in Figure 1.

THE MANY IMPURITY PROBLEM

One of the conclusions which can be drawn from the result of the previous section is that for $D \geq 10$ the two impurity scattering process can be regarded as independent, i.e., there are no interference effects. Therefore, it is possible to treat the many impurity problem in the dilute limit assuming independent scattering without introducing significant errors, which we have recently done for the sine-Gordon⁷ and Nonlinear Schrödinger⁸ models. In this section we present the former analysis.

The equation we study is

$$u_{tt} - u_{xx} + \left(1 + \epsilon \sum_n \delta(x - a_n)\right) \sin u = 0, \quad (4)$$

where the distances $b_n = a_{n+1} - a_n$ are randomly distributed with probability $p(b) = b_0^{-1} \exp(-b/b_0)$. If the mean distance between impurities is large, we can use the previous section results to treat independently the scattering by each impurity. This is done in the framework of the collective-coordinate formalism, in which solitons are considered as particles and then δ -functions are substituted by equivalent sech-shaped potentials of width Δ (see Ref. 6,7 for details). The key point now is to describe the scattering in terms of the time distribution of the impurities instead of the spatial one; i.e., to study the problem by dealing with the time intervals τ_n elapsed when the kink travels between the n th and the $(n+1)$ th scatterers, and the (constant) intervals t_0 that separate them, during which the kink travels through one impurity. By doing this, it is not difficult to obtain the statistical properties of the kink; in this way, we have been able to compute the mean kink position $X(t)$ (and any other time-dependent function).

As the expression is actually very cumbersome, we do not write it down here. Instead, we have evaluated it numerically for different cases; as an example, in Figure 2 we show two plots of the asymptotic difference L_{as} , defined as the difference between the kink position and the one it should have if it would have traveled with the asymptotic velocity, which from our calculation turns out to be⁷

$$V_{as} = \frac{V_0 \tau_0 + \Delta}{\tau_0 + t_0}, \quad (5)$$

τ_0 being the mean temporal distance between impurities and V_0 the kink initial velocity. Figure 2 shows that, after a short period, in fact, after the kink crosses the length of one impurity, $L_{as} \rightarrow 0$, which implies that we can already estimate the kink position by using Eq. (5) for its speed. This outcome is the most important one of our work, as it allows to predict the kink behavior in the random medium from the knowledge of a few parameters of it. We can also conclude that the important parameter to decide when the asymptotic regime starts is t_0 , the time for the kink to travel through a single impurity.

The procedure we have sketched here is general and can be applied to any NKG system, irrespective of its integrability. We do not expect radiative corrections to be important in the dilute limit, due to the absence of interference. However, as a final remark, we would like to point out that numerical work is needed to check the validity of the independent scattering approximation.

ACKNOWLEDGMENTS

We have greatly benefited from discussions with O. A. Chubykalo, S. A. Gredeskul, and A. M. Kosevich. Partial financial support from CICyT (Spain) through project MAT90-0544 is gratefully acknowledged.

REFERENCES

1. S. E. Trullinger, V. E. Zakharov, and V. L. Pokrovsky, eds., "Solitons," North-Holland, Amsterdam (1986).
2. A. Sánchez and L. Vázquez, Nonlinear wave propagation in disordered media, *Int. J. Mod. Phys. B* 5:2825 (1991).
3. Z. Fei, Y. S. Kivshar, and L. Vázquez, Resonance phenomena in soliton-impurity interactions, in "Future Directions of Nonlinear Dynamics in Physical and Biological Systems" (this volume).
4. A. Barone and G. Paternó, "Physics and Applications of the Josephson Effect," John Wiley & Sons, New York, (1982).
5. Yu. S. Kivshar, A. Sánchez, O. A. Chubykalo, A. Kosevich, and L. Vázquez, Interference effects in soliton scattering by impurities, *J. Phys. A*, submitted (1992).
6. Yu. S. Kivshar and B. A. Malomed, Dynamics of solitons in nearly integrable systems, *Rev. Mod. Phys.* 61:763 (1989).
7. S. A. Gredeskul, Yu. S. Kivshar, L. K. Maslov, A. Sánchez, and L. Vázquez, Kink propagation through disordered media, *Phys. Rev. A*, in press (1992).
8. Yu. S. Kivshar, S. A. Gredeskul, A. Sánchez, and L. Vázquez, Localization decay induced by strong nonlinearity in disordered systems, *Phys. Rev. Lett.* 64:1693 (1990).

SELF-FOCUSSING OF COUPLED GUIDED ACOUSTIC WAVES AT A NONLINEAR RESONANCE

A.P. Mayer

Institut für Theoretische Physik
Universität Regensburg
W-8400 Regensburg
Germany

INTRODUCTION

Guided acoustic waves, especially surface acoustic waves and waves in elastic plates, have attracted considerable interest for a number of years, mainly because of their applicability in signal processing devices¹. Due to the concentration of energy at the waveguide, nonlinear effects are readily observable¹. This has stimulated a large number of theoretical investigations on various effects of nonlinearity on the propagation of guided acoustic waves. In certain geometries with material properties homogeneous along an axis vertical to the direction of propagation, the shear-horizontal component of the displacement field decouples from the components of sagittal polarization. In the presence of nonlinearity, acoustic waves of purely sagittal polarization can still exist. However, shear-horizontal acoustic waves can generate sagittal components of the displacement field via the second-order nonlinearity even in isotropic elastic media^{2,3}. In derivations of evolution equations for slow variations of the envelope of shear-horizontal guided acoustic waves, these sagittal components may usually be eliminated adiabatically giving rise to an effective third-order nonlinearity in the evolution equation of the nonlinear Schrödinger type³. In situations where the second harmonic of a sinusoidal shear-horizontal wave with wavenumber q has frequency equal or close to a sagittal guided mode with wavenumber $2q$, an adiabatic elimination is no longer possible. This nonlinear resonance of shear-horizontal and sagittal waves has been discussed in more detail in Ref. 4 for the case of plate modes. The purpose of this contribution is to incorporate dispersion and diffraction into the evolution equations for the envelopes of the two nonlinearly coupled carrier waves and to discuss, on the basis of these equations, the possibility of the formation of coupled solitary channels in this system.

EVOLUTION EQUATIONS

The displacement field $\tilde{u}(\vec{x}, t)$ in an elastic plate has to satisfy the equation of motion

$$\rho \ddot{u}_m = T_{Mm,M} \quad (1)$$

with the stress tensor (T_{Mm}) having components

$$T_{Mm} = S_{mMnN}u_{n,N} + \frac{1}{2}S_{mMnNlL}u_{n,N}u_{l,L} \quad (2)$$

up to cubic anharmonicity. Here, ρ is the mass density of the elastic medium and (S_{mMnN}) and (S_{mMnNlL}) are material constants. In addition to the equation of motion (1), the displacement field has to satisfy the boundary conditions $T_{3m} = 0$ at the upper and lower surface of the plate which we choose to be orthogonal to the z -axis. Following Ref. 4, we write the displacement field in the form of an asymptotic expansion

$$\vec{u} = \epsilon \vec{u}^{(1)} + \epsilon^2 \vec{u}^{(2)} + \dots \quad (3)$$

the first-order term of which consists of a shear-horizontal wave with wavenumber q and a sagittal wave with wavenumber $2q$:

$$\vec{u}(\vec{x}, t) = \begin{pmatrix} 0 \\ \cos(\kappa z + \phi) \\ 0 \end{pmatrix} e^{i(qx - \bar{\omega}t)} A + \begin{pmatrix} w_1(z, 2q) \\ 0 \\ w_3(z, 2q) \end{pmatrix} e^{i(2qx - \omega t)} \tilde{B}. \quad (4)$$

Here, the propagation direction has been chosen to be the x -direction. The amplitudes A and \tilde{B} depend on stretched coordinates $X_1, Y_1, T_1, X_2, Y_2, T_2, \dots$. In order to obtain the dominant nonlinearity as well as diffraction and dispersion in the evolution equations for A and \tilde{B} , we have to scale these stretched coordinates in powers of $\epsilon^{1/2}$ rather than in powers of ϵ , i.e. $X_1 = \epsilon^{1/2}x, X_2 = \epsilon x, \dots$. This means that the effect of the second-order nonlinearity is enhanced as compared to the case of nonresonant coupling since it acts on shorter scales. Carrying out the multiple scales analysis, we are led to the following pair of coupled evolution equations:

$$i(B_t + V B_x) + \frac{1}{2}g_{\parallel} B_{xx} + \frac{1}{2}g_{\perp} B_{yy} + (2\bar{\omega} - \omega)B = M^* A^2 \quad (5)$$

$$i(A_t + \bar{V} A_x) + \frac{1}{2}\bar{g}_{\parallel} A_{xx} + \frac{1}{2}\bar{g}_{\perp} A_{yy} = M A^* B, \quad (6)$$

where $B = \tilde{B} \exp[i(2\bar{\omega} - \omega)t]$. \bar{V} is the group velocity of the shear-horizontal mode and \bar{g}_{\parallel} and \bar{g}_{\perp} are the second derivatives of the linear mode frequency with respect to the wavevector component in x - and y -direction, respectively. The corresponding quantities without overbar refer to the sagittal mode. The coupling constant M is essentially an overlap integral involving the second- and third-order elastic moduli and the displacement profiles of the two modes. In order to study self-focussing and the formation of coupled channels in this system, we consider a stationary situation and neglect the second derivatives with respect to x in comparison to the first derivatives⁵. After rescaling, the system of evolution equations takes the form

$$iB_x + \Omega B_{yy} + \Delta B = A^2 \quad (7)$$

$$iA_x + A_{yy} = \pm 2A^* B. \quad (8)$$

The lower sign in equ. (8) corresponds to the case of V and \bar{V} having different sign, and the upper sign corresponds to the opposite case which we shall consider here. Furthermore, $\Omega = (g_{\perp} \bar{V})/(\bar{g}_{\perp} V)$ and Δ is proportional to the frequency mismatch $2\bar{\omega} - \omega$. In the following, we assume Ω to be positive.

SPECIAL SOLUTIONS

The simplest nontrivial solutions of the coupled nonlinear system of equations (7) and (8) are homogeneous in the y -direction,

$$A(x, y) = A_0 e^{-iKx} \quad (9)$$

$$B(x, y) = B_0 e^{-2iKx}, \quad (10)$$

where

$$K = -\frac{1}{4}\Delta + \left[\left(\frac{1}{4}\Delta \right)^2 + |A_0|^2 \right]^{1/2}. \quad (11)$$

An analysis of the linear stability of these solutions against modulations $\sim \exp[\pm i(qy - \kappa x)]$ reveals two branches for the dispersion relation $\kappa(q)$, one "optical" branch with $\kappa(q \rightarrow 0) \neq 0$ and one "acoustic" branch with $\kappa(q \rightarrow 0) = 0$. Defining $F = (4 + \Delta/K)^2 - 4$ and $H = (2 + 2\Omega + \Delta/K)(2 + \Delta/K)$, we find, in the limit $q \rightarrow 0$, that the optical branch is unstable if $F < 0$, i.e. for $-6 < \Delta/K < -2$, whereas the acoustic branch is unstable for $H/F < 0$.

In analogy to the single soliton solutions of the nonlinear Schrödinger equation, the system of equations (7), (8) has solutions which correspond to coupled channels of the shear-horizontal and sagittal mode. Such solitary wave solutions can be obtained by the following reduction of the system (7), (8) to ordinary differential equations in the same way as demonstrated by Parker and Newbould⁶ for a different system of coupled nonlinear evolution equations:

$$A(x, y) = \sqrt{\Omega} a(y) e^{i\alpha x} \quad (12)$$

$$B(x, y) = b(y) e^{2i\alpha x}. \quad (13)$$

For convenience, we introduce the parameters $p^2 = \alpha\Omega/(2\alpha - \Delta)$ and $q = (2\alpha - \Delta)\alpha/\Omega$. Changes of the parameter q at fixed p result in a simple rescaling of the solutions (12), (13). Fig. 1 shows a profile of two coupled channels for the case $p = 0.5$. It can be seen easily that for $p = 1$, both a and b have sech^2 -shape.

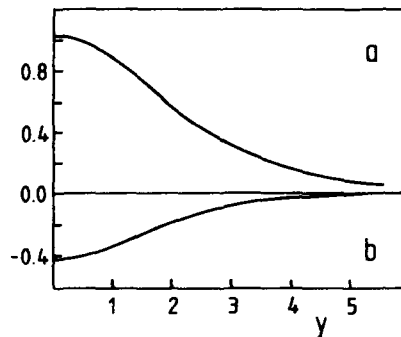


Figure 1. Coupled channel profiles for $p = 0.5$ (arbitrary units).

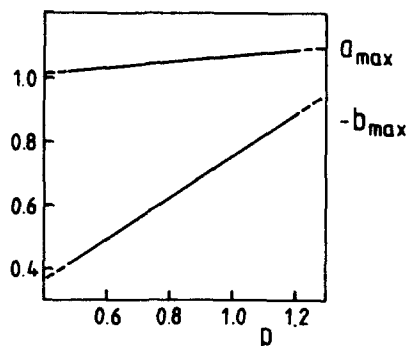


Figure 2. Dependence of the profile maxima on the parameter p ($q = 1$).

For certain ranges of the parameters, "dark" channels can be found with $a(y)$ and $b(y)$ approaching finite nonzero limiting values for $y \rightarrow \pm\infty$. The stability of these various types of coupled channels and the influence of higher order nonlinearity remain to be investigated.

REFERENCES

1. G.I. Stegeman and F. Nizzoli, Surface vibrations, in: "Surface Excitations," V.M. Agranovich and R.Loudon, eds., North-Holland, Amsterdam (1984).
2. G.A. Maugin, "Nonlinear Electromechanical Effects and Applications," World Scientific, Singapore (1985).
3. A.A. Maradudin and A.P. Mayer, Surface acoustic waves on nonlinear substrates, in: "Nonlinear Waves in Solid State Physics," A.D. Boardman, M. Bertolotti, and T. Twardowski, eds., Plenum, New York (1990).
4. A.P. Mayer, D.F. Parker, and A.A. Maradudin, On the role of second-order nonlinearity in the evolution of shear-horizontal guided acoustic waves, *Phys. Lett. A* 164:171 (1992).
5. V.I. Karpman, "Non-Linear Waves in Dispersive Media," Pergamon, Oxford (1974) [Russ. edition: Nauka, Moscow (1973)].
6. D.F. Parker and G.K. Newbould, Coupled nonlinear Schrödinger equations arising in fibre optics, *J. Phys. Colloq.* 50:C3-137 (1989).

SOME EXACT WAVE SOLUTIONS IN TERMS OF THE WEIERSTRASS FUNCTIONS FOR NONLINEAR HYPERBOLIC EQUATIONS

Alexander M. Samsonov

Theoretical Department, A.F.Ioffe Physico-Technical
Institute of Russian Academy of Sciences
St.Petersburg, 194021 Russia

INTRODUCTION AND GENERAL RESULTS

When the long wave propagation problem in the 1-D wave guide of various physical nature is considered, the following nonlinear hyperbolic equation (NHE)

$$u_{tt} - u_{xx} = (P_k(u) + au_{tt} - bu_{xx})_{xx} + (\epsilon u^2 + fu)_{xt} + gu_{txx}, \quad (1)$$

seems to present the quite general description for the evolution of the unknown function $u(x, t)$ of the space coordinate x and time t , in which a polynomial nonlinearity $P(u)$ of order k , the dispersion and dissipation are taken into account. The aim of the study is to propose an approach for exact explicit travelling wave solutions (TWS) of (1), which seems not to be integrable by means of the inverse scattering transform (IST) method. Introducing the phase variable $z = x \pm Vt$, after integration twice of the result, we have a nonlinear second order O.D.E with respect to the new unknown u , in the form

$$u'' = Au' + Q(u), \quad (2)$$

which is, indeed, the equation, describing a nonlinear oscillator with damping (or the generalized Duffing equation). Here primes denote differentiations with respect to z , $Q(u)$ is a polynomial, and u is assumed to get the constant values at infinity. Two conditions are important for the approach under consideration, namely, that the differential function (DF) should be polynomial, and it should not contain z (at least, the equation (2) should be reducible to an autonomous one). The following *theorem*, proved¹ recently:

the generalized Duffing equation $u'' = u' + Q(y)$, containing an *arbitrary* polynomial nonlinearity $Q(u)$, can be reduced to the Abel equation: $v' = v^3 + F(y)$,
the non-autonomous one with *cubic* nonlinearity,

provides the further necessary reduction of the integration problem for (2). Moreover the classical results of the 1st order nonlinear O.D.E. theory can be used, and the *theorem* by Hermite² for integrals of an autonomous equation of 1st order $P(u', Q(u)) = 0$ is of crucial importance:

if $P(\cdot)$ has no movable critical points, the genus of corresponding Riemann surface is either 0 or 1, and then the integral is the rational function of z , or the rational one with respect to $\exp(z)$ and/or to an elliptic function, respectively.

The question arises how to find an integral for $P(u', Q(u)) = 0$ explicitly, and for this purpose one can use the well known (Whittaker & Watson³) and the most general representation for any elliptic function in terms of the Weierstrass function $\wp(z)$ or $\wp(\exp(z))$ as follows:

$$u(z) = A(\wp(\cdot)) + B(\wp(\cdot))\wp'(\cdot), \quad (3)$$

with rational functions A and B with respect to their arguments.

The advantage of this approach consists in the possibility to exploit for dissipative problem the following proposition: an autonomous equation $v'(z) = q(v)$ with a polynomial $q(v)$ can be solved in terms of $\exp(\alpha z)$ and of the Weierstrass function $\wp(z + c)$ among the special functions of mathematical physics, because any derivative of both mentioned can be expressed in terms of a polynomial with respect to the function itself.

However, the Abel equation is not integrable in general case. Therefore we try to find the solution in the form (3) for the Duffing equation (2) of 2nd order with rational (or even polynomial) A and B ; this attempt results in various periodic, doubly periodic, and localized solutions of the NHE with dissipation. The procedure seems to be quite simple: one should substitute the expression (3) into (2), make independently the coefficients at each order of \wp and \wp' equal to zero, and obtain the (overdefined) set of coupled algebraic equations. When a solution of the system exists, perhaps, under some restrictions for coefficients of equation, we obtain a solution of initial NHE. Moreover, any mathematical symbolic software for PC can be used very effectively for an algebra at this stage.

TRAVELLING WAVE SOLUTIONS FOR DISSIPATIVE PROBLEMS OF NONLINEAR DYNAMICS

To demonstrate the use of the approach we begin with the Duffing *quadratic* equation, that corresponds to the problem of TWS of the famous KdV-Burgers equation. For $k = 2$ we have from (2)

$$u'' = au' + cu^2 + du + e, \quad (4)$$

and finding the solution in the form (3), we get

$$u = \alpha \exp 2\gamma(z + z_0)\wp[\beta \exp \gamma(z + z_0)], \quad (5)$$

where α, β, γ are constants. Solving the set of corresponding algebraic nonlinear equations for coefficients one easily obtains: $d < 0$, $e = 0$, $\operatorname{sgn}(\alpha) = -\operatorname{sgn}(c)$, $25d = -6a^2$, $\gamma = a/5$, therefore the exact solution has the form

$$u = \alpha y^2 \wp[(25c\alpha/(6a^2))^{1/2}y, 0, g_3], \quad y = \exp \gamma(z + z_0), \quad (6)$$

and contains two free parameters α and g_3 , and a shift constant z_0 . We are sorry for misprints in this formula in the paper¹. If the coefficients in (4) are that an additional restriction $g_3 = 0$ is valid, one can conclude for roots e_i of the characteristic polynomial for $\wp(\cdot)$ that either $e_1 = e_2$ or $e_2 = e_3$, and this leads to the *kink solution* in the form

$$u = \alpha + \beta y^2 / (y + \kappa)^2, \quad (7)$$

that was obtained⁴ recently by means of the Painleve equation analysis.

For cubic nonlinearity it follows from (2), that $u'' = au' + bu^3 + cu^2 + du + e$, and after substitution $y = \exp \gamma(z + z_0)$ it results in a more complicated form:

$$y^2 \gamma^2 u'' = (a\gamma - \gamma^2) y u' + b u^3 + c u^2 + d u + e. \quad (8)$$

Nevertheless, assuming the solution has the form:

$$u = y^q A(\varphi) + y^n \varphi^m (\beta y^k) \varphi', \quad (9)$$

we obtain : $q = 0, n = k = 1, \gamma = a/3, m = -1, g_3 = 0$, and the exact solution is:

$$u = -c/3b + y \varphi' / [(2b)^{1/2} \varphi(y, g_2, 0)], \quad (10)$$

if two additional conditions for coefficients in (8) are satisfied: $b(2a^2 + 9d) = 3c^2$, $c(8a^2 + 9d) = -81eb \rightarrow b \neq 0$.

The use of the approach is not restricted by the second order problems. For example, following the famous book by Alwyn Scott⁵, containing FitzHugh-Nagumo (FHN) model's description of the problem of nonlinear nerve pulse transmission, we consider the coupled nonlinear equations for the unknown function $u(x, t)$, that are presented nowadays as

$$u_{xx} - u_t = F_3(u) + R, \quad R_t = \epsilon(u + a - bR), \quad (11)$$

with recovery function R and cubic source term $F_3(u) = q_0 + q_1 u + q_2 u^2 + q_3 u^3$.

Looking for TWS, we reduce these equations to the third order O.D.E., corresponding to the FHN model, as follows:

$$u''' + \alpha u'' + u'(3q_3 u^2 + 2q_2 u + \rho) + n + m u + \delta q_2 u^2 + \delta q_3 u^3 = 0. \quad (12)$$

where $\alpha = V - \epsilon b/V, \delta = -\epsilon b/V, \rho = -\epsilon b - q_1, n = \delta q_0 + \epsilon a/V, m = \delta q_1 + \epsilon/V$. To find a solution we assume $u = A(\varphi) + B(\varphi)\varphi', \varphi = \varphi(z + z_0)$ with both functions A and B being polynomials with respect to φ , and we obtain exact explicit TW solution of FHN equation in the form $u = A\varphi + B\varphi'/\varphi$, where A, B are constants now, $(A/B)^2 = -2(1 - \epsilon b^2)/(3b)$, while the parameters of the Weierstrass function φ are:

$$g_3 = 0, \Delta = g_2^3 < 0, 2g_2 = 3\epsilon b/(V^2),$$

for the source function F :

$$q_3 = -1/(2B^2), q_2 = (1 - \epsilon b^2)/(bA),$$

$$q_1 = -1/b, q_0 = -2AV^2(-\epsilon b + 1/b)/(3\epsilon^2 b^3) - a/b,$$

and

$$\pm 2B^2 = [-Vb/(54(1 - \epsilon b^2))]^{1/2} - 1,$$

while V (wave velocity) and z_0 are free parameters.

The same approach can be used for fourth order O.D.E. of the form $u'''' = \alpha u'' + Q_k(u)$. Following the proposition (3) with $B = 0$ and polynomial $A(\cdot)$ of order m , i.e., $u = A_m(\varphi(z))$, we obtain the condition $m(k-1) = 2$, that for cubic nonlinearity $k = 3$ means $m = 1$, hence the exact solution is $u = a\varphi(\gamma z)$, while for $k = 2$ the equality

$m = 2$ is valid, and therefore $u = \alpha\varphi(\gamma z) + \beta\varphi^2(\gamma z)$. The last formula provides to obtain TWS for the Kuramoto-Sivashinsky equation.

We note in addition that to apply the approach for non-autonomous equation $P(u, u', z) = 0$ one should follow the *theorem* by Poincare⁶ :

if all critical points of the equation are unmovable, it can be reduced to the Riccati equation for genus $p = 0$, while for $p = 1$ its solution is expressed in terms of the Weierstrass elliptic \wp -function.

This approach can be useful in various physical problems, dealing with nonlinear P.D.E. with dissipation to obtain some new exact solutions and to study their stability .

REFERENCES

1. Samsonov A.M., On some exact travelling wave solutions for nonlinear hyperbolic equations, in: "Nonlinear waves and dissipative effects", D.Fusco, A.Jeffrey eds., Longman, London, pp.123-132 (1991).
2. Hermite C. Course Lithographie de l'Ecole Polytechnique, Paris (1873).
3. Whittaker E.T., G.N.Watson G.N. A Course of Modern Analysis, vol.2., Cambridge University Press, Cambridge (1962).
4. Samsonov A.M., On some exact solutions of nonlinear longitudinal wave equations with dispersion and dissipation, in: "Dispersive waves in dissipative fluids - Proc. Euromech Coll. 240, Bologna", D.G.Crighton, F.Mainardi eds., Tecnoprint, Bologna, pp.56-57 (1988).
5. Scott A. Active and Nonlinear Wave Propagation in Electronics. Wiley, New York et al. (1970).
6. Poincare H. Sur un theoreme de M.Fuchs. *Acta Mathematica*, 7 (1885).

CONTROLLING CHAOS IN HAMILTONIAN SYSTEMS

Ying-Cheng Lai^{1,2}, Mingzhou Ding³ and Celso Grebogi^{1,4}

¹Labotatory for Plasma Research
University of Maryland, College Park, MD 20742

²Department of Biomedical Engineering
The Johns Hopkins University School of Medicine
Baltimore, MD 21205

³Center for Complex Systems and Department of Mathematics
Florida Atlantic University, Boca Raton, FL 33431

⁴Department of Mathematics
Institute for Physical Science and Technology
University of Maryland, College Park, MD 20742

Abstract

An unstable periodic orbit in Hamiltonian systems often possesses complex conjugate eigenvalues at one or more of its orbit points. This renders the stabilization method used for controlling chaos proposed by Ott, Grebogi, and Yorke (OGY) not directly applicable to Hamiltonian systems. By introducing the notion of stable and unstable directions at each orbit point and incorporating such directions into a control scheme, we extend the original OGY method to the control of Hamiltonian chaos. Our method also includes an efficient algorithm for calculating the stable and unstable directions at each point of a given trajectory. Other issues related to controlling chaos in Hamiltonian systems are also discussed.

1. Introduction

It is highly desirable in many situations to control chaos in nonlinear dynamical systems^{1,2}. One of the most successful methods so far is the one proposed by Ott, Grebogi, and Yorke (the OGY method)². In this method, a chaotic trajectory can be converted into a periodic one by applying small, judiciously chosen temporal perturbations to an accessible system parameter. The method is advantageous in several regards. First, it does not require *a priori* knowledge of the system equations. A time series from measuring one of the system's dynamical variables in conjunction with the delay-coordinate embedding method³ is often sufficient to achieve the desired control. Second, the method is extremely flexible in that one can select to control any of the infinite number of unstable periodic orbits embedded in a chaotic attractor. This method has attracted a growing interest from a variety of scientific disciplines⁴⁻¹². It has been implemented experimentally to control chaotic motions in a host of physical systems,

including a magnetic ribbon⁵, a fluid convection system⁶, a spin-wave system⁷, a chemical system⁸, an electric diode⁹, and a laser system¹⁰. Extensions of the original method to control high dimensional dynamical systems¹¹ and to control transient chaos¹² have also been addressed.

In practical situations where chaotic systems are often situated in a noisy environment and the orbit to be controlled is of relatively high period, it is important to apply the parameter perturbations at each time step^{2,11}. Such a formalism has been proposed² for dissipative dynamical systems. It makes use of the eigenvalues and eigenvectors of the Jacobian matrix evaluated at each point of the unstable periodic orbit to be controlled. In Hamiltonian systems, however, an unstable periodic orbit typically has complex conjugate eigenvalues on the unit circle at one or more of its orbit points. In this case, the eigenvectors are not defined in the real plane. This fact can be illustrated by using the extensively studied standard map¹³, whose dynamical properties are believed to be typical in Hamiltonian chaotic systems,

$$(x_{n+1}, y_{n+1}) = [(x_n + y_n) \bmod(2\pi) - \pi, y_n + p \sin(x_n + y_n)], \quad (1)$$

where p is the control parameter. Figure 1 shows an unstable periodic orbit of period-7 superposed on a long chaotic trajectory in the chaotic sea for $p = 1$. The centers of the plus signs indicate the locations of the periodic points. The horizontal and vertical directions at each point signify the real and imaginary axes in the complex plane spanned by the eigenvalues. The nature of the eigenvalues is then schematically represented by two dots plotted on the plane. For the case shown in the figure, two of the seven orbit points have complex conjugate eigenvalues. We have also examined a large number of other periodic orbits and found similar mixings of real and complex conjugate eigenvalues along these orbits. In fact, one can show analytically that this is a general feature of the standard map, which is nonhyperbolic for $p = 1$. Here by "nonhyperbolic" we mean the existence of KAM surfaces in the chaotic sea.

Due to the existence of complex conjugate eigenvalues along the unstable periodic orbit, the original OGY formula for calculating the temporal parameter perturbation *at each time step* fails to apply in Hamiltonian systems. A possible remedy is to apply such perturbations at every m -th time step, assuming the period of the orbit is m . This approach is viable for noise-free Hamiltonian systems, but, as we have remarked earlier, it is extremely vulnerable to external or system noise, particularly if the period of the desired orbit is large¹⁴. Thus, it is imperative to devise an extension of the OGY method to allow for parameter perturbations at *each* time step of the system evolution.

To achieve this we first make the following observation. Let \mathbf{X}_n be the n -th point on a periodic trajectory. Consider a small circle around \mathbf{X}_n . Iterate the circle backward one step. The image is typically an ellipse around the point \mathbf{X}_{n-1} . This indicates that there is a direction in the neighborhood of \mathbf{X}_{n-1} along which the distance contracts and another direction along which the distance expands. If we use such directions in place of the eigenvectors in the original OGY formula, problems associated with complex eigenvalues become nonexistent. Our numerical examples show that the resulting control scheme works remarkably well. Thus a key question now is to find such stable and unstable directions¹⁵ at each periodic point. In the Appendix, we will discuss one such algorithm originally developed for dissipative systems¹⁵.

Another issue not associated with controlling dissipative chaos concerns the length of the initial chaotic transient τ before a trajectory can be controlled. In dissipative chaotic systems, for randomly chosen initial conditions, τ has an exponential probability distribution¹⁶, i.e., $P(\tau) \sim \exp[-(\tau / \langle \tau \rangle)]$ for large τ , where $\langle \tau \rangle$ is the average length of the transient and it scales algebraically with the range of the maximum allowable parameter perturbations². Thus $\langle \tau \rangle$ is always finite. In Hamiltonian systems, however, the probability distribution of τ is algebraic¹⁷⁻¹⁹:

$$P(\tau) \sim \tau^{-\alpha}, \quad (2)$$

due to the presence of KAM surfaces. Here α is the decay exponent with a value between 1 and 2. Thus the average transient time $\langle \tau \rangle$ in this case is infinite regardless of the range of the parameter perturbation. Such a long transient time τ may pose a major difficulty in controlling Hamiltonian chaos if the physical system operates under a constrained time frame. This issue is addressed to a certain degree by the recent

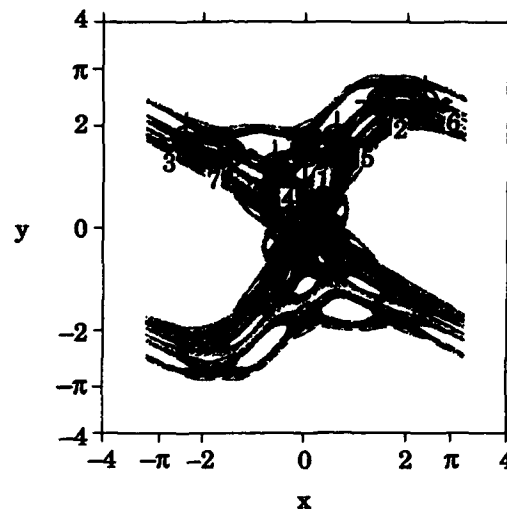


Figure 1: A period-7 orbit superposed on a long chaotic trajectory initiated at $(x, y) = (0.5, 0.5)$. The white regions $\{(x, y) \in [-\pi, \pi]\}$ denote the KAM islands. The locations of the periodic points are indicated by the plus signs. The horizontal and vertical lines at each point signify the real and imaginary axes in the complex plane spanned by the eigenvalues. If the two dots are on the horizontal axis the periodic point has real eigenvalues. If the two dots are one on the unit circle then the point possesses complex conjugate eigenvalues. The integers denote the order of orbit points under iterations of the map.

advances in an area called 'targeting' in which an initial condition is rapidly guided to a desired location in the phase space using parameter perturbations. The algorithm currently proposed for dissipative systems²⁰ appears to be directly applicable to cases we consider in this paper²¹. But features novel to Hamiltonian systems seem to suggest that a more sophisticated routine be needed to form a general targeting package for Hamiltonian problems. We will discuss some of these features in Sec. 3.

The organization of the paper is as follows. In Sec. 2, we review the basic theory of the OGY method and derive an expression for temporal parameter perturbations that explicitly involves the stable and unstable directions discussed earlier. In Sec. 3, we present our numerical results for the standard map and briefly discuss the issue of 'targeting' and the effect of external noise. In Sec. 4, we present the conclusion. In the Appendix, we describe a method to calculate the stable and unstable directions along a trajectory (which can be either periodic or chaotic).

2. The Method of Controlling Chaos

We formulate the theory for discrete dynamical systems or maps of the form

$$\mathbf{X}_{i+1} = \mathbf{F}(\mathbf{X}_i, p), \quad (3)$$

where $\mathbf{X}_i \in \mathbb{R}^2$, $p \in \mathbb{R}$ is an adjustable parameter, and \mathbf{F} is a smooth function in both variables. We restrict the parameter perturbation to be small, i.e.,

$$|p - p_0| < \delta, \quad (4)$$

where p_0 is some nominal parameter value and δ is a small number defining the range of p variation. The procedure of controlling chaos works as follows. First, we choose an unstable periodic orbit embedded in the chaotic sea that yields the best system performance according to some criterion. We next define a small region around each of the periodic point whose size is proportional to δ . Suppose that an initial condition is chosen randomly in the chaotic sea. Due to ergodicity, the resulting trajectory will enter the small region about one of components of the periodic orbit. After this takes place, we perturb the parameter in such a way that the system is stabilized around the chosen periodic orbit.

More specifically, assume that an unstable orbit of period- m is $\mathbf{X}_{O1}(p) \rightarrow \mathbf{X}_{O2}(p) \rightarrow \dots \rightarrow \mathbf{X}_{Om}(p) \rightarrow \mathbf{X}_{O(m+1)}(p) = \mathbf{X}_{O1}(p)$. The linearized dynamics in the neighborhood of the period- m orbit is then

$$\mathbf{X}_{n+1} - \mathbf{X}_{O(n+1)}(p_n) = \mathbf{M} \cdot [\mathbf{X}_n - \mathbf{X}_{On}(p_n)], \quad (5)$$

where \mathbf{M} is the two-dimensional Jacobian matrix at the orbit point \mathbf{X}_{On} , $p_n = p_0 + (\Delta p)_n$, $(\Delta p)_n \leq \delta$. The shift in the locations of these periodic points can be written as:

$$\mathbf{X}_{On}(p_n) - \mathbf{X}_{On}(p_0) \approx (\Delta p)_n \mathbf{g}_n, \quad (6)$$

where $\mathbf{g}_n = \partial \mathbf{X}_{F(n)}(p) / \partial p|_{p_0}$.

In Eq. (5), the Jacobian matrix \mathbf{M} will not be expressed in terms of eigenvalues and eigenvectors, because there may exist complex conjugate eigenvalues at some of the periodic points. Instead we explore the stable and unstable directions associated with these points. It is worthy noting that the stable and unstable directions do not necessarily coincide with the eigenvectors¹⁵ at a given periodic point if $m \neq 1$. To see how such stable and unstable directions arise at a periodic point, let us choose a small circle of radius ϵ around the point \mathbf{X}_{On} . In Cartesian coordinates with the origin at \mathbf{X}_{On} , the circle can be expressed as $dx^2 + dy^2 = \epsilon^2$. After one backward iteration, the image of the circle under \mathbf{F}^{-1} in Cartesian coordinates with the origin at $\mathbf{X}_{O(n-1)}$ can be expressed as $A(dx')^2 + B(dx')(dy') + C(dy')^2 = 1$ which is typically an ellipse, where A, B and C are functions of the entries of the Jacobian matrix at \mathbf{X}_{On} . This means that distances along the major axis of the ellipse contracts as a result of the map. Similarly distances along the minor axis expand under \mathbf{F} . The images of the

major and minor axes of the ellipse at $\mathbf{X}_{O(n-1)}$ under \mathbf{F} approximate the stable and unstable directions at $\mathbf{X}_{O(n)}$. A systematic method of finding these stable and unstable directions for general two-dimensional maps will be presented in the Appendix.

Let $\mathbf{e}_{s(n)}$ and $\mathbf{e}_{u(n)}$ denote the stable and unstable vectors at $\mathbf{X}_{O(n)}$, and let $\mathbf{f}_{s(n)}$ and $\mathbf{f}_{u(n)}$ be the corresponding contravariant vectors such that $\mathbf{f}_{u(n)} \cdot \mathbf{e}_{u(n)} = \mathbf{f}_{s(n)} \cdot \mathbf{e}_{s(n)} = 1$ and $\mathbf{f}_{u(n)} \cdot \mathbf{e}_{s(n)} = \mathbf{f}_{s(n)} \cdot \mathbf{e}_{u(n)} = 0$. The central point of the OGY method is to require that the iteration of a trajectory point in the small neighborhood around $\mathbf{X}_{O(n)}$ lies on the stable direction at $\mathbf{X}_{O(n+1)}$, i.e.,

$$[\mathbf{X}_{n+1} - \mathbf{X}_{O(n+1)}(p_n)] \cdot \mathbf{f}_{u(n+1)} = 0. \quad (7)$$

Substituting Eqs. (5) and (6) into Eq. (7), we obtain the following expression for the parameter perturbations,

$$(\Delta p)_n = \frac{\{\mathbf{M} \cdot [\mathbf{X}_{n+1} - \mathbf{X}_{O(n+1)}(p_n)]\} \cdot \mathbf{f}_{u(n+1)}}{[(\mathbf{M} \cdot \mathbf{g}_n) - \mathbf{g}_{n+1}] \cdot \mathbf{f}_{u(n+1)}}, \quad (8)$$

where \mathbf{M} is evaluated at $\mathbf{X}_{O(n)}$. Note that the quantities in Eq. (7) are all experimentally accessible through the time-delay embedding method. In particular, the Jacobian matrices and their inverses along a periodic orbit can be obtained by using the algorithm proposed by Eckmann and Ruelle²². It should be emphasized that the parameter perturbations calculated from Eq. (8) apply to the system at *each* time step. This is essential to minimize the effect of external noise^{2,11,14} when the system is in a noisy environment.

3. Numerical Results and Discussions

In this section we apply the method developed in Sec. 2 to control chaotic motions in the standard map. The periodic orbit we choose to stabilize is the one shown in Fig. 1. The result is shown in Fig. 2 where the x coordinate of the trajectory point is plotted in the vertical direction and time is plotted in the horizontal direction. The control region near every periodic point on the period-7 trajectory is a small circle of radius 0.01. The range of parameter perturbation is $\delta = 0.01$. An interesting feature of the time series in Fig. 2 is the appearance of 'holes' in the uncontrolled trajectory. These holes are due to the presence of KAM islands. Specifically, when the trajectory approaches the neighborhood of some KAM islands associated with an elliptic periodic orbit, it tends to stay near the islands for a long period of time. When this occurs, the trajectory only wanders around the KAM islands and spares the chaotic region between the KAM islands, thus leaving unfilled regions in the projection of the trajectory on the x axis.

The extremely long chaotic transient (on the order of 10^4 in Fig. 2 and even on the order of 10^6 for some other cases we have examined) before the trajectory can be stabilized is caused by the stickiness effect of KAM surfaces. The average transient time is in fact infinite according to Eq. (2). This situation is fundamentally different from that in the control of dissipative chaotic systems. A possible solution to this problem is to introduce the 'targeting'²⁰ technique in which a point is brought rapidly to the desired place (the 'target') via small parameter perturbations. For the case shown in Fig. 2, the targeting algorithm proposed for dissipative systems is directly applicable. The reason is that the initial condition and the target are located in the same ergodic component of the phase space separated from other components by the Cantori²³, fractal remains of KAM surfaces. It is not at all clear whether such a targeting method works effectively in bringing particles from one ergodic component to another and then to the target. Thus devising a general scheme of targeting suitable to the Hamiltonian phase space structure remains an open question.

The influence of external noise on control can be severe. A trajectory stabilized around a unstable periodic orbit may be occasionally 'kicked' out of the controlling region². The effect of noise is reduced in some cases by allowing the magnitude of the parameter perturbation to exceed the average amplitude of the noise. Even in such

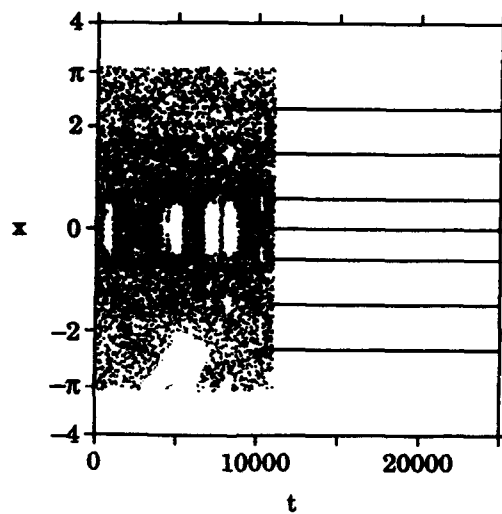


Figure 2: The x coordinate of the trajectory versus time. After the control is turned on the motion is stabilized around the desired unstable period-7 orbit. Notice that the initial chaotic transient is quite long in this case (on the order of 10^4), as compared with the typical initial transient in dissipative chaotic systems². The "holes" in the time series of the uncontrolled chaotic transient is due to the "stickiness" effect of the KAM surfaces.

cases, there is still a probability of the controlled trajectory being kicked out. In dissipative systems, this is not such a serious problem because, after a rather short chaotic transient, the trajectory comes back to the desired controlling region. In Hamiltonian systems, however, when this occurs, the trajectory will experience an extremely long transient before it comes close to the controlling region, as discussed above. Thus the two ingredients discussed in this paper, namely, targeting and applying parameter perturbation at every time step, appear to be essential to achieve satisfactory control of chaotic motions in Hamiltonian systems.

4. Conclusion

In this paper, the original OGY method of controlling chaos is extended to Hamiltonian systems. The extended method allows one to apply parameter perturbations at each time step, thus minimizing the effect of noise. Specifically, we obtain an expression for the temporal parameter perturbation using the stable and unstable directions at each periodic point, overcoming the difficulty presented by the fact that unstable periodic orbits in Hamiltonian systems often possess complex conjugate eigenvalues²⁴. We also discuss the effect of KAM islands on the control, which leads us to believe that a practical control of Hamiltonian chaos should include a general targeting algorithm as an integral part.

Appendix: Calculating Stable and Unstable Directions

From the Jacobian matrices one can calculate the stable and unstable directions at each orbit point, from which one obtains $f_{u(n+1)}$ in Eq. (8). To this end we discuss an algorithm developed in Ref. [15]. This algorithm also works for chaotic trajectories.

To find the stable direction at a point X , we first iterate this point forward under the map N times and get a trajectory $F^1(X)$, $F^2(X)$, ..., $F^N(X)$. Now imagine we put a circle of arbitrarily small radius ϵ at the point $F^N(X)$. If we iterate this circle backward once, the circle will become an ellipse at the point $F^{N-1}(X)$ with the major axis along the stable direction of the point $F^{N-1}(X)$. We continue iterating this ellipse backwards, while at the same time keeping the ellipse's major axis of order ϵ via certain normalization procedures. When we iterate the ellipse all the way back to the point X , the ellipse becomes very thin with its major axis along the stable direction at point X .

In practice, instead of using a small circle, we take a unit vector at the point $F^N(X)$ since the Jacobian matrix of the *inverse map* F^{-1} rotates a vector in the tangent space of F towards the stable direction. Thus, we iterate a unit vector backward to point X by multiplying by the Jacobian matrix of the inverse map at each point on the *already existing* orbit. We normalize the vector after each multiplication to the unit length. For sufficiently large N , the unit vector we get at point X is a good approximation of the stable direction at X . A key point in the calculation is that we do *not* actually calculate the inverse Jacobian matrix along the trajectory *by* iterating the point $F^N(X)$ backwards using the inverse map F^{-1} . The reason is that if we do so, the trajectory will usually diverge from the original trajectory $F^N(X)$, $F^{N-1}(X)$, ..., $F^1(X)$ after only a few backward iterations. What we do is to store the inverse Jacobian matrix at every point of the orbit $F^i(X)$ ($i = 1, \dots, N$) when we iterate forward the point X beforehand.

Similarly, to find the unstable direction at point X on the chaotic set, we first iterate X backward under the inverse map N times to get a backward orbit $F^{-j}(X)$ with $j = N, \dots, 1$. We then choose a unit vector at point $F^{-N}(X)$ and iterate this unit vector forward to point X by multiplying by the Jacobian matrix of the map N times since the Jacobian matrix of the forward map rotates a vector towards the unstable direction. We normalize the vector to the unit length at each step. The final vector at point X is a good approximation of the unstable direction at that point if N is large enough. Again, to avoid divergence from the original trajectory, we do not actually iterate the inverse map. What we do in this case is to choose X to be the end point of a forward orbit, all the points before X are the inverse images of X and we store the

Jacobian matrix of forward map at those points.

The method so described is very efficient. Particularly, it converges fast. For $N = 20$, the error between the calculated and real stable (or unstable) directions is on the order of 10^{-10} for chaotic trajectories in the Hénon map¹⁵. For the standard map we find similar rate of convergence.

Acknowledgement

We thank Tamás Tél for discussions. This work was supported by the Department of Energy (Scientific Computing Staff, Office of Energy Research).

References

1. A. Hubler, *Helv. Phys. Acta.* **62**, 343(1989); T. B. Fowler, *IEEE Trans. Autom. Control* **34**, 201(1989); B. A. Huberman and E. Lumer, *IEEE Trans. Circuits Syst.* **37**, 547(1990).
2. E. Ott, C. Grebogi and J. A. Yorke, *Phys. Rev. Lett.* **64**, 1196(1990); and in *Chaos: Soviet-American Perspectives on Nonlinear Science*, Edited by D. K. Campbell (American Institute of Physics, New York, 1990).
3. N. H. Packard *et al.*, *Phys. Rev. Lett.* **45**, 712(1980); F. Takens, in *Dynamical Systems and Turbulence*, Edited by D. Rand and L. S. Young (Springer, Berlin, 1981).
4. U. Dressler and G. Nitsche, *Phys. Rev. Lett.* **68**, 1(1992).
5. W. L. Ditto, S. N. Raaseo and M. L. Spano, *Phys. Rev. Lett.* **65**, 3211(1990).
6. J. Singer, Y. -Z. Wang and H. H. Bau, *Phys. Rev. Lett.* **66**, 1123(1991).
7. A. Azevedo and S. M. Rezende, *Phys. Rev. Lett.* **66**, 1342(1991).
8. B. Peng, V. Petrov and K. Showalter, *J. Phys. Chem.* **95**, 4957(1991).
9. E. R. Hunt, *Phys. Rev. Lett.* **67**, 1953(1992).
10. R. Roy, T. W. Murphy, Jr., T. D. Maier and Z. Gills, *Phys. Rev. Lett.* **68**, 1259(1992).
11. F. J. Romeiras, C. Grebogi, E. Ott and W. P. Dayawansa, *Physica* **58D**, 165(1992).
12. T. Tél, *J. Phys. A: Math. Gen.* **24**, L1359(1991).
13. B. V. Chirikov, *Phys. Rep.* **52**, 263(1979).
14. Note that a trajectory originally in the neighborhood of a period- m orbit leaves the orbit exponentially like $\exp(\lambda_u m)$, where $\exp(\lambda_u) > 1$ is the unstable Lyapunov number of the orbit. Under the influence of noise, if control is applied at every m th time step, the trajectory will deviate from the orbit rapidly before the next parameter control can be applied and the orbit may be decontrolled. Hence, it is desirable that the control be applied at *each* time step.
15. Y. C. Lai, C. Grebogi, J. A. Yorke and I. Kan, "How often are chaotic saddles nonhyperbolic?", to be published in *Nonlinearity*.
16. C. Grebogi, E. Ott and J. A. Yorke, *Physica* **7D**, 181(1983); P. Romeiras, C. Grebogi, E. Ott and J. A. Yorke, *Phys. Rev. A* **36**, 5365(1987).
17. C. F. F. Karney, *Physica* **8D**, 360(1983).
18. B. V. Chirikov and D. L. Shepelyansky, *Physica* **13D**, 395(1984).

19. J. D. Meiss and E. Ott, Phys. Rev. Lett. **55**, 2741(1985) and Physica **20D**, 387(1986).
20. T. Shinbrot, E. Ott, C. Grebogi and J. A. Yorke, Phys. Rev. Lett. **65**, 3215(1990).
21. T. Shinbrot, private communication.
22. J. -P. Eckmann and D. Ruelle, Rev. Mod. Phys. **57**, 617(1985).
23. R. S. Mackay, J. D. Meiss and I. C. Pervival, Phys. Rev. Lett. **52**, 697(1984) and Physica **13D**, 55(1984).
24. After we completed the present work, we received a preprint by C. Reyl, L. Flepp, R. Badii and E. Brun who demonstrated the control of NMR-Laser chaos in high-dimensional embedding space. In their system, there also exist complex eigenvalues. Since the system is dissipative, those complex eigenvalues are not on the unit circle. They developed a modified OGY method in which parameter perturbations are chosen to minimize the norm $\|X_{n+1} - X_{F(n+1)}(p_n)\|$ in Eq. (4). Their method does not make use of the geometric structure of unstable periodic orbits, and consequently, is quite different from the method we presented in this paper.

DETERMINISTIC DISORDER IN TWO-DIMENSIONAL MEDIA

Mikhail I. Rabinovich and Anatoly L. Fabrikant

Institute of Applied Physics
Russian Academy of Science
603600 Nizhny Novgorod, Russia

INTRODUCTION

The idea that random distributions of physically meaningful fields in space may be deterministically generated was put forth considerably after the discovery of dynamical chaos.^{1,2,3,4} Such investigations, however, could have been expected much earlier, in the beginning of the seventies, because of a very close analogy between the time series generated by dynamical systems and one-dimensional spatial field distributions described by ordinary differential equations in which spatial coordinate plays the part of time.

Radically new problems arise in the analysis of spatial chaos even in a one-dimensional case. They are, in the first place, the evolutionary origin of disorder (i.e. its birth out of regular initial distribution), stability of disorder to small perturbations (detection among different statical irregular distributions of stable, metastable and unstable ones), and, finally, grouping of various field distributions according to their degree of complexity. The latter is not an easy task because nearly identical spatial correlation functions or Fourier spectra may correspond to spatial distributions of different complexities.

Irregular spatial field distributions are now being broadly investigated in various branches of micro- and macrophysics. Aspects of interest are, for example, topological disorder of defects in a crystal lattice,⁵ chaotic distribution of field intensity across a Fabry-Perot resonator at large Fresnel numbers in nonlinear optics,⁶ the distribution of vertical velocity component in a horizontal layer of fluid in Rayleigh-Bénard convection,⁷ density distribution of matter in Galaxy, etc. The universal language of nonlinear dynamics is a useful tool in understanding the origin of spatial disorder in different fields of physics. Thus, experience gained in the investigation of turbulence, for instance, may be employed in the theory of superconductivity.

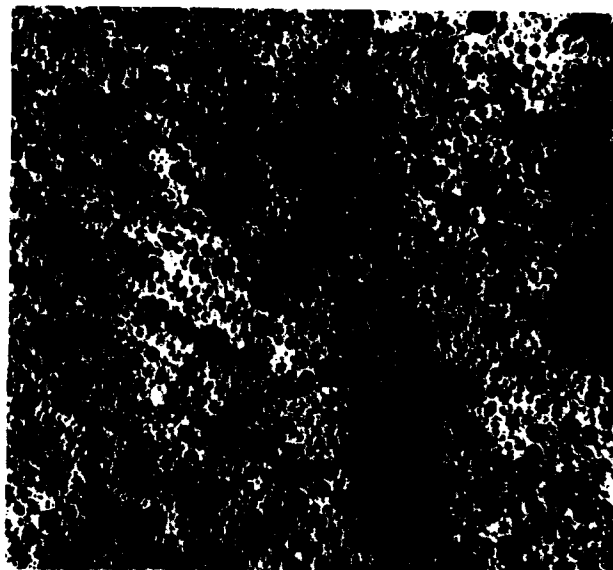


Figure 1: Disorder of bubbles in soapy foam.

This paper is concerned, primarily, with ideas and results related to analysis of two-dimensional spatial field distributions. The architecture of the paper is as follows. Deterministically generated disorder of two-dimensional fields is defined in Section 2 in which a method for the diagnostics of finite-dimensional spatial chaos using analysis of a translational dynamical system with two times is also considered. Typical scenarios of the birth of finite-dimensional spatial disorder (the "crystal - quasicrystal - disorder" transitions, as well as transitions through defect formation and intermittency) are analysed in Section 3. The evolution of regular field states to disorder through the birth of localized structures, their random pinning and the resulting stochastic spatial patterns is investigated in Section 4. Section 5 is devoted to perspectives in the development of ideas on deterministic disorder; diagnostics of fields of different physical origins (wind waves, in particular) using a method for the calculation of spatial correlation dimension is also considered.

SPATIAL CORRELATION DIMENSION OF A SNAPSHOT

Can a given spatial disorder such as, for example, the one depicted in Fig. 1 be deterministically generated? This question may be answered using the processing of spatial distributions of multidimensional fields that was proposed in.⁸ This method is essentially as follows.

We introduce the notion of phase space for a two-dimensional space series $u(x_i, y_i)$ (like in the case of one-dimensional time series). To this end, we make the snapshot of the two-dimensional space series $u(x, y)$ discrete, i.e. we represent it as a grid with the x_i, y_j -nodes and consider the values of the space series for each of them: $u_{i,j} = u(x_i, y_j)$. Each node has two indices, it has neighbours on the left and on the right, as well as on top and at the bottom. We introduce a discrete final clus-

ter $A_{K,L}^{(m)} = \{(u_{i,j}), i = K, \dots, K+m-1, j = L, \dots, L+m-1\}$ that is determined by $(m \times m)$ points. By shifting this cluster (which is now not a set of numbers like in a one-dimensional case but a square matrix) along the space series we obtain a trajectory in a matrix space that can also be called phase space.

Using this approach, like for time series, we can determine correlation dimension and all the characteristics that were formerly used for the description of stochastic sets in an ordinary phase space, we mean entropy, Lyapunov exponents, etc. If the stochastic set determined in this fashion has a finite dimension, then the snapshot of interest may be referred to as finite-dimensional disorder.

This program may be implemented using a formal mathematical language. Consider a set of continuous (vector) functions $u(x), x \in R^d, u \in R^p$ employing conventional procedures of summation and scaling up. Introducing into this set a distance we obtain a metric space B that will be referred to as the phase space of the system. To each d -dimensional vector $\alpha = (\alpha_1, \dots, \alpha_d) \in R^d$ we associate the translation map $T^\alpha : B \rightarrow B$ that is determined by the expression $T^\alpha u(x) = u(x + \alpha)$. Thus we determine the action of the group R^d on B or, in other words, we have a dynamical system with d times that will be referred to as a translational dynamical system.

If the process under study is such that knowing the initial state (initial field distribution) one can unambiguously determine the subsequent states at any moment of time, then a semigroup of evolution operators $\{S^t\}_{t \geq 0}$ also acts on B , i.e. an evolutionary dynamical system is determined as well. The behaviour of the trajectories of translational and evolutionary dynamical systems in the common phase space B gives a full mathematical description of the spatio-temporal properties of the nonequilibrium medium of interest.

Generalizing the algorithms presented in,⁹ we can propose the algorithms for the calculation of correlation and pointwise dimensions of the snapshots. Let us take a two-dimensional snapshot u in the form of an array $(u_{i,j}, i, j \in Z_+)$. In practice, the array, naturally, has a limited size: $i \leq N_1, j \leq N_2$, but N_1 and N_2 are supposed to be sufficiently large numbers. For each integer $m \geq 1$ we can construct from the array $\{u(i,j)\}$ $(m \times m)$ matrices: $A_{K,L}^{(m)} = \{(u_{k,l}), k = K, \dots, K+m-1, l = L, \dots, L+m-1\}$. Let us define the correlation integral in the form

$$C^{(m)}(\varepsilon) = \frac{R^{(m)}(\varepsilon)}{[(N_1 - m)(N_2 - m)]^2}; \quad (1)$$

$$R^{(m)}(\varepsilon) = \#\{((K, L), (K', L')) : \text{dist}(A_{K,L}^{(m)}, A_{K',L'}^{(m)}) \leq \varepsilon\}, \quad (2)$$

where $\#(E)$ is the number of elements in the set E . Then, it can be shown that for sufficiently small ε , the $\log C^{(m)}(\varepsilon) / \log \varepsilon$ ratio will be approximately equal to the correlation dimension D_s of the two-dimensional snapshot in m -dimensional embedding space.

Following¹⁰ we will estimate the minimal size of the array $(u_{i,j})_{N_1 \times N_2}$ that is needed for correct calculation of the dimension on the interval $[\varepsilon_1, \varepsilon_2]$. Because

$$D_s \cong \frac{\log_2 C^{(m)}(\varepsilon'') - \log_2 C^{(m)}(\varepsilon')}{\log_2 \varepsilon'' - \log_2 \varepsilon'}, \quad (3)$$

where $C^{(m)}(\varepsilon') \geq \frac{1}{N_1^2 N_2^2} \cdot C^{(m)}(\varepsilon'') \leq 1$, then, assuming $\varepsilon'' = 2^k \cdot \varepsilon'$, we will estimate the dimension:

$$D_s \leq \frac{2}{K} \cdot \log_2(N_1 \cdot N_2) \quad (4)$$

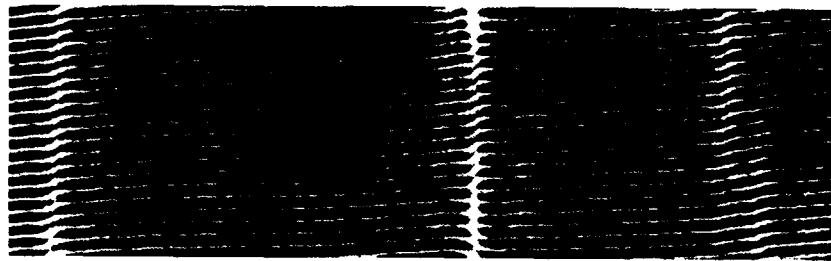


Figure 2: Transverse defects against the background of rolls in a liquid crystal.

Thus, when determining the correlation dimension of a multidimensional snapshot one must bear in mind that the number of discretization points along each time coordinate may be much smaller than in the case of one-dimensional time.

SCENARIOS OF THE BIRTH OF FINITE-DIMENSIONAL SPATIAL DISORDER

Because spatial disorder may be considered only within large-box problems we will analyse only the two groups of physical experiments which meet this requirement. We will take Faraday ripples on the surface of a parametrically excited horizontal layer of liquid and Bénard-Marangoni convection with large aspect ratio.

One might think that Nature has designed these flows purposefully for the investigation of spatial disorder. In both cases, static spatial structures are born near the threshold of spontaneous symmetry breaking. The difference is that they are actually static ones in the case of convection, while for capillary ripples the entire picture oscillates with a frequency equal to half-frequency of gravity field oscillations. The structures in the latter case are static if they are observed stroboscopically with appropriate period. Note that capillary ripples are of particular interest to experimenters because they can use an additional control parameter: the frequency of parametrically excited capillary waves. As frequency changes, resonant interaction between excited waves and, consequently, the behaviour of spatial structures change too. Besides, spatial structures may appear according to different scenarios depending on the parameters.

Modulation Disorder

Examples of modulation disorder are transverse chaotic modulation against the background of a regular lattice of Faraday ripples¹¹ and irregular sequence of transverse defects against the background of rolls (see Fig. 2) in magnetohydrodynamic convection in a liquid crystal.¹² A single defect of this type may look like two identical lattices of rolls, that fill the upper and lower half-spaces and are displaced half a period relative to one another. These transverse defects are, as a rule, repeated irregularly along the y -axis.

The disorder of transverse defects reminds the disorder of localized structures that

was discussed in.¹³ The similarity will be even more complete if we filter the initial periodic lattice. This can be done by representing the initial field in the form $u(x, y, t) = A(y, t)e^{ix} + c.c.$ (the lattice period is supposed to be equal to 2π). Substituting this solution into initial equations we obtain a fourth-order Newell-Whitehead-Sigel (NWS) equation for complex amplitude along y :

$$\frac{\partial A}{\partial t} = A + \gamma A^* - \frac{\partial^4 A}{\partial y^4} - A |A|^2 \quad (5)$$

When $\gamma \neq 0$, this equation takes into account periodic (with the period π) inhomogeneity of the medium. In the case of convection, this is, for example, a periodic inhomogeneous temperature distribution at the lower boundary of the layer.

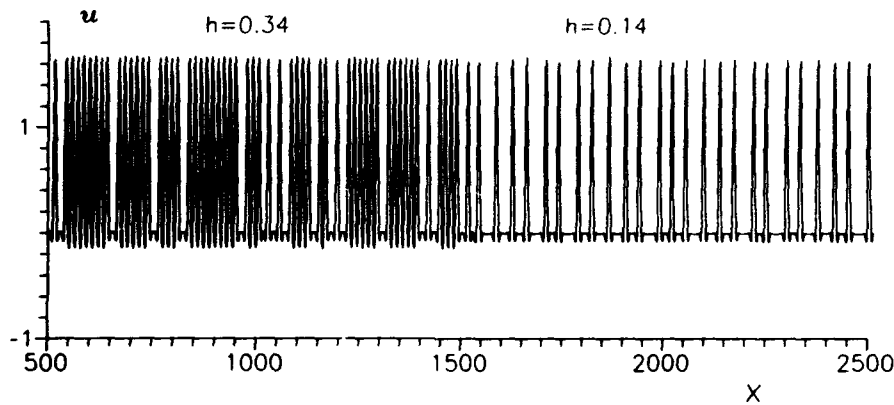


Figure 3: Disorder of solitons in a one-dimensional analog of (7).

The solutions of (5) that describe stationary jumps of the phase $A(y)$ by π correspond to defects. The absolute value of $A(y)$ then tends to constant A_0 as $y \rightarrow \pm\infty$. Equation (5) is also a gradient model. Therefore all statical regimes that are established in our system as $t \rightarrow \infty$ (the ones with defects – jumps – including) must be described by ordinary differential equation

$$A_{yyyy} - A(1 - |A|^2) + \gamma A^* = 0 \quad (6)$$

We can show that there exists in the phase space of this dynamical system a countable set of homoclinic trajectories which correspond to localized structures of phase and amplitude.

Single defects correspond only to the simplest homoclinic trajectory in the phase space of (6). This equation must describe, besides simplest localized states, more complicated combinations of "solitons", including their chaotic sequences like the ones presented in Fig. 3.

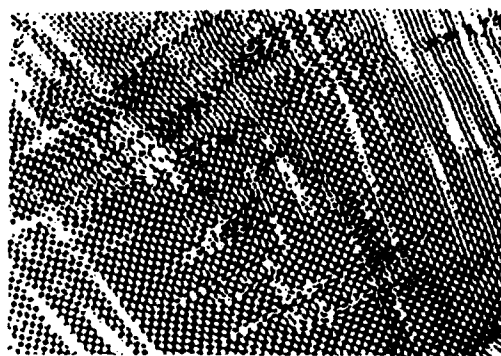


Figure 4: Disorder of defects in capillary ripples.

Note that such chaotic distributions of transverse defects also exist in the absence of periodic inhomogeneity along x , i.e. when $\gamma = 0$. They agree qualitatively with the picture observed in experiments (see Fig. 2).

Finite-Dimensional Topological Disorder

As supercriticality (the Rayleigh or Marangoni number in convection, a relative amplitude of the oscillating portion of gravity field in Faraday ripples) increases, the spatial picture of the flow in the form of a square or a hexagonal lattice or a simple one-dimensional lattice of rolls loses its stability, as a rule, due to the birth of defects¹ (Fig. 4). The increase in supercriticality results in the growth of the number of defects randomly placed in the lattice and, thus, spatial disorder emerges. Is this disorder deterministically generated? The answer to this question can be found by calculating the spatial correlation dimension of the snapshot. The results are presented in Fig 5. One can see that the dimension is, actually, finite! The dimension grows with increasing supercriticality, which confirms our intuitive ideas that the development of spatial disorder implies the birth of new independent spatial excitations. To put it in other words, spatial correlation dimension may be used as a qualitative characteristic of the complexity of inhomogeneous distribution of a two-dimensional field.

We would like to add to this that in the case of capillary ripples a dynamical system capable of generating snapshots like the ones depicted in Fig. 4 may be obtained from initial equations of motion for liquid surface, given that spatial interaction of counter-propagating capillary waves with unfixed transverse structure are taken into account (see also¹⁴). Apparently, it would be interesting to calculate the correlation dimension of computer snapshots and compare the obtained dependence of D , on supercriticality with the one given in Fig. 5b.

Capillary Quasicrystals

It was only yesterday that stable quasicrystal structures appeared to be inher-

¹Using a spectral language one can consider many defects of two-dimensional fields as a superposition of several spatial modes having close wave numbers.

ent solely in objects of microphysics.⁵ However quite recently there have appeared remarkable experiments in which macro-quasicrystals have been observed in capillary ripples.^{16,17}

The structure of the patterns observed on the surface of a parametrically excited liquid layer at small supercriticality depends on the type of nonlinearity and on the extent of dissipation. By varying the amplitude of external oscillating field and its frequency one can control these properties of the medium, even if the liquid remains unchanged. At sufficiently strong dissipation, only simple regular lattices with square cells (given small square field nonlinearity) or hexagonal cells (when this nonlinearity is strong enough) are observed on the surface. A square lattice is a superposition of two mutually orthogonal standing waves having equal absolute values of the wave number k that is determined by dispersion law for capillary ripples: $ga^2k^3 \approx \pi^2 f_p^2$ (here f_p is the frequency of oscillating gravity field, a stands for capillary length, and g is acceleration of gravity). All standing or travelling waves with the wave numbers $|\vec{k}| = k$ that make

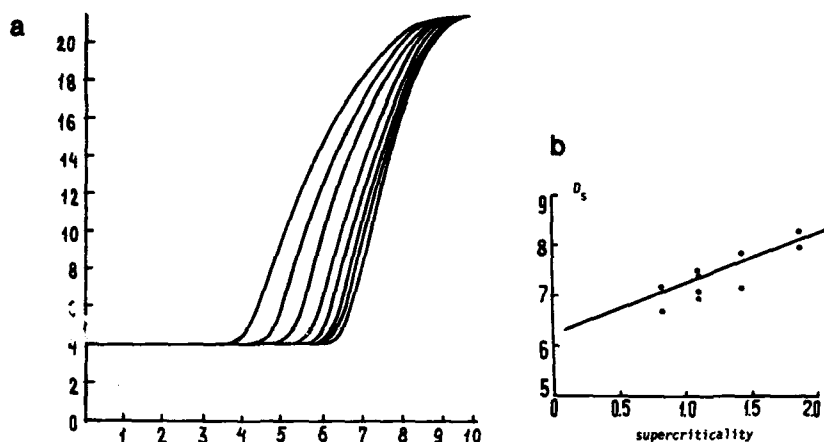


Figure 5: a. Correlation integral corresponding to Fig. 4. b. Correlation dimension of snapshots of capillary ripples as a function of supercriticality.

an arbitrary angle with the observed patterns have, in principle, equivalent conditions for the excitation in a linear approximation. At a nonlinear stage, however, they are suppressed due to mode competition. In view of equal potentialities of all waves having equal absolute values of k , the orientation of the established lattice depends only on random initial conditions.

For sufficiently strong nonlinearity, the capillary waves with $\vec{k}_{1,2,3}$ ($|\vec{k}_{1,2,3}| = k$) making an angle of 60° relative to one another are coupled resonantly. The resonant condition, $\vec{k}_1 + \vec{k}_2 = \vec{k}_3$, is met in this case, which guarantees the onset of a hexagonal lattice.

As supercriticality increases, the effect of competition becomes less significant and the picture gets more complicated: now several (> 2) standing waves, the angle between which is determined by the condition of interaction minimum, may steadily co-exist in the regime established. We would like to remind our reader that, for given k , identical cells may fill the plane only if these cells are squares or hexagons. Consequently, only four or six excited travelling waves produce a crystal lattice of capillary ripples. The excitation of eight (or four standing) waves gives a quasicrystal structure! Christiansen and his co-authors¹⁸ observed such a quasicrystal structure (see Fig. 6).

Stable observation of capillary quasicrystals enables one to reveal, as the control parameter is changed, the "quasicrystal - spatial disorder" transition. Relevant exper-

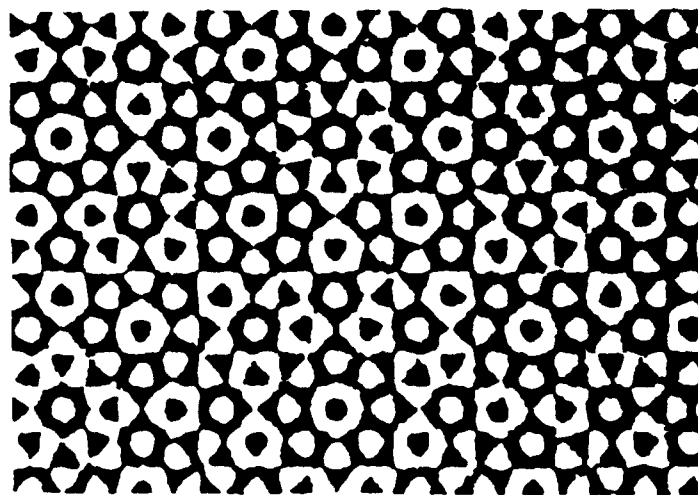


Figure 6: Capillary quasicrystals formed by four standing waves.

iments are now being carried out by our group (Nizhny Novgorod) employing as an additional parameter periodicity of the bottom. Note that a similar transition, "incommensurability - spatial chaos", is well known for the case of one spatial coordinate. The destruction of an open winding on a torus as a result of additional forcing and formation of a stochastic set corresponds to such a transition in the phase space of a dynamical system (see also¹⁷).

RANDOM PINNING OF LOCALIZED STRUCTURES

While discussing possible scenarios of the birth of spatial disorder we were concerned only with fairly small supercriticality and were interested, primarily, in the destruction of "weakly nonlinear lattices". In the case of supercritical bifurcations, when trivial equilibrium is unstable, the variation of the control parameter or in time leads to successive formation of new, nearly harmonic, spatial excitations. The situation is usually different in the case of subcritical bifurcations. Elementary excitations are strongly nonlinear, which means, if we employ a spectral language, that they contain a great number of spatial harmonics. The most significant example of such strongly nonlinear excitations are localized states of a two-dimensional field. The interaction of such excitations may give rise to both a regular lattice and topological disorder, like that observed in solids. We will consider the onset of such a disorder in time assuming nearly harmonic conditions.¹⁸

Consider a generalized Swift-Hohenberg equation that describes subcritical bifurcation:

$$\frac{\partial u}{\partial t} = -u + \beta u^2 - u^3 - (\kappa_0^2 + \nabla^2)^2 u \quad (7)$$

The parameter β determines the instability threshold (only disturbances of finite amplitude $u > u_0$, where $u_0 = [\frac{L}{2} - (\beta^2/4 - (1 + \kappa_0^4))^{1/2}]$ and L/κ_0 is the characteristic spatial scale of the system, increase). Such a model describes many bistable systems.

In order to describe the transformation of spatial field distribution we analyse the spatial spectrum of space series and the evolution of spatial entropy in time in a one-dimensional case. We show that a nearly harmonic initial field distribution transforms in the course of time into a lattice of solitons that move apart, due to instability, at a random distance from one another and stick at potential minima forming, as $t \rightarrow \infty$, a static disordered lattice. The statistical characteristics of this lattice depend on the period of initial field distribution. If the initial distribution has different periods in different portions, then, as $t \rightarrow \infty$, an inhomogeneous static regime with "different" disorder is established for which piece-wise constant dependence of entropy on coordinate is typical. We would like to note that the mechanism responsible for the birth of spatial chaos due to random pinning of defects in an oscillating potential of one another was proposed within a one-dimensional model with supercritical bifurcation by Coulet, Elphick and Repaux.¹

We will be interested in the time evolution of spatial distributions of a two-dimensional "field" that is described by Eq. (7) that may be represented in a gradient form

$$\frac{\partial u}{\partial t} = -\frac{\delta F}{\delta u}, \quad (8)$$

where $F = \int_{\Omega} [\frac{1}{2}u^2 - \frac{\beta}{3}u^3 + \frac{u^4}{4} + \frac{1}{2}((\kappa_0^2 + \nabla^2)u)^2] d\vec{r}$ is a free energy functional. Only static attractors may exist in the phase space of this system because F may only decrease along the trajectory $\frac{dF}{dt} = -\int (\frac{\partial u}{\partial t})^2 d\vec{r} \leq 0$. Periodic, quasiperiodic or chaotic spatial distributions may correspond to these attractors. The number of attractors may, in principle, be arbitrary great. Indeed, according to (7) all static solutions that are established as $t \rightarrow \infty$ meet a translational dynamical system $(\kappa_0^2 + \nabla^2)^2 u + f(u) = 0$, where $f(u) = \beta u^2 + u^3$.

Representing initial periodic state of the field as a point in the phase space of the gradient system of interest, we can formulate the problem of the birth of disorder in the form of a simple question: Is this point contained in the attraction basin of the attractor corresponding to disordered field distribution as $t \rightarrow \infty$? Physically, however, this formulation of the problem does not sound natural enough. We must be concerned with a set of close initial field distributions rather than with one particular distribution. An initial phase volume with a characteristic size $\varepsilon \ll 1$ and not a point corresponds to such a set in phase space. Then the question will have a quite different formulation: Will an irregular state of the field the statistical characteristics of which depend only on the period of initial distribution and are independent of ε (with $\varepsilon \rightarrow 0$ including) set in as $t \rightarrow \infty$? Numerical experiment must be performed along these lines.

Equation (7) was solved in our numerical experiment employing a spectral method for $N = 128 \times 128$ harmonics with boundary conditions $u(0) = u(l)$ for $l = 100$, $\kappa_0 = 1$ and $\beta = 2.9$. We took a nearly harmonic initial field distribution

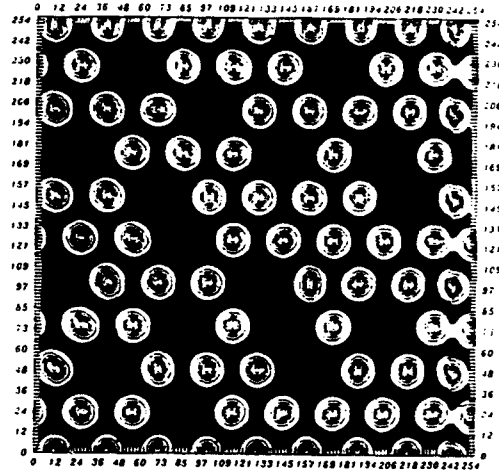
$$u(x) = a \sin K_x x \sin K_y y + \varepsilon f(x, y), \quad (9)$$

where $\varepsilon \ll a$ and $f(x, y)$ is a random function.

The wave number K of harmonic distribution was chosen so that a periodic lattice of localized structures emerging from it when $\varepsilon = 0$ should correspond to the local maximum of free energy in Eq. (7), i.e. that such a lattice should be unstable relative to small disturbances. Small irregular component $\varepsilon \ll 1$ acts in this case only as a "trigger" to initiate instability. Then, a solution like the one shown in Fig. 7 is established as $t \rightarrow \infty$ for $a = 1.8$ and $\varepsilon = 0.3 - 0.01$.

The numerical experiment illustrates the birth of spatial chaos whose properties are universal in that they do not depend on statistical characteristics of $f(x, y)$ but,

Figure 7: Stable irregular distributions of two-dimensional solitons.



instead, are determined by the dynamical system itself.

The time dependence of Kolmogorov-Sinai entropy calculated for one-dimensional space series shows that entropy grows monotonically from zero and tends to a constant when $t \rightarrow \infty$. The increase of entropy and, eventually, its asymptotic form indicate that static disorder sets in.

Numerical experiment demonstrated that finite-dimensional disorder is formed in two stages. At the first (fast) stage of evolution, the initial field distribution transforms in time $t \leq \beta$ into a lattice of solitons that are slightly shifted (for small ϵ) with respect to equidistant arrangement. If we have a nearly periodic initial distribution, the soliton lattice is nearly periodic too. The medium remembers initial conditions at this stage of evolution. As t increases ($t > \beta$), the solitons slowly shift relative to one another and the initial conditions are no longer remembered if the lattice is unstable.

Results of computer experiment may be interpreted pictorially within the following model. For not too short distances between the neighbouring solitons (on the order of their characteristic size or larger), the asymptotic method enables us to describe the soliton motion as the dynamics of a chain of particles with specific interaction potential that is determined by the structure of the "tails" of localized structures:

$$M \frac{dx_{ij}}{dt} = \frac{\partial}{\partial x_{ij}} u_{ij}, \quad M \frac{dy_{ij}}{dt} = \frac{\partial}{\partial y_{ij}} u_{ij} \quad (10)$$

Here x_{ij} and y_{ij} are coordinates of the center of the i, j -th soliton, $M = \int (\nabla u^{(0)})^2 dr$ is mobility of the soliton having the structure $u^{(0)}(x)$, and u_{ij} is the potential produced by all solitons except the i, j -th one at the point x_{ij} :

$$u_{ij} = \sum_{m,n} u_{ij}^{mn}, \quad u_{ij}^{mn} = e^{-\nu R_{ij}^{mn}} \cos(\mu R_{ij}^{mn} + \varphi_0), \quad (11)$$

where $\nu = Re\sqrt{i - \kappa_0^2}$, $\mu = Im\sqrt{i - \kappa_0^2}$, and φ_0 is a numerical constant,

$$R_{ij}^{mn} = \sqrt{(x_{mn} - x_{ij})^2 + (y_{mn} - y_{ij})^2},$$

and summation takes into account only interaction with nearest neighbours.

The equilibrium states of system (10) are described by periodic, quasiperiodic and stochastic solutions which enclose either the entire plane or part of it. Rectangular and hexagonal lattices of solitons with arbitrary lattice constants correspond to simplest

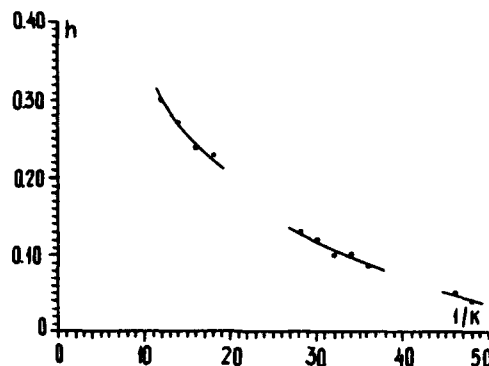


Figure 8: Kolmogorov-Sinai entropy versus a period of initial perturbation $\sim \sin kx$ in one-dimensional analog.

periodic solutions. Lattices in which the distance between particles corresponds to minima (or maxima) of the pair interaction potential (11) have highest (lowest) stability. Note that simplest stable stochastic solutions that are contained within (10)-(11) may be constructed out of stable periodic lattices by omitting in the lattice an arbitrary amount of particles.

What happens if the period of initial distribution is such that the emerging periodic structure is unstable? Arbitrary disturbance as $t \rightarrow \infty$ may lead either to regular periodic and quasiperiodic distribution of "particles" or to chaotic distribution of particles - solitons.

It follows from analysis of system (7) that different unstable soliton lattices and, consequently, different established distributions must correspond to initial distributions with different periods - the effect of multistability. Because of instability, the neighbouring solitons may either move apart by "one minimum" (one oscillation of a soliton tail) or move towards one another by the same "unit length". Then it appears obvious that the degree of disorder may only decrease with increasing period of initial distribution! This guess was proved completely in a computer experiment (Fig. 8).

APPLICATIONS AND PERSPECTIVES

The considered theory of deterministic spatial disorder of multidimensional fields is now at its most intriguing stage of development. Very little has been done yet but perspectives seem to be highly optimistic. Therefore we will mention only a few problems, picked out almost at random, to demonstrate the resources and potentialities of this fascinating and extremely attractive branch of science.

1. Computer and laboratory experiments show that the degree of disorder of a two-dimensional field increases with the growing number of localized states (particles, defects, etc.). Apparently, if these states do not interact with one another, the dimension D_s will be infinite, like for complete thermodynamical disorder. There arises a question: What kinds of particle interactions transform infinite-dimensional disorder into finite-dimensional one? Finally, is there any relation

between thermodynamical and dynamical characteristics for finite-dimensional disorder?

2. Is it possible to reconstruct the properties of deterministic chaos for large-box problems by measuring the dimension of a time series at one point? The answer is "yes", but the time series must be very long, which makes the problem unsolvable, in fact. A natural impulse in this situation is to use several time series measured at different points in space. The algorithm for calculation of the correlation dimension of time series can be readily generalized for this problem. However, there arises a new task: to choose the points at which the time series should be measured. Apparently, solution of this problem is extremely important for the prognosis of spatial fields, for example, for weather prediction.
3. Up to now, we have considered an ideal situation when finite-dimensional disorder exists "all by itself", i.e. without uncontrolled spatial inhomogeneities. Whereas real snapshots always contain different noises of unknown origin that have a rather broad Fourier spectrum. The noises may be produced by technical details of diagnostics, as a result of signal transmission through communication channel, by inhomogeneity of photo materials, etc. It is an extremely difficult task to detect finite-dimensional disorder against the background of spatial noise using traditional statistical methods. However, the experience gained with time series shows that use of even simplest forms of "dynamical" processing of snapshots (calculation of D_2 , spatial entropy, etc.) makes the problem sound a little more optimistic.¹⁸
4. A rather broad spectrum of propagating waves, including the ones with a nearly saturation amplitude, is typical for real wave fields that exist in the Nature (in atmosphere, in the ocean, in space plasma, and so on). With the excess over the saturation amplitude, wave dissipation caused by breaking (i.e. by the formation of small-scale, most often turbulent, perturbations on wave crests) increases sharply. The interaction of propagating waves is then described in a weakly nonlinear approximation. Whereas breaking is a strongly nonlinear process and the resulting turbulence may be considered as a random field. This picture of turbulence is usually observed for internal gravity waves propagating in atmosphere with density decaying exponentially along the vertical¹⁹ or for wind waves at sufficiently strong wind.²⁰

It is almost impossible to distinguish the wave and turbulent components using traditional methods (except the cases when the components have strongly differing space or time scales). Besides, researchers usually have at their disposal only snapshots of spatial fields while phase velocities of different spectral components are unknown. We believe therefore that a method for calculation of the spatial dimension of snapshots may be a useful tool that will enable one to separate small-scale structures related to propagating waves from a chaotic component of higher dimension.

References

1. P.Coullet, C.Elphick and D.Repaux, Nature of spatial chaos, *Phys. Rev. Lett.* 58:431 (1987).
2. S.Aubry, in: "Solitons and Condensed Matter Physics", Springer, ser. Solid State Physics, vol.8, A.R.Bishop and T.Schneider, eds., Springer, Berlin (1979).

3. S.Aubry and G.Abramovici, Chaotic trajectories in the standard map. The concept of anti-integrality, *Physica D* 43:199 (1990).
4. K.A.Gorshkov, L.A.Ostrovsky, V.V.Papko, and A.S.Pikovsky, On the existence of stationary solitons, *Phys. Lett. A* 74:177 (1979).
5. J.M.Ziman. "Models of Disorder", Cambridge University Press, Cambridge (1979).
6. L.A.Lugiato and R.Lefevr, Spatial dissipative structures in passive optical systems, *Phys. Rev. Lett.* 58:2209 (1987).
7. P.Manneville. "Dissipative Structures and Weak Turbulence", Academic Press (1990).
8. V.S.Afraimovich, A.B.Ezersky, M.I.Rabinovich, M.A.Shereshevsky, and A.L.Zheleznyak, Dynamical description of spatial disorder, *Physica D* (to be published in 1992).
9. I.Procaccia, P.Grassberger, and H.G.E.Heitschel, On the characterization of chaotic motions, in: "Lect. Notes in Physics", Springer, 179:212 (1983).
10. D.Ruelle, Deterministic chaos: the science and the fiction, *Proc. R. Soc. Lond. A* 427:1873:241 (1990).
11. A.B.Ezersky, M.I.Rabinovich, V.P.Reutov, and I.M.Starobinets, Spatio-temporal chaos in parametric excitation of capillary ripples, *Sov. Phys. JETPH* 64:1228 (1986).
12. E.Bodenschatz et al., Patterns and defects in liquid crystals, in: "New Trends in Nonlinear Dynamics and Pattern-Forming Phenomena (The Geometry of Nonequilibrium)", Pierre Couillet and Patric Huerre, eds., Plenum Press, N.Y. (1988).
13. L.Korsinov, M.I.Rabinovich, and L.Sh.Tsimring, Breaking symmetry in nonequilibrium systems. Interfaction of defects, *Phys. Rev. A* (to be published).
14. M.I.Rabinovich, V.P.Reutov, and A.V.Rogalsky, Defects of nonlinear fields of capillary ripples, *Phys. Lett.* 144:259 (1990).
15. B.Christiansen, P.Alstrom, M.T.Levinsen, Ordered capillary-wave states: quasicrystals, hexagons, and radial waves, *Phys. Rev. Lett.* 68:14:2157 (1992).
16. W.S.Edwards and S.Fauve, *Phys.Rev.Lett.*, (to be published).
17. M.I.Rabinovich, A.L.Fabrikant, and L.Sh.Tsimring, Finite-dimensional spatial disorder, *Sov. Phys. Uspekhi* 167:4 (1992).
18. K.A.Gorshkov, L.N.Korzinov, M.I.Rabinovich, and L.Sh.Tsimring, submitted to *Phys. Rev. Lett.*
19. D.C.Fritts, T.Tsuda, T.Sato, S.Fukao, and S.Kato, Observational evidence of a saturated gravity wave spectrum in the proposphere and lower stratosphere, *J. Atmos. Sci.* 45:12:1741 (1988).
20. M.S.Longuet-Higgins, Capillary rollers and bores, submitted to *J. Fluid. Mech.*

PHASE SHIFTS AND NONLINEAR EFFECTS IN STOCHASTIC RESONANCE

MI Dykman¹, R Mannella², PVE McClintock³ and NG Stocks³

¹Physics Department, Stanford University, Stanford, CA 94305, USA

²Dipartimento di Fisica, Università di Pisa

Piazza Torricelli 2, 56100 Pisa, Italy

³Physics Department, Lancaster University, Lancaster LA1 4YB, UK

Suppose one wants to look at a weak periodic signal within a random noise: a way to improve the Signal to Noise Ratio (SNR) is to use a lock-in amplifier, but the frequency of the periodic component must be known to achieve a high amplification. A different method is offered by the mechanism of Stochastic Resonance (SR)^{1,2}. SR is a mechanism which uses a nonlinear device (a bistable system could be an example, but other possibilities are known³) to enhance the SNR even if the frequency of the periodic modulation is not exactly known. Most intriguing and counterintuitive, there exists a range of noise intensities for which the SNR increases as the noise intensity is increased. The effect is shown in Fig.1 where (left hand side) we send a periodic signal plus a random term to a nonlinear filtering device (middle, a bistable electronic circuit) and we obtain a strong filtered signal (right hand side, jagged line) at the driving frequency; by comparison, on the right hand side we report with a dashed line the periodic component buried in the noisy input signal, amplified by a factor 10.

It is very simple to understand the physical mechanism of SR. Suppose one has a filter: this filter will be described by its transfer function (or susceptibility) $\chi(\Omega)$. If the form of the transfer function is known, the behaviour of the filter will be known too. For systems

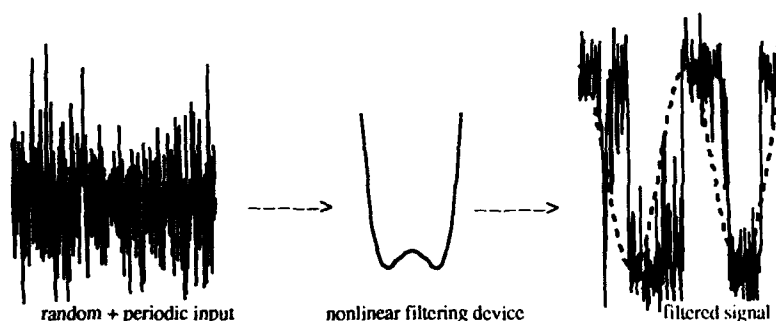


Figure 1. Schematic view of the SR phenomenon (see text for more details).

in thermal equilibrium (at a temperature T) it is straightforward to derive $\chi(\Omega)$. Using the Linear Response Theory^{4,5} one gets

$$\operatorname{Re} \chi(\Omega) = \frac{2}{T} \int_0^\infty dx \frac{Q(x) x^2}{x^2 - \Omega^2} \quad \operatorname{Im} \chi(\Omega) = \frac{\pi \Omega Q(\Omega)}{T} \quad (1)$$

where $Q(\Omega)$ is the spectral density of fluctuations in the system. If the external forcing has an amplitude A and its frequency is ω , the SNR can be written as

$$\text{SNR} = \frac{A^2}{4} \frac{|\chi(\omega)|^2}{Q(\omega)} \quad (2)$$

and it is clear from the above equations that we only need to know $Q(\Omega)$. Very roughly, a quick power counting of T in Eqs 1 and 2 shows that we may expect SR if at the driving frequency $Q(\Omega)$ depends more than quadratically on the temperature T .

A typical SNR vs T plot for a given driving frequency will look like Fig. 2. We show next on Fig. 3 the SNR enhancement as measured in a electronic circuit^{4,5}; crosses are the theoretical predictions using Eq. (1) (from measured $Q(\Omega)$), squares are the SNR's measured

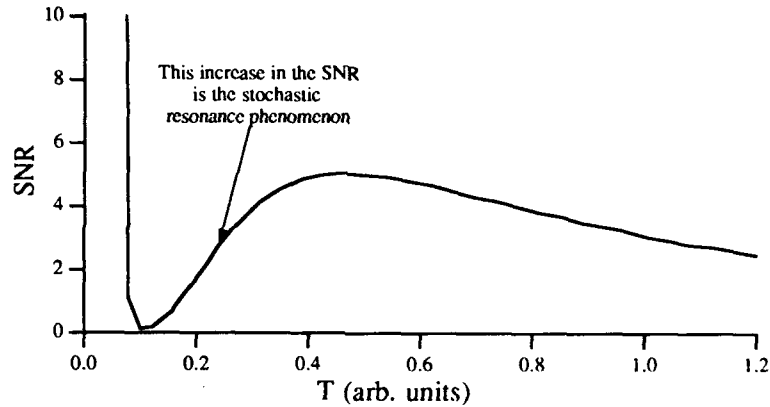


Figure 2. The SNR ratio vs. T , showing the SR phenomenon.

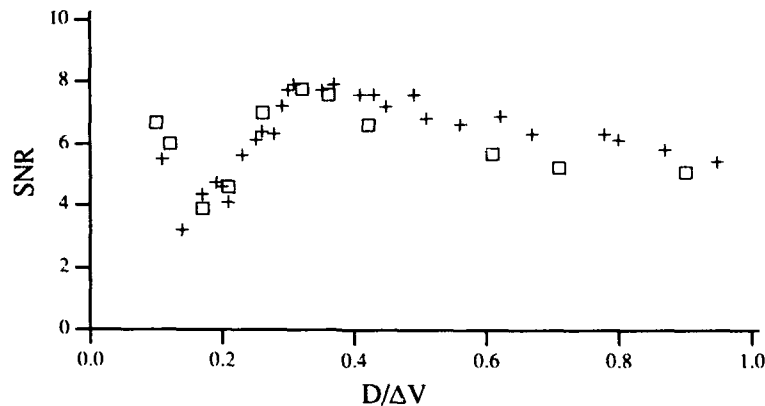


Figure 3. SNR (squares) measured in a bistable system vs noise intensity (in scaled units, see text); crosses are theoretical predictions.

in the circuit. Note that both in Fig.2 and Fig. 3 the fact that the maximum of the SNR vs. T is very broad implies that the SR mechanism should work even if the frequency of the driving forcing is not precisely known⁶. A typical electronic bistable system, used to study SR, could be

$$\dot{x} = x - x^3 + f(t) + A \cos \omega t \quad (3)$$

where $f(t)$ is a gaussian random noise, delta correlated and of intensity D (which plays the role of the temperature T). Eq. (3) describes a symmetric bistable system, the simplest model where SR can be found; the term $A \cos \omega t$ represents the weak external periodic force, and we look at the response of the variable x . Notice that the noise intensity has been scaled on units of the potential barrier between the two minima ($\Delta V=0.25$ for the model of Eq. (3)), because this is the main quantity which determines the onset of SR in bistable systems.

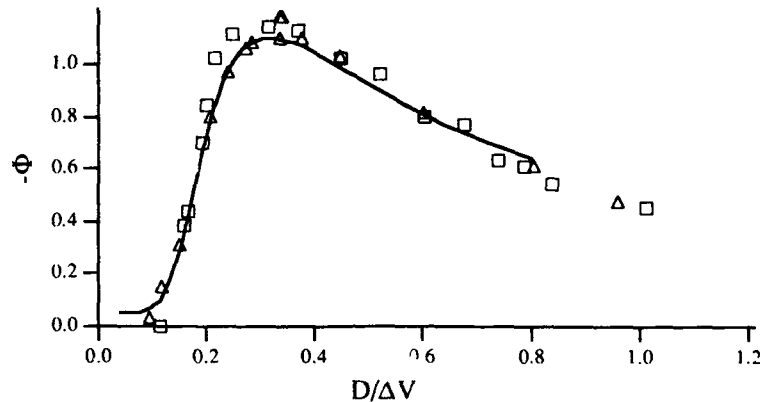


Figure 4. Phase lag between average signal and periodic forcing (symbols refer to two different amplitudes of the periodic forcing) vs noise intensity. The full line is the theoretical prediction.

As clear from Eqs. 1, the response can have an imaginary part. We expect then that the system should display a phase shift between external forcing and average response, and that this phase shift should not be function of A ⁷. Fig. 4 proves that this conjecture is true: we plot the phase shift ($-\Phi$, different symbols correspond to different A 's) between response and external driving for the model of Eq. (3), compared with the theoretical prediction (solid line). Contrary to the case of Fig. 3, here $Q(\Omega)$ has been derived theoretically from first principles, not from a simulation. The agreement between simulations and theory is remarkable.

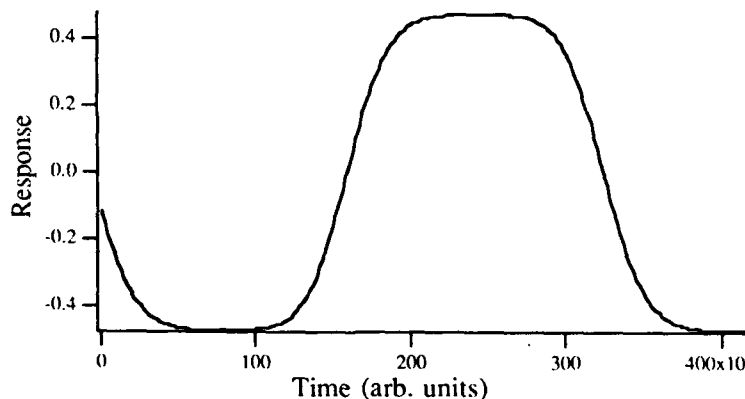


Figure 5. Expected response in the very nonlinear regime

Finally, it is possible to investigate theoretically the SR phenomenon even in a (very) nonlinear regime^{4,8}. In this case the response of the system is no longer sinusoidal, as shown on Fig. 5. The idea is to use an expansion of the response in terms of Bessel functions, given that for a bistable system the dynamics (and hence $Q(\Omega)$) is dominated by an activation process (across the potential barrier) of exponential form.

In Fig. 6 we show a typical power spectral density in the nonlinear regime, obtained from a numerical simulation of Eq. (3) in the appropriate range of parameters. Satellite peaks at frequencies odd multiples of the driving frequency ω are visible (in particular the one at 3ω). In the inset we report the theoretical predictions for the first three harmonics (triangles) and the result of the numerical simulation (squares with error bars). We regard the agreement as very satisfying.

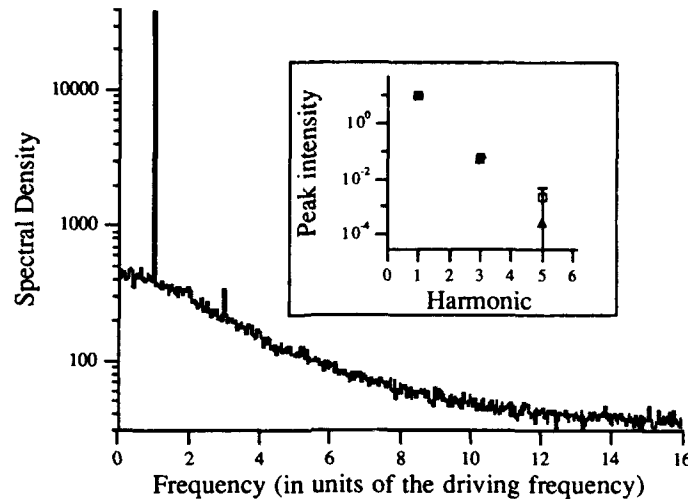


Figure 6. Measured spectral densities in the nonlinear regime. Inset: comparison between experiment (triangles) and theory (squares).

ACKNOWLEDGEMENTS

This work was partly supported by the EC under contract n. SC1*-CT91-0697 (TSTS), and by the Science and Engineering Research Council (UK)

REFERENCES

1. Early work on stochastic resonance: R Benzi et al., J. Phys. A **14**, L453 (1981), Tellus **34**, 10 (1982); C Nicolis, Tellus **34**, 1 (1982)
2. Reviews on SR: F. Moss, in Some Problems in Statistical Physics, edited by GH Weiss (SIAM, Philadelphia, 1992); MI Dykman et al., Pis'ma Zh. Exsp. Teor. Fiz. **53**, 182 (1991) (JETP Lett. **53**, 193 (1991)); see also the monograph issue of J. Stat. Phys. on SR, January 1993, and MI Dykman⁷.
3. NG Stocks et al. "Stochastic Resonance in Monostable Systems" (submitted to PRL); MI Dykman et al., "High Frequency Stochastic Resonance for Periodic Attractor" (submitted to PRL); see also J. Stat. Phys., Jan. 1993.
4. MI Dykman et al., Pis'ma Zh. Exsp. Teor. Fiz. **52**, 780 (1990) (JETP Lett. **52**, 144 (1990))
5. MI Dykman et al., Phys. Rev. Lett. **65**, 2606 (1990)
6. Private communication from A Bulsara.
7. MI Dykman et al., Phys. Rev. Lett. **68**, 2985 (1992) and references therein; see also L. Gammaitoni et al., Phys. Rev. Lett. **67**, 1799 (1991); Phys. Lett. A **158**, 449 (1991).
8. MI Dykman et al., "Nonlinear effects in Stochastic Resonance" (in preparation).

CONTROLLING DEPENDENCE ON INITIAL CONDITIONS IN CHAOTIC SYSTEMS

T. Kapitaniak

Division of Control and Dynamics
Technical University of Łódź
Stefanowskiego 1/15
90-924 Łódź, Poland

Aperiodic excitation of a dynamical system can be advantageous in many practical systems, for example it can reduce fatigue of materials in number of mechanical systems (gear boxes are the classical systems of this type). Sensitive dependence on initial conditions which is characteristic for all chaotic systems makes that the response trajectory is not only aperiodic but unpredictable as well. That is why it is difficult to use chaotic systems in practice. Recently the problem of controlling chaos i.e., to convert the chaotic behaviour found in many physical systems to a periodic time dependence or aperiodicity which is predictable, has attracted great interest [1-6]. The method of Ott, Grebogi and Yorke [1] (OGY) has the unique feature that it enables one to select predetermined time-periodic behaviour by making only small time-dependent perturbations. They show that permanent chaos can always be depressed by stabilizing one of many periodic orbits embedded in the chaotic attractor. The idea is to start with any initial condition, wait until the trajectory falls into a target region around the desired periodic orbit and then apply feedback control. The applications of OGY method to stabilized higher periodic orbits in chaotic diode resonator have been demonstrated by Hunt [2]. A modification of this method to control chaos using time delay coordinates has been presented by Nitsche and Dressler [3]. Besides the described above feedback methods it is possible to stabilize periodic orbits by nonfeedback methods [4,5]. In this note we show two techniques of controlling chaos which allow to generate aperiodic trajectory which is predictable by a small change of system parameters.

The first method is applicable to the systems which behaviour depends on a control parameter - c in such a way that they have a chaotic attractor for one value of c , let's say c_1 and strange repeller together with periodic attractor for the other value of $c - c_2$. Systems with strange repeller exhibit transient chaos [6]. Trajectories started from randomly chosen initial points then approach the attractor with probability one. Before reaching it, however, they might come close to the strange repeller and stay in its vicinity for shorter or longer time. Long lived chaotic transients are often present around crisis configurations [6], at parameters values just beyond the disappearance of the chaotic attractor. It is worth

mentioning that systems with fractal basin boundaries are also accompanied by transient chaos since such boundaries are, in general the stable manifolds of chaotic repeller. Computation of transient Lyapunov exponents for the systems with chaotic repellers often shows such a property that their values become nonpositive far before the transient died i.e. before trajectory reaches attractor [7,8].

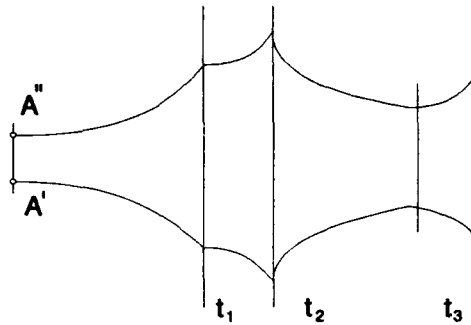


Figure 1 Behaviour of nearby trajectories.

The main idea of our method is described in Figure 1. Let's consider two trajectories which start from nearby initial conditions A' and A'' which lie on or close to a strange chaotic attractor. For $t_0 < t < t_1$ these trajectories represent evolution of the system for a value of control parameter $c=c_1$ and for $t_1 < t < t_3$ the evolution is shown for control parameter $c=c_2$. In the first time interval we observe exponential divergence of trajectories described by positive Lyapunov exponent - $\lambda(t) > 0$. At time $t=t_1$ we are changing a value of control parameter from c_1 to c_2 . For a new value of control parameter our system has a strange repeller and we observe first a further divergence of trajectories and a positive transient Lyapunov exponent $\lambda(t) > 0$ for $t_1 < t < t_2$. At time t_2 a transient Lyapunov exponent changes sign from positive to negative and for $t_2 < t < t_3$ we observe a convergence of trajectories. At time t_3 we are changing a value of control parameter to c_1 again, etc. If t_3 is chosen in such a way that the period of time $t_3 - t_2$ is not sufficient for a system to reach periodic attractor and

$$\int_{t_0}^{t_2} \lambda(t) dt \approx \int_{t_2}^{t_3} \lambda(t) dt \quad (1)$$

then we do not observe divergence of trajectories in time. As a part of trajectory evolves on the strange chaotic attractor the switches between c_1 and c_2 will take place in different points of phase space so the trajectory is aperiodic (not t_3 -periodic).

As an example of our method let us consider:

$$\ddot{x} + a\dot{x} - (1 + c \cdot \cos(\omega t))x + bx = 0 \quad (2)$$

where a , b , c and ω are constant. In this note we took $a=0.1$, $b=1$, $\omega=1$ and c as a control parameter. We took two values of c : $c_1=0.35$ and $c_2=0.34$. For c_1 the behaviour of the system is chaotic and for c_2 the system is characterized by above described transients [8]. In numerical investigations $t_1=10^5 T_1$ and $t_3=3 \cdot 10^5 T_1$, $T_1=2\pi/\omega$ have been taken and we considered the behaviour of a system:

$$\ddot{x} + a\dot{x} - (1 + c(t)\cos(\omega t))x + bx = 0 \quad (3)$$

where $c(t)=c_1$ for $t_0 < t < t_1$ and $c(t)=c_3$ for $t_1 < t < t_3$. Generally T_1 and $T_2=t_3$ are incommensurate so eq.(3) has four-dimensional phase-space $(x, \dot{x}, \omega t, (2\pi/t_3)t)$ and can have strange nonchaotic attractor. The value of the largest Lyapunov exponent averaged over time T_2 is negative and close to -0.001 so we do not observe exponential divergence of trajectories in time. This result shows that applying our control procedure we manage to build aperiodic trajectory which is predictable in that sense that nearby trajectories do not diverge exponentially as it is shown in Figure 2. Figure 2 presents the distance $x'(t+nT_2) - x''(t+nT_2)$; where $n = 1, 2, \dots$, x' is a trajectory for initial conditions $x(0)=0.1$, $\dot{x}(0)=0$ and x'' is a trajectory for $x(0)=0.101$, $\dot{x}(0)=0$.

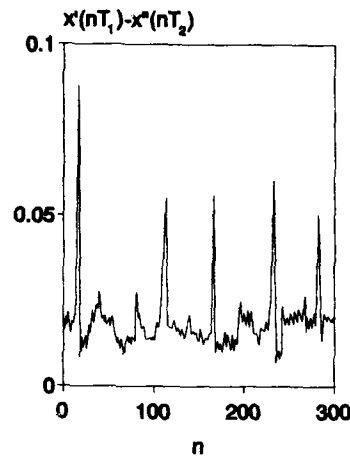


Figure 2 Distance between nearby trajectories of eq.(3) versus time.

The second method allows to convert the unknown chaotic trajectory to a desired aperiodic trajectory. The idea of this method is to perturb one of the system parameters, for example c in eq.(2), as:

$$\dot{c} = \zeta((x - x_n) - (\dot{x} - \dot{x}_n)) \quad (4)$$

where (x_n, \dot{x}_n) is a known aperiodic trajectory (it could come from chaotic system), ζ is the stiffness of the control and $x(t)$ is actual output of the system. In our numerical experiments we considered the system given by eq. (2) for $c=0.35$ and as x_n we took a chaotic trajectory obtained for this system with initial conditions $x_0=0.01$, $\dot{x}_0=0$. When the control dynamics (4) is applied our system evolves and reaches the desired trajectory $x_n(t)$. We have studied the dependence of the recovery time τ_R (the time after which the trajectory from randomly chosen initial condition reaches the desired trajectory with the assumed precision 10^{-4} , on ζ . For ζ in the interval (0.01-0.1) we estimated τ_R for randomly chosen 500 initial conditions and averaged them. As expected the recovery time decreases when ζ increases - Figure 3.

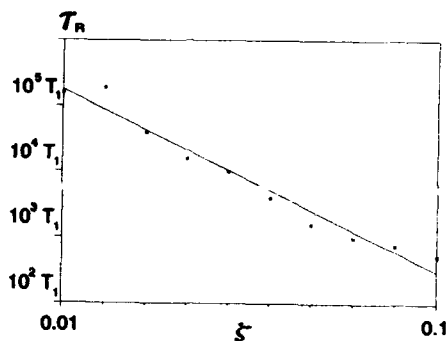


Figure 3 Recovery time τ_R versus stiffness coefficient ζ .

The presented methods are less general than the OGY method. They can be applied only to the systems which displayed specific apriori known behaviour. This requires the knowledge of equations of motion. On the other hand, to apply this method we do not have to follow the trajectory and wait till it will be in the appropriate target region. As an effect of control it is possible to obtain aperiodic trajectory which is different from original chaotic trajectory in such a way that it can be predictable (it is characterized by nonpositive Lyapunov exponents). These methods allow to control dependence on initial conditions in chaotic systems and can encourage practical applications of them.

Acknowledgment

This work has been supported by KBN (Poland) under the project no.333579102.

REFERENCES

1. E. Ott, C. Grebogi, and Y.A. Yorke, Controlling chaos, *Phys. Rev. Lett.* 64, 1196, (1990)
2. E.R. Hunt, Stabilizing high-periodic orbits in a chaotic system: the diode resonator, *Phys. Rev. Lett.* 67, 1953 (1991)
3. G. Nitsche and U. Dressler; Controlling chaotic dynamical systems using time delay coordinates, *Physica D* (in press) (1990)
4. T. Kapitaniak, "Chaos in Systems with Noise", World Scientific (1988)
5. Y. Braiman and I. Goldhirsch, Taming chaotic dynamics with weak periodic perturbations, *Phys. Rev. Lett.* 66, 2545 (1991)
6. T. Tel, Transient chaos, In: "Directions in Chaos", vol. 3, Hao Bai-Lin (ed.), World Scientific, Singapore (1990)
7. S. V. Ershov, A.B. Potapov; On the nature of nonchaotic turbulence, Preprint (1991)
8. T. Kapitaniak, Strange nonchaotic transients, *J. Sound Vibr.* (in press)

DYNAMICAL SYSTEMS ANALYSIS OF AN AERODYNAMIC DECCELERATOR: BIFURCATION TO DIVERGENCE AND FLUTTER

Louis J. Piscitelle

Aero-Mechanical Engineering Directorate
U.S. Army Natick Research, Development and Engineering Center
Natick, MA 01760-5017

INTRODUCTION

The prediction of a circular decelerator's behavior during the initial phase of the opening process is an important technical barrier for researchers in the airdrop community. As a parachute is expected to open successfully at higher speeds and lower altitudes, the ability to predict the stability of the initial interaction between the decelerator and the flow field becomes crucial. A stability analysis of a mathematically rigorous model for this process would predict which conditions would result in various types of stable and unstable behavior. The analysis would provide details about the shape of the canopy just prior to the inflation process. Currently, all models of the opening process (Steeves, 1989; Ross, 1971; Purvis, 1982) apply only after the decelerator has attained some assumed initial shape.

The subject of this paper is the development of a mathematical model of a canopy's behavior just after the canopy is extracted. This model requires the development of a partial differential equation (PDE), which governs the interaction of the canopy with the flow field. The derived model could be analyzed using dynamical system theory to determine the stability of the canopy as a function of the values of various physical parameters (e.g., airspeed and line tension).

There are numerous models in the open literature for the interaction of a flexible structure with a flow field; for an overview see Dowell, 1980. Typically, these models were created to analyze the aerodynamic flutter problem of a structure in a supersonic flow field. Since most Army airdrops are performed at subsonic speeds, these models are not directly applicable. Work has been published for problems where a pipe either conveys fluid or is in a flow field (Paidoussis and Issid, 1974; Paidoussis, 1966). These models were either not applicable, such as those for pipes conveying fluid, or too restrictive, such as the linear models of Paidoussis, 1966. Hence, the development of an applicable model was essential.

The application of dynamical system theory to aerodynamic stability problems is not new. In fact, the supersonic flutter problem has been examined in some detail (Holmes and

Marsden, 1983; Dowell, 1966, 1980). The stability of pipes conveying fluid has also been examined by Holmes, 1977. The idea is to use dynamical system techniques to find the "essential generic models" from the full system of PDEs (Holmes, 1977).

PHYSICAL MODEL

The decelerator is modelled as a long thin tube, with mass per unit length m , which is simply supported at each end. The tube is immersed in a fluid which is flowing with a free stream velocity U parallel to the initial (undeformed) axis of the tube. The tube may also be subject to an initial axial load, T_0 , applied at the right support by displacing the right support.

The boundary conditions are chosen to model the attachment of the decelerator to the payload at one end and to the extraction chute at the other end. The boundary conditions wherein both ends are fixed or one end is fixed with the other free may also be used.

The material is assumed to be viscoelastic and to obey the Kelvin-Voight model, as assumed by Holmes, 1977 and Paidoussis and Issid, 1974. The axial extension, $w(x)$, induced by the lateral deflection $y(x)$ is given by $\int (y')^2 dx$.

Paidoussis, 1966 used the result of Lighthill, 1960 for the resultant relative velocity, $v(x,t)$, between the tube and the flow to derive a linearization (first order approximation) to the drag experienced by the tube. To derive a better approximation, it is necessary to examine more closely the drag equation and the geometry of interaction of the tube with the flow field. Taylor, 1952 based his model for the effect of tube inclination to the flow on a curve fitted to laminar flow data in which sine squared worked well. The difficulty with this work is that the sine squared term leads to terms in the PDE which are even in y . This result is not physical. The same data have been fitted well by the current author using sine cubed for the nonlinear extension and this fitting leads to physically meaningful terms for the PDE, i.e., terms which are odd in y .

A new drag equation was derived to include the effect of the tube's velocity in the y direction on both the magnitude and direction of the total fluid velocity relative to the tube and the new nonlinear extension to the drag. Expanding the resulting equation in a Taylor series and retaining the first set of higher order terms, the normal drag force becomes

$$F_N = \frac{1}{2} \rho D C_f [U^2 y' + U y] + \frac{1}{2} \rho D [U^2 (C_D, -\frac{1}{2} C_f) (y')^3 + U (3 C_D, -\frac{1}{2} C_f) (y')^2 \dot{y}] \quad (1)$$

The longitudinal drag force is the one used by Paidoussis, 1966. Thus, the equation of motion may be written as (see Paidoussis, 1966; Holmes, 1977), with simple supports,

$$\begin{aligned} \alpha \dot{y}'''' + y'''' + [u^2 (1 - \frac{1}{2} \zeta_c \mu (\frac{1}{2} - x)) - \Gamma - \kappa \int_0^1 (y')^2 dx - \sigma \int_0^1 y' \dot{y}' dx] y'' \\ + 2 \beta^{1/2} u \dot{y}' + \zeta_c \mu^2 y' + \frac{1}{2} \beta^{1/2} \zeta_c \mu \dot{y} \\ + \dot{y} + \frac{1}{2} \zeta_c \mu^2 C_f (R - \frac{1}{2}) (y')^3 + \frac{1}{2} C_f \beta^{1/2} \zeta_c \mu (3R - \frac{1}{2}) (y')^2 \dot{y} = 0 \end{aligned} \quad (2)$$

Equation 2 is in dimensionless form. If only the linear terms in equation 2 are retained, the resulting equation is equivalent to the linear PDE examined by Paidoussis, 1966. If the last two nonlinear terms on the left hand side (LHS) of equation 2 are eliminated, the resulting equation is similar to that derived in Holmes, 1977.

DERIVATION OF LOW-DIMENSIONAL MODELS

The eigenfunctions for simple supports are $\sin(j\pi x)$. Using Galerkin averaging (see Dowell, 1966; Holmes, 1977) of equation 2 with $y_s = \sum_{j=1}^n r_j(\tau) \sin(j\pi x)$ gives a set of n second order ordinary differential equations (ODEs) in the time coefficients $r_i(\tau)$. Truncating the series at $n = 1$, and 2, gives two low-dimensional models:

for $n = 1$:

$$\begin{aligned} \ddot{r}_1 + A_1 \dot{r}_1 + B_1 r_1 + \kappa \frac{\pi^4}{2} r_1^3 \\ + \sigma \frac{\pi^4}{2} r_1^2 \dot{r}_1 + \frac{\pi^2 c_T \zeta \beta^{1/2} (3R - \frac{1}{2})}{8} r_1^2 \dot{r}_1 = 0 \quad , \end{aligned} \quad (3)$$

for $n = 2$:

$$\begin{aligned} \ddot{r}_1 + A_1 \dot{r}_1 + B_1 r_1 + \frac{32}{9} \zeta c_T \mu^2 r_2 - \frac{16}{3} \beta^{1/2} u \dot{r}_2 \\ + \kappa \pi^4 [\frac{1}{2} r_1^2 + 2 r_2^2] r_1 + \sigma \frac{\pi^4}{2} [r_1 \dot{r}_1 + r_2 \dot{r}_2] r_1 \\ + \pi^2 \zeta c_T \mu^2 (R - \frac{1}{2}) [\frac{4}{5} r_1^2 r_2 - \frac{144}{35} r_2^3] \\ + \pi^2 c_T \zeta \beta^{1/2} u (3R - \frac{1}{2}) [\dot{r}_1 r_2^2 + \frac{1}{8} r_1^2 \dot{r}_1] = 0 \quad , \end{aligned} \quad (4a)$$

$$\begin{aligned} \ddot{r}_2 + A_2 \dot{r}_2 + B_2 r_2 + \frac{8}{9} \zeta c_T \mu^2 r_1 - \frac{16}{3} \beta^{1/2} u \dot{r}_1 \\ + \kappa \pi^4 [2 r_1^2 + 8 r_2^2] r_2 + \sigma \frac{\pi^4}{2} [4 r_1 \dot{r}_1 + 16 r_2 \dot{r}_2] r_2 \\ + \pi^2 \zeta c_T \mu^2 (R - \frac{1}{2}) [\frac{176}{35} r_1 r_2^2 + \frac{4}{5} r_1^3] \\ + \pi^2 c_T \zeta \beta^{1/2} u (3R - \frac{1}{2}) [\frac{1}{2} r_2^2 \dot{r}_2 + \frac{1}{4} r_1^2 \dot{r}_2] = 0 \quad , \end{aligned} \quad (4b)$$

$$\text{Where, } A_s = \pi^4 s^4 \alpha + \frac{1}{2} \beta^{1/2} \zeta c_T \mu, \quad B_s = \pi^4 s^4 + [\Gamma - u^2] \pi^2 s^2 \quad (5)$$

RESULTS

This section describes the use of dynamical system theory to investigate the bifurcation behavior of the low dimensional model given by equation 3.

Equation 3 has equilibrium points at

$$\begin{aligned} x_2 = 0 \quad , \\ \frac{\kappa \pi^4}{2} x_1^3 + B_1 x_1 = 0 \quad . \end{aligned} \quad (6)$$

Equation 6 agrees with the results obtained by Holmes, 1977. If $B_1 > 0$, then $(0,0)$ is a unique fixed point and it is a sink. This means that the undeflected shape is stable. If $B_1 < 0$, there exist three equilibrium points given by $(0,0)$ and $([\pm 2B_1/\kappa\pi^4]^{1/2}, 0)$. Unlike the problem examined by Holmes, 1977, a three parameter bifurcation space $(u, \Gamma, R) \in \mathbb{R}^3$ exists because of the new parameter R , defined as $R = C_D/C_T$. The tube is now unstable since the center fixed point is a saddle and, for R large enough, the other two are sinks (see Holmes, 1977). Note also that the change in sign of B_1 from positive to negative takes place at the Euler buckling mode. For the case where $R < R_\alpha$ (where R_α is the critical value above which the results agree with Holmes, 1977), different results are obtained. For $B_1 > 0$ there still exists a unique fixed point at $(x_1, x_2) = (0,0)$. For $B_1 < 0$ and $R > R_\alpha$, the structure is identical to that found by Holmes, 1977 and there are three equilibrium points, one saddle and two sinks. If, however, R is reduced to a value below R_α , then the two sinks become sources and a pair of limit cycles is born. Physically, these limit cycles correspond to the canopy oscillating about either one of the displaced positions, i.e., fluttering.

REFERENCES

- DOWELL, E. H., 1966. Nonlinear Oscillations of a Fluttering Plate, *AIAA Journal* 4;7:1267-1275.
- 1980. *New Approaches in Nonlinear Problems in Dynamics*, Philadelphia: SIAM. Nonlinear Aeroelasticity.
- HOLMES, P., 1977. Bifurcations to Divergence and Flutter in Flow-Induced Oscillations: A Finite Dimensional Analysis, *J. Sound Vib.* 53;4:471-503.
- HOLMES, P. and J. MARSDEN, 1983. Bifurcation to Divergence and Flutter in Flow Induced Oscillations; an Infinite Dimensional Analysis, *Automatica* 14:367-384.
- LIGHTHILL, M. J., 1960. Note on Swimming of Slender Fish, *J. Fluid Mech.* 9:305-317.
- PAIDOUSSIS, M. P., 1966. Dynamics of Flexible Slender Cylinders in Axial Flow: I-Theory, *J. Fluid Mech.* 26:717-736.
- PAIDOUSSIS, M. P. and N. T. ISSID, 1974. Dynamic Stability of Pipes Conveying Fluid, *J. Sound Vib.* 33:267-294.
- PURVIS, J. W., 1982. Theoretical Analysis of Parachute Inflation Including Fluid Kinetics, *J. Aircraft* 19;4:290-296.
- ROSS, E. W., 1971. A General Theory of Parachute Opening, U.S. Army Natick RD&E Center Technical Report TR-71-32-OSD.
- STEEVES, E. C., 1989. Analysis of Decelerators in Motion Using Computational Fluid Dynamics, *Proc. AIAA 10th Aerodynamic Decelerator and Balloon Tech. Conf.*, Cocoa Beach, FL.
- TAYLOR, G. I., 1952. *Proc. Roy. Soc. A*;214:158.

CHAOS IN A MODEL OF A RAILWAY WHEELSET

Eva Slivsgaard^{1,3} and Carsten Knudsen^{2,3}

¹Laboratory of Applied Mathematical Physics

²Physics Laboratory III

³MIDIT

The Technical University of Denmark

INTRODUCTION

There are a variety of nonlinear topics in railway vehicle dynamics. In this paper we examine a simple nonlinear model of the motion of a suspended railway wheelset in the low velocity range between 0 and 13 m/s. The wheels have conical wheel profile and roll on a straight and horizontal track unaffected by external torques. The suspension elements have linear characteristics. The *nonlinear part* is given by the relation between the creepage and the creep forces in the ideal contact point between the wheel and the track. The effect of flange contact is modelled by a very stiff spring with a dead band.

A Chaotic motion is presented by a one-dimensional bifurcation diagram where the wheelset velocity, V , is used as control parameter. A first return map in the chaotic region is examined by symbolic dynamics.

EQUATIONS OF MOTION

According to Vermeulen and Johnson⁴ the resulting creep-force is given by

$$F_R(u) = \mu N \begin{cases} u - \frac{1}{3}u^2 + \frac{1}{27}u^3, & u < 3 \\ 1, & u \geq 3 \end{cases}, \quad u = (G\pi a_e b_e / \mu N) \xi_R, \quad (1)$$

$$\xi_R = \sqrt{(\xi_x/\psi)^2 + (\xi_y/\psi)^2}, \quad \xi_x = \frac{1}{V} \frac{dx}{dt} - \psi, \quad \xi_y = \frac{a}{V} \frac{d\varphi}{dt} + \frac{\lambda x}{r_0}.$$

The lateral creep-force component, F_x , and the longitudinal creep-force

component, F_y , is then determined by

$$F_x = (\xi_x/\psi)F_R/\xi_R, \quad F_y = (\xi_y/\psi)F_R/\xi_R. \quad (2)$$

When the flange of the wheelset touches the rail, a restoring force on the lateral displacement occur momentarily. This force is called the flange force and is given by

$$F_T(x) = \begin{cases} k_0(x - \delta), & \delta < x, \\ 0, & -\delta \leq x \leq \delta, \\ k_0(x + \delta), & x < -\delta, \end{cases} \quad (\delta = 0.0091 \text{ m}). \quad (3)$$

The equations of motion for the wheelset are obtained by including the suspension, friction, and flange forces in Newton's equation

$$\begin{aligned} md^2x/dt^2 + 2k_1x + 2F_x + F_T(x) &= 0, \\ Id^2\psi/dt^2 + 2aF_y &= 0, \end{aligned} \quad (4)$$

x denotes the lateral displacement, ψ the yaw angle.

Through a change of variables these equations of motion are converted to a fourth order autonomous dynamical system. We have used the software package PATH² to follow both stable and unstable periodic solutions as the control parameter, V , is varied.

NUMERICAL RESULTS

Figure 1 shows a bifurcation diagram of the dynamics up to $V = 10.8$ m/s. The stationary solution remains stable until the speed reaches 10.050 m/s, where a supercritical Hopf bifurcation creates a stable limit cycle. The amplitude of the limit cycle increases rapidly with the velocity until flange contact occurs at $V = 10.056$ m/s. A magnification of the bifurcation diagram just after flange contact reveals the transition to chaos: First a symmetry breaking pitchfork bifurcation, followed by a complete period doubling cascade. These bifurcations appear in a very small range in speed ($\Delta V = 0.0003$ m/s).

A crisis¹ is evident at $V \approx 10.183$ m/s, where three-band chaos develops. The bands narrow with growing speed. Especially, the center band narrows onto flange contact. At $V \approx 10.21$ m/s the bands vanish to periodic solutions. Immediately after, a Floquet multiplier leaves the unit disc at +1 and large scale chaos develop. Calculating a return map of the value of the lateral deviation at the $n + 3$ 'rd intersection (of the trajectory with the maximum value of the lateral deviation) against its value at the n 'th intersection at $V = 10.215$ m/s reveals that the transition to chaos is through type-I intermittency.

At $V \approx 10.26$ m/s, the symmetric chaotic attractor splits up into two asymmetric chaotic attractors with two-band chaos. The four bands decrease in amplitude, and at $V \approx 10.3025$ m/s they are replaced by two asymmetric period-2 oscillations. These limit cycles exist for an extremely narrow speed range, and they undergo a reverse period doubling at $V = 10.303$ m/s. Decreasing the speed instead shows that the period-2 solutions bifurcate exactly at the value where flange contact

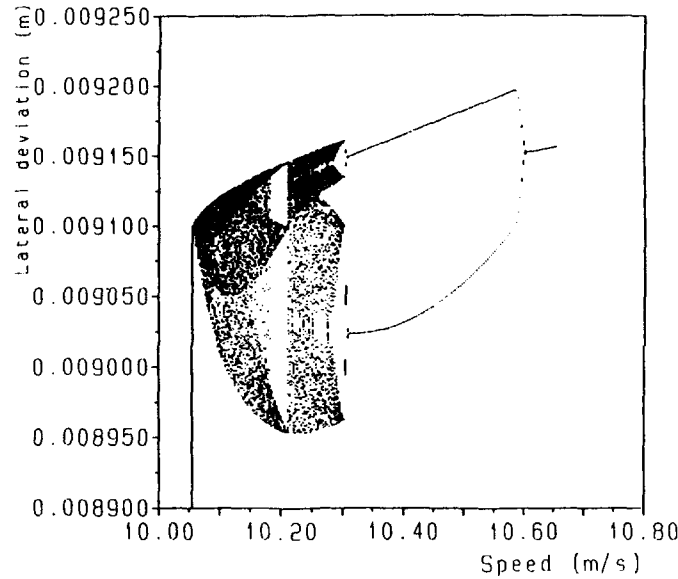


Figure 1. Bifurcation diagram showing the maximum lateral deviation versus the speed.

occurs. The transition to chaos is through type-III intermittency as indicated by a return map at $V = 10.295$ m/s.

At $V = 10.50$ m/s a pitchfork bifurcation restore the symmetric oscillations. The symmetric limit cycle exists up to $V = 13.81$ m/s.

SYMBOLIC DYNAMICS

Figure 2 shows a return map of the value of the lateral deviation at the $n + 1$ 'st intersection of the trajectory with the maximum value of the lateral deviation against its value of the n 'th intersection at $V = 10.215$ m/s. Inspired by the strong influence of flange contact, the interval of the return map, I , will be divided into five subintervals $I_1 - I_5$ (see the figure). We can construct the transition matrix⁵

$$A = \begin{pmatrix} 0 & 0 & 1 & 1 & 1 \\ 1 & 1 & 0 & 0 & 0 \\ 1 & 1 & 0 & 0 & 0 \\ 0 & 0 & 1 & 1 & 1 \\ 0 & 0 & 1 & 1 & 1 \end{pmatrix}. \quad (5)$$

The return map on I is topologically conjugate to a shift map on the set of all possible itineraries allowed by A . This means that for each itinerary allowed by A , there exists one and only one orbit for the return map and vice versa (for more details see Knudsen *et al.*³).

The number of prime periodic orbits of period k can be calculated as

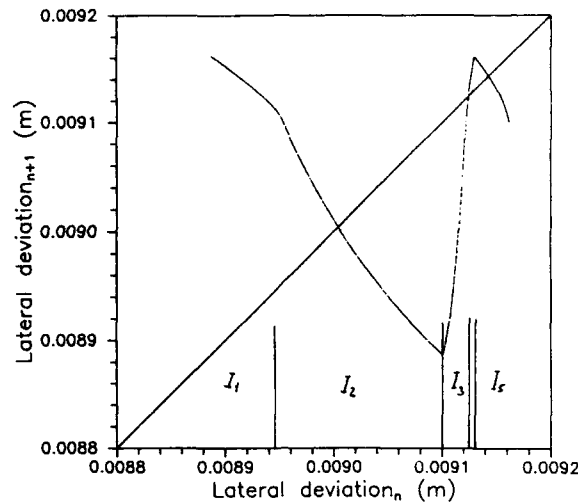


Figure 2. A first return map for the chaotic attractor at $V = 10.215$ m/s.

$$N(k) = (\text{tr}(A^k) - \sum_{1 \leq i < k; i|k} N(i) \cdot i) / k. \quad (6)$$

An analytic calculation of the topological entropy yields

$$h = \log((3 + \sqrt{5})/2). \quad (7)$$

The positive value of the topological entropy implies so-called topological chaos, meaning that at least chaotic transients exist.

DISCUSSION

The numerical results help us to understand the complicated behavior of a rolling wheelset.

The trivial solution loses its stability in a supercritical Hopf bifurcation. Hereafter periodic and chaotic motions can exist, but the periodic oscillations dominate the examined speed range. We emphasize that our symbolic dynamics calculations show the existence of topological chaos.

More detailed investigations of the dynamics of the rolling wheelset can be found in Knudsen *et al.*³

REFERENCES

1. Grebogi, C., Ott, E. and Yorke, J.A., 'Chaotic attractors in crisis', *Physical Review Letters*, **48** (22), (1982) 1507-1510.
2. Kaas-Pedersen, C., *PATH user's guide*, Laboratory of Applied Mathematical Physics, The Technical University of Denmark (1989).
3. Knudsen, C., Feldberg, R. and True, H., 'Bifurcations and chaos in a model of a rolling railway wheelset', *Phil. Trans. R. Soc. London Ser. A*, **338** (1992) 455-469.
4. Vermeulen, P. J. and Johnson, K. L., 'Contact of nonspherical elastic bodies transmitting tangential forces', *J. of Appl. Mech.*, **31** (1964) 338-340.
5. Wiggins, S., *Global Bifurcations and Chaos*, Springer-Verlag New York (1989).

NONLINEAR MODELLING OF SHIMMYING WHEELS

Gábor Stépán

Department of Applied Mechanics
Technical University of Budapest
H-1521 Budapest, Hungary

INTRODUCTION

The problem of the so-called shimmying wheel has been studied in the special literature for several years (see e.g. the early paper of Schlippe and Dietrich, 1941). These investigations are stimulated by the studies of the dynamical behaviour of trailers or those of the steered wheels of cars, landing gears of aeroplanes, etc. (see e.g. Scheidl et al., 1985). The complex dynamical behaviour of these wheels clearly refer to nonlinear vibrations.

The present paper summarizes the model considerations of a single towed wheel from the view-point of nonlinear dynamics only. The wheel is considered with an elastic tyre characterized by the creep force presented by Pacejka (1966b). Similar creep forces are often used in railway dynamics (see e.g. True, 1987), too.

The existence of chaotic shimmy motion is shown by Stépán (1991) when the wheel itself is rigid and the king pin is elastic, i.e. when the classical Coulomb friction is used to describe the contact of the wheel and the ground. The Coulomb friction is strongly nonlinear, but it cannot model the real contact forces if the elastic element of the structure is at the wheel, and the contact region is not a single point. This explains the present analysis of the nonlinear creep force and nonlinear geometry in the dynamical model.

MECHANICAL MODEL

The top- and side-view of a wheel rolling on the plane (x, y) is presented in Figure 1. The figure also explains the basic notation: l stands for the carcass length, the half contact length is denoted by a and the so-called relaxation length of the tyre is the constant σ . The towing speed v is constant and prescribed for the king pin A .

UNSTABLE PERIODIC MOTION

Introducing the carcass angular velocity $\nu = \dot{\psi}$ as a new variable and using a third order truncated system of (1), we rewrite the motion equations in the form

$$\frac{d}{dt} \begin{pmatrix} \psi \\ \nu \\ q \end{pmatrix} = \begin{pmatrix} 0 & 1 & 0 \\ 0 & -\frac{k}{I_A} & -\frac{c_1}{I_A} \\ v & l-a & -\frac{\sigma}{I_A} \end{pmatrix} \begin{pmatrix} \psi \\ \nu \\ q \end{pmatrix} + \begin{pmatrix} 0 \\ \frac{c_3}{I_A} q^3 \\ -\frac{v}{6} \psi^3 + \frac{v}{2\sigma} \psi^2 q \end{pmatrix} + \text{h.o.t.}, \quad (2)$$

where c_1 and c_3 come from the power series: $lF_y(q) + M_{Ox}(q) = c_1 q - c_3 q^3 + \dots$. If the viscous damping is neglected then a clear analytical calculation can be carried out. With $k = 0$, the Routh-Hurwitz criterion gives the stability condition of the trivial solution in the form: $l > l_{cr} = a + \sigma$. At the critical parameter value $l = l_{cr}$, the characteristic roots are given by

$$\lambda_{1,2} = \pm i\omega = \pm \sqrt{\sigma \frac{c_1}{I_A}} \Big|_{l=l_{cr}}, \quad \lambda_3 = -\frac{v}{\sigma}.$$

Following the Hopf bifurcation calculation method of Hassard et al. (1981) or Stépán (1989), we can prove the existence of a subcritical Hopf bifurcation at this critical point. Neglecting the details of the lengthy algebraic work, we present only the final result here: the approximation of the unstable periodic motion which exists around the stable equilibrium for $l > l_{cr}$:

$$\begin{pmatrix} \psi \\ \nu \\ q \end{pmatrix} = 2\sqrt{\frac{l-a}{\sigma} - 1} \begin{pmatrix} \sin(\omega t) \\ \omega \cos(\omega t) \\ \sigma \sin(\omega t) \end{pmatrix}. \quad (3)$$

As there is no damping, there is no attractor outside this unstable limit cycle since the nonlinear creep force is potential in this case.

NUMERICAL SIMULATION

The simulation results of (1) has confirmed the Hopf bifurcation calculation. Figure 2 shows the unstable periodic solution (3) in the attractive centre manifold which is approximated by the plane spanned by the corresponding eigenvectors of $\lambda_{1,2}$. If a solution starts outside the cylinder (the domain of attractivity of the equilibrium) at $(\psi_0; \nu_0; q_0) = (-0.2; 3.0 [1/s]; 0.02 [m])$ then it spirals outwards without finding another attractor. If it starts inside, at $(0.2; -5.5 [1/s]; -0.03 [m])$, then it spirals towards the stable equilibrium. The other parameter values are fixed as follows: $I_A = 0.3576 [kg m^2]$, $c_c = 10^5 [N/m^2]$, $a = 0.04 [m]$, $\sigma = 0.12 [m]$, $l = 0.1605 [m]$, $v = 10 [m/s]$, $\mu F_z = 800 [N]$.

When the damping factor is not zero, e.g. $k = 0.3 [Nms]$, and the carcass length is reduced to $l = 0.155 [m]$, the trajectories starting at $\psi_0 = 0.2, 0.25$ and 0.45 while $\nu_0 = q_0 = 0$ clearly refer to two periodic motions: a stable one appears around the original unstable limit cycle. However, this new stable limit cycle is caused by the damping and not by the nonlinearity of the creep force. This attractor may seem to be a limit cycle, but if its amplitude is greater than q_{sl} , full sliding occurs and (1b) does not hold anymore. A correct modification of equ. (1) could show a chaotic solution there as in the case of Stépán (1991).

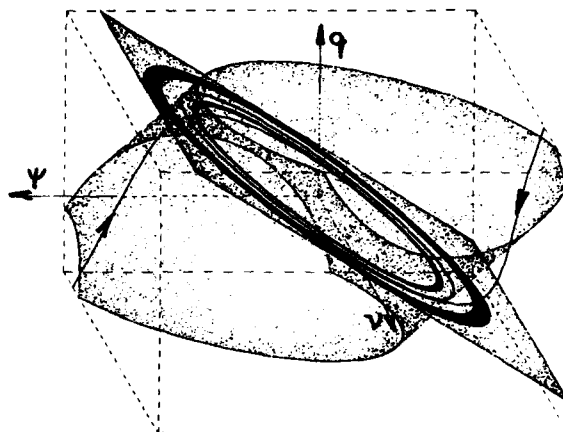


Figure 2. Trajectories in the phase space of the undamped system.

CONCLUSIONS

The existence of the unstable limit cycle in the dynamics of shimmying wheels is due to the nonlinear geometry of the structure. The presence of dry friction at the king pin (as used by Pacejka, 1966a) is not essential to explain the experimentally also verified unstable periodic motion (see Pacejka, 1966b). The fact that the nonlinear creep force cannot stabilize the system without additional viscous damping refers to an important approximation in the mathematical model (1), namely that a stationary (or quasi-stationary) creep force is applied in the dynamical equations. This requires further analysis.

ACKNOWLEDGEMENTS

This work was supported by the Danish Council for Scientific and Industrial Research under grant nr. 16-4786.M and also by the Hungarian Scientific Research Foundation under grant nr. OTKA 5-328.

The author wishes to thank Prof. H. True and Prof. H. Pacejka for discussions of current problems during this work.

REFERENCES

- Hassard, B. D., Khazarinoff, N. D. and Wan, Y. H., 1981, "Theory and Applications of Hopf Bifurcations", London Mathematical Society Lecture Note Series 41, Cambridge.
- Pacejka, H. B., 1966a, Analysis of the shimmy phenomenon. *Automobile Division, IMechE* 180:2A:1.
- Pacejka, H. B., 1966b, "The Wheel Shimmy Phenomenon," Delft Univ. Techn. WTHD:48.
- Pacejka, H. B., 1988, "Modelling of the Pneumatic Tyre and Its Impact on Vehicle Dynamic Behaviour," Delft Univ. Techn. i72B.
- Scheidl, R., Stribersky, A., Troger, H. and Zeman, K., 1985, Nonlinear stability behaviour of a tractor-semitrailer in downhill motion, *Proc. 9th IAVSD-Symposium (Linköping)*, 509.
- von Schlippe, B. and Dietrich, R., 1941, Das Flattern eines bepneuten Rades, *Ber. Lilienthal Ges.* 140:35.
- Stépán, G., 1989, "Retarded Dynamical Systems," Longman, Harlow Essex.
- Stépán, G., 1991, Chaotic motion of wheels, *Vehicle System Dynamics* 20:341.
- True, H., 1987, Bifurcation problems in railway vehicle dynamics, *Proc. Bifurcation: Analysis, Algorithms, Applications (Dortmund)*, ISNM 79:319.

CHAOTIC SOLITONS AND VACUUM

P. J. Werbos and P. A. Hansson¹ *

N.S.F, Engineering Div, Washington DC, USA

¹ Editor-in-chief, NANOBIOLOGY, Department of
Medical Electronics, St Bartholomew's Hospital
West Smithfield, London EC1A 7BE, UK

INTRODUCTION

The most fundamental change in Physics this century has been in the role of the observer. One consequence of the latter is symmetry, i.e., that two observers must perceive the same physical reality structure, as in relativity, and a second consequence is Quantum Mechanics. What we propose here is that an underlying nonlinear partial differential equation (PDE) can describe high-energy physics phenomena.

Classical PDEs are local and realistic, but they violate causality as formulated by Bell [1]. Bell's assumption has two parts:

- 1) There exists a conditional probability, dependent upon the inputs of the experiment, for the state of a photon coming out of a scattering experiment.
- 2) This conditional probability density is the correct basis for predicting the outcome of an experiment, regardless of what measurements are made, so long as the inputs to the experiment are the same.

In PDEs, the expected outcome would correspond to the probability of measurement dependent on all the information available. (Inputs and choice of measurement device are important boundary conditions in solving PDEs). The implicit assumption of time-forward causality is, however, not valid at the microscopic level; as shown in [2], the time-symmetric character of quantum calculations explains why QFT is consistent with Bell.

The notion that classical theory is the limit of QFT as Planck's constant tends to zero is true only for classical theories based on point particles. PDE theories need not lead to this. In fact, we will argue that it is natural to think of particles as chaotic solitons. By this we mean some form of stable localized excitation, rather than a static object (to within translation). It will not be possible to deal here with the entire structure of QFT [3,4].

SOLITONS

Although solitons in two-dimensional systems like the Korteweg-DeVries system, are well known [5] very little is known about solitons in higher dimensions. Roger Newton [6] has argued that generalized methods for locating solitons are extremely difficult to apply in four dimensions. *Ad hoc* approximations from four to two dimensions, or topological shapes (like in the fluxes of fusion reactors) have been used [7].

We are developing a theory which, like QFT, has a unitary scattering matrix, and in which particles are assumed to be some form of solitons. The calculations are based on a scalar field (ϕ). De Broglie proposed that particles are waves with a linear and a nonlinear region. The nonlinear PDE would generate stable, quantized local excitations. Here we will assume that free particles are chaotic solitons as defined above. The quantitative development of De Broglie's ideas was always limited. Even Norbert Wiener [8], when developing a statistical formalism for classical, failed to reproduce the linearity of QFT.

Our formalism builds on an existing one which has been successful in engineering [9]. The approach by Paul Martin does not yield an hermitian dynamical matrix H and thus a unitary scattering matrix ($S = \lim e^{iHt}$), but we have showed that we can overcome that problem, at least for nondissipative systems with time symmetry.

The input is represented by a vector p_- . The initial state of the field is $\phi(x, t_-)$ at all points x at the starting time t_- . At a later time t_+ we will have $\phi(x, t_+)$ at p_+ . The probability of a conditional output is based on a differential equation which describes the dynamics between t_- and t_+ .

In quantum scattering we can only estimate a probability distribution

$$P_r(p_+/p_-) = f(p_-) \int P_r(p_+) \phi(x, t_-) P_r(\phi(x, t_-/p_-) d^\infty \phi(x, t_-) \quad (1)$$

These are in our view incorrect boundary conditions since they force us to have time-forward causality. We suggest that the probability of any result comes from convoluting distributions

$$P(\text{final state}) = \text{Tr}(P_f P_{eg}) \quad (2)$$

where $P(g)$ is a 'density matrix'

$$P(g) = W(g) P(0) W(g)^H \quad (3)$$

and P is the result of transforming the matrix R

$$R_{nm}(x_1, \dots, x_n, y_1, \dots, y_m) = E(\phi(x_1), \dots, \phi(x_n), \phi(\bar{y}_1), \dots, \phi(\bar{y}_m)) \quad (4)$$

In classical chaos theory a strange attractor is an equilibrium set of states and the states near the attractor must show stability by moving towards the attractor as time goes to zero [11]. In our approach, since we have no time-forward causality, we define stability as dispersion away from the soliton. One of us (P.W.) calls this 'emissive stability'. Also, deviations that "boost" the soliton (change its momentum) before dispersing are allowed.

It has been possible to show how methods from QFT can 'detect' chaotic solitons in solutions of PDEs with a hermitian operator \hat{H} [10]. In short, it can be shown that the usual QFT method to locate 'bound states' provides a way to detect chaotic solitons in PDEs. We have classical fields, rather than operator fields. It is interesting to note that the method works best for PDEs of polynomial type, using calculating procedures in the neoclassical view.

VACUUM

Paul Dirac and Pascual Jordan showed that bosons and fermions may be described as excitations of quantum fields regardless whether they are photons, electrons or protons. Thus the vacuum should not contain any particles. In non-relativistic QFT there are no zero-point fluctuations, while in the relativistic vacuum there is no empty space, based on the particle concept. The vacuum in the standard model of particle physics is nearly reminiscent of the 19th century ether since it is a ferromagnet, a dielectric, a superconductor and a thermodynamic phase. The non-zero vacuum expectation values of Higgs and Goldstone fields are different from zero-point fluctuations, since the latter follow from the fundamentals of quantum theory. The vacuum of a quantum field can have no unique definition in terms of particle number alone.

The vacuum in Dirac's Quantum electrodynamics was an infinite negative energy electron state. This sea was soon eliminated (with no meaning for of the antimatter at the level of one particle) but with gauge covariance and microcausality and not the canonical basis of quantum mechanics. Or 'first we had the luminiferous ether, then we had the electromagnetic ether and now we haven't e(i)ther' [12]. Our idea is that zero-point fluctuations are due to the soliton nature of particles.

CONCLUSIONS

HERA (Hadron Electron Ring Accelerator) will be able to probe the internal structure of the proton. This will make it possible to test whether the point like assumption of QFT is correct. The lack of size of the electron is a problem waiting for understanding.

A demonstration on how to use chaos in a physical system has already been published [13]. In 1989 one of us (PAH) [14] suggested that a chaotic state could make it possible to transfer nonkinetic energy into work. The problem therefore was to solve the phase space topology of the non kinetic energy term in nuclei, to perturb into an analytically solvable form and move the energy out for work. The difference between the latter and Maxwell's demon is that the latter is not a statistical 'spill over' problem but a problem of topology of chaotic regions.

We are confronted by that similar nonlinearities occur in general in Korteweg-DeVries equation as in supersymmetry [15]. This, together with the measurements of weak vector bosons seems necessary to explain high energy physics.

Finally, our view of measurement and observation leads to predictions like those of the usual observer formalism of QFT, but there are some important differences. Here, it is the measurement apparatus (e.g. polarizers set up where reaction products come

out) rather than the act of observation (humans looking at the results) which has an impact on the outcome and the impact arises because the measurement apparatus, like the apparatus which generates the incoming particles, is part of the boundary conditions. There is never a time when the 'wave function is crystallized'. Indeed, our intuitive talk about 'retroactive causation' really refers to the reason why certain configurations of space-time never occur; it does not imply any kind of change in what happened in the past. (Likewise, we never actually change the future in a four-dimensional regime).

* These are personal views and not part of our respective activities at NSF and Nanobiology.

REFERENCES

- [1] Clauser, J.F. et al, Phys. Rev. Lett. 23, p.880-884 (1969)
- [2] De Beauregard, O.C., Krafatos, ed., Proceedings of a Workshop on Bell's Theorem, Quantum Theory and Concepts of the Universe, Kluwer Academic Publishers (1989)
- [3] Mandl, "Introduction to Quantum Field Theory", Wiley, N.Y. (1959)
- [4] Itzykson and Zuber, "Quantum Field Theory", McGraw-Hill, N.Y. (1980)
- [5] Whitham, G., "Linear and Nonlinear Waves", Wiley Interscience, N.Y. (1974)
- [6] Newton, R.G. "Three-dimensional Inverse Scattering", Springer-Verlag (1989)
- [7] Eilenberger, G., "Solitons: Mathematical Methods for Physicists", Springer-verlag, (1983)
- [8] Siegel and Khang, J. Fluid Mech. 41, 593 (1970)
- [9] Martin, P. et al, Phys. Rev. A 8, 423 (1983)
- [10] Werbos, P., "Chaotic solitons and the Foundations of Physics : A Potential Revolution", Appl. Math. & Comput. (*in press*)
- [11] Grebogi, C. et al, Science, 238, p632-638 (1987)
- [12] Hoffmann, B. 'The Strange Story of the Quantum', Penguin Books, Harmondsworth, p. 37 (1963)
- [13] Shinbrot, T, et al, Phys. Rev. Lett. 68:19 (1992)
- [14] Hansson, P.A., IAA-89-667 (1989)
- [15] Wess, J., Bagger Supersymmetry and Supergravity, Princeton University Press, Princeton (1983)

Q-HERMITIAN CONJUGATION, QUANTUM GROUPS AND SQUEEZING

E.Celeghini¹, M.Rasetti² and G.Vitiello³

¹Dipartimento di Fisica and Sezione I.N.F.N.
Universita' di Firenze, Italy

²Dipartimento di Fisica and Unita' I.N.F.M.
Politecnico di Torino, Italy

³Dipartimento di Fisica, Universita' di Salerno
and I.N.F.N. Sezione di Napoli, Italy

Quantum groups have shown to be an exceptionally promising and rich structure whereby one can expect a growing wealth of new results in statistical mechanics and quantum field theory¹. Stemmed out of the algebraic structure dictated by integrability conditions (quantum Yang-Baxter (q -Y.-B.) equations) for a class of integrable systems, quantum groups can be intuitively thought of as the deformation of the universal enveloping algebra of some given Lie algebra \mathcal{L} of dynamical variables induced by replacing the Jacobi identities with the q -Y.-B. equations, yet preserving the associativity properties of \mathcal{L} . As usual, quantum groups is synonymous of Hopf algebra.

On a different side, it has been recognized that squeezed coherent states^{2,3} constructed as generalized coherent states for suitable algebras may describe a wide class of systems characterized by reduced quantum fluctuations⁴⁻⁷.

In a recent paper⁸, we have shown how the two concepts of quantum groups and squeezing can be bridged in the simple setting provided by a set of states which are a modified version of the states introduced by Biedenharn and McFarlane⁹ (B - McF). We conjecture that the notion of quantum group coherent state is in general the natural candidate to describe squeezed quantum states of matter. In this report we closely follow ref. 8 and 11 to which the reader is addressed for more details.

The quantum version of the Jordan-Wigner map is generated by the set of operators $\{a_q, \bar{a}_q, N_q; q \in \mathbb{C}\}$, with relations

$$[N_q, a_q] = -a_q \quad ; \quad [N_q, \bar{a}_q] = \bar{a}_q \quad , \quad (1)$$

$$a_q \bar{a}_q - q^{\frac{1}{2}} \bar{a}_q a_q = q^{-\frac{1}{2}} N_q \quad . \quad (2)$$

The structure lying behind (1) and (2) has been shown to be a quantum super-algebra¹⁰ $S \sim osp_q(1/2)$.

As we intend to discuss the property of squeezing of the generalized coherent states $(G.C.S)_q$ associated with S , we have to equip first the realization (1), (2) of S with the notion of hermiticity. We work in the customary Fock space \mathcal{F} , which will make the physics of squeezing much more transparent. This also implies that $N_q^\dagger = N_q \equiv N$, where $N = N_{q=1}$ is the usual boson number operator.

It is worth stressing that the notion of q -hermiticity may be introduced in discussing eq. (2). Let us briefly illustrate this point.

We assume the usual set of (q -independent) operators $\{a, a^\dagger, N = a^\dagger a\}$, with relations

$$[N, a] = -a \quad ; \quad [N, a^\dagger] = a^\dagger \quad , \quad (3)$$

and with $a^\dagger a |n\rangle = n |n\rangle$, $a |0\rangle = 0$. We denote by $\{|n\rangle | n \text{ integer } \geq 0\}$ the usual basis of \mathcal{F} . Thus a^\dagger denotes the conventional hermitian conjugate of a . However, we now also introduce the operator $\hat{a}(q) \equiv \hat{a}_q$ with the requirements

$$[N, \hat{a}_q] = \hat{a}_q \quad (4a)$$

$$\hat{a}_q \rightarrow a^\dagger \text{ for } q \rightarrow 1 \quad (4b)$$

In other words, we introduce the notion of q -dependent hermitian conjugation by defining the q -hermitian operator \hat{a}_q for each point q of the complex plane excluded the origin 0 (see below). Although the operator a does not depend on q , as said above, however we also write $a_q \equiv a$ for homogeneity of notation. From the assumption (4a) it follows that

$$\hat{a}_q |n\rangle = g(n, q) |n+1\rangle \quad (5)$$

By using $a |n\rangle = n^{\frac{1}{2}} |n-1\rangle$ we also have

$$a_q \hat{a}_q |n\rangle = (n+1)^{\frac{1}{2}} g(n, q) |n\rangle \quad (6a)$$

$$\hat{a}_q a_q |n\rangle = n^{\frac{1}{2}} g(n-1, q) |n\rangle \quad (6b)$$

where $g(n, q)$ is a function to be found and on which we put the requirement of boundness for any $q \in (\mathbb{C} - 0)$ (see below). We also assume for any nonzero q the normalization $g(0, q) = 1$ and $g(-m, q) \equiv 0$, $m > 0$.

From (6) it follows

$$\langle n | a_q \hat{a}_q - \hat{a}_q a_q | n \rangle = f(n, q) \quad (7)$$

with

$$f(n, q) \equiv F(n+1, q) - F(n, q) \quad (8a)$$

$$F(n, q) \equiv n^{\frac{1}{2}} g(n-1, q) \quad (8b)$$

Of course, from our hypotheses it also follows that, for any $q \in (\mathbb{C} - 0)$, $f(0, q) = 1$, $F(0, q) = 0$ and

$$f(n, q) \rightarrow 1 \text{ for } q \rightarrow 1 \text{ and for any integer } n > 0 \quad (9a)$$

$$F(n, q) \rightarrow n \text{ for } q \rightarrow 1 \text{ and for any integer } n > 0 \quad (9b)$$

The assumption of boundness of $g(n, q)$, and therefore of $F(n, q)$ and of $f(n, q)$, leads us to express $F(n, q)$ in its most general form as

$$F(n, q) = \sum_{m=0}^{\infty} c_m(n) q^{-m}, \quad q \in (\mathbb{C} - 0), \quad n > 0. \quad (10)$$

From (10) and (8a) we finally find that one possible solution for the coefficients $c_m(n)$ brings us to

$$F(n, q) = \sum_{m=0}^{n-1} q^{-m} = q^{-\frac{n-1}{2}} [n]_q, \quad n > 0 \quad (11)$$

and

$$g(n, q) = (n+1)^{-\frac{1}{2}} q^{-\frac{n}{2}} [n+1]_q, \quad q \in (\mathbb{C} - 0), \quad n \geq 0 \quad (12a)$$

$$f(n, q) = q^{-n}, \quad q \in (\mathbb{C} - 0), \quad n \geq 0 \quad (12b)$$

where

$$[n]_q \equiv \frac{q^{\frac{1}{2}n} - q^{-\frac{1}{2}n}}{q^{\frac{1}{2}} - q^{-\frac{1}{2}}} = \frac{\sinh(\frac{1}{2}nz)}{\sinh(\frac{1}{2}z)}$$

with $z \equiv \ln q = x + iy$.

Eq.(2) is then obtained from (7) by using the rescaled $\bar{a}_q \equiv \hat{a}_q q^{\frac{1}{2}N_q}$. Eqs. (1) are also satisfied. We notice that $[a_q, \bar{a}_q] = [n+1]_q - [n]_q$, which is now symmetric under $q \rightarrow q^{-1}$ (contrarily to eq. (7), see also eq. (12b)), and that (11) is consistent with the co-covariance of such a commutator.

Under the assumptions made above, from the point of view of the space of states the q-hermitian conjugation leads to the construction of $\mathcal{F}_q = \{|0\rangle, |n\rangle_q = (n!)^{\frac{1}{2}} ([n]_q!)^{-1} (\bar{a}_q)^n |0\rangle; n > 0\}$ for any $q \in (\mathbb{C} - 0)$. In other words, we have a fiber bundle with fibers \mathcal{F}_q and basis $(\mathbb{C} - 0)$.

To proceed in our discussion is now also convenient to introduce a_q^\dagger and \bar{a}_q^\dagger .

Conjugation of (1) and (2) immediately leads then to

$$a_q^\dagger = \bar{a}_{q^*} [\chi_q(N)]^{-1}, \quad \bar{a}_q^\dagger = \chi_q(N) a_{q^*}, \quad (13)$$

where $\chi_q(N)$ is a function to be determined by suitable self-consistency conditions. We fix it so that a_q, a_q^\dagger are canonically conjugate with each other, i.e. so that in the corresponding sector \mathcal{S} be identical with the usual Weyl-Heisenberg algebra, namely $[a_q, a_q^\dagger] = 1$. This condition is implemented by the choice

$$\chi_q(N) = \frac{([N+1]_{q^*} [N+1]_q)^{\frac{1}{2}}}{N+1}, \quad (14)$$

One has as well $a_{q^*} = a_q \left(\frac{[N]_{q^*}}{[N]_q} \right)^{\frac{1}{2}}$ and $\bar{a}_{q^*} = \left(\frac{[N]_{q^*}}{[N]_q} \right)^{\frac{1}{2}} \bar{a}_q$.

Notice that as $q \rightarrow 1$, $a_q^\dagger \rightarrow \bar{a}_q \rightarrow a^\dagger$, $\bar{a}_q^\dagger \rightarrow a_q \rightarrow a$, $a_q^\dagger a_q \rightarrow a^\dagger a \equiv N$ (recall that $a_q^\dagger a_q = \frac{N}{[N]_q} \bar{a}_q a_q$).

In view of (13), (14),

$$\begin{aligned} a_q |n\rangle &= \left(\frac{[n]_q}{[n]_{q^*}} \right)^{\frac{1}{2}} n^{\frac{1}{2}} |n-1\rangle, \\ \bar{a}_q |n\rangle &= \left(\frac{[n+1]_q}{[n+1]_{q^*}} \right)^{\frac{1}{2}} \left(\frac{[n+1]_q [n+1]_{q^*}}{n+1} \right)^{\frac{1}{2}} |n+1\rangle, \end{aligned} \quad (15)$$

whence $\bar{a}_q a_q |n\rangle = [n]_q |n\rangle$. $|0\rangle$ is the highest weight vector of S : $a_q |0\rangle = 0$.

If one defines now the coherent states $\{|\alpha; q\rangle : |\alpha, q \in \mathbb{C}\}$ by

$$a_q |\alpha; q\rangle = \alpha |\alpha; q\rangle, \quad (16)$$

it is straightforward to check that

$$|\alpha; q\rangle = \mathcal{N}(|\alpha|) \exp_q(\alpha \bar{a}_q) |0\rangle, \quad (17)$$

where $\exp_q(x) \equiv \sum_{n=0}^{\infty} \frac{x^n}{[n]_q!}$ is the quantum version of the exponential function ($[n+1]_q! \equiv [n+1]_q [n]_q!$), and $\mathcal{N}(|\alpha|)$ is a normalization factor which with the above choice turns out to be independent of q : $\mathcal{N}(|\alpha|) = \exp(-\frac{1}{2}|\alpha|^2)$.

Then also,

$$|\alpha; q\rangle = \exp(-\frac{1}{2}|\alpha|^2) \sum_{n=0}^{\infty} \frac{\alpha^n}{\sqrt{n!}} \left(\frac{[n]_{q^*}!}{[n]_q!} \right)^{\frac{1}{2}} |n\rangle. \quad (18)$$

We notice that in the limit $q \rightarrow 1$, $|\alpha; q\rangle$ turns into a customary Glauber coherent state¹².

We can thus define the quantum analog of position (Q_q) and momentum (P_q) operators :

$$\begin{aligned} P_q &\equiv i \left(\frac{m\hbar\omega}{2} \right)^{\frac{1}{2}} (\bar{a}_q - a_q^\dagger), \\ Q_q &\equiv \left(\frac{\hbar}{2m\omega} \right)^{\frac{1}{2}} (\bar{a}_q + a_q^\dagger). \end{aligned} \quad (19)$$

Q_q and P_q are hermitian and have commutation relation

$$[Q_q, P_q] = i\hbar \left(\frac{[N+1]_q [N+1]_{q^*}}{N+1} - \frac{[N]_q [N]_{q^*}}{N} \right) \equiv i\hbar_q. \quad (20)$$

Operators (20) give rise to a quantum version of the quantized harmonic oscillator (*q.h.o.*), with hamiltonian

$$\begin{aligned} H_q &\equiv \frac{1}{2m} P_q^2 + \frac{1}{2} m\omega^2 Q_q^2 = \frac{1}{2} \hbar\omega (\bar{a}_q^\dagger \bar{a}_q + a_q \bar{a}_q^\dagger) \\ &= \frac{1}{2} \hbar\omega \left(\frac{[N+1]_q [N+1]_{q^*}}{N+1} + \frac{[N]_q [N]_{q^*}}{N} \right). \end{aligned} \quad (21)$$

Eq. (21) suggests a possible experimental test of the q -effects through the spectrum of the q .h.o. for large N . If one considered indeed eq. (20) - in the low z limit - as a canonical form with $\hbar_q = \hbar (1 + \frac{1}{4} \text{Re}(z^2)N(N+1) + \mathcal{O}(z^4))$, the q .h.o. hamiltonian would then be written, up to the same order, as $H_q = \hbar_q \omega_q (N + \frac{1}{2})$, with $\omega_q = \omega (1 - \frac{1}{6} \text{Re}(z^2)N(N+1) + \mathcal{O}(z^4))$. In this perspective the spectrum of H_q can be thought of as that of the usual harmonic oscillator in which the level spacing is deformed in such a way that it increases with n (up to $\mathcal{O}(z^4)$ as $\hbar\omega (1 - \frac{1}{2} \text{Re}(z^2)(n+1)^2)$).

In order to show that the $(G.C.S)_q \{|\alpha; q\rangle\}$ are squeezed, we proceed now to evaluate the variances of Q_q and P_q . Denoting, as customary,

$$(\Delta Q_q)^2 = \langle Q_q^2 \rangle - \langle Q_q \rangle^2, \quad (\Delta P_q)^2 = \langle P_q^2 \rangle - \langle P_q \rangle^2, \quad (22)$$

where $\langle \bullet \rangle \equiv \langle \alpha; q | \bullet | \alpha; q \rangle$, one can readily check that one can write $(\Delta Q_q)^2 = \frac{\hbar}{2m\omega} (A_q + B_q)$, $(\Delta P_q)^2 = \frac{1}{2} m\hbar\omega (A_q - B_q)$, with

$$A_q \equiv \langle \bar{a}_q^\dagger \bar{a}_q \rangle + \langle \bar{a}_q \bar{a}_q^\dagger \rangle - 2 \langle \bar{a}_q \rangle \langle \bar{a}_q^\dagger \rangle, \quad B_q \equiv (\Delta \bar{a}_q^\dagger)^2 + (\Delta \bar{a}_q)^2. \quad (23)$$

For simplicity of notation, we shall henceforth use units such that $m\omega = 1$.

Due to (20), we say that one has *strong squeezing* in P_q (respectively Q_q) if $\Delta P_q < \left(\frac{1}{2} |\langle \hbar_q \rangle|\right)^{\frac{1}{2}}$ (respectively $\Delta Q_q < \left(\frac{1}{2} |\langle \hbar_q \rangle|\right)^{\frac{1}{2}}$). Analogously we say that one has *weak squeezing* if \hbar_q is replaced by \hbar in the above inequalities. It should be pointed out that the $\{|\alpha; q\rangle\}$'s are not minimum uncertainty states[†]. Thus, not surprisingly, the locus of points C for which $B_q = 0$ does not necessarily separate, in the (α, q) space (isomorphic to $\mathbb{C} \times \mathbb{C}$) regions characterized by weak squeezing in P_q from regions with weak squeezing in Q_q , as one has with conventional squeezed states¹³.

The calculations are lengthy but straightforward. Notice that $|\alpha|^2 = \langle N \rangle$, therefore in our numerical analysis we confine our attention to relatively low $|\alpha|$ ($< \sim 10$). One finds

$$\langle \bar{a}_q \rangle \langle \bar{a}_q^\dagger \rangle = \frac{e^{-2|\alpha|^2}}{4|\alpha|^2 |\sinh(\frac{1}{2}z)|^2} \left| e^{|\alpha|^2 \exp(\frac{1}{2}z)} - e^{|\alpha|^2 \exp(-\frac{1}{2}z)} \right|^2, \quad (24a)$$

$$\begin{aligned} \langle \bar{a}_q^\dagger \bar{a}_q + \bar{a}_q \bar{a}_q^\dagger \rangle &= \frac{e^{-|\alpha|^2}}{4|\alpha|^2 |\sinh(\frac{1}{2}z)|^2} \\ &\left\{ 2 \left[e^{|\alpha|^2 \cosh x} \cosh(|\alpha|^2 \sinh x) - e^{|\alpha|^2 \cos y} \cos(|\alpha|^2 \sin y) \right] \right. \\ &\left. + |\alpha|^2 \left[\text{Ei}(|\alpha|^2 e^x) + \text{Ei}(|\alpha|^2 e^{-x}) + 2 \text{Re Ei}(-|\alpha|^2 e^{iy}) \right] \right\}, \end{aligned} \quad (24b)$$

[†] This is related to the fact that also the states (17), as the B.-McF. states are not coherent states for the q -W.H. group, in that they do not have the right transformation properties under the quantum group action.

$$B_q = \frac{e^{-|\alpha|^2}}{2|\alpha|^2} \operatorname{Re} \left\{ \frac{e^{-2i\varphi_\alpha}}{\{\sinh(\frac{1}{2}z)\}^2} \left[\exp\left(-\frac{1}{2}z + |\alpha|^2 e^z\right) + \exp\left(\frac{1}{2}z + |\alpha|^2 e^{-z}\right) - 2 \cosh\left(\frac{1}{2}z\right) e^{|\alpha|^2} - e^{-|\alpha|^2} \left(\exp\left(|\alpha|^2 e^{\frac{1}{2}z}\right) - \exp\left(|\alpha|^2 e^{-\frac{1}{2}z}\right) \right)^2 \right] \right\} ; \quad (24c)$$

where φ_α denotes the phase of α , whereas $\operatorname{Ei}(\zeta)$ and $\operatorname{E1}(\zeta)$ denote the exponential integral functions. Numerical results show that there is a rich structure with interesting squeezing phenomena. In ref. 8 plots in the α -plane are reported which show squeezing regions.

For different q 's near 1 we find regions in the α -plane of strong squeezing and curves C along which $\Delta P_q = \Delta Q_q = \left(\frac{1}{2}\hbar\mathcal{A}_q\right)^{\frac{1}{2}}$, crossing which one switches from a regime with $\Delta P_q > \Delta Q_q$ to the one where $\Delta P_q < \Delta Q_q$.

For q not too close to the unit circle, it is always $\hbar_q > \hbar$, which corresponds to the property that along the curves C $|\alpha|$ grows monotonically and smoothly with φ_α .

The regions of both weak and strong squeezing manifest the feature of symmetry under exchange of Q_q and P_q , which geometrically corresponds to a rotation in the α -plane by $\frac{1}{2}\pi$.

The relevance of the states for which $|q| \approx 1$ but the phase of q is nonvanishing, which exhibit such a rich structure of squeezing features, is worth stressing. Moreover, in view of the physical applications of q -coherent states, the combined notions of deformed Planck constant \hbar_q and of weak and strong squeezing may make the states $\{|\alpha; q\rangle\}$'s the appropriate tools for a phenomenological understanding of the deformation parameter q .

ACKNOWLEDGEMENT

Finally, we would express our great pleasure in contributing this paper to honour Professor Alwyn. C. Scott.

REFERENCES

1. M. Jimbo, *Lett. Math. Phys.* **10**, 63 (1985); **11**, 247 (1986)
2. D. Stoler, *Phys. Rev. D* **1**, 3217 (1970)
3. H.P. Yuen, *Phys. Rev. A* **13**, 2226 (1976)
4. J. Katriel, A.I. Solomon, G. D'Ariano, and M. Rasetti, *Phys. Rev. D* **34**, 2332 (1986); *J. Opt. Soc. Am. B* **4**, 1728 (1987)
5. G. D'Ariano, and M. Rasetti, *Phys. Lett.* **107 A**, 291 (1985)
P.D. Drummond, and S.J. Carter, *Phys. Rev. Lett.* **58**, 1841 (1987); *J. Opt. Soc. Am.* **4**, 1565 (1987)
6. M. Artoni, and J.L. Birman, *Quantum Opt.* **1**, 91 (1989)
7. C.W. Gardiner, A.S. Parkins, and M.J. Collett, *J. Opt. Soc. Am.* **4**, 1683 (1987)
8. E. Celeghini, M. Rasetti, and G. Vitiello, *Phys. Rev. Lett.* **66**, 2056 (1991)
9. L.C. Biedenharn, *J. Phys. A: Math. Gen.* **22**, L873 (1989)
A.J. MacFarlane, *J. Phys. A: Math. Gen.* **22**, 4581 (1989)
10. E. Celeghini, T.D. Palev, and M. Tarlini, *Mod. Phys. Lett. B* **5**, 2056 (1991)

11. E. Celeghini, M. Rasetti and G. Vitiello, *On q-hermitian conjugation*, in preparation
12. R.J. Glauber, *Phys. Rev.* **130**, 2529 (1963); **131**, 2766 (1963)
13. M.N. Nieto, in *Non-Equilibrium Quantum Statistical Physics*, G. Moore, and M.O. Scully, eds.; Plenum Press, New York, 1985

LARGE-AMPLITUDE NARROW SOLITONS IN LATTICES

K.A.Gorshkov, O.A.Druzhinin and L.A.Ostrovsky

Applied Physics Institute, Academy of Sciences
603600 Nizhny Novgorod, Russia

1. INTRODUCTION

Discrete systems have drawn much interest recently in the context of the nonlinear wave theory. Propagation of waves in electric transmission lines, solitary waves in molecular chains dynamics of lattices of non-linear oscillators may serve as an examples where nonlinear processes are described by discrete-difference equations and discreteness of a system may become important¹⁻⁷.

Lattices with nonlinear interaction between nearest neighbouring particles often represent a good model relevant to those in real systems. Usually, one can consider Hamiltonian of a lattice in the form

$$H = \sum_{n=1}^N p_n^2 / 2 + \Phi(q_n - q_{n-1}), \quad (1)$$

where $\Phi(x)$ is the interaction potential.

Dynamics of such a lattice is described by the equations of motion

$$\ddot{q}_n = F(q_{n+1} - q_n) - F(q_n - q_{n-1}), \quad (2)$$

where $F(q) = \partial\Phi/\partial q$.

Travelling waves in discrete lattices have been considered by many authors. However, only in the case of Toda lattice with exponential potential a solitary wave solution was derived in an explicit form. Results obtained for non-integrable lattices with polynomial potential with the use of various approximations evidence that these lattices also can support discrete solitary waves⁸⁻¹¹.

If spatial variations of a wave substantially exceed a length of a lattice cell, one can expand forces in (2) to obtain a PDE with quasi-continuous coordinate n . For example, in cases of quadratic and cubic nonlinearities equations of motion are reduced to Boussinesq equations which is known to be completely integrable¹²⁻¹⁴. For waves propagating in one direction these equations in their turn can be reduced to KdV and m-KdV equations, respectively, and corresponding solitary waves solutions are easily derived.

The problem becomes much more complicated for essentially discrete dynamical regimes when scales of spatial variations are of the order of one lattice cell. In this case the motion of the lattice can not be described by equations obtained in the continuum limit and other approximations should be used to obtain a form of a solitary wave and relation between its parameters.

Some useful compromises can be achieved by using "quasi-continuum" methods based on a more sophisticated approximation of difference of forces in (2). Corresponding solutions obtained are more exact compared to solutions obtained in the continuum limit and take into account discreteness to some extent.¹⁰ Methods using weak and variational formulations give equations describing parameters of solitary waves which are approximated by a set of trial functions with a soliton-like form.

Another approach is that based on a "narrow soliton" approximation, when one considers high and short solitary waves. In this essentially discrete case equation (2) can again be reduced to nonlinear ODE which gives an approximate solution for a central part of the soliton in an explicit form. This approach was proposed in and applied to the case of quadratic nonlinearity. Solution obtained describes a discrete solitary wave with large amplitude which occupies only a few lattice cells and essentially differs from the Boussinesq soliton obtained in the continuum limit.

In this paper using a similar but somewhat extended approach we study solitary waves in the lattice with cubic nonlinearity. By regular procedure we derive a solution describing both a central part of the soliton and its wings. In order to check the robustness of the approach we apply the narrow soliton approximation also to the case of Toda lattice. Comparison of the exact solution shows very good agreement. We also consider processes of interactions (collisions) between discrete solitons.

2. SOLITARY WAVE SOLUTIONS

Let us consider a lattice of N particles with Hamiltonian (1) and interaction potential with cubic nonlinearity:

$$\Phi(x) = a \cdot (x^2/2 + bx^4/4). \quad (3)$$

Corresponding equations of particle motion is given by eq. (2) with force

$$F(x) = a \cdot (x + bx^3). \quad (4)$$

It is convenient to introduce displacement variables $U_n = q_n - q_{n-1}$ and rewrite (2) in the form

$$\ddot{U}_n = F(U_{n+1}) + F(U_{n-1}) - 2F(U_n) \quad (5)$$

Let us consider a solution in the form of a stationary wave:

$$U_n(t) = U_0 f(\xi), \quad \xi = \frac{n-ct}{cT} \quad (6)$$

where c and T are characteristic velocity and duration, and $\delta^{-1} = cT$ is a characteristic wave width. Note, that equation (5) is invariant under transformation $U \rightarrow -U$. Without loss of generality we assume $U_0 > 0$.

Then, substitution of (6) into eq.(5) gives an ordinary differential-difference equation for dimensionless function $f(\xi)$ in the form

$$\frac{1}{aT^2} f''(\xi) = f(\xi+\delta) + f(\xi-\delta) - 2f(\xi) + bU_0^2 \cdot [f^3(\xi+\delta) + f^3(\xi-\delta) - 2f^3(\xi)] \quad (7)$$

In continuum limit $\delta \ll 1$ (or $cT \gg 1$) using Taylor series of $F[f(\xi \pm \delta)]$ and performing twice integration over ξ one obtains in particular the well known mKdV soliton

$$U_n(t) = U_0 \operatorname{sech}[\delta \cdot (n - cT)], \quad c = \sqrt{a} \cdot (1 + bU_0^2/2), \quad \delta = (6bU_0^2)^{1/2}. \quad (8)$$

We are interested, however, in narrow solitons with large amplitudes when $bU_0^2 \gg 1$.

Then, only a few particles effectively take part in wave motion simultaneously. Nonlinearity is strong so that linear terms in eq.(7) can be neglected almost everywhere. Of course, at larger $|\xi|$ the solution becomes linear and proportional to $\exp(-\lambda|\xi|)$ with exponent λ easily found. However, this part of the solution is vanishingly small.

The equation for $f(\xi)$ takes an approximate form

$$\frac{1}{aT^2} f''(\xi) = bU_0^2 \cdot [f^3(\xi+\delta) + f^3(\xi-\delta) - 2f^3(\xi)] \quad (9)$$

We assume that for large bU_0^2 soliton width $\delta^{-1} = cT$ does not depend on the amplitude and remains constant close to unity rather than decreases to zero (as it does e.g. in the case of Toda soliton),

$$\delta \approx \text{const} \sim 1 \text{ for } bU_0^2 \gg 1. \quad (10)$$

Later this assumption is verified numerically. Then, $f'' \sim f$ and it immediately follows from (9) that soliton duration is of the order of

$$T^2 \approx 1/abU_0^2. \quad (11)$$

Taking into account (12) one finds approximate expression for soliton velocity

$$c \approx \sqrt{ab} U_0. \quad (12)$$

Using (9) one can derive two equations describing the main body and wings of a discrete soliton. Let us denote corresponding parts of function f as f_0 and f_1 .

The first equation is obtained in the region of small $|\xi|$, when terms $f'(\xi \pm \delta)$ in eq.(9) are small compared to $f^3(\xi)$ and can be omitted. Thus, corresponding equation takes the form

$$f''_0(\xi) \approx -\sqrt{2} \alpha \cdot f_0^3(\xi), \quad (13a)$$

where $\alpha = \sqrt{2}abU_0^2T^2 \sim 1$. Also, conditions $f_0(0)=1$ and $f'_0(0) = 0$ should be taken into account.

Equation for wings of the soliton is derived from (9) in the region $\xi \sim \pm\delta$, when terms $f^3(\xi)$ and $f^3(\xi \pm \delta)$ are small compared to term $f^3(\xi \mp \delta) = f_0^3(\xi \mp \delta) \sim 1$ and can be neglected,

$$f''_1(\xi) \approx \alpha/\sqrt{2} \cdot f_0^3(\xi \mp \delta). \quad (13b)$$

Note, that from eqs.(13a,b) follows that

$$f_1''(\xi) = -1/2 f_0''(\xi \mp \delta).$$

This equation can be integrated to give the following expression for soliton wings

$$f_1(\xi) = -\frac{1}{2} f_0(\xi \mp \delta) + s_1(\xi \mp \delta) + s_2, \quad \xi \sim \pm \delta, \quad (14)$$

where constants $s_{1,2}$ are determined by conditions

$$f_1(\xi) \rightarrow 0, \quad f_1'(\xi) \rightarrow 0 \text{ for } \xi \rightarrow \infty. \quad (15)$$

Thus, integrating eq.(13a) one obtains a solution describing the main body of the soliton. Then, substitution of this solution into (14) gives expression for soliton wings in the region $\xi \sim \delta$.

Note, that solution f_0 and f_1 should be joined at some point ξ_0 , where

$$f_0(\xi_0) = f_1(\xi_0), \quad f_0'(\xi_0) = f_1'(\xi_0) \quad (16)$$

Matching procedure gives two equations for two unknown values ξ_0 and δ .

Simple integration procedure⁸ leads to the solution of (13a) expressed in terms of elliptic functions,

$$\Psi[\arccos f_0(\xi), k] = \alpha \xi, \quad (17)$$

where $\Psi(z, k) = \int_0^z \frac{dx}{(1-k^2 \sin^2 x)^{1/2}}$, $k \approx 0,8$. Moreover, since modulus k is close to unity one has $\text{cn } \Psi \approx \text{sech } \Psi$, and the approximate solution for the main body of discrete soliton can be written in the form

$$U_n(t) = U_0 \cdot f_0(\xi), \quad f_0 = \text{sech } \alpha \xi \quad (18)$$

Note, that substituting (18) into (14) one can not fulfill conditions (15) which is explained by the fact that (18) is a good approximation for (14) only in the central region of the soliton. Thus, one should use more exact expression (17), or integrate (13b) numerically with function f_0 given by (18) (which gives main contribution to the integral).

Substituting solution (18) into the r.h.s. of (13b) we obtain the following equation for wings

$$f_1''(\xi) \approx \alpha/\sqrt{2} \cdot \text{sech}^3[\alpha \cdot (\xi \mp \delta)], \quad (19)$$

where $\xi \sim \pm \delta$. Taking into account conditions (15) we can integrate eq.(19) numerically to find soliton wings. Comparison with numerical results shows that analytical solution (18) is close to the actual form of the soliton in the region $|\xi| < 0,4$ (long dashed line in fig.1a). We obtained form of the soliton wings by numerical integration of eq.(19) with conditions (15) (short dashed line in fig.1a). Joining procedure gives values $\xi_0 \approx 0,4$ and $\delta \approx 0,3$. Note good agreement with actual form of the soliton practically everywhere..

Dependences of soliton velocity c and width δ^{-1} on so-

lition amplitude U_0 are shown in fig.2a and 2b, respectively. Dependence $c(U_0)$ is fairly well described by approximate expression $c \approx \sqrt{a}(1 + bU_0)^{1/2}$ which for large amplitudes coincides with (12) and for small amplitudes with (8). Similar expression is obtained in quasi-continuum approaches⁹.

For large amplitudes ($bU_0^2 \gg 1$) the width becomes constant and does not decrease which confirms our assumption. Similar result was obtained in the case with quadratic nonlinear-

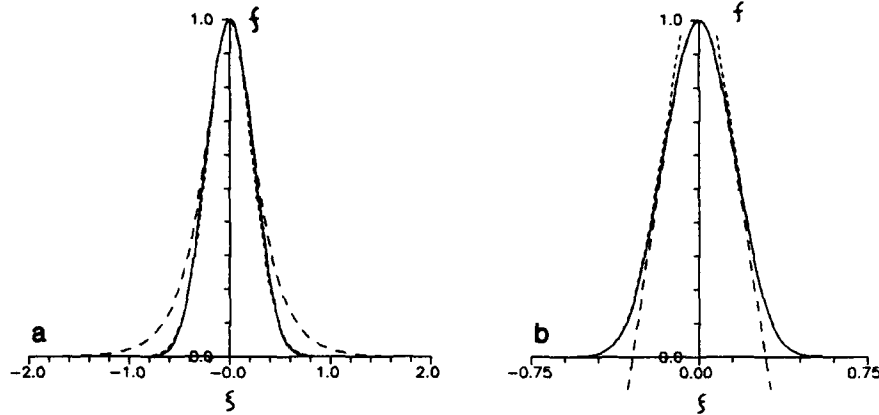


Fig.1 Solutions (15,17) (a) and (20,22) (long dashed curves for the central part and short dashed curves for soliton wings) compared with actual form of solitons in the lattice with cubic nonlinearity ($U_0 = 4,3$; $c = 3,5$) (a) and Toda lattice ($U_0 = 4,5$) (b) (full curves). Parameters $a = 1$; $b = 1$.

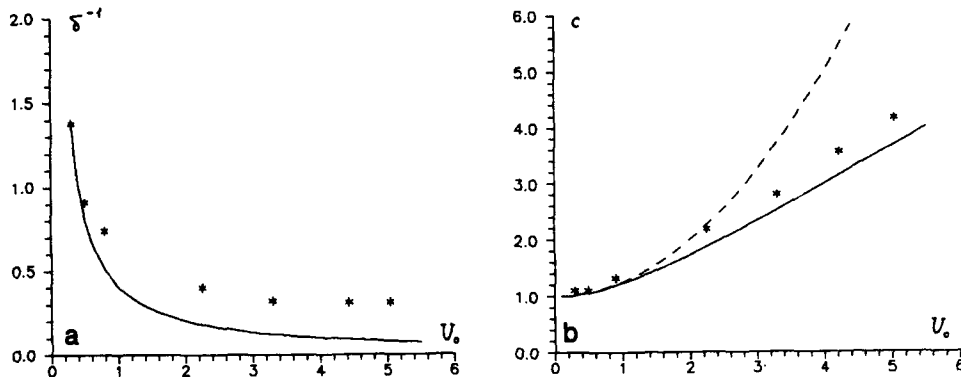


Fig.2 Dependences of soliton width $\delta^{-1} = cT$ vs. soliton amplitude (a) and soliton velocity c vs. soliton amplitude U_0 (b). Full curve corresponds to solution (8) obtained in the continuum limit, stars correspond to numeric results.

ity⁸. This saturation effect can also be deduced from solutions obtained with the use of quasi-continuum methods and variational approaches^{9,10}.

It is of interest to apply the narrow soliton approximation to the completely integrable case of the lattice with exponential potential $\Phi(x) = a \cdot \exp(bx)$ (Toda lattice) in order

to compare corresponding solution with exact analytical form of the soliton.

According to approximation used above, the central part of the soliton is described by function $f_0(\xi)$ which is obtained after integration of the following equation

$$f''_0(\xi) = -2 a T^2 U_0^{-1} \exp [b U_0 f_0(\xi)], \quad (20)$$

with conditions $f(0) = 1$ and $f'(0) = 0$. The corresponding expression takes the form

$$f_0(\xi) = (b U_0)^{-1} \ln(\operatorname{sech}^2 \alpha \xi) + 1, \quad (21)$$

with coefficient $\alpha = T (ab)^{1/2} \exp(b U_0 / 2)$.

In the region $\xi = \pm \delta$ the soliton is described by function $f_1(\xi)$ which is found from the equation (14) together with conditions (15) in the form

$$f_1(\xi) = -f_0(\xi \mp \delta) / 2 \pm \frac{\alpha}{b U_0} (\xi \mp \delta) + 1/2 + \ln 2 / b U_0, \quad (22)$$

where $\xi \sim \pm \delta$.

Exact solution is given by the following expression³

$$f(\xi) = (b U_0)^{-1} \ln(1 + \operatorname{sh}^2 \delta \cdot \operatorname{sech}^2 \xi), \quad (23)$$

and parameters U_0 and T are expressed through parameter $\delta = 1/cT$ as

$$T = 1/\operatorname{sh} \delta, \quad U_0 = 1/b \ln(1 + \operatorname{sh}^2 \delta). \quad (24)$$

Comparison of exact solution (23) with solution (21,22) obtained under narrow soliton approximation shows very good agreement (fig.1b).

Moreover, one can easily see that the matching condition in this case implies that the approximate solution can be written in the form

$$f^a(\xi) = f_0(\xi) - \frac{1}{2} [f_0(\xi + \delta) + f_0(\xi - \delta)]. \quad (25)$$

After substitution (21) into (25) and taking into account that factor α tends to 1 for sufficiently large amplitude, we find that f^a coincides with exact solution (23).

Note also that in the case of Toda lattice there is no saturation effect. Indeed, from (24) one finds for large amplitudes

$$\delta \sim b U_0.$$

Thus, the width of Toda soliton always depends on the amplitude and no saturation takes place.

3. INTERACTIONS OF DISCRETE SOLITONS

As it was mentioned above, in the continuum limit system (4) becomes completely integrable and solitary wave solutions correspond to mKdV-solitons. It is well known that collisions of solitons cause only phase shifts while each interacting soliton retains its identity. Generally, it is believed that such interactions of solitary waves may serve as an indication

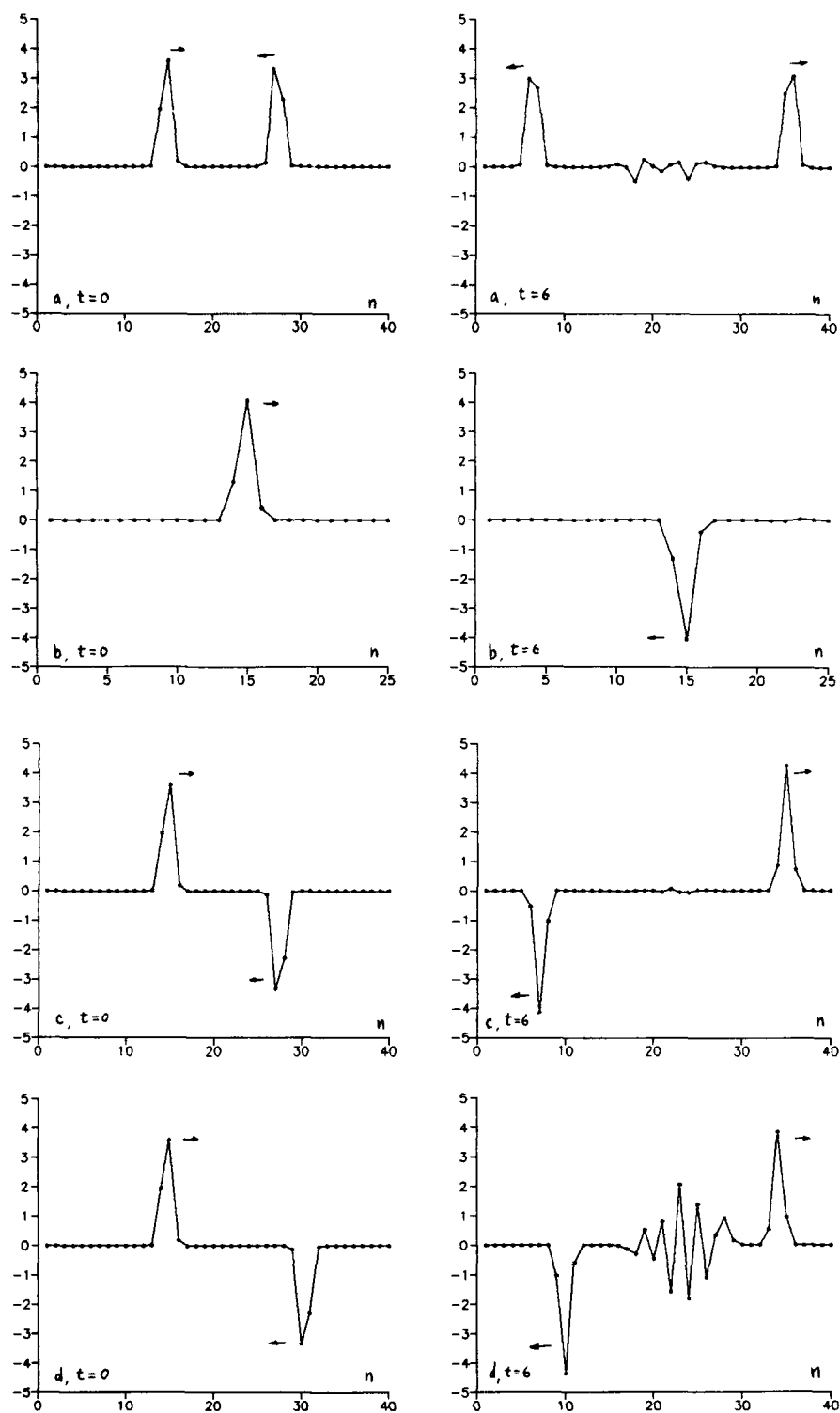


Fig.3 Different stages of collisions of two discrete solitons of the same polarity (a), of different polarities (c,d) and the process of reflection of the discrete soliton from the fixed (right) boundary (b).

that system is completely integrable, i.e. has the number of independent integrals equal to the number of degrees of freedom, or infinite number of integrals in the case of a continuum system¹⁵. However, in the non-integrable case under study collisions of discrete solitons typically result in additional effects such as radiation.

We studied numerically processes of collisions of discrete solitons and reflection of a soliton from the fixed boundary (figs.3). We found that collisions of two discrete solitons generally result in some radiation (fig.3a). Reflection of the soliton from the fixed boundary only changes its polarity, the radiation being considerably smaller than that after collision in fig.3a (fig.3b). Note, that amount of radiation released due to collision may be very sensitive to initial conditions. Namely, if initial positions of solitons are chosen in such a way that collision of solitons is effectively equivalent to reflection, the radiation is very small (fig.3b). However, if initial positions of solitons are changed, the radiation is much stronger (fig.3c). A possible reason for it is the strong influence of the cell located between solitons: in case of an exact antisymmetry of collision (or reflection) this cell remains fixed throughout all interaction time (which automatically is fulfilled for reflection).

Note, that the radiation field is small compared to solitons amplitude, so that solitons practically do not change. However, after several collisions radiation may become substantial which results in an irregular motion of the lattice.

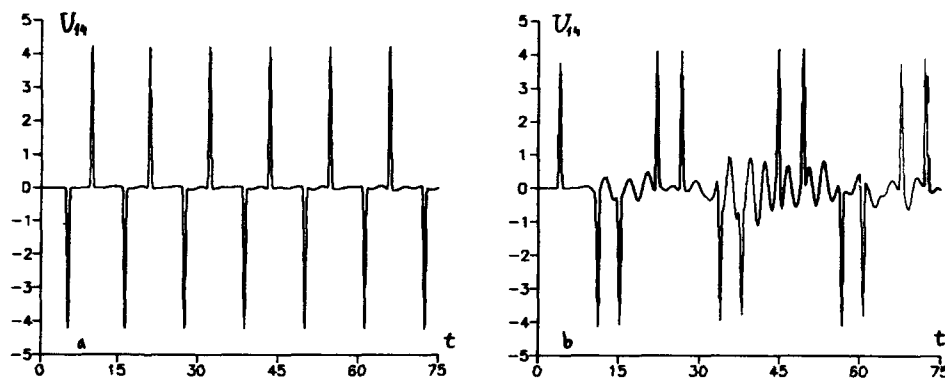


Fig.4 Dependence of displacement U_{14} vs. time for initial conditions similar (a) to those in fig.4a (one soliton) (a) and (b) in fig.3a (two solitons).

In order to demonstrate how long soliton pattern can exist in FPU-lattice, we performed numerical integration of dynamics of solitons in a resonator with fixed ends ($U=0$ at the boundaries) for two different initial conditions. If initially only one soliton is given, motion of the lattice remain regular for a considerable time (fig.4a). In this case weak radiation is released due to reflections of the soliton from boundaries, and the form of the soliton as well as its energy practically does not change. On the other hand, if two solitons are present initially, their multiple collisions lead to substantial radiation and subsequent irregular motion of the lat-

tice (fig.4b). This may serve as demonstration of an essential role of collisions of discrete solitons collisions in the process of thermalization in FPU-lattice.

4. DISCUSSION

The main subject of this paper are discrete solitary waves in lattices with cubic nonlinearity. The wave amplitude is large enough, so that soliton is localized at a scale of one lattice cell and only a few particles take part in motion at a time. Using the narrow soliton approximation we construct an analytical solution describing both the main body and wings of the soliton. Soliton width is found to be independent of the amplitude as the latter becomes large, so that a situation takes place. Velocity of the soliton is proportional to its amplitude in the limit of large amplitudes.

In order to demonstrate the robustness of the approach used we applied it to the case of Toda lattice and compared an approximate solution with an exact one. We find that for large amplitudes there is a fairly good agreement.

We also studied numerically processes of collisions of discrete solitons. We found that generally some radiation is released. The radiation is very sensitive to initial conditions. For example, in fully antisymmetric case, when collision of two solitons with different polarities and close amplitudes is equivalent to reflection of one soliton from the fixed boundary, the radiation produced is notably smaller.

Multiple collisions bring about irregular motion of the lattice which can be regarded as a source of stochastization in FPU-lattices.

As inviting future developments we consider application of the developed analytical approach to the problem of evolution of discrete soliton under the action of a small perturbation (e.g. energy losses), generalization of the theory to 2D- and 3D-systems and consideration of FPU-problem from the point of view of the models of discrete solitons ensembles.

Another class of problems related to discrete description and associated with soliton motion include "soliton lattices" first mentioned in¹⁷. Here solitons are not necessarily discrete and can even be described by the continuum limit equations. There is an ensemble of solitons with close velocities which can be described as classical particles interacting with some potential¹⁶.

It is of interest to note that since a soliton typically has an exponential asymptotic form $f(\xi) = \exp(-\lambda\xi)$ the interaction potential is also exponential and the lattice of solitons is equivalent to Toda lattice¹⁷. Thus, there is a solution corresponding to Toda soliton which may be considered as a modulation soliton. The Toda lattice equation plays here the same role as the nonlinear Schrödinger equation for quasiharmonic waves.

If modulation of the lattice of solitons is strong, i.e. there is a large velocity difference, its dynamics constitutes more readily propagation of a dislocation than oscillations of solitons relative to one another. In fact, this case corresponds to the essentially discrete dynamics discussed above.

A greater variety of processes is exhibited for lattices of solitons with oscillating asymptotic fields (complex λ) such as in the case of Kawahara equation. There is a countable family of bound states of such solitons as well as unstable

lattices, the instability leading to a disordered motion¹⁷.

Another interesting class of problems relates to "really distributed" systems in a form of a continuous wave system periodically loaded with discrete nonlinear elements which form a kind of lattice, e.g. a transmission electric line with nonlinear capacities or mechanical system of domains with nonlinear wall motions¹⁸. Note, that in linear approximation dispersive curves in (ω, k) -plane form a typical multizonal structure in case of weak coupling. Then, phase velocities of a set of wave harmonics may be close to each other not only for very low frequencies (in the limit of the first zone) but in case when each next harmonic lies in the subsequent zone (because main part of dispersion curves lies close to the line $\omega = ck$). Thus, there exists a class of waves with the scale much smaller than the lattice period. They can be described as stationary progressive waves on the lattice.

REFERENCES

1. Yu.K.Bogatyryov and L.A.Ostrovsky. Propagation of Electromagnetic Waves in Nonlinear Lumped Transmission Lines: The Structure of the Shock Waves Front. *Izv.VUZov Radiofizika* 4, no.5, 1063 (1963) (in Russian).
2. E.Fermi, J.Pasta, S.Ulam, Collected Papers of Enrico Fermi (Univ. of Chicago Press, Chicago 1965) vol.11, p.978.
3. M.Toda, Theory of Nonlinear Lattices, Springer-Verlag, Berlin Heidelberg New-York 1981.
4. J.H.Batteh and J.D.Powell. Propagation of Solitons in One-Dimensional Chain Under Shock Compression, in *Solitons in Action* (Academic Press, New-York 1978).
5. P.L.Christiansen and A.C.Scott. *Davydov Soliton Revisited* Plenum, New-York (1990).
6. N.Zabusky, M.Kruskal, *Phys.Rev.Lett.* 15, 240 (1965).
7. P.Rosenau. Dynamics of Dense Lattices. *Phys.Rev.A* 36, 5868 (1987).
8. J.C.Eilbeck and R.Flesch. Calculation of Families of Solitary Waves on Discrete Lattices. *Phys.Lett.A* 149, 200 (1990).
9. O.A.Druzhinin and L.A.Ostrovsky. Solitons on Discrete Lattices. *Phys.Lett.A* 160, no.11, 357 (1991).
10. J.A.D.Wattis, Approximations to solitary waves on lattices:1, preprint (1992).
11. D.B.Duncan and J.A.D.Wattis Approximations to solitary waves on lattices:2, preprint (1992).
12. C.Gardner, G.Green, M.Kruskal, R.Miura, *Phys.Rev.Lett.* 19 (1967), 1095.
13. V.E.Zakharov, L.D.Faddeev, *Functional Analysis* 5 (1971), no.4, 18 (in Russian).
14. V.E.Zakharov, *JeTPh* 67, 219 (1973) (in Russian).
15. P.Zhang, *J.Math.Phys.* 32 (1991) no.11, 3055.
16. K.A.Gorshkov, L.A.Ostrovsky and V.V.Papko, *Sov.Phys.JETP* 44, 306 (1976).
17. K.A.Gorshkov and V.V.Papko. Dynamic and Stochastic Oscillations of Soliton Lattices. *Sov.Phys. JETP* 46(1), 92, (1977).
18. Yu.K.Bogatyryov, K.A.Gorshkov and L.A.Ostrovsky. Nonlinear Waves in Periodic Structures. *Radiotekhnika i Elektronika* 3, 461 (1976) (in Russian).

DYNAMICAL STRUCTURES IN 2D LATTICES

M. Remoissenet¹, J. Pouget² and J.M. Tamga¹

¹Laboratoire O.S.C, 6 Blvd Gabriel 21000 Dijon, France

²Laboratoire de Modélisation en Mécanique
Université P. et M. Curie 75252 Paris Cedex 05, France

1. INTRODUCTION

Very little is known about nonlinear entities in dimension higher than one, their formation and dynamics are of great interest in various branches of science¹. Two dimensional structures²⁻³ (domain walls, vortices) play an important role in the material properties and they become crucial in nonlinear physics involved in the problem of adsorbates deposited on crystal surfaces. In this paper we focus on the formation of localized states mediated by modulational instability in a two-dimensional (2D) lattice. The paper is organized as follows. In section 2 we introduce our model which is a two-dimensional non-dissipative Frenkel-Kontorova model with additional nonlinear interactions. In section 3 the discrete equations governing the dynamics of the lattice are reduced to a two-dimensional nonlinear Schrödinger equation in the low amplitude and semi discrete limit. Then, in section 4, the modulational instability conditions of this equation are calculated. Section 5 deals with numerical simulations, we investigate the role played by modulational instability on the evolution into localized states of an initial plane wave, with low amplitude, propagating on the lattice.

2. LATTICE MODEL

The basic model is made of a two-dimensional lattice equipped, at each node, with a *rotator* or *rigid rotating molecule*. Namely, each molecule can rotate in the lattice plane. At site (m, n) the angle of rotation is $\Phi_{m,n}$. Each molecule interacts *nonlinearly* with its first-nearest neighbors and with a *periodic substrate potential*. Under these conditions the equation of motion of the molecule at site (m, n) is :

$$\ddot{\Phi}_{m,n} = \frac{G_L}{J}(\Phi_{m+1,n} + \Phi_{m-1,n} - 2\Phi_{m,n}) + \frac{G_T}{J}(\Phi_{m,n+1} + \Phi_{m,n-1} - 2\Phi_{m,n})$$

$$\begin{aligned}
& + \frac{B_L}{J} [(\Phi_{m+1,n} - \Phi_{m,n})^3 - (\Phi_{m,n} - \Phi_{m-1,n})^3] \\
& + \frac{B_T}{J} [(\Phi_{m,n+1} - \Phi_{m,n})^3 - (\Phi_{m,n} - \Phi_{m,n-1})^3] - \omega_0^2 \sin \Phi_{m,n}
\end{aligned} \quad (1)$$

Here, J is the inertia of the molecules, G_L and G_T are the linear coupling coefficients in the longitudinal and transverse directions while the parameters B_L and B_T are the nonlinear coupling coefficients in the longitudinal and transverse directions, respectively. The last term in Eq.(1) is due to the substrate potential where ω_0^2 is the strength of the potential barrier and ω_0 can be interpreted as the frequency of small oscillations in the bottom of potential wells. Note that if the nonlinear couplings is removed ($B_L = 0$ and $B_T = 0$) Eq.(1) reduces to the 2-D Frenkel-Kontorova or 2-D discrete sine-Gordon model⁴. Next, we derive the nonlinear dispersion relation corresponding to (1). To calculate the nonlinear dispersion relation, we assume *plane wave solutions* with slowly varying envelope $\psi_{m,n}$:

$$\Phi_{m,n}(t) = \epsilon \psi_{m,n} \exp[i(\omega t - k_L m a - k_T n a)] + cc \quad (2)$$

Here cc denotes the complex conjugate, k_L and k_T are the components of the wave vector $\vec{k} = (k_L, k_T)$, ω is the circular frequency of the carrier wave which varies rapidly, and $\epsilon \ll 1$. The small amplitude limit is considered, this allows us to expand the sine function with respect to $\Phi_{m,n}$ up to the third order. On inserting (2) into (1) and neglecting the third order harmonic terms we obtain the *nonlinear dispersion relation*

$$\begin{aligned}
\omega^2 = & \omega_0^2 + 4 \frac{C_{0L}^2}{a^2} \sin^2\left(\frac{k_L a}{2}\right) + 4 \frac{C_{0T}^2}{a^2} \sin^2\left(\frac{k_T a}{2}\right) \\
& + \epsilon^2 \left[\frac{48 B_L}{J} \sin^4\left(\frac{k_L a}{2}\right) + \frac{48 B_T}{J} \sin^4\left(\frac{k_T a}{2}\right) - \frac{1}{2} \omega_0^2 \right] |\psi|^2
\end{aligned} \quad (3)$$

Where $C_{0L}^2 = G_L a^2 / J$ and $C_{0T}^2 = G_T a^2 / J$. The first three terms in the right hand side of Eq.(3) represent the linear contribution to the dispersion relation whereas the last term corresponds to the nonlinear contribution. In the above calculations we have used the continuum approximation and the slow envelope was considered as constant in comparison to the rapid carrier oscillations.

3. DERIVATION OF THE 2D NONLINEAR SCHRÖDINGER EQUATION (2D-NLS)

We consider slow modulation in space and time of a carrier wave with given wave numbers k_{Lc} and k_{Tc} . Restricting our attention to the case of a carrier wave propagating in the x direction i.e $k_{Lc} = k_c$ and $k_{Tc} = 0$ we can reduce Eq.(1) to a *2D nonlinear Schrödinger equation* by using the multiple scales perturbative technique or consider the nonlinear dispersion relation(3). We have verified that both methods give the same result. Under this condition we get

$$i\epsilon(\psi_{t_1} + V_{gL}\psi_X) + \epsilon^2 P_1 \psi_{XX} + \epsilon^2 P_2 \psi_{YY} + \epsilon^2 Q |\psi|^2 \psi = 0 \quad (4)$$

where

$$P_1 = \frac{1}{2} \left(\frac{\partial^2 \omega}{\partial k_L^2} \right)_c, P_2 = \frac{1}{2} \left(\frac{\partial^2 \omega}{\partial k_T^2} \right)_c, Q = - \left(\frac{\partial \omega}{\partial |\psi|^2} \right)_c, V_{gL} = \left(\frac{\partial \omega}{\partial k_L} \right)_c$$

Considering a frame moving with group velocity V_{gL} and using the transformation $\xi = X - V_{gL}t_1$, $\eta = Y$, $\tau = \epsilon t_1$ next (V_{gL} being the group velocity in the longitudinal direction), we transform Eq.(4) into the *standard 2D Nonlinear Schrödinger equation* :

$$i\psi_\tau + P_1\psi_{\xi\xi} + P_2\psi_{\eta\eta} + Q|\psi|^2\psi = 0 \quad (5a)$$

where

$$P_1 = [C_{0L}^2\omega_c^2 a^2 \cos(k_c a) - C_{0L}^4 \sin^2(k_c a)]/2a^2\omega_c^3, P_2 = C_{0T}^2/2\omega_c \quad (5c)$$

$$Q = [\frac{1}{2}\omega_0^2 - 48\frac{B_L}{J} \sin^4(\frac{k_c a}{2})]/2\omega_c \quad (5d)$$

This equation has been extensively studied especially in plasma physics, hydrodynamics and optics⁵. We now restrict our study to the isotropic case, i.e $G_L = G_T = G$ ($C_{0L} = C_{0T} = C_0$) and $B_L = B_T = B$. Proceeding as Yuen and Lake⁶ for their study of hydrodynamic waves it is convenient to reduce Eq.(5a) to a 1D equation, that is to consider plane modulation at an angle α from the direction of propagation of carrier wave. Namely we introduce the oblique coordinate

$$S = \xi \cos \alpha + \eta \sin \alpha$$

Equation(5a) is then transformed into the *1D Nonlinear Schrödinger equation (NLS)*

$$i\psi_\tau + P\psi_{SS} + Q|\psi|^2\psi = 0 \quad (6)$$

where the dispersion coefficient P is given in Appendix. Equation(6) describes the evolution of the envelope ψ in the S direction of a carrier wave propagating in the x direction.

4. MODULATIONAL INSTABILITY

Using Eq.(6) we can investigate the stability of a plane wave propagating on the lattice. A linear analysis of a small perturbations of this elementary plane wave solution yields a criterion of instability named modulational or Benjamin-Feir instability. Skipping all the analytical details the region of instability is given by

$$0 < q < q_l = \psi_0 \sqrt{Q/P}$$

with $PQ > 0$ and where q is a real wave number in the S direction. Thus a perturbation with a wave vector $\vec{q}=(q_L, q_T)$ satisfying $0 < q_L < q_l \cos \alpha$ and $0 < q_T < q_l \sin \alpha$ can trigger instability in the lattice. Here q_L and q_T are the wave numbers of the perturbation in the longitudinal and transverse directions. α is an angle defined by $\alpha = \tan^{-1}(q_L/q_T)$. The maximum instability occurs at $q_{Lmax} = (q_l/\sqrt{2})\cos \alpha$ and $q_{Tmax} = (q_l/\sqrt{2})\sin \alpha$ with a maximum growth rate given by $\sigma_{max} = |\nu| = Q\psi_0^2$. The modulational instability criterion depends on the sign of PQ which depends itself on the carrier wave number and on the modulational propagation direction, for $\alpha = 0$ the instability is longitudinal, for $\alpha = \pi/2$ the instability is transverse. In the first Brillouin zone three cases are possible (see Appendix) : (i) for $0 < k_c < k_{c2}$, $PQ > 0$ for all α , (ii) for $k_{c2} < k_c < k_{c1}$, PQ is always negative, (iii) if $k_{c1} < k_c < \pi/a$, then we have $PQ > 0$ for $\alpha < \alpha_c$ and $PQ < 0$ for $\alpha > \alpha_c$. In this last case, like for hydrodynamic waves⁶ there is a limiting angle which can be calculated from model parameters. However, in the following the influence of this limiting angle will not be examined. We will restrict ourselves to case (i).

5. NUMERICAL SIMULATIONS AND CONCLUSION

Now, we want to clarify the role played by modulational instabilities on the response of the lattice to an initial homogeneous disturbance with low amplitude. Furthermore, we attempt to elucidate the dynamics of nonlinear structures which should appear in the long time evolution of the lattice and cannot be predicted from the 2D-NLS model.

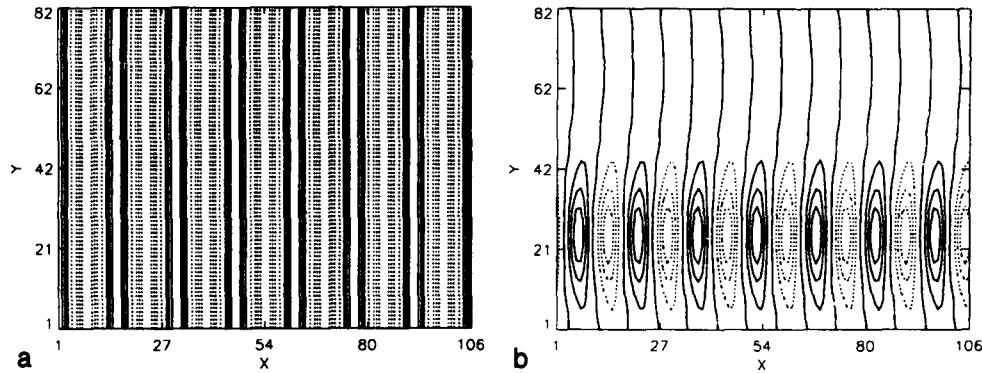


Figure 1. Contour plots corresponding to Φ^2 for $\alpha = \pi/2$ (full line for $\Phi > 0$, dashed line for $\Phi < 0$): (a) initial condition, (b) recurring patterns at time $T = 2000$.

At this end we use *numerical simulations which are directly performed on the original microscopic equations* [see Eq.(1)] which govern the dynamics of the 2D lattice. Specifically, we consider a lattice plane made of 106×82 points along with periodic boundary conditions on left and right sides and on lower and upper boundaries, as well. The initial conditions are provided by an harmonic wave carrier traveling in the x direction and homogeneous in the transverse direction with amplitude A , wavenumber k_c and frequency ω which satisfies the dispersion relation (3) where $k_T = 0$. This dispersion relation implies a nonzero phase velocity because a forbidden band exists for $0 < \omega < \omega_0$ as given by Eq.(3) in the linear limit. We take $A = 0.35$ and we have 7 periods within the longitudinal length of the lattice plane which leads to $k_c \simeq 0.415$. The simulations are carried out for the discrete sine-Gordon system, that is with zero nonlinear coupling ($B = 0$). The strength of the substrate potential is $\omega_0^2 = 0.09$ (the linear coupling G is set to the unity). In order to trigger the instability, small ($\simeq 10^{-3}$) random or coherent perturbations are superposed to the initial velocity $\dot{\Phi}$ and removed afterwards. We have first checked that for $\alpha = 0$ a small coherent modulational perturbation the initial sinusoidal wave breaks into a train of envelope-solitons we recover the classical modulational instability which occurs in 1D system. Otherwise, in the transverse case the coherent perturbation gives rise to transverse instability; beyond this instability periodic patterns appear which recur, in the Fermi Pasta Ulam sense, to the initial state and so on [see figure 1]. For $0 < \alpha < \pi/2$, the initial plane wave (see figure 1.a), modulated by

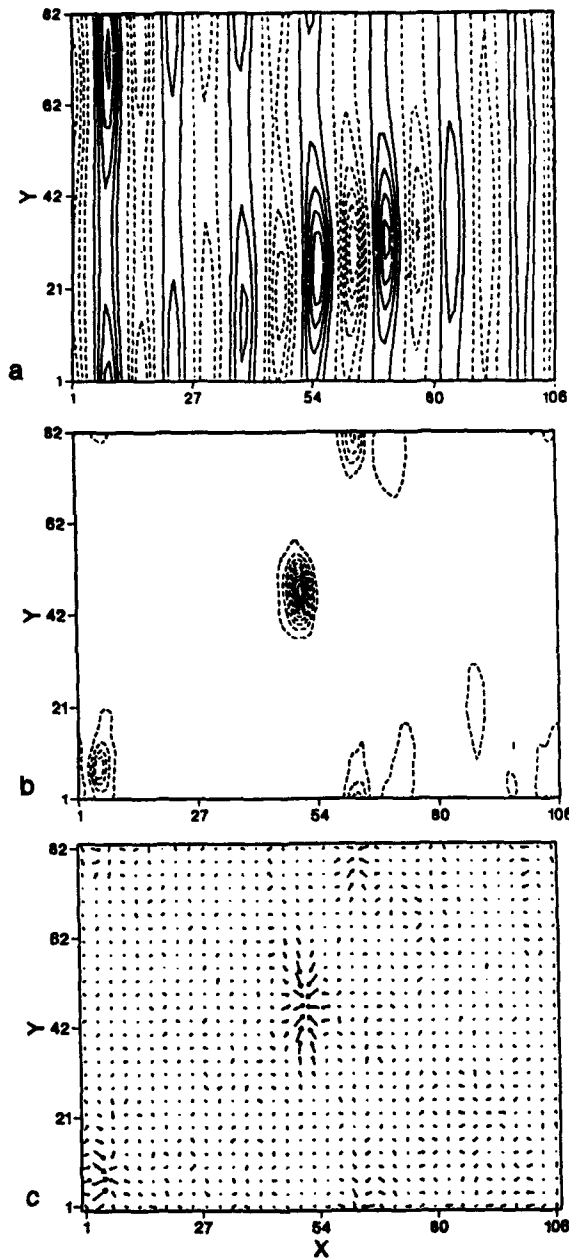


Figure 2. (a) the birth of localized structures at time $T = 1280$, (b) moving pulsons at time $T = 4200$, (c) patterns corresponding to figure 2 (b). the arrows depict the rotation gradient.

a random or coherent perturbation, evolves into localized structures inhomogeneously distributed on the lattice. The results are collected together in figure 2 where we have the contour line plots for $\text{sign}(\Phi)\Phi^2$. Then, as predicted by the NLS model, the instability occurs and after a lapse of time $T = 1280$, the small initial perturbation gives rise to stretched localized structures along the transverse direction. At time $T = 4200$, we observe very clearly some localized structures which are ellipse-shaped

as shown in figure 2.b. They look like the ring solitons or pulsons observed numerically in 2D sine-Gordon system with different boundary conditions⁷. When time further increases, these localized structures still persist and look like stable. No recurrence to the initial state of these structures was observed for these set of simulations. The characteristic extends of these structures are about 10 lattice spacings in x direction and 21 lattice cells in y direction. We attribute this anisotropy to the discreteness effects which could be important in x direction while the continuum limit seems to be acceptable in the transverse direction. In figure 2 (c) we have represented the finite differences gradient of the rotation $\Phi_{m,n}$ in x and y directions. The resulting structures present some similarities with vortex-like structures⁸.

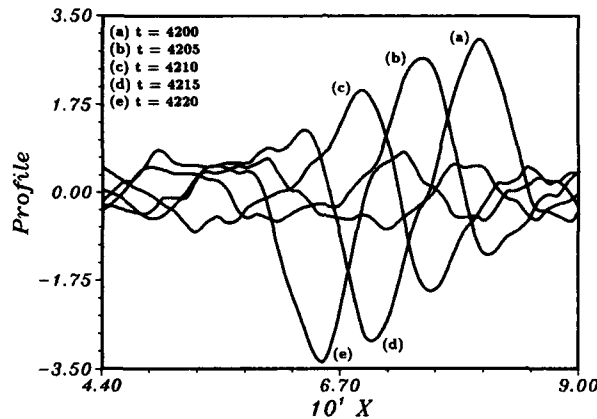


Figure 3. Evolution of the profile of a typical structure between times $T = 4200$ and $T = 4220$. The profile shows that the pulson breathes while moving in the x direction.

In order to obtain more details about the dynamics of a particular structure we have plotted the profile, in x direction, of the structure located in the middle of the lattice between times $T = 4200$ and $T = 4220$, the results are shown in figure 3. It is now clear that the structure is moving in the x direction while oscillating like a breather or a pulson. From these results we can estimate the traveling velocity of the pulson $V_{trav} \simeq 0.55$ and its circular frequency : $\Omega \simeq 0.2$. It is very interesting to note that this frequency is smaller than the cut-off frequency $\omega_0 = 0.3$: it lies in the lower linear gap of the lattice. Finally, we note that the amplitude of the pulsons is large and such that : $-4\pi/3 < \Phi < 4\pi/3$, thus the (molecular) rotations overcome collectively the potential barrier, but they do not reach the bottom of the next well. By increasing the nonlinear coupling we can change the sign of the coefficient Q in the nonlinear Schrödinger equation[see eq.(5d)]. This implies that PQ can become negative and the instabilities disappear as we have checked numerically.

In conclusion, our present study shows, that the complex physics of nonlinear oscillations in extended systems such as 2D lattices allows the jumping of energy from an initial extended state weakly excited, into local pulses. All our results indicate that the 2D-NLS model is efficient to predict the instabilities of an initial steady state on the lattice. Nevertheless, such a model does not allow to approach the long time regime which is characterized by the appearance of localized breathing modes or pulsons. The properties of these pulsons, their number and their distribution, must be further studied both numerically and theoretically.

APPENDIX

The dispersion coefficient P of nonlinear Schrödinger equation [see Eq.(6)] is given by

$$P = f(k_c) \cdot [g(k_c) - \cos^2 \alpha] \quad (C.1)$$

where

$$f(k_c) = \frac{4C_0^4 \sin^4(k_c a/2) + (4C_0^4 + 2C_0^2 \omega_0^2 a^2) \sin^2(k_c a/2)}{2\omega_0^3 a^2} \quad (C.2)$$

$$g(k_c) = \frac{4C_0^2 \sin^2(k_c a/2) + \omega_0^2 a^2}{4C_0^2 \sin^4(k_c a/2) + (4C_0^2 + 2\omega_0^2 a^2) \sin^2(k_c a/2)} \quad (C.3)$$

For $g(k_c) > 1$ i.e $k_c < k_{c1} = \frac{2}{a} \sin^{-1} \left(\sqrt{\frac{\omega_0^2 a^2 + \sqrt{\omega_0^4 a^4 + 4C_0^2 \omega_0^2 a^2}}{4C_0^2}} \right)$, P is always positive. Otherwise if $k_c > k_{c1}$, then P is positive for $\alpha > \alpha_c$ and negative for $\alpha < \alpha_c$ where α_c is given by

$$\alpha_c = \cos^{-1} \left(\sqrt{\frac{4C_0^2 \sin^2(k_c a/2) + \omega_0^2 a^2}{4C_0^2 \sin^4(k_c a/2) + (4C_0^2 + 2\omega_0^2 a^2) \sin^2(k_c a/2)}} \right) \quad (C.4)$$

Let us define the critical wave number k_{c2} for which Q becomes zero. Q is positive for $k_c < k_{c2}$ and negative for $k_c > k_{c2}$. k_{c2} is given by

$$k_{c2} = \frac{2}{a} \sin^{-1} \left[\left(\frac{J\omega_0^2 a^4}{96B_L} \right)^{\frac{1}{4}} \right] \quad (C.5)$$

In the first Brillouin zone $[0, \frac{\pi}{a}]$, we deduce that if $0 < k_c < k_{c2}$ then PQ is positive for all angles. If $k_{c2} < k_c < k_{c1}$ then $PQ < 0$ for all α . If $k_{c1} < k_c < \pi/a$ then we have $PQ > 0$ for $\alpha < \alpha_c$ and $PQ < 0$ for $\alpha > \alpha_c$.

REFERENCES

1. A.V. Gaponov-Grekhov and M.I. Rabinowich, Physics Today, 43,30(1990)
2. F. Falo, A.R. Bishop, P.S. Lomdahl and B. Horovitz, Physic. Rev.B 43,8081(1991)
3. P. Coullet and D. Walgraef, Europhys. Lett, 10, 525(1991)
4. J. Pouget, S. Aubry, A.R. Bishop and P.S. Lomdahl, Phys.Rev.B39,9500(1989)
5. V.E. Zakharov, Sov. Phys. JETP 35, 908 (1972).
6. H.C. Yuen and B.M. Lake Phys. Fluids, Vol.18, pp. 956-960 (1975).
7. P.L. Christiansen and P.S. Lomdahl, Physica 2D, pp 482-494(1981)
8. Y. Ishimori, J. Phys. Soc. Jpn. 55, 82(1986).

MODEL HAMILTONIAN, COHERENT STATE AND ANHARMONIC LOCALIZED MODES AS DYNAMICAL SELF-TRAPPING IN NONLINEAR SYSTEMS AND BIOLOGICAL MACROMOLECULES

Shozo Takeno

Laboratory of Physics
Faculty of Engineering and Design
Kyoto Institute of Technology
Kyoto 606, Japan

I. Introduction

The soliton theory in mathematical physics has been generally established for spatially one-dimensional(1D), continuous systems except for a few exceptional cases such as the Toda lattice.¹ Underlying concepts are the inverse-scattering-theory formalism,² the Hirota bilinear form using the D -operators,³ the Sato τ -function theory⁴ and so on. An open question and issue are whether or not the concepts developed in mathematical physics and mathematics are equally applicable to realistic problems in physics, such as higher dimensional continuous systems, discrete lattices, solids, small molecules, macromolecules, etc. and biological systems. In field theory, finite-energy, stable localized classical solutions of nonlinear differential equations have often been identified as solitons,⁵ while nonlinear differential difference equations in solid state physics, biophysics and biochemistry have been reduced to differential equations by using the continuum approximation to get solitons.

On the other hand, recent studies on the vibrational properties of perfect anharmonic crystal lattices have shown the existence of stationary (immobile) localized modes above the top of the harmonic frequency band.⁶ For 1D lattices with the hard quartic anharmonicity, approximate analytical calculations and numerical experiments^{7,8} have been performed to show the existence of moving anharmonic localized modes. Also shown are the existence in d -dimensional lattices of exact analytical solutions of moving anharmonic localized modes for specific nonlinear exciton transfer problems.⁹ It has been shown that some of the moving anharmonic localized modes in these cases look like solitons under favorable conditions.

Generally speaking, solitons in solids, molecular and biological systems, if any, can be considered as nonlinear, particlelike collective modes born out of a sea of small

amplitude atomic or molecular motion, in which a large number of quanta are involved. Then, questions are: (a) what are natures of quantum states of solitons obtained as classical solutions in nonlinear physics. (b) how the classical solutions emerge from quantum states? (c) what are associated quantum fluctuations?

The purpose of this paper is threefold: (A) To introduce a concept of anharmonic localized modes originally motivated in solid state physics into the soliton theory to obtain solitonlike nonlinear modes in discrete systems, such as lattices including higher dimensional cases, molecules, and biological systems. (B) To apply a coherent state path integral formalism to study the concept of solitons in strongly nonlinear quantum systems. (C) To study vibron soliton problems¹⁰ in dynamical self trapping problems in polypeptides¹¹ and molecular crystals¹² from the viewpoint of anharmonic localized modes.

II. Stationary Anharmonic Localized Modes

First, we illustrate an anharmonic localized mode, put forward by Sievers and the present author in 1988⁶, by studying its simplest form for stationary modes. Let us consider a perfect anharmonic lattice with harmonic and hard quartic potential governed by the equation

$$\ddot{u}_n(x) = - \sum_{x_1} J_2(x, x_1) u(x_1) - \sum_{x_1, x_2, x_3} J_4(x, x_1, x_2, x_3) u(x_1) u(x_2) u(x_3). \quad (1)$$

with

$$J_2(x, x_1) = K_2(x, x_1)/M, \quad J_4(x, x_1, x_2, x_3) = K_4(x, x_1, x_2, x_3)/M, \quad (2)$$

where, $u_\alpha(n)$ with $x = (n, \alpha)$ is the α component of the displacement from its equilibrium position of an atom with atomic mass M at an n th lattice site. The K_2 's and the K_4 's are the force constants derived from the harmonic and quartic potentials, respectively. We look for stationary vibrational modes of the system by setting

$$u(x) = 2 \sum_{p=1}^{\infty} \cos[(2p+1)\omega t] \phi_p(x), \quad (3)$$

where the $\phi_p(x)$'s are profile functions of the modes with frequency $(2p+1)\omega$, all of which are assumed to be independent of time variable t . For simplicity, we use a rotating-wave approximation (RWA) from the outset to obtain

$$\phi(x) = 3 \sum_{x_1, x_2, x_3} G(x, x'; \omega) J_4(x', x_1, x_2, x_3) \phi_1(x_1) \phi_1(x_2) \phi_1(x_3). \quad (4)$$

Here

$$G(x, x'; \omega) = \sum_{\mu} \frac{\varphi_{\mu}(x) \varphi_{\mu}^*(x')}{\omega^2 - \omega(\mu)^2} \quad (5)$$

is the lattice Green's function for the harmonic lattice, in which the $\omega(\mu)^2$ and the $\varphi_{\mu}(x)$'s are the squared-frequency eigenvalues and the corresponding eigenfunctions, respectively, characterized by the index μ for the harmonic lattice. Close similarity of Eq.(4) to eigenvalue equations for harmonic localized modes due to an impurity¹³ is noted. It is shown that Eq.(4) exhibit localized mode solutions with eigenfrequencies outside the harmonic frequency band $\omega(\mu)$ under certain conditions.

Analytical solutions to Eq.(4) can be obtained by considering the extreme localization limit for a mode lying far above the top of the harmonic frequency band. The result for

a d -dimensional simple cubic lattice with the nearest neighbor harmonic and quartic-anharmonicity force constants, K_2 and K_4 , is given by

$$\omega^2 = \frac{2dK_2}{M} \left[1 + \frac{1}{2d} + 3\frac{J_4}{J_2}\alpha^2 \left\{ 1 + \left(\frac{1}{2d} \right)^3 \right\} \right], \quad (6)$$

$$u_0 = \alpha, \quad u_1 = -(1/2d)\alpha. \quad (7)$$

Here we have taken the central position of the localized mode at the origin of the coordinate, in which u_0 , u_1 , and α are the displacement of the atom at the origin, that of its nearest neighbors and the amplitude of the localized mode, respectively. It is also shown that the amplitude of higher harmonics with eigenfrequencies $3\omega, 5\omega, \dots$ are much smaller than that of the fundamental mode with eigenfrequency ω .

Because of the formal generality of Eq.(4), the ubiquity of the existence of stationary anharmonic localized modes in nonlinear lattices including higher dimensional cases can be seen. By suitable re-definition of the Green's, Eq.(4) is also applicable to molecular systems.

III. Moving Anharmonic Localized Modes and Solitons

The existence of moving anharmonic localized modes in a specific form of Eq.(1) for a 1D lattice with nearest neighbor interactions can most easily be shown by introducing the relative displacement

$$v_n = u_{n+1} - u_n \quad (8)$$

to write the equation of motion in the form

$$\ddot{v}_n(x) = J_2(v_{n+1} + v_{n-1} - 2v_n) + J_4(v_{n+1}^3 + v_{n-1}^3 - 2v_n^3), \quad (9)$$

where $u_n \equiv u(n)$ is the displacement for the 1D case, and J_2 and J_4 are the nearest neighbor harmonic and quartic mass-reduced force constants, respectively. We use the RWA and look for solutions to Eq.(9) in the form

$$v_n = 2\phi_n \cos(kna - \omega t), \quad (10)$$

where ϕ_n , k , ω , and a are an envelope function which is also a function of t , wave number, frequency and the lattice constant of the system, respectively. Inserting Eq.(10) into Eq.(9), we obtain a pair of equations for the coefficients of $\sin(kna - \omega t)$ and $\cos(kna - \omega t)$:

$$\dot{\phi}_n = -\frac{J_2 \sin(ka)}{2\omega}(\phi_{n+1} - \phi_{n-1}) \left[1 + 3\frac{J_4}{J_2}(\phi_{n+1}^2 + \phi_{n+1}\phi_{n-1} + \phi_{n-1}^2) \right], \quad (11)$$

$$\begin{aligned} \ddot{\phi}_n - \omega^2 \phi_n &= J_2 [\cos(ka)(\phi_{n+1} + \phi_{n-1}) - 2\phi_n] \\ &+ 3J_4 [\cos(ka)(\phi_{n+1}^3 + \phi_{n-1}^3) - 2\phi_n^3]. \end{aligned} \quad (12)$$

Approximate analytical solutions to Eqs.(11) and (12) can be obtained by noting that the sech function,

$$\phi_n \equiv C \operatorname{sech}[K(na - Vt)] \quad (13)$$

is an exact solution to both of the equations

$$-\frac{\dot{\phi}_n}{1 + \phi_n^2} = J_2 \sin(ka)(\phi_{n+1} - \phi_{n-1}), \quad (14)$$

$$\frac{(\epsilon - \omega)\phi_n}{1 + \phi_n^2} = J_2 \cos(ka)(\phi_{n+1} + \phi_{n-1}), \quad (15)$$

with

$$C = (\pm 1)^{|n|} \sinh(Ka), \quad (16)$$

$$V = \pm(2/K)J_2 \sinh(Ka) \sin(ka), \quad (17)$$

$$\omega = \epsilon \mp 2J_2 \cosh(Ka) \cos(ka). \quad (18)$$

In the above equations, ϵ and K are a constant and a parameter, respectively. Then, it is a straightforward matter to show that approximate analytical solutions to Eq.(9) can be obtained as follows

$$v_n = 2(\pm 1)^{|n|} \sqrt{J_2/6J_4} \sinh(Ka) \operatorname{sech}[K(na - Vt)] \cos(kna - \omega t), \quad (19)$$

with

$$\omega^2 = 2J_2 [1 \mp \cosh(Ka) \cos(ka)] + K^2 V^2, \quad (20)$$

$$V = \pm J_2 \sinh(Ka) \sin(ka) / K\omega. \quad (21)$$

In the above equations, the plus and minus signs correspond to the modes appearing below or above the squared frequency band

$$\omega^2 = 2J_2 [1 - \cos(ka)] \equiv \omega(k)^2 \quad (22)$$

of the harmonic lattice. In the former case, the upper limit of K exists to ensure that $\omega^2 \geq 0$. It is clearly seen that envelope lattice solitons given by Eq.(19) are moving anharmonic localized modes lying outside the harmonic squared frequency band $\omega(k)^2$.

It is noted that the result obtained above for the mode lying below the squared frequency band reduces, in the limit $k \rightarrow 0$ and $\omega \rightarrow 0$ and for small K at the same time, to conventional pulse soliton solutions

$$v_n = \sqrt{\frac{J_2}{6J_4}} Ka \operatorname{sech}[K(x - Vt)], \quad (23)$$

with

$$V = C_0 [1 + (K^2 a^2 / 12)]^{1/2}, \quad (24)$$

obtained by using the continuum approximation to Eq.(9). It is therefore seen that the moving anharmonic localized mode contains the conventional pulse solitons reducible to those governed by the modified KdV equation in an asymptotic limit.

Original equations for the displacement field u from which Eq.(9) is derived, is of the form

$$\ddot{u}_n = J_2 (u_{n+1} + u_{n-1} - 2u_n) + J_4 [(u_{n+1} - u_n)^3 - (u_n - u_{n-1})^3]. \quad (25)$$

Using the same procedure as before, we can show that approximate analytical anharmonic localized mode solutions to Eq.(25) are of the form

$$u_n = 2(\pm 1)^{|n|} (1/D) \sinh(Ka) \operatorname{sech}[K(na - Vt)] \cos(kna - \omega t), \quad (26)$$

where

$$D = \sqrt{(12J_4/J_2) [1 - \cos(ka)]}, \quad (27)$$

with k and ω satisfying entirely the same form of equations as Eqs.(20) and (21). Equations (26) and (27) are a different type of moving anharmonic localized modes from those described by Eq.(19). In particular, the result obtained here for the u -field does not reduce to the conventional pulselike soliton solution in the limit $k \rightarrow 0$ and $\omega \rightarrow 0$.

Owing to the approximate nature of the analytical solutions so obtained, these results should be tested by numerical experiments. This was done for various values of K and k . The result obtained here for the modes appearing above the squared frequency band $\omega(k)^2$ may be summarized as follows: (1) Smooth and very stable propagation of a localized mode for small K in both cases. (2) For both of small and large values of K for the u -field, solitons emerge from collision processes with their identity preserved. Thus, moving anharmonic localized modes for the 1D anharmonic lattices governed by Eqs.(9) and (25) can be identified as solitons under favorable conditions.

The concept of anharmonic localized modes appearing outside the squared frequency band of the harmonic lattice provides us with a wider view of solitons as compared with that in the conventional soliton theory. By such a concept characteristic to the solid state physics, we may gain a clue to seek another kind of solitonlike nonlinear modes, stationary or immobile and mobile, to higher dimensional lattice systems, disordered lattices, molecular systems, biological systems, and so on.

VI. Quantum Mechanical Concepts of Solitons. Path Integral Formulation

It is seen from Eqs.(19) and (26) that the solutions for moving anharmonic localized modes contain the quartic-anharmonicity force constant K_4 in the denominator. This shows that solitonlike modes in quantum systems are unattainable by the conventional perturbation method. Generally speaking, solitonlike modes can be considered as large-amplitude collective modes with which a large number of quanta are associated. One of good candidates for quantum states for such highly excited states is coherent states characterized by the indefiniteness of the number of relevant quanta¹⁴.

Let us consider a many-boson system the Hamiltonian H of which is given, in terms of a set of creation and annihilation operators, $\{a_\nu\}$ and $\{a_\nu^\dagger\}$, specified by indices ν as

$$H = H(\{a_\nu^\dagger\}, \{a_\nu\}). \quad (28)$$

The boson coherent state $|A\rangle$ of the system are defined by^{14,15}

$$|A\rangle = \prod_\nu \exp\left(-\frac{|\alpha_\nu|^2}{2}\right) \exp(\alpha_\nu a_\nu^\dagger) |0\rangle, \quad (29)$$

where the symbol $|0\rangle$ denotes the vacuum state of the boson system, and α_ν is a complex quantity. By using the well-known completeness relation of the coherent states,^{14,15} the functional integral representation for the matrix element of the evolution operator $\exp(-iHt/\hbar)$ between an initial state $|A_i\rangle$ and a final state $|A_f\rangle$ can be written in the form^{16,17}

$$\begin{aligned} \langle A_f | \exp(-iHt/\hbar) | A_i \rangle \\ = \int D(A) \exp\left[(i/\hbar) \int L(\{\alpha_\nu\}, \{\alpha_\nu^*\}, \{\dot{\alpha}_\nu\}, \{\dot{\alpha}_\nu^*\}) dt\right], \end{aligned} \quad (30)$$

with

$$L = \frac{1}{2} \sum_\nu \left(\alpha_\nu^* i \hbar \frac{d\alpha_\nu}{dt} - \alpha_\nu i \hbar \frac{d\alpha_\nu^*}{dt} \right) - \langle A | H | A \rangle, \quad (31)$$

in which

$$\langle A | H | A \rangle = H_N(\{\alpha_\nu^*\}, \{\alpha_\nu\}), \quad (32)$$

where $H_N(\{\alpha_\nu^*\}, \{\alpha_\nu\})$ is the normal ordered form of $H \equiv H(\{\alpha_\nu^*\}, \{\alpha_\nu\})$, and the symbol $D(A)$ denotes a sum over all paths moving forward in time t .

Without any approximation procedure, the formal result using the coherent state path integral method is of little practical use. A working procedure is the stationary phase approximation combined with the use of the Hubbard-Stratonovich transformation.^{18,19} Here we illustrate the simplest stationary phase approximation $\delta S = 0$ to obtain

$$i\hbar \frac{d\alpha_\nu}{dt} = \frac{\partial \langle A | H | A \rangle}{\partial \alpha_\nu^*} \quad \text{and c.c.} \quad (33)$$

Let us apply the above result to the quantum dynamics of a phonon system. Let $u(x)$ and $p(x)$ be a c-number form of the displacement and the momentum of an atom at the site $x = (n, \alpha)$ (cf. Eq.(1)). Then, Eqs.(30) are equivalent to

$$\frac{\partial u(x)}{\partial t} = \frac{\partial \langle H \rangle}{\partial p(x)}, \quad \frac{\partial p(x)}{\partial t} = -\frac{\partial \langle H \rangle}{\partial u(x)} \quad (34)$$

where $\langle H \rangle$ is the diagonal coherent state representation of H . Equations (33) or (34) constitute a basis for a theory of vibron solitons developed by the present author¹⁰.

V. Vibron Solitons in Polypeptides

Let us illustrate how the concept of anharmonic localized modes and that of the coherent-state-based path integral¹⁷ can be applied to the dynamical self-trapping of amide-I vibrations by acoustic phonons on hydrogen bonding in polypeptides. Let us assume that the representation $\langle H \rangle$ with respect to the boson coherent state of the Hamiltonian H for a vibron-phonon system that we study is given by

$$\langle H \rangle = H_{\text{vib}} + H_{\text{ph}} + H_{\text{int}}, \quad (35)$$

with

$$H_{\text{vib}} = \sum_n \left(\frac{p_n^2}{2\mu} + \frac{\mu\omega_0^2}{2} q_n^2 \right) - \frac{1}{2} \sum_{n,m} L(n,m) q_n q_m, \quad (36)$$

$$H_{\text{ph}} = \sum_n \left[\frac{P_n^2}{2\mu} + V(u_{n+1} - u_n) \right], \quad (37)$$

$$H_{\text{int}} = \sum_n \left[\frac{\lambda_+}{2} q_n^2 (u_{n+1} - u_n) + \frac{\lambda_-}{2} q_n^2 (u_n - u_{n-1}) \right]. \quad (38)$$

Here H_{vib} is the Hamiltonian of vibrons simulating a set of amide-I oscillators in a polypeptide chain, in which q_n , p_n and $L(n,m)$ are the displacement of an n th oscillator with eigenfrequency ω_0 and effective mass μ from its equilibrium position, its momentum and the coefficient of the dipole-dipole interaction energy between the n and m oscillators, respectively. The quantity H_{ph} is the Hamiltonian for an anharmonic phonon system simulating longitudinal acoustic phonons in the hydrogen-bonded polypeptide chain, where u_n , P_n , and $V(u_{n+1} - u_n)$ are the displacement of an n th molecule (peptide unit) with mass M from its equilibrium position, its momentum and the intermolecular potential energy, respectively. The potential energy term in Eq.(37) can be well approximated by the Morse potential function²⁰

$$V(u_{n+1} - u_n) = U_0 \{1 - \exp[-\beta(u_{n+1} - u_n)]\}, \quad (39)$$

where U_0 and β are constants. The quantity H_{int} is the Hamiltonian describing vibron-phonon interactions, where λ_{\pm} are interaction constants.

From Eqs.(34), equations of motion satisfied by q_n and $v_n = u_{n+1} - u_n$ are written as the

$$\begin{aligned} \mu \ddot{q}_n + \mu \omega_0^2 q_n - \sum_m L(n, m) q_m \\ + \lambda_+ v_n q_n + \lambda_- v_{n-1} q_n = 0, \end{aligned} \quad (40)$$

$$\begin{aligned} M \ddot{v}_n - [f(v_{n+1}) + f(v_{n-1}) - 2f(v_n)] \\ - \frac{1}{2} [\lambda_- (q_{n+2}^2 + q_n^2 - 2q_{n+1}^2) + \lambda_+ (q_{n+1}^2 + q_{n-1}^2 - 2q_n^2)] = 0. \end{aligned} \quad (41)$$

In Eq.(41), $f(v_n) = -dV(v_n)/dv_n$ is the intermolecular force. We take an approximate analytical solutions to Eq.(41) to be of the form

$$f(v_n) = -D(\lambda_+ q_{n+1}^2 + \lambda_- q_n^2), \quad (42)$$

where D is a constant. Inserting this into Eq.(40), we obtain

$$\ddot{q}_n + \omega_0^2 q_n - \frac{1}{\mu} \sum_m L(n, m) q_m - \gamma_1 q_n^3 - \gamma_2 (q_{n+1}^2 + q_{n-1}^2) q_n = 0, \quad (43)$$

where

$$\gamma_1 = D(\lambda_+^2 + \lambda_-^2)/\mu, \quad \gamma_2 = D\lambda_+ \lambda_- / \mu. \quad (44)$$

As in the case of Eqs.(9) and (25), we seek solutions to Eq.(43) in the form of Eq.(10). In doing this, we assume that the $L(n, m)$'s are nonvanishing only for nearest neighbor pairs. Writing the nearest neighbor interaction constant as L , setting $J = L/\mu$ and using the same procedure as before, we obtain a pair of equations

$$\dot{\phi}_n = -\frac{J \sin(ka)}{2\omega} (\phi_{n+1} - \phi_{n-1}) \left[1 + \frac{2\gamma_2 \cos(ka)}{J} (\phi_{n+1} + \phi_{n-1}) \phi_n \right], \quad (45)$$

$$\begin{aligned} (\omega_0^2 - \omega^2) \phi_n + \ddot{\phi}_n - 3\gamma_1 \phi_n^3 - \gamma_2 (\phi_{n+1}^2 + \phi_{n-1}^2) \phi_n \\ = J \cos(ka) \left[\phi_{n+1} + \phi_{n-1} + \frac{2\gamma_2 \cos(ka)}{J} (\phi_{n+1}^2 + \phi_{n-1}^2) \phi_n \right]. \end{aligned} \quad (46)$$

These equations are similar in form to Eqs.(11) and (12). Thus, using the same procedure, we obtain approximate anharmonic localized mode solutions in the form

$$\phi_n = 2A \sinh(Ka) \operatorname{sech}[K(na - Vt)], \quad (47)$$

with

$$\omega^2 = \omega_0^2 - 2J \cosh(Ka) \cos(ka) + K^2 V^2 \equiv \omega_v^2, \quad (48)$$

$$V = \frac{J \sinh(Ka) \sin(ka)}{K\omega}, \quad (49)$$

where

$$A = \sqrt{\frac{J}{4\gamma_2 \cos(ka)}}. \quad (50)$$

The obtained result represents vibron solitons¹⁰ having the form of lattice envelope solitons with eigenfrequency appearing below the linear vibron frequency band

$$\omega^2 = \omega_0^2 - 2J \cos(ka) \equiv \omega_v^{(0)2}. \quad (51)$$

In terms of

$$\Delta\omega_v^2 = \omega_v^2 - \omega_v^{(0)2}, \quad (52)$$

the binding energy E_B of the vibron solitons is written as

$$E_B = \hbar (\omega_v - \omega_v^{(0)}) \simeq \frac{\hbar \Delta\omega_v^2}{2\omega_0}. \quad (53)$$

The corresponding solutions for the phonon field is of the form

$$f(v) = -B \operatorname{sech}^2 [K(na - Vt)], \quad (54)$$

where B is a constant, and we have used the RWA. In accordance with Eq.(39), we take the leading term in $f(v)$ to be of the form

$$f(v) = K_2 v - K_3 v^2, \quad (55)$$

where K_2 and K_3 are harmonic and cubic-anharmonicity force constants, respectively. Equation (54) is consistent with Eqs.(41), (42) and (55) at least for small K .

Equations (47),(48) and (49) clearly show that the dynamical self-trapping of vibrons by anharmonic acoustic phonons in polypeptides can be regarded as anharmonic localized modes.

The results obtained above are supplemented by those obtainable from the continuum approximation to Eqs.(40) and (41). Here we present only the results of calculations,

$$\Delta\omega_B^2 = \frac{(\lambda_+ + \lambda_-)B}{2\mu}, \quad (56)$$

$$K = \sqrt{\frac{2K_3 B}{K_2 a^2}}, \quad (57)$$

$$V = c_1^2 - \frac{(\lambda_+ + \lambda_-)M c_2^2}{4K_3 \mu}, \quad (58)$$

$$B = \frac{B_c}{2} + \sqrt{\left(\frac{B_c}{2}\right)^2 + \frac{3}{2} \frac{\lambda_+ + \lambda_-}{K_3} A^2}, \quad (59)$$

$$B_c = \frac{3(V^2 - C_2^2)M}{2K_3 a^2}, \quad (60)$$

where

$$c_1 = \sqrt{\frac{La^2}{\mu}}, \quad \text{and} \quad c_2 = \sqrt{\frac{K_2 a^2}{M}}, \quad (61)$$

are the velocity of vibrons and that of the acoustic phonons, respectively.

Using numerical values of relevant physical parameters derived from the numerical data by Pierce²⁰, we obtain the following numerical results for polypeptides

$$\begin{aligned} \omega_0 &= 3.7 \times 10^{-20} \text{ J}, & c_1 &= 1.6 \times 10^4 \text{ m/s}, & c_2 &= 4.6 \times 10^3 \text{ m/s}, \\ V &= 5.7 \times 10^3 \text{ m/s}, & J_L &\equiv \frac{\hbar L}{2\mu\omega_0} = 1.8 \times 10^{-22} \text{ J}, & E_B &\simeq 1.5J. \end{aligned} \quad (62)$$

The above results suggest a possible existence of supersonic, rather than subsonic, vibron solitons in polypeptide systems.

VI. Concluding Remarks

The concept of anharmonic localized modes is an approach to the soliton problem from the standpoint of solid state physics. Here, solitons are regarded as localized modes appearing outside the energy or frequency band for linear or harmonic part in the properties of systems induced by their intrinsic nonlinearity. Such a concept is particularly useful to study solitonlike modes in discrete lattices, molecular systems and biological systems including higher dimensional cases. By their nature, the anharmonic localized modes are divided into two types, stationary or immobile and mobile. The former is characterized by the ubiquity of their existence, while the existence of the latter, which has been shown to possess close similarity to conventional solitons in mathematical physics, appears more restrictive. By its nature, the concept of anharmonic localized modes may provide us with a wider view of solitons in solid state physics, chemical physics and biophysics as compared with that of the conventional soliton theory. It is particularly useful when considering solitonlike modes in discrete 1D and higher dimensional systems including small and macro molecules and biological systems. It is noted in passing that breather modes and envelope solitons in the soliton theory can be naturally understood as a kind of anharmonic localized modes.

In the theory of anharmonic localized modes, emphasis has always been placed on physical aspects, rather than mathematical aspects, of the problem with particular attention paid to discrete systems. The cost of the utility and the ubiquity of the concept is paid by the difficulty of attaining mathematical rigor and beauty in many cases. In addition to applying its concept to real physical, chemical and biological problems, much therefore remains to be done to develop its mathematical aspect.

Acknowledgements

The author would like to express his sincere thanks to Mr. K. Hori for his close cooperation in this work, including his extensive numerical experiments and the preparation of the manuscript.

This paper is dedicated to Prof. A.C. Scott on the occasion of his sixty years birth day.

References

1. M.Toda, J. Phys. Soc. Jpn. 22:431(1967); 23:501(1967).
2. See for example, A.J.Ablowitz and H.Segur, Solitons and the Inverse Scattering Transform, SIAM Studies in Applied Mathematics, Philadelphia (1981).
3. R.Hirota, "Direct method of finding exact solutions of nonlinear evolution equations, in Bäcklund Transformation", A.Dold and B.Eckmann eds., Springer, Berlin, Heidelberg and New York (1974).
4. M.Sato, RIMS Kokyuroku, 439(1981), 31. See also, Y.Ohta, J.Satsuma, D.Takahashi and T.Tokihiro, Prog. Theor. Phys. Suppl. No. 94:210(1988).
5. See for example, R.Rajaraman, Solitons and Instantons (North Holland, 1982).

6. A.J.Sievers and S.Takeno, Phys. Rev. Lett.61:970 (1988).
7. S.Takeno and K.Hori, J. Phys. Soc. Jpn. 59:3037 (1990); K.Hori and S.Takeno, J. Phys. Soc. Jpn. 61(1992), to be published.
8. S.R.Bickham, A.J.Sievers and S.Takeno, Phys. Rev. B45:10334(1992).
9. S.Takeno, J. Phys. Soc. Jpn. 61:1433(1992).
10. S. Takeno, Prog. Theor. Phys. 69:1796(1983), 71: 395(1984); 73:853(1985); J. Phys. Soc. Jpn. 59:3127 (1990).
11. See for example, A.S.Davydov, Solitons in Molecular Systems, D.Reidel Pub. Com., Dordrecht, Boston and Lancaster (1985).
12. For a review, see A.C.Scott, to be published in Phys. Reports.
13. For a review, see for example, A.A.Maradudin, E.W. Montroll, C.H. Weiss and I.P. Ipatova, Theory of Lattice Dynamics in the Harmonic Approximation, Solid State Phys. Suppl.3, F. Seitz and D. Turnbull, eds., Academic Press, New York (1971).
14. R.J.Glauber, Phys. Rev.131:2766(1963).
15. J.M.Radcliffe, J. Phys. A4:313(1971).
16. R.P.Feynman and A.R. Hibbs, Quantum Mechanics and Path Integration, McGraw-Hill, New York (1967).
17. L.S.Schulman, Techniques and Applications of Path Integration, Wiley, New York, (1981).
18. Hubbard, Phys. Rev. Lett. 3:77(1959).
19. R.L. Stratonovich, Sov. Phys.-Doklady 2:416(1958).
20. B.M.Pierce, "Quantum Chemical Calculations of Molecular Parameters Defining Davydov Soliton Dynamics in Polypeptides" in Davydov's Soliton Revisited.- Self-Trapping of Vibrational Energy in Protein, P.L. Christiansen and A.C. Scott, eds., Plenum Press, New York,(1990).

QUANTUM HOLSTEIN POLARON MODEL AND CLASSICAL CHARGED GAS ON A RING

Xidi Wang

Institute for Pure and Applied Sciences
University of California, San Diego
La Jolla, California 92093
U. S. A.

A great many techniques have been developed so far for solving polaron problems. Frequently used analytical approaches, in the context of the Fröhlich model, Holstein model, and Davydov model, are variational methods [1], perturbative treatments [2], and Ansatz methods [3]. Great success has been achieved in obtaining accurate results for such physical quantities as polaron energy and effective mass, e.g. by Feynman's variational method for the Fröhlich polaron problem. There are however still some subtle issues that need to be made clear. To list a few from the author's interests: a) How abrupt is the self-trapping transition?¹ b) Can the translational symmetry be broken due to the self-trapping? c) How does one describe the polaron dynamics at general temperatures? Numerical simulations, such as the Quantum Monte Carlo method [4], can provide us in principle, with exact answers within error bars for certain physical observables. However, there are still many difficulties in obtaining definitive answers these problems.

In contrast to conventional routes, this paper approaches the problem rigorously by reducing the fully quantum problem to a classical one. It is hoped that this alternative method may provide insights which are hard to obtain from conventional perspectives.

As a special class of polaron problems, the Holstein model describes the motion of an electron in quasi-one-dimensional materials coupled with optical phonons of the crystal [2] (molecular crystal model). This paper focuses on the Holstein model due to the apparent simplicity of its Hamiltonian and the richness of its physical phenomena. It is shown that the Holstein model is thermodynamically equivalent to a problem of *classical* charges on a ring. Some of the above mentioned questions can thus be reduced to find the phase diagram of the classical charges. The polaron energy band, effective mass, and polaron conductivity, for example, can be expressed as some averages over the grand canonical ensemble of the charges. Many of the formal relations derived in the current paper can be generalized straightforwardly to other types of phonons and higher dimensions.

¹Feynman's answer for the Fröhlich polaron problem in continuum is smooth transition rather than sharp transition, however, there is no reason to believe that the discrete polaron problem behaves the same as the continuum one. Most of the results obtained in this paper are direct consequences of the discreteness of the Hamiltonian.)

The Hamiltonian of the Holstein polaron model in one dimension (1-d) is given by

$$H = -t \sum_n (A_n^\dagger A_{n+1} + A_{n+1}^\dagger A_n) + \chi \sum_{n,q} e^{-iqn} (B_q^\dagger + B_{-q}) A_n^\dagger A_n + \sum_q B_q^\dagger B_q. \quad (1)$$

Here A_n^\dagger (A_n) is the electron creation (annihilation) operator on the n^{th} site of a N -site chain. B_q^\dagger (B_q) is the optical phonon creation (annihilation) operator at the n^{th} site transformed to Fourier space. All energies are measured in the unit optical phonon quantum $\hbar\omega$.

The Hamiltonian (1) is invariant under discrete translations, so that the total crystal momentum is conserved. One can then transform H into momentum sectors (labeled by the total crystal momentum quantum number k) with a unitary transformation $U = e^{-i\hat{X}\hat{P}}$ [5,6], where $\hat{X} = \sum_n n A_n^\dagger A_n$ is the electron position operator; $\hat{P} = \sum_q q B_q^\dagger B_q$ is the phonon crystal momentum operator. In terms of the transformed variables, the new Hamiltonian is given by

$$H = \sum_k H_k a_k^\dagger a_k, \quad H_k = -2t \sum_q \cos(\hat{P} - k) + \sum_q b_q^\dagger b_q + \chi \sum_q (b_q^\dagger + b_q). \quad (2)$$

Here a_k are the "dressed" electron operators in Fourier space, i.e. the Fourier transform of $A_n e^{-in\hat{P}}$; $b_q^\dagger = B_q e^{-iq\hat{X}}$ are the "dressed" phonon operators. It is interesting to note that if one starts from a dressed electron eigenstate with *arbitrary* initial phonons, the dressed electron remains in its momentum eigenstate without being scattered by the dressed phonons. In particular, if the phonons are in eigenstates with eigenvalue E_k , then E_k are the exact polaron energy band levels.

When there is only one electron present, the partition function becomes the simple sum of phonon partition functions of each momentum sector.

$$Z = \text{Tr} e^{-\beta H} = \sum_k Z_k, \quad Z_k = \text{Tr}_{ph} e^{-\beta H_k}, \quad E_k = \lim_{\beta \rightarrow \infty} \frac{1}{\beta} \ln(Z_k). \quad (3)$$

Thus, by computing the partition function Z_k , one can find the polaron energy band E_k . The trace over phonon Tr_{ph} can be evaluated by employing the functional integral over *coherent state variables* β_q provided that $\cos(\cdot)$ term is properly normal ordered. The partition function Z_k can then be obtained as [7]

$$Z_k = \int \prod_q d\beta_q^* d\beta_q e^{-\sum_q \int_0^\beta dx \left[\beta_q^* \frac{\partial}{\partial x} \beta_q + \mathcal{H}_k(\beta^*, \beta) \right]}, \quad (4)$$

$$\mathcal{H}_k(\beta^*, \beta) = -t \sum_{n=-1} e^{-iek} e^{\sum_q \zeta_q^* \beta_q} + \chi \sum_q (\beta_q^* + \beta_{-q}) + \beta_q^* \beta_q. \quad (5)$$

Here by definition, $\zeta_q^* = e^{iq} - 1$.

The nonlinearity of the polaron problem is displayed in the nested exponentials in (4) and (5). In order to eliminate the functional integrations over β_q^* and β_q , one can expand the first exponential

$$\exp \left[t \int_0^\beta dx \sum_{n=1} e^{iek - \sum_q \zeta_q^* \beta_q^*} \right] = \sum_{n=0}^{\infty} \frac{t^n}{n!} \int_0^\beta dx_1 \cdots \int_0^\beta dx_n \sum_{\epsilon_1, \dots, \epsilon_n} e^{\sum_{j=1}^n \left[i\epsilon_j k - \sum_q \zeta_q^* \beta_q^* \right]} \quad (6)$$

Now the phonon action is expressed in terms of bilinear forms, meanwhile, n charge variables have been introduced for the n^{th} order Taylor expansion. One can then carry out the

Gaussian integrations over all β_q^* and β_q and obtain [7]

$$Z_k = Z^{ph} \sum_{n=0}^{\infty} \frac{t^n}{n!} \int_0^\beta dx_1 \dots \int_0^\beta dx_n \sum_{\epsilon_1, \dots, \epsilon_n} e^{-ik\epsilon_n} e^{A(x, \epsilon)}. \quad (7)$$

Here Z^{ph} is the free phonon partition function given by $Z^{ph} = (1 - e^{-\beta})^{-N}$. The definition $\epsilon_n = \sum_{j=1}^n \epsilon_j$ is used. The quantity $-A(x, \epsilon)$ can be regarded as the action of n classical charges on a ring of length β with charge ϵ_i located at x_i . Given the ordering of the charges on the ring, $0 < x_1 < x_2 < \dots < x_n < \beta$, the action $-A(x, \epsilon)$ can be written as

$$A(x, \epsilon) = \frac{s}{2\sinh(\beta/2)} \sum_{j>i} e^{-\Delta x_{ij}} \theta_{ij} + A(\epsilon), \quad (8)$$

where $s = N\chi^2$ by definition. Δx_{ij} is defined as the distance from x_i to x_j in counter-clockwise direction on the ring. θ_{ij} and $A(\epsilon)$ are independent of the coordinate of the charges but dependent on the charge distribution $\{\epsilon\}$. With the definition of ϵ_{x_i, x_j} as the $\sum_{i=x_i}^{x_j} \epsilon_i$, where the sum is in counter-clockwise direction from ϵ_i to ϵ_j on the ring, one can obtain

$$\theta_{ij} = \theta(\epsilon_{x_{i+1}, x_{j-1}}, \epsilon_n) + \theta(\epsilon_{x_i, x_j}, \epsilon_n) - \theta(\epsilon_{x_{i+1}, x_j}, \epsilon_n) - \theta(\epsilon_{x_i, x_{j-1}}, \epsilon_n), \quad (9)$$

$$A(\epsilon) = \frac{s}{2\sinh(\beta/2)} \left[(\beta - n)(e^{\beta/2} + \theta(\epsilon_n, \epsilon_n)e^{-\beta/2}) + e^{\beta/2} \sum_{i=1}^n \theta(\epsilon_i, \epsilon_n) + e^{-\beta/2} \sum_{i=1}^n \theta(\epsilon_n - \epsilon_i, \epsilon_n) \right] \quad (10)$$

$$\theta(\epsilon_{x, x}, \epsilon_n) = (1 - e^{-\beta}) \sum_{p=0}^{\infty} \delta_p \epsilon_{x, x} e^{-p\beta}. \quad (11)$$

At low temperatures, where $e^\beta \gg 1$, the classical action can be simplified as

$$\theta(\epsilon_{x_i, x_j}, \epsilon_n) = \delta(\epsilon_{x_i, x_j}), \quad A(x, \epsilon) = s(\beta - n) + 2s \sum_{j>i} e^{-\Delta x_{ij}} \theta_{ij}. \quad (12)$$

The sign of the interaction among the charges is determined by the factor θ_{ij} .

Recalling the definition of the grand canonical partition function in statistical mechanics, one can regard $\sum_{n=0}^{\infty} \dots$ as the sum over all the canonical ensembles with n charges, and regard $\sum_{\epsilon_1, \dots, \epsilon_n} \dots$ as the sum over all the charge distributions. Thus both sums give rise to a grand canonical ensemble for the case of $k=0$. From this perspective, one can define a grand canonical partition function as

$$\Theta = \sum_{n=0}^{\infty} \frac{t^n}{n!} \int_0^\beta dx_1 \dots \int_0^\beta dx_n \sum_{\epsilon_1, \dots, \epsilon_n} e^{A(x, \epsilon)} = \sum_{n=0}^{\infty} t^n \sum_{\epsilon_1, \dots, \epsilon_n} \int_0^\beta dx_1 \dots \int_0^\beta dx_n e^{A(x, \epsilon)}, \quad (13)$$

where the hopping integral t behaves as the fugacity of the grand canonical ensemble, and inverse temperature β behaves as the volume (length of the ring) within which the classical charges exist.

Physical observables can be written as thermodynamical averages over the grand canonical ensemble defined

$$\langle Q_n \rangle = \frac{\sum_{n=0}^{\infty} t^n \sum_{e_1, \dots, e_n} \int dx_1 \dots \int dx_n Q_n e^{A(x, e)}}{\sum_{n=0}^{\infty} t^n \sum_{e_1, \dots, e_n} \int dx_1 \dots \int dx_n e^{A(x, e)}} \quad (14)$$

Due to the fact that all e 's are summed symmetrically with respect to inversion $e \rightarrow -e$, one can replace $e^{-iek} \rightarrow \cos(ek)$, such that the partition function for the k^{th} sector can be written as

$$Z_k = \langle \cos(\tilde{e}_n k) \rangle \Theta Z_{ph} \quad (15)$$

The polaron energy band levels can be found

$$E_k - E_0 = \lim_{\beta \rightarrow \infty} -\frac{1}{\beta} \ln \langle \cos(\tilde{e}_n k) \rangle \quad (16)$$

The polaron effective mass can also be obtained similarly

$$\frac{1}{2m^*} = \langle \tilde{e}_n^2 \rangle \quad (17)$$

The simplest approximation one can make is to ignore the interactions among the charges. The partition function can be calculated easily in this case, so that the polaron band can be found as $E_k = 2te^{-i} \cos(k) - s$, which is the well-known Holstein small polaron band. However, this approximation (trivial here) cannot describe the behavior of the classical charges in general, especially since as can be shown that the interactions between the charges are often *attractive*. This attraction can result in dramatic changes in the polaron band in comparison with the small polaron band [7].

In summary, it is demonstrated that the finite temperature partition function of the Holstein polaron model can be expressed as a grand canonical partition function of a 1-d classical charged gas on a ring. Thus the two systems are thermodynamically equivalent. It is shown that the interesting physical observables of the original problem, such as the polaron energy band, effective mass, and polaron conductivity, can be expressed as thermodynamical averages in terms of this classical grand canonical ensemble. The generalizations to multi-electron/polaron systems and higher dimensions are shown elsewhere [7]. The form of the interactions among the classical charges is derived rigorously at arbitrary temperatures. The classical charges interact with each other via an exponential interaction with a constant coefficient, which depends on the charge distribution. In the case of the trivial free particle approximation, the current formalism gives the well-known Holstein small polaron band result. Numerical simulations of the grand canonical classical charged gas are underway.

ACKNOWLEDGEMENTS

The author would like to acknowledge many useful discussions with David W. Brown and David K. Campbell. This work is supported by NSF ASC 90-14996.

REFERENCES

1. R. P. Feynman, *Statistical Mechanics*, (W. A. Benjamin, Inc., Reading, Mass., 1972).
2. T. D. Holstein, *Ann. Phys. (N.Y.)* 8, 325 (1959); 343 (1959). T. D. Holstein, L. A. Turkevich, *Phys. Rev. B* 38, 1923 (1988).
3. A. S. Davydov, *Solitons in Molecular Systems*, (D. Reidel Publishing Company, Boston 1985).
4. Xidi Wang, D. W. Brown and K. Lindenberg, in *Davydov Soliton Revisited*, ed., P. Christiansen and A. Scott (Plenum 1991). Xidi Wang, D. W. Brown and K. Lindenberg, *Phys. Rev. Lett.*, 62, 1796 (1989).
5. T. D. Lee, F. E. Low and D. Pines, *Phys. Rev.*, 90, 297 (1952).
6. G. Venzl and S. F. Fischer, *J. Chem. Phys.*, 81, 6090 (1984); *Phys. Rev. B*, 32, 6437 (1985).
7. Xidi Wang, in preparation.

THE QUANTUM ABLOWITZ-LADIK EQUATION AS A Q-BOSON SYSTEM

R.K. Bullough, N.M. Bogoliubov¹ and G.D. Pang²

Department of Mathematics, UMIST, P.O. Box 88
Manchester, M60 1QD, U.K.

¹Royal Society Ex-Agreement Visitor from Steklov
Mathematical Institute, Fontanka 27, St. Petersburg

²Royal Society Royal Fellow on leave from Institute of
Physics, Beijing

In this note we comment on the 'quantum Ablowitz-Ladik equation' and on its solutions referred to by Alwyn Scott (ACS) in his paper¹. We show how both the equation and its solutions are related to the new so-called q-bosons and thus to the quantum groups. In his paper 'There's more than one way to skin Schrödinger's cat'¹ presented at this meeting, his 60th Birthday Celebration meeting, ACS reminded us that it was possible to get, rather easily, numerical values for the low-lying energy eigenvalues and eigenstates for both integrable and non-integrable quantum models providing a number operator \hat{N} commuting with the Hamiltonian \hat{H} , $[\hat{N}, \hat{H}] = 0$, could be found. Amongst the two quantum integrable models in 1 + 1 dimensions he discussed was the quantum Ablowitz-Ladik equation (or quantum difference differential nonlinear Schrödinger model²)

$$-i\partial/\partial t B_n = (B_{n-1} + B_{n+1})(1 + \frac{1}{2} \gamma_G B_n^\dagger B_n) - 2 B_n \quad (1)$$

now written in our notation² in terms of the operators B_n, B_n^\dagger for convenience of reference. The model was introduced in Ref.3 and the Bethe equations derived through the algebraic Bethe ansatz of the quantum inverse scattering method (QISM) were given for it later⁴. ACS was concerned to compare, for two integrable models, the results of the QISM with those obtained through the 'standard number state method' (SNSM) which uses only $[\hat{H}, \hat{N}] = 0$. The A-L system was one of these two integrable models (the other was the dimer of the discrete self-trapping equation¹).

ACS also commented on the 'quantum discrete nonlinear Schrödinger model' which is $-i\partial/\partial t \phi_n = \phi_{n+1} + \phi_{n-1} + \gamma \phi_n^\dagger \phi_n \phi_n$ with $[\phi_n, \phi_m^\dagger] = \delta_{nm}$ and is not integrable (the appropriate integrable model here is the lattice bose gas²). The quantum A-L model (1) is integrable^{1,2}. The coupling constant γ_G in (1) is the coupling constant γ used in Refs. 3,4 as described by ACS, and the B_n, B_n^\dagger (ACS uses b_j, b_j^\dagger) satisfy unusual commutation relations namely

$$[B_n^\dagger, B_m^\dagger] = [B_n, B_m] = 0; [B_n, B_m^\dagger] = (1 + \frac{1}{2} \gamma_G B_n^\dagger B_n) \delta_{nm}. \quad (2)$$

Kulish³ gave these commutation relations as well as the number operator

$$\hat{N} = \sum_{n=1}^f \ell n (1 + \frac{1}{2} \gamma_G B_n^\dagger B_n) / \ell n (1 + \frac{1}{2} \gamma_G). \quad (3)$$

With the commutation relations (2) the Hamiltonian \hat{H} for (1) is

$$\hat{H} = - \sum_{n=1}^f [B_n^\dagger (B_{n+1} + B_{n-1}) - 2 \ell n (1 + \frac{1}{2} \gamma_G B_n^\dagger B_n) / \ell n (1 + \frac{1}{2} \gamma_G)] \quad (4)$$

taken under periodic boundary conditions (b.c.s) so that $n + f \equiv n$: $[\hat{H}, \hat{N}] = 0$ and the system can be solved for its energy eigenvalues and eigenstates by the SNSM.

Each single site number operator $N_m \equiv \ell n (1 + \frac{1}{2} \gamma_G B_m^\dagger B_m) / \ell n (1 + \frac{1}{2} \gamma_G)$ has eigenstates $|n\rangle_m$: $N_m |n\rangle_m = n |n\rangle_m$ and the n are non-negative integers: the vacuum state $|0\rangle_m$ has $B_m |0\rangle_m = 0$ and

$$\begin{aligned} B_m^\dagger |n\rangle_m &= \sqrt{2[(1 + \frac{1}{2} \gamma_G)^{n+1} - 1] / \gamma_G} |n+1\rangle_m \\ B_m |n\rangle_m &= \sqrt{2[(1 + \frac{1}{2} \gamma_G)^n - 1] / \gamma_G} |n-1\rangle_m. \end{aligned} \quad (5)$$

In his talk¹ ACS compared specific solutions of the algebraic Bethe ansatz (QISM) for equation (1) with solutions found by the SNSM. For fixed n , and f even, the QISM gives n -particle eigenenergies in the form $E_{n,j} = 2n + (2/\gamma_G)(\alpha_{\frac{1}{2}f-1} + \alpha_{1-\frac{1}{2}f})$. The α 's are found through the Bethe equations and depend on the index j . For $n = 2^1$, $E_{2,j} = 4 - \zeta_j(1 + t^{-1}) - \zeta_j^{-1}(1 + t)$ where the ζ_j are roots of $\zeta^{f+2} - t g \zeta^f - g \zeta^2 + t = 0$ in which t is an f th root of unity, $t = \exp(2\pi i k/f)$, and (for $n=2$) the pairs of roots are related as $\zeta_i \zeta_j = t$. In the case $f = 4$ with $n = 2$ there is an 8-fold degenerate set of energies $E_{2,j} = 4$ ($j = 1, \dots, 8$) and a 2-fold degenerate set $E_{2,j} = 4 + 2\sqrt{4 + \frac{1}{2} \gamma_G}$ ($j = 9, 10$). The 10 possibilities j will arise by assuming^{1,5} that the n particles are placed on f sites as bosons; but the algebra (2) is not a boson algebra, and we remark further on this energies count below. These results from the QISM were compared with those found by the SNSM (primarily found in this case for f odd) with some advantage to the SNSM where for f odd one needs only to diagonalise an $\frac{1}{2}(f+1) \times \frac{1}{2}(f+1)$ matrix. For the QISM, numerical solutions could be found relatively easily for $f \leq 8$ and $n \leq 7$. On the other hand while $n = 2$ and f arbitrary is easy by the SNSM, $n \geq 4$ and large f is also not convenient⁵ by the SNSM.

Our interest in the A-L system² has arisen in a rather different way. ACS et al.⁵ recognise the 'funny bosons' (ACS's phrasing¹), which have the commutation relations (2), as 'deformations' (namely as deformations of Lie algebras⁶ to the so-called 'quantum groups'). Our interest has arisen directly from a study of the properties of the q-bosons (algebra (2) is a q-boson algebra²), and of the position of the q-bosons within the general theory of the quantum groups^{2,6-10}. Vitiello in his paper 'Squeezing and quantum groups'¹¹ illustrated some of this same aspect. Our interest has also concerned the thermodynamics of q-boson models¹² and so with the case of very large f-values - namely $f \rightarrow \infty$ in thermodynamic limit^{2,10,12}. Only the Bethe Ansatz, the QISM, or their generalisations¹³, are currently available for this purpose as far as we know at present.

The q-boson algebra is a group contraction of the quantum group $su_q(2)$ ^{2,6-10}, it follows from the Primakov-Holstein transformation for $su_q(2)$ ⁷⁻¹⁰, and it is a natural q-deformation of the Heisenberg-Weyl algebra for ordinary bosons. The algebra is

$$a_n a_n^\dagger - q a_n^\dagger a_n = q^{-N_n}, \quad [N_n, a_n^\dagger] = a_n^\dagger, \quad a_n = (a_n^\dagger)^\dagger, \quad (6)$$

with other operators for different n,m commuting. This becomes the algebra (2) through

$$B_n = q^{-\frac{1}{2}N_n} a_n = a_n q^{-\frac{1}{2}(N_n-1)}, \quad B_n^\dagger = (B_n)^\dagger \quad (7)$$

with $-(1 - q^{-2}) = \frac{1}{2} \gamma_G$, on the Fock space (8). We shall use $q = e^\gamma$ with $\gamma > 0$ and q real and > 1 in this note. This confines us to the 'repulsive' case of (1) and there are no quantum soliton solutions. The 'attractive' case obtained through $q = e^{i\gamma}$ is, in effect, described in^{9,10}. Evidently $\gamma \rightarrow 0$ ($q \rightarrow 1$) reduces (6) to the Heisenberg-Weyl algebra.

The q-boson algebra (6) has a representation on the Fock space formed from the q-boson states $|n\rangle_m$, $m = 1, \dots, f$ defined above equation (5). The normalised state vectors are then

$$|0\rangle = \prod_{m=1}^f |0\rangle_m, \quad |n\rangle = \prod_{m=1}^f |n\rangle_m = \prod_{m=1}^f ([n_m]!)^{-\frac{1}{2}} (a_m^\dagger)^{n_m} |0\rangle. \quad (8)$$

The notation is now $[n]! \equiv [1].[2] \dots [n]$ and $[n] \equiv (q^n - q^{-n})/(q - q^{-1})$. We call $[n]$ 'the box notation' for n defined this way⁹. On this Fock space one proves

$$a_n^\dagger a_n = [N_n], \quad a_n a_n^\dagger = [N_n + 1] \quad (9)$$

in which the box notation is extended to operators. In terms of ordinary boson operators b_n, b_n^\dagger , with $[b_n, b_m^\dagger] = \delta_{nm}$, a representation of the a_n, a_n^\dagger and N_n is

$$a_n = \left\{ \frac{[N_n + 1]}{N_n + 1} \right\}^{\frac{1}{2}} b_n, \quad a_n^\dagger = (a_n)^\dagger, \quad N_n = b_n^\dagger b_n = N_n^\dagger. \quad (10)$$

In this representation the Fock space (8) is identical with the Fock space for f ordinary bosons. In this way we could be concerned in the energies count (see above) with the p ways n bosons can be placed on f sites. However, the QISM actually works with a Pauli principle on the creation operators of the theory, and the issue is then whether the f th roots of unity to be associated with each root λ_ℓ of the Bethe equations (13) below can be identical or not. ACS *et al.*^{1,5} show they can be equal for $f = 4$, $n = 2$: we have shown the same for $f = 2$, $n = 2$. This situation could be important to the thermodynamic limit $f \rightarrow \infty$ if it actually occurs there, a situation we are investigating.

There is also the number phase representation for the q -boson algebra (6): $[N_m, \phi_n] = i \delta_{nm}$ and $a_n = e^{i\phi_n} ([N_n])^{\frac{1}{2}}$, $a_n^\dagger = (a_n)^\dagger$. In this way we can show that the Hamiltonian (4) of the A-L system is, upto a factor of one half, equivalently

$$\hat{H} = -\frac{1}{2} \sum_{n=1}^f \{ Z_n e^{-i(\phi_n - \phi_{n-1})} Z_{n-1}^\dagger + \text{h.c.} - 2 N_n \} \quad (11)$$

with $Z_n \equiv \left\{ (1 - e^{-2\gamma N_n}) / (1 - e^{-2\gamma}) \right\}^{\frac{1}{2}}$. It is also clear, from (3) or from (9), that with \hat{H} from (4) conveniently taken as $\hat{H} = -\frac{1}{2} \sum_{n=1}^f \{ (B_{n-1}^\dagger B_n + \text{h.c.}) + \gamma^{-1} \ln(1 - Q B_n^\dagger B_n) \}$ with an extra factor $\frac{1}{2}$ and $Q = (1 - q^{-2}) \equiv (1 - e^{-2\gamma})$

$$\hat{H} = -\frac{1}{2} \sum_{n=1}^f (B_{n-1}^\dagger B_n + \text{h.c.} - 2 N_n), \quad (12)$$

our 'q-boson hopping model'.² Thus (upto a factor of 2) the eigenenergies found by ACS are eigenenergies of the two other models (11) and (12) and the eigenstates found by ACS are eigenstates of these models. It would be interesting and even instructive to apply the SNSM to both of (11) and (12) directly - since each model has a commuting number operator \hat{N} .

Our solution of these three models (4), (11) and (12) is a QISM solution depending on the roots of the Bethe equations

$$e^{-12\gamma\lambda_\ell f} = \prod_{j=1, j \neq \ell}^n \exp\{i\Phi(\lambda_\ell - \lambda_j)\}, \quad (13)$$

in which the 2-body phase shifts are $\Phi(\lambda) = 2 \tan^{-1}((\tan \lambda \gamma) \coth \gamma)$. For chemical potential $\bar{\mu}$, the n -particle eigenenergies are

$$E_n = \sum_{\ell=1}^n (2 \sin^2(\gamma \lambda_\ell) - \bar{\mu}) = \sum_{\ell=1}^n (1 - \cos(2\gamma \lambda_\ell) - \bar{\mu}). \quad (14)$$

For $\bar{\mu} = 0$ this expression can be identified as $2E_n = 2n + 2 \gamma_G^{-1} (\alpha_{\frac{1}{2}f-1} + \alpha_{1-\frac{1}{2}f})$ as given by ACS and colleagues^{1,5}. The Bethe equations (13) become their Bethe equations by $i\gamma\lambda_\ell \rightarrow \lambda_\ell$, $\gamma \rightarrow -\eta$ where $2\eta \equiv \ln(1 + \frac{1}{2})$

γ_G). We also find an explicit solution of (13) for $\gamma \rightarrow \infty$ for any n and f^2 .

The Bethe equations (13) and the n -particle energies (14) were found² by a limit $\Lambda \rightarrow \infty$ on a more complicated q -boson lattice model^{9,10}. This more complicated lattice model replaces the ordinary bosons of the lattice Bose gas model by q -bosons^{9,10}. The Hamiltonian remains local, but it depends on the real parameter Λ , and involves interactions between four nearest neighbours. The Hamiltonians (4), (11) and (12) found through $\Lambda \rightarrow \infty$ involve only nearest neighbour interactions. The q -boson hopping model (12) looks particularly simple. But it is a hopping model for the (nonlinear) q -bosons. It is linear in terms of ordinary bosons for $q \rightarrow 1$, but for $q \neq 1$ involves an additional set of nonlinearities in all powers of the number operators N_m .

In thermodynamic limit, where $f \rightarrow \infty$ at finite density, we have derived² the Yangs' equation at zero temperature, $T = 0$,

$$\varepsilon(k) = 2 \sin^2(\frac{1}{2}k) - \bar{\mu} + (2\pi)^{-1} \int_{-\kappa}^{\kappa} \{\partial\Phi(k-k')/\partial k\} \varepsilon(k') dk' \quad (15)$$

with $\varepsilon(\pm\kappa) = 0$: $-\kappa \leq k \leq \kappa$ defines the Fermi sphere. We find the density D of particles in the form $D = \lim_{f \rightarrow \infty} (n/f) = \int_{-\kappa}^{\kappa} \rho(k) dk$ and the mode particle densities $\rho(k)$ satisfy an integral equation with the same kernel as (15)². The pressure p of q -bosons is then $p = -\frac{1}{2}\pi^{-1} \int_{-\kappa}^{\kappa} \varepsilon(k') dk'$. The excitation energies $\varepsilon(k)$ from (15) also determine the ground state energy density $\lim_{f \rightarrow \infty} (E/f) = -p + \bar{\mu} D$ as well as the energies of excitation from that ground state. It would be interesting and rather important to try to infer this ground state energy from the SNSM; but, as $f \rightarrow \infty$ in thermodynamics limit, $n \rightarrow \infty$, so that D is a finite density. Other results include the pressure p at finite temperatures $p = - (2\pi\beta)^{-1} \int_{-\infty}^{\infty} \ln(1 + e^{-\beta\varepsilon(k')}) dk'$ where $\beta^{-1} = k_B T$ and the $\varepsilon(k')$ solve the finite T form of (15) which replaces $\varepsilon(k')$ under the integral sign by $\beta^{-1} \ln(1 + e^{-\beta\varepsilon(k')})$ making that integral equation nonlinear. We have also, calculated asymptotically the correlation functions in thermodynamic limit².

To sum up: As was well recognised by ACS in his paper¹ the SNSM has certain very real advantages - notably simplicity for the calculation of low-lying eigenenergies and states, and versatility in that it is applicable to discrete integrable and non-integrable systems (lattices) if there is an operator \hat{N} such that $[\hat{H}, \hat{N}] = 0$. On the other hand the QISM, as in Refs. 2,9,10 e.g., displays the mathematical structure, a

quantum group structure, but is limited to the integrable systems which however can be lattices or field theories. However in this case it is also possible to go to the thermodynamic limit and construct the thermodynamics as well as the asymptotics of the correlation functions at zero T and very small T . Analytical methods for the correlation functions at all values of T are currently being developed and depend on the classical form of the inverse method.

REFERENCES

1. A.C.Scott, with V.Z.Ehol'skii, M.Salerno, and J.C.Eilbeck, 'There's more than one way to skin Schrödinger's cat'. This meeting.
2. N.M.Bogoliubov, R.K.Bullough and G.D.Pang, 'Exact solution of a q-boson hopping model', submitted to *Phys. Rev. Lett.* July 17, 1992, and references.
3. P.P.Kulish, *Lett. Math. Phys.*, 5 :191 (1981).
4. V.S.Gerdjikov, M.I.Ivanov and P.P.Kulish, *J. Math. Phys.* 25 :25 (1984).
5. V.Z.Ehol'skii, M.Salerno, A.C.Scott and J.C.Eilbeck, Preprint, 'There's more than one way to skin Schrödinger's cat' March 13, 1992, submitted to *Physica D*.
6. R.K.Bullough, S.Olafsson, Yu-zhong Chen and J.Timonen, in: "Diff. Geo. Methods in Theor. Phys" Ling-Lie Chau and W.Nahm eds., Plenum, New York, NATO ASI Series B 245:47, (1990).
7. R.K. Bullough and N.M. Bogoliubov in: "XXth Intl. Conf. on Diff. Geom. Methods in Theor. Phys", Sultan Catto and Alvany Rocha eds., World Scientific, Singapore (1992), pp.488 - 504.
8. R.K. Bullough and N.M. Bogoliubov, in: "Proc. III Potsdam - V Kiev Intl. Workshop on Nonlinear Systems in Physics" A.S. Fokas and D. Kaup eds., Springer-Verlag, Berlin (1992). To appear.
9. N.M.Bogoliubov and R.K.Bullough, *J.Phys.A:Math. Gen.*25:4057 (1992).
10. N.M.Bogoliubov and R.K.Bullough, 'Completely integrable model of interacting q-bosons', *Phys. Letts. A*. In Press.
11. G. Vitiello 'Squeezing and quantum groups'. This meeting.
12. N.M.Bogoliubov, R.K.Bullough and G.D. Pang. To be published.
13. See e.g. J. Timonen, M. Stirland, D.J. Pilling, Yi Cheng, and R.K.Bullough, *Phys. Rev. Lett* 56: 2233 (1986); R.K.Bullough, Yu-zhong Chen, and J. Timonen, 'Soliton statistical mechanics' in "Nonlinear World Vol.2" V.G. Bar'yakhtar et al. eds., World Scientific, Singapore (1989), pp.1377-1422 and refs.

MOVING LOCALIZED MODES IN NONLINEAR LATTICES

Ch. Claude, Yu. S. Kivshar *, O. Kluth
and K. H. Spatschek

Institut für Theoretische Physik I, Heinrich-Heine-
Universität Düsseldorf, D-4000 Düsseldorf 1, Germany

*Institute for Low Temperature Physics and Engineer-
ing, 310164 Kharkov, Ukraine

Recently interest in localized modes for strongly anharmonic lattices was growing mostly due to the paper by Sievers and Takeno¹, who proposed a new kind of localized mode in nonlinear lattices. Because the lattice is *without* impurities, they called this mode as an *intrinsic localized mode* in order to distinguish it from the impurity-induced localized mode. Different properties of the intrinsic localized mode have been discussed in a number of papers (see, e.g., Refs. 2,3) for 1D and 3D cases. The original model for the intrinsic localized mode is the so-called Fermi-Pasta-Ulam (FPU) model. It describes a 1D chain composed of atoms with masses m , in which each atom interacts only with its nearest neighbors. If $u_n(t)$ is the displacement of the n th atom from its equilibrium position and k_2 and k_4 are nearest neighbor harmonic and quartic anharmonic force constants, respectively, the equations of motion are given by

$$\frac{d^2}{dt^2} u_n = k_2(u_{n+1} + u_{n-1} - 2u_n) + k_4[(u_{n+1} - u_n)^3 + (u_{n-1} - u_n)^3]. \quad (1)$$

For sufficiently strong anharmonicity, stable odd-parity localized modes are possible with the frequency ω given by $\omega^2 = \frac{3}{m}(k_2 + \frac{27}{16}k_4 A^2)$. Here the localized pattern is $u_n(t) = A(\dots, 0, -\frac{1}{2}, 1, -\frac{1}{2}, 0, \dots) \cos \omega t$; the approximation is valid for larger $(k_4/k_2)A^2$. Some authors have proposed another variant of a stationary self-localized mode, i.e. an even parity localized mode, $u_n(t) = A(\dots, 0, -1, 1, 0, \dots) \cos \omega t$, which has been found to be extremely stable.

Another type of intrinsic localized modes may be analysed for a model with nonlinearity produced by an on-site potential², e.g. as it is in the nonlinear Klein-Gordon (KG) model,

$$\frac{d^2}{dt^2} u_n = K(u_{n+1} + u_{n-1} - 2u_n) - \alpha u_n + \frac{1}{3}\beta u_n^3. \quad (2)$$

Here highly localized modes exist with frequencies *below* ($\beta > 0$) the frequency gap $\omega_0^2 = \alpha/m$ or *above* ($\beta < 0$) the cut-off frequency $\omega_{max}^2 = \omega_0^2 + 4K$.

One of the main problems in the theory of intrinsic localized modes is to prove that they can move along the chain. Since there is no analytical expression for moving intrinsic localized modes, in a recent paper by Bickham *et al.*³ this study has been carried out numerically, and the authors made measurements of the shape and the dispersion relation for moving anharmonic modes in the model (1). However, this measurement did not show *why* the moving intrinsic localized modes are possible even under the strong influence of discreteness effects, and *which kind* of relations exists between different types of models for intrinsic localized modes. The purpose of our work is to apply a simple analytical approach to investigation of moving intrinsic localized modes in the models (1) and (2) and to compare the results for both the models. One of the most important issues of our analysis is to show that nonintegrability of the discrete models (1) and (2) gives rise to an effective periodic (Peierls-Nabarro) potential, which may capture the mode at the atom site or between the sites. Nevertheless, the model (1) does support moving localized modes in a wide region of the system parameters, but the model (2) cannot support propagating localized modes if the mode amplitude exceeds a certain threshold value, so that strongly localized modes will be always *captured* by the lattice discreteness.

The main idea of our approach is to use the integrable discrete Ablowitz-Ladik (AL) model⁴ as a basis of a perturbation theory for models (1) and (2). We make the so-called "rotating wave approximation", i.e. only the terms proportional to the main harmonic are taken into account. In the framework of this approach the intrinsic localized modes for the models (1) and (2) are treated as perturbed lattice solitons.

Let us start first from the KG chain (2). Substituting the ansatz $u_n = \exp(-i\omega_0 t)\Psi_n + \text{c.c.}$ into Eq.(2), where $\omega_0^2 = \alpha/m$ is the gap frequency of the linear spectrum of the chain, we keep only the terms $\sim \exp(-i\omega_0 t)$ so that under the assumption $d\Psi_n/dt \ll \omega_0 \Psi_n$ Eq.(2) will reduce to the discrete nonlinear Schrödinger (NLS) equation

$$2im\omega_0 \frac{d\Psi_n}{dt} + K(\Psi_{n+1} + \Psi_{n-1} - 2\Psi_n) + \beta|\Psi_n|^2\Psi_n = 0. \quad (3)$$

Equation (3) may be written as a perturbed AL equation

$$2im\omega_0 \frac{d\Psi_n}{dt} + K(\Psi_{n+1} + \Psi_{n-1} - 2\Psi_n) + \frac{1}{2}\beta(\Psi_{n+1} + \Psi_{n-1})|\Psi_n|^2 = R(\Psi_n), \quad (4)$$

where

$$R(\Psi_n) = \frac{1}{2}\beta|\Psi_n|^2(\Psi_{n+1} + \Psi_{n-1} - 2\Psi_n). \quad (5)$$

As is well known, the AL model given by Eq.(4) with $R = 0$ is exactly integrable and it supports (moving) nonlinear localized excitations in the form of lattice solitons⁴, the latter may be highly localized objects involving only a few particles. The exact soliton solution of the AL model can be presented in the form

$$\Psi_n(t) = \frac{\sinh \mu \exp[ik(n - x_0) + i\alpha]}{\cosh[\mu(n - x_0)]}, \quad (6)$$

where in the unperturbed case $\dot{\mu} = 0$, $\dot{k} = 0$, $\dot{x}_0 = (2/\mu) \sinh \mu \sin k$, and $\dot{\alpha} = 2[\cosh \mu \cos k - 1]$. In Eq. (6) and the subsequent calculations related to Eqs. (4), (5) we have used the renormalized variables: $t \rightarrow (2m\omega_0/K)t$ and $\Psi_n \rightarrow (2K/\beta)^{1/2}\Psi_n$.

Considering now the r.h.s. of Eq.(4) as a perturbation (that is certainly valid for not strongly localized modes), we will use the perturbation theory for the AL model

based on the inverse scattering transform⁵. According to this approach, the parameters of the solution (6), i.e. μ , k , α and x_0 , are assumed to be slowly varying in time. The equations describing their evolution in the presence of the perturbation may be simplified using the well-known Poisson formula to evaluate the sums appearing as a result of discreteness of our primary model,

$$\frac{dx_0}{dt} = \frac{2}{\mu} \sinh \mu \sin k, \quad \frac{dk}{dt} = \frac{2\pi^3 \sinh^2 \mu \sin(2\pi x_0)}{\mu^3 \sinh(\pi^2/\mu)}, \quad (7)$$

and also $d\mu/dt = 0$ as above. In Eq.(7) we keep only the contribution of the first harmonic because the higher harmonics of the order of s will always appear with the additional multiplier $\sim \exp(-\pi^2 s/\mu)$ which is assumed to be exponentially small (even for $\mu \sim 1$). As μ is constant, the system (7) may be easily analysed on the phase plane (k, x_0) assuming a parametrical dependence on μ . As follows from our analysis, there exists a critical value, $\mu_c \approx 3.6862$. Below the critical value, $\mu < \mu_c$, there are phase trajectories describing moving localized modes. Small values of the parameter μ correspond to the quasi-continuous approximation when the lattice equations are transformed to the continuous ones and they may be described by the continuous NLS equation. However, if the parameter μ exceeds the critical value μ_c , the phase plane does not have trajectories describing moving localized modes. This result simply means that if the nonlinearity exceeds the threshold value, there are no propagating localized modes in the chain. All such modes will exist only in a trapped state.

Let us now consider the similar problem for the FPU chain, being the original model used by Sievers and Takeno¹. To derive the perturbed AL equation in this case we use the ansatz: $u_n = (-1)^n [\exp(i\omega_m t) \Psi_n + \text{c.c.}]$, where $\omega_m^2 = 4k_2/m$ is the cut-off frequency of the spectrum of the linear chain. Substituting this ansatz into Eq.(1) and keeping again only the terms proportional to the first harmonic, under the same assumptions as above we obtain the equation

$$2im\omega_m \frac{d\Psi_n}{dt} + k_2(\Psi_{n+1} + \Psi_{n-1} - 2\Psi_n) + 24k_4 |\Psi_n|^2 (\Psi_{n+1} + \Psi_{n-1}) = R(\Psi_n), \quad (8)$$

where now

$$\begin{aligned} R(\Psi_n) = & -3k_4 \{ |\Psi_{n+1}|^2 \Psi_{n+1} + |\Psi_{n-1}|^2 \Psi_{n-1} + 2|\Psi_n|^2 \Psi_n + (\Psi_{n+1}^2 + \Psi_{n-1}^2) \Psi_n^* \\ & + 2\Psi_n (|\Psi_{n+1}|^2 + |\Psi_{n-1}|^2) + \Psi_n^2 (\Psi_{n+1}^* + \Psi_{n-1}^*) - 6|\Psi_n|^2 (\Psi_{n+1} + \Psi_{n-1}) \} \end{aligned} \quad (9)$$

is an effective perturbation to the AL model.

Applying again the perturbation theory⁵, we obtain the system of *three* coupled equations for the soliton parameters,

$$\frac{dx_0}{dt} = \frac{2}{\mu} \sinh \mu \sin k, \quad \frac{dk}{dt} = \frac{2\pi^3 \sinh^2 \mu \sin(2\pi x_0)}{\mu^3 \sinh(\pi^2/\mu)} g(k, \mu), \quad (10)$$

$$\frac{d\mu}{dt} = \frac{2\pi^3 \sinh^2 \mu \sin(2\pi x_0)}{\mu^3 \sinh(\pi^2/\mu)} \tanh \mu f(k, \mu), \quad (11)$$

with $g(k, \mu) = (\cos k / \cosh \mu) - 2 \cos(2k)$ and $f(k, \mu) = (\sin k / \cosh \mu) - 2 \sin(2k)$. To write Eqs. (10), (11), we have renormalized Eq.(8) as follows: $t \rightarrow (2m\omega_m/k_2)t$ and $\Psi_n \rightarrow (k_2/24k_4)^{1/2} \Psi_n$.

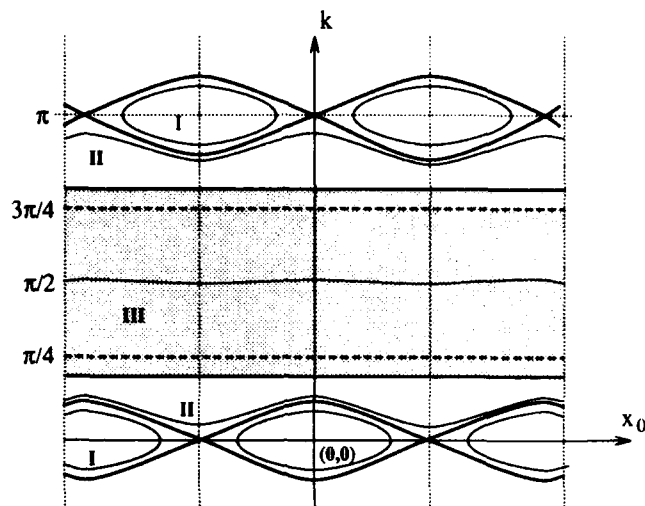


Fig.1 Phase plane (k, x_0) corresponding to Eqs.(10) for fixed μ .

Considering the system (10) for fixed μ we can use the phase plane (k, x_0) to show different types of the nonlinear dynamics. In Fig.1 we find the presence of two straight lines for each value of the parameter μ ($0 < \mu < \infty$, the solid lines for $\mu = 0$ and the dashed ones for $\mu \rightarrow \infty$, all other values of μ will give lines in between) which separate two different kinds of the system dynamics and they *never* disappear, even for the cases of very large μ . Within the region separated by these two lines the FPU model *always* admits moving localized modes (lattice solitons), and this result confirms numerical observations of moving localized modes³. For the complete model (10) to (11) we have found that in the region III (see Fig.1) the solutions depend *very weakly* on the variation of μ , at least in the middle part of this region. As a result, the main conclusion for moving intrinsic localized modes remains valid even if the evolution of μ (small in the numerical results) is taken into consideration.

In conclusion, we have shown that intrinsic localized modes in a chain with nonlinear interparticle interaction may *always* exist as moving excitations, but for intrinsic localized modes in a chain with nonlinear on-site potential, there is a threshold value of the nonlinearity parameter above which the modes will be *always* captured by the lattice discreteness.

REFERENCES

1. A.J. Sievers and S. Takeno, *Phys. Rev. Lett.* 61: 970 (1988).
2. S. Takeno, K. Kisoda and A.J. Sievers, *Progr. Theor. Phys. Suppl.* 94: 242 (1988).
3. S.R. Bickham, A.J. Sievers and S. Takeno, *Phys. Rev. B* 45: 10344 (1992).
4. M.J. Ablowitz and J.F. Ladik, *J. Math. Phys.* 17: 1011 (1976).
5. A.A. Vakhnenko and Yu.B. Gaididei, *Theor. Mat. Fiz.* 68: 350 (1986) [*Theor. Math. Phys.* 68: 873 (1987)].

QUANTUM SOLITONS IN THE DNLS AND HUBBARD MODELS

H Gilhøj*, J C Eilbeck†, A C Scott*

* Laboratory of Applied Mathematical Physics
The Technical University of Denmark
DK-2800 Lyngby, Denmark

† Department of Mathematics
Heriot-Watt University, Riccarton
Edinburgh EH14 4AS, UK

Abstract

We extend the results of a previous calculation concerning the existence of soliton bands in anharmonic quantum lattices. In particular we consider the case where the periodicity f of the lattice is even rather than odd, and we also show that for the two quanta case, the eigenvalues of the discrete nonlinear Schrödinger equation (a boson model) are equivalent to those of the Hubbard model (a fermion model).

1 Introduction

In a previous calculation [1], we studied the existence of soliton bands in 1-D anharmonic quantum lattices, for the case where the periodicity of the lattice f was an odd integer, and the number of quanta n was two, the simplest nontrivial case. Four models were considered, the Discrete Nonlinear Schrödinger equation (DNLS), the Ablowitz-Ladik model, a fermionic polaron model, and the Hubbard model. The tool used in this study is the Number State Method (NSM), so-called to distinguish it from the Quantum Inverse Scattering method, which can also be applied to all but the first of these models. Limitations of space prevent us from reviewing the details here: see [1, 2].

In this note we extend the calculations in [1] in two ways: (i) we show how to modify the calculations for the *even* f case for the DNLS model (the theory for the A-L model and the fermionic polaron model follows in a similar way), and (ii) we show how the calculations for the Hubbard model can be recast so as to exhibit the equivalence of this model in the $n = 2$ case with the DNLS model.

2 The Discrete Nonlinear Schrödinger lattice, even f case

The quantum DNLS model is a special case of the quantum discrete self-trapping equation (DST), which has been proposed in a variety of applications, including the description of molecular vibrations in one-dimensional chains [2].

The DNLS equation has the following Hamiltonian

$$\hat{H}_{dnls} = - \sum_{j=1}^f \left(\frac{\gamma}{2} b_j^\dagger b_j^\dagger b_j b_j + b_j^\dagger b_{j-1} + b_j^\dagger b_{j+1} \right),$$

which commutes with the number operator $\hat{N}_{dnls} = \sum_{j=1}^f b_j^\dagger b_j$ where b_j^\dagger (b_j) are bosonic raising (lowering) operators satisfying the commutation relations $[b_i, b_j^\dagger] = \delta_{ij}$, $[b_i^\dagger, b_j^\dagger] = [b_i, b_j] = 0$. The most general eigenfunction of \hat{H}_{dnls} and the translation operator \hat{T} is a sum of products of elementary number states of the form $|n_1\rangle|n_2\rangle\ldots|n_f\rangle \equiv [n_1 n_2 \ldots n_f]$, where $n = n_1 + n_2 + \ldots + n_f = 2$ in the case we consider here.

In the *even* f calculation, there are two cases depending on whether the integer ν in the eigenvalue $t = \exp 2\pi i \nu / f$ of the translation operator is odd or even. The wavefunction corresponding to ν even is

$$|\Psi_{dnls}\rangle = \frac{1}{\sqrt{f}} \sum_{j=1}^f (t\hat{T})^{j-1} [20 \ldots 0] + \frac{1}{\sqrt{f}} \sum_{j=1}^f (t\hat{T})^{j-1} [110 \ldots 0] + \frac{1}{\sqrt{f}} \sum_{j=1}^f (t\hat{T})^{j-1} [1010 \ldots 0] + \ldots + \frac{1}{\sqrt{(f/2)}} \sum_{j=1}^f (t\hat{T})^{j-1} [10 \ldots 010 \ldots 0]$$

whereas for ν odd the last term in the sum is omitted.

The requirement of $\hat{H}_{dnls} |\Psi_{dnls}\rangle = E |\Psi_{dnls}\rangle$ leads to a block diagonalised matrix

$$\mathbf{H} = \text{diag}[Q_\nu^{dnls}]_{\nu=0}^{f-1}.$$

where for even ν , Q_ν^{dnls} is a $(f/2 + 1) \times (f/2 + 1)$ matrix

$$Q_\nu^{dnls} = - \begin{pmatrix} \gamma & q^* \sqrt{2} & & & & \\ q \sqrt{2} & 0 & q^* & & & \\ & q & 0 & q^* & & \\ & & \ddots & \ddots & \ddots & \\ & & & q & 0 & \sqrt{2} q^* \\ & & & & \sqrt{2} q & 0 \end{pmatrix} \quad (2.1)$$

where $q = (1 + t)$. For odd ν , Q_ν is the $(f/2) \times (f/2)$ matrix formed from (2.1) by omitting the final row and column.

A plot of eigenvalues of \mathbf{H} for the even f case almost identical to that for the odd f case shown in [1]. The calculations for the even f case for the A-L scheme and the fermionic polaron model goes through in a similar way, again the corresponding eigenvalue plot looks identical to the odd f case.

3 The Hubbard Model

We consider here the Hubbard model, a quasi-one-dimensional equation arising in the description of ferromagnetism and superconductivity [3]. The Hamiltonian is

$$\hat{H}_{Hub} = - \sum_{j=1}^f (a_j^\dagger a_{j+1} + a_j^\dagger a_{j-1} + b_j^\dagger b_{j+1} + b_j^\dagger b_{j-1} + \gamma a_j^\dagger a_j b_j^\dagger b_j).$$

$a_j^\dagger(a_j)$ and $b_j^\dagger(b_j)$ are creation (annihilation) operators for different spin states, and both obey fermionic anticommutation relations: $\{a_i, a_j^\dagger\} = \delta_{ij}$, $\{a_i, a_j\} = \{a_i^\dagger, a_j^\dagger\} = 0$. The Hamiltonian in this case commutes with two number operators, one for each spin state. So, an elementary product state consists of two rows one for each spin state and each column corresponding to a degree of freedom.

As in [1], we consider here only the case where one quanta lies in each spin state. In [1] we used the notation $[0 \dots 0 \dots 1 \dots 0 \dots]$ for this sort of state, here for conciseness we use ϕ_j^i for a state with one quanta in the "up" state at site i and one quanta in the "down" state at site j .

The Hamiltonian has an additional symmetry property besides the translational symmetry; the interchange of the two rows introduced through an operator which we will call \hat{X} . In [1] this symmetry was not used, but a general eigenfunction of \hat{N} , \hat{T} and \hat{X} and even f can be constructed in a straightforward way. Again the result depends on whether ν is even or odd. For even f and even ν define

$$\begin{aligned} |\Psi_{Hub}\rangle &= \frac{c_1}{\sqrt{f}} \sum_{j=1}^f (t\hat{T})^{j-1} \phi_1^1 + \frac{c_2}{\sqrt{2f}} \sum_{j=1}^f (t\hat{T})^{j-1} (\phi_2^1 + \phi_1^2) + \dots \\ &+ \frac{c_{f/2}}{\sqrt{2f}} \sum_{j=1}^f (t\hat{T})^{j-1} (\phi_{f/2}^1 + \phi_1^{f/2}) + \frac{c_{f/2+1}}{\sqrt{f}} \sum_{j=1}^f (t\hat{T})^{j-1} \phi_{f/2+1}^1 \\ &+ \frac{c_{f/2+2}}{\sqrt{2f}} \sum_{j=1}^f (t\hat{T})^{j-1} (\phi_2^1 - \phi_1^2) + \dots + \frac{c_f}{\sqrt{2f}} \sum_{j=1}^f (t\hat{T})^{j-1} (\phi_{f/2}^1 - \phi_1^{f/2}) \end{aligned}$$

Again \mathbf{H} block diagonalises with the Q matrices

$$Q_\nu^{Hub}(t) = \begin{pmatrix} Q_{\nu+}^{Hub}(t) & 0 \\ 0 & Q_{\nu-}^{Hub}(t) \end{pmatrix}, \quad (3.1)$$

where $Q_{\nu+}^{Hub}(t)$ is exactly the same matrix as in the DNLS case (2.1), and

$$Q_{\nu-}^{Hub}(t) = - \begin{pmatrix} 0 & q^* & 0 & \cdot & \cdot & 0 \\ q & 0 & q^* & & & 0 \\ 0 & q & 0 & q^* & & \\ & & \ddots & \ddots & \ddots & \\ & & & q & 0 & q^* \\ 0 & 0 & \cdot & \cdot & q & 0 \end{pmatrix}_{f/2-1 \times f/2-1} \quad (3.2)$$

with q as defined in the DNLS case.

For even f and odd ν define

$$\begin{aligned} |\Psi_{Hub}\rangle &= \frac{c_1}{\sqrt{f}} \sum_{j=1}^f (t\hat{T})^{j-1} \phi_1^1 + \frac{c_2}{\sqrt{2f}} \sum_{j=1}^f (t\hat{T})^{j-1} (\phi_2^1 + \phi_1^2) + \dots \\ &+ \frac{c_{f/2}}{\sqrt{2f}} \sum_{j=1}^f (t\hat{T})^{j-1} (\phi_{f/2}^1 + \phi_1^{f/2}) + \frac{c_{f/2+1}}{\sqrt{2f}} \sum_{j=1}^f (t\hat{T})^{j-1} (\phi_2^1 - \phi_1^2) + \dots + \\ &+ \frac{c_{f-1}}{\sqrt{2f}} \sum_{j=1}^f (t\hat{T})^{j-1} (\phi_{f/2}^1 - \phi_1^{f/2}) + \frac{c_f}{\sqrt{f}} \sum_{j=1}^f (t\hat{T})^{j-1} \phi_{f/2+1}^1 \end{aligned}$$

again $Q_\nu^{Hub}(t)$ is split as in (3.1), but now $Q_{\nu+}^{Hub}(t)$ is the same as in the even ν case except that the final row and column is removed, and $Q_{\nu-}^{Hub}(t)$ is as before, except that

the row and column removed from $Q_{\nu+}^{Hub}(t)$ is added at the end of the matrix, giving two $f/2 \times f/2$ matrices.

In the *odd* f case, the procedure is similar except the $\phi_{f/2+1}^1$ term is omitted, and $Q_{\nu+}^{Hub}(t)$ is now identical to the corresponding DNLS matrix (c.f. (3.5) in [1]), and $Q_{\nu-}^{Hub}(t)$ is the same as $Q_{\nu+}^{Hub}(t)$ with the *first* row and column removed.

It can be shown that the matrices $Q_{\nu-}^{Hub}(t)$ merely add more quasicontinuum states to $Q_{\nu+}^{Hub}(t)$, so the overall picture is almost identical to the DNLS results. We have exactly the same soliton and quasi-continuum bands, except the quasi-continuum band now has a denser packing of states for a given f . We show in Fig. 1 a typical plot of E v. ν for the Hubbard model.

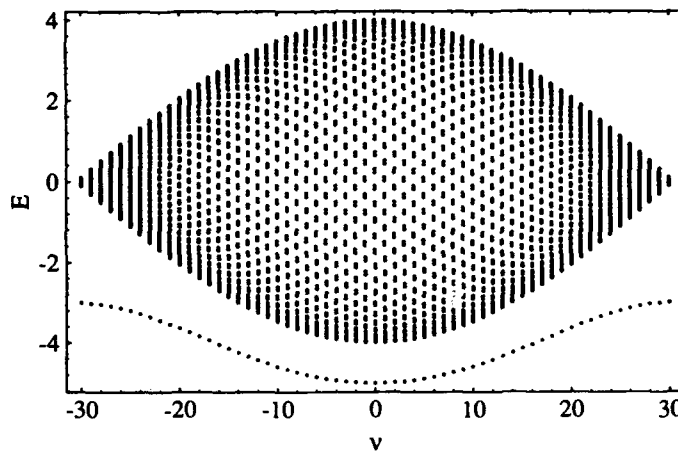


Figure 1. Spectrum of the Hubbard model for $f = 61$, $\gamma = 3$

References

- [1] J C Eilbeck, H Gilhøj, A C Scott, "Soliton bands in anharmonic quantum lattices", Phys. Lett. A, 1992 (in press).
- [2] A C Scott and J C Eilbeck, Phys. Lett. **119A** (1986) 60; A C Scott and J C Eilbeck, Chem. Phys. Lett. **132** (1986) 23; A C Scott, L Bernstein and J C Eilbeck, J. Biol. Phys. **17** (1989) 1; L Bernstein, J C Eilbeck and A C Scott, Nonlinearity **3** (1990) 293. P D Miller, A Scott, J Carr and J C Eilbeck, Physica Scripta **44** (1991) 509-516. H Gilhøj, Masters thesis: *Classical and Quantum Mechanical Properties of the DST Equation*, Laboratory of Applied Mathematical Physics, Technical University of Denmark, 1992.
- [3] R Micnas, J Ranninger and S Robaszkiewicz, Rev. Mod. Phys. **62** (1990) 113; M Wadati, E Olmedilla and Y Akutsu, J. Phys. Soc. Japan **56** (1987) 1340.

STATIONARY SOLITONS IN DISCRETE LATTICES OF DIFFERENT DIMENSIONALITY

V.A.Kuprievich

Bogolyubov Institute for Theoretical Physics
Academy of Sciences of Ukraine
252143 Kiev, Ukraine

The problem of the self-trapping (ST) exciton (or, equivalently, electron) as a result of its interaction with a crystal lattice, in the recent time is broadly discussed in connection with the question of soliton energy transport in the quasi-1-d peptide chains¹. The 2-d ST problems are considered with application to the surface states and Langmuire-Bladgett films; the matter of particular interest is the bipolaron mechanism of high- T_c superconductivity in oxide ceramics with 2-d layered structure².

Most of the studies of 2-d and 3-d ST states (^{3,4} and references therein) are based on the continuum models, commonly using the Gaussian approximation for the electronic wave function. Successive discrete consideration is applied mostly to 1-d cases⁵⁻⁸. Again, the 2-d and 3-d ST states are usually considered within the infinite isotropic lattices, whereas one can point out a number of interesting applications which requires a study of ST states in anisotropic models, with finite-size effects being important as well.

To consider the above aspects of the ST problem we present a discrete-model study of stationary self-trapped states of exciton adiabatically interacting with the rectangular D -dimensional $N_1 \times N_2 \dots \times N_D$ lattice. These states can be obtained from the stationary conditions of the energy functional

$$E = \sum_m \epsilon_m \Phi_m^2 - 2 \sum_{m\alpha} t_\alpha \Phi_m \Phi_{m+\alpha} + \frac{1}{2} \sum_{m\alpha} w_\alpha q_{m\alpha}^2. \quad (1)$$

Site number m in the lattice is assumed to be a vector with components m_1, m_2, \dots, m_D , nearest neighbour sites in the direction α ($\alpha = 1, 2, \dots, D$) are represented by the vectors $m \pm \alpha$, Φ_m is real wave function, t_α are hopping parameters, $q_{m\alpha}$ is the change of the bond length between sites $m - \alpha$ and m , and w_α is an elastic constants along the direction α . The electron-lattice coupling is introduced, like in the Davydov soliton model¹, through the dependence of the site energies ϵ_m on the lengths of the adjacent bonds

$$\epsilon_m = \epsilon_0 + \sum_\alpha \chi_\alpha (q_{m\alpha} + q_{m+\alpha,\alpha}), \quad (2)$$

where χ_α are coupling parameters. The cyclic boundary conditions in each dimension are assumed.

Using the stationarity conditions of E with respect to $q_{m\alpha}$ to exclude the lattice coordinates we obtain ($\epsilon_0 = 0$)

$$E = - \sum_\alpha t_\alpha \sum_m \left[2\Phi_m \Phi_{m+\alpha} + \frac{1}{4} g_\alpha (\Phi_m^4 + \Phi_m^2 \Phi_{m+\alpha}^2) \right], \quad g_\alpha = 4\chi_\alpha^2 / w_\alpha t_\alpha \quad (3)$$

Finally, the stationarity conditions of E with respect to Φ_m yields

$$\sum_\alpha t_\alpha \left[\Phi_{m-\alpha} + \Phi_{m+\alpha} + \frac{1}{4} g_\alpha (2\Phi_m^2 + \Phi_{m-\alpha}^2 + \Phi_{m+\alpha}^2) \Phi_m \right] = \theta \Phi_m, \quad (4)$$

where θ is Lagrangian multiplier taking into account the normalization. Equation (4) admits the solution $\Phi_m^0 = C$, plain wave with zero momentum, describing a free (F) state; the constant C is determined by the normalization. The conditions which ensure that the F state is stable (i.e. corresponds to an energy minimum) can be found, like for 1-d case⁷, using the Fourier transformation to obtain the eigenvalues of the Hessian matrix defined in the terms of denormalized Φ_m . As a result, the critical coupling ensuring stability of the solution $\Phi_m = C$ is determined by the smallest of g_α which satisfy the equalities

$$\sum_\beta t_\beta g_\beta - g_\alpha t_\alpha \sin^2(\pi/N_\alpha) = 2t_\alpha C^{-2} \sin^2(\pi/N_\alpha), \quad \alpha = 1, 2 \dots D \quad (5)$$

For the isotropic lattice ($t_\alpha = t$, $g_\alpha = g$, $N_\alpha = N$) one can obtain from (5) the expression for the critical coupling

$$g_0 = 2N^D / [D \sin^2(\pi/N) - 1]. \quad (6)$$

When $N \gg 1$ an approximate formula $g_0 = 2\pi^2 N^{D-2} / D$ shows that in infinite lattice the F state is always unstable for $D = 1$ ($g_0 \sim 1/N$) and stable for $D = 3$ ($g_0 \sim N$); for 2-d lattice $g_0 \approx \pi^2$, so the F state is stable at $g < g_0$ and unstable at $g > g_0$.

The obtained stability condition for the F state represents only its correspondence to a local minimum and doesn't exclude the existence of deeper minima corresponding to ST states. To analyze the problem we apply the Hartree-type approximation for the wave function Φ_m choosing it as a product of the normalized one-dimensional functions $\phi_{\alpha m}$. The energy expression (3) is thus reduced to

$$E = \sum_\alpha t_\alpha F_\alpha, \quad F_\alpha = -T_\alpha - G_\alpha P_\alpha / 4, \quad (7)$$

$$T_\alpha = 2 \sum_m \phi_{\alpha m} \phi_{\alpha, m-\alpha}, \quad P_\alpha = \sum_m (\phi_{\alpha m}^4 + \phi_{\alpha m}^2 \phi_{\alpha, m+\alpha}^2), \quad (8)$$

where the effective coupling parameter for dimension α is

$$G_\alpha = g_{\alpha m} \prod_{\beta, (\beta \neq \alpha)} R_\beta, \quad R_\alpha = \sum_m \phi_{\alpha m}^4, \quad (9)$$

The values of R_α range from the minimum equal to $1/N_\alpha$ (F state) to the maximum equal to 1 (for the state localized on one site).

Qualitatively the influence of several dimensions upon self-trapping can be considered for the case of 2-d lattice ($\alpha = x, y$). The dependence of the energy on $\phi_{\alpha m}$ can be identified with that in the 1-d case, $E = -t(T + \tilde{g}P/4)$, if the effective coupling \tilde{g} is

$$\tilde{g} = g_x R_y + g_y t_y P_y / 2t_x, \quad (10)$$

Thus the degree of localization in x direction also depends on the y parameters and, through R_y and P_y , on the shape of ϕ_{ym} . Due to the increase of corresponding R_α and P_α localization in some direction favors the localization along other directions.

To simplify the calculations of ST states we use the analytical approximation^{6,7} $\phi_{\alpha m} \sim \exp(-a_\alpha |m - N_\alpha/2|)$, where $a_\alpha \geq 0$ are variational parameters. Then

$$F_\alpha = F(a_\alpha, G_\alpha, N_\alpha), \quad F(a, G, N) = 2/\cosh a + G \tanh(a/4) \tanh(Na/2), \quad (11)$$

$$R_\alpha = R(a_\alpha, N_\alpha), \quad R(a, N) = \tanh(a/2) \tanh(Na/2). \quad (12)$$

The set of a_α which corresponds to the stationary states can be obtained from the energy minimum conditions with respect to all the variables a_α . Functions T_α drop with rising a_α , so at $g_\alpha = 0$ the point $a_\alpha = 0$ (F state) is a minimum. Because P_α

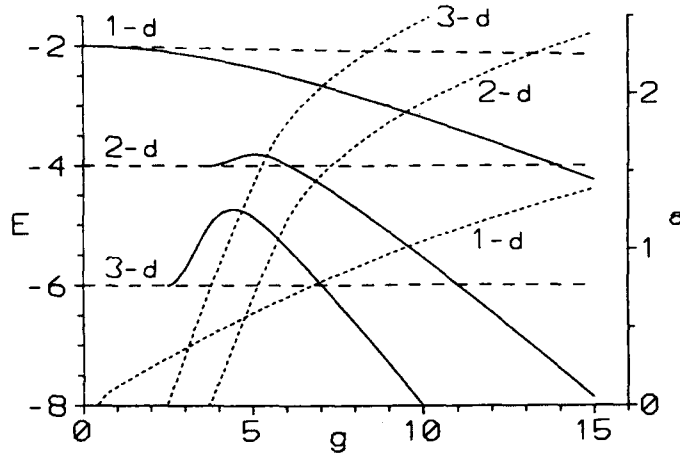


Figure 1. Energies of the self-trapped states (solid lines), free states (dashed lines) and the width parameter a (dotted lines) in the minimum points as functions of the coupling g for the isotropic lattices of different dimensionality with $N_\alpha = 50$

and R_α are increasing function of a_α , other minimum points are possible, at least when coupling exceeds its critical magnitude.

For the isotropic lattice of the same size $N = 2M$ for each of D dimensions the energy expression is

$$E = -D[2/\cosh a + G \tanh(a/4) \tanh(Na/2)], \quad G = g \tanh(a/2) \tanh(Na/2)^{D-1} \quad (13)$$

In the 1-d case considered in⁶ the energy $E = F(a, g, N)$ has a single stationary point at $a > 0$, which always is a minimum of $E(a)$. For the 2-d and 3-d cases the characteristics of the curves $E(a)$ strongly depends on the magnitude of coupling. For the weak coupling the function $E(a)$ has a single minimum at $a = 0$, which corresponds to the F state. With greater g an additional minimum appears on the energy curve but its energy is higher than that of the F state, so the corresponding ST state is metastable. Subsequently increasing g makes the second minimum more and more deep, thus stabilizing the ST state; the F state, the energy of which weakly affected by the

coupling, becomes metastable; the height of the energetic barrier which separates the energy minima can be estimated from the dependence $E(a)$. Under strong coupling, $g > g_0$ the point $a = 0$ becomes maximum, thus the F state turns out to be unstable and only the ST states remain. The corresponding quantitative data are given in Figure 1 which displays the calculated energies of the ST and F states and width parameter a corresponding to the minima of $E(a)$ in the 1-d, 2-d and 3-d lattices.

Various interesting cases can be considered in a simple way basing on the described approach. In particular, the treatment of 2-d system as two coupled 1-d ones allows us to consider the problem of 1-d-like states in 2-d structures. These states have the form $\Phi_{mn} = \phi_m$ or $\Phi_{mn} = \phi_n$ and can be formally regarded as a special case of factorized states. The corresponding analysis shows that the states with the symmetry breaking along single direction are not stable in the isotropic lattice with $N_x = N_y$ (they do not correspond to energy minima but to saddle points). The folded structure is possible when $N_x \gg N_y$; this quasi-1-d system can be considered as a model of the long stack of ring molecules. The consideration of Hartree-like equation shows that the symmetry breaking of ϕ_x with the symmetric ϕ_y in this system is possible even in the absence of the coupling along the stack ($g_x = 0$).

The presented approach in its general formulation provides a unified natural background for studying ST-state properties in various anisotropic 2-d and 3-d discrete systems. So, the soliton formation in the discrete quasi-1-d system involving interchain coupling can be considered in a similar way. Among other important applications, the 3-d ST problem in the 2-d layered structures like that of high- T_c oxide superconductors is worth of studying.

REFERENCES

1. "Davydov's soliton revisited. Self-trapping of vibrational energy in protein", P.L.Christiansen and A.C.Scott,eds., Plenum, N.-Y., (1990).
2. A.S.Davydov, Theoretical investigation of high-temperature superconductivity, *Phys. Reports* 190:192 (1990).
3. Toyozawa, Y.Shinozuka, Stability of an electron in deformable lattice - Force range, dimensionality and potential barrier, *J.Phys.Soc.Jpn.* 48:472 (1980).
4. P.Nagy, P.Markos, On the nature of the self-trapping of different types of polarons, *Phys.Stat.Sol.(b)* 151:571 (1989).
5. G.Venzl, S.F.Fischer, Theory of exciton-phonon coupling in one-dimensional molecular crystals: A variational treatment with delocalized solitary waves, *Phys.Rev.B* 32:6437 (1985).
6. V.A.Kuprievich, Variational study of stationary autolocalized states in a discrete model, *Theor. Math. Phys.(USSR)* 64:269 (1985).
7. V.A.Kuprievich, On autolocalization of the stationary states in a finite molecular chain, *Physica D* 14:395 (1985).
8. H.Bolterauer, M.Opper, The quantum lifetime of the Davydov soliton, *Z.Phys.B* 82:95 (1991).

NUMERICAL AND EXPERIMENTAL STUDIES ON THE AC-DRIVEN DAMPED TODA LATTICE

T. Kuusela¹, J. Hietarinta²

¹Department of Applied Physics, University of Turku
20500 Turku, Finland

²Department of Physics, University of Turku
20500 Turku, Finland

The Toda lattice, sometimes referred to as the exponential lattice, has been used to model the nonlinear effects of lattice vibrations in crystals in an effort to study e.g. the partition of energy among various modes of vibration, thermal expansion under excitation, the finiteness of the thermal conduction etc. The Toda lattice with dissipation and an external ac-drive can be written in the form

$$\partial_t^2 \ln(1 + V_n) + \alpha \partial_t \ln(1 + V_n) = V_{n-1} + V_{n+1} - 2V_n + 2(-1)^n \epsilon \cos(\omega t), \quad (1)$$

where α , ϵ and ω are the dissipation factor, the drive amplitude and frequency, respectively. If $\alpha = \epsilon = 0$ we have an integrable system with all solitonic properties. Then the single soliton solution is

$$V_n(t) = \sinh^2(\mu) \operatorname{sech}^2(\mu n \pm \sinh(\mu)t). \quad (2)$$

In the case of $\alpha > 0$, $\epsilon = 0$ the system has decaying solitary wave solution because of dissipation, but nevertheless many solitonic properties remain.^{1,2,3}

The dissipation in the Toda lattice can be compensated with an external ac-drive, as it has been recently suggested⁴. Analytical results⁴ and direct numerical simulations⁵ of the system (1) have demonstrated that stable propagation of solitons with the velocity v is possible, if

$$\omega = (2N + 1)\pi v, \quad N = 0, 1, 2, \dots \quad (3)$$

and if $\epsilon > \epsilon_{thr}$, where ϵ_{thr} is the threshold value of the drive parameter. It has been

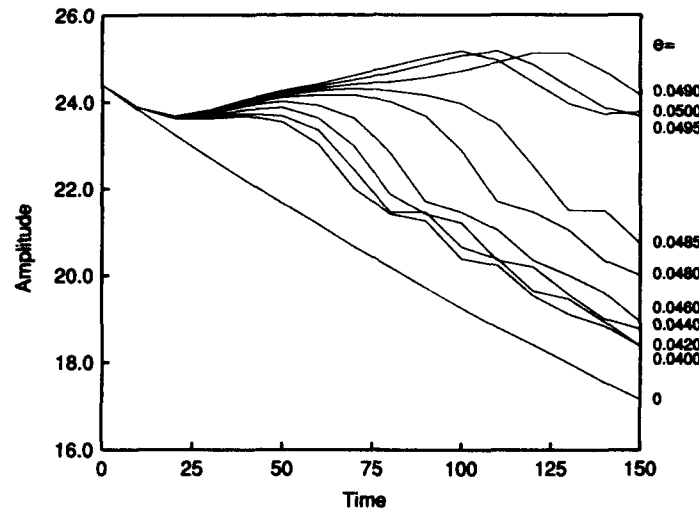


Figure 1. The amplitude of the soliton as a function of time with different values of the drive parameter ϵ .

shown analytically⁴ that for a sufficiently large velocity ($N = 0$)

$$\epsilon_{thr} \approx 4\alpha\omega \ln(v). \quad (4)$$

The sign-changing factor $(-1)^n$ in (1) is absolutely necessary to provide for real input of energy from the ac-drive. Without this factor the amplitude of a soliton decays even if the drive amplitude is very large.

We have numerically integrated equation (1) with periodic boundary conditions⁵. As an initial state we have used the ideal 1-soliton solution (2). In order to examine the evolution of the soliton under external drive we have solved numerically the eigenvalue problem of the Toda lattice at the moments of time $t = 0, 10, \dots, 150$. The amplitude $A = \sinh^2(\mu)$ of the soliton corresponding to the dominant eigenvalue is shown in Figure 1 as a function of time for different values of the drive parameter ϵ ($\mu = 2.30$, $v = 2.14$, $\alpha = 0.002$ and $\omega = 6.774$). There is clear threshold value at $\epsilon = 0.0490 \pm 0.0005$. With smaller values the amplitude decays exponentially but with higher values the mean amplitude is constant.

In Figure 2 we have collected the threshold data for three different dissipation factors, each one with five different velocities. The drive parameter is normalized with the dissipation factor in order to compare directly the theoretical prediction (4) with numerical results. With large amplitudes all curves converge and approach the theoretical curve. In the limit of minimum velocity $v = 1$ the threshold value tends to increase rapidly. This is because of the width of the soliton: when the soliton extends over several lattice points, the drive partially cancels itself. We also observe that with small dissipation a relatively stronger drive is needed. The rate of energy losses is a sum of the dissipative part proportional to α and the constant radiative part independent of α , and therefore the normalized drive parameter approaches infinity when α goes to zero.

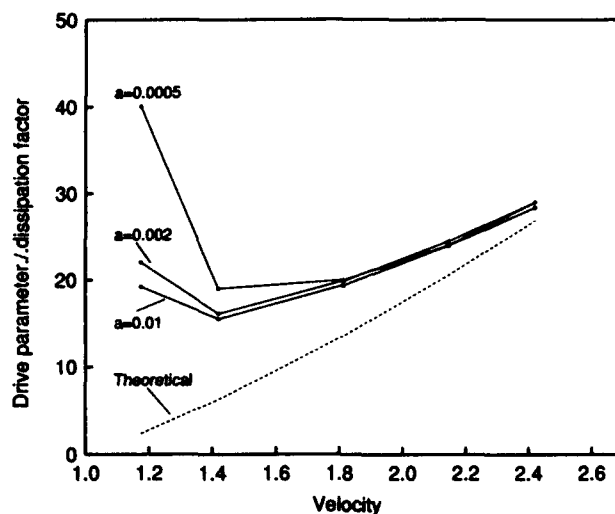


Figure 2. The threshold values of the drive parameter normalized with the dissipation factor as a function of the soliton velocity. The theoretical prediction (4) is drawn with dashed line.

The numerical results show clearly that soliton dissipation can be compensated in a discrete lattice with an ac-drive which has alternating sign in adjacent lattice points. One can expect that this effect can be seen in real solitons propagating in an ac-driven quasi-one-dimensional ionic lattice or in an ion-doped polymer chain. One experimental realization of this phenomenon has been performed using nonlinear electrical transmission lines, which serve a practical tool to investigate soliton phenomena in nonlinear discrete systems. The external sinusoidal drive is included using inductive coupling of the drive generator⁶, as shown in Figure 3. By choosing the values of the components properly, this circuit very well approximates the system (1), and the energy input and threshold effect (in a agreement with numerical results) are easily observed.

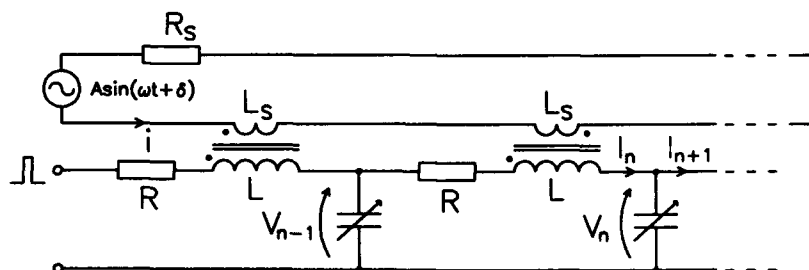


Figure 3. The nonlinear electrical transmission line with the inductively coupled drive.

REFERENCES

1. T. Kuusela, J. Hietarinta, Elastic scattering of the solitary waves in the strongly dissipative Toda lattice, *Phys. Rev. Lett.* 62:700 (1989)
2. T. Kuusela, J. Hietarinta, Numerical, experimental and analytical studies of the dissipative Toda lattice. I The behaviour of a single solitary wave, *Physica D* 41:322 (1990)
3. T. Kuusela, J. Hietarinta, Numerical, experimental and analytical studies of the dissipative Toda lattice. II Elastic scattering of solitary waves, *Physica D* 46:1 (1990)
4. B. A. Malomed, Propagating solitons in damped ac-driven chains *Phys. Rev. A* 45:4097 (1992)
5. T. Kuusela, J. Hietarinta, B. A. Malomed, Numerical study of solitons in the damped ac-driven Toda lattice, submitted to *J. Phys. A*
6. T. Kuusela, Soliton experiments in a damped ac-driven nonlinear electrical transmission line, *Phys. Lett. A* 167:54 (1992)

QUANTUM EFFECTS IN THE NONLINEAR NONADIABATIC DIMER

Riccardo Mannella, David Vitali, Luca Bonci and Paolo Grigolini

Dipartimento di Fisica dell' Università di Pisa
Piazza Torricelli 2, 56100 Pisa, Italy

Kenkre and Wu ¹ have studied the nonadiabatic effects on the nonlinear dimer, assuming a finite relaxation time for the vibrations.

They have considered a model in which each site interacts with an overdamped classical oscillator

$$\begin{aligned}
 i \dot{c}_1(t) &= V c_2(t) - \lambda \beta_1(t) c_1(t) \\
 i \dot{c}_2(t) &= V c_1(t) - \lambda \beta_2(t) c_2(t) \\
 \dot{\beta}_1(t) + \Gamma \beta_1(t) &= \frac{\Gamma \chi}{\lambda} |c_1(t)|^2 \\
 \dot{\beta}_2(t) + \Gamma \beta_2(t) &= \frac{\Gamma \chi}{\lambda} |c_2(t)|^2
 \end{aligned} \tag{1}$$

With the following definitions

$$\langle \sigma_x(t) \rangle = |c_1(t)|^2 - |c_2(t)|^2 \tag{2a}$$

$$\langle \sigma_y(t) \rangle = i [c_1(t) c_2^*(t) - c_1^*(t) c_2(t)] \tag{2b}$$

$$\langle \sigma_z(t) \rangle = [c_1(t) c_2^*(t) + c_1^*(t) c_2(t)] \tag{2c}$$

$$y(t) = \frac{\lambda}{\chi} (\beta_1(t) - \beta_2(t)) \tag{2d}$$

it is possible to rewrite eqs.(2) in the form

$$\begin{aligned}
\langle \dot{\sigma}_x(t) \rangle &= 2 V \langle \sigma_y(t) \rangle \\
\langle \dot{\sigma}_y(t) \rangle &= -2 V \langle \sigma_x(t) \rangle - \chi \langle \sigma_z(t) \rangle y(t) \\
\langle \dot{\sigma}_z(t) \rangle &= \chi \langle \sigma_y(t) \rangle y(t) \\
\dot{y}(t) + \Gamma y(t) &= \Gamma \langle \sigma_x(t) \rangle.
\end{aligned} \tag{3}$$

We have investigated the effects of relaxing the classical assumption on the vibrations, by studying a Fröhlich-type quantum mechanical Hamiltonian, which reproduces the semiclassical set of equations (3). We have considered the spin-boson Hamiltonian of Leggett *et al.*², in which the overdamped oscillator y is replaced by a continuous distribution of quantum oscillators

$$H = -\frac{\omega_0}{2} \sigma_z + g \sigma_x \sum_i \Gamma_i (b_i^\dagger + b_i) + \sum_i \omega_i b_i^\dagger b_i \tag{4}$$

supplemented with the following ohmic spectral density

$$J(\omega) \equiv g^2 \sum_i \Gamma_i^2 \delta(\omega - \omega_i) = g^2 \omega \exp(-\omega/\omega_c) \tag{5}$$

The relationship between the parameters is the following:³

$$V \rightarrow \frac{\omega_0}{2} \quad \chi \rightarrow 4\Delta = 4g^2\omega_c \quad \Gamma \rightarrow \frac{2}{\pi} \omega_c \tag{6}$$

We have focused on $\langle \sigma_x(t) \rangle$, the probability difference between the two sites, and we have derived the following nonlinear and nonstationary integrodifferential equation for its dynamics:³

$$\begin{aligned}
\langle \dot{\sigma}_x(t) \rangle &= -\omega_0^2 \int_0^t ds \langle \sigma_x(s) \rangle \operatorname{Re} \left\{ \exp \left[-4g^2 \int_0^{t-s} dt_1 \int_0^{t_1} dt_2 \langle \tilde{x}^{(0)}(t_2) \tilde{x}^{(0)}(0) \rangle \right] e^{-4i\Delta(t-s)} \right. \\
&\times \exp \left[4i g^2 \int_s^t d\tau \int_0^\tau d\tau' \sum_i \Gamma_i^2 \sin \omega_i(\tau - \tau') (1 - \langle \sigma_x(\tau') \rangle) \right] \left. \right\}
\end{aligned} \tag{7}$$

where $\tilde{x} = \sum_i \Gamma_i (\tilde{b}_i + \tilde{b}_i^\dagger)$ is the quantum counterpart of y of eq.(2.1) and it is the collective coordinate describing the molecular vibrations.

Our equation (7) corresponds to the nonlinear nonadiabatic dimer of eq.(3) in presence of the quantum fluctuations of the oscillators (first exponential factor in eq. (7)). Our

approach (7) also provides a nonlinear generalization of the noninteracting blip approximation (NBA) theory of Leggett *et al.* ³. In fact, we get the NBA equation by neglecting the nonlinear factor (the last exponential term) in eq.(7).

The stability of self-trapping against thermal and quantum fluctuations is a crucial question in the nonlinear dimer because self-trapping is necessary for the manifestation of Davydov's soliton along molecular chains. The nonlinear nonadiabatic dimer is characterized by a transition to localization ($\langle \sigma_x \rangle_{eq} \neq 0$) at sufficiently large nonlinearity parameter χ . There are two stable equilibrium broken-symmetry states corresponding to the stationary states of the DNSE, that are irreversibly reached due to the coupling to the dissipative oscillator. The self-trapping transition has the form of a second order phase transition which takes place at $\chi_c = 2V$

It is interesting and a little bit surprising that also the linear integrodifferential equation derived from the NBA shows a very similar transition to localization at zero temperature. It is again a second order phase transition, but at a larger threshold, $\chi_c = \pi\Gamma$, ($V \ll \Gamma$ due to time-scale separation).

Our theory recovers under specific conditions both the NBA and the nonlinear nonadiabatic dimer theory, each of them leading to localization. Thus one would be tempted to conclude that also our equation implies localization. The main result of our investigation is that this intuitive conclusion is wrong and that even if one starts from $\langle \sigma_x \rangle = 1$, there is no self-trapping. The joint action of nonlinearity and quantum mechanical fluctuations leads to localization breakdown, in spite of the fact that their separate action would support localization.

We have performed an asymptotic analysis of eq. (7) by assuming that $\langle \sigma_x(t) \rangle$ tends to a well defined limit, $\langle \sigma_x(\infty) \rangle$, and we have studied which are the asymptotic values allowed by this equation.

We have found the following results: ⁴

- i) the "delocalized" solution $\langle \sigma_x(\infty) \rangle = 0$ is admitted for any value of the coupling strength g .
- ii) for $g > 1/2$ also the fully broken-symmetry state, namely $\langle \sigma_x(\infty) \rangle = 1$, would seem possible. Nevertheless, this additional solution must be disregarded because for any finite value of the tunneling frequency ω_0 the state of $\sigma_x = 1$ cannot be an eigenstate of the spin-boson Hamiltonian.

Thus we conclude that our approach (7) is incompatible with any self-trapping, even if it interpolates between two theories (NBA and Kenkre-Wu theory) which both yields localization.

To confirm this asymptotic analysis we have solved eq.(7) numerically in the ohmic case at zero temperature (see figures 1 and 2).

Since the self-trapping mechanism is the key for solitonic behavior in the DNSE, our results seems to suggest that quantum fluctuations can be quite effective in the destruction of solitonic propagation in molecular chains.

It is still an open question whether our results can be extrapolated from the dimer to the

infinite chain and how much they depend on the details of the quantum mechanical model Hamiltonian we have chosen.

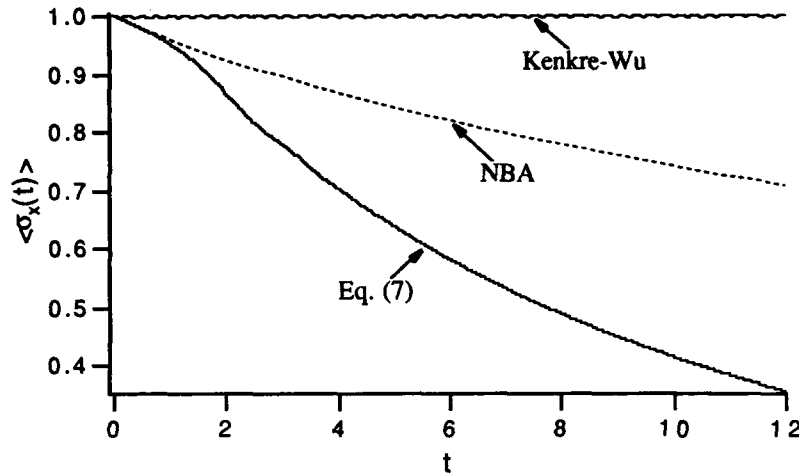


Figure 1. $\langle \sigma_x \rangle$ versus time at zero temperature. The values of the parameters are: $\omega_0=1$, $\omega_c=20$, $g=0.55$

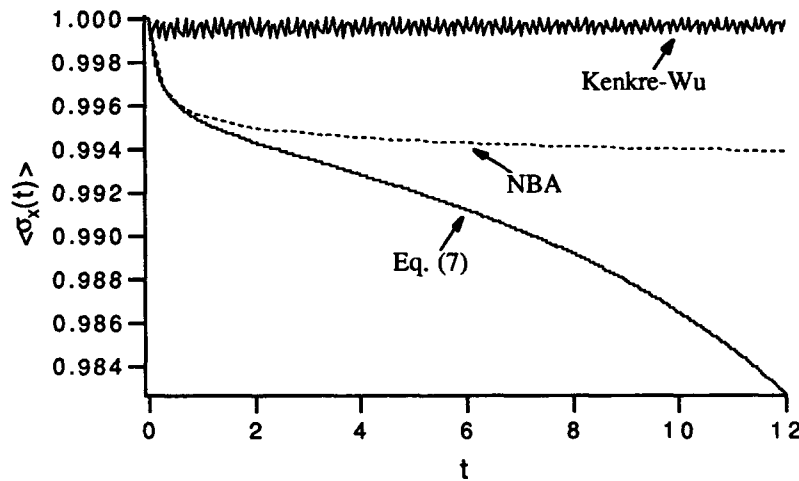


Figure 2. $\langle \sigma_x \rangle$ versus time at zero temperature. The values of the parameters are: $\omega_0=1$, $\omega_c=20$, $g=0.75$

REFERENCES

1. V.M. Kenkre, and H.-L. Wu, Phys. Rev. B 39, 6907 (1989); Phys. Lett. A 135, 120 (1989).
2. A.J. Leggett, S. Chakravarty, A.T. Dorsey, M.P.A. Fisher, A. Garg, and W. Zwerger, Rev. Mod. Phys. 59, 1 (1987).
3. D. Vitali, P. Grigolini, Phys. Rev. A, 42, 7091 (1990).
4. D. Vitali, L. Bonci, R. Mannella, P. Grigolini, Phys. Rev. A 45, 2285 (1992).

ON THE DISCRETE AND CONTINUUM INTEGRABLE HEISENBERG SPIN CHAIN MODELS

K. Porsezian

Centre for Nonlinear Dynamics
Department of Physics
Bharathidasan University
Tiruchirapalli 620 024, India

INTRODUCTION

It has been realized in recent times that the elementary excitations in Heisenberg ferromagnetic systems can be characterized by spatially compact solitons in addition to the linear spin waves (magnons).¹⁻⁴ Hence rigorous attempts were made after the discovery of the concepts of soliton and inverse scattering transform to identify soliton possessing integrable spin models. It was successful in the case of simple spin models like one-dimensional classical isotropic and anisotropic spin chains.^{1,5} At the same time Lakshmanan¹ approached the spin chain problem through an understanding of the underlying geometry of the system. This enabled Lakshmanan and his co-workers^{2,3} to investigate a large class of integrable spin chain models by including different kinds of magnetic interactions. Some of the systems in this list include bilinear, biquadratic, deformed, site dependent, and radially symmetric Heisenberg ferromagnetic spin chains. Similarly gauge equivalence formalism introduced by Zakharov and Takhtajan⁴ connects the integrable nonlinear Schrödinger (NLS) family of equations with integrable spin models. The main advantage of the above equivalence method is that individual treatment of each one of them would become unnecessary and full information about only a few basic equations would be sufficient to solve the rest generated from them. In this paper we discuss the connection between various spin systems and nonlinear Schrödinger family of equations through geometrical and gauge equivalence methods.

GEOMETRICAL EQUIVALENCE¹

Consider the evolution of spins in a chain and map the same to a moving helical space curve in E^3 at a given time by identifying the spin vector with the unit tangent vector of the space curve. It is known that at any arbitrary instant of time, the state of this space curve with given curvature $\kappa(x,t)$ and torsion $\tau(x,t)$ is governed by the following Serret-Frenet (SF) equations.

$$e_{ix} = d \wedge e_i, \quad d = \kappa e_3 + \tau e_1 \quad (1)$$

Here e_i , $i = 1, 2, 3$ are the tangent, normal and binormal (trihedral) vectors. Using the SF equation and the spin evolution equation (after replacing the spin vector S by e_1) the time evolution of the trihedral can be written as

$$e_{it} = \omega \wedge e_i, \quad \omega = \omega_1 e_1 + \omega_2 e_2 + \omega_3 e_3 \quad (2)$$

$\omega_1, \omega_2, \omega_3$ are functions of x, t, κ, τ and their derivatives.

The compatibility of eqs. (1) and (2) (i.e.) $\frac{\partial e_{ix}}{\partial t} = \frac{\partial e_{it}}{\partial x}$ gives a set of coupled partial differential equations in κ and τ which on making the complex transformation

$$q = \kappa(x,t) \exp\left\{i \int_{-\infty}^x \tau(x',t) dx'\right\} \quad (3)$$

lead to different nonlinear evolution equation in the NLS family depending on the nature of magnetic interactions of the system.

GAUGE EQUIVALENCE⁴

Consider the linear problem of Lax pair associated with the integrable equation $Lq = 0$.

$$\varphi_x = U\varphi, \quad \varphi_t = V\varphi \quad (4)$$

where the Jost function φ and the Lax pair U, V are complex

matrix functions of the field $q, q_x \dots$, the independent variables x and t and the spectral parameter λ . The compatibility of (4), i.e., $\varphi_{xt} = \varphi_{tx}$, $U_t - V_x + [U, V] = 0$ yields the original nonlinear system. In order to construct the equivalent new evolution equation, we introduce the gauge transformation

$$\varphi' = g^{-1}\varphi \quad (5)$$

where φ' is the Jost function for the new system and $g \in GL(2, \mathbb{C})$ is a unitary matrix function of x and t . Using (5) in (4), we obtain the new linear eigen value problem

$$\varphi'_x = U'\varphi', \quad \varphi'_t = V'\varphi' \quad (6)$$

with $U' = g^{-1}Ug - g^{-1}g_x$, $V' = g^{-1}Vg - g^{-1}g_t$. The compatibility of (6) gives the new equivalent integrable evolution equation for which the Lax pair is given by U' and V' . Now, to connect NLS type equations with the Heisenberg ferromagnetic spin systems we introduce the transformation $S = g^{-1}\sigma_3g$. The applicability of the above two methods is given in Table 1.

CONCLUSION

We have demonstrated that through geometrical and gauge equivalence methods it is possible to 'unify' a large number of integrable systems, pinpointing a few basic ones. Application of these methods also allows us to generate new integrable systems along with their Lax pairs.

ACKNOWLEDGEMENT

The author is thankful to Prof. M. Lakshmanan for introducing him into the exciting area of nonlinear dynamics and for his guidance. He also wishes to thank Dr M. Daniel for his useful discussions. He wishes to thank the Department of Science and Technology, Government of India for the financial support in the form of a young scientist project and the NBHM for travel support.

Table 1. Completely integrable classical continuum Heisenberg ferromagnetic spin chains and their connection with NLS family

System	Spin equation	NLS family	Equivalence
Some ferromagnetic systems			
1. Isotropic ¹	$S_t = S \wedge S_{xx}$	$i q_t + q_{xx} + 2 q ^2 q = 0$	Geometrical/ Gauge
2. Isotropic + External field ⁵	$S_t = S \wedge S_{xx} + \mu [S \wedge h]$	-do-	Gauge
3. Isotropic + Anisotropy + External field ⁵ (Easy axis $A > 0$)	$S_t = S \wedge S_{xx} + 2A(S \wedge S^2 e_3) + \mu [S \wedge h e_3]$	-do-	Gauge
4. Doubly anisotropic ⁶	$S_t = S \wedge S_{xx} + S \wedge \tau S$ $= \text{diag}(\tau_1, \tau_2, \tau_3)$	-do- ($\tau_1 = \tau_2 < \tau_3$)	Gauge
5. Deformed ⁷	$S_t = S \wedge S_{xx} + \epsilon (S_x)^3$	$i q_t + q_{xx} + 2 q ^2 q - i \epsilon (q ^2 q)_x = 0$	Geometrical/ Gauge
6. Site dependent ⁸	$S_t = (\alpha x + \beta) S \wedge S_{xx} + \alpha S \wedge S_x$	$i q_t + (\alpha x + \beta)(q_{xx} + 2 q ^2 q)$ $+ 2\alpha(q_x + q \int q ^2 dx) = 0$	Geometrical/ Gauge
7. Circularly ⁸ symmetric	$S_t = S \wedge S_{rr} + (S \wedge S_r)/r$	$i q_t + q_{rr} + (q_r/r) - q/r^2 + 2 q ^2 q$ $+ 4q \int \frac{ q ^2}{r'} dr' = 0$	Geometrical/ Gauge
8. Biquadratic ⁹	$S_t = S \wedge (S_{xx} + \gamma S_{xxxx} + 5S(S_{xx}) + \frac{5}{2} S_{xx}^2 S)$	$i q_t + q_{xx} + 2 q ^2 q + \gamma q_{xxxx} + 8 q ^2 q_{xx}$ $+ 2q^2 q_{xx}^* + 4q q_x ^2 + 6q_x^2 q^* + 6 q ^4 q = 0$	Geometrical/ Gauge

Some mathematical generalizations

9. Generalized isotropic¹⁰

$$S_t = \alpha(S \wedge S_{xx}) + 8(S_{xx} \wedge \frac{3}{2} S_x^2 S_x)$$

Geometrical/
Gauge

10. Generalized linearly x-dependent¹¹

$$S_t = (\alpha_1 x + \beta_1) S \wedge S_{xx} + \alpha_1 S \wedge S_x - (\alpha_2 x + \beta_2) S_x + \alpha_3 (S_{xx} \wedge \frac{3}{2} S_x^2 S_x) + i(\alpha_2 x + \beta_2) q_x + i\alpha_3 (q_{xxx} + 6|q|^2 q_x) = 0$$

Geometrical/
Gauge

11. Higher dimensional generalization¹²

$$S_t = S \wedge (S_{xx} + \alpha S_{yy}) + \varphi_x S_y + \varphi_y S_x$$

$$\varphi_{xx} = \alpha^2 \varphi_{yy} + 2\alpha^2 S(S \wedge S_y) = 0$$

Gauge

Some discrete models

12. $S_{n,t} = \frac{S_n \wedge S_{n+1}}{1 + S_n \cdot S_{n+1}} + \frac{S_n \wedge S_{n-1}}{1 + S_n \cdot S_{n-1}}$ (Ref. 13)

Gauge

13. $S_{n,t} = \frac{(S_n \cdot S_{n+1}) S_n - S_{n+1}}{1 + S_n \cdot S_{n+1}} + \frac{S_{n-1} - (S_n \cdot S_{n+1}) S_n}{1 + S_n \cdot S_{n-1}}$ (Ref. 14)

Gauge

14. $S_{n,t} = a \left[\frac{S_n \wedge S_{n+1}}{1 + S_n \cdot S_{n+1}} + \frac{S_n \wedge S_{n-1}}{1 + S_n \cdot S_{n-1}} \right] + b \left[\frac{(S_n \cdot S_{n+1}) S_n - S_{n+1}}{1 + S_n \cdot S_{n+1}} + \frac{S_{n-1} - (S_n \cdot S_{n+1}) S_n}{1 + S_n \cdot S_{n-1}} \right]$ (Ref. 15)

Gauge

REFERENCES

1. M. Lakshmanan, Continuum spin system as an exactly solvable dynamical system, **Phys. Lett.** A61:53(1977).
2. M. Daniel, "Nonlinear excitations in the Heisenberg ferromagnetic spin chain," Ph.D. thesis, University of Madras (1983).
3. K. Porsezian, "On the nonlinear dynamics of the discrete and continuum spin systems," Ph.D. thesis, Bharathidasan University (1990).
4. V. E. Zakharov and L. A. Takhtajan, Equivalent of the nonlinear Schrödinger equation and the equation of a Heisenberg ferromagnet, **Theor. Math. Phys.** 38:17(1979).
5. A. F. Borovik, Exact integration of the nonlinear Landau-Lifshitz equation, **Solid State Commun.** 34:721(1980).
6. E. K. Sklyanin, The complete integrability of the Landau-Lifshitz equation, Lomi preprint (1979).
7. K. Porsezian, M. Lakshmanan and K. M. Tamizhmani, Geometrical equivalence of a deformed Heisenberg spin equation and the generalized nonlinear Schrödinger equation, **Phys. Lett.** A124:159(1987).
8. K. Porsezian and M. Lakshmanan, On the dynamics of the radially symmetric Heisenberg ferromagnetic spin system, **J. Math. Phys.** 32:2923(1991).
9. K. Porsezian, M. Daniel and M. Lakshmanan, On the integrability aspects of the one-dimensional classical continuum isotropic biquadratic Heisenberg spin chain, **J. Math. Phys.** 33:(1992) (in press)
10. Y. Ishimori, A relationship between the AKNS and WKI schemes of the inverse scattering method, **J. Phys. Soc. Japan** 51:394(1983).
11. M. Lakshmanan and S. Ganesan, Geometrical and gauge equivalence of the generalized Hirota, Heisenberg and WKIS equation with linear inhomogeneties, **Physica** A132:117(1985).
12. B. G. Konopelchenko and B. J. Matkarimov, On the inverse scattering transform for the Ishimori equation, **Phys. Lett.** A135:183(1989).
13. Y. Ishimori, An integrable spin chain, **J. Phys. Soc. Japan** 51:3417(1989).
14. V. S. Gerdjikov, M. I. Ivanov and Y. S. Vaklev, Gauge transformations and generating operators for the discrete Akharov-Shabat system, **Inverse Prob.** 2:413(1986).
15. K. Porsezian and M. Lakshmanan, Discretized Hirota equation equivalent spin system and Bäcklund transformations, **Inverse Prob.** 5:L15(1988).

DYNAMICS AND INSTABILITY OF NONLINEAR PATTERNS IN PHASE TRANSFORMATION PROBLEMS

J. Pouget

Laboratoire de Modélisation en Mécanique (associé au CNRS)
Université Pierre et Marie Curie, 4 Place Jussieu
75252 Paris Cédex 05, France

Abstract : Nonlinear dynamics and instability mechanism of a lattice model for elastic phase transformations are presented. On the basis of a two-dimensional lattice model involving nonlinear and competing interactions the formation and dynamics of twinning in alloys are examined. The emphasis is placed especially on the instability mechanisms of a strain band and modulated structure with respect to the transverse perturbations producing then localized structures on the lattice. The physical conjectures are illustrated by means of numerical simulations. The results are interpreted as microtwinning formation in crystalline alloys.

INTRODUCTION

Research in recent years has received a great interest in *complex spatial structures* and *nonlinear dynamics* taking place in numerous fields of physical sciences. These structures become fundamental in the study of *phase transitions* which are usually accompanied by the appearance of defects : dislocation motions, grain boundaries, domain wall structures and twinings [1,2]. Here, we want to illustrate the formation of spatial and temporal patterns in two-dimensional systems occuring for *phase transformations in alloys* such as ferroelastic-martensitic transformations. The main motivation of this work is the understanding how spatial structure formation and related dynamics arising at the *microscale* are able to organize the system at the *macroscale*. Ferroelastic-martensitic transformations are characterized by involving lattice distortions, usually shear displacements. The transformation is accompanied by the dynamics of twin interfaces and twin bands [3,4]. On the other hand, the nucleation process can be seen as a pretransformation phenomenon where modulated strain structures are developed within the high-temperature or parent phase. However, the *instability phenomena* can be considered as the growth of martensitic phases producing thus localized structures or elastic domains. These *microstructures* are well described at an intermediate scale where the microscopic physics provides *competing* and *strongly nonlinear* interactions. This

underlines the interest of lattice models, since the latter possess the physical ingredients which are the basis of the relevant effects.

Starting with a two-dimensional lattice model which allows us to describe a cubic-tetragonal transformation, an instability mechanism for martensitic twinning is examined [5,6]. The existence of low-lying transverse acoustic phonons propagating along the $[110]$ direction is responsible for lattice instability [7]. The system exhibits structures made of spatially periodic arrangements of martensites referred to as "tweed patterns" occurring in some range of temperatures and followed, at lower temperature, by the martensitic phase. First, the quasicontinuum approximation of the lattice model leads to an asymptotic model which describes the long-time evolution of the nonlinear structures emerging from the instability. Second, by means of semi-discrete approach and in the low-amplitude limit an envelope equation is then deduced from the microscopic system and provides a criterion of stability for modulated structures.

THE MODEL

a. Lattice Interactions

Let us consider an atomic plane made of squares parallel to the i and j directions (see fig. 1) (In-Tl, Fe-Pd are good examples). A particle of the lattice plane is located by (i, j) . After deformation of the lattice, the particle experiments a displacement in the plane defined by $u(i, j)$ and $v(i, j)$ along the i and j directions, respectively.

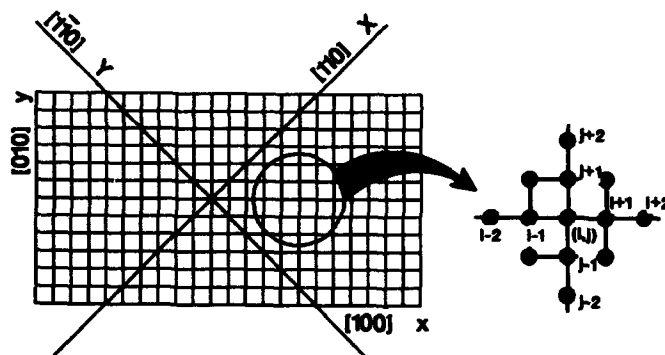


Fig. 1 : Two-dimensional lattice model and details of the interactions by pairs and noncentral forces

We assume that the particles interact through two types of interatomic potential : (i) interatomic interactions between first-nearest neighbors considered as functions of particle pairs in the i and j directions and in the diagonal directions as well and (ii) interactions involving *noncentral forces* or three-body interactions between *first-* and *second-nearest neighbors* in the i and j directions. These interactions provide competing interactions which are equivalent to bond bending forces due to the long-range atomic interactions. Then, we can propose the following lattice energy [6,8]

$$\begin{aligned} \nu = \sum_{(i,j)} \left\{ \Phi(S(i,j)) + \frac{1}{2} \beta (G(i,j))^2 + \frac{1}{2} \delta \left[(\Delta_L^+ S(i,j))^2 + (\Delta_T^+ G(i,j))^2 \right] \right. \\ \left. + \frac{1}{2} \eta \left[(\Delta_L^+ (S(i+1,j) + 2S(i,j) + S(i-1,j)))^2 \right. \right. \\ \left. \left. + (\Delta_T^+ (G(i,j+1) + 2G(i,j) + G(i,j-1)))^2 \right] \right\} , \end{aligned} \quad (1)$$

where we have defined the discrete deformations

$$S(i, j) = u(i, j) - u(i-1, j), \quad G(i, j) = u(i, j) - u(i, j-1), \quad (2)$$

and the potential Φ is given by

$$\Phi(S) = \frac{1}{2}\alpha S^2 - \frac{1}{3}S^3 + \frac{1}{4}S^4. \quad (3)$$

The equations are written in nondimensional unit and the coefficients α , β , δ and η are the parameters of the model. The first two terms in Eq.(1) are the nonlinear and linear potentials emerging from the interactions by pairs. The lattice potential (3) is the expansion up to the fourth order of the interactions by pairs in the i direction. The third and fourth parts of the lattice energy represent the noncentral interactions in the i and j directions between first- and second-nearest neighboring particles. The operators Δ_L^+ and Δ_T^+ denote the forward first-order finite differences: $\Delta_L^+ f(i, j) = f(i+1, j) - f(i, j)$ and $\Delta_T^+ f(i, j) = f(i, j+1) - f(i, j)$.

b. Equations of Motion

Adding the kinetic energy to the lattice energy (1) we can write the following equation for the discrete displacement $u(i, j)$

$$\ddot{u}(i, j) = \Delta_L^+ \Sigma_L(i, j) + \Delta_T^+ \Sigma_T(i, j), \quad (4)$$

where we have defined some discrete stresses

$$\Sigma_L(i, j) = \sigma(i, j) - \Delta_L^- \chi_L(i, j), \quad (5.a)$$

$$\Sigma_T(i, j) = \beta G(i, j) - \Delta_T^- \chi_T(i, j), \quad (5.b)$$

$$\sigma(i, j) = \alpha S(i, j) - S(i, j)^2 + S(i, j)^3, \quad (5.c)$$

$$\chi_L(i, j) = \Delta_L^+ (\delta S(i, j) + \eta (S(i+2, j) + 4S(i+1, j) + 6S(i, j) + 4S(i-1, j) + S(i-2, j))) , \quad (5.d)$$

$$\chi_T(i, j) = \Delta_T^+ (\delta G(i, j) + \eta (G(i, j+2) + 4G(i, j+1) + 6G(i, j) + 4G(i, j-1) + G(i, j-2))) . \quad (5.e)$$

The operators Δ_L^- and Δ_T^- represent the backward first-order finite differences in the i and j directions, respectively. Equations (5.a) and (5.b) define the discrete macroscopic stresses and Eqs (5.d) and (5.e) are the microscopic stresses due to the noncentral interactions. Note that the nonlinear stress (5.c) derives from the potential (3).

QUASICONTINUUM MODEL

In order to describe, at the continuum scale, the lattice dynamics, we then consider the *long-wavelength limit* of Eqs (4) and (5). After some classical algebras we arrive at the equation of motion for the continuous deformation $S(x, y, t)$

$$S_{tt} = \Sigma_{Lxx} + \Sigma_{Tyy}, \quad (6)$$

with

$$\Sigma_L = \sigma(S) - \delta_1 S_{xx}, \quad (7.a)$$

$$\Sigma_T = \beta S - \delta_2 S_{yy}, \quad (7.b)$$

where we have set $\delta_1 = \delta + 16\eta - \alpha/12$ and $\delta_2 = \delta + 16\eta - \beta/12$. Note that we recover the macro-stresses $\sigma(S)$ and βS in Eqs (7.a) and (7.b) and the last terms in Eqs (7.a) and (7.b) stand for the microscopic stresses which emerge both from the noncentral interactions and discreteness effects. It should be noticed that the quasicontinuum model thus deduced from the lattice model is somewhat similar to a continuum model derived from nonlinear elasticity including strain gradient [4].

DYNAMICS OF NONLINEAR STRUCTURES

a. Numerical simulations

Here, we are interested in the *instabilities with respect to the transverse disturbances* of a strain band moving in the x direction and homogeneous in the y direction. A question can be risen, what is the new spatial structures emerging from the instability process and we want to know whether they are coherent and stable or not. The numerical scheme is provided by the set of difference-differential equations (4)-(5). The results of the numerics are shown in Fig.2. Figure 2.a is the initial condition, that is a localized deformation in the x direction and homogeneous along the other direction which is however a solution to the 1D problem. Some time later, perturbations are developing along the transverse direction as depicted in Fig. 2.b. The instabilities are growing showing that the nonlinear structure is no longer stable with respect to the transverse perturbations. After a rather long time, the resulting pattern consisting in a disk-shaped structure is created as shown in Fig. 2.c. This structure turns out to be robust and stable [6,8].

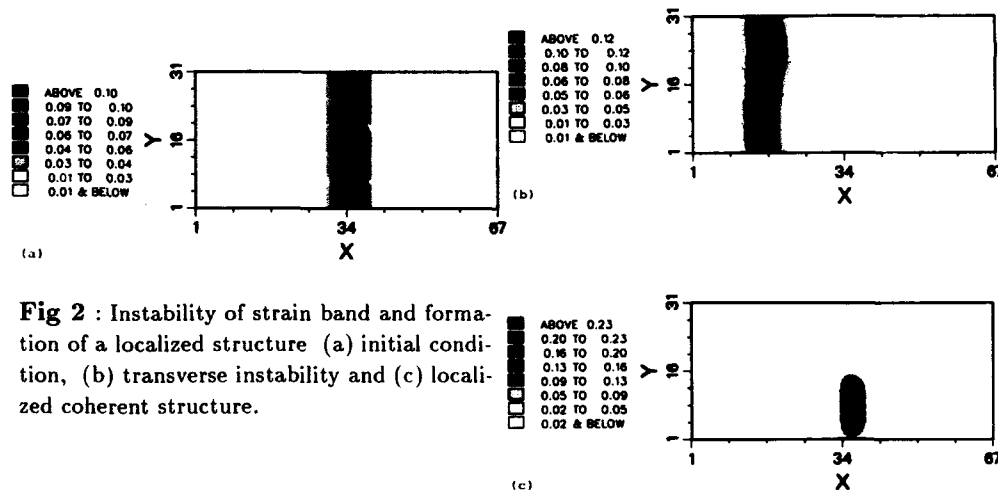


Fig 2 : Instability of strain band and formation of a localized structure (a) initial condition, (b) transverse instability and (c) localized coherent structure.

b. Asymptotic model

In order to understand the evolution of the localized structure over large scale of time, we derive an asymptotic model from the quasicontinuum model (6). By means of a multiscale technique an equation for the strain ψ (the zero-order of the expansion) is obtained at the lower order in a small parameter ϵ (which is associated with the weak nonlinearity) and it can be written as [8]

$$\left(\psi_T + (\psi^2 - \psi^3)_\xi + \delta_1 \psi_{\xi\xi\xi} \right)_\xi = \beta \psi_{YY} . \quad (8)$$

where we have introduced the new variables

$$\xi = \epsilon^{1/2}(x - vt) , \quad Y = \epsilon y , \quad T = -\epsilon^{3/2}t/v . \quad (9)$$

and we have set $v = \sqrt{\alpha}$ the sound velocity in the x direction. Accordingly, the long-time evolution of the nonlinear structure (see Fig. 2.c) is governed by Eq. (8) which is of the Kadomtsev-Petviashvili type (KP equation). We notice that, in the standard KP equation, the third-order nonlinear term does not exist [9]. It can be proved that localized solutions to Eq. (8) are stable [9].

STABILITY OF MODULATED STRUCTURES

a. Linear analysis

Going back to the discrete system, we consider the linearized equations (4) about a uniform deformation S_0 corresponding to a stable minimum of the lattice potential (3). By looking for harmonic solutions to the discrete linearized equations of motion of the microscopic model, we obtain the dispersion relation of waves traveling in the i direction

$$\omega^2 = 4 [\hat{\alpha}(S_0) \sin^2(p/2) + 4\delta \sin^4(p/2) + \eta \sin^4(p)] , \quad (10)$$

where $\hat{\alpha}(S_0) = (\partial^2 \Phi / \partial S^2)_{S=S_0}$, p is the wavenumber and ω is the circular frequency. The details of the dispersion curves ω^2 as a function of p are drawn in Fig. 3. The curves exhibit a softening at a nonzero wavenumber. For a particular value of α curve (c) corresponds to the critical situation for which we must have $\omega^2(p_0, \alpha_0) = 0$ and $(d\omega^2/dp)_{(p_0, \alpha_0)} = 0$. Then, the stability condition is $\omega^2 > 0$ for all p (see curve (b)). The critical situation occurs when ω^2 vanishes for $\alpha = \alpha_0$ at $p = p_0$ while ω^2 remains positive for all other p 's. Then α_0 denotes the critical value of the control parameter or the elastic modulus for which a periodic state of strain with wave number p_0 takes place on the lattice.

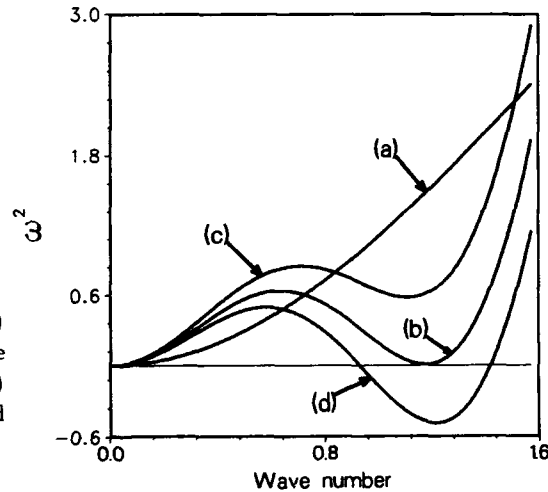


Fig. 3 : Phonon dispersion curves : (a) classical atomic chain, (b) stable case ($\alpha > \alpha_0$), (c) critical situation ($\alpha = \alpha_0$) (d) small zone of instability around the critical wavenumber p_0 ($\alpha < \alpha_0$).

b. Nonlinear analysis

In the vicinity of the critical point, the linear approximation breaks down after a time of the order $1/\omega$ and the nonlinear terms would no longer be ignored. With the view of examining the influence of nonlinearities on the structure stability we must consider a semi-discrete approach and multiscale technique in order to derive an amplitude equation [10]. We first introduce a small parameter as follows

$$\alpha = \alpha_0 + \lambda \epsilon^2 , \quad (11)$$

which can be connected with the characteristic time and length scales around the critical point. Now, we look for solutions to the complete nonlinear equations of motion (4) as an asymptotic series of $S(n, m)$ in ϵ and in harmonics of the phase variable

$$S(n, m) = \epsilon A(n, m)e^{in p_0} + \epsilon^2 (B_1(n, m)e^{in p_0} + B_2(n, m)e^{2in p_0}) + c.c. \quad (12)$$

The method consists in separating the fast changes of the periodic structure involving the discrete phase $n p_0$ while the amplitude parts (A , B_1 and B_2) are treated in the continuum limit, knowing that the solution (12) is valid in the vicinity of the critical point. Without getting into the algebraic manipulations, we finally arrive at

$$A_{\tau\tau} - (\omega^2)_{pp} A_{XX} - \beta A_{YY} + \bar{\lambda} A - \mu |A|^2 A = 0, \quad (13)$$

where we have set

$$\bar{\lambda} = 4\lambda \sin^2(p_0/2), \quad (14.a)$$

$$\mu = 4\sin^2(p_0/2) (-3 + 8\sin^2(p_0)/\omega^2(2p_0)), \quad (14.b)$$

and $(\omega^2)_{pp}$ holds for the second derivative of ω^2 with respect to p taken at $p = p_0$. Moreover, we have introduced a slow time variable $\tau = \epsilon t$ and stretching space variables $X = \epsilon x$ and $Y = \epsilon y$. We remark that Eq. (13) obtained at the third order in ϵ is of *Ginzburg-Landau type*. We can relate the amplitudes B_1 and B_2 to A . In fact, Eq.(13) describes how the amplitude of the strain of the first order deviates locally from the basic periodic homogeneous strain structure. The study of homogeneous solutions to Eq. (13) provides the growth rate of the transverse perturbations, hence a stability criterion.

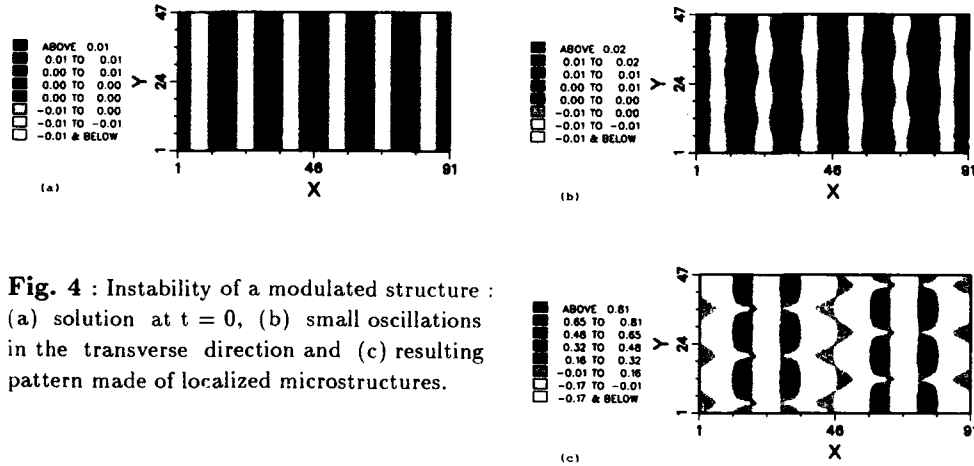


Fig. 4 : Instability of a modulated structure : (a) solution at $t = 0$, (b) small oscillations in the transverse direction and (c) resulting pattern made of localized microstructures.

c. Numerical simulations

Using the microscopic equations as a numerical scheme we illustrate the evolution of the nonlinear structure beyond the instability. The results are presented in Fig. 4. The initial structures which consists in spatially sinusoidal strain in the x direction and homogeneous in the y direction is given in Fig. 4.a. The wavelength of the periodic structure corresponds to that of the critical wavenumber p_0 . The elastic constant α

is slightly shifted just below the critical value α_0 . After a short lapse of time, small oscillations are taking place along the transverse direction as shown in Fig. 4.b. Latter on, we observe that the instability has produced an array of localized structures in both directions of the lattice (Fig. 4.c).

CONCLUSIONS

Our main objective was merely to briefly describe the *physical mechanisms* of nonlinear structure formation occurring in ferroelastic-martensitic transformations. On the basis of a two-dimensional lattice model two interesting problems related to twinning dynamics have been examined. We have pointed out the importance of the microscopic point of view, because of the softening of the acoustic phonon branch which triggers lattice instabilities and gives rise thus to complex patterns. The latter can be considered as the partial growth of martensitic domains in the high-temperature phase. These domain structures are usually observed by means of high-resolution electron microscopy which reveals very fine microtextures in various alloys [11].

Nevertheless, further extensions of the model can be studied both in the framework of the discrete system and continuum limit. In addition, the dynamics of the elastic structures is certainly influenced by applied stresses and damping leading to hysteresis effects.

REFERENCES

- [1] A.R. BISHOP. In *Nonlinear Structures in Physical Systems. Pattern Formation, Chaos and Waves*, Eds L. Lui & M.C. Hedlay, Springer-Verlag, Berlin (1990).
- [2] K. PARLINSKI. *Phys. Rev. B* **35**, 8680 (1987).
- [3] A.L. ROITBURD. In *Solid State Physics* **33**, Eds H. Ehenreich, F Seitz & D. turnbull, Academic Press, New York (1978).
- [4] G.R. BARSCH and J.A. KRUMHANSL. *Metall. Trans.* **19A**, 761 (1987).
- [5] J. POUGET. *Phys. Rev. B* **43**, 3575 & 3582 (1991).
- [6] J. POUGET. *Phase Transitions* **34**, 105 (1991).
- [7] S.M. SHAPIRO. In *Competing Interactions and Microstructures : Static and Dynamics*. Eds R. Lesar, A.R. Bishop & R. Heffner, Springer-Verlag, Berlin. (1988).
- [8] J. POUGET. *Phys. Rev. B* **46**, 10554 (1992).
- [9] R. BLAHA, E.W. LAEDKE and K.H. SPATSCHEK. *Physica D* **40**, 249 (1989).
- [10] M. REMOISSENET. *Phys. Rev. B* **33**, 2386 (1986).
- [11] D. BRODDIN *et al.* *Phil. Mag.* **A59**, 47 (1989).

DISCRETE MODULATED WAVES

M. Rose

Laboratory for Applied Mathematical Physics
The Technical University of Denmark
DK-2800, Lyngby, Denmark

Abstract

The continuous nonlinear Schrödinger equation has both nonintegrable and integrable discretizations. In this paper we consider the question of whether these discretizations are equivalent as models for modulated waves on nonlinear lattices. The evolution equations for the envelope of discrete modulated waves on the sine-Gordon lattice are derived by the method of multiple scales. Both the standard discrete nonlinear Schrödinger equation and its integrable variant are obtained. The integrable variant is not generic.

1 Introduction

The nonlinear Schrödinger (NLS) equation is the generic evolution equation for the envelope of modulated waves in continuous systems with periodic boundary conditions [1],

$$iu_t + u_{xx} + 2|u|^2u = 0. \quad (1.1)$$

Two discretized versions of the NLS equation have been used to study its properties numerically. Applying the central difference approximation to the spatial derivative one obtains the diagonal discrete nonlinear Schrödinger (DDNLS) system,

$$i\dot{u}_n + \frac{u_{n+1} - 2u_n + u_{n-1}}{h^2} + 2|u_n|^2u_n = 0. \quad (1.2)$$

A different approach was taken by Ablowitz and Ladik [2]. They developed a method to explicitly construct completely integrable differential-difference equations and in this context derived the integrable discrete nonlinear Schrödinger (IDNLS) system,

$$i\dot{u}_n + \frac{u_{n+1} - u_{n-1}}{2} + 2|u_n|^2(u_{n+1} + u_{n-1}) = 0. \quad (1.3)$$

For certain parameter values DDNLS exhibits chaotic behavior while IDNLS, being integrable, can never have chaotic behavior [3]. Some progress has been made in the analysis of these different behaviors by considering DDNLS as a perturbation of IDNLS [4,5]. The issue of interest in these studies is the use of discrete equations as approximations to the continuous NLS equation. Equation (1.1) may also be derived as the continuum limit of modulated waves on a nonlinear lattice [6,7]. In these cases the question arises as to which of the discretizations may be more appropriate for numerical simulations of modulated waves on the particular lattice being studied.

In this paper we demonstrate these considerations with the sine-Gordon (DsG) lattice,

$$\ddot{u}_n = u_{n+1} - 2u_n + u_{n-1} - \sin u_n. \quad (1.4)$$

It arises as a model of arrays of point Josephson junction contacts or of torsional pendula [8]. We will derive the governing equation for the discrete envelope of modulated waves for the DsG lattice and show that DDNLS and IDNLS are accurate to the same order as envelope equations. This provides a derivation of IDNLS in a physical context. We will also show that IDNLS is not a generic envelope equation.

2 Derivation

It is assumed that the DsG lattice with periodic boundary conditions has small amplitude solutions which may be expanded in terms of the parameter ϵ ,

$$u_n = \epsilon u_{n,0} + \epsilon^2 u_{n,1} + \epsilon^3 u_{n,2} + O(\epsilon^4). \quad (2.1)$$

The amplitude is assumed to vary with the slow time scales $T_1 = \epsilon t$ and $T_2 = \epsilon^2 t$, so the first order solution is of the form

$$u_{n,0} = a_n(T_1, T_2) e^{i(n\theta - \omega t)} + a_n^*(T_1, T_2) e^{-i(n\theta - \omega t)}, \quad (2.2)$$

where θ = the wave number of the carrier wave and ω = the carrier wave frequency. It is also assumed that the nearest neighbor amplitude variation is $O(\epsilon)$. Using the calculus of forward differences this assumption is expressed as

$$Da_n = a_{n+1} - a_n = O(\epsilon). \quad (2.3)$$

In this formalism the second difference is

$$D^2 a_n = Da_{n+1} - Da_n = a_{n+2} - 2a_{n+1} + a_n = O(\epsilon^2). \quad (2.4)$$

The expansion (2.1) is substituted into (1.4) and the terms are grouped by powers of ϵ . At first order the relation

$$-\omega^2 a_n = a_{n+1} e^{i\theta} - 3a_n + a_{n-1} e^{-i\theta} \quad (2.5)$$

is obtained. The difference (2.3) is used to write a_{n+1} and a_{n-1} in terms of a_n and one obtains the dispersion relation,

$$\omega^2 = 3 - 2 \cos \theta, \quad (2.6)$$

and carries the differences $Da_n e^{i\theta} - Da_{n-1} e^{-i\theta}$ to next order. It is worth noting that (2.5) can also be written as

$$\begin{aligned} a_n &= \frac{1}{3 - \omega^2} (a_{n+1} e^{i\theta} + a_{n-1} e^{-i\theta}) \\ &= \frac{1}{\cos \theta} (a_{n+1} e^{i\theta} + a_{n-1} e^{-i\theta}) \end{aligned} \quad (2.7)$$

At order ϵ^2 a discrete version of the conservation of wave-number is obtained,

$$a_{nT_1} + \frac{\sin \theta}{\omega} D a_{n-1} = 0. \quad (2.8)$$

Here we have used the second difference (2.4) and carried the $D^2 a_{n-1} e^{-i\theta}$ term to order ϵ^3 . The ϵ^3 equation is

$$-2i\omega a_{nT_2} + a_{nT_1T_1} = \frac{1}{2} |a_n|^2 a_n + D^2 a_{n-1} e^{-i\theta} \quad (2.9)$$

From (2.8) we obtain

$$a_{nT_1T_1} = \frac{\sin^2 \theta}{\omega^2} D^2 a_{n-1}, \quad (2.10)$$

and so (2.9) can be written

$$ia_{nT_2} + \left(\frac{e^{-i\theta}}{2\omega} + \frac{\sin^2 \theta}{2\omega^2} \right) D^2 a_{n-1} + \frac{1}{4\omega} |a_n|^2 a_n = 0. \quad (2.11)$$

The relation (2.7) can be used in the nonlinear term to write

$$ia_{nT_2} + \left(\frac{e^{-i\theta}}{2\omega} + \frac{\sin^2 \theta}{2\omega^2} \right) D^2 a_{n-1} + \frac{1}{4\omega \cos \theta} |a_n|^2 (a_{n+1} e^{i\theta} + a_{n-1} e^{-i\theta}) = 0. \quad (2.12)$$

These relations are valid for arbitrary values of the wavenumber θ .

When the carrier wave is long the coefficients of (2.11) and (2.12) may be expanded about $\theta = 0$. The following systems are obtained

$$2ia_{nT_2} + a_{n+1} - 2a_n + a_{n-1} + |a_n|^2 a_n = 0. \quad (2.13)$$

and

$$2ia_{nT_2} + a_{n+1} - 2a_n + a_{n-1} + |a_n|^2 (a_{n+1} + a_{n-1}) = 0. \quad (2.14)$$

These are the DDNLS and IDNLS systems, respectively, for the sine-Gordon lattice.

3 Discussion

These methods may also be applied to other systems, such as waves on large biomolecules, where modulated waves are possible but taking the continuum limit is undesirable. It is, however, important to note that the IDNLS system (2.14) was obtained because of the specific form of equation (2.7). In general the relation between a_n , a_{n+1} and a_{n-1} will depend on the underlying lattice. For example, when the same expansion is applied to the KdV lattice,

$$\dot{u}_n = e^{u_{n+1}} - e^{u_{n-1}}, \quad (3.1)$$

one obtains the first order relation

$$-i\omega = a_{n+1} e^{i\theta} - a_{n-1} e^{-i\theta}. \quad (3.2)$$

This will not yield an IDNLS system and so it would be inappropriate to use (1.3) as a discretization for studying modulated waves on (3.1).

Much work remains to be done in understanding the behavior of the discrete forms of the NLS equation. In the case where both DDNLS and IDNLS can be derived at

the same order, one should check that they exhibit similar behavior over the range of parameter values for which the derivation is valid. In addition, as (2.13) and (2.14) have been derived directly, the higher order terms of each are available. This provides for the ability to perform a more physical perturbation analysis of these systems.

Acknowledgements

The author would like to thank Peter Miller and Alwyn Scott for many stimulating discussions.

This work was funded by the Danish Council for Scientific and Industrial Research, Grant no. 16-4786.m

References

- [1] A. C. Newell, *Solitons in Mathematics and Physics*, Society for Industrial and Applied Mathematics, Philadelphia, PA, 1985.
- [2] M. J. Ablowitz & J. F. Ladik, "A nonlinear difference scheme and inverse scattering," *Stud. Appl. Math.* 55 (1976), 213-229.
- [3] M. J. Ablowitz & B. M. Herbst, "On the homoclinic structure and numerically induced chaos for the nonlinear Schrödinger equation," *SIAM J. Appl. Math.* 50 (1990), 339-351.
- [4] M. J. Ablowitz & P. A. Clarkson, *Solitons, Nonlinear Evolution Equations and Inverse Scattering*, London Mathematical Society Lecture Note Series #149, Cambridge Univ. Press, New York, NY, 1991.
- [5] D. W. McLaughlin & C. M. Schober, "Chaotic and homoclinic behavior for numerical discretizations of the nonlinear Schrödinger equation," *Phys. D* to be published.
- [6] J. Pouget & M. Remoissenet, "Modulational instability and two-dimensional dynamical structures," in *Nonlinear Coherent Structures in Physics and Biology*, M. Remoissenet & M. Peyrard, eds., Lect. Notes in Phys. #393, Springer-Verlag, New York-Heidelberg-Berlin, 1991, 227-233.
- [7] K. Yoshimura & S. Watanabe, "Envelope solitons as an intrinsic localized mode in a one-dimensional nonlinear lattice," *J. Phys. Soc. Japan* 60 (1991), 82-87.
- [8] A. C. Scott, F. Y. F. Chu & D. W. McLaughlin, "The soliton: A new concept in applied science," *Proc. of the IEEE* 61 (1973), 1443-1483.

TODA SOLITONS AND THE MÖSSBAUER EFFECT

M.V. Sataric,¹ R.B. Žakula,² S. Zeković,² and J.A. Tuszynski³

¹Faculty of Technical Science, Novi Sad, Yugoslavia

²Institute of Nuclear Sciences "Boris Kidrič, Belgrade, Yugoslavia

³Department of Physics, University of Alberta
Edmonton, Alberta, T6G 2J1, Canada

ABSTRACT

In this paper we investigate anharmonic lattices that support the formation and propagation of Toda solitons along their chains. The main objective is to examine the influence of Toda solitons (TS) on the Mössbauer emission of gamma photons. Furthermore we conclude that it can be expected that the emission of hard gamma rays may be instrumental in producing narrow Toda solitons even at low temperatures. A manifestation of this phenomenon could be through an anomalous increase of the coefficient of thermal conductivity.

1. INTRODUCTION

The objective of this paper is to examine the applicability of Toda model lattices exhibiting the Mössbauer effect (ME) and study the consequences. Our model will employ an anharmonic monoatomic chain with Toda interactions between sites whose nuclei are capable of emitting gamma photons (GP). When a nucleus centered at a lattice site is caused to emit a GP, the transition energy $\Delta E_{n,m}$, in principle, may be distributed among: a) the GP, b) the nucleus that emits the GP, c) the chain as a whole and, finally, d) a part of the energy can be absorbed by the vibrational degrees of freedom of the chain. In the case under consideration these vibrational degrees of freedom may both involve pure phonon modes (PMs) and localized TSs.

A Mössbauer transition occurs when a TS state remains unchanged before and after the emission, so that the GP involved absorbs the entire energy of transition. In other words, the emission is an elastic process.

2. THE TODA LATTICE AND THE MÖSSBAUER TRANSITION PROBABILITY

We begin by briefly considering a Toda lattice (TL) of molecules located along the x-axis with equilibrium distances R_0 between neighboring sites. The equation of motion

for such a one-dimensional monoatomic TL with the nearest-neighbor interaction potential U expressed by¹

$$U = \frac{k}{b} \left\{ u_n - u_{n-1} + \frac{1}{b} [\exp(b(u_{n-1} - u_n)) - 1] \right\} \quad (1)$$

is given by

$$M \frac{d^2 u_n}{dt^2} = \frac{k}{b} [\exp(bu_n) - \exp(bu_{n+1})] \quad (2)$$

where M denotes the mass and u_n the displacement of n -th particle. The parameter k represents the coefficient of longitudinal elasticity of the corresponding harmonic chain while b denotes the magnitude of anharmonicity. Introducing the relative displacement as $\rho_n = u_{n-1} - u_n$ a one-soliton solution of the TL problem is then given by

$$\beta_n(t) = \frac{1}{b} \ln \left\{ 1 + \frac{\sinh^2(\mu)}{\cosh^2\left[\frac{\mu}{R_0}(nR_0 - vt)\right]} \right\} \quad (3)$$

which describes a compressional pulse propagating along the TL with the velocity v below

$$v = \frac{v_0}{\mu} \sinh(\mu) \quad (4)$$

and $v_0 = R_0 \left(\frac{k}{M}\right)^{1/2}$ represents the longitudinal sound velocity for $b = 0$. Here μ denotes the parameters of TS which defines the domain of localization (length) of a TS through $\Delta n = 2\pi\mu^{-1}$. It is evident from eq. (4) that the TS propagation velocity v always exceeds the sound velocity ($v > v_0$). Moreover, TS's with larger amplitudes (and thus larger parameters μ) propagate faster.

Provided the requirements for the applicability of the continuum approximation are fulfilled, i.e. that $\Delta n \gg 1$ or $\mu \ll 2\pi$, eq. (3) may be simplified as

$$\rho(x,t) = b^{-1} \frac{\sinh^2(\mu)}{\cosh^2\left(\frac{\mu}{R_0} \xi\right)}, \quad \xi = x - x_0 - vt \quad (5)$$

Here x_0 represents the position of the TS's center and $\rho(x,t)$ replaced the discrete variable ρ_n and, in the continuum limit we have

$$\rho(\xi) = -R_0 \frac{\partial}{\partial x} u(\xi) \quad \text{or} \quad u(\xi) = \left(\frac{2}{3b\mu^2}\right) \frac{[1 - \tanh(\frac{\mu}{R_0} \xi)] \sinh^2(\mu)}{1 + 2\cosh^2(\frac{\mu}{R_0} \xi)} \quad (6)$$

The proper normalization of the mass density distribution of eq. (5) finally gives

$$|p\rangle = \frac{1}{2} (3\mu)^{1/2} \text{sech}^2 \left[\frac{\mu}{R_0} (x - vt) \right]; \quad x_0 = 0 \quad (7)$$

The energy of a single GP typically ranges from about 10 keV to approximately 5 MeV which corresponds to wavelengths from about 1 Å to about 10^{-3} Å, respectively. It

is well-known that for GP energy of $\hbar\omega = 100$ keV and an emitting nucleus with $M = 10^{-25}$ kg the recoil energy of nucleus is $E_R = 0,05$ eV and the width of a Doppler line at room temperature is $\Delta E_D = 0,2$ eV. The above results pertain to harmonic crystals. Since a TL is a model of highly anharmonic crystal it is clear that the local displacements of molecules involved in the formation of a TS can cause an additional Doppler effect. In order to estimate its magnitude we calculate the velocity $v_{osc} = du/dt$ using eq. (6). In order to come up with numerical estimate v_{osc} for emitting nuclei, we can use data for propagation of TS in DNA molecules² as follows

$$R_0 = 3 \cdot 10^{-10} \text{ m}; k = 5,13 \cdot 10^{-10} \text{ N}; b = 6,18 \cdot 10^{10} \text{ m}^{-1}; v_0 = 1,69 \cdot 10^3 \text{ ms}^{-1}.$$

Below, we consider two limiting pictures of a TS: (a) a broadly spread soliton, over many lattice sites and (b) a narrowly localized soliton involving only a few lattice sites. In the first case, we take $\Delta n = 50$ and obtain $\mu \sim 0,1$ so that $\sinh(\mu) \sim \mu$. Consequently we assess $v = v_0$ and $\bar{v}_{osc} = 1 \text{ ms}^{-1}$. In the opposite case, however, when we take $\Delta n = 5$ and $\mu = 2$ it follows that $v = 1,8 v_0$ and $\bar{v}_{osc} = 250 \text{ m/s}$. It is therefore apparent that a broadly spread TS will provide a negligible contribution to the Doppler effect. On the other hand, a highly localized soliton pulse can cause a Doppler effect which is comparable to that due to thermal motion at room temperature.

Consequently, when a nucleus located at a crystal lattice site emits or absorbs a quantum of GP, the following processes may occur:

- (1) A change in the vibrational state of lattice, i.e. a phonon excitation, provided the recoil energy exceeds the Debye energy: $E_R \geq k_B T_D$, where T_D is the Debye temperature.
- (2) We predict that by virtue of a significant local displacement of the emitting nucleus, a Toda soliton may be generated, provided the recoil energy is sufficiently large and exceeds the energy of a strongly localized TS. Namely with $\hbar\omega > 100$ keV the recoil energy can be of the order of 1 eV. This is comparable to the energy of a single TS which is given by $E_s = 2 k b^{-1} [\sinh(\mu) \cosh(\mu) - 1]$. For strongly localized solitons spread over 3-5 chain sites we obtain $\mu = 2$ and using above mentioned data for DNA we find that $E_s = 2$ eV. Thus, it can be envisaged that an atom emitting a gamma quantum receives the entire recoil energy E_R and then it may collide with a neighboring atom. As a result of this collision and owing to the anharmonicity of the lattice a strongly localized TS may be created. To produce a broadly spread soliton ($\mu \ll 1$) several atoms would have to be set in motion nearly simultaneously which is rather improbable. We therefore conclude that it can be expected that the emission of hard GPs may be instrumental in producing narrow TSs even at low temperatures. A manifestation of this phenomenon could be through an anomalous increase of the coefficient of thermal conductivity.³
- (3) If a narrow TS already exists in the immediate vicinity of emitting nucleus, Doppler broadening of its spectral line takes place.
- (4) If the recoil energy is smaller than the values required in both (1) and (2) then elastic resonant emission or absorption of a GP takes place. This gives rise to the ME in its standard form.

We calculated the emission probability of a GP in the standard form.⁴ The wave function of lattice is represented as a tensor product of the envelope of a TS (see eq. (7)) and the quantum (PMs) of the lattice $|v_q\rangle = (b_q)^{v_q} (v_q!)^{-1/2} |0\rangle$, where $v_q = 1, 2, \dots$ and b_q, b_q^+ represents the annihilation and creation operators, respectively, for longitudinal phonons with a wave vector q . As usual, $|0\rangle$ denotes the phonon vacuum. After cumbersome calculation the probability of ME is given by

$$\bar{W}_{if} = \frac{1}{2} \left(\frac{\pi}{D} \right)^{1/2} \Phi(D^{1/2}) \left\{ 1 + 0.084 \frac{\sigma^2}{D} - 0.168 \sigma^2 \frac{\partial}{\partial D} \ln [\Phi(D^{1/2})] \right\} \quad (8)$$

where we introduced the following set of denotations

$$\begin{aligned} \Phi(\lambda) &= \frac{2}{\sqrt{\pi}} \int_0^\lambda \exp(-t^2) dt \\ D &= \frac{3}{2} \frac{E_R}{k_B T_D} \\ \sigma &= \frac{2}{3} \left[\frac{\sinh(\mu)}{\mu} \right]^2 \left(\frac{\hbar p}{b} \right) \end{aligned} \quad (9)$$

and p is the momentum of emitted GP.

It is obvious that the impact of TSs on the value of the ME probability, \bar{W}_{if} is quite sensitive to the propagation velocity v through the relation $\sigma^2 \sim v^4$. Estimating \bar{W}_{if} in the special case of $D = 1/4$ and $\sigma = 1/2$ results in $\bar{W}_{if} = 0.85$ which means that at low temperatures the ME is characterized by a high probability under the specified conditions.

REFERENCES

1. M. Toda, *J. Phys. Soc. Jpn.* 22:431; 23:501 (1967).
2. V. Muto, A.C. Scott and P.L. Christiansen, *Physica* D44:75 (1990).
3. G. Casati, J. Ford, F. Vivaldi and W.M. Visscher, *Phys. Rev. Lett.* 53:1120 (1984).
4. Z. Ivić, M. Satačić, Z. Shemesedini and R. Žakula, *Phys. Scr.* 37:564 (1988).

**BIPOLARONIC CHARGE DENSITY WAVES,
POLARONIC SPIN DENSITY WAVES
AND HIGH T_c SUPERCONDUCTIVITY**

Serge Aubry*

CNLS, Los Alamos National Laboratory
Los Alamos, NM 87545, USA

Abstract: At large enough electron phonon coupling, the existence of bipolaronic, polaronic and mixed states is rigorously proven for the adiabatic Holstein model at any dimension and any band filling¹. The ground-state is one of them which then prove the existence of insulating Bipolaronic Charge Density Waves (BCDW). The role of the quantum lattice fluctuations is analysed and found to be negligible in that regime but to become essential in case of phonon softening then favouring the occurrence of superconductivity^{2,3}. When a strong Hubbard term is also present, the bipolarons break into polarons and the ground state is expected to be a Polaronic Spin Density Wave (PSDW). If the repulsive Hubbard term is comparable to the electron-phonon coupling, the energy for breaking a bipolaron into two polarons can become small and we get instead of these two degenerate structures, a pair of polarons bounded by a spin resonance which we call "spin resonant bipolaron". This resonant bipolaron is still strongly bound, but the role of the quantum lattice fluctuations becomes now very important and yields a sharp broadening of the band width of this resonant bipolaron. Thus, the strong quantum character of these resonant bipolarons could prevent their localization into real space structures which could be insulating BCDWs or PSDWs, then favouring the formation of a superconducting coherent state with a possible high T_c . (For details see ref.4)

REFERENCES

- [1] S.Aubry, G.Abramovici and J.L. Raimbault *J. Stat.Phys.* **67** 675-780 (1992)
- [2] S.Aubry, G. Abramovici, D.Feinberg, P. Quemerais and J.L. Raimbault in *Non-Linear Coherent Structures in Physics, Mechanics and Biological Systems (Lect. Notes in Physics, Springer vol 353 p.103-116 (1989)*
- [3] S.Aubry in *Microscopic Aspects of Non-Linearity in Condensed Matter Physics* ed. A.R.Bishop, V.L.Pokrovsky and V.Tognetti NATO ASI Series, Series B vol **264** Plenum p.105-114 (1991)
- [4] S.Aubry *Bipolaronic Charge Density Waves, Polaronic Spin Density Waves and High T_c Superconductivity* submitted to Proceeding on "Phase separation in Cuprate Superconductors" May 6-12, 1992 Erice, Sicily, Italy World Scientific Pub. ed.K.A. Müller and G.Benedek (1992)

* On leave of *Laboratoire Leon Brillouin, (Laboratoire commun CEA-CNRS) CE Saclay 91191-Gif-sur-Yvette (France)*

INDUCTIVELY COUPLED LONG JOSEPHSON JUNCTIONS: COLLECTIVE COORDINATE ANALYSIS AND I-V CHARACTERISTICS

Tassos Bountis and Takis Skiniotis

Department of Mathematics
University of Patras
Patras 26110, Greece

Dedicated to Al Scott, on the occasion of his 60th birthday

INTRODUCTION

The collective coordinate analysis of soliton dynamics developed by McLaughlin and Scott for perturbed sine-Gordon equations is applied here to **two inductively coupled** Long Josephson Junctions (LJJ's). It is found that the motion of fluxon (antifluxon) pairs -one fluxon on each junction- is described very well by the ode's of the collective coordinates, representing the "center of mass" position and velocity of each fluxon. The formation of **bifluxon states**, which either oscillate or travel in phase-locked fluxon pairs along the LJJ's is accurately predicted and verified by the numerical solution of the pde's.

We also carry out a stability analysis of the McCumber branches of our two LJJ's and successfully determine the I, V values at which the first three zero-field steps (ZFS) occur. Increasing then the coupling parameter ϵ , we discover that these ZFS appear at lower and lower voltage values. The I-V characteristics we obtain exhibit certain strong entrainment properties which may be of experimental interest, especially if they persist in the case of many coupled LJJ's.

The plan of the paper is as follows: In the first section, we present the collective coordinate analysis of the bifluxon states predicted by the ode's and verified by the solution of the pde's of the two LJJ's. We then describe our stability analysis of the McCumber solutions and show that it accurately predicts the formation of the first few ZFS, corresponding to the appearance of 1, 2, 3, etc fluxons on the LJJ's. Finally, we present the I-V characteristics of the system and discuss their physically interesting entrainment properties.

COLLECTIVE COORDINATES FOR BIFLUXON STATES

It is a well-known fact that the literature on the theory and applications of Josephson junctions has been growing steadily in the last 15 years¹⁻¹¹. One of the more common approaches in many analytical and simulation studies of these junctions (in the so-called **overlap geometry**) is to consider the perturbed sine-Gordon equation^{1,2,5,9} in the dimensionless form

$$\varphi_{tt} - \varphi_{xx} + \sin\varphi = -\alpha\varphi_t + \beta\varphi_{xx} + \gamma \quad (1)$$

describing the phase difference $\varphi(x,t)$ of the eigenfunctions of the two superconductors separated by a thin insulating barrier of length $L \gg \lambda_J$ (λ_J being the Josephson penetration length). These are the so-called Long Josephson Junctions (LJJ's), in which the $\alpha\varphi_t$ and $\beta\varphi_{xx}$ loss terms are due to normal electrons tunneling across and normal electrons flowing along the barrier respectively.

If these losses are small enough, they can be "balanced" by the bias current term γ on the rhs of (1), in such a way that the LJJ can still support **fluxon** (soliton-like) waveforms similar to the exact kink(+) or antikink(-) soliton solutions

$$\varphi_s(x,t) = 4 \tan^{-1} \left\{ \exp \left[\pm \frac{x - ut - x_0}{(1 - u^2)^{1/2}} \right] \right\} \quad (2)$$

of the unperturbed ($\alpha=\beta=\gamma=0$) sine-Gordon equation (1). In a remarkable paper by McLaughlin and Scott¹, it was shown that, within the framework of perturbation theory, such fluxon solutions of (1) can exist, in the form

$$\varphi(x,t) = 4 \tan^{-1} \left\{ \exp \left[\pm \frac{x - X(t)}{(1 - U^2(t))^{1/2}} \right] \right\} \quad (3)$$

where the so-called **collective coordinates** $X(t)$, $U(t)$ have replaced the constant x_0 , u parameters of the solution (2) of the unperturbed problem.

In a series of earlier papers¹²⁻¹⁴, we have demonstrated that the collective coordinate approach can be used to accurately describe the motion of fluxons in single LJJ's in the presence of inhomogeneities (impurities) modeled by the term¹

$$- \sin\varphi \sum_{i=1}^N \mu_i \delta(x - a_i)$$

on the rhs of (1). In both the case of "microshort" ($\mu_i > 0$) and "microresistor" ($\mu_i < 0$) inhomogeneities, we showed that the ode's derived for the variables $X(t)$ and $U(t)$, reproduced very well a number of fluxon "trapping" phenomena observed near such inhomogeneities.

In this paper, we wish to turn our attention to the study of fluxon dynamics in two

"inductively" coupled LJJ's⁸⁻¹⁰ described by the system of pde's

$$\varphi_{tt} - \varphi_{xx} + \sin \varphi = -\alpha_1 \varphi_t + \gamma_1 + \beta_1 \varphi_{xtt} + \epsilon \psi_{xx} \quad (4a)$$

$$\psi_{tt} - \psi_{xx} + \sin \psi = -\alpha_2 \psi_t + \gamma_2 + \beta_2 \psi_{xtt} + \epsilon \varphi_{xx} \quad (4b)$$

where the α_i , β_i , γ_i are as described above and $\epsilon \geq 0$ is a small coupling parameter. In a recent work¹⁴, we have considered fluxon solutions of (4a,b) of the form

$$4 \tan^{-1} \left\{ \exp \left[\sigma_i \frac{x - X_i}{(1 - U_i^2)^{1/2}} \right] \right\} = \begin{cases} \varphi(x, t) & , i=1 \\ \psi(x, t) & , i=2 \end{cases} \quad (5)$$

$\sigma_i = \pm 1$, where $X_i(t)$, $U_i(t)$, $i=1,2$, are the collective variables for the two fluxons.

Inserting (5) in (4) and using the McLaughlin-Scott approach leads to the system of ode's¹⁴

$$\left(\frac{dV_i}{dt} \equiv \dot{V}_i \right) = -\alpha_i V_i + \sigma_i \gamma_i \frac{\pi}{4} \pm \frac{\epsilon \sigma_1 \sigma_2}{2} \frac{I}{(1 + V_1^2)^{1/2} (1 + V_2^2)^{1/2}} \begin{cases} + : i=1 \\ - : i=2 \end{cases} \quad (6a)$$

$$(6b)$$

with

$$\dot{X}_i = U_i, \quad V_i \equiv U_i / (1 - U_i^2)^{1/2}, \quad i=1, 2, \quad (7)$$

$$I = \int_{-\infty}^{\infty} \text{sech} \xi \tanh \xi \text{sech}[\rho(\xi + \theta)] d\xi, \quad (8)$$

and

$$\theta \equiv \frac{X_2 - X_1}{(1 - U_2^2)^{1/2}}, \quad \rho \equiv \left[\frac{1 - U_2^2}{1 - U_1^2} \right]^{1/2} \quad (9)$$

where we have taken, for simplicity, $\beta_1 = \beta_2 = 0$, since these terms do not significantly affect the behavior of the system.

Note that equations (6), in the case $\alpha_1 = \alpha_2 = \alpha$, add up to yield a linear equation for the motion of the "center of mass" of the two fluxons

$$\dot{V} = -\alpha V + \frac{\pi}{4} (\sigma_1 \gamma_1 + \sigma_2 \gamma_2) \quad , \quad V \equiv V_1 + V_2$$

This means, of course, that the "center of mass" of the fluxons, as $t \rightarrow \infty$, will approach the limiting velocity

$$V_{\infty} = \frac{\pi}{4\alpha} (\sigma_1 \gamma_1 + \sigma_2 \gamma_2) \neq 0 \quad ,$$

or be stationary, if $\sigma_1 \gamma_1 + \sigma_2 \gamma_2 = 0$. The behavior of the **distance between** the fluxons, on the other hand, can be found by subtracting equations (6a,b) from each other.

This was first done by Kivshar and Malomed⁸ in the non-relativistic limit $|U_i| \ll 1$, $i=1,2$, in which $V_i \approx U_i$, $\rho \approx 1$ in (9), and the integral (8) can be explicitly evaluated. Upon subtraction of (6a) from (6b) one finally derives

$$\ddot{X} = -\alpha \dot{X} + \gamma - \frac{2\epsilon \sigma_1 \sigma_2}{\sinh X} \left(1 - \frac{X}{\tanh X} \right) \quad (10)$$

with $X \equiv X_2 - X_1$, $\alpha = \alpha_1 = \alpha_2$ and

$$\gamma = \frac{\pi}{4} (\sigma_2 \gamma_2 - \sigma_1 \gamma_1) \quad (11)$$

It is now easy to investigate the behavior of $X(t)$ by plotting the potential

$$W(X) = -\gamma X + \frac{AX}{\sinh X} \quad , \quad A = 2\epsilon \sigma_1 \sigma_2 \quad (12)$$

as a function of X , in the "attractive" ($A < 0$) as well as "repulsive" ($A > 0$) case^{8,14}.

For example, in the "repulsive" case, $A > 0$, the height of the "barrier" at $X \approx 0$, $W_0 \equiv A$ (for small γ) gives the energy threshold above which the two fluxons will not be able to form a bound state and will simply pass through each other. In Fig. 1a we have put $\alpha = 0$ and plotted the solution curves of (10) in the X, U plane, for a kink-antikink pair ($\sigma_1 = -\sigma_2 = 1$, $A = 1$, $\gamma_1 = \gamma_2 = 0.2/\pi$). Starting our fluxon pair with $X(0) = 10.0$ and $U(0) = 0$ we observed that the solution of the pde gave us a bound bifluxon state oscillating inside the closed homoclinic loop of Fig. 1a, as shown in Fig. 2a.

On the other hand, the same fluxon-antifluxon pair, with $X(0) = 10.1$, finds itself **just outside** the separatrix of Fig. 1a and breaks apart failing to form a bound state, as shown in Fig. 2b. Note that with the addition of dissipation (see Fig. 1b), the region of attraction of the bound state increases considerably and the fluxons eventually come to a stop at a distance $X \approx 4.1$ of from each other.

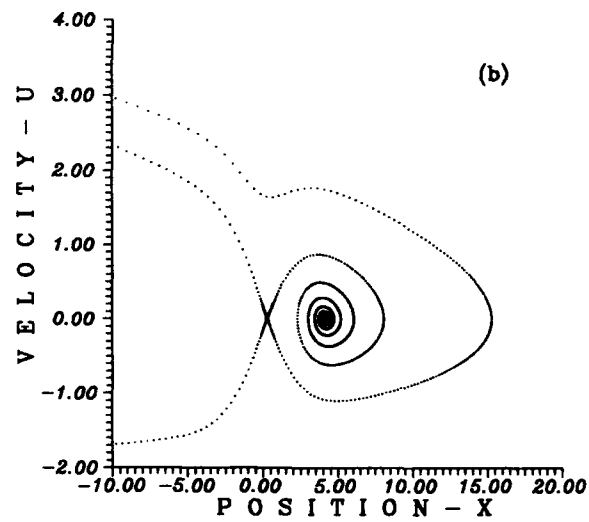
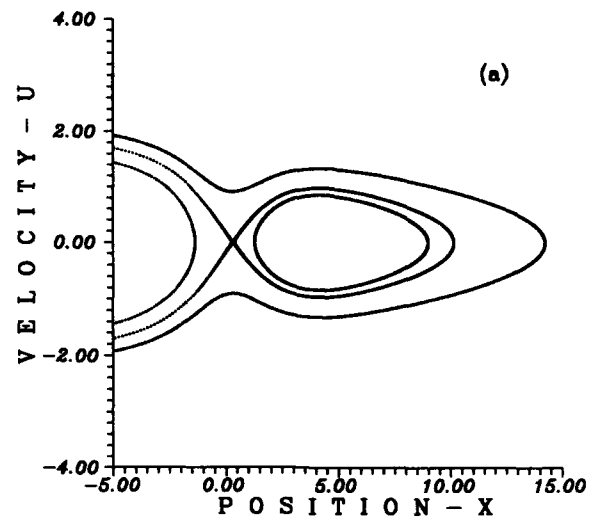


Figure 1. Phase plane (X,U) with parameters (a) $\alpha=0$, $\sigma_1=-\sigma_2=1$, $A=1$, $\gamma_1=\gamma_2=0.2/\pi$, (b) $\alpha=0.048$.

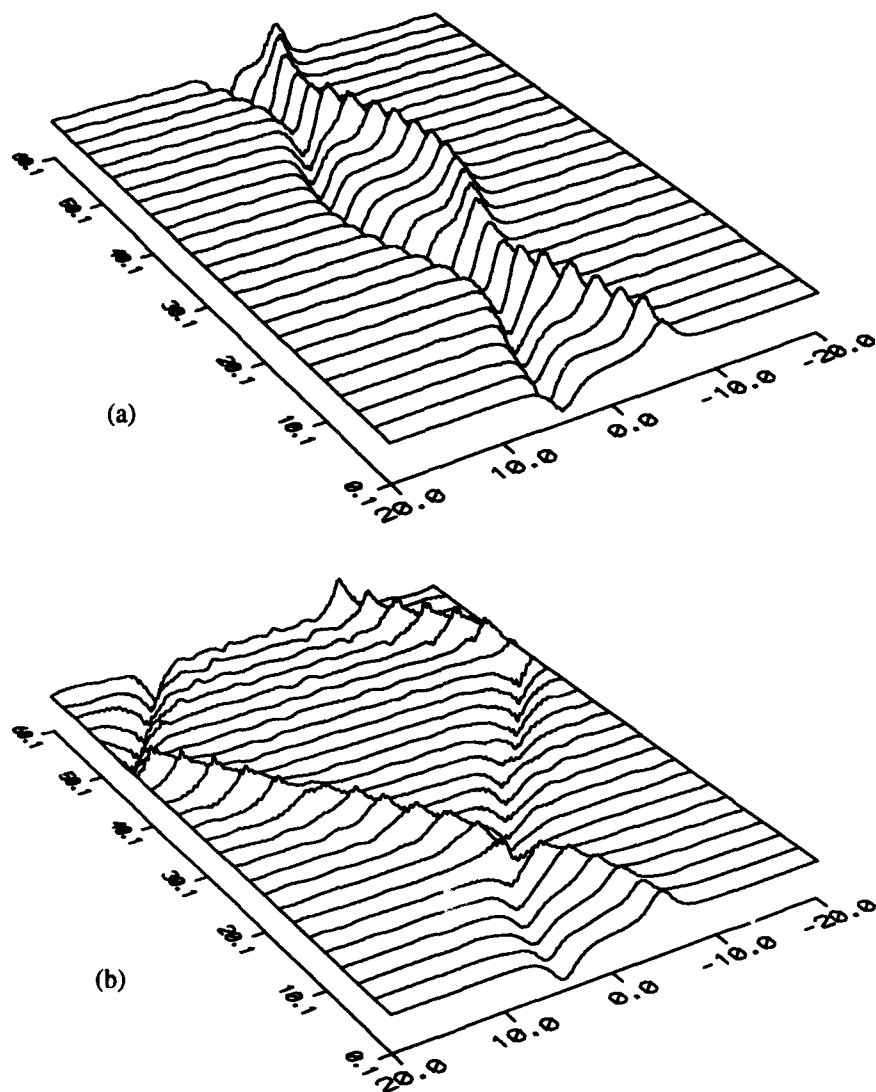


Figure 2. Evolution of ϕ_x , ψ_x in time and space from the numerical solution of pde's (4), with (a) $X(0)=10.0$ and (b) $X(0)=10.1$. (The parameters correspond to those of Fig.1a).

Had one wanted to keep them going, however, one could simply introduce an ac-current in the LJJ's, setting e.g. $\gamma_i = \gamma_{i0} + e \cos \Omega t$ in equations (4). Phase-locked oscillations are then observed for the bound bifluxon state with frequency Ω . Moreover, for very small damping, the fluxons are seen to get "trapped" for a while in the homoclinic "tangle" of the intersecting manifolds of the central unstable fixed point of Fig.1 (which becomes an unstable periodic orbit of period $2\pi/\Omega$ on a Poincare surface of section). All these phenomena will be described in more detail in a forthcoming publication¹⁵.

Finally, we remark that the "non-relativistic" approximation leading to eq. (10) turned out to work very well, in all the cases we tried. Although it is not too time-consuming to compute numerically the integral (8) at every integration step, this may be avoided, in general, since the predictions of eqns (6) turn out to differ very little from those of the non-relativistic limit¹⁵.

STABILITY ANALYSIS OF THE McCUMBER SOLUTIONS

We then went on to apply the stability analysis of Pagano⁵ and Costabile et al¹⁶ to the McCumber solutions

$$\varphi_0 = 2am(t/k, k) \quad , \quad \psi_0 = 2am(t/k, k) \quad (13)$$

of the unperturbed ($\alpha_i = \beta_i = \gamma_i = e = 0$, $i=1,2$) solutions of eqns (4). These are the well known Jacobi "amplitude" elliptic functions of modulus k ¹⁷, corresponding to energies larger than those required for the kink-like and periodic solutions of the associated "pendulum" equations: $\varphi_{0,tt} + \sin \varphi_0 = 0$ and $\psi_{0,tt} + \sin \psi_0 = 0$.

Substituting in eqns (4) the Fourier expansions

$$\begin{Bmatrix} \varphi(x, t) \\ \psi(x, t) \end{Bmatrix} = \sum_{j=0}^N \begin{Bmatrix} \varphi_j(t) \\ \psi_j(t) \end{Bmatrix} \cos \omega_j x \quad , \quad \omega_j \equiv \frac{\pi j}{L} \quad (14)$$

and using the orthogonality of the $\cos \omega_j x$ functions one obtains one equation for each spatial mode of φ

$$\ddot{\varphi}_j + \omega_j^2 \varphi_j + \frac{2}{L} \int_0^L \sin \varphi \cos \omega_j x \, dx = -(\alpha_1 + \omega_j^2 \beta_1) \dot{\varphi}_j - e \omega_j^2 \psi_j \quad (15)$$

and a corresponding one for ψ , replacing $\varphi_j \rightarrow \psi_j$ and $\alpha_1 \rightarrow \alpha_2$, $\beta_1 \rightarrow \beta_2$ in (15). Considering then small perturbations $\varphi = \varphi_0 + \Delta\varphi$, $\psi = \psi_0 + \Delta\psi$ about the McCumber branches (13) and using some simple elliptic function identities, one derives, for each mode j , two linear Lamé-type equations,

$$\ddot{\phi}_j + (\alpha_1 + \beta_1 \omega_j^2) \dot{\phi}_j + [\omega_j^2 + 1 - 2sn^2(t/k, k)] \phi_j + \epsilon \omega_j^2 \psi_j = 0 \quad (16)$$

and one with $\phi_j \rightarrow \psi_j$, $\alpha_1 \rightarrow \alpha_2$, $\beta_1 \rightarrow \beta_2$ in (16).

In the case of identical junctions, $\alpha_1 = \alpha_2 = \alpha$, $\beta_1 = \beta_2 = \beta$ eqns (16) separate in the sum and difference variables

$$s_j \equiv \phi_j + \psi_j, \quad u_j \equiv \phi_j - \psi_j$$

into two uncoupled Lamé equations

$$\ddot{s}_j + (\alpha + \beta \omega_j^2) \dot{s}_j + [\omega_j^2 (1 + \epsilon) + 1 - 2sn^2(t/k, k)] s_j = 0 \quad (17a)$$

$$\ddot{u}_j + (\alpha + \beta \omega_j^2) \dot{u}_j + [\omega_j^2 (1 - \epsilon) + 1 - 2sn^2(t/k, k)] u_j = 0 \quad (17b)$$

whose stability (instability) regions can be separately plotted for $j=1,2,3$ on a $\langle V \rangle$, L graph, where $\langle V \rangle = \langle \phi \rangle$ is the (time) averaged voltage along each junction and L is the length of the junctions, see Fig.3.

Making use of the Floquet theoretic analysis of Lamé equations^{5,16} we plot in Fig.3 by solid curves the "cusp-like" instability regions of eq.(17a) and by dashed curves those of eq.(17b). Note that the distinction between them becomes clear as ϵ increases from $\epsilon=0.1$ (Fig.3a) to $\epsilon=0.5$ (Fig.3b). Outside these regions, the solutions of (17) die out and the McCumber branches are recovered. Within the boundaries of these "cusps", however, the solutions of (17) (and hence ϕ_j and ψ_j) grow exponentially and the LJJ's can support 1,2, or 3 stable fluxons each, for $j=1,2$ and 3 respectively.

This is how the zero field steps ZFS1, ZFS2 and ZFS3 are formed, as we discuss in the next section. The way we verify the validity of the above stability analysis is as follows: Fixing α , β , ϵ and L we start increasing our bias currents $\gamma_1 = \gamma_2 = \gamma$ in (4), following the McCumber branches along the I-V characteristics of the LJJ's, see Fig.4. Then, at the point of Fig.3, where we cross the lowest instability curve (cf. eq. (17b)), of the $j=1$ "cusp" say, we introduce one fluxon on each LJJ and find that they persist, moving up and down the LJJ's in a stable form, for very long times.

Excellent agreement is found between the predictions of Fig.3 and the points of formation of the first 3 ZFS even for ϵ as high as 0.1 and 0.5. In fact, similar results were found when we deviated from the case of identical LJJ's. Varying α_1 and β_1 in such a way as to satisfy $\alpha_1 + \beta_1 \omega_j^2 = \alpha_2 + \beta_2 \omega_j^2$ - so that the equations for ϕ_j and ψ_j cf.(16), can still be uncoupled into equations of the form (17)- we also found, for different j , very good agreement between the predictions of stability analysis and the formation of the j th ZFS on the I-V characteristics, see Fig.5 for $j=1,2$.

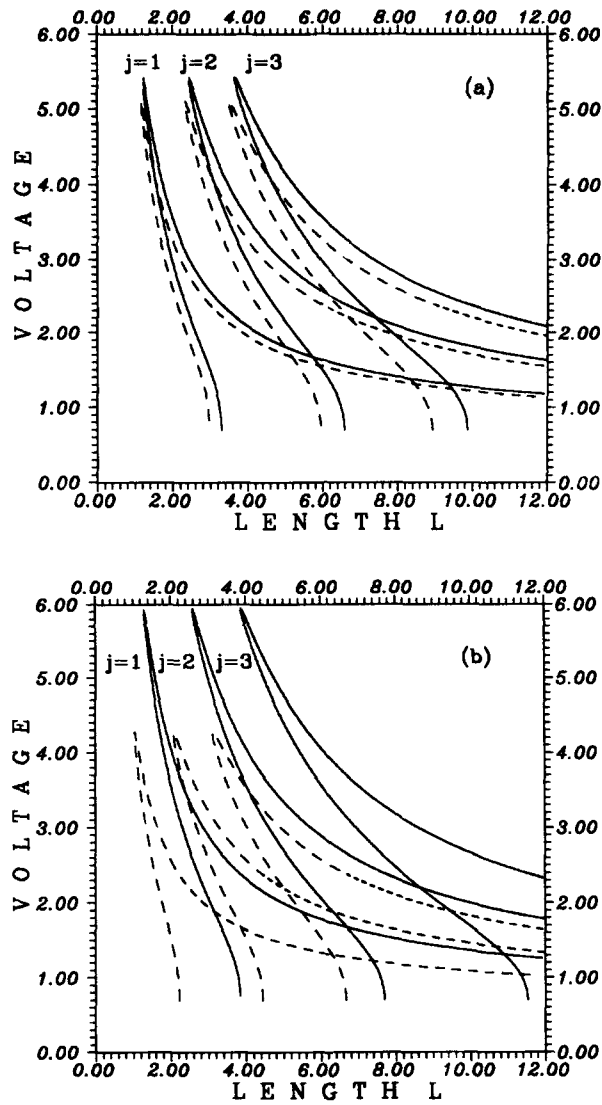


Figure 3. Instability transitions for the McCumber branch, for two inductively coupled junctions with parameters $\alpha_1=\alpha_2=0.05$, $\beta_1=\beta_2=0.02$ and (a) $\epsilon=0.1$, (b) $\epsilon=0.5$.

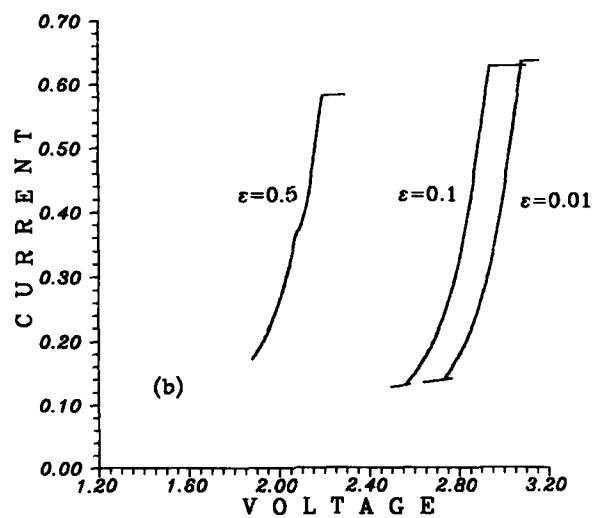
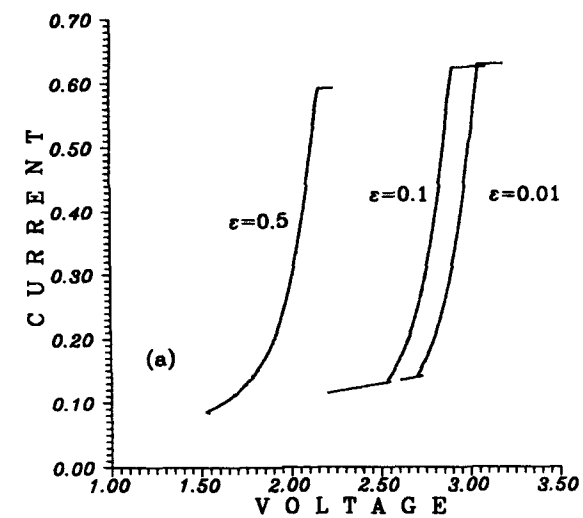


Figure 4. I-V characteristics for identical junctions with different values of coupling parameter ϵ .
 (a) ZFS-1 for length $L=2.0$, (b) ZFS-2 for length $L=4.0$. ($\alpha_1=\alpha_2=0.05$, $\beta_1=\beta_2=0.02$)

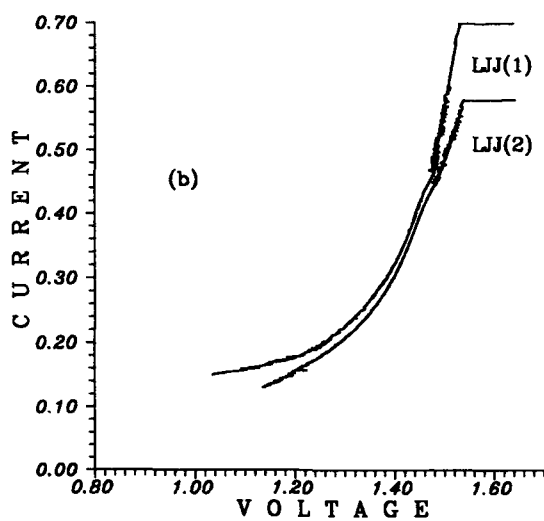
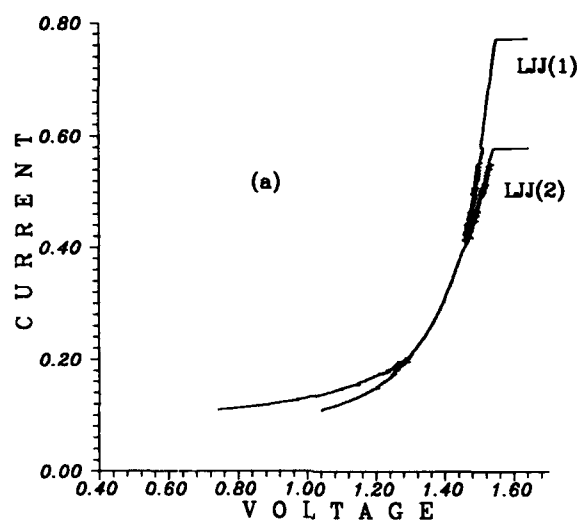


Figure 5. I-V characteristics for different junctions with length $L=4.0$, $\alpha_1=0.08$, $\alpha_2=0.05$, $\beta_1=0.02$, $\beta_2=0.0686$ and initial bias currents (a) $\gamma_1=\gamma=0.11$, (b) $\gamma_1=0.15$, $\gamma_2=0.13$.

I-V CHARACTERISTICS AND FLUXON ENTRAINMENT

It is well-known that, for practical applications, one would like to be able to estimate, control and maximize the superconducting current flowing through a Josephson junction device. In our system of coupled LJJ's, we find that we can do all this by studying the I-V characteristics of each junction individually.

We may think of our two LJJ's as coupled in parallel, with free boundary conditions

$$\phi_x(0,t) = \phi_x(L,t) = \psi_x(0,t) = \psi_x(L,t) = 0 \quad (18)$$

interacting via the "inductive" terms ϕ_{xx} , ψ_{xx} of eq. (4a,b) respectively. We start by following the McCumber branch for each junction, on the plane of (time) averaged voltage $\langle V \rangle$ and current γ , by eliminating the modulus k between the equations of junction 1

$$\langle V \rangle_1 = \langle \dot{\phi}_0 \rangle = \frac{\pi}{kK(k)} \quad , \quad \gamma_1 = \frac{4\alpha_1 E(k)}{\pi k} \quad (19)$$

where ϕ_0 is given by (13) and K , E are elliptic integrals of the first and second kind. Similarly, for junction 2, we replace $\phi_0 \rightarrow \psi_0$ and $\gamma_1 \rightarrow \gamma_2$, $\alpha_1 \rightarrow \alpha_2$ in (19).

Then, at the γ_i -values where the ZFS's are expected to appear, we place on each junction one kink (antikink) waveform, cf.(2), moving with a velocity $u=u_i$ which satisfies^{5,14}

$$\gamma_i = \frac{4u_i}{\pi\sqrt{1-u_i^2}} \left[\alpha_i + \frac{\beta_i}{3(1-u_i^2)} \right] \quad , \quad i=1,2 \quad (20)$$

and solve the pde's (4) numerically until the motion of the fluxons becomes stabilized¹⁸. Then, we compute the space and time averaged voltages $\langle V \rangle_1 = \langle \dot{\phi}_i \rangle$, $\langle V \rangle_2 = \langle \dot{\psi}_i \rangle$ and plot them against γ_1 and γ_2 respectively in Figs.4,5.

Observe in Fig.5a that the ZFS1 of the two junctions, with different α_i and β_i , coincides near the middle of the graph, if the initial γ_i 's we use are the same. We can, however, split the two ZFS1's apart, if we wish, provided we start our simulations with different γ_i 's, see Fig.5b. We have examined carefully the lower parts of the ZFS1's of Fig.5a and have found that the periods of the two fluxons, traveling up and down the junctions, undergo a series of transitions, until these periods finally coincide, at the point where the two curves meet¹⁵.

A similar phenomenon of fluxon "entrainment" is observed when the coupling parameter ϵ is increased. As we demonstrate in Fig.6 the two ZFS1's become **identical** over the full range of their existence as ϵ varies from 0.01 to 0.5.

We also wish to draw the attention of the reader to an interesting **shift** of the ZFS's of the system as the coupling becomes stronger. This effect is clearly evident in Fig.4 where we have taken identical junctions with $\alpha_1 = \alpha_2$, $\beta_1 = \beta_2$. In Fig.7 we also show it for ZFS3. We believe that this is an important phenomenon, since it demonstrates that the **closer** one brings the LJJ's together the easier it is to observe these current "jumps" in the performance of the system, as they occur at lower and lower values of $\langle V \rangle$ and γ .

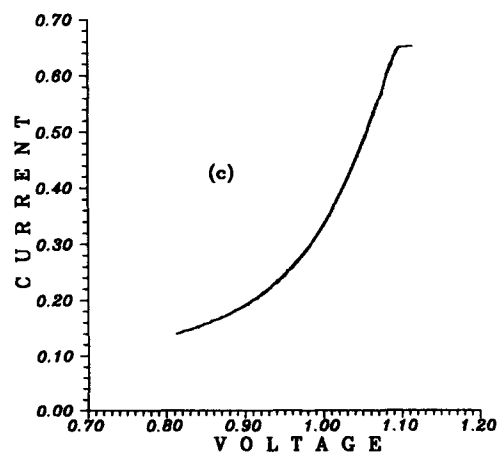
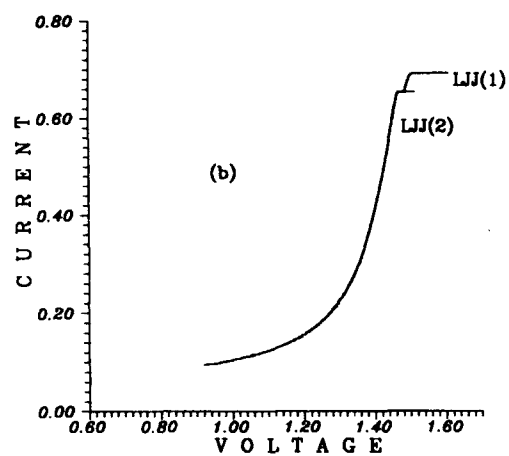
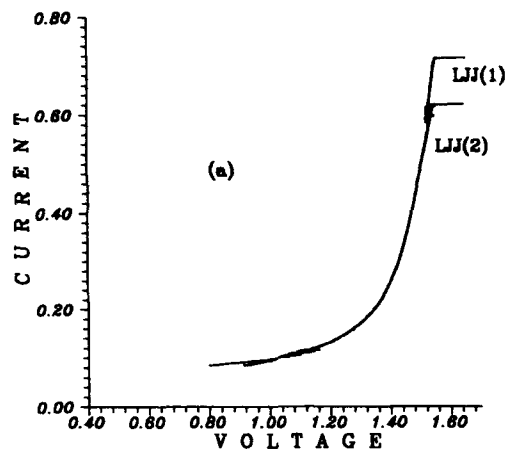


Figure 6. I-V curves for junctions with length $L=4.0$, $\alpha_1=0.06$, $\alpha_2=0.05$, $\beta_1=0.02$, $\beta_2=0.0362$ and coupling (a) $\epsilon=0.01$, (b) $\epsilon=0.1$, (c) $\epsilon=0.5$.

Clearly, it would be interesting to study how these phenomena change when one imposes a magnetic field through different boundary conditions¹⁹, or examines junctions with different characteristics⁸. We plan to report on these questions in another publication¹⁵.

Finally, our results may be of relevance in connection with a recent study of fluxon dynamics in "stacked" superconducting Josephson layers²⁰. In that study, the problem is approached from first principles and interestingly enough, in the 2-junction case, equations very similar to our eqns (4) are derived. Thus, we hope that our investigations will be of some use to some actual experiments, currently under way on such Josephson junction devices, at Lungby and other laboratories around the world.

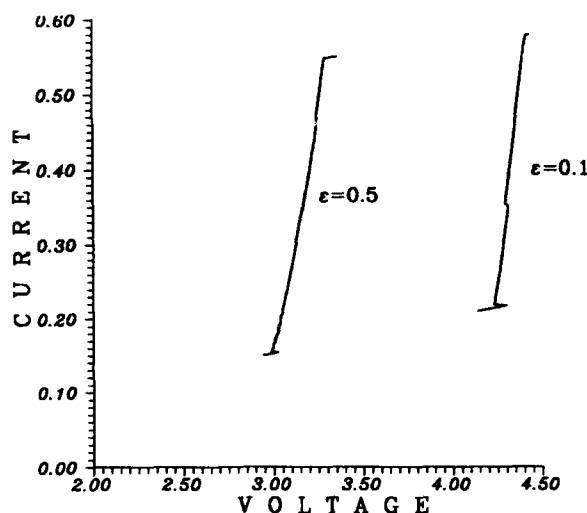


Figure 7. ZFS-3 for coupled junctions with different values of coupling parameter ϵ and $L=4.0$.

ACKNOWLEDGEMENTS

Some of the results of this paper have been inspired by many discussions with our dearest friend and collaborator, the late Stephanos Pnevmatikos. We wish to express here, one more time, our deepest feelings of sorrow for the loss of such a brilliant human and scientific presence from our midst.

Thanks and congratulations are due to Peter Christiansen and Bob Parmentier for an excellently organized meeting. We also thank the Research Center and University of Crete for their hospitality, as well as Prof. N. Flytzanis for his help and advice at different stages of this work. One of us (T.S.) expresses his gratitude to the EC-SCIENCE-0229-C(AM) program for supporting his participation at this meeting. Useful discussions on Josephson junction problems, with N.F.Pedersen, A.Ustinov and Y.Kivshar are also acknowledged here.

REFERENCES

1. D.W. McLaughlin and A.C. Scott, Phys. Rev. A18, 1672, (1978).
2. A. Barone and G. Paternó, "Physics and Applications of the Josephson Effect", Wiley, Interscience, New York (1982).
3. K.K. Likharev, "Dynamics of Josephson Junctions and Circuits", Gordon and Breach, New York (1986).
4. N.F. Pedersen, Physica Scripta, Vol. T13, 129, (1986).
5. S. Pagano, "Nonlinear Dynamics in Long Josephson Junctions", PhD Thesis, report N. S42, The Technical University of Denmark, Lungby, Denmark (1987).
6. I.L. Serpuchenko and A.V. Ustinov, JETP Lett. 94, 297, (1987).
7. A.A. Golubov, I.L. Serpuchenko and A.V. Ustinov, JETP. 94, 297, (1988).
8. Y.S. Kivshar and B.A. Malomed, Phys. Rev. B37, 9325, (1988).
9. P.L. Christiansen and N.F. Pedersen, in "Singular Behaviour and Nonlinear Dynamics", St. Pnevmatikos, T. Bountis and Sp. Pnevmatikos eds., World Scientific, Singapore, (1989).
10. J. Grønbech-Jensen, et al Phys. Rev. B42, 7, (1990).
11. See several papers in "Nonlinear Superconductive Electronics and Josephson Devices" ed. by G. Costabile, S. Pagano, N.F. Pedersen, M. Russo, Plenum, London, (1992).
12. T. Bountis and St. Pnevmatikos, Phys. Lett. 143A (4,5), 221, (1990).
13. T. Bountis, St. Pnevmatikos, St. Protogerakis and G. Sohos, in Lecture Notes in Phys. 353, Springer, New York, (1990).
14. T. Skiniotis, T. Bountis and St. Pnevmatikos, in the volume of ref. 11 above.
15. T. Skiniotis and T. Bountis, in preparation.
16. G. Costabile, S. Pagano and R.D. Parmentier, Phys. Rev. B36(20), 5225, (1987).
17. A.H. Nayfeh and D.T. Mook, "Nonlinear Oscillations", Wiley Intersciences, New York (1979) Chapt.5.
18. T. Skiniotis, "Analytical and Numerical Solutions of Nonlinear Wave Equations", PhD Thesis, Department of Mathematics, University of Patras, Greece (1993).
19. N.F. Pedersen and A. Davidson, Phys. Rev. B41(1), 178, (1990).
20. S. Sakai, P. Bodin and N.F. Pedersen, "Fluxons in Thin Film Superconductor-Insulator Super Lattices", preprint, subm. for publication (1992).

THE SINE-GORDON EQUATION AND SUPERCONDUCTING SOLITON OSCILLATORS

Stephanos Pnevmatikos¹ and Niels F. Pedersen²

¹Research Center of Crete, P.O. Box 1529
711 10 Heraklion, Crete, Greece

²Physics Lab. 1, The Technical University of Denmark
DK-2800 Lyngby, Denmark

This paper was finished shortly before the tragic death of Stephanos Pnevmatikos in the Autumn of 1990.

It was felt appropriate not to make changes even if his death caused a delay in the publication.

The Editors

ABSTRACT

Long Josephson junctions have a potential as narrow linewidth oscillator at millimeter and submillimeter frequencies. Such oscillators are suitable for use as local oscillators in integrated superconducting receivers. The oscillator derives its existence from fluxon motion governed by the sine-Gordon equation. The properties of this dynamical system are discussed both analytically and by comparison to a mechanical system with similar properties. The state of the art for low temperature experiments with superconducting microwave - and millimeter wave oscillators is reviewed. Typically the low power output of a single junction must be enhanced by inserting it in a resonant structure or by having several junctions phaselocked to each other. Such systems have demonstrated power output of the order a microwatt at frequencies between 10 and 500 GHz. An integrated receiver with all component fabricated by superconducting thin film technology is predicted.

I. INTRODUCTION

Solitons have recently attracted a lot of interest for fundamental studies and applications in many branches of modern technology, such as superconducting transmission lines and optical fibers. An early review by Scott et al [1] considered soliton propagation in a number of different physical systems within science and technology. Here we will concentrate on soliton propagation in long Josephson

junctions or Josephson transmission lines. The idea is to use perturbational methods to derive properties of a lightly damped system from those of a rather similar undamped system for which an analytical solution is known. Since our system is highly nonlinear such an approach is by no means trivial, and the validity of a solution can often only be proven by a comparison to numerical solutions. Many of the ideas here follow the original paper by McLaughlin and Scott [2] which was later expanded and modified towards practical use in the review paper by Pedersen [3]. A good deal of the theoretical description which for the purpose of this school is very tutorial - is adapted from lecture notes for a course given at the University of Thessaloniki by Pnevmatikos [4]. Finally we want to point out that a very recent extensive review by Kivshar and Malomed [5] on solitons in nearly integrable systems is a good continuation of some of the topics discussed here.

The present paper is very tutorial, but has one specific aim in mind - the use of long Josephson junctions (LJJ) as a soliton microwave oscillator to be used in an integrated superconducting microwave amplifier. In such an amplifier one would take advantage of the large number of other superconducting thin film components that have already been developed for high frequency use. Such single components include mixers, parametric amplifiers, bolometers, filters, transmission lines, etc. They have been tested in many experiments and are often found to be superior to conventional components. The local oscillator is a crucial component and the soliton oscillator is a very promising technique for that. Work in this direction is presently going on in several research laboratories around the world. In such a Josephson transmission line system a soliton is a quantum of magnetic flux, $\Phi_0 = 2 \times 10^{-15}$ Vs, that moves much like a particle under the influence of bias current and losses.

It should be mentioned here that the recent discovery of high transition temperature superconductivity has stimulated tremendously the interest in developing superconducting thin films components. If progress in materials technology can be made the problem of cooling can be reduced considerably since nitrogen could be used instead of liquid helium or cryocoolers.

The paper is organized in the following way: Section II describes an easily comprehended mechanical system that obeys the same equation as our superconducting non-linear transmission line. This system is a chain of coupled pendula. Section III describes the properties of the sine-Gordon equation, and section IV discusses the basic properties of the long superconducting Josephson junction. Section V expands on the previous section by discussing several technical details relating to long Josephson junctions. Section VI treats the experimental situation in relation to using superconducting soliton microwave oscillators. The paper is summarized in section VII.

II. MECHANICAL ANALOG OF THE SINE-GORDON EQUATION

The most pedagogical way to introduce the concept of topological solitons is to use one-dimensional series of simple pendula the points of support of which are connected in an elastic way through springs (Fig. 2.1). The dynamic behaviour of this mechanical system presents a fascinating resemblance to the dynamics of fluxons in a Long Josephson Junctions (LJJ). In the following we will show that the configuration of Figure 2.1 is the mechanical analog of the sine-Gordon equation (SG), [6]-

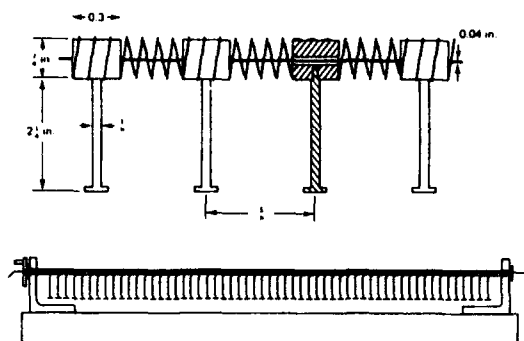


Fig. 2.1: Mechanical analog of the sine-Gordon (SG) equation. In the upper part the details for the chain of coupled pendula are given [6,7].

We suppose that each pendulum can rotate around its supporting axis without being able to move along it. Due to the elastic coupling through the spring the transverse oscillation of each pendulum affects the equilibrium of the neighbouring pendula. Thus if θ_n is the angle of deviation of the n th pendulum from its vertical equilibrium position then the equations of motion for the system of pendula take the form:

$$I \frac{d^2 \theta_n}{dt^2} = -Mgl \sin \theta_n + K(\theta_{n+1} - \theta_n) - K(\theta_n - \theta_{n-1}) \quad (2.1)$$

$$n=1, 2, \dots, N$$

which expresses the fact that the moment of inertia of the pendulum times its angular acceleration is equal to the sum of the applied torques. The chain is considered to be long enough so that we are not interested in the special form that the equations take at the two ends of the chain ($n=1$ and $n=N$) which is determined by the type of boundary conditions we consider (fixed ends, periodic boundary conditions, etc.). The equations (2.1) can be derived from the Hamiltonian:

$$H(p_n, \theta_n) = \sum \left[\frac{1}{2} I \dot{p}_n^2 + Mgl (1 - \cos \theta_n) + \frac{1}{2} K (\theta_{n+1} - \theta_n)^2 \right] \quad (2.2)$$

through the Hamilton equations:

$$\frac{d\theta_n}{dt} = \frac{\partial H}{\partial p_n}, \quad \frac{dp_n}{dt} = -\frac{\partial H}{\partial \theta_n} \quad (2.3)$$

From equation (2.1) we can now easily derive the more practical form:

$$\frac{d^2 \theta_n}{dt^2} = \omega_0^2 (\theta_{n+1} - 2\theta_n + \theta_{n-1}) - \Omega_0^2 \sin \theta_n \quad (2.4)$$

where

$$\omega_0 = (K/I)^{1/2}, \quad I = MI^2, \quad \Omega_0^2 = Mgl/I \quad (2.5)$$

l being the length of the pendulum and I its moment of inertia, M its mass and g the acceleration of gravity. In the previous model we considered springs which obey Hookes law, K being the spring's constant, so that the interactions between first

neighbours are harmonic. When $K = \omega_0 = 0$, then the pendula are uncoupled and each of them behaves like an independent oscillator. In the opposite case the deviation of a pendulum from its equilibrium position entails the deviation of its neighbouring pendula. The excitation that is caused by the deviation of a pendulum is spread along the chain, the more, the stronger the coupling between the pendula is (collective excitation). In this way, applying a whole rotation at one of the pendula, we create a localized excitation which behaves like a topological soliton whose properties we are going to study in the following. Of course, topologically, the rotation of the pendulum creates a soliton only when it is done from the end of the chain. In the opposite case it creates a soliton and an antisoliton (Fig. 2.2), something that finally leaves the asymptotic values of the excitations at the end of the chain unchanged.

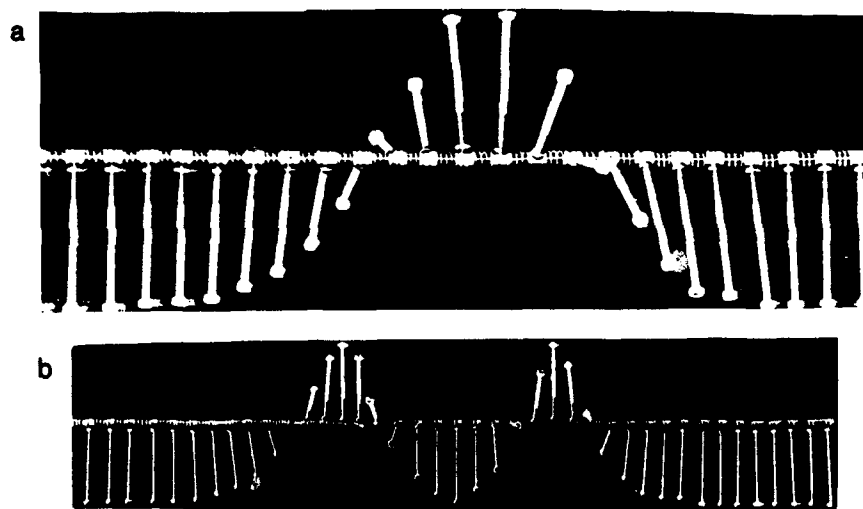


Fig. 2.2. a) Soliton in the coupled pendula chain. b) Soliton and antisoliton at the middle of the chain.

When the deviation of the pendula from the vertical equilibrium position is small enough, one can expand the sine of the non-linear term of equation (2.4) and suppose that $\sin \theta_n \sim \theta_n$. Thus equation (2.4) becomes a linear difference differential equation, which can be solved in classical ways. In this approximation we suppose that the coupling between neighbouring pendula is quite strong, so that the deviation of the pendulum causes a perturbation with large width. Then the deviations of neighbouring pendula won't differ too much, so that we can write:

$$\theta_{n \pm 1} = \theta \pm l_0 \theta_x + \frac{l_0^2}{2} \theta_{xx} \pm \dots \quad (2.6)$$

where l_0 is the distance between two successive pendula, $\theta(x,t) \sim \theta_n(t)$ and $\theta_x = \partial \theta / \partial x$. Substituting relation (2.6) in the equations (2.4), we easily arrive at the following partial differential equation, which is the SG equation:

$$\theta_{tt} - c_0^2 \theta_{xx} + \Omega_0^2 \sin \theta = 0 \quad (2.7)$$

where $c_0 = 1_0 \omega_0$ is the characteristic velocity of small amplitude transverse waves propagation in the chain.

2.1 Topological solitons of the SG equation

Introducing the following new system of coordinates

$$X = \alpha x, \quad T = \beta t, \quad \text{where } \alpha = \Omega_0 / c_0, \quad \beta = \Omega_0 \quad (2.8)$$

we obtain the dimensionless form of the SG equation:

$$\theta_{TT} - \theta_{XX} + \sin \theta = 0 \quad (2.9)$$

for which we should define the proper boundary conditions, eg. free ends:

$$\theta_X(T, 0) = \theta_X(T, L) = 0 \quad (2.10)$$

where L is the length of the chain; or periodic boundary conditions:

$$\theta(T, 0) = \theta(T, L) = 0, \quad \text{mod } (2\pi) \quad (2.11)$$

In case that the chain has "infinite" length the periodic boundary conditions are written as:

$$\theta(T, -\infty) = \theta(T, \infty) = 0, \quad \text{mod } (2\pi) \quad (2.12)$$

Searching for travelling wave solutions which propagate with constant velocity we can make the transformation:

$$\theta(X, T) = \theta(s), \quad \text{where } s = X - vT \quad (2.13)$$

where v is the constant velocity of the wave in the (X, T) system of coordinates. Now the partial differential equation (2.9) turns to the following ordinary differential equation:

$$(1 - v^2) \theta_{ss} = \sin \theta \quad (2.14)$$

which we are able to integrate. Multiplying (2.14) by θ_s and integrating we obtain the equation:

$$\frac{1}{2} (1 - v^2) (\theta_s)^2 = -\cos \theta + \chi_1 \quad (2.15)$$

where χ_1 is the integration constant. This constant is determined by the boundary conditions of the wave. In the general case, the wave solutions are expressed as a combination of elliptic functions [8,9] and represent periodic wave (see fig. 2.3).

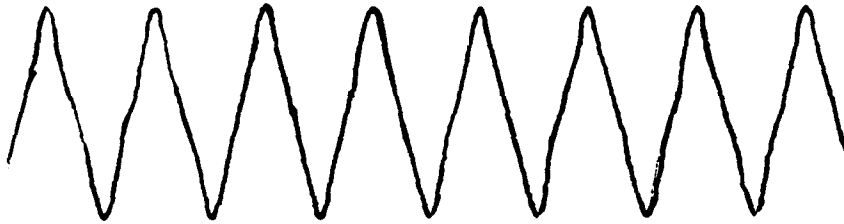


Fig. 2.3: An anharmonic form of periodic solution of the SG equation [8].

If our interest is to search for solutions of the form of figure 2.2, then we should apply the boundary conditions:

$$\theta \rightarrow 0, \text{ mod}(2\pi) \quad \text{and} \quad \theta_s, \theta_{ss} \rightarrow 0, \quad \text{when } |s| \rightarrow \infty \quad (2.16)$$

which correspond to spatially-localized solutions. In the case the constant K_1 equal to unity ($\chi_1 = 1$) the relation (2.15) turns to:

$$\pm (s - s_0)/(1 - v^2)^{1/2} = \int \frac{d(\theta/2)}{2 \sin \theta}$$

where s_0 is the integration constant. Calculating the integral and inverting we finally find the solution:

$$\theta = 4 \arctan \left\{ \exp [\pm (s - s_0)/(1 - v^2)^{1/2}] \right\} \quad (2.17)$$

which in the original system of coordinates becomes:

$$\theta(x,t) = 4 \arctan \{ \exp[\pm \gamma(x-x_0-vt)/d] \} \quad (2.18)$$

where x_0 is a constant which determines the position of the center of mass of the solution, $v=vc_0$ is the wave velocity, $\gamma=(1-v^2/c_0^2)^{-1/2}$ is the Lorentz factor and $d=c_0/\Omega_0$.

The plot of solution the (2.18) is a "kink" which represents a whole rotation of the pendula chain around its axis ($\theta:0 \rightarrow 2\pi$). This rotation is realized around the position x_0 and is done within an area which is approximately determined by the quantity:

$$D = 2\pi \frac{d}{\gamma} \quad (2.19)$$

which is the width of the solution. The more the coupling of the pendula becomes stronger than the gravitational attraction ($c_0 > \Omega_0$), the bigger the quantity D becomes, which means that the width of the soliton is getting larger. The width D depends also on the wave velocity (through parameter γ). For $v=0$ we have $\gamma=1$ and the which D takes its maximum value which corresponds to the static form of the solution. When the velocity v increases, the soliton becomes narrower increasing its slope, but it always remains "subsonic" ($v < c_0$). When $v \rightarrow c_0$, the soliton becomes very narrow and the approximation of the continuum limit no longer holds. Then the discreteness effects appear. If we want the continuum limit to hold then we should always have $d/\gamma \gg l_0$. Only in this way the SG equation describes correctly the dynamical behaviour of the figure's 2.1 system. In the opposite case we should return to the equations (2.4). The (\pm) signs in (2.18) solution determine the polarity of the wave (see fig. 2.4). The $(+)$ sign corresponds to a kink (positive rotation) and the $(-)$ sign to an antikink (negative rotation).

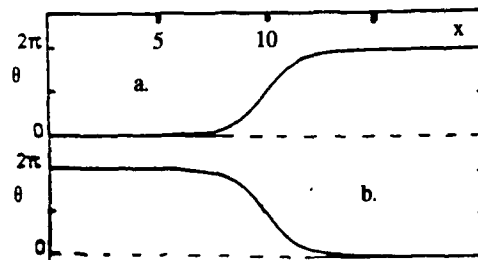


Fig. 2.4 Typical form of the kink (a) and antikink (b) solutions of SG equation.

The SG equation is a totally integrable nonlinear differential equation with partial derivatives which can be solved and studies analytically with much more elegant and mathematically complete methods.

2.2 Energy and particle character of soliton

The SG equation can be derived from a Hamiltonian density which has the form:

$$H(p, \theta) = \frac{1}{2} [p^2 + \theta_x^2 + 4 \sin^2(\theta/2)] \quad (2.20)$$

through the field equations:

$$\theta_T = \frac{\delta H}{\delta p} \quad (2.21)$$

$$p_T = - \frac{\delta H}{\delta \theta} = - [-\theta_{XX} + 2\sin(\theta/2) \cos(\theta/2)] \quad (2.22)$$

these equations are the continuous analog of equations (2.3). Substituting the kink or antikink solution (2.17), where $s = X - vT$, into the Hamiltonian density (2.21) and integrating, we take the soliton energy in the dimensionless form:

$$E_s^* = \int_{-\infty}^{\infty} H(p, \theta) dX = 8\gamma \quad (2.23)$$

We can also make this calculation in the original system of coordinates. From the solution (2.18) we notice that:

$$\theta_x = (2\gamma/d) \operatorname{sech}\phi \quad \text{and} \quad \theta_t = -v\theta_x \quad (2.24)$$

$$\frac{1}{2\gamma^2} (\theta_x)^2 = - \frac{1}{2} (c_0/\Omega_0\gamma)^2 (\theta_x)^2 = 1 - \cos\theta \quad (2.25)$$

Combining (2.24) and (2.25), the soliton energy in full dimensions:

$$E_s^* = (l/2) \int_{-\infty}^{\infty} [\theta_t^2 + c_0^2 \theta_x^2 + 2\Omega_0^2 (1 - \cos\theta)] \frac{dx}{l_0} \quad (2.26)$$

takes the form:

$$E_s(v) = (8c_0^2 I / l_0 d) \gamma \quad (2.27)$$

which can also be rewritten as

$$E_s = mc_0^2 \quad (2.28)$$

where c_0 is the characteristic velocity for the medium (the velocity of "sound" in the chain) and

$$m = m_0 \gamma = m_0 (1 - v^2/c_0^2)^{-1/2} \quad (2.29)$$

The quantities

$$m_0 = 8I/l_0 d \quad \text{and} \quad E_s(0) = m_0 c_0^2 \quad (2.30)$$

are the mass and the rest energy of the soliton (static soliton) respectively. The relation (2.28) is the well-known Einstein's relativistic formula. The SG soliton has a relativistic particle character, since its mass increases with velocity and becomes infinity when $v \rightarrow c_0$. We notice that the soliton energy can never be zero. The minimum value of the energy that a soliton can have is the rest energy. The least possible rest energy of the soliton is needed in order to make a rotation of the pendula chain. Thereafter every offer of energy to the soliton changes only its kinetic situation, changing its width (mass), until a second soliton is created and so on.

The SG equation of the form (2.9) seems, thus, to be the "model" equation both for the mechanical system of figure 2.1 as well as for the Josephson transmission line as we shall see next. It is thus worth, in the next chapter, to proceed in a deeper analysis of the SG equation and its solutions. The mechanical analog will be very useful to us in understanding what is going on inside a Josephson transmission line (JTL).

III. THE SINE-GORDON EQUATION

The sine-Gordon (SG) equation can be derived from a Lagrangian density of the form:

$$L = \frac{1}{2} [\dot{\phi}_x^2 + \phi_t^2 - 2(\cos\phi - 1)] \quad (3.1)$$

where $\varphi(x,t)$ represents a continuous field changing in spaces and time and $\varphi_x = \partial\varphi/\partial x$, $\varphi_t = \partial\varphi/\partial t$. For example $\varphi(x,t)$ may be the function of the pendula displacements of the mechanical analog of figure 2.1 in the continuum limit. If we insert equation (3.1) into an Euler-Lagrange equation of the type:

$$\frac{\partial}{\partial t} \left(\frac{\partial L}{\partial \dot{\varphi}} \right) + \frac{\partial}{\partial x} \left(\frac{\partial L}{\partial \varphi_x} \right) - \frac{\partial L}{\partial \varphi} = 0 \quad (3.2)$$

we have the partial differential SG equation:

$$\phi_{tt} - \phi_{xx} + \sin\phi = 0 \quad (3.3)$$

As it is known every solution of (3.2) satisfies Hamilton's principle, which supposes that the integral $\int L dx dt$, is an extremum. With the choice of signs we have made, the stable solutions of the SG equation will correspond to a minimum and the unstable to a maximum of this integral. Inserting now the corresponding momentum density:

$$\Pi = \frac{\partial L}{\partial \dot{\varphi}} = -\dot{\varphi} \quad (3.4)$$

we take the Hamiltonian density H with the help of a Legendre transformation of the type

$$H = L - \Pi \dot{\varphi} \quad (3.5)$$

where

$$H = \int_{-\infty}^{\infty} H dx = \int_{-\infty}^{\infty} \left\{ \frac{1}{2} [(\phi_x)^2 + (\phi_t)^2 + 2(1 - \cos\phi)] \right\} dx \quad (3.6)$$

is the total energy of the system (Hamiltonian).

If we concentrate our interest in solutions for which

$$\lim_{x \rightarrow +\infty} \phi = 2\pi m \quad \text{and} \quad \lim_{x \rightarrow -\infty} \phi = 2\pi n \quad (3.7)$$

where m and n integers, then beside the total energy H which is conserved we can define the density of rotations:

$$\rho = \frac{\partial L}{\partial \phi_x} = \phi_x \quad (3.8)$$

so that the total number of rotations

$$R = \int_{-\infty}^{\infty} \rho dx = 2\pi(m-n) \quad (3.9)$$

is also a conserved quantity. In fact the quantity R equals the number of fluxons (positive rotations) minus the number of antifluxons (negative rotations).

In addition to the quantities (3.6) and (3.9), another conserved quantity is the total momentum of the system

$$P = - \int_{-\infty}^{\infty} dx \phi_x \phi_t \quad (3.10)$$

One can show that the SG equation has an infinite number of first integrals (conservation laws), thus being a totally integrable system [8,10]. This means that we can exactly equation (3.3) and calculate the whole spectrum of it's solutions. In the following, however, we won't enter into such a detailed mathematical study.

The potential $V(\phi) = 1 - \cos \phi$ of Hamiltonian (3.6) creates for the system an infinite number of ground states. Thus, every change of the function $\phi(x,t)$ by 2π leaves the system unchanged. Moreover, the SG equation is invariant under Lorentz transformations of the type:

$$\begin{pmatrix} t' \\ x' \end{pmatrix} = \gamma \begin{pmatrix} 1 & -v \\ -v & 1 \end{pmatrix} \begin{pmatrix} t \\ x \end{pmatrix} \quad (3.11)$$

where $\gamma = (1-v^2)^{-1/2}$ is the Lorentz factor and v is the relative velocity of the two reference systems (X,t) and (X',t') .

3.1 Small Amplitude Waves

If we expand the potential $V(\phi) = 1 - \cos \phi$ around zero, assuming that $\phi < 1$, then equation (3.3) takes the very well-known form of Klein-Gordon equation:

$$\phi_{xx} - \phi_x = \phi \quad (3.12)$$

which admits plane wave solutions of the form:

$$\phi(X,t) = \text{Re} \{ \phi_0 \exp [i (kx - \omega t)] \} \quad (3.13)$$

obeying the dispersion relation:

$$\omega^2 = 1 + k^2 \quad (3.14)$$

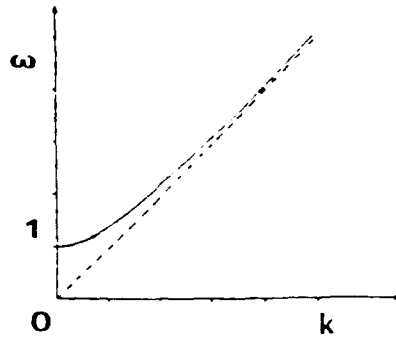


Fig. 3.1 Dispersion relation for small amplitude waves of the linearized SG equation.

The dispersion relation (3.14) resembles to the corresponding relation for the transverse waves in plasma. Thus, in correspondence the solutions (3.19) are called "plasma waves" and the frequency $\omega = 1$, which determines the beginning of the zone for the allowed frequencies is called "plasma frequency". We can easily see, using the mechanical analog, that excitations with frequency $\omega < 1$ do not propagate in these media. From the relation (3.14) the propagation medium is "dispersive", that means that the group velocity ($v_g = d\omega/dk$) and the phase velocity ($v_{ph} = \omega/k$) of a wave packet are different and depend on the wavevector k of each component. As a result the wave packet progressively decomposes when it propagates in the nonlinear medium mentioned above.

3.2 Simple Solutions of SG Equation

If we do not restrict ourselves to the study of small amplitude waves then the nonlinearity of the potential $V(\phi) = 1 - \cos \phi$ balance the dispersion of the propagation medium and permits the SG equation to admit even localized solutions with the characteristic stability of solutions.

If we set the condition that we look for travelling wave solutions, that is waves that are propagating with a constant velocity v , we can perform the transformation $s = x - vt$, where $v = v/c$, v being the wave's velocity in the original system and c is a characteristic velocity of the system (e.g. the light velocity). Thus, partial differential equation SG turns to the ordinary differential equation:

$$(1-v^2) \phi_s = \sin \phi \quad (3.15)$$

where $\phi_s = d\phi/ds$. Multiplying by ϕ_s and integrating equation (3.15) we get:

$$(1-v^2) \phi_s^2 = 2(E - \cos \phi) \quad (3.16)$$

where E is a constant of integration. The values of the parameters E and v are crucial for the definition of the type of solitons.

Equation (3.16) admits two groups of solutions, the "magnetic" solutions, which propagate with velocities less than the characteristic velocity c_0 ($v^2 < 1$), and the "electric", which propagate with velocities larger than c_0 ($v^2 > 1$) [9].

3.2.1 "Magnetic" type solutions

In the case, where $v^2 < 1$, equation (3.16) turn to:

$$\pm 2^{1/2} \gamma (s-s_0) = \int d\phi (E - \cos \phi)^{-1/2} \quad (3.17)$$

where $\gamma = (1-v^2)^{-1/2}$ is the Lorentz factor and s_0 is the new constant of integration. In this point it is better to distinguish three cases: $E=1$, $E>1$ and $E<1$.

a) 1st case ($E=1$): Solitary waves

Calculating the integral (3.17) when $E=1$ and inverting the expression that comes out, we end with the solution:

$$\phi(s) = 4 \arctan [\exp \{\pm \gamma(s-s_0)\}] \quad (3.18)$$

The solution (3.18) represents a spatially localized "kink" wave. For the (+) sign inside the argument, the wave is coming with zero value from $-\infty$ and ends with the 2π value at $+\infty$. For the (-) sign we have the opposite (see fig. 2.4). The values 0 and 2π represent two energetically different degenerate ground states of the original system. The $(1-\cos \phi)$ potential gives to the Hamiltonian (3.6) an infinity of such ground states. The transition from one ground state to the other is realized in a localized (limited) region of space and the waveform that results is named kink (antikink) respectively for the + (-) sign. Such a transition between two different ground states gives to the wave an additional topological stability and permits its existence even when its velocity is zero (static kink). These properties lead us to give at the sine-Gordon kink the characterization of a topological soliton. For the dimensionless form of SG the width of the wave (3.18) is defined only by the parameter $\gamma = (1-v^2)^{-1/2}$. The transition width between the two ground states is proportional to the quantity $\lambda = 2\pi/k$, where $k=\gamma$. Thus, when $v=0$ the kink takes the largest possible

transition region in space before ending at the constant asymptotic values. When $v \rightarrow 1$, then the kink becomes infinitesimally narrow (step function).

From the relation (3.18) we can show that:

$$\phi_x = \phi_s = \pm 2\gamma \operatorname{sech}[\gamma(X-s_0-vt)] \quad (3.19)$$

which has the form of a positive (negative) pulse for the $+$ ($-$) signs respectively. When $v \rightarrow 1$, the pulse (3.19) tends to a " δ -function".

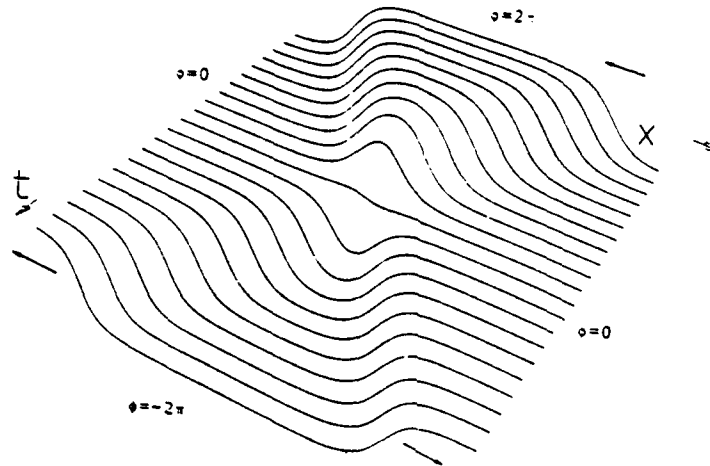


Fig. 3.2: Head-on collision of a pair of kink-antikink solitons of the SG equation [8].

In figure 3.2 we give the results of a simulation of the interaction between two kink-antikink solutions of SG equation representing the quantity ϕ_x . the finite length of the chain in the numerical simulation does not affect the solution which was calculated for an infinite length system (SG equation) because the soliton solution is localized.

We may show that:

$$\phi_t = -v\phi_x \quad (3.20)$$

where γ is given by (3.18) and therefore the momentum (3.10) of the system when it includes one such soliton is given by the relation:

$$P(\phi_{sol}) = v \int_{-\infty}^{\infty} dx \phi_x^2 \quad (3.21)$$

The energy of the kink solution will respectively be given by the integral (3.6). So, if

we use the relation:

$$\frac{1}{2} (1-v^2) \phi_x^2 = 1 - \cos\phi \quad (3.22)$$

we get:

$$E = \int_{-\infty}^{\infty} \phi_x^2 dx \quad (3.23)$$

Thus, calculating the integrals (3.23) and (3.21) for the solutions (3.20), we have:

$$E_s = 8\gamma \quad (3.24a)$$

and

$$P_s = 8v\gamma = vE_s \quad (3.24b)$$

which are the energy and momentum of the kink/antikink soliton, for the dimensionless form (3.3) of the sine-Gordon equation, related by $E_s = (8^2 + P_s^2)^{1/2}$.

b) 2nd case ($E > 1$): Helicoidal waves

In the case where $E > 1$, equation (3.17) takes the form:

$$\pm 2\gamma s = \int_{\pi}^{\phi(s)} d\phi [A + \sin^2(\phi/2)]^{-1/2} \quad (3.25)$$

where $A = (E-1)/2 > 0$ and $0 \leq A \leq 1$. So, defining the new variable $\tau = \cos(\phi/2)$ and inserting the parameter k ($0 < k < 1$), where

$$A = k_1^2/k^2 \quad \text{and} \quad k_1^2 = 1 - k^2 \quad (3.26)$$

the integral (3.25) becomes:

which is an elliptic integral [11]. The final solution for $\phi = \arccos(2\tau)$, is [9]:

$$-\gamma s/k = \int_0^s d\tau [(1-\tau^2)(1-k^2\tau^2)]^{-1/2} \quad (3.27)$$

$$\phi(s) = 2 \arcsin[\pm \operatorname{sn}(\gamma s/k, k)] + \pi \quad (3.28)$$

where $\operatorname{sn}(\gamma s/k, k)$ is the well known Jacobian elliptic function [8] and $K^2 < 1$. For small values of k^2 , the function $\phi(s)$ increases (decreases) monotonically for the + (-) sign.

If $\phi(s)$ represents an angle, then this solution represents a monotonic rotation towards one direction, that is a helicoidal wave. In the limit $k^2 \rightarrow 0$, we have $\operatorname{sn}(\gamma s/k, k) = \sin(\gamma s/k)$, hence $\phi(s) = \pi \pm 2\gamma s/k$. Finally in the limit where $K_1^2 = 1 - k^2 < 1$ the $\operatorname{sn}(\gamma s/k, k)$ periods is infinite and the elliptic function turns to the $\tanh(\gamma s/k)$ hyperbolic function, so the solution (3.28) takes the form of the kink solution (3.18).

c) 3rd case ($E < 1$): Oscillatory waves.

In the case where $E < 1$, equation (3.17) takes the form:

$$\pm 2\gamma s = \int_0^{\phi(s)} ds [\sin^2(\phi/2) - E]^{-1/2} \quad (3.29)$$

where

$$2B = 1 - E > 0 \quad \text{and} \quad 0 < B < 1/2 \quad (3.30)$$

if now

$$B = k_1^2 = 1 - k^2 \quad \text{and} \quad \tau = \sin(\phi/2) \quad (3.31)$$

then

$$\pm \gamma s = \int_1^{\tau} d\tau [(1-\tau^2)(\tau^2 - K_1^2)]^{-1/2} \quad (3.32)$$

which is an elliptic integral. The final solution for $\phi = \arcsin(2\tau)$ is:

$$\phi(s) = 2 \arcsin [dn(\gamma s/k, k)] \quad (3.33)$$

The solution (3.33) represents a nonlinear oscillation around the ground state.

3.2.2 "Electric" field solutions

In the case the solutions are always accompanied by "Cherenkov" radiation while they propagate, which is not included in the mathematical expression of the solutions [9]. For $v^2 > 1$, equation (3.16) becomes:

$$\pm 2^{1/2} \gamma_0 (s-s_0) = \int d\phi (\cos \phi - E)^{-1/2} \quad (3.34)$$

where $\gamma_0 = (v^2 - 1)^{-1/2}$. We can now distinguish, as previously, three cases: $E > 1$, $E = 1$, $E < 1$ and obtain solutions of similar form with those of the previous paragraph. One can look, though, for more details in [9], since the case $v^2 > 1$ is of less physics importance.

3.2.3 "Breather" waves

Using more complicated techniques [8-10] we are able to calculate solutions with two, or even more solitons and antisolitons. The superposition principle does not hold here. The two soliton solutions, which are in certain finite distance from each other, will also contain a term that describes their interaction.

Under certain conditions a kink and an antikink can form a bound state with less energy than the one that the original compounds had. Such a solution [8-10] is called "breather" (see fig. 3.3) and is given by the formula

$$\phi_B(X,t) = 4 \arctan[(1/\omega_B^2 - 1)^{1/2} \operatorname{sech} \theta_E \sin \theta_0] \quad (3.35a)$$

where

$$\theta_E = \gamma(1 - \omega_B^2)^{1/2} (X - s_0 - vt) \quad , \quad \theta_0 = \gamma \omega_B [t - v(X - s_0)] \quad (3.35b)$$

The breather is a packet of oscillations, whose envelope waveform oscillates in time (see fig. 3.3.) with frequency ω_B ($0 < \omega_B < 1$). Inserting the solution (3.35) in Hamiltonian (3.6) and integrating, we calculate breather's energy:

$$E_B = 16\gamma (1 - \omega_B^2)^{1/2} \quad (3.36)$$

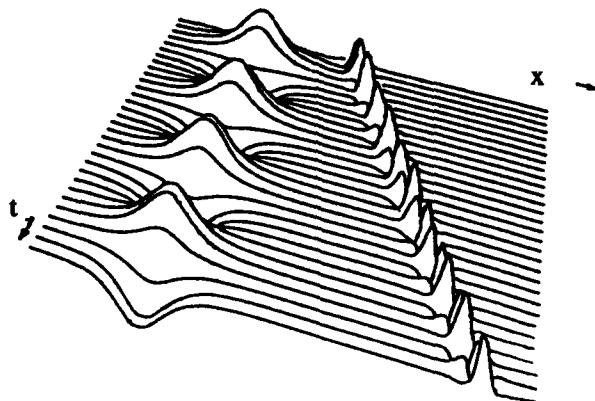


Fig. 3.3: Evolution of two breather solitons of the SG equation. The first has zero velocity of propagation while the second is moving to the right [8].

where 8γ is the energy of one kink. From (3.36) we get that:

$$\text{For } \omega_B \rightarrow 0: \quad E_B \rightarrow 16\gamma \quad (2\text{kinks})$$

$$\text{For } \omega_B \rightarrow 1: \quad E_B \rightarrow 0 \quad (\text{small amplitude oscillations})$$

it is worth noticing that since $\omega_B < 1$, breather's frequency lies inside the gap of the dispersion relation of figure 3.1. From the relation (3.36) it is obvious that energetically, breather is more economic than a kink and an antikink together, a fact that explains breather's stability. The breather soliton is a non-topological soliton, because it corresponds to an excitation of the same ground state. The pendula start from zero angle, in some region of the chain they make a π -angle and without performing a rotation they return back to zero angle. The breather soliton cannot exist static. Even though it does not move from its position, at least its internal degree of freedom (internal oscillation) will evolve ($\omega_B \neq 0$).

The solutions we calculated in this chapter correspond to a system with infinite degrees of freedom, where we don't have to define boundary conditions. The simulations we presented correspond though to limited systems. The reader who has the mathematical interest to investigate SG solutions for specific boundary conditions can look at the references [8,10,12,13].

A complete (general) solution of the SG equation will be composed of kinks, antikinks, breathers (discrete spectrum) and oscillatory (periodic) wave solutions (continuous spectrum). An arbitrary wavepacket, with given energy, which is initially offered to a system which is exactly described by the SG equation, will asymptotically decompose to a well defined number of kinks, antikinks, breathers and periodic waves. The quantity, the quality and the exact values of their parameters and the dynamics of the solutions which will arise can be exactly predicted by the SG equation with the

help of the mathematical technique: "Inverse Scattering Method" [8,10,14,15] which is something like a nonlinear generalization of Fourier transform, where the Fourier components are now the kinks, antikinks, breathers and the nonlinear periodic oscillations.

IV. LONG SUPERCONDUCTING JOSEPHSON JUNCTIONS

One of the most characteristic applications of the sine-Gordon equation and of the theory of topological solitons in general, is the physics of long superconducting Josephson junctions.

4.1 The Josephson effect

Several years after the discovery of superconductivity [16] and five years beyond its theoretical interpretation [17], Cambridge's postgraduate student **Brian Josephson** published the "possible" theoretical realization of the superconducting tunneling effect [18]. One year later Anderson and Rowell verifies experimentally Josephson's discovery [19].

When we have two simple conductors (1 and 2) which are separated by a thin oxide layer, in the general case, the insulating oxide acts like a potential barrier which stops the flow of electrons between the two superconductors. When, though the insulator is thin enough (10-20Å) then, applying a small external potential difference, some electrons are able to penetrate the potential barrier and give conductivity. This is the well known quantum tunneling effect. The current-voltage relation for small voltage is ohmic.

When the temperature gets low enough (lower than some critical temperature T_c) some materials become superconductors. That is, they present zero electric resistance and become perfect diamagnet (the magnetic field penetrates the material only into a depth λ_L , which is called London penetration depth, while in the interior of the material we have $B=0$). Josephson wanted to investigate if tunneling effect exists when we have a junction between two superconductors separated by a thin insulating oxide.

If we consider two conductors S_1 and S_2 (see fig. 4.1) then as soon as the temperature of the system gets below the critical temperature T_c , many of the electrons of the two superconductors form pairs (Cooper pairs) in which the two electrons have opposite momentum and spin. Due to their bosonic character Cooper pairs are able to "condense" in large superconductive states for each superconductor. If Ψ_1 is the probability amplitude for the superconducting electrons in the first superconductor and Ψ_2 in the second, then the two wavefunctions will satisfy the following system of time-dependent Schrödinger's equations [20].

$$i\hbar \frac{\partial \Psi_1}{\partial t} = E_1 \Psi_1 + K \Psi_2 \quad (4.1a)$$

$$\hbar \frac{\partial \Psi_2}{\partial x} = E_2 \Psi_2 + K \Psi_1 \quad (4.1b)$$

where $\hbar = h/2\pi$ is Planck's constant and K is a constant which depends on the junction and expresses the possibility that each wavefunction can spread to

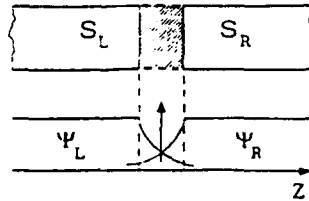


Fig. 4.1: Superconducting junction and the corresponding wavefunctions

the other superconductor. (See fig. 4.1). For reasons of simplicity we consider that K constant is the same for both the superconductors and $E_1 = -E_2 = E$. While

$$E_1 - E_2 = 2E = qV \quad (4.2)$$

where $q=2e$ is the charge of one Cooper pair. The Ψ_1 and Ψ_2 wavefunctions are complex functions, so they can be written in the form:

$$\Psi_1 = \rho^{1/2} \exp(i\phi_1) \quad \text{and} \quad \Psi_2 = \rho^{1/2} \exp(i\phi_2) \quad (4.3)$$

where ρ is the Cooper pairs density and ϕ the common phase for all the pairs. For reasons of simplicity we use again the symmetry of figure 4.1 and suppose that $\rho_1 = \rho_2 = \rho$.

In such a superconductor the current density which penetrates is given by

$$J = \rho \frac{e}{m_e} (\hbar \nabla \phi - 2eA) \quad (4.4)$$

where e and m_e are the electronic charge and mass respectively and A is the vector potential [7,20].

When the thickness d of the insulator which separates the two superconductors become very small ($d < 100\text{\AA}$), then we initially notice that free electrons start to penetrate it, forming the so called quantum tunneling effect. When the thickness is further reduced ($d < 30\text{\AA}$) then the first Cooper pairs also begin to penetrate the insulator. In this state the two phases ϕ_1 and ϕ_2 are no longer independent since they start to have overlap with their opposite superconductor over the insulator. This is the so called Josephson effect.

Inserting the wave functions (4.3) in the equations (4.1) and combining the previous relations Josephson proved the two following important equations which are known as "Josephson equations":

$$J = J_0 \sin \phi \quad (4.5a)$$

$$\frac{\partial \phi}{\partial t} = \frac{2e}{\hbar} V \quad (4.5b)$$

where

$$\phi = \phi_2 - \phi_1 \quad (4.5c)$$

$$J_0 = 2K\rho/\hbar \quad (4.5d)$$

ϕ being the phase difference between the two wavefunctions and J_0 the maximum amplitude of the current density that penetrates the insulator. Josephson's first relation tells us that the current density which flows in the junction depends on the phase difference ϕ having J_0 as a maximum value. Josephson's second relation tells us that the voltage drop between the two superconductors is proportional to the time variation of the phase difference ϕ . From relation (4.5b) one can calculate the phase difference ϕ with the approximation of a constant:

$$\phi(t) = \phi_0 + (2e/\hbar) \int V(t) dt \quad (4.6)$$

a) DC Josephson effect: If we suppose that $V=0$, then from (4.6) we can see that the phase is constant but not necessarily zero. When, though, $\phi = \phi_0 \neq 0$ then relation (4.5a) tells us that the current $I = I_0 \sin \phi$ is different from zero, and it can reach the maximum value I_0 . That is, if one considers a closed superconducting loop, it is enough to stop somewhere the continuity of the superconducting phase with a thin insulating layer and one will observe the appearance of small supercurrents with biggest possible intensity the quantity I_0 ($J_0 \times$ surface), without the presence of an electric source. This remarkable prediction was made for the first time in 1962 by Josephson [18] and was experimentally verified one year later by Anderson and Rowell [19].

b) AC Josephson effect: If we now apply a constant voltage $V = V_0$, then integration of relation (4.6) will give: $\phi = \phi_0 + 2eV_0 t/\hbar$ and Josephson's first relation (4.5a) will turn to:

$$J = J_0 \sin (\phi_0 + 2eV_0 t/\hbar) \quad (4.7)$$

hence an alternating current will appear in the junction, having the frequency:

$$\omega_J = 2\pi f_J = 2eV_0/\hbar \quad (4.8)$$

Since \hbar is a very small number, the frequency ω_J with which the current oscillates is very large, hence for small voltages no remaining current that can be measured is observed. In fact, since the temperature is never zero, a small current due to the "normal" electrons is observed.

The total behaviour of DC and AC Josephson effects is demonstrated in figure 4.2, showing the IV characteristic of a Josephson junction. The dotted line represents the current-voltage relation in a usual junction between metals. In a superconducting junction, for $V=0$, a current that can reach up to the maximum value I_0 appears. This state corresponds to a static value of the phase $\phi = \arcsin(I/I_0)$. As soon as we give small dc values to the voltage between the two superconductors the current takes negligible values due to the enormous frequency of its oscillation. The small non-zero value in the theoretical curve, is due to the thermal flow of normal electrons through the insulator. Since the temperature of the junction in the experimental curve (4.2b) is very low ($T=1.52K$), this branch is inexistent until a critical voltage value. For junctions that work at higher temperatures this branch become more obvious and is called the quasiparticle or McCumber branch. When the voltage reaches a critical value ($2\Delta \sim \pm 2.5mV$), then the McCumber branch has an abrupt ascent and tends to follow the dotted line of the ohmic behaviour. This critical value of the voltage corresponds to the energy that is higher than the electronic energy gap Δ between the two superconductors that form the junction, hence the phase ϕ is changing in time with a frequency proportional to the external dc voltage.

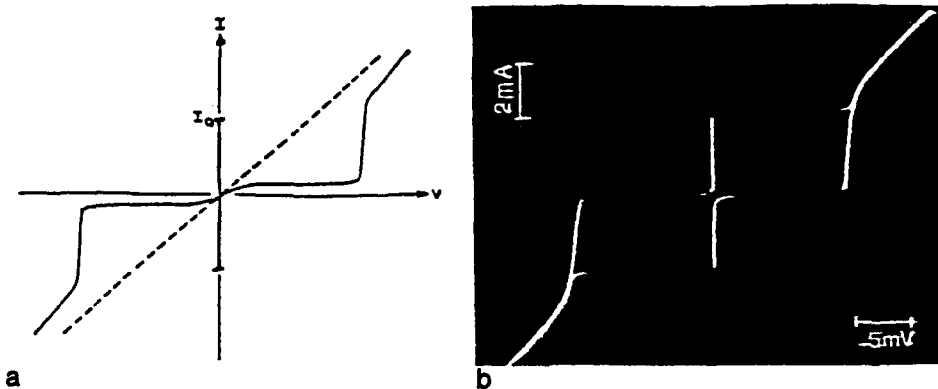


Fig. 4.2: IV characteristic for a Josephson junction. a) Theoretical curve from Josephson's relation. b) typical experimental IV characteristic for a Sn-Sn_xO_y-Sn junction at $T=1.52K$ temperature [7].

Another way to obtain supercurrent, using relatively small voltages is to consider a small alternating current:

$$V = V_0 + V_a \cos \omega t \quad (4.9)$$

where

$$\phi(t) = \phi_0 + 2eV_0 t / \hbar + (2eV_a / \hbar \omega) \sin \omega t \quad (4.10)$$

hence, using the approximation: " $\sin(x + \Delta x) = \sin x + \Delta x \cos x$ ", when Δx is small, we obtain:

$$J = J_0 [\sin(\phi_0 + 2eV_0 t / \hbar) + (2eV_a / \hbar \omega) \sin \omega t \cos(\phi_0 + 2eV_0 t / \hbar)] \quad (4.11)$$

The first term in relation (4.11) has zero mean value, but the second one does not if $\omega = 2eV_0 / \hbar$. This resonance phenomenon was experimentally observed by Shapiro [21].

4.2 Influence of an external magnetic field

Considering an arbitrary geometry of a Josephson junction and taking a cross-section of it we have the figure 4.3. In order to derive the equations that govern the electrodynamics of such a Josephson junction we will follow Barone and Paterno's presentation [7,22].

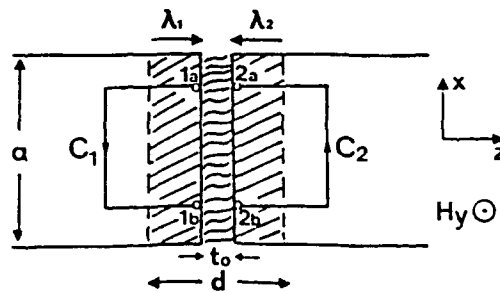


Fig. 4.3: Cross-section of a Josephson junction. The magnetic field is applied in y-direction. The dashed parts show the penetration depth λL of the field in the two superconductors [7].

Let us consider the Josephson junction under the influence of a magnetic field B which is applied in the y-direction (see fig. 4.3). The relation (4.4) for the current density of each superconductor easily takes the form:

$$\phi_{1,2} = (2e/\hbar) (m_p J / 2e^2 \rho + A) \quad (4.12)$$

where A is the vector potential which is connected to the magnetic field B through the relation $\nabla \times A = B$. Integrating along C_1 and C_2 contours we have:

$$\phi_{1b}(x+dx) - \phi_{1a}(x) = (2e/\hbar) \int_{C_1} (A + mJ/2e^2\rho) dl \quad (4.13a)$$

$$\phi_{2b}(x) - \phi_{2a}(x+dx) = (2e/\hbar) \int_{C_2} (A + mJ/2e^2\rho) dl \quad (4.13b)$$

In the choice of the integration paths we take care that C_1 and C_2 do not penetrate deeper than the dashed regions of figure 4.3 outside of which the supercurrent J is zero (London penetration depth). We also take care that J is perpendicular to the parts of the contours C_1 and C_2 which are orientated towards the x -direction, hence the second parts of the integrals (4.12) can be omitted, thus:

$$\begin{aligned} \phi(x+dx) - \phi(x) &= [\phi_{1b}(x+dx) - \phi_{2b}(x+dx)] - [\phi_{1a}(x) - \phi_{2a}(x)] = \\ &= (2e/\hbar) \left[\int A \cdot dl + \int A \cdot dl \right] \end{aligned}$$

If we also neglect the width of the insulating barrier, we have:

$$\phi(x+dx) - \phi(x) = (2e/\hbar) \int A \cdot dl \quad (4.14)$$

Using Stoke's theorem integral (4.14) can be replaced by the surface integral of the magnetic field, hence:

$$\int A \cdot dl = \int_s (\nabla \times A) ds = B_y (\lambda_1 + \lambda_2 + t_0) dx \quad (4.15a)$$

and so

$$d\phi/dx = \frac{2ed}{\hbar} B_y \quad (4.15b)$$

where $d = \lambda_1 + \lambda_2 + t_0$, λ_1 , λ_2 being London's penetration depths and t_0 the thickness of the dielectric barrier. Integration relation (4.15) we have:

$$\phi = \frac{2eB_y d}{\hbar} x + \phi_0 \quad (4.16)$$

Thus, relation (4.5a) of Josephson effect in the presence of an external magnetic field becomes:

$$J = J_0 \sin \left(\frac{2edB_y}{\hbar} x + \phi_0 \right) \quad (4.17)$$

which indicates that the penetration supercurrent is spatially modulated by the magnetic field.

4.3 Electrodynamics of Josephson junction

Supposing now that the magnetic field has a contribution to the x and y directions ($B_z=0$):

$$\frac{\partial \phi}{\partial x} = \frac{2eb_y d}{\hbar}$$

$$\frac{\partial \phi}{\partial y} = \frac{2eB_x d}{\hbar}$$

and differentiating we obtain:

$$\frac{\partial^2 \phi}{\partial x^2} = \frac{2ed}{\hbar} \frac{\partial B_y}{\partial x} \quad (4.18a)$$

$$\frac{\partial^2 \phi}{\partial y^2} = \frac{2ed}{\hbar} \frac{\partial B_x}{\partial y} \quad (4.18b)$$

From Ampere-Maxwell's law from electromagnetism we have:

$$\nabla \times \mathbf{B} = m_0 \mathbf{J} + e\mu_0 \frac{\partial \mathbf{E}}{\partial t} \quad (4.19)$$

which in our case turns to

$$\frac{\partial B_y}{\partial x} - \frac{\partial B_x}{\partial y} = \mu_0 J_z + \epsilon \mu_0 \frac{\partial E}{\partial t} \quad (4.20)$$

and from the Josephson relation $J = J_0 \sin \phi$ we get:

$$\frac{\hbar}{2ed} \left(\frac{\partial^2 \phi}{\partial x^2} + \frac{\partial^2 \phi}{\partial y^2} \right) = \mu_0 J_0 \sin \phi + \frac{\mu_0 \epsilon}{t_0} \frac{dV}{dt} \quad (4.21)$$

where $\epsilon = \epsilon_r \epsilon_0$ is the dielectric constant, μ_0 is the magnetic permeability of vacuum and $E = V/t_0$. Thus, using Josephson's second relation we obtain the following two dimensional SG equation:

$$\phi_{xx} - c_0^2 (\phi_{xx} + \phi_{yy}) + \Omega_J^2 \sin \phi = 0 \quad (4.22)$$

where

$$c_0 = (t_0 / \epsilon \mu_0 d)^{1/2}, \quad \Omega_J = (2e J_0 t_0 / \hbar e) \quad (4.23)$$

Equation (4.22) determines the spatially two dimensional spatiotemporal dynamics of the phase difference ϕ between the two superconductors, which is connected with the current density J and the potential difference V between the two superconductors. The typical thickness of each superconductor in a classical geometry [3,7,22] is 4000 Å. The London coefficient λ_1 of the magnetic field's penetration depth inside the superconductors, is 500-1000 Å, while the supercurrent's penetration depth which is defined by the Josephson coefficient:

$$\lambda_J = (\hbar / 2e \mu_0 J_0 d)^{1/2} = c_0 / \Omega_J \quad (4.24)$$

is of the order of 100 μm . The maximum value for the density of supercurrent lies between $1 \cdot 10^6 \text{ A/cm}^2$. The characteristic Josephson frequency $f_J = \Omega_J / 2\pi$ (the so called plasma frequency) takes values $10^8 \cdot 10^{11} \text{ Hz}$, where $\Omega_J = c_0 / \lambda_J$ and c_0 is the light velocity inside the dielectric being typically 5 percent of the velocity c of light in vacuum.

We can very easily understand the physical meaning of the three parameters λ_J , c_0 and Ω_J making the following simplifications:

Let us consider the one dimensional, static form of equation (4.22):

$$\frac{\partial^2 \phi}{\partial x^2} = \frac{1}{\lambda_J^2} \sin \phi \quad (4.25)$$

where $\phi = \phi(x)$, then for $\phi \ll 1$ we have $\sin \phi \sim \phi$ and the linearized form of (4.25) will accept solutions of the form:

$$\phi(x) = Ae^{x/\lambda_J} + Be^{-x/\lambda_J} \quad (4.26)$$

which means that λ_J is the characteristic length for an essential change of the phase. Beyond this length the phase $\phi(x)$ is zero, hence we do not have supercurrent. The λ_J , penetration depth of the supercurrent (Josephson penetration depth) also defines whether a junction is called "small" or "long" in a certain direction.

4.4 Small Josephson junction

If we consider a junction with figure's 4.4 geometry, where W and L are small enough that $W, L \ll \lambda_J$, then the phase $\phi(t)$ has no longer spatial dependence, hence equation (4.22) takes the simpler form:

$$\phi_{xx} + \Omega_J^2 \sin \phi = 0 \quad (4.27)$$

which describes a simple harmonic oscillator ("pendulum") which for small amplitudes of oscillation (where $\sin \phi \sim \phi$) oscillates approximately with the high eigenfrequency Ω_J , while the phase is the same everywhere in the junction's surface at a given time.

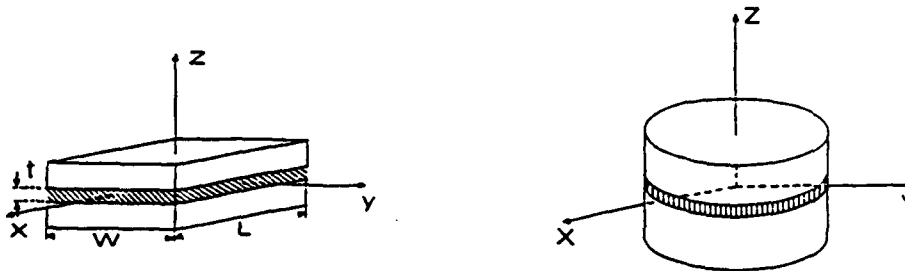


Fig. 4.4: Small Josephson junction (two different geometries).

The frequency Ω_J is called plasma frequency and for the linearized form of equation (4.27) one obtains the dispersion relation of figure 3.1 which is given from the formula:

$$\omega^2 = \Omega_J^2 + c_0^2 k^2 \quad (4.28)$$

For frequencies lower than the plasma frequency Ω_J , the oscillations decay inside the dielectric. Thus, Ω_J represents the lowest frequency with which an electromagnetic wave can pass through a Josephson junction. This frequency is typically of the order of 10^{10} Hz. The extremely high frequency Ω_J and the remarkable properties of such a junction make it an interesting electronic device for applications [7,23].

4.5 Josephson transmission line

A typical geometry for a Josephson junction is that of figure's 4.5. The construction of this junction is such that only in the x-direction the insulator has length larger than the Josephson penetration length ($L \gg \lambda_J$, while $W \ll \lambda_J$ and $t \ll W$). Then the Josephson junction takes the form of a waveguide.

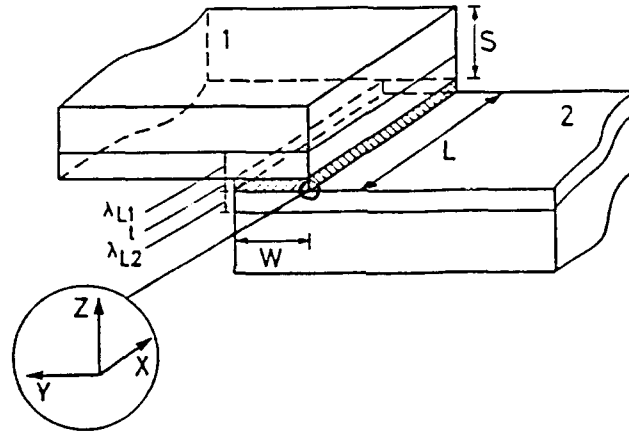


Fig. 4.5: Typical configuration for a long superconducting Josephson junction [22].

The junction of figure 4.5 is a long superconducting Josephson junction and it is described by the equation:

$$\phi_{xx} - c_0^2 \phi_{xx} + \Omega_J^2 \sin \phi = 0 \quad (4.29)$$

where c_0 plays the role of a limiting velocity with which the phase $\phi(x,t)$ wave solutions of equation (4.29), cannot exceed. Swihart has shown that c_0 is the light's velocity inside the dielectric of the junction [24] which is sufficiently smaller than the velocity c of light in vacuum ($c_0 \sim c/20$). The velocity c_0 in a LJJ is often called Swihart velocity.

One can describe the LJJ with the help of the hypothetical equivalent circuit which is called "Josephson Transmission Line" (LTJ).

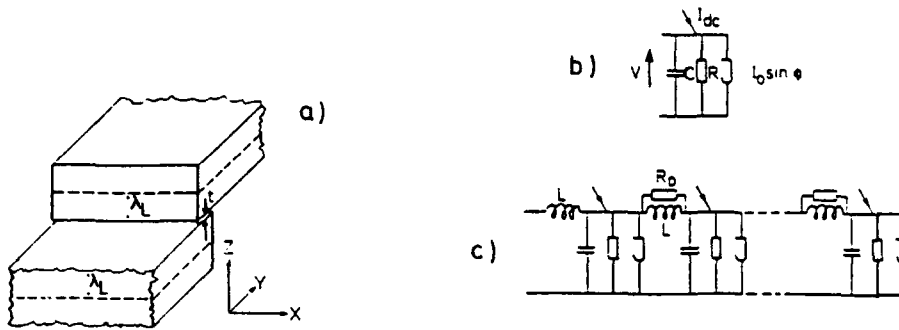


Fig. 4.6: a) Long Josephson Junction (LJJ) b) Simple Josephson oscillator (electric analog of a small Josephson junction) c) Josephson transmission line (electric analog of a long Josephson junction).

If we call L the inductance per unit length that the long Josephson junction has due to the storing of magnetic energy in the two superconductors, which reaches the λ_L depth (London penetration depth) and in the insulator with t_0 thickness, then in MKSA units, L is given by the type:

$$L = \mu_0 (2\lambda_L + t_0)/W = \mu_0 d/W \quad (4.30)$$

where $\mu_0 = 4\pi \times 10^{-7}$ H/m is vacuum's magnetic permeability, W is the width of the junction and t_0 the insulator's thickness.

If we also call C the parallel capacitance of the superconducting line per unit length which is caused by the electric energy stored in the dielectric, then:

$$C = We/t_0 \quad (4.31)$$

where $\epsilon = \epsilon_T \epsilon_0$ and $\epsilon_0 = (1/36\pi) \times 10^9$ F/m is the dielectric susceptibility of vacuum and ϵ_T the relative susceptibility which depend on the junction material. Thus, defining an inductance and a capacitance per unit length for a LJJ, we are able to use the electric circuit of figure 4.6c. Thus, applying Kirshhoff's low we can write:

$$Ldx \frac{\partial i}{\partial t} = (V - dV) - V \quad (4.32a)$$

$$i - (i + di) = Cdx \frac{\partial V}{\partial t} + J_0 dx \sin \phi \quad (4.32b)$$

where di and dV are the variations of current and voltage in the elementary section of the line dx . Simplifying relations (4.32) we get:

$$\frac{\partial V}{\partial x} = -L \frac{\partial i}{\partial t} \quad (4.33a)$$

$$\frac{\partial i}{\partial x} = -C \frac{\partial V}{\partial t} - J_0 \sin \phi \quad (4.33b)$$

Differentiating (4.33a) with respect to x and substituting in (4.33b) we have:

$$\frac{\partial^2 V}{\partial x^2} = -L \frac{\partial^2 i}{\partial x \partial t} = L \frac{\partial}{\partial t} \left(C \frac{\partial V}{\partial t} + J_0 \sin \phi \right) \quad (4.34)$$

Hence, differentiating Josephson's second relation and substituting in (4.34) we get:

$$\frac{\hbar}{2e} \phi_{xx} = \frac{\hbar}{2e} LC \phi_{xt} + LJ_0 \frac{\partial}{\partial t} \sin \phi \quad (4.35)$$

from where, integrating with respect to t and making the integration constant zero (external current doesn't exist) we obtain equation (4.29) with

$$c_0 = (LC)^{-1/2} \quad \text{and} \quad \Omega_J = (2eJ_0/\hbar C)^{1/2} \quad (4.36)$$

where L and C are given from relations (4.30) and (4.31).

4.6 The Fluxon

If we now use as a length unit $\lambda_J = (\hbar/2eJ_0L)^{1/2}$ and as a time unit $\Omega_J^{-1} = (\hbar C/2eJ_0)^{1/2}$, then equation (4.29) takes the following dimensionless form of SG equation:

$$\phi_{TT} - \phi_{XX} + \sin \phi = 0 \quad (4.37)$$

where

$$T = t/\Omega_J^{-1} \quad \text{and} \quad X = x/\lambda_J \quad (4.38)$$

Everything we have previously said for SG equation obviously holds now for LJJ. The soliton solution of (4.37) has the form:

$$\phi = 4 \arctan \{ \exp[\pm \gamma(x - x_0 - vT)] \} \quad (4.39)$$

where v is the soliton's relative velocity, $\gamma = (1 - v^2)^{-1/2}$ is Lorentz factor and x_0 is it's initial position (for $T=0$).

Having now the form of the spatiotemporal variation of the phase $\phi(x,t)$, we can substitute (4.39) into Josephson's second relation (4.5b) and estimate the voltage V between the two superconductors.

$$V = \frac{\hbar}{2e} \phi_t \quad (4.40)$$

while from relation (4.33a) we can respectively estimate the supercurrent that penetrates the junction:

$$i = - \frac{\hbar}{2eL} \phi_x \quad (4.41)$$

In fact, of course, the mean values of ϕ_x and ϕ_t should be measured in order to obtain the i and V quantities.

The phase ϕ is also related to the magnetic flux Φ of the junction through the relation:

$$\phi = 2\pi \frac{\Phi}{\Phi_0} \quad (4.42)$$

where $\Phi_0 = \hbar/2e = \pi\hbar/e$ is one flux quantum. Since the solution (4.39) entails a change of phase by 2π , this means that the magnetic flux changes by a flux quantum Φ_0 . Hence, the propagation of a soliton along the junction is equivalent to a magnetic flux's quantum penetration through the junction. This is a reason why the soliton (and the antisoliton) in LJJ is called fluxon (and antifluxon). From the relations (4.40) and (4.41) we can connect the magnetic flux with the potential difference between the two superconductors and the supercurrent that penetrates the insulator respectively:

$$V = \frac{\partial \Phi}{\partial t} \quad , \quad i = - \frac{1}{L} \frac{\partial \Phi}{\partial x} \quad (4.43)$$

It is obvious that since $\phi(x,t)$ and $\Phi(x,t)$ have the form of kink/antikink the $V(x,t)$ and $i(x,t)$ quantities will have the form of positive/negative pulse respectively. Thus, applying a potential difference between the two superconductors we expect to detect at the ends of the junction the periodic appearance of current and voltage pulses. Depending on the intensity of the applied voltage we will have one or more fluxons.

The small amplitude of the magnetic flux quantum ($\Phi_0 \sim 2 \times 10^{-15}$ Vs) and the large velocity of the response of a Josephson junction ($\Phi_J \sim 10^{11}$ Hz) make the experimental measurement of these quantities very difficult. The first succeeded measurement of a many-fluxon waveform was made in 1976 by Scott and his collaborators [25]. While the experimental detection of a single fluxon was performed in 1982 by Matsuda and Uehara [26]. It is obvious that the technological completion of the methods which will make worthy fluxon physics is still in progress.

From the first Josephson's relation we obtain the density of supercurrent. Substituting the one soliton in this relation we have the plot of figure 4.7 from which we see that the passage of the supercurrent in a certain time is made in a localized portion of the junction. Letting the time evolve the penetration window of the supercurrent scans the whole length of the junction in the x-direction. From figure 4.7 it is understood that the supercurrent makes a loop of entry and exit for the Cooper pairs, which circulate from one superconductor to the other without going away from the insulator more than distances of order v_J . The loop (fluxon) moves forth and back along the junction reflecting each time at the ends of the junction.

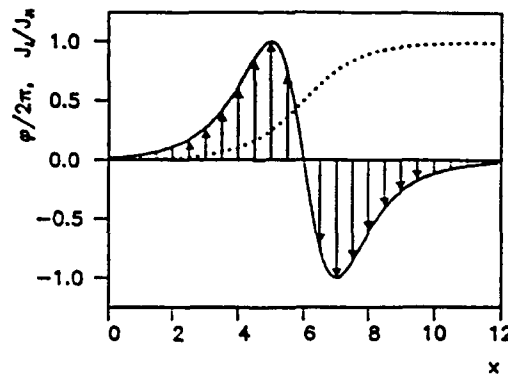


Fig. 4.7: The kink soliton (dotted line) for the phase $\phi/2\pi$ and the current fluxon (continuous line) [27].

The use however of the integrable SG equation (4.37) for the description of the dynamics of a LJJ is only academic. The quantitative derivation of the results we discussed and their connection with experiments demand the presence of a number of terms in SG equation which are related to the losses of the system, which up to now for pedagogical reasons had been omitted.

V. PERTURBED SINE-GORDON EQUATION

The more careful derivation of Josephson's equations makes us realize that the current density that flows through the separating insulator of the junction has not only the contribution of the supercurrent $J_0 \sin \phi$ only. A more complete expression for the density of current in a LJJ is given by the type [18,22]:

$$J = J_0(V) \sin \phi + \left[\frac{1}{R_1(V)} \cos \phi + \frac{1}{R_0(V)} \right] V \quad (5.1)$$

which contains the contribution of the current due to the normal electrons (last terms) and that the Cooper pairs interference current. $R_0(V)$ and $R_1(V)$ are the resistances for these two currents respectively. The second term in (5.1) is usually for simplicity omitted. Also for simplicity, we may assume that J_0 and R_0 are not functions of the voltage V .

5.1 More realistic equation for a LJJ

Combining relation (5.1) with Maxwell's equations we obtain a more realistic equation for the LJJ, which has the form [22]:

$$J_0 \sin \phi + \frac{\hbar}{2e} \left(\frac{1}{R_0} + \frac{\cos \phi}{R_1} \right) \frac{\partial \phi}{\partial x} = \frac{\hbar}{2e} \frac{1}{\mu_0 d} \frac{\partial^2 \phi}{\partial x^2} - \frac{\hbar}{2e} \frac{\epsilon}{t_0} \frac{\partial^2 \phi}{\partial x^2} + e R_s \frac{\partial^3 \phi}{\partial x \partial x^2} \quad (5.2)$$

where R_s is the resistance per unit length due to the surface currents which are created in the London penetration layers around the insulator and the other constants are defined in the same way as in relations (4.21) and (5.1). Inserting the quantities (4.23) and (4.24) in (5.2) we have:

$$\frac{\partial^2 \phi}{\partial x^2} - \frac{1}{c_0^2} \frac{\partial^2 \phi}{\partial t^2} - \frac{1}{\lambda_J^2} \sin \phi = \mu_0 d \left(\frac{1}{R_0} + \frac{\cos \phi}{R_1} \right) \frac{\partial \phi}{\partial x} - e R_s \frac{\partial^3 \phi}{\partial x \partial x^2} \quad (5.3)$$

Thus, measuring length in λ_J units (Josephson penetration depth) and time in $\Omega_{J,1}$ units (inverse Josephson plasma frequency) and inserting the constants:

$$\alpha = \frac{\omega}{\epsilon \Omega_J R_0}, \quad \beta = \epsilon R_J \Omega_J, \quad \gamma = \frac{R_0}{R_1} \quad (5.4)$$

we obtain the following perturbed sine-Gordon equation (P-SG):

$$\phi_{XX} - \phi_{TT} - \sin\phi = \alpha (1 + v \cos\phi) \phi_T - \beta \phi_{XIT} - \gamma \quad (5.5)$$

where $\gamma = I/I_0$, I being an external current which we apply in order to balance the losses and I_0 the maximum Josephson current. We usually assume that $v=0$.

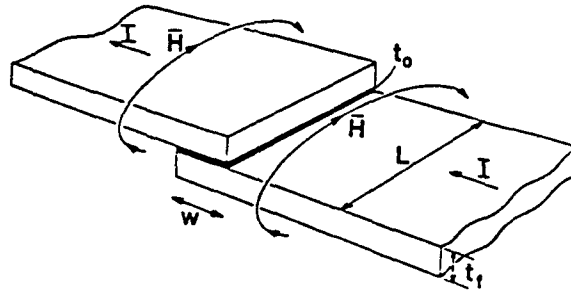


Fig. 5.1: a) Typical geometry for a LJJ. b) Josephson transmission line; $j_0 dx = I$ is the external current (bias current). The typical values of the parameters are [28]:
 $t_0 (10^{-9}m) \ll \lambda_L (5 \times 10^{-7}m) \ll h (2 \times 10^{-7}m) \ll W (5 \times 10^{-5}m) \ll \lambda_J (2 \times 10^{-4}) \ll L (10^{-3}m)$.

The dimensionless equation (5.5) describes the dynamical behavior of the phase difference $\phi(x,t)$ in a realistic LJJ (see figure 5.1a). The last two terms of equation (5.5) insert into the LJJ's equivalent circuit two resistances parallel to the shunt capacitance and the series inductance respectively (see figure 5.1b).

5.2 Perturbation theory for the P-SG

If we consider that the conductivity of the quasiparticles that penetrate the insulator is constant (we usually consider that $V=0$ in equation (5.5) and we adjust the value of α) and we assume that a bias current is applied to the junction ($\gamma = \text{const.}$), having no influence of an external magnetic field, then the P-SG equation:

$$\phi_{TT} - \phi_{XX} + \sin\phi = \gamma - \alpha \phi_T + \beta \phi_{XIT} \quad (5.6)$$

describes very satisfactorily the dynamic behavior of the phase difference $\phi(X,T)$ on the LJJ.

When $\alpha = \beta = \gamma = 0$, then equation (5.6) takes the form of SG equation, which

we extensively discussed in chapter III. Now, very naturally, one wonders how for all these solutions of SG equation and especially the soliton solution exist and how much relation they have with the much more realistic P-SG equation? The first to face this question were McLaughlin and Scoot [2], proposing two different approaches of equation (5.6) where it's right hand side is considered as a simple perturbation of the SG equation.

Considering that α , β and γ are different from zero then all the other solutions of the SG equation become asymptotically unstable and the LJJ which is initially excited by them tends to return to it's ground state. This, though, does not happen for fluxons and antifluxons which become the main carriers of the dynamics of the P-SG equation. The two last terms on the right-hand side of equation (5.6) which express the losses of the system, without being able to destroy the fluxons, tend to "ruin" their kinetic energy and trap them at some point of the junction. The external bias term (bias current) on the contrary, tends to accelerate fluxons and antifluxons in opposite directions. Finally, if that is possible, one expects that a balance will occur and the fluxons/antifluxons will move towards the direction which the field imposes which a certain velocity which is defined by the losses of the system.

If $\phi(X,T)$ is a solution of equation (5.6) then we can show that it holds:

$$\frac{d}{dt} H_{SG}(\phi) = - \int_{-\infty}^{\infty} (\gamma \phi_T + \alpha \phi_T^2 + \beta \phi_{XT}^2) dx \quad (5.7)$$

where $H_{SG}(\phi) = 8\gamma$ with $\gamma = (1-v^2)^{-1/2}$, is the energy of the SG equation fluxon/antifluxon, thus:

$$\frac{d}{dt} H_{SG}(\phi) = 8v (1-v^2)^{-3/2} \frac{dv}{dt} \quad (5.8)$$

The velocity v of the soliton is no longer a constant parameter, but at least for an initial transient period it has a dependence on time which is defined by the perturbation terms.

Consider α , β and γ small we can assume that besides the modulation of the velocity the perturbation terms have no other influence on the soliton's form. Thus putting the SG solution in equation (5.8) we obtain the relation:

$$\frac{dv}{dt} = \pm \frac{1}{4} \pi \gamma (1-v^2)^{-3/2} - \alpha v (1-v^2) - \frac{1}{3} \beta v \quad (5.9)$$

If the length of the LJJ is considered infinite (very large) then asymptotically we expect that we will have a balance between the competitive perturbation terms of equation (5.6), hence finally we will have $dv/dt=0$. Thus, from (5.9) we can easily

calculate the asymptotic value v_∞ of the velocity of the fluxon/antifluxon which will be given by the relation:

$$\gamma = \frac{4v_\infty}{\pi(1-v_\infty^2)} \left[\alpha + \frac{\beta}{3(1-v_\infty^2)} \right] \quad (5.10)$$

For $\beta=0$ we can easily obtain the equation:

$$v_\infty = [1 + (4\alpha/\pi\gamma)^2]^{-1/4} \quad (5.11)$$

The above calculation is not exact and it is not easy to be done for more than one fluxon/antifluxon. Beyond the modulation of the velocity the perturbation of (5.6) equation will cause other changes of the SG equation solutions. For instance, we expect a small change in the energy of fluxons/antifluxons which will be the cause of radiation of small oscillations. The reader who wants to use more complete methods for the study of equation (5.6) should study references [2,7,22].

5.3 I-V characteristic

In order to create a transition to the next section, which is experimental, we will discuss here the role of I-V characteristics. The experimental identity of a Josephson junction is its I-V characteristic (that is the current-voltage curve). Such a typical I-V characteristic is that of figure 5.2. As soon as we apply a small bias current to the junction the vertical branch of zero voltage appears (dc Josephson effect). Continuing to increase the current and right after we exceed the maximum value of Josephson current I_0 , we observe a steep shift of the curve (see dotted lines) to finite voltage values which are located in the McCumber branch (quasiparticle branch). This branch initially presents a steep ascent of the current and ends in an ohmic behavior.

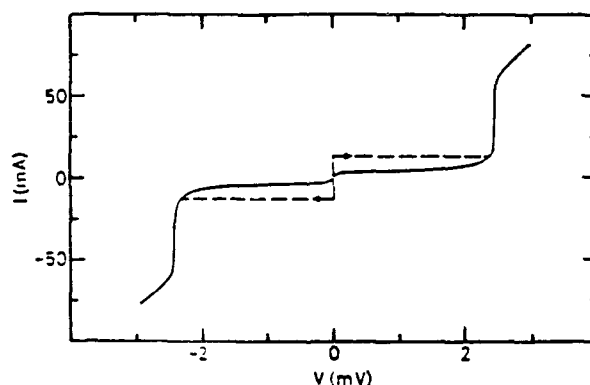


Fig. 5.2: Typical I-V characteristic of a Josephson junction [27]. The arrows show the shift from the zero voltage current to the McCumber branch.

In 1964 M.D. Fiske, applying an external magnetic field observed the appearance of current peaks on the low current part of the McCumber branch (far enough from the ohmic behavior) [29]. These singularities are called "Fiske steps".

If we now consider a LJJ, then even in the absence of a magnetic field we observe the formation of similar current peaks (see fig. 5.3) which for this reason are called Zero Field Steps or simply ZFS. In figure 5.3a we represent the first three ZFS which are located in distance between them while the first ZFS is located approximately at the position $34 \mu\text{V}$. The height of each ZFS is approximately 1mA . If an external magnetic field is applied to the junction, Fiske steps (ZFS) appear in the I-V characteristic (fig. 5.3b). In order to place a LJJ working at a certain ZFS, one starts from the McCumber branch and diminish the bias current until the value that lies right under the foot of the ZFS. Next, increasing again the current little by little the voltage stays and LJJ enters into the corresponding ZFS state.

The first to detect the existence of ZFS were Chen, Finnegan and Langenberg [30]. Fulton and Dynes [31] related for the first time the ZFS with the propagation of fluxons in the LJJ. The fluxon's propagation is related to the propagation of a voltage pulse ($V \sim \langle \phi_t \rangle$) which can be experimentally detected at the ends of the junction.

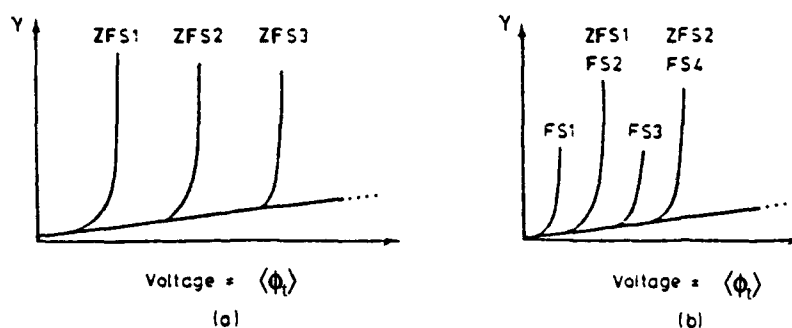


Fig. 5.3: a) I-V characteristic of a LJJ with three ZFS's. b) I-V characteristic in the presence of external magnetic field.

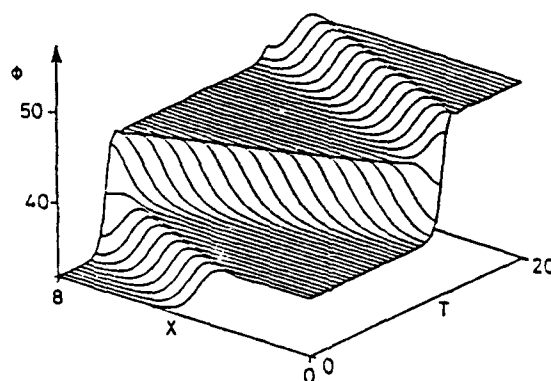


Fig. 5.4: Numerical simulation for the propagation of a fluxon (kink) on a LJJ which works at the 1st ZFS conditions. The parameters have the following values: $\alpha=0.05$, $\beta=0.02$, $\gamma=0.5$ and $L=8$ and we have considered free boundary condition [22].

Let us assume that a single fluxon propagates in the junction. After exactly one period $T_0 = 2L/v$ (where L is the junction length and v the soliton velocity) the fluxon returns back to the position from where it started. At the ends of the junction we have considered free boundary conditions, that is $\phi_x = 0$, where the soliton (kink) is reflected and changes polarity (see fig. 5.4). Thus, in a complete period, the phase has changed by 4π . If we have N kinks on the junction the phase changes by $4N\pi$.

In general, we have the relation:

$$\frac{1}{T} \int_0^{T_0} \phi_t dt = \frac{1}{T} [\phi(T_0) - \phi(0)] = \frac{2e}{h} V_{dc} \quad (5.12)$$

from where we find

$$V_{dc} = \frac{4\pi N}{T_0} \frac{h}{2e} = \frac{Nv}{L} \Phi_0 \quad (5.13)$$

which tell us that for a certain bias current I_{dc} , the dc voltage depends on the number of flux quanta (fluxons), the length of the junction and the velocity of fluxons. The velocity v is no longer a free parameter, as it was for the SG equation, but it is defined through the balance between the influence of the external field (bias current) and the losses.

1st ZFS

If we set the LJJ working at the 1st ZFS we have the picture of figure 5.5. In this case there is only a single fluxon on the junction, which is assumed to move initially to the left, be reflected at the free ends and change polarity. At the main figure we present the ϕ_x quantity, which as it is known is related to the current. The mean value in a $2L$ period of ϕ_x is zero. Thus the total current i which flows in the insulator towards a direction is zero. In contrast, ϕ_T which is related to the voltage and is represented at the insert part of figure 5.5, is not zero over the period which corresponds at a $2L$ length path of the pulse. In the insert figure we observe that the pulse does not change sign after the reflections at the ends. This is due to the fact that $\phi_T = -v_x$, where the velocity v also changes sign after each reflection at the boundaries.

2nd ZFS

If we set the LJJ working at the 2nd ZFS then we have the picture of figure 5.6. In this case in the LJJ two fluxons exist which can be propagated either to the same direction (Fig. 5.6a) or to different directions (fig. 5.6b).

The mean value for the voltage $\langle V \rangle$ is almost the same for both the dynamic states of the 2nd ZFS and corresponds to a value of voltage approximately

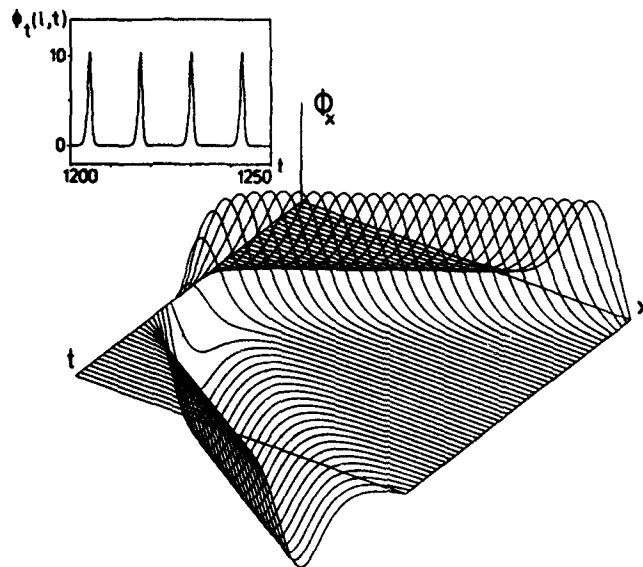


Fig. 5.5: Numerical simulation of equation (5.5) with $\alpha=0.05$, $\beta=0.02$, $\gamma=0.35$ and $L=6$. A period of spatial propagation corresponds to approximately 10 time units [32].

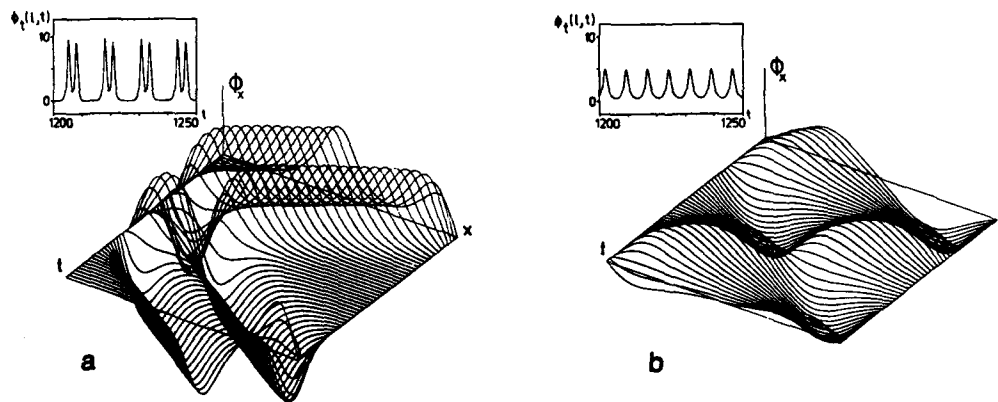


Fig. 5.6: Numerical simulation of equation (5.5) for the dynamic state of the 2nd ZFS. a) The two fluxons propagate towards the same direction $\alpha=0.05$, $\beta=0.02$, $\gamma=0.3$ and $L=6$ b) The fluxon and antifluxon propagate towards opposite directions $\alpha=0.005$, $\beta=0.02$, $\gamma=0.125$ and $L=6$.

double the value of the 1st ZFS. In contrast, the maximum current is slightly smaller than that of the 1st ZFS and this is due to the fact that the dynamic state of two fluxons is less stable than the state of one fluxon. In figure 5.7 we symbolically represent the fluxon's path for the several dynamic states of 1st and 2nd ZFS. We can also obtain such pictures for the next ZFS's, where their representation is more complicated [32].

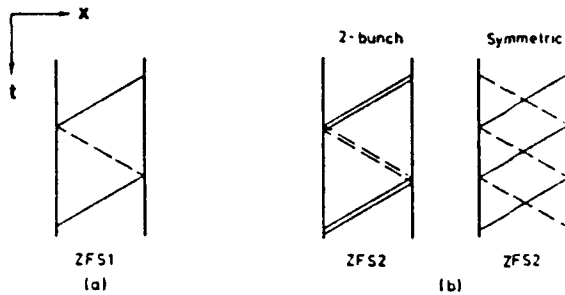


Fig. 5.7: Paths of fluxons while they propagate on the LJJ [27].

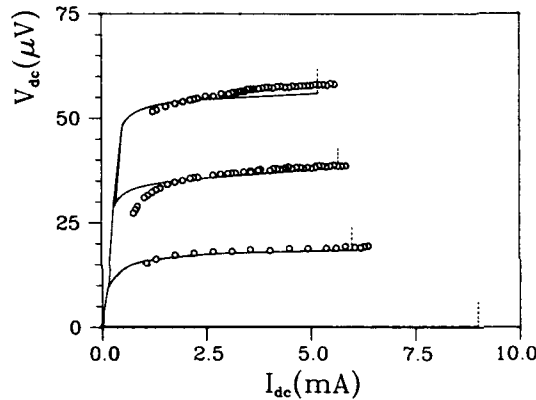


Fig. 5.8: I-V characteristic for a LJJ. The circles indicate experimental results while the continuous lines numerical results [28].

The comparison between numerical results which are obtained from equation (5.5) and experimental results is very satisfactory. In figure 5.8 we show such a comparison.

5.4 Estimate of emitted power

Since for most of the applications the soliton microwave oscillator is biased on one of the ZFS's it is of interest here to make a very rough estimate of the potential available power. Let us for simplicity assume a 100 GHz soliton oscillator in Niobium technology. The length L would be about $50 \mu\text{m}$ and the voltage of the first ZFS about $200 \mu\text{V}$. With reasonable values of the tunneling current density the junction could carry 200 mA with bias on the first ZFS. The power delivered from the bias circuit to the junction is then $4 \mu\text{W}$. A good fraction of that power (for example $1 \mu\text{W}$) exists as intrinsic power in the junction at the fundamental frequency. With a good coupling circuit about 10% ($0.1 \mu\text{W}$) could be coupled to an external circuit. This power can be enhanced considerably by biasing on higher order ZFS's or by phase locking several long Josephson junctions. Incidentally we note from our simple estimate that for the soliton oscillator the power increases with frequency since the voltage of the ZFS increases. This is an unusual property of any high frequency oscillator.

On the other hand it may be difficult to obtain a 10% coupling efficiency specially at the higher frequencies. Very elaborate microwave designs are necessary to bridge the gap from the transmission line to the 100 Ohm level of traditional microwave components and antennas. In the next section we will discuss various designs and the results that have actually been obtained experimentally.

IV. EXPERIMENTAL RESULTS

6.1 Single Soliton oscillators

A soliton bouncing back and forth in a long junction is perhaps the simplest way of realizing a local oscillator. A schematic drawing is shown in figure 6.1. When the soliton is reflected at the right end of the junction a fraction of the power is coupled to the microstrip. Since this crude coupling scheme only gives a very weak coupling, it is possible to study the bare fluxon motion by coupling the microstrip to a conventional microwave receiver. This was done for example in [33], where it was realized, that multisoliton propagation could take place. Such multisoliton motion may keep the fundamental oscillator frequency unchanged but enhances the power emitted, since more solitons are involved. The crude coupling shown in figure 6.1 does not provide enough power to be useful as a local oscillator however. A typical number at 10 GHz is 10^{-11} - 10^{-13} Watt. To provide more power more elaborate coupling schemes such as cavity coupling, slot lines, etc. must be used.

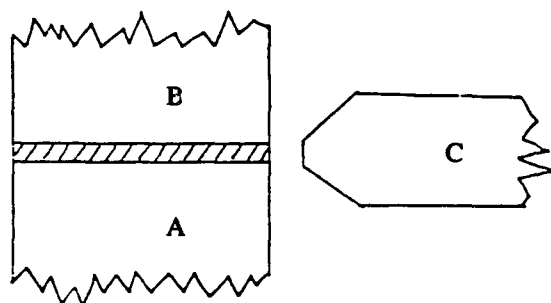


Fig. 6.1: Schematic drawing of a soliton oscillator. Films A and B overlap and are separated by a thin insulator layer. C is the microstripline.

The simple setup shown in figure 6.1 also made it possible to obtain a measurement of the linewidth of the radiation [34]. Again at 10 GHz this turned out to be of order of a few kHz, which is a very satisfactory number. Of course at 10 GHz many other techniques can be used to produce narrow linewidth oscillators, however, the single junction soliton oscillator can easily be scaled to 100 GHz, or even 500 GHz, without special technological problems. The available power scales at least proportional to the frequency (possible to the square of the frequency) to make it even more useful at higher frequencies. At 35 GHz output powers of order tens of nanowatts was measured in a single junction soliton generator [35].

A more elaborate coupling scheme may include the use of a resonant circuit between the long junction and the microstrip in figure 6.1. Recently numerical simulations have been performed [36] with the purpose of studying the interaction mechanism between a long junction and a cavity. These simulations demonstrated that it was possible to have a soliton phase lock to the cavity at its resonance frequency. In that process power was delivered to the cavity thereby charging it.

With the cavity further coupled to a microstrip circuit the power could be coupled out. A typical problem in connection with coupling the power out is that the long Josephson junction often has an impedance level below $1\ \Omega$ while the microstrip circuit has an impedance level of order $50\ \Omega$. Thus either cavity coupling or microstrip impedance transformers or a combination must be used. Figure 6.2 shows a clever design used by the group in Salerno, Italy [37]. It incorporates a resonant structure one half wavelength long and a microslot line. This circuit will be dealt with in more detail below.

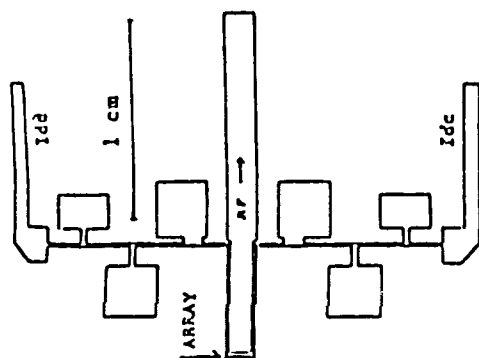


Fig. 6.2: Sample and stripline geometry for the 20 junction array used in [37].

For some local oscillator applications (for example some parametric amplifiers) the impedance level of the receiving end is also low. Thus both the local oscillator and the parametric amplifier or mixer may be on the same chip and $50\ \Omega$ circuits at microwave frequencies can be avoided altogether. The coupling loss from the long Josephson junction can be reduced considerably. In such an experiment with both the soliton generator and the detector on the same chip Cirillo et al [38] measured about $0.1\ \mu\text{W}$ generated at about $75\ \text{GHz}$.

It should be kept in mind however, that for many applications, including astronomy, the impedance level of incoming signals (antenna) is hundreds of ohms so that somewhere the inconvenient impedance transformation must be made.

A quite different single junction single fluxon oscillator was described by Sakai et al [39]. In this remarkable experiment a circular long Josephson junction with a load resistor in one end and a feedback resistor between the two ends was used, and the oscillation waveform at $24\ \text{GHz}$ was measured by using a superconducting (Josephson junction) sampling circuit.

6.2 Coupled (phase-locked) soliton oscillators

If two soliton oscillators can be synchronized to phase-lock the output voltage would double and hence the power increase a factor of 4. With N junctions locked the

output power would increase as N squared. In a remarkable experiment by the Salerno group [37,40] they used 20 long junctions and obtained as much as $0.35 \mu\text{W}$ at x-band in a 50Ω line. This is more than adequate for driving an SIS mixer or a Josephson junction parametric amplifier. Linewidths down to about 5 kHz were measured. The coupling scheme they used is the one shown in figure 6.2.

The success of the above experiment is remarkable, however the details of the phase-locking is not understood. For example, do the junctions couple along their long parallel sides or can interaction only take place at the ends, where solitons are reflected and electromagnetic generation created? Presently experimental work with a simple system consisting of only two junctions is being pursued to clarify this question [41].

Numerically the interaction of two long junctions end-coupled to each other through a common cavity has been studied in [36]. An example of such phase-locking is shown in figure 6.3, which displays quite clearly the synchronization (with a small phaseshift) of the solitons in the two junctions, even though the damping parameters were chosen 10% different in the two junctions. The interaction mechanisms between the two junctions and the cavity is quite complicated: in parts of the period current is transferred from a junction to the cavity, and in other parts the current direction is reversed [36]. Coupling circuits other than a cavity have been studied in [42] (inductance, including experiments), [43] (capacitance) and [44] resistance. In an approximate manner, described in [45], a system consisting of 8 long junctions coupled to the same cavity was investigated [46].

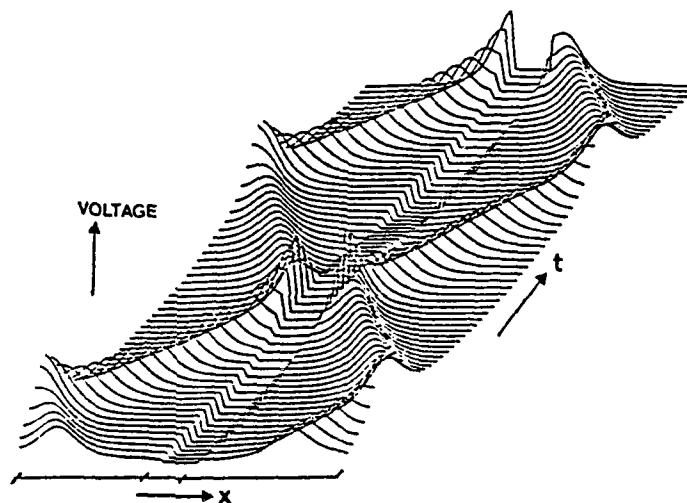


Fig. 6.3: Synchronization of two solitons through a cavity in the middle of the line.

It should be noticed that the Salerno group also tried a 100 junction sample. In this case however only very few junctions coupled, and only little output power was measured. Because of the success with the basic 20 junction circuit we expect more work in this direction in the future.

6.3 Flux flow oscillators

A device that is somewhat similar to the single long Josephson soliton oscillator is the so called flux flow oscillator developed and described in a series of important papers by the Japanese group at Kyushu University [47,48,49,50]. In the flux flow oscillator a magnetic field is applied to the long Josephson junction, and the almost symmetric configuration considered in sections 6.1 and 6.2 is broken. Fluxons are created in one end of the junction and annihilated in the other end, i.e. transferred to an external circuit. With a sufficiently large magnetic field the pulse character of the individual fluxons is changed to an overlapping train of fluxons propagation in one direction. The results that have been obtained are impressive [48,49,50]. In a low impedance receiver on chip was measured about $1 \mu\text{W}$ tunable between 100 GHz and 500 GHz by means of the magnetic field. No direct experimental measurement of the linewidth has been obtained, in [49] an estimation based on the dynamic resistance of the zero field step predicts the possibility of a linewidth of a few kHz.

In summary the flux flow oscillator seems to be very well developed by the Japanese group and should be mature for applications. Work has been taken up by other groups such as described in [51].

6.4 Small single Josephson oscillators

The main reason for using the long Josephson junction oscillators instead of small junction ones is firstly the narrower linewidth, but also the larger potential power. Nevertheless it is worth briefly considering the situation if small Josephson junctions are used. In the next section dealing with coupled (phase-locked) small see that such samples are certainly competitive for use as microwave generators.

A single junction generator is discussed in [52]. The high current density oscillator junction produces $0.5 \mu\text{W}$ of radiation and about 10 nW is coupled to an on chip detector. The frequency is from 300 GHz to well above 1 THz. There are no results for the linewidth, but it is expected to be large compared with the numbers cited in the previous sections.

6.5 Phase-locked arrays of small junctions

By phase-locking an array of small junction [53,54] it is possible to increase the emitted power by a factor N squared and decreasing the linewidth by $1/N$ where N is the number of phase-locked junctions ([53] is good for references on the subject of arrays of junctions).

Typically the junctions must be very small and have large current density, and the coupling circuitry tends to be complicated; fabrication involves E-beam lithography. However, recent results [55] are very promising. A 40 junction array delivered up to $1 \mu\text{W}$ of power into a 60Ω on chip detector at frequencies about 350-380 GHz, and the potential for higher power and higher frequencies exists. No measurement of the linewidth were reported [55] however earlier work at lower frequencies has confirmed the $1/N$ dependence of the linewidth [53]. Even so we expect the linewidth to be larger than the kHz results reported for long Josephson junctions.

6.6 Integrated amplifier

The ultimate aim is to build an on chip receiver with local oscillator, mixer/-amplifier, if circuit, filters and antenna on the same chip. Work in this direction is taking place in several countries, but no finished system has been reported yet.

VII. CONCLUSIONS AND DISCUSSION

The properties of the sine-Gordon equation for fluxon motion on the Josephson transmission line were discussed. The dynamics was visualized by a comparison to a mechanical system with simple properties, the chain of coupled pendula. From all the SG equation solutions, these who conserve their physical importance in a realistic system as that of one LJJ are the fluxon/antifluxon solutions. The LJJ is a typical nonlinear system, where one can study experimentally all the known phenomena of Nonlinear Physics, starting from solitons and ending in chaos [56-58]. Many aspects of this Physics are not discussed here, especially those who are related with recent theoretical and experimental results involving new interesting applications.

One ultimate aim of this research is to utilize the fluxon motion in Josephson transmission line for the purpose of constructing an oscillator at millimeter and submillimeter frequencies. The state of the art for such oscillators was discussed by reviewing the experimental results obtained so far. It is concluded that in order to have a margin in power for the use as local oscillators in superconducting receivers, phase locking of several long Josephson junctions may offer an advantage.

The role of the recently discovered high transition temperature superconductors may be very important in the future. This is because the frequency range may potentially be extended by factor of 10 to the 10 THz range, and further cooling problems may be simplified considerably. However, the fundamental component "the thin film superconductor-insulator-superconductor Josephson junction" has not yet been made for those very complicated ceramic materials. If such junctions become available there are reasons to believe that the formulas derived here will still be applicable, although of course the materials parameters are changed.

Acknowledgments

It is a pleasure to acknowledge discussions and assistance on the preparation of the manuscript by Stavros Protogerakis (University of Crete). We also acknowledge the permission to use many plots from the references [7,8,22,27,28]. This work was supported by the EEC stimulation grant: ST2J-0267-C and a H.E.N.E. Δ. program of the Greek Ministry for Research and Technology.

REFERENCES

- [1] A.C. Scott, F.Y.F. Chu and D.W. McLaughlin: "The Soliton: A new concept in Applied Sciences", Proc. IEEE, 61(10) (1973) 1443.

- [2] D.W. McLaughlin and A.C. Scott: "Perturbation analysis of fluxon dynamics", *Phys. Rev. A*, 18(4) (1978) 1652.
- [3] N.F. Pederson: "Solitons in Josephson Transmission Lines", Ch.9, p.p. 469-501, in "Solitons", eds. S.E. Trullinger et al (Elsevier Science Publ. B.V. 1986).
- [4] St. Pnevmatikos: "Sine-Gordon solitons and long Josephson Junctions", lectures at the European Erasmus graduate program: "Mathematics and Fundamental Applications", University of Thessaloniki, 1988.
- [5] Yu.S. Kivshar and B.A. Malomed: "Dynamics of solitons in nearly integrable systems", *Rev. Mod. Phys.* 61 (1989) 763.
- [6] A.C. Scott: "A nonlinear Klein-Gordon equation", *Am. J. Physics*, 37(1) (1969) 52.
- [7] A. Barone and G. Paterno: "Physics and applications of the Josephson effect" (J. Wiley, New York 1982).
- [8] R.K. Dodd, J.C. Eilbeck, J.D. Gibbon and H.C. Morris: "Solitons and nonlinear wave equations" (Academic Press, London 1982).
- [9] A.S. Davydov: "Solitons in molecular systems" (D. Reidel, Dordrecht 1985).
- [10] G.L. Lamb, Jr: "Elements of Soliton theory" (J. Wiley, New York 1980).
- [11] P.F. Byrd and M.D. Friedman: "Handbook of Elliptic Integrals", 2nd edition (Springer, Berlin 1971).
- [12] R.D. Parmentier: "Fluxons in long Josephson junctions", p.173, in "Solitons in Action", eds. K. Lonngren and A.C. Scott, (Academic Press, New York 1978).
- [13] G. Costabile, R.D. Parmentier, B. Savo, D.W. McLaughlin and A.C. Scott: "Exact solutions of the sine-Gordon equation describing oscillations on a long (but finite) Josephson junction", *Appl. Phys. Lett.*, 32 (1978) 587.
- [14] M.J. Ablowitz, D.J. Kaup, A.C. Newell and H. Segur: "Method for solving the sine-Gordon equation", *Phys. Rev. Lett.* 30 (1973) 1262.
- [15] L.A. Takhtadzhyan and L.D. Faddeev: "Essentially nonlinear one-dimensional model of classical field theory", *Theor. Math. Phys.* 21 (1974) 1046.
- [16] H.K. Onnes, *Commun. Phys. Lab., Univ. Leyden*, Nos. 119, 120, 122, (1911).
- [17] J. Bardeen, L.N. Cooper and J.R. Schrieffer: "Theory of Superconductivity", *Phys. Rev.* 108 (1957) 1175.
- [18] B.D. Josephson: "Possible new effects in superconductivity tunneling", *Phys. Lett.* 1 (1962) 251.
- [19] P.W. Anderson and J.M. Rowell: "Probable Observation of the Josephson Superconducting Tunnel Effect", *Phys. Rev. Lett.* 10 (1963) 230.

- [20] R.P. Feynman, R.B. Leighton and M. Sands: "The Schrödinger equation in a classical context: a seminar on Superconductivity", *The Feynman Lectures on Physics*, Vol. III, chapt. 21 (Addison-Wesley 1965).
- [21] S. Shapiro: "Josephson currents in superconducting tunneling: The effect of microwaves and other observations", *Phys.Rev.Lett.* 11 (1963) 80.
- [22] S. Pagano: "Nonlinear dynamics in long Josephson junctions", PhD thesis (report no. S42), The Technical University of Denmark, 1987.
- [23] K.K. Likharev: "Dynamics of Josephson junction and circuits" (Gordon and Breach, New York 1986).
- [24] J.C. Swihart: "Field solution for a thin film superconducting strip transmission line", *J.Appl.Phys.*, 32 (1961) 461.
- [25] A.C. Scott, F.Y.F. Chu and S.A. Reibel: "Magnetic flux propagation on a Josephson Transmission Line", *J.Appl.Phys.* 47 (1976) 3272.
- [26] A. Matsuda and S. Uehara: "Observation of fluxon propagation on Josephson transmission lines", *Appl.Phys.Lett.* 41 (1982) 770.
- [27] M.P. Soerensen: "Josephson junctions and sine-Gordon systems", PhD Thesis (report no. S27), The Technical University of Denmark, 1984.
- [28] P.S. Lomdahl: "Solitons in Josephson Junctions: An Overview", *J.Stat.Phys.* 39(5/6), 551-561, 1985; P.S. Lomdahl, O.H. Soerensen and P.L. Christiansen: "Soliton excitations in Josephson tunnel junctions", *Phys.Rev.B*, 25(9) (1982) 5737.
- [29] M.D. Fiske: "Temperature and magnetic field dependence of the Josephson tunneling current", *Rev.Mod.Phys.* 36 (1964) 221.
- [30] J.T. Chen, T.F. Finnegan and D.N. Langenberg: "Anomalous d.c. current singularities in Josephson tunnel junctions", *ICSS*, 413 (1969); see also *Physica* 55 (1971) 413.
- [31] T.A. Fulton and R.C. Dynes: "Single vortex propagation in Josephson tunnel junction", *Solid State Commun.* 12 (1973) 57.
- [32] P.S. Lomdahl: "Soliton dynamics in non-integrable sine-Gordon systems", PhD Thesis, (report no S20), The Technical University of Denmark 1982.
- [33] B. Dueholm, O.A. Levring, J. Mygind, N.F. Pedersen, O.H. Soerensen and M.Cirillo: "Multisoliton excitations in long Josephson junctions", *Phys.Rev. Lett.* 46 (1981) 1299.
- [34] E. Joergensen, V.P. Koshelets, R. Monaco, J. Mygind, M.R. Samuelsen and M. Salerno: "Thermal fluctuations in resonant motion of fluxons on a Josephson transmission line: Theory and experiment", *Phys.Rev.Lett.* 49 (1982) 1093.
- [35] G. Hohenwarter: Private communication.

- [36] N. Groenbech-Jensen, N.F. Pedersen, A. Davidson and R.D. Parmentier: "Numerical study of long Josephson junctions coupled to high Q cavity", Appl. Phys.Lett. (submitted).
- [37] S. Pagano, R. Monaco and G. Costabile: "Microwave oscillator using arrays of long Josephson junctions", IEEE Trans. Mag. MAG-25, 1080 (1989); G. Costabile, D. Andreone and V. Lacquaniti: "Series array of highly hysteretic Josephson junctions coupled to a microstrip resonator", J.Appl.Phys. 58 (1985) 1072.
- [38] M. Cirillo, I. Modena, P. Carelli and V. Foglietti: "Millimeter wave generation by fluxon oscillations in a Josephson Junction" J.Appl.Phys. 65 (1989) 2376.
- [39] S. Sakai, H. Akoh and H. Hayakawa: "Fluxon feedback oscillator", Jpn. J.Appl.Phys. 23 (1984) L610.
- [40] R. Monaco, S. Pagano and G. Costabile: "Superradiant emission from an array of long Josephson junctions", Phys.Lett. A131 (1988) 122.
- [41] T. Holst, J. Bindslev Hansen, N. Groenbech-Jensen and J.A. Blackburn: "Phase locking between Josephson soliton oscillators", Preprint, 1989.
- [42] M. Cirillo: "Inductively coupled fluxon oscillators", J.Appl.Phys. 58 (1985) 3217.
- [43] H.S. Newman and K.L. Davis: "Fluxon propagation in Josephson junction transmission lines coupled by resistive network", J.Appl.Phys. 53 (1982) 7026.
- [44] M. Cirillo, A.R. Bishop, P.S. Lomdahl and S. Pace: "Analysis of the capacitive coupling of Josephson transmission lines", Phys.Rev. B39 (1989) 4804.
- [45] N. Groenbech-Jensen, R.D. Parmentier and N.F. Pedersen: "Phase locking of fluxon oscillations in long Josephson junction coupled through a resonator", Phys.Lett. A. 142 (1989) 427.
- [46] N. Groenbech-Jensen, R.D. Parmentier and N.F. Pedersen, under preparation.
- [47] T. Nagatsuma, K. Enpuku, F. Irie and K. Yoshida: "Flux-flow type Josephson oscillator for millimeter and submillimeter wave region", J.Appl.Phys. 54 (1983) 3302.
- [48] T. Nagatsuma, K. Enpuku, K. Yoshida and F. Irie: "Flux-flow-type Josephson oscillator for millimeter and submillimeter wave region II. Modeling", J.Appl.Phys. 56 (1984) 3284.
- [49] T. Nagatsuma, K. Enpuku, K. Sueoka, K. Yoshida and F. Irie: "Flux-flow-type Josephson oscillator for millimeter and submillimeter wave region III. Oscillation stability", J.Appl.Phys. 58 81985) 441.
- [50] J. Qin, K. Enpuku and K. Yoshida: "Flux-flow-type Josephson oscillator for millimeter and submillimeter wave region IV. Thin film coupling", J.Appl. Phys. 63 (1988) 1130.

- [51] Y.M. Zhang, P.H. Wu and T. Claeson: "Numerical calculation of the height of velocity matching step of flux flow type Josephson oscillator", Preprint 1989.
- [52] P. Robertazzi and R.A. Buhrman: "NbN Josephson tunnel junctions for Terahertz local oscillators", Appl.Phys.Lett. 53 (1988) 2441.
- [53] A.K. Jain, K.K. Likharev, J.E. Lukens and J.E. Sauvageau: "Josephson junction array", Phys.Rep. 109 (1984) 309.
- [54] P. Hadley, M.R. Beasley and K. Wiesenfeld: "Phase locking of Josephson junction series arrays", Phys.Rev. B38 (1988) 8712.
- [55] J.E. Lukens, A.K. Jain and K.L. Wan: "Applications of Josephson effect arrays for submillimeter sources", Nato ASI (1988); K. Wain, A.K. Jain and J.E. Lukens: "Submillimeter wave generation using Josephson junction arrays", Appl.Phys.Lett. 54 (1989) 1805.
- [56] N.F. Pedersen: "Noise and Chaos in Josephson junctions", Physica Scripta, TL3 (1986) 129.
- [57] G. Reinisch, J.C. Fernandez, N. Flytzanis, N. Taki and St. Pnevmatikos: "Phase-lock of a weakly biased inhomogeneous long Josephson junction to an external microwave source", Phys.Rev. B, 38 81988) 11284.
- [58] T. Bountis and St. Pnevmatikos: "Josephson junction dynamics in the presence of inhomogeneities", Phys.Lett. A, 143 (1990) 221.

STATIC SOLUTIONS OF A TWO DIMENSIONAL JOSEPHSON WINDOW JUNCTION

J. G. Caputo ¹, M. Devoret ² and N. Flytzanis ³

¹ LMI, INSA, BP 8, 76131 Mont-Saint Aignan cedex France

² CEA, CEN, Saclay, France

³ Physics Department, University of Crete, Iraklion, Greece

Abstract

We studied the static "soliton" solutions of a two dimensional window Josephson junction. The junction is surrounded by a region with no tunneling with inductive properties similar or different from the window. We have varied the aspect ratios of the junction and its environment with respect to the Josephson characteristic length λ_J . In all cases the fluxon width is much larger than λ_J . It depends in a complicated way on the geometry when λ_J is smaller than the width of the junction. On the contrary for long and narrow junctions it increases like λ_J^2 . This strong increase of the fluxon width leads to its destruction due to the finiteness of the junction.

A simplified but rather successful modeling of the fluxon dynamics in a one dimensional Josephson junction is the sine-Gordon equation [1,2,3] describing the phase difference of the Cooper pair condensate in the superconducting films. However in a particular device called a window junction one should expect important two dimensional effects to appear [4]. Such a junction consists of an active window surrounded by an "idle" region with no tunneling. This will modify the properties of the junction. This geometry allows for better quality junctions [4,5], in particular the edges are better defined and don't deteriorate with time as shown by the LTSEM technique [6]. In this paper we consider the static fluxon solution in a window junction with zero bias current and magnetic field. The I-V characteristics of a junction depend also on static properties i.e. the static field configuration. In the one dimensional case this is adequately given by the sine-Gordon static kink of width λ_J . For the general window junction the phase $\phi(x,y)$ will not be describable with a few parameters. There are however geometries in which this is possible. It should also be mentioned that these fluxons are marginally stable when the junction is infinite. The numerical algorithms

used [7,8] preserve the initial antisymmetric character of the solution. Besides small external fields can stabilise these solutions which are a good description of a low velocity kink away from the boundaries.

The method of solution presented here is a downhill minimisation of the total energy starting from a pure sine-Gordon kink solution E consists of a magnetic like energy due to the surface currents E_m and the Josephson part E_j :

$$E = \sum_{i \neq j} \frac{1}{2L_{ij}} (\phi_i - \phi_j)^2 + \sum_i \frac{I_{ji}}{\lambda_j^2} (1 - \cos(\phi_i)) \quad (1)$$

where L_{ij} is the inductance between sites i and j and the summation is on nearest neighbors only. We have used a two dimensional distributed Josephson circuit model with grid size a . The dimensions of the window are $l \times w$, those of the idle region $L \times W$. The parameter I_{ji} is the critical current inside the window and zero outside. Here L_{ij} will be considered uniform. This discrete model can be shown to be completely equivalent to Maxwell's equations and the Josephson constitutive equation. In this model the normal derivative is zero on the outside boundary and the normal component of the surface current is continuous across the junction boundary.

In an infinite one dimensional junction with no idle region the non-dimensional phase is given by:

$$\phi(x) = 4 \tan^{-1}(e^{-\frac{x}{\alpha}}) \quad (2)$$

with $\alpha = \lambda_j$ the fluxon width. The dimensionless Josephson and magnetic energies are:

$$E_j = \frac{4\alpha}{\lambda_j^2} \quad (3.a)$$

$$E_m = \frac{4}{\alpha} \quad (3.b)$$

Minimising the total energy with respect to α gives as expected $\alpha = \lambda_j$ and $E_j = E_m$. The same result holds true if the junction is two dimensional with no idle region except that the expressions in (3) are multiplied by w . In a more general two dimensional geometry the phase lines outside the junction will be spread out since this minimises the gradient of ϕ , the Josephson energy will be minimum for $\phi = 0$ or 2π and this will tend to reduce the width of the kink. The competition of these two effects leads to phase lines that are strongly curved as they leave the junction.

For a large idle region one can distinguish two regions depending if the ratio $\frac{\lambda_j}{w}$ is smaller or greater than 1. In the former case there is a significant transverse structure of the phase in the junction. The phase cannot except for some specific geometries be described by a few parameters. The width of the kink increases faster than linearly with λ_j . When the ratio $\frac{\lambda_j}{w}$ becomes greater than 1 the phase lines in the junction become straight. This geometry in the case where λ_j is much smaller than the length of the junction l is amenable to a simple modeling. The magnetic energy in the idle region can be computed by using the analogy of two conductors of finite length l and infinitely small width placed on a line such that they are at a distance 2α of each other. The two conductors are at potentials 0 and 2π respectively. The field can be obtained by conformally mapping the upper half-plane to a rectangular domain where the field is constant [9]. The energy is then given in terms of elliptic integrals and reduces when $\frac{\lambda_j}{w}$ becomes small to:

$$E_m = 4\pi \ln\left(\frac{l}{2\alpha}\right) \quad (4)$$

which is the energy contained within a circle of diameter l . The convergence of the energy to (4) is fast so that it holds within 10 % even when $\frac{a}{l}$ is about .2.

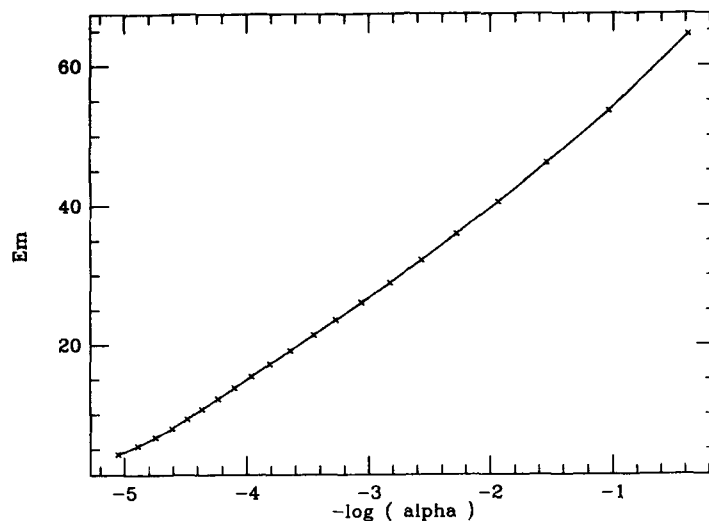


Figure 1: The magnetic energy vs. $\log(\alpha)$ for a long narrow junction in a wide environment. ($l=351$, $w=3$, $L=601$, $W=353$)

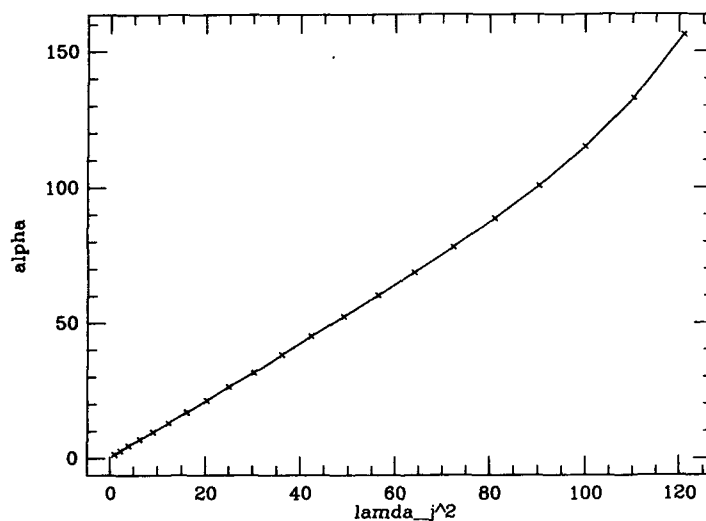


Figure 2: α as a function of λ_j^2 for the long narrow junction of figure 1.

Because the phase lines are approximately straight in the junction the Josephson energy can be approximated by (3.a) in which the right hand side is multiplied by w . Minimising the total energy with α we obtain

$$\alpha = \frac{\pi}{w} \lambda_j^2 \quad (5)$$

i.e. the soliton width varies quadratically with λ_j in this particular geometry. Figure 1 shows the magnetic energy vs. $\ln\alpha$ obtained by varying λ_j . It can be seen that for a

wide range of values of λ_j the curve is linear with a slope close to 4π . The departure from linearity at large λ_j is due to the soliton being affected by the boundary while for small λ_j the shape of the phase in the junction is crucial to define the magnetic energy [7]. Figure 2 shows α vs. λ_j^2 and the region where the curve is linear is consistent with the linear portion in figure 1. The slope is very close to $\frac{\pi}{w}$. The agreement with (4) is very good and is due to the fact that when λ_j becomes larger than w the magnetic energy in the junction becomes much smaller than the one in the idle region. In figure 3 we plot the contour lines of the phase field in the junction. Some lines are closed indicating for example that the region where $\phi = 0$ is surrounded by a region where $\phi > 0$. It is then possible that an increase of λ_j leading to an increase of the width of the soliton can cause its annihilation.

In the study presented above the size of the idle region was large so that there could be no influence from the boundaries. In realistic situations the idle region is not so large. It is therefore expected to change significantly the magnetic energy because the contributions from the electrical images of the junction will be significant. This effect is currently being investigated together with the dynamic behavior of these fluxons.

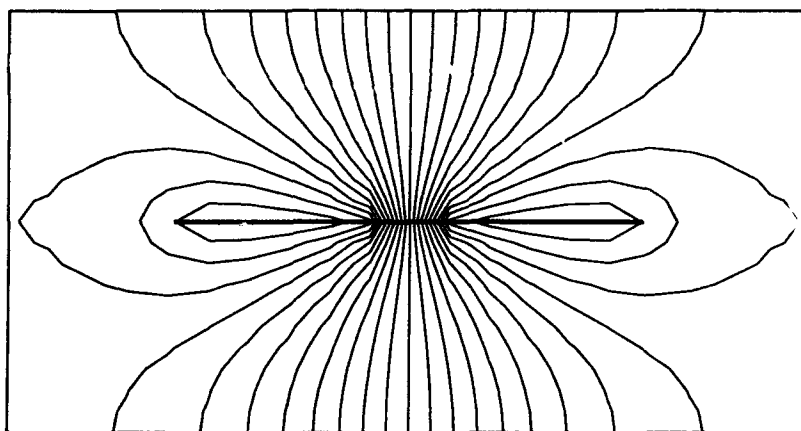


Figure 3: Contour lines of the phase for the junction of figure 1 with $\lambda_j = 4$. The computed phase field has been scaled down for representation.

Acknowledgements

This work is supported by the EEC Science project Number SC1*-CT91-0760 and a Greek-French collaboration agreement. The authors acknowledge many discussions with G. Reinisch, J. C. Fernandez and C. Roblin.

REFERENCES

- [1] A. C. Scott, F. Y. Chu and S. A. Reible, *J. Applied Physics* **47**, 3272, (1976)
- [2] A. Barone and G. Paterno, "Physics and applications of the Josephson effect", Wiley Interscience, New York (1982)
- [3] R. D. Parmentier in "Solitons in action", Academic Press New York (1978), p. 173
- [4] J. M. Pritchard and W. H. Schroen, *IEEE, Trans. Mag. MAG-4*, 320, (1968)
- [5] A. Ustinov, private communication
- [6] R. P. Huebener, *Rep. Prog. Phys.* **47**, 175, (1984)
- [7] J. G. Caputo, M. Devoret and N. Flytzanis, preprint
- [8] M. Vavalis, J. G. Caputo and N. Flytzanis, preprint
- [9] K. J. Binns and P. J. Lawrenson, "Analysis and computation of electric and magnetic field problems", Pergamon Press, (1973)

FLUXON OSCILLATIONS IN A PARALLEL BIASED ARRAY OF SMALL JOSEPHSON JUNCTIONS

G. Costabile and P. Sabatino

Dipartimento di Fisica
Universita' di Salerno
I-84081 Baronissi, Italy

INTRODUCTION

The purpose of this paper is to report some of the results obtained from the numerical simulation of the dynamical behaviour of a parallel biased array of small Josephson junctions. The interest for this topic was stimulated by the participation of the authors to a research program concerning the flux flow in grain boundary junction arrays, that is going to be started with the support of the EEC. Moreover, since the model equations are essentially the same as the ones obtained to integrate numerically the Perturbed Sine Gordon Equation, which models the dynamics in long Josephson junctions,¹ there was some interest to explore the effects originated by an extreme spatial discretization. The emphasis has been put on the calculation of I-V characteristics and their interpretation, in order to compare the results of the simulations with the experimental work in progress in our laboratory.

THE MODEL

Let us consider an array of N parallel biased Josephson junctions (JJ) (Fig.1) consisting on $N-1$ superconductive loops of equal area, each incorporating two JJ's. In what follows we will assume that the bias current is uniformly distri-

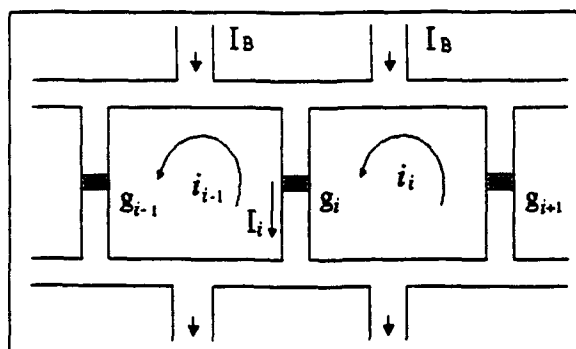


Figure 1. Geometry of the parallel biased Josephson junctions array.

buted and that no external magnetic field is applied. With these hypotheses, imposing the fluxoid to be quantized in each loop, we obtain from the RSJ model¹ the following differential equation for the time evolution of the quantum phase difference φ_i across the i -th JJ:

$$\ddot{\varphi}_i + \alpha \dot{\varphi}_i + \sin(\varphi_i) - \beta^{-1}(\varphi_{i-1} - 2\varphi_i + \varphi_{i+1}) - \gamma = 0 \quad (1 < i < N). \quad (1)$$

Here $\gamma = I_B/I_0$ is the bias current normalized to the junction critical current, the time is normalized with respect to the inverse of the plasma frequency $\omega_J = (2eI_0/\hbar C)^{-1/2}$, $\alpha = (\omega_J RC)^{-1}$ is the damping parameter depending on the quasiparticle resistance R and the junction capacitance C and $\beta = 2\pi LI_0/\Phi_0$, where L is the loop inductance and Φ_0 is the magnetic flux quantum. For the first and the last junctions one must take into account that they are not comprised between two contiguous loops. Therefore, their equations take the form:

$$\ddot{\varphi}_1 + \alpha \dot{\varphi}_1 + \sin(\varphi_1) - \beta^{-1}(\varphi_2 - \varphi_1) - \gamma = 0 \quad (2)$$

and

$$\ddot{\varphi}_N + \alpha \dot{\varphi}_N + \sin(\varphi_N) - \beta^{-1}(\varphi_{N-1} - \varphi_N) - \gamma = 0. \quad (3)$$

We observe that, as in the case of a long JJ, the array has a mechanical analog, i.e., a chain of elastically coupled pendula with negligible losses in the springs, but the intrinsic discretization makes more strict the analogy.

THE NUMERICAL RESULTS

The numerical calculations that we report in this paper are based on the following set of parameters: $N=10$, $\alpha=0.25$, $\beta=1$. These parameters are suggested by the opportunity to obtain a realistic simulation of a device made of 10 Nb-AlOx-Nb junctions that will be tested in our laboratory. The system of Eqs. 1,2,3 has been integrated using the Bulirsch-Stoer algorithm² with the error parameter $\epsilon \leq 10^{-6}$. To obtain the I-V characteristics the current γ was incremented in steps of 10^{-3} ; after each increment the system was allowed to run 100 integration steps for the sake of stabilization, then the average voltage was calculated using the successive 200 steps.

In Fig. 2 we show the I-V characteristic of the array calculated assuming as initial conditions $\varphi_i=0$, $\dot{\varphi}_i=0$ ($i=1\dots N$). As expected, it is identical to the I-V characteristic of a single JJ, because static and uniform initial conditions make ineffectual the coupling term in Eqs. 1-3. The dynamics becomes much more interesting if we choose as initial conditions a magnetic flux quantum (or fluxon) trapped in the array, i.e. $\varphi_1, \dots, \varphi_5=0$, $\varphi_6, \dots, \varphi_{10}=2\pi$, $\dot{\varphi}_i=0$. In this case, if we start the integration from $\gamma=0$, the static fluxon turns out to be unstable: we found that the phases realign themselves to a common value (i.e., the fluxon is destroyed) within few integration steps, and the I-V characteristic reduces to the one in Fig. 2. The value of γ at which the static fluxon disappears is a monotonically growing function of β ; when β is increased to about 4, the static fluxon

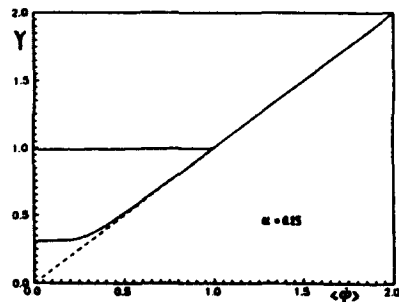


Figure 2. I-V characteristic with uniform initial conditions.

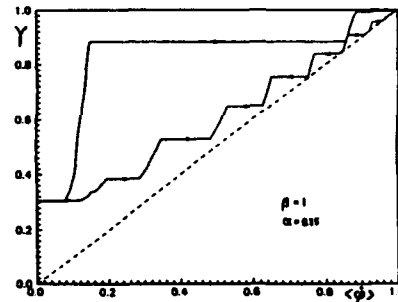


Figure 3. I-V characteristic with one static fluxon as initial conditions.

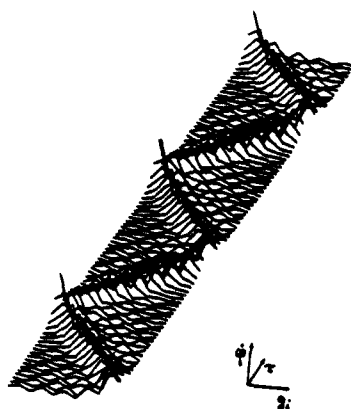


Figure 4. Fluxon oscillations.

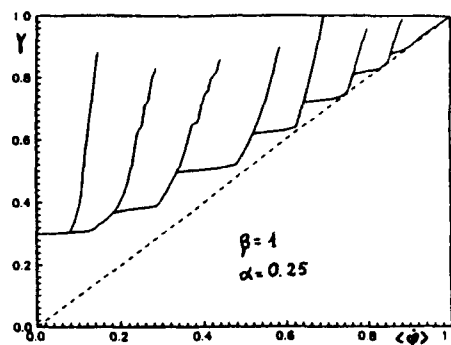


Figure 5. Full I-V characteristic.

stays in the array until γ becomes so large that it starts moving. To generate a steady state with one (or more) stable oscillating fluxon when $\beta < 4$ one must provide from the very beginning a finite amount of energy exceeding some threshold that also depends on α . For $\alpha = 0.25$ and one fluxon in the array the threshold current is $\gamma_s = 0.302$. The calculated characteristic is then shown in Fig.3, where the first vertical branch at nonzero voltage identifies the stable oscillations of a single fluxon. Since the phenomenon retains the same physical meaning as fluxon oscillations in a long JJ, we will refer to this (and to higher voltage branches) as to Zero Field Step¹ (ZFS). The time evolution of the array when biased on the ZFS1 is plotted in Fig.4 that clearly shows the succession of reflections of a fluxon into an antifluxon (and viceversa). In Fig.3 we note that exceeding $\gamma = 0.884$ there is a large voltage jump from the ZFS1; this happens because six more fluxons are suddenly generated. Increasing further γ , the system stays on the ZFS7 until it collapses to the state of uniform rotation of ϕ . Decrementing γ from the ZFS7, the fluxons are progressively lost and therefore the characteristic goes through the lower order ZFS's. From Fig.3 one can deduce the threshold current for each ZFS and calculate the full I-V characteristic (Fig.5) adding successively one static fluxon to the initial conditions for each ZFS to be calculated. The same characteristic was obtained, alternatively, repeating the procedure described above to illustrate the I-V characteristic reported in Fig.3, but increasing again γ whenever, descending the I-V characteristic, the number of fluxons was reduced to the desired value. We remark that, no matter where the fluxons were localized in the array by the initial conditions, the steady state turned out to be the same.

Insofar the dynamics reminds closely the case of a long JJ (but for the large current threshold to start the fluxon motion). But an effect of the strong discretization can be seen on the ZFS2 and the ZFS3 in Fig.5 and, more clearly,

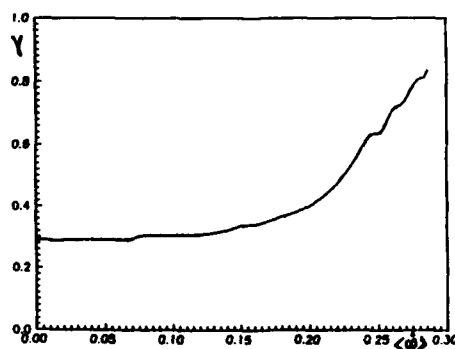


Figure 6. Enlarged view of the ZFS2.

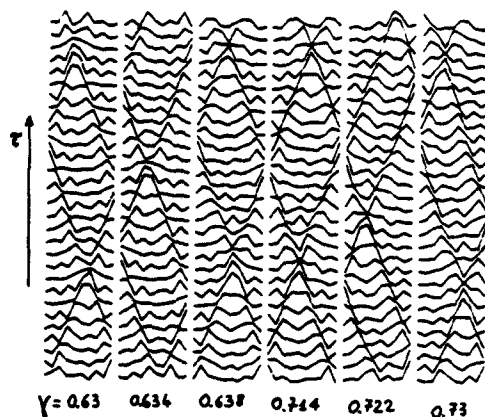


Figure 7. Fluxon-antifluxon collisions on ZFS2.

in Fig.6, which provides an enlarged view of the ZFS2. The evident structure of the step, that is obtained both incrementing and decrementing γ , can be possibly explained analyzing the plots in Fig.7, which shows the time evolution of the voltage across the junctions for values of γ corresponding to the first and the second transition in the structure. It can be seen that in the first case the peak voltage of the fluxon-antifluxon collision, initially localized either on the fourth or on the seventh junction ($\gamma=0.63$), moves to the fifth and the sixth ($\gamma=0.638$); the behaviour is reversed in the second transition ($\gamma=0.714$ and $\gamma=0.73$). In the middle ($\gamma=0.634$ and $\gamma=0.722$), the peak is evenly spread between two JJ's (fourth-fifth and sixth-seventh) and, since it never grows as large as the voltage produced by a collision localized on a junction, less energy is comparatively dissipated, so that a small current increment causes a relatively larger velocity (i.e., voltage) increment.

CONCLUSION

These simulations show that the parallel biased Josephson junction array shares many features with the long Josephson junction, as was expected on the ground of both physical and mathematical considerations. However, it departs to some extent from the well known dynamics of the long junction due to the discretization and to the effect of the large loop inductance. We intend to investigate further this subject and to extend the simulation to the effect on the array of an rf signal.

REFERENCES

1. A. Barone and G. Paternò, "Physics and Applications of the Josephson Effect" Wiley, New York (1967).
2. W.H. Press, B.P. Flannery, S.A. Teukolsky, and W.T. Wetterling, "Numerical Recipes", Cambridge University Press (1986).

LINEWIDTH OF JOSEPHSON OSCILLATIONS IN $\text{YBa}_2\text{Cu}_3\text{O}_{7-x}$ STEP EDGE GRAIN BOUNDARY JUNCTIONS

Yu. Ya. Divin^{1,3,4}, A. V. Andreev^{1,4}, A. I. Braginski²,
G. M. Fischer^{1,5}, K. Herrmann², J. Mygind¹, N. F. Pedersen¹
and M. Siegel²

¹Physics Laboratory I, B 309, Technical University of Denmark
DK-2800 Lyngby, Denmark

²Institut für Schicht- und Ionentechnik, Forschungszentrum Jülich
D-W5170 Jülich, Germany

³Institut für Festkörperforschung, Forschungszentrum Jülich
D-W5170 Jülich, Germany

⁴Institute of Radioengineering and Electronics of the Russian
Academy of Sciences, Moscow 103907, Russia

⁵Lehrstuhl Experimentalphysik II, University of Tübingen
D-W7400 Tübingen, Germany

INTRODUCTION

Recently many different types of high- T_c superconducting weak links have been studied and some of them have shown Josephson behaviour¹. One of the promising types is the step edge grain boundary junction (SEJ)². These junctions are fabricated by epitaxial growth of a high- T_c thin film onto a steep step etched into the substrate. As follows from High Resolution Electron Microscopy (HREM) studies³ the SEJ actually is a series connection of at least two grain boundary junctions formed at the upper and the lower edges of the step. We have studied the ac Josephson effect in $\text{YBa}_2\text{Cu}_3\text{O}_{7-x}$ step edge grain-boundary junctions in the temperature range from 4 K to 90 K. The temperature dependence of the linewidth of millimeter-wave Josephson oscillations was measured and it was shown that the effective noise temperatures of a SEJ may be as low as the physical temperature in the temperature range investigated. An excess $1/f$ -type fluctuation contribution to the observed linewidth may be explained by an inhomogeneous spatial distribution of the current. The SEJ studied may be considered as multi-junction multi-loop interferometers, in which excess noise can be attributed to spontaneous transitions between different states.

EXPERIMENTAL TECHNIQUES

A step of $\sim 120\text{nm}$ height and $\sim 80^\circ$ angle had been etched on a LaAlO_3 substrate by Ar^+ ion milling. Then a $\text{YBa}_2\text{Cu}_3\text{O}_{7-x}$ thin film was deposited by pulsed laser ablation⁴. The width of the junction was defined by patterning 2 to $32\text{ }\mu\text{m}$ wide bridges across the step using photolithography and Ar^+ ion beam etching. The sample holder was placed inside a sealed vacuum can immersed directly in a liquid helium bath. The temperature of the copper sample holder was measured by two calibrated thermometers in connection with a temperature controller. A coil wound around the vacuum can could supply a dc magnetic field perpendicular to the substrate. All data were measured for magnetic fields maximizing the critical current of the SEJ. The cryostat was electrically shielded and surrounded by a double μ -metal shield. All measurement were made in an rf shielded room.

The indirect measurement technique of the Josephson linewidth is the same as used in the study of the linewidth of low- T_c microcontacts⁵. This technique is based on the analytical properties of the voltage dependent response, $\Delta V(V)$, which is the difference between the unperturbed IV -curve and the curve obtained with applied electromagnetic radiation. The response $\Delta V(V)$ shows an odd-symmetric resonance at the voltages $V = \pm(h/2e)f$. The voltage difference, δV , between the maximum value V^+ and the minimum value V^- of the response $\Delta V(V)$ in this region gives us the linewidth δf according to the relation $\delta f = (2e/h) \delta V$.

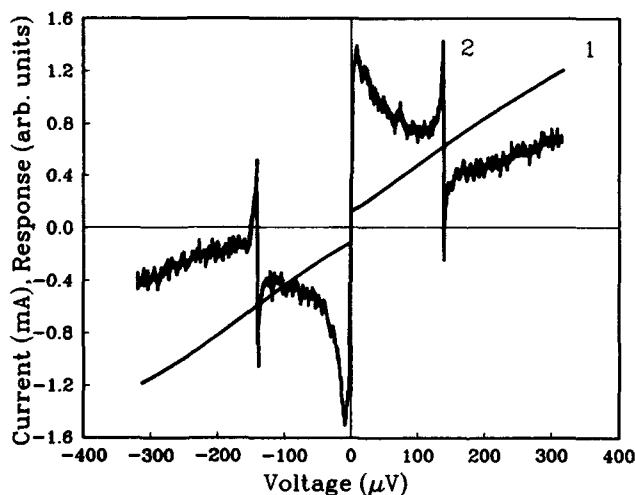


Figure 1: The IV -curve (1) and the voltage response $\Delta V(V)$ (2) to 70.2 GHz irradiation for a $32\text{ }\mu\text{m}$ wide SEJ at 77.3 K.

RESULTS AND DISCUSSION

Figure 1 shows the 77.3 K IV -curve (curve 1) and the voltage response $\Delta V(V)$ (curve 2) to mm-wave radiation with frequency $f = 70.2\text{GHz}$ for a SEJ with the width $W = 32\text{ }\mu\text{m}$. Two odd-symmetric resonances at voltages $V \simeq \pm(h/2e) f = \pm 145\text{ }\mu\text{V}$ were observed on the $\Delta V(V)$ response, thus demonstrating the nonlinear interaction of the weak mm-wave radiation with the Josephson-oscillations. The width, δV , of the resonant structure was $(2.5 \pm 0.4)\text{ }\mu\text{V}$ and this value corresponds to the Josephson linewidth $\delta f = (2e/h)\delta V = (1.2 \pm 0.2)\text{ GHz}$. The measured value of the linewidth is close to the value $\delta f = 0.9\text{ GHz}$ estimated for this SEJ using the RSJ model with Nyquist thermal fluctuations at 77.3 K. In a recent study⁶ of the Josephson oscillation

linewidth in bicrystal grain boundary junctions it was shown that thermal fluctuations could be dominant in the linewidth from liquid nitrogen to liquid helium temperatures, but for the SEJ we find a different temperature behaviour.

At temperatures below 77.3 K the response $\Delta V(V)$ showed an unusual behaviour with applied magnetic fields of the order of 10^{-5} T. Figure 2 shows an example of this at 70.3 K. In order to maximize the resonance response for positive current bias (Figure 2a) and negative current bias (Figure 2b) different magnetic fields were applied. Not only the IV -curve (curve 1) but also the response $\Delta V(V)$ (curve 2) became strongly asymmetric. In some cases no coherent response was observed at negative bias, when the response was maximized at a positive bias (Figure 2a). For some temperatures below 60 K switching and chaotic behaviour in the IV -curves and $\Delta V(V)$ curves were observed. At lower temperatures the IV -curves showed a hysteresis which was dependent on the maximum bias current used in the previous measurement. The linewidth also depended on the applied magnetic field. For example a small decrease in the critical current by the magnetic field could decrease the linewidth by a factor of two at 70 K.

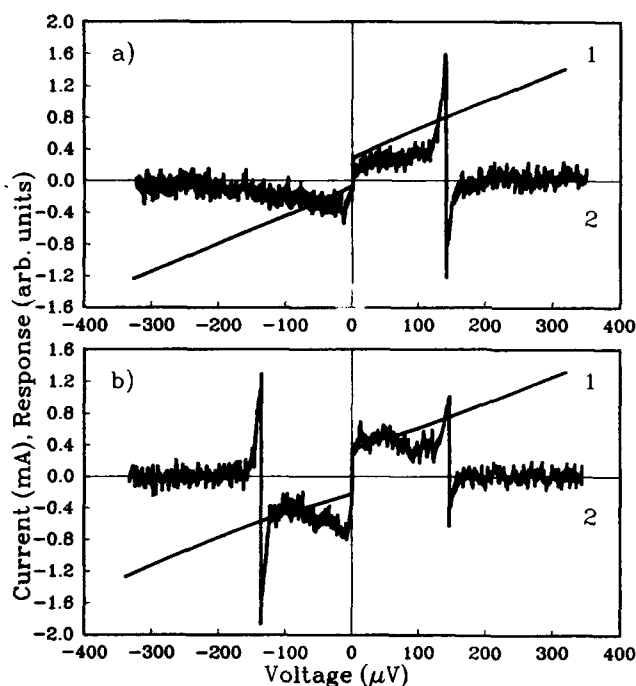


Figure 2: IV -curve (1) and response $\Delta V(V)$ (2) maximized by applying an additional magnetic field of 10^{-5} T at positive current bias (a) and negative current bias (b) at 70.3 K.

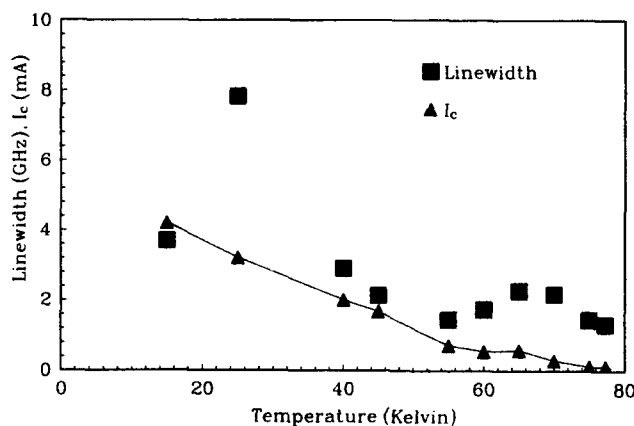


Figure 3: The linewidth of 70 GHz Josephson oscillations (Squares) and the critical current (Triangles) versus temperature for a $32\mu m$ SEJ at 70.2 GHz.

The temperature dependence of the linewidth of the 70 GHz radiation detected from a 32 μm wide SEJ is shown in Figure 3 (filled squares). It is a general trend that the linewidth does not increase proportional to temperature as it is expected in the case where thermal fluctuations were dominating. Alternatively a $1/f$ -type critical current fluctuation ⁷ might be responsible for the excess contribution to the linewidth at lower temperatures. From Figure 3 it is clear, that the variation of the critical current (Triangles) and the linewidth is not directly proportional, but the data seem to be better accounted for by $1/f$ -noise in the critical current.

A possible explanation could be that a spatially inhomogeneous current distribution in the SEJ causes the peculiarities in both the averaged dc characteristic and in the linewidth, which actually is determined by the integrated spectral density of the voltage fluctuations of the junction. According to this approach the SEJ may be considered as a multi-junction (with different I_{ci}) multi-loop (with different inductances L_k) interferometer, where the characteristic energies $E_{\Phi k} = \frac{\Phi_0^2}{8L_k}$ and $E_{Jk} = \frac{hI_{ck}}{2e}$ may be larger than kT at lower temperatures. This increases the complexity of the system studied and introduces new available states with closely spaced energy levels between which spontaneous transitions may take place, resulting in an increase of the non-thermal noise of the SEJ.

ACKNOWLEDGEMENTS

This work was partially supported by the Danish Technical Research Council (STVF) HTSC program, the Danish Research Academy, the German Academic Exchange Service (DAAD), and the German Ministry for Research and Technology.

REFERENCES

1. R. Gross and P. Chaudhari, Status of dc-SQUIDS in the high temperature superconductors, in: *Principles and Applications of Superconducting Quantum Interference Devices*, A. Barone, ed., World Scientific, Singapore (1991).
2. R. W. Simon, J. F. Burch, K. P. Daly, et al. in: *Science and Technology of Thin Film Superconductors 2*, R. D. McConell and R. Noufi, ed., Plenum Press, New York (1990).
3. C. L. Jia, B. Kabius, K. Urban, K. Herrmann, J. Schubert, W. Zander and A. I. Braginski, *Physica C* 196:211 (1992).
4. K. Herrmann, Y. Zhang, H.-M. Mück, J. Schubert, W. Zander and A. I. Braginski, *Supercond. Sci. Technol.* 4:583 (1991).
5. Yu. Ya. Divin, N. A. Mordovets, *Sov. Tech. Phys. Lett.* 9:245 (1983); Yu. Ya. Divin, N. A. Mordovets, *Ext. Abstracts 9 Int. Conf. IR & MM waves*, Takarazuka, 427, (1984).
6. Yu. Ya. Divin, J. Mygind, N. F. Pedersen and P. Chaudhari (submitted to *Appl. Phys. Lett.*).
7. M. Kawasaki, P. Chaudhari and A. Gupta, $1/f$ noise in $\text{YBa}_2\text{Cu}_3\text{O}_{7-\delta}$ superconducting bicrystal grain-boundary junctions, *Phys. Rev. Lett.*, 68:1065 (1992).

FLUXON DYNAMICS IN DISCRETE SINE GORDON SYSTEM

G. Filatrella^{1,2}, S. Matarazzo³, S. Pagano³

¹ LAMF and Physics Laboratory 1, Technical University of Denmark
DK-2800 Lyngby, Denmark

² Physics Department, University of Salerno
I-84081 Baronissi, Italy

³ Istituto di Cibernetica del CNR
I-80042 Arco Felice, Italy

INTRODUCTION

Fluxon propagation in Long Josephson Junctions (LJJ) has been thoroughly investigated in past years both as a model system for soliton dynamics¹ and in view of possible practical applications². The electrodynamics of a LJJ is described by a perturbed version of the well known sine-Gordon Equation (PSGE), its kink solution corresponding to a magnetic flux quantum propagating in the junction barrier. Recently has attracted considerable interest solitons propagation in arrays of small coupled Josephson junctions³. In this paper we focus our attention on a system constituted of by a one dimensional array of coupled Josephson Junctions, designed in such a way to generate microwave radiation through a controlled fluxon dynamics.

MODEL

In Fig. 1a is shown a sketch of the device investigated, constituted by 3 basic elements: 1) an array of coupled Josephson junctions, each appearing as a small micro-bridge between the two superconducting electrodes; 2) a control line (on the left of the device) generating a local magnetic field when a current I_L is passing through it; 3) a detector junction (on the right of the device) which is coupled to the array through a resistor R_d .

The equivalent electrical model is shown in Fig. 1b, where additional current control inputs have been considered: I_c as an additional current bias for the first junction of the array, and I_m which generates a magnetic field uniformly coupled to the array. Junctions are modelled by the usual Resistive Shunted Junction (RSJ) model, which well describes both SIS and SNS type junctions, and the loops self inductances are represented by inductors series connecting the junctions. The bias current I_b is supposed

to be spatially uniform. For simplicity we will assume that all the junctions are equal, as well as all the loop inductances. We parenthetically note that the circuit in Fig. 1b is formally equivalent to a lumped-element model of a Josephson transmission line, the only difference being the finite spatial junctions separation.

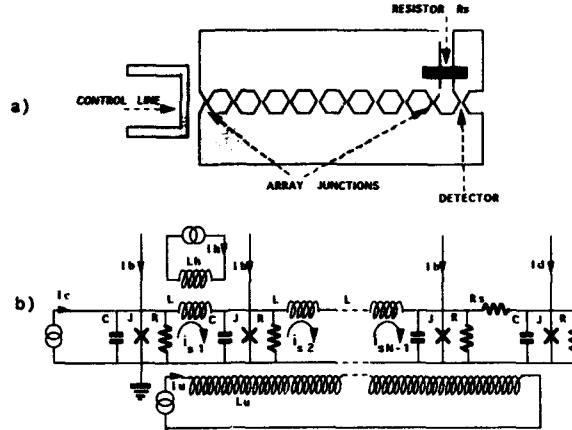


Figure 1. a) sketch of the proposed device, b) its electrical model

By writing the equation for the current in each junction, taking into account the flux quantization in the superconducting loop⁴, and applying the usual normalization we obtain a set of coupled ordinary differential equations describing the time evolution of the phase ϕ of the N junctions in the array and of the detector:

$$\gamma + \gamma_c + \frac{2\pi}{\beta}(\eta_L^{(1)} + \eta_u) - \frac{1}{\beta}(\phi_1 - \phi_2) = \sin\phi_1 + \alpha\dot{\phi}_1 + \tilde{\phi}_1 \quad (1a)$$

$$\gamma + \frac{2\pi}{\beta}(\eta_L^{(n)} - \eta_L^{(n-1)}) - \frac{1}{\beta}(2\phi_n - \phi_{n-1} - \phi_{n+1}) = \sin\phi_n + \alpha\dot{\phi}_n + \tilde{\phi}_n \quad (1b)$$

$$\gamma - \frac{2\pi}{\beta}(\eta_L^{(N-1)} + \eta_u) - \frac{1}{\beta}(\phi_N - \phi_{N-1}) - \alpha\rho(\dot{\phi}_N - \dot{\phi}_D) = \sin\phi_N + \alpha\dot{\phi}_N + \tilde{\phi}_N \quad (1c)$$

$$\gamma_D + \alpha\rho(\dot{\phi}_N - \dot{\phi}_D) = \sin\phi_D + \alpha\dot{\phi}_D + \tilde{\phi}_D \quad (1d)$$

where the current is normalized to the junction critical current I_0 , time is normalized to the inverse of the plasma frequency ω_p , $\alpha = 1/\omega_p RC$, $\beta = 2\pi LI_0/\Phi_0$ is the well known SQUID screening parameter and is also a measure of the array discreteness, (it is easy to see that $\beta = \Delta x^2/\lambda_J^2$, Δx being the junction spacing), $\rho = R/R_s$ represents the coupling between the array and the detector, γ_c is the normalized control current, η_u and $\eta_L^{(n)}$ the normalized uniform and local magnetic flux, respectively, and $2 \leq n \leq N-1$.

RESULTS

We have numerically integrated Eqs. (6) using parameters close to the experimentally reasonable values. In particular we investigated high damping configurations ($\alpha \simeq 1$) typical of high T_c superconductors devices. In Fig. 2 is shown a typical IV characteristic of an array of 10 junctions in presence of weak uniform magnetic field ($\eta_u = 0.1$), weak dissipations ($\alpha = 0.3$) and no coupling to the detector. The phase evolutions corresponding to the points (A) and (B) of the IV curve are shown in the inserts. From the inserts is easily inferred that point A belongs to the first zero field step (ZFS1) of the LJJ (a single fluxon (antifluxon) propagating along the junction

at almost constant speed and being reflected at the edge as an antfluxon (fluxon)). Likewise the point (B) on the small step at $V \approx 1.3$, is on the fifth order Fiske step (FS5) (a periodic motion consisting of 3 fluxons moving in the positive x-direction until they reach the array edge where only 2 are reflected as antfluxons). We note that those two different dynamical states are obtained with a very tiny change (0.01) of the bias current.

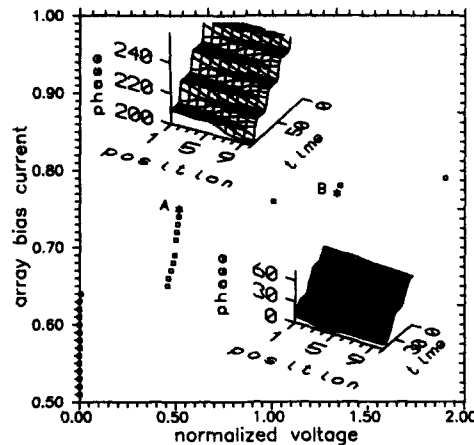


Figure 2. IV characteristic of a 10 junctions array. The two inserts show 3d plots of the phase evolution corresponding to the bias point (A) and (B) in the Figure.

To investigate the behavior of the device as a microwave oscillator⁵ we have chosen the parameters in order to produce a one direction fluxon motion (flux flow). In this state the magnetic field present at the left edge of the array injects fluxons that are then driven by the bias current with an almost constant speed toward the right end of the array. There the fluxons are absorbed generating a microwave radiation.

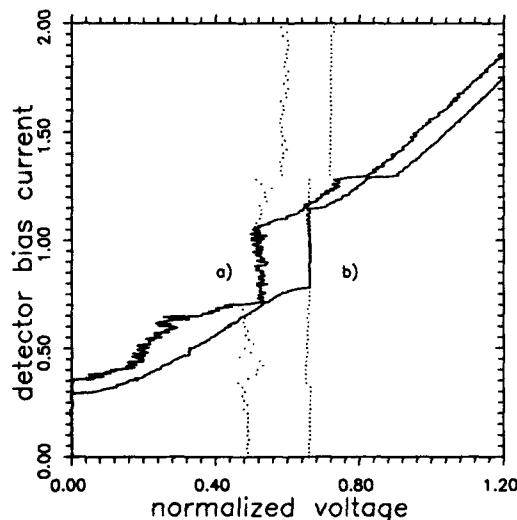
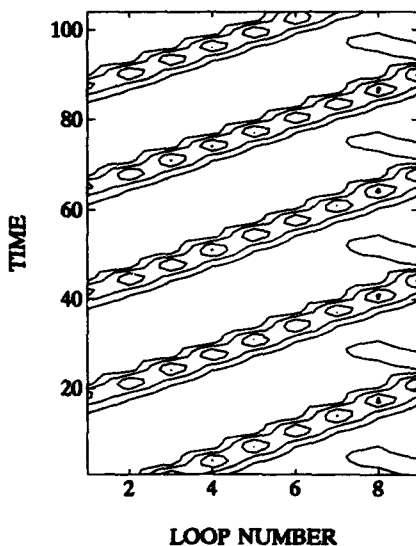


Figure 3. (left) Contour plot of the magnetic field inside the array when biased in the flux flow regime. Figure 4. (right) Detector (solid line) and array (dotted line) voltage vs the detector current for different values of the magnetic field: a) $\eta_u = 0.1$, b) $\eta_u = 0.5$.

The rate of injection (which determine the frequency ν of the radiation, and also the dc array voltage $V = 2\pi\Phi_0\nu$) depends upon the value of the external magnetic field η (or the control current γ_c) and the bias current γ . As an example of this dynamical state we show in Fig. 3 a contour plot of the magnetic field inside the array. The parameters value are $N = 10$, $\gamma = 0.17$, $\eta_L = 0.5$, $\eta_u = 0$, $\rho = 0$, $\alpha = 1$, $\beta = 5$. The high α value is responsible of the absorption of the fluxon at the right edge in the absence of load ($\rho = 0$). The value of β is such that a fluxon can almost be fully trapped in a single loop, and the resulting motion is nonuniform. When a load junction is attached to the array ($\rho > 0$) it senses the electromagnetic field generated at the array edge. In the flux flow regime this electromagnetic field will have a strong component at $\nu = \frac{V}{2\pi\Phi_0}$, which can interact with the detector generating for instance the well known rf-induced steps in the IV characteristic. The situation is shown in Fig. 4 where we have chosen the same parameters as for Fig. 3 but $\rho = 0$. Fig. 4 shows the detector (solid line) and the array (dotted line) voltages vs the detector current γ_D for $\eta_u = 0.1$ and it is well clear a region of phase locking $0.75 \leq \gamma_D \leq 1.05$. Fig. 4b shows the same situation but for $\eta_u = 0.5$. The main effect of changing the magnetic field is a change in the generated frequency, thus demonstrating the tunability of the oscillator. In both Figs. 4a and 4b it is possible to observe a small change in the array voltage when the detector current is varied, this loading effect should be avoided in a real application, possibly using a series dc-block capacitor between the oscillator and the load.

CONCLUSIONS

We have investigated the dynamics of an array of inductively coupled Josephson Junctions and shown its feasibility as a microwave generator when operated in the flux flow regime. The device can be realized within the present high Tc junctions technology, and work in this direction is in progress.

ACKNOWLEDGEMENT

The authors wish to thank A. Barone, G. Costabile, R. Cristiano, and R.D. Parmentier for helpful discussions and suggestions. S.P. is grateful to the MIDIT (Denmark) for hospitality during part of this work. The financial supports of the Progetto Finalizzato "Superconducting and Cryogenics Technologies" of the National Research Council (CNR) of Italy and of EEC through Contract No. SC1*-CT91-0760 (TSTS) are acknowledged.

REFERENCES

1. T.A. Fulton and R.C. Dynes, "Single vortex propagation in Josephson tunnel junctions", *Solid State Commun.* **12** (1973) 57.
2. D.W. McLaughlin and A.C. Scott, "Perturbation analysis of fluxon dynamics", *Phys. Rev A* **18**, (1978) 1652.
3. S. Hontsu and J. Ishii, "Fluxon propagation on a parallel array of microbridge-type Josephson junctions" *J. Appl. Phys.* **63** (1988) 2021.
4. see e.g. A. Barone and G. Paternó, "Physics and Applications of Josephson Effect", Wiley, New York (1982).
5. S. Pagano, R. Monaco and G. Costabile, "Microwave oscillator using arrays of long Josephson Junctions" *IEEE Trans. Magn. MAG-25*, 1080 (1989).

NONLINEAR INTERACTION OF FLUXON AND PLASMA WAVES IN A FINITE JOSEPHSON JUNCTION

Marek Jaworski

Institute of Physics
Polish Academy of Sciences
Al. Lotników 32/46
02-668 Warszawa, Poland

It is well known that a lossless one-dimensional Josephson junction can be described by the Sine-Gordon (SG) equation in laboratory coordinates¹:

$$u_{xx} - u_{tt} = \sin u, \quad (1)$$

where u denotes the phase difference between the wavefunctions in both superconducting electrodes of the junction. Furthermore, u_x is proportional to the magnetic field, while u_t — to the electric field within the junction.

The fluxon plasma interaction plays an important role in the analysis of time-dependent phenomena in long Josephson junctions^{2,3}. More generally, the interaction between a strongly nonlinear (soliton-like) component of the solution and a quasi-linear small-amplitude oscillation is discussed also in other contexts, such as dynamics of the SG kink in the presence of perturbation⁴, and the quasi-particle (de Broglie-like) state of the SG system.⁵

Usually, a small-amplitude contribution v is determined approximately by the linearization of eq.(1) about a strongly nonlinear solution u_0 :

$$u = u_0 + v, \quad v \ll u_0. \quad (2)$$

Substituting (2) into (1) and retaining only linear terms we obtain a linear partial differential equation with respect to v , which can be solved for a relatively simple unperturbed term u_0 , e.g. for a static kink⁶.

The aim of this paper is to present a more general and practically useful perturbation method, making possible to linearize eq. (1) in the presence of arbitrary nonlinear solution u_0 .

A general multiperiodic solution of eq. (1) can be written as ^{7,8}

$$u = 2i \ln \frac{\Theta(z + e/2 | B)}{\Theta(z | B)}, \quad (3)$$

where B is a $g \times g$ Riemann matrix, e denotes the g -dimensional unit vector, $z \in C^g$ is a linear function of space and time coordinates

$$z_j = k_j x + \omega_j t + z_j^0, \quad x, t \in R, \quad z^0 \in C^g, \quad j = 1, 2, \dots, g$$

and $\Theta(z | B)$ denotes the g -dimensional Riemann theta function

$$\Theta(z | B) = \sum_{n \in Z^g} \exp(i2\pi n z + i\pi n B n). \quad (4)$$

Let us consider a $(g+1)$ -periodic solution (3) where g denotes strongly nonlinear components (soliton trains, breathers etc.), while the term labelled by $g+1$ represents a small-amplitude quasi-linear contribution. The reality conditions imply that⁹

$$B_{jj} = 1/2 + i\beta_{jj}, \quad B_{ij} = \alpha_{ij},$$

$$\alpha_{ij}, \beta_{ij} \in R, \quad i = 1, 2, \dots, g, \quad j = g+1.$$

The expression (4) describing the $(g+1)$ -dimensional theta function can be rewritten as

$$\Theta(\tilde{z} | \tilde{B}) = \sum_{n_j} \exp(i2\pi n_j z_j + i\pi n_j^2 B_{jj}) \Theta(z + \alpha_j n_j | B), \quad (5)$$

where \tilde{z} , \tilde{B} denote a $(g+1)$ -dimensional vector argument and a $(g+1) \times (g+1)$ Riemann matrix, respectively. In the small-amplitude limit we have $\beta_{jj} \gg 1$, $q_j = \exp(-\pi\beta_{jj}) \ll 1$, thus the summation over n_j can be restricted to the leading terms $n_j = 0, \pm 1$ and

$$\Theta(\tilde{z} | \tilde{B}) \simeq \Theta(z | B) + iq_j [e^{-i\eta_j} \Theta(z - \alpha_j | B) + e^{i\eta_j} \Theta(z + \alpha_j | B)], \quad (6)$$

where $\eta_j = 2\pi z_j = \mu_j x + \Omega_j t$, and the dispersion relation for the perturbation term is $\Omega_j^2 = \mu_j^2 + 1$.

Substituting (6) into (3) and retaining only the terms linear in q_j we obtain

$$u_{g+1} = u_g + q_j v_j + O(q_j^2), \quad j = g+1, \quad (7)$$

where

$$v_j = 2 \left[\frac{e^{-i\eta_j} \Theta(z + e/2 - \alpha_j | B) + e^{i\eta_j} \Theta(z + e/2 + \alpha_j | B)}{\Theta(z + e/2 | B)} + \frac{e^{-i\eta_j} \Theta(z - \alpha_j | B) + e^{i\eta_j} \Theta(z + \alpha_j | B)}{\Theta(z | B)} \right]. \quad (8)$$

It should be noted that the small-amplitude solution exists both for $\Omega_j < 1$ and $\Omega_j > 1$.

For $\Omega_j < 1$ we have μ_j imaginary, and consequently the small-amplitude solution is decaying rather than propagating in the x direction. The single perturbation term is complex, hence in order to keep the solution real we have to combine two perturbation terms, i.e. $\eta = \mu x \pm \Omega t$. Such a combination is equivalent to a breather train, which oscillates in time, but is stationary and localized in space.

For $\Omega_j > 1$, both Ω_j and μ_j are real, and the small-amplitude wave is propagating in the x direction.

The dispersion parameters $k_j, \omega_j, \mu_j, \Omega_j$ as well as elements of the matrix B can be obtained from the spectral analysis⁸. Here, however, we have used another approach based on the Schottky parametrization of the Riemann surface¹⁰.

As an example, let us consider a one-dimensional Josephson junction of finite length L , immersed in the external uniform magnetic field. Assuming time-periodic dynamics of the junction we can formulate the problem as solving eq. (1) for u subject to the following boundary conditions:

$$u_x(0, t) = u_x(L, t) = \beta, \quad (9a)$$

$$u(x, t) = u(x, t + T) + 2\pi n. \quad (9b)$$

where β is a constant proportional to the external magnetic field.

As an unperturbed solution we take two fluxon (antifluxon) trains moving in opposite directions with the same velocity¹¹. The static magnetic field is taken into account as the third stationary soliton train. Unfortunately, such a solution does not satisfy the boundary conditions (9a,b), thus we try to solve the problem by consecutive approximations, including more and more quasi-linear components (plasma waves).

A more detailed analysis shows that plasma waves do not interact with each other in the small-amplitude limit, thus

$$u_x(0, t) = u_{0,x}(0, t) + \sum_{j=1}^{\infty} q_j v_{j,x}(0, t), \quad (10)$$

where $u_{0,x}$ denotes the unperturbed solution, q_j — a free amplitude, and $v_{j,x}$ — a plasma wave with the time-period commensurate with that of the unperturbed solution.

For given boundary condition $u_x(0, t) = \beta$, one can determine the coefficients q_j using standard methods. (Because of symmetry it is sufficient to consider only one end of the junction). Fig. 1 shows an approximate solution $\tilde{u}_x(0, t)$ for $\beta \simeq .5$ and $N = 15$ small-amplitude terms taken into account. One can see that the convergence to the exact solution $u_x(0, t) = \beta$ is very poor, and the problem of completeness of the set $v_{j,x}$ is still open. Nevertheless, both sides of the Parseval's relation differ by less than 5 per cent, what indicates that the set of small-amplitude terms is probably complete.

Similar calculations performed for $\beta \simeq 1.25$ yield qualitatively the same result. In the language of fluxon dynamics it means that in both cases we deal with the same mechanism corresponding to the zero-field steps (ZFS). On the other hand, the above solution is not unique, and one can consider also other mechanisms of fluxon reflection from the boundary¹², giving rise to the Fiske steps (FS).

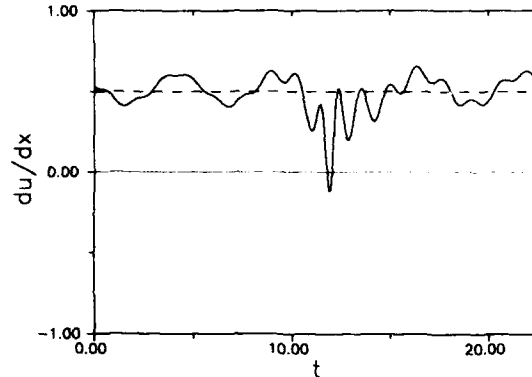


Figure 1. Approximate solution $\bar{u}(0,t)$ for $N = 15$ perturbation terms taken into account (solid line) and exact boundary condition $u(0,t) = \beta$ (dashed line). The time-period is $T = 22.74$.

Thus, on the basis of a lossless model (1) we are not able to determine what kind of mechanism is preferable for given value β of the external magnetic field. It seems that the analysis of a perturbed SG model is needed to clarify this problem.

ACKNOWLEDGMENTS

This work was supported by Grants No. PB 2-0479-91-01 and PB 2-0480-91-01.

REFERENCES

1. A. Barone and G. Paterno, "Physics and Application of the Josephson Effect," Wiley, New York (1982).
2. O.H. Olsen and M.R. Samuelsen, Phys. Rev. B 33:595 (1986).
3. M. Cirillo and A. Cutolo, Fluxon-radiation interactions in long Josephson junctions, Università di Salerno, preprint.
4. O. Legrand and M. Taki, Phys. Lett. A 110:283 (1985).
5. J.C. Fernandez, J.J.P. Leon, and G. Reinisch, Ann. Fond. L. de Broglie 10:37 (1985).
6. J. Rubinstein, J. Math. Phys. 11:258 (1970).
7. V.O. Kozel and V.P. Kotlarov, Dop. AN UkrSSR A 10:878 (1976), (in Ukrainian).
8. M.G. Forest and D.W. McLaughlin, J. Math. Phys. 23:1248 (1982).
9. J. Zagrodsinski and M. Jaworski, Z. Phys. B 49:75 (1982).
10. A.I. Bobenko and L.A. Bordag, J. Phys. A 22:1259 (1989).
11. R.D. Parmentier, Fluxons in long Josephson junctions, in: "Solitons in Action," K. Lonngren and A. Scott, eds, Academic, New York (1978).
12. B. Dueholm, E. Jorgensen, O.A. Levring, J. Mygind, N.F. Pedersen M.R. Samuelsen, O.H. Olsen, and M. Cirillo, Physica 108B:1303 (1981).

OBSERVATION OF MULTIPLE PARTICLE TUNNELING IN HIGH QUALITY SUPERCONDUCTING TUNNEL JUNCTIONS

A. Oliva¹ and R. Monaco²

¹Dipartimento di Fisica - University of Salerno - Italy

²Istituto di Cibernetica - C.N.R. - Napoli - Italy

We report on the temperature dependence ($1.2\text{K} < T < 4.2\text{K}$) of the subgap current in high quality superconducting tunnel junctions (STJ's), that is the tunnel current in the voltage range $0 < V < V_g$, where $V_g = (\Delta_1 + \Delta_2)/2e$ is the gap voltage and Δ_1 and Δ_2 are the forbidden energy gaps for the electrodes.

In the BCS model the subgap current of an ideal loss-free barrier in a STJ is mainly due to the tunneling of the thermally excited quasiparticles (single electron tunneling)[1]. However, in real devices, it has been found that, in the voltage range $V_g/2 < V < V_g$, the measured current is slightly higher than the expected single electron tunnel current [2]; the agreement between theory and experiment is recovered considering another intrinsic transport mechanism: the multiple particle tunneling (MPT) [3], [4].

The MPT is a tunneling process according to which one or more Cooper pairs in one superconductor tunnel into the other superconductor and dissociate in two or more (m) quasiparticles (or vice versa). The MPT appears, for a symmetric junction, as current jumps in the I-V characteristic, at voltages V_g/m and is proportional to e^{-ms} where m is the tunneling order and s is related to the barrier thickness and height [5]. This suggests that, to a second order of approximation, also the two particle tunneling ($m=2$) has to be taken into account and, in fact, on this process we will focus our attention in what follows.

A simple relation for a symmetrical junction at $T=0$ can be derived between the ratio $\Delta I_{V_g/2}/\Delta I_{V_g}$ of the step height at $V=V_g/2$ and the one at $V=V_g$ and the normal conductance per unit area G_{nn}/A :

$$\Delta I_{V_g/2}/\Delta I_{V_g} = K G_{nn}/A$$

where K is a numerical constant roughly equal to $10^{-2} \Omega \mu\text{m}^2$ [3], [5]. Moreover, the step height and width are slowly dependent on the temperature and slowly dependent on small magnetic fields.

The junctions investigated were obtained from Nb/Al-AlO_x/Nb trilayers using different processes, all based on the selective anodization of the top Nb electrode. In the table the most relevant parameters for eight STJ's having different areas and normal conductances are listed.

Table 1. Experimental parameters.

SAMPLE	A μm^2	G _{nn} ¹ /A mho μm^{-2}	$\Delta V_{g/2}$ μV	ΔV_g μV	$(\Delta V_{g/2})/(\Delta V_g)$	K ohm μm^2	T-gain ²	V _m ³ mV
5H10=1	138	6.3E-04	0.096	230	4.2 E-04	0.70	1500	83
38E2=3	14	26E-04	0.220	100	22 E-04	0.85	500	55
46E6=3	1200	1.2E-04	0.058	430	1.3 E-04	1.0	1800	73
46E1=3	1200	2.1E-04	0.260	720	3.6 E-04	1.7	9500	64
30E5=1	1600	5.0E-04	2.800	2700	10 E-04	2.0	62	50
15H5=2	820	3.7E-04	0.64	840	7.6 E-04	2.1	50	48
12H2=1	138	2.3E-04	0.10	90	11 E-04	4.8	109	51
12H4=4	2300	2.0E-04	2.3	1400	16 E-04	8.2	58	58

¹G_{nn}: normal state conductance

²T-gain= $I_{sg}(1.2\text{K}, 0.5\text{mV}) / I_{sg}(4.2\text{K}, 0.5\text{mV})$

³V_m= $0.7\Delta V_g R$; $R=2\text{mV} / I_{sg}(4.2\text{K}, 2\text{mV})$

The quality factor value $V_m=2.7\text{V}$ at the lowest temperature ($T=1.18\text{K}$) is a remarkable result, although according to the theory this value should be about 1000 times larger. To better understand this point the I-V characteristic at different temperatures is reported in Fig.1: as the temperature decreases the subgap current quickly decreases.

When the temperature is sufficiently reduced ($T<3\text{K}$) step-like subharmonic structures begin to be observable in the I-V characteristic first at $V=V_g/2$ and later on at $V=V_g/3$ (as indicated by arrows); in

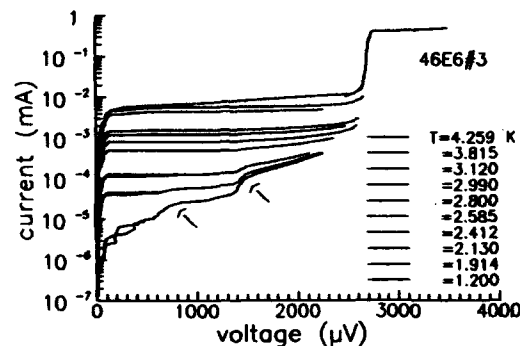


Fig.1: Experimental I-V characteristics at different temperatures.

these measurements the Josephson current was almost completely suppressed by a rather small magnetic field (~ 100 Gauss). We report a list of experimental elements indicating that these structures are due to the MPT:

- 1) weak dependence on small magnetic fields and on the temperature;
- 2) step like structures;
- 3) absence of higher order mechanisms ($m > 3$); (the probability to observe multiparticle tunneling decreases strongly with the order m).

For the same sample, we report (Fig.2) the temperature dependence of the subgap current I_{sg} , compared to the theoretical single electron current I_{se} , at different voltages. At $V=2$ mV and at $T=4.2$ K the junction is practically ideal, but a saturation is observed as the temperature is decreased. At $V=0.1$ mV the experimental points are well fitted by the theoretical curve. A small residual current can be attributed to ohmic losses through or parallel to the barrier; this results in a very low spurious loss for the barrier so that $R_{spurious} > 10^4 R_{nn}$ (R_{nn} is the normal resistance).

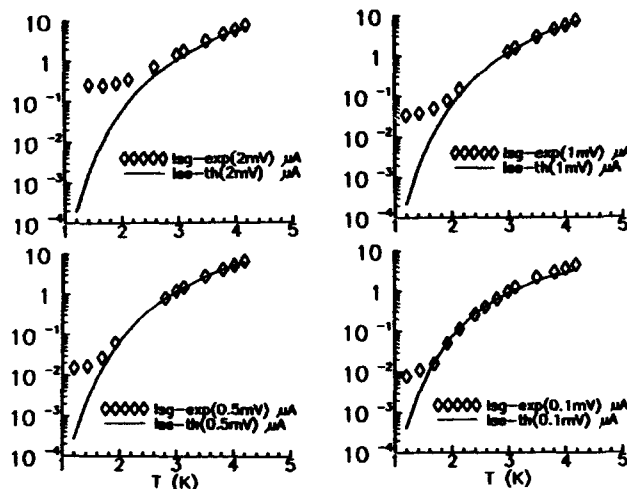


Fig.2: Temperature dependence of the subgap current I_{sg} , compared to the theoretical single electron current I_{se} , at different voltages.

The subgap current in a STJ can be thought of as the sum of three independent contributions, i.e., single electron tunneling current, two particle tunneling current and excess current due to ohmic losses in the barrier; the relative amplitudes of these parallel transport mechanisms depend on the temperature and on the quality of the barrier. The two particle contribution to the tunnel current determines the main observed departure from the single electron theory in the voltage range $V_g/2 < V < V_g$.

The plot in Fig.3 reveals more clearly the relative magnitudes and widths of the structures at $V_g/2$ and at V_g . It seems clear that the current increase at $V_g/2$ is appreciably broader than the one at V_g ; a clear explanation of this effect is not known at the present time.

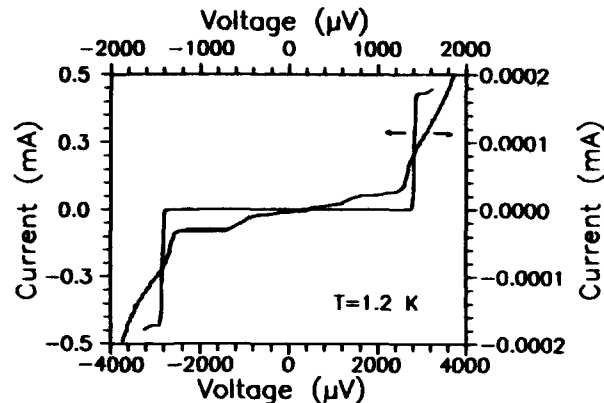


Fig.3: The I-V characteristics near V_g and $V_g/2$. The V_g region is referred to the left and bottom scales while the $V_g/2$ region to the right and top scales.

In the table we report the experimental K values calculated from the measured value of the ratios $\Delta I_{V_g/2}/\Delta I_{V_g}$ and G_{nn}/A . We can observe that the smallest K value is about a factor 100 greater than that predicted by the theory; this implies that the two particle step is much larger than the expected theoretical value. It can be stressed also that the disagreement is greater the smaller is the temperature current gain (T-gain); in other words, smaller spurious resistance junctions seem to have a smaller two particle step height. This observation is consistent with the possible explanation of the disagreement between the theory and the experiments in terms of barrier non uniformities proposed by many authors [6], [7].

ACKNOWLEDGMENT

We wish to thank R.Cristiano, L.Frunzio and M.Del Prete for the precious collaboration and the interesting discussions. This work was supported by C.N.R. under Progetto Finalizzato "Superconductive and Cryogenic Technologies".

REFERENCES

- [1] E.L.Wolf, Principles of Electron Tunneling Spectroscopy, Oxford (1985).
- [2] R.Monaco, R.Cristiano et al., J.Appl.Phys., 71, 4 (1992).
- [3] J.R.Shrieffer and J.W.Wilkins, Phys. Rev.Letters,10,1 (1963).
- [4] B.N.Taylor and E.Burnstein, Phys. Rev. Letters, 10, 1 (1963).
- [5] L.E.Hasselberg, M.T.Levinsen, M.R.Samuelsen, Phys. Rev. B, 9, 9 (1974).
- [6] C.L.Foden et al., Submitted to Phys.Rev.B, April (1992).
- [7] J.M.Rowell and Feldman, Phys.Rev., 172, 2 (1968).

NONLINEARITY IN BCS MODELS OF HIGH- T_c SUPERCONDUCTORS

T. Pavlopoulos² N. Lazarides¹, P.L. Christiansen¹,
M.P. Sørensen¹, and P.N. Spathis³

¹Laboratory of Applied Mathematical Physics
The Technical University of Denmark
DK-2800 Lyngby, Denmark

²Department of Mathematics
University of Patras
Patras, Greece

³Max-Planck-Institut für Plasmaphysik
Garching bei München, D-8046, Germany

INTRODUCTION

A large number of explanations for superconductivity in high- T_c materials have been proposed. In particular efforts are devoted to detailed understanding of the pairing interaction mechanism. When a pairing potential has been established the Bardeen, Cooper, and Schrieffer (BCS) approach is often used to find T_c and other relevant physical quantities¹. In the following we shall apply the BCS strategy to high- T_c superconductors using a phenomenological pairing interaction without discussing the detailed microscopic origin of this interaction. Particular emphasis will be put on the nonlinear properties of the BCS gap equation with anisotropic gap parameter.

MODEL DESCRIPTION

In the description of the pairing interaction of ordinary low-temperature superconductors extended electron wave functions are employed. In the high- T_c materials we shall instead start from a tight-binding model of the electronic states with the energy dispersion relation¹⁻⁴

$$\epsilon_{\mathbf{k}} = A[-2(\cos(k_x a_x) + \cos(k_y a_y)) + 4B\cos(k_x a_x)\cos(k_y a_y) - 2C\cos(k_z a_z) - \mu] \quad (1)$$

μ denotes the chemical potential and a_x , a_y , a_z are the lattice constants. Here we shall

assume $a_x = a_y$. The parameters A, B, and C are related to the hopping probabilities from site to site in the crystal². k_x , k_y , and k_z are the components of the electron wavevector \mathbf{k} .

Assuming onsite and intralayer nearest neighbour attraction, the pairing potential becomes^{3,4}

$$V_{\mathbf{k}\mathbf{k}'} = g_0 + 2g_x \cos((k_x - k'_x)a_x) + 2g_y \cos((k_y - k'_y)a_y) \quad (2)$$

g_0 is the strength of the onsite pairing interaction and g_x , g_y denote the pairing interaction strength in the x- and y-direction, respectively. The BCS gap equation reads

$$\Delta_{\mathbf{k}} = \frac{1}{N} \sum_{\mathbf{k}'} V_{\mathbf{k}\mathbf{k}'} F_{\mathbf{k}'} \quad (3)$$

N is the number of lattice sites and $F_{\mathbf{k}}$ is defined by

$$F_{\mathbf{k}} = \frac{\Delta_{\mathbf{k}}}{2E_{\mathbf{k}}} \tanh\left(\frac{1}{2}\beta E_{\mathbf{k}}\right) \quad (4)$$

where $\beta = 1/(k_B T)$ and k_B is Boltzmann's constant. $E_{\mathbf{k}} = \sqrt{\epsilon_{\mathbf{k}}^2 + \Delta_{\mathbf{k}}^2}$ is the quasiparticle excitation energy. In order to solve the gap equation we use the following solution ansatz^{2,3}

$$\Delta_{\mathbf{k}} = \Delta_0 + 2\Delta_x \cos(k_x a_x) + 2\Delta_y \cos(k_y a_y) \quad (5)$$

which leads to three coupled nonlinear algebraic equations

$$\begin{aligned} \Delta_0 &= \frac{g_0}{N} \sum_{\mathbf{k}} F_{\mathbf{k}} \quad , \\ \Delta_x &= \frac{g_x}{N} \sum_{\mathbf{k}} \cos(k_x a_x) F_{\mathbf{k}} \quad , \\ \Delta_y &= \frac{g_y}{N} \sum_{\mathbf{k}} \cos(k_y a_y) F_{\mathbf{k}} \quad . \end{aligned} \quad (6)$$

In (6) we set both A and k_B equal to unity which is equivalent to measuring all the energies in units of A and the temperature in units of A/k_B . A physical representative value of A is about 0.05eV which leads to $A/k_B = 580\text{K}$.

NUMERICAL SOLUTIONS

In Ref.2 a detailed study of the solutions to Eq.(6) has been done for the case of absent onsite pairing, i.e. $g_0=0$. It is there shown that the transition from the normal state with vanishing gap to the superconducting state with nonzero gap results from a pitchfork bifurcation as the absolute temperature is lowered from above the transition temperature T_c to below. Depending on the value of the chemical potential μ , the superconducting state can either have s-wave symmetry ($\Delta_x = \Delta_y$) or d-wave symmetry ($\Delta_x = -\Delta_y$). Furthermore, it was found in Ref.4 that a second phase transition from either s-wave or d-wave symmetry to a mixed s- and d-wave solution could take place at a transition temperature $T_{c1} < T_c$ for a certain range of μ -values. Note that changing μ corresponds to changing the filling of the conduction band of the electrons responsible for superconductivity². Pitchfork bifurcations in the gap equation have dramatic effects on measurable physical quantities, as e.g. the electron specific heat, spin susceptibility, etc. In the electronic specific heat C given by²

$$C = \frac{1}{2} k_B \beta^2 \sum_k \left(E_k + \beta \frac{dE_k}{d\beta} \right) E_k \operatorname{sech}^2 \left(\frac{1}{2} \beta E_k \right) , \quad (7)$$

each pitchfork bifurcation leads to a discontinuous jump. From calculations of C versus T in the case $g_0=0$ and $\mu=-2.0$ it is evident that the two transition temperatures T_c and T_{c1} are too far apart in comparison with experiments⁵. This deficiency can be resolved by including the onsite pairing interaction g_0 .

In Fig. (1) we show C/T versus T calculated from Eqs.(6) and (7) using the parameter values

$$g_x = g_y = 1.2, \quad \mu = -2.0, \quad B = 0.45, \quad C = 0.1 , \quad (8)$$

and $g_0 = 0.3$. The chosen value of μ give rise to a double phase transition which leads

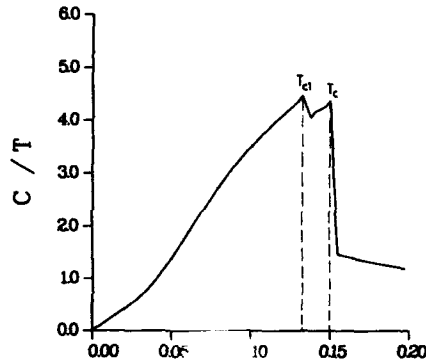


Figure 1. The electronic specific heat C/T versus T at $g_0 = 0.3$. The other parameter values are given by Eq. (8).

to two peaks in the electronic specific heat. By including the onsite pairing we have been able to position the two peaks close to each other as observed in experiments. In order to demonstrate the variation in distance between the two transition temperatures we show T_c and T_{c1} as function of g_0 in Fig. (2).

SUMMARY

The influence of adding an onsite pairing interaction in a BCS approach to describe high- T_c superconductivity has been investigated. Previously, it has been demonstrated that depending on the value of the chemical potential a phase transition between two different superconducting states may occur resulting in a double peaked structure of the electronic specific heat. Here we have shown that including an onsite pairing makes it possible to adjust the distance between the two transition temperatures and thereby fit the calculated electronic specific heat to experimental findings.

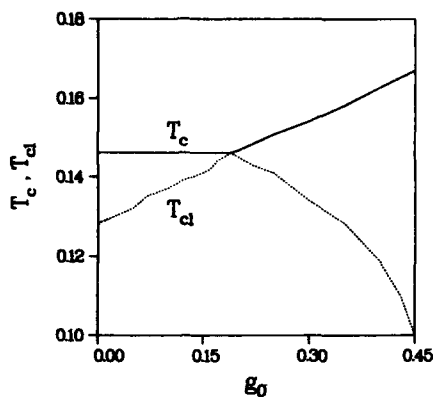


Figure 2. The transition temperatures T_c and T_{c1} as function of g_0 . Parameter values as given by Eq. (8).

ACKNOWLEDGEMENTS

This work is supported by the Danish National Science Research Council [Grant Nos. 11-7075 and 11-9706] and the EC Science programme [Contract No. SCI/0229-C(AM)]. Special thanks goes to T. Schneider for valuable discussions.

REFERENCES

1. H. De Raedt, T. Schneider, and M.P. Soerensen, *Z. Phys. B-condensed Matter* **79**, 327:332 (1990).
2. P.N. Spathis, M.P. Soerensen, and N. Lazarides, *Phys. Rev. B* **45**(13), 7360:7367 (1992).
3. T. Schneider, and M.P. Soerensen, *Z. Phys. B-condensed Matter* **81**, 3:12 (1990).
4. T. Schneider, M. Frick, and M.P. Soerensen, *Dynamics of Magnetic Fluctuations in High-Temperature Superconductors*, Ed. G. Reiter et al., Plenum Press, New York, 219:231 (1991).
5. T.C. Choy, M.P. Das, Hongxing He, *Phase Transitions*, **20**, 1:25 (1990).

STATICS AND DYNAMICS OF FLUX VORTICES IN DISCRETE SYSTEMS

G. Rotoli

Department of Physics, University of Salerno
I-84081 Baronissi (SA), Italy

Discrete Josephson Structures (DJS) are involved in different fields of low temperatures physics. Here we focus our attention on 1d arrays and 2d square arrays of short Josephson junctions (cfr. Fig.1). While 1d arrays are interesting for the development of Flux-Flow based devices [1,2], 2d arrays, besides their intrinsic properties [3], were proposed as models to explain some properties of High T_c Superconductors [4]. In both these structures the non-linearity present in the Josephson element plays a fundamental role permitting solitonic solutions [5] called fluxons (often also flux-quanta or 'vortices' in the 2d arrays).

Equations for the gauge-invariant phases of each junction ϕ_i in a DJS can be written utilizing in our case the equivalent circuits of Fig.1. Here we report the equations for the 1d case only (2d equations can be found in [6]) that are:

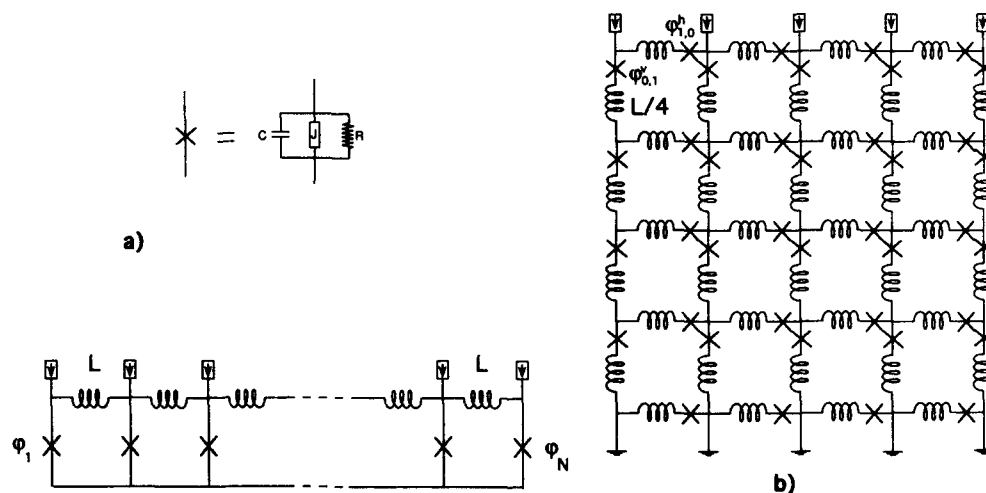


Fig.1: a) 1d array; b) 2d array.

Equations for the gauge-invariant phases of each junction ϕ_i in a DJS can be written utilizing in our case the equivalent circuits of Fig.1. Here we report the equations for the 1d case only (2d equations can be found in [6]) that are:

$$\frac{d^2\phi_i}{dt^2} = (\beta)^{-1}[\phi_{i-1} - 2\phi_i + \phi_{i+1}] - \alpha \frac{d\phi_i}{dt} - \sin \phi_i. \quad (1)$$

here $\beta = 2\pi LI_0/\Phi_0$ with L the single loop inductance and I_0 the Josephson current. Times are normalized to the inverse of the Josephson frequency $\omega_J = (2\pi I_0/C\Phi_0)^{1/2}$ with C the single junction capacitance; α is the quasiparticle loss [7]. Boundary equations are:

$$\frac{d^2\phi_1}{dt^2} = (\beta)^{-1}[\phi_2 - \phi_1] - \alpha \frac{d\phi_1}{dt} - \sin \phi_1 + \eta_1. \quad (2a)$$

$$\frac{d^2\phi_N}{dt^2} = (\beta)^{-1}[\phi_{N-1} - \phi_N] - \alpha \frac{d\phi_N}{dt} - \sin \phi_N + \eta_N. \quad (2b)$$

Where η_1 and η_N are the normalized magnetic fields at the arrays ends. These equations look like a discretized version of the Sine-Gordon (more properly Perturbed Sine-Gordon) equation. The discreteness effects in such systems are linked to the parameter β well-known in SQUID theory. Essentially β controls the number of flux quanta per cell of the array. In fact β is simply related to λ_J , the so-called Josephson length, by the relation $\lambda_J = a/\beta^{1/2}$, where a is the cell dimension. From Long Josephson Junction (LJJ) theory we know that fluxons extend $\simeq \lambda_J$, so for $\beta \ll 1$ the fluxon extends over several cells, while for $\beta \simeq 1$ we have substantially one fluxon per cell; finally for $\beta \gg 1$ more than a fluxon can be put in a single cell.

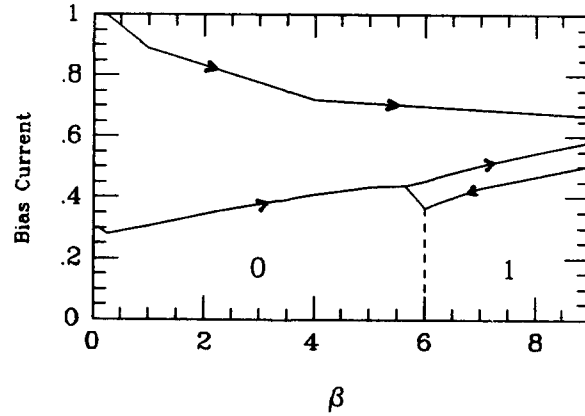


Fig.2: Dynamical range of ZFS1 in a 1d array as a function of β . Arrows indicate the switch direction; here $\alpha = 0.25$ and $N = 20$.

Though many properties of 1d and 2d systems are essentially the same we stress that important differences exist between them. In particular we remark the presence of frustration effects on the phases of the wavefunction associated to each superconducting island, i.e. the spins in the glass analogy, in a 2d array, that no have analog in the 1d case (we remember that spins were introduced in HTC theory by Ebner and Stroud [4] to explain the glassy properties of these systems).

1D ARRAYS

Dynamical solutions of Eq.s (1) were found by numerically integrating it with a Bulirsh-Stoer algorithm. We have to distinguish two type of solutions: 1) free running fluxons, that are the Discrete Sine-Gordon analog of ZFS in LLJ; 2) Flux-Flow solutions in which an external static field generates fluxons at one edge of the array. ZFS1 dynamical range as a function of β is shown in Fig.2. We note the progressive reduction of the dynamical region: from below due to pinning of a fluxon between two junctions, and from above due to the increase of oscillations on the trailing edge that kills the fluxon over a given bias current. We note also the presence of hysteresis above $\beta = 2\pi$ where sweeping the current toward 0, the fluxon does not annihilate at the depinning current but survives again until it remains pinned in a cell of the array. Some Flux-Flow results are collected in Fig.3, here we report the dynamic range of Flux-Flow Steps as a function of η for two different values of α and for $\beta = 1$; the region below the depinning current is the first lobe of the magnetic field pattern of the array (the field is supposed to be uniform over the array). We note the presence of resonances (typical steps are presented in the inset) both near the McCumber branch of I-V and above this, these are due to the interaction of Flux-Flow with array resonances in magnetic field (Fiske steps in LLJ).

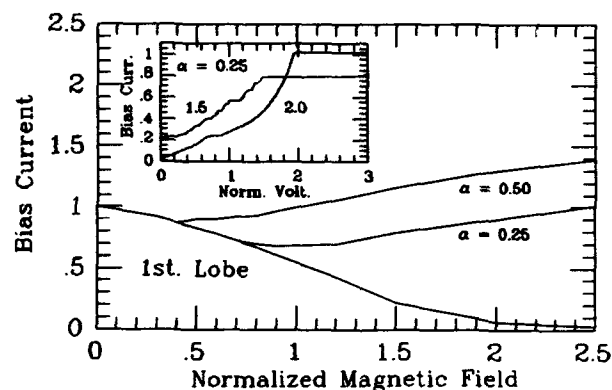


Fig.3: Dynamical range of Flux-Flow steps in a 1d array as a function of η for two different values of α . For these simulations $\beta = 1$ and $N = 20$.

2D ARRAYS

An interesting question is the presence of an auto-induced frustration over the spin system; this is another aspect of Self-Induced Magnetic Field effects (SIMF) that recently [8] was introduced by some authors in the study of 2d arrays. For finite values of β each flux quantum induces frustration over the spin system associated with the square array. We can see this in Fig.4 where the spin system over an array was rebuilt from the junction phases (differences) by 'integrating' the junction phases first along the horizontal line of array, next along the vertical line and viceversa giving two plots for a single values of β . For $\beta = 10^{-3}$ the two plots appear practically identical

confirming that no frustration was induced by the self-field of flux-quanta, but for $\beta = 10^{-1}$ we see clearly a difference between the two plots, so the spin system does not have a preferred state. These considerations can be carried on until β becomes $\geq 2\pi$, in fact beyond this point it is impossible assign a definite value of phase at a superconducting island because $\lambda_{2\pi} = 2\pi a/\beta$, the typical distance over which the phase changes by 2π in a superconductor, becomes comparable with a , i.e. the island dimension.

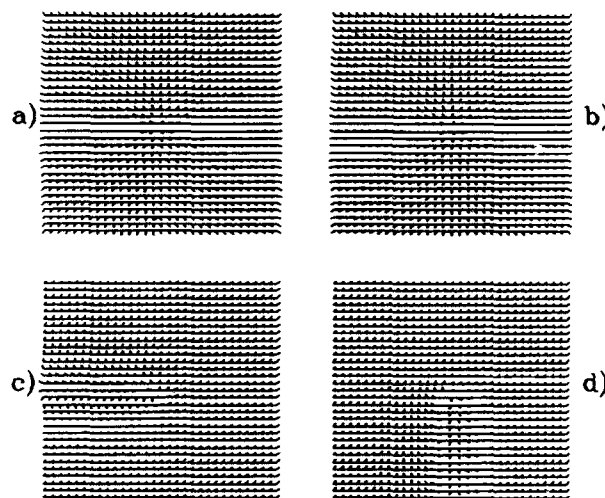


Fig.4: Spin system obtained by phase-differences: a) $\beta = 10^{-3}$ horizontal before vertical; b) $\beta = 10^{-3}$ vertical before horizontal; c) and d) the same for $\beta = 10^{-1}$.

ACKNOWLEDGEMENT

I wish to thank R.D. Parmentier for illuminating comments and for a critical reading of the manuscript. I had several interesting discussions with M.Cirillo, R.De Luca, G. Filatrella, S.Pace, S. Pagano, A.Petraglia, A.Saggese and M. Salerno.

REFERENCES

- [1] J.S.Martens et al., IEEE Trans. on Mag., MAG-27, 3284, 1991.
- [2] G.Filatrella, S.Matarazzo and S.Pagano, Poster Session to this Workshop.
- [3] H.S.J.van der Zant et al., J.Low Temp.Phys.79, 289, 1990 and 82, 67, 1991; S.P.Benz et al. Phys.Rev.Lett.64, 693, 1990.
- [4] C.Ebner and D.Stroud, Phys.Rev.B31, 165, 1985.
- [5] N.J.Zabusky e M.D.Kruskal, Phys. Rev. 15, 240, 1965.
- [6] K. Nakajima and Y. Sawada, Journ. Appl. Phys.52, 5732 (1981).
- [7] A.Barone and G.Paterno', *Physics and Application of Josephson effect*, Wiley NY, 1982.
- [8] A.Majhofer, T.Wolf and W.Dieterich, Phys.Rev.B44, 9634, 1991.

SOLITON TYPE PROPAGATION IN HTcS MATERIALS

Jerzy A. Zagrodzinski

Institute of Physics
Polish Academy of Sciences
02-668 Warsaw, Poland

INTRODUCTION

The aim of this paper is to discuss the model^{1,2} of a planar thin film made of high temperature superconductive (HTcS) granular material. The model exhibits the soliton type effects in the form of solitary waves or even periodic wavetrains.

It is worthwhile to note that the discussed model reflects to some extent the commonly spread opinion that the properties of HTcS materials essentially depend on the tunnel junctions formed between the grains but weakly on the bulk material properties, especially in cases when the propagational effects are considered. This conclusion is confirmed also by the fact that in the discrete version, the discussed model coincides with the system of algebraic equations used in the past to describe the regular array of short Josephson junctions^{1,2}.

So far there is no proof that the model leads to the system of completely integrable partial differential equations (PDEs) and its general solution is unknown. Nevertheless one can construct a rich class of particular solutions on a basis of reduction to the two dimensional case, (more precisely by the reduction of 2+1 case to 1+1 or 2+0).

We report a few classes of such solutions and, as an example, we show a vortex - like pattern in the dynamic case. The reader will observe close resemblance with the two-dimensional XY models of statistical mechanics applied often in the analysis of two dimensional arrays of superconducting islands^{3,5}.

The last part of this report is devoted to the hexagonal array in order to compare at least the equation structure with those of regular array ones.

REGULAR ARRAY

The system of PDEs which describes the regular network of short Josephson junctions in the continuous limit can be derived starting from Hamiltonian \mathcal{H} , which depends on two variables ϕ_1 and ϕ_2 being the order parameters ascribed to the horizontal or vertical branches of the network.

$$\mathcal{H} = \int h(x,y,t) dx dy. \quad (1)$$

In the discrete version φ_1 and φ_2 represent the phase differences across each of horizontal and vertical junctions, respectively.

Starting from the density

$$h = [\varphi_{1,t}^2 + \varphi_{2,t}^2 + (\varphi_{1,y} - \varphi_{2,t})^2]/2 + 2 - \cos\varphi_1 - \cos\varphi_2, \quad (2)$$

where φ_1 and φ_2 depend on space coordinates x, y and t being the real time multiplied by the Swihart velocity, a standard procedure leads to the system of equations

$$\begin{aligned} \varphi_{1,yy} - \varphi_{1,tt} - \sin\varphi_1 &= \varphi_{2,xy}, \\ \varphi_{2,xx} - \varphi_{2,tt} - \sin\varphi_2 &= \varphi_{1,xy}. \end{aligned} \quad (3)$$

Observe that the dissipative terms in this system are neglected although dissipation plays an important role when the theory is compared with experimental data. However, the analytical solutions if exist, can be found only under this simplification. If it concerns the static version, some consequences of the set (3) were discussed also in ².

It is seen that if $\varphi_1 = \varphi_1(y, t)$ and $\varphi_2 = \varphi_2(x, t)$ the system (3) reduces to uncoupled sine-Gordon equations (sGe).

Another solution in form of the plane wave leads as usually to ordinary differential equation (ODE). Namely, if $z = \kappa x + \nu y + \omega t$ and $\varphi_i = \varphi_i(z)$, $i=1,2$, then for $\varphi_2 = \varphi$ ODE takes the form

$$[1 + a^2(1 - a^2 \sin^2 \varphi)^{-1/2} \cos \varphi] \varphi_{,zz} + a^2(a^2 - 1)(1 - a^2 \sin^2 \varphi)^{-3/2} \varphi_{,z}^2 = \sin \varphi, \quad (4)$$

and putting $\sin \varphi_2 = \sin \varphi_1 / a$ we obtain two branches: static ($\omega=0$) and dynamic ($\omega^2 = \kappa^2 + \nu^2$) with $a = -\nu/\kappa$ and $a = \kappa/\nu$, respectively.

The next class solutions follows from an observation, that if $\phi = \phi(\zeta, \tau)$ satisfies sGe (ζ -space, τ -time), then

$$\varphi_2 := \phi(\delta x + t, -\varepsilon \delta y + t) \text{ and } \varphi_1 := \varepsilon \varphi_2 + \pi, \quad (5)$$

with $\delta = \pm 2^{1/2}$ and $\varepsilon = \pm 1$, (where both signs can be taken independently), also satisfy (3).

Solutions of this type can be either solitonic or quasi-periodic or even mixed but always of a dynamic character.

As an example of solutions following from (5) we show in Fig.1 a two-soliton solution in (ζ, τ) with different soliton velocities. In the left hand side, the "arrows" represent $\varphi_2 \in (0, 2\pi]$ and in the right hand side we plot the quantity defined as $H := \varphi_{2,y} - \varphi_{1,x}$. H is interpreted physically as the unique component of magnetic field perpendicular to the array plane, (continuous lines denote positive field, dotted lines - negative).

One can find a close resemblance of the patterns in the left column with the drawing of vortex structures obtained as the result of application of XY models to Josephson arrays. There are however some differences. In the most papers starting from XY model, there is considered a different array topology. Here, we consider an array constructed from junctions arranged in such a manner that there are two components of the current and hence two order parameters. The usually discussed structure deals with "overlap" geometry, (which is convenient for fabrication), and involves only one component of the current and thus it requires an unique order parameter. We are convinced that the topology considered here is more adequate for a thin film granular medium.

Comparing the left and the right plots of Fig.1 one can observe that the structures of both fields i.e. ϕ and H are qualitatively similar if both solitons have nearly the same velocities, but when the velocities are different, the patterns differ significantly too. Since $\sin\phi_1$ determines



Fig.1. Vortices of ϕ_2 (on the left) and magnetic field H (on the right) according to (5), if 2-soliton solution of sGe is applied.

Soliton velocities:

a) 0 and .55;

b) .42 and .55;

c) .943 and .946.

a current, the current vortices do not coincide with maxima of magnetic field in strongly dynamic case. Physically, this effect can be explained by the rising contribution of terms $\phi_{i,n}$, which also have a meaning of the currents, but of course they vanish completely in static case.

This stresses the significance of truly dynamic effects.

In order to verify that the discussed system (3) coincides with the description of the regular network of tunneling junctions, observe that the discrete version of (3) coincides with the system of algebraic equations for the regular (rectangular) array of short junctions. For details reader is referred to references^{1,2}.

HEXAGONAL ARRAY

A model of granular medium which pretends to be correct should at least qualitatively be independent on shape of the elementary cell. This is the reason that we report here the system of equations for a hexagonal array. Although there is no evidence that both regular and hexagonal structures lead to the same results, nevertheless the similarity of equations seems to be promising.

We report below the system of equations, which involves now three dependent functions $\phi_i(x,y,t)$, $i=1,2,3$. Starting from the discrete system, described by three ϕ_i , at the beginning of discrete space variables and assuming the coordinate system as in Fig.2, (with axes 1,2,3), we arrive in continuous limit at the following set of equations

$$(\sin\varphi_i + \varphi_{i,u})_{,i} = 0, \quad H_{i'} = \sin\varphi_i + \varphi_{i,u}, \quad \varphi_{j,j'} = sH/2, \quad (6)$$

where indices i or i' denote the differentiation with respect to the indicated axis, s denotes the surface of the hexagonal elementary cell and the Einstein summation rule is adopted. Equations (6) represent, in order of appearance: the generalized Kirchhoff equation, the definition of mag-

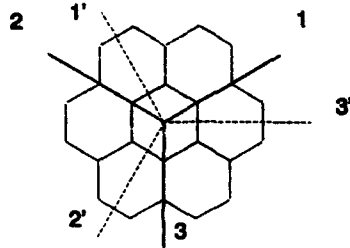


Fig.2.
Coordinate system for the
hexagonal array;
(axes i' and i are
perpendicular).

netic field and the generalized fluxoid equation. From (6) the second order equations can be derived

$$\varphi_{j,j'} = s(\sin\varphi_i + \varphi_{i,u})/2, \quad \text{for each } i. \quad (7)$$

In Cartesian coordinate system ($3=y$, $3'=x$) these reduce to ($\mu=3^{1/2}$)

$$(\varphi_1 + \varphi_2 - 2\varphi_{33})_{,xx} + 3(\varphi_1 - \varphi_2)_{,yy} + 2\mu(\varphi_1 - \varphi_2)_{,xy} = 2sj_1, \quad (8)$$

$$(\varphi_1 + \varphi_2 - 2\varphi_{33})_{,xx} - 3(\varphi_1 - \varphi_2)_{,yy} - 2\mu(\varphi_1 - \varphi_2)_{,xy} = 2sj_2, \quad (9)$$

$$2\varphi_{3,xx} - sj_3 = (\varphi_1 + \varphi_2)_{,xx} + \mu(\varphi_1 - \varphi_2)_{,xy} \quad \text{where } j_i = \sin\varphi_i + \varphi_{i,u}. \quad (10)$$

It is seen that for φ_3 , with Cartesian y -axis coincident with 3 -axis and x with $3'$ -axis, equation (10) is analogous to the equation (3) for the regular structure. Since the equations (7) relate to nonorthogonal coordinate system, sometimes in application, it is more convenient to take (10) and to complete the system by the first order equations (6).

We have no strong arguments, so far, that regular and hexagonal models lead to the same results. In the static case ($\partial/\partial t=0$) however, the rectangular sample biased by dc external current gives qualitatively the same results both for regular and hexagonal arrays. The current flows only on the border of the sample and the pattern becomes asymmetrical in the presence of an external magnetic field. This can be read in favor of the equivalency of both structures.

ACKNOWLEDGEMENTS

The Author is thankful to Dr S.Lewandowski for useful discussions. This work was supported by Polish 2-480-91-01 and 2-479-91-01 Grants.

REFERENCES

1. K.F.Nakajima and Y.Sawada, Numerical analysis of vortex motion in two-dimensional array Josephson junctions, *J.Appl.Phys.*52:5732 (1981).
2. J.Zagrodzinski, The Josephson Junction Array as a Model of HTcS Granular Medium, *Physica C* 180:216 (1991).
3. Conference in Supercond. Networks, *Physica B* 152:No 1/2 (1988).
4. T.P.Orlando, J.E.Mooij and H.S.J. van der Zant, Phenom. model of vortex dynamics in arrays of Joseph. junct., *Phys.Rev.B.*43: 10218 (1991).
5. H.S.van der Zant, Vortex Dynamics in Artif. Fabricated Superconductive Networks, PhD Thesis, Technische Universiteit Delft (1991).

DYNAMICS OF SOLITARY WAVES IN NEMATIC LIQUID CRYSTALS

F.Kh.Abdullaev¹, A.A.Abdumalikov², E.N.Tsoi¹

¹Thermophysics Department, Uzbek Academy of Sciences

²Tashkent State University
Tashkent, 700135, Uzbekistan

INTRODUCTION

The liquid crystals (LC) demonstrate a broad spectrum of nonlinear static and dynamic structures in phenomena of various nature (see [1-3]). One can distinguish some causes determined the interest to a nonlinear LC dynamics. Firstly one can examine the LC as the models of other physical systems described by a same equations. On the other hand, the LC are in many respects exceptional objects for nonlinear dynamics investigation, allowing to sharpen the nonlinear intuition, to check the different principles of theory of nonlinear waves propagation in active, inhomogeneous, dissipative media. It is necessary to note, that in many cases a nonlinear excitations in LC can be observed visually [1,4], without using a complex devices, that is undoubtedly considerable advantage. After all, the investigation of nonlinear LC dynamics allow better to comprehend the nature of this state, to determine the various LC parameters, to work out a new principles for LC devices.

Apparently the existence of a solitary orientational waves in nematic LC (NLC) has been first discussed by W.Helfrich, P.G.de Gennes, F.Brochard [5]. L.Leger [6] observed this waves (walls) in experiments on a reorientation of NLC director by magnetic fields (Frederiks's effect). At present many nonlinear phenomena in LC are being explained on the basis of solitons theory, these are the vortex dynamics in the region of electrohydrodynamic (EHD) instability, the motion of boundary between a domains with opposite polarizations in chiral smectic C, the solitary director waves in shear-flow, the various kinds of defects and inhomogeneity of structure and transition between them under the action of an external fields. To describe these effects the sine-Gordon (SG), the modified Korteweg-de Vries, the nonlinear Schrodinger, the generalized Boussinesq equations, ϕ^4 -model are used.

In present paper the dynamics of a nonlinear objects - breathers and nonlinear periodic waves - in LC are considered. It is found the condition for existence of quasistationary SG breather state. The parameters regions for

stability of nonlinear periodic waves of modified Boussinesq (mBq) equation are obtained.

THE BREATHING DYNAMICS IN NLC

It is known that the LC state (structure, hydrodynamical flow) at fixed temperature is characterized by the director $\vec{n}(\vec{r}, t)$ ($(\vec{n})^2 = 1$), indicating a primary direction of molecules long axes, by the velocity $\vec{v}(\vec{r}, t)$ and by the pressure $P(\vec{r}, t)$, where \vec{r} is coordinate, t is time. In accordance with this the main set of equations describing LC dynamics include the continuity equation, the fluid motion equation and the equation of director evolution [7]. The variation of director field can initiate the macroscopic LC flow ("back" flow) even in absence of internal causes evoked hydrodynamical current. However on choice of a special kind geometry (e.g. pure twist deformation) and at small couple between hydrodynamical and orientational subsystems the flows influence can be neglected. On the other hand it is known, that the back flow influence leads mainly to redefinition of dissipative coefficients in the director motion equation. In view of this arguments we come to simplified variant of obtaining of LC dynamic equations, reducing them to director motion equation only. Let us describe the system Hamiltonian, depending on director distribution in following form [7]:

$$H = \frac{1}{2} \int [J(\partial \vec{n} / \partial t)^2 + K_1 (d \vec{n} / d x)^2 + K_2 (\vec{n} \cdot \text{rot} \vec{n})^2 + K_3 (\vec{n} \times \text{rot} \vec{n})^2 - \chi_a (\vec{n} \cdot \vec{H})^2] d\vec{r}, \quad (1)$$

where K_1, K_2, K_3 , are Frank coefficients for splay, torsion, and bending deformations, J is the density of inertia moment, χ_a is the anisotropic part of magnetic susceptibility, \vec{H} is the external magnetic field. Using this Hamiltonian and including the dissipation, we obtain the equation describing NLC director evolution.

Let us consider the thin homeotropic layer of NLC. The constant magnetic field \vec{H} is perpendicular to the layer (Z-axis), the additional time-varying magnetic field \vec{h} is directed along Y-axis ($\vec{h} \perp \vec{H}$). We suppose, that initial conditions are selected so that the director deviation occur in YOZ-plane, i.e. we have the pure twist deformation, $\vec{n} = (0, \sin \theta, \cos \theta)$, where $\theta(x, t)$ is an angle between Z-axis and director \vec{n} .

The LC energy in θ variable can be written as:

$$H = \frac{1}{2} \int [J(\theta_t)^2 + K_2 (\theta_x)^2 - \chi_a (\vec{n} \cdot \vec{H}_s)^2] dx, \quad (2)$$

Here $\vec{H}_s = \vec{H} + \vec{h}$ is total magnetic field.

Then the equation of NLC director motion in dimensionless variables is

$$u_{\tau\tau} - u_{\xi\xi} + \sin(u) = 2\varepsilon(\tau)\cos(u) - \Gamma u_\tau, \quad (3)$$

where

$$\begin{aligned}\tau &= \omega_0 t, \quad \xi = x/d_0, \quad \Gamma = \frac{\gamma_1}{H} (\chi_a J)^{-1/2}, \quad c = (K_2/J)^{1/2}, \\ d_0 &= (K_2/\chi_a)^{1/2}/H, \quad \varepsilon(\tau) = h(t)/H = \varepsilon_0 \sin(\Omega\tau), \\ \omega_0 &= c/d_0, \quad \Omega = \omega/\omega_0, \quad u = 2\theta.\end{aligned}\quad (4)$$

Here c is characteristic velocity, $1/\omega_0$ and d_0 are time and space scale respectively, γ_1 is viscosity coefficient. The equation (3) is the perturbed SG equation. In this paper we suppose the dissipative coefficient is small, i.e. we believe, that the inertia effects predominate in LC dynamics. It is necessary to note, that in main situation the dissipative effects determine the LC dynamics. However if one consider the temperature region near nematic-isotropic transition, where the viscosity coefficient γ_1 become small or the lyotropic LC, where a molecules associate in massive complexes with large inertia moment, then the contribution of dissipative effects can be supposed small. Below we imply just such physical situation and study the dissipation influence by perturbation theory. On the other hand even if the viscosity coefficients are not small, our approach give a qualitative notion about the initial stage of process on the time $t < J/\gamma_1$.

We note, that the arguments for magnetic field are valid for electric field also, it is enough to replace in a formulae and equations the magnetic field \vec{H} by an electric field and the anisotropic part of magnetic susceptibility χ_a by the anisotropic part of dielectric permittivity ε_a . But the values of electric field must be less then the threshold of EHD instability.

We write the breather solution of unperturbed SG equation as:

$$u_b(\xi, \tau) = -4 \operatorname{arctg} \left[\frac{\nu \cos(\psi)}{\eta - \operatorname{ch}(z)} \right] \quad (5)$$

where

$$\begin{aligned}\psi &= \varphi(\tau) - \frac{\eta}{\nu} z \nu, \quad z = \frac{\nu}{|\lambda|} \frac{\xi - \xi_0(\tau)}{(1 - \nu^2)^{1/2}} \\ \nu &= \frac{1 - 4|\lambda|^2}{1 + 4|\lambda|^2}, \quad \lambda = \eta + i\nu, \quad (\nu, \eta > 0),\end{aligned}$$

$$d\varphi/d\tau = (\eta/|\lambda|)(1 - \nu^2)^{1/2}, \quad d\xi_0/d\tau = \nu.$$

Unlike the soliton, the breather is characterized also by a frequency of internal oscillations $d\varphi/d\tau$. Further we shall consider the small-amplitude ($\gamma = \operatorname{arctg}(\nu/\eta) \ll 1$) breather. If initially breather is in rest (velocity $\nu=0$), then $\psi = \varphi(\tau)$.

The perturbation in the equation (3) is not localized, therefore to use the standard perturbation theory [8] the

solution must be represented in form [9]:

$$u(\xi, \tau) = u_{br}(\xi, \tau) + u_b(\tau), \quad (6)$$

where $u_{br}(\xi, \tau)$ is breather part, $u_b(\tau)$ describe the background oscillations and satisfy the linearized equation (3). Then we obtain the set of ordinary equations for amplitude γ and phase φ :

$$d\gamma/d\tau = [\pi\bar{E}(\tau)\gamma^2 \cos^2(\varphi) - 2\Gamma\gamma \sin(\varphi)] \sin(\varphi), \quad (7)$$

$$d\varphi/d\tau = 1 - \gamma^2/2 + \frac{2}{3} \pi\bar{E}(\tau)\gamma \cos^3(\varphi) - \\ - \Gamma \sin(\varphi) \cos(\varphi)[1 + 2\gamma^2 \sin^2(\varphi)],$$

where $\bar{E}(\tau) = [\sin u_b - 2\varepsilon(\tau)\cos u_b] \approx A \sin(\Omega\tau + \delta)$,

$$A = 2\varepsilon_0[\alpha^2 + 1 - 2\alpha \cos\delta_0]^{1/2}, \quad \tan\delta = \alpha \sin\delta_0/(1 - \alpha \cos\delta_0),$$

$$\tan\delta_0 = \Gamma\Omega/(\Omega^2 - 1), \quad \alpha = [(\Omega^2 - 1)^2 + \Gamma^2\Omega^2]^{1/2}.$$

Using the method of sequential approximations one can obtain, that at $\Omega \neq \Omega_0 = 1$ or 3 the breather amplitude oscillating decrease. But in region $\Omega \approx \Omega_0$ the parametric resonance, and consequently the quasistationary breather state with constant average amplitude are possible. Let us choose $\Omega = 3 - \delta\Omega$, where $\delta\Omega$ is small deviation, the case $\Omega \approx 1$ we discuss below.

Dividing the phase into fast and slow parts

$$\varphi = [(\Omega\tau + \delta) + \Delta(\tau)]/3,$$

and averaging (7) over fast variable, we obtain the set for mean amplitude $\bar{\gamma}$ and "slow" phase $\bar{\Delta}$:

$$d\bar{\gamma}/d\tau = \pi A/8 \bar{\gamma}^2 \cos(\bar{\Delta}) - \Gamma \bar{\gamma}, \quad (8)$$

$$d\bar{\Delta}/d\tau = \delta\Omega - (3\gamma^2/2) - \pi A/4 \gamma \sin(\bar{\Delta}).$$

The phase portrait of system (8) is shown in Fig.1. The character of phase trajectories is determined on a value of parameter R :

$$R = \left| \frac{\delta\Omega/2 - 96\Gamma^2/(\pi^2 A^2)}{[(\delta\Omega/2)^2 + \Gamma^2]^{1/2}} \right|.$$

It is seen, that at $R > 1$ (Fig.1a) the breather amplitude tend to zero. At $R < 1$ (Fig.1b) two stationary points (saddle and focus) appear. The stability of focus point can

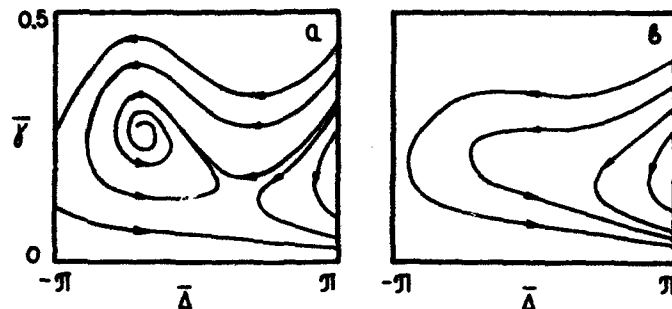


Figure 1. Phase portrait of system (8): a) $R < 1$, b) $R > 1$.

be determined by coefficients matrix of linearized system (8). It can be shown, that trace of matrix is equal to $-\Gamma < 0$, i.e. the focus is stable. Thus we obtain, that at $R < 1$ we have the stationary state.

As to the perturbation frequency $\Omega \approx 1$, one can see, that it is the resonance frequency both for background and for small-amplitude breather oscillations. This fact leads to arising of hysteresis phenomena in breathers dynamics [10]. However for rather small strength of perturbation our results qualitatively remain valid at $\Omega \approx 1$.

Analogously one can show that at $\vec{h} \parallel \vec{E}$ the breather synchronized with external field exists (in region $\Omega_0 = 2$). The existence of similar states is concerned with compensation of a dissipative losses of energy by energy flow from magnetic field.

In conclusion of this section we mention, that at some parameters Ω and ε_0 a stochastic breather dynamics is possible. The chaotic NLC director motion takes place if the following condition is satisfied:

$$\frac{1 - \exp(-\Gamma)}{\Gamma} \left(\frac{\varepsilon_0 \Omega}{\cos(\gamma)} \right)^{2/3} \geq 1$$

THE STABILITY OF SOLITONS AND NONLINEAR PERIODIC ORIENTATIONAL WAVES

As a rule the expansion of nematic free energy is restricted to terms with quadratic space derivatives. This approach is using for static and linear processes. However at study of evolution of nonuniform director distribution or at investigation long-time LC dynamics the account of next terms in free energy are required. In [11] it is shown that the account of highest gradient terms leads to mKdV equation integrated by inverse scattering transform method. In this case a nonlinearity is connected not with external fields, but with anharmonicity, which the terms of four and highest

order introduce.

Thus the energy density has form [11]:

$$H = \frac{1}{2} [J(\theta_t)^2 + K_2(\theta_x)^2 + A(\theta_x)^2 - B(\theta_{xx})^2], \quad (9)$$

where A, B are the combinations of coefficients at four order invariants.

Then the director motion equation is written on dimensionless variables as

$$u_{\tau\tau} - u_{\xi\xi} - \text{sign}(\alpha)6(u_\xi)^n u_{\xi\xi} - \text{sign}(\beta)u_{\xi\xi\xi\xi} = \Gamma_0 u_\tau, \quad (10)$$

where

$$\tau = \omega_0 t, \quad \xi = x/|\beta|^{1/2}, \quad u = \alpha\theta, \quad \alpha = A/K_2, \quad \beta = B/K_2,$$

$$\alpha = |\alpha/\beta|^{1/2}, \quad \varepsilon = \chi_a H^2 |\alpha\beta|^{1/2} / (2K_2),$$

$$\Gamma_0 = 1/2 \gamma_1 (|\beta|/(JK_2))^{1/2}, \quad n = 2.$$

The equation (10) is the perturbed mBq equation. We note, that this equation also arise at study of mono- and diatomic chains with a certain kind of interaction between particles [12]. We shall investigate the linear stability of solitons and onoidal waves (at $\Gamma_0 = 0$) by Whitham method which is very effective for Lagrange systems. The study of stability is of interest for experimental observation of nonlinear excitations in LO. At $n = 1$ in (10) we have Boussinesq equation (Bq) integrated unlike the mBq equation by IST method. The stability of solitons and periodic waves of Bq was considered by J.G.Berryman [13], Fal'kovich et al [14]. In particular in [14] by using Shabat method it is shown that Bq soliton is stable at velocities $v > 1/2$ and unstable at $v < 1/2$. The parameters regions for stable nonlinear waves was obtained also. Same result for solitons was found from analysis of conservative laws and was confirmed by numerical calculation in [15]. The unstable Bq soliton is divided on two stable ones.

At first let us consider the stationary solutions of mBq, that we shall study there. This are

a) The nonlinear periodic wave corresponding to spiral distribution of LO director:

$$u(\xi, \tau) = \alpha m(2K\theta/\pi) + \pi/2, \quad \theta = k\xi - \omega\tau \quad (11a)$$

with dispersion relation :

$$\omega^2 - k^2 + (2K/\pi)^2 \cdot k^4 (2 - m^2) = 0. \quad (12a)$$

We shall name such wave as "rotations wave" (RW).

b) The nonlinear periodic wave, corresponding to director distribution, in that the molecules is deviated from vertical line on an angle less than π :

$$u(\xi, \tau) = \text{sign}^{-1}(m \cdot \text{sn}(2K\theta/\pi)) + \pi/2, \quad (11b)$$

with dispersion relation :

$$\omega^2 - k^2 + (2K/\pi)^2 \cdot k^4 (2m^2 - 1) = 0 \quad (12b)$$

We shall name it "oscillations wave" (OW).

o) Solitary wave (soliton):

$$u(\xi, \tau) = 2\tau m^{-1} [\exp(m_0 \theta)] \quad (11a)$$

with dispersion relation :

$$m_0^2 = (1 - v^2)/(k^2) \quad (12a)$$

Here k is the wave number, ω is the frequency, m is the form-factor (elliptic functions modulus), am and sn are the elliptic amplitude and sine respectively, $K = K(m)$ is the complete elliptic integral of the first kind. To use the Whitham method let us introduce Lagrange function, corresponding to equation (10):

$$L_0 = \frac{1}{2} \int_{-\infty}^{+\infty} [(u_t)^2 - (u_x)^2 + (u_x)^4 - (u_{xx})^2] dx \quad (13)$$

Then the set of equations, describing the evolution of stationary waves $u(\theta)$ modulations has the form [16]:

$$\partial/\partial t(L_\omega) - \partial/\partial x(L_k) = 0, \quad \partial k/\partial t + \partial \omega/\partial x = 0, \quad (14)$$

$$\text{where } L(k, \omega, m) = \frac{1}{2\pi} \int_0^{2\pi} L_0 dx$$

is the averaged Lagrangian (for soliton the integration limits must be changed for $-\infty$ and $+\infty$), indexes denote partial derivatives on corresponding variables. To close the set (14) it needs to append the dispersion relation (12), then we have complete system of equations on 3 parameters $k(x, t)$, $\omega(x, t)$, $m(x, t)$.

The stability of stationary solutions one can judge from the type of modulation equations (14). Namely, if the type of the set (14) is hyperbolic, then the perturbations of initial wave are finite on time, but if the type of set (14) is elliptic, the perturbations grow exponentially. The type of modulation equations is determined by the sign of discriminant:

$$D = r^2 - pq, \quad (15)$$

where

$$p = L_{\omega\omega} L_{mm} - L_{\omega m}^2, \quad q = L_{kk} L_{mm} - L_{km}^2, \quad r = L_{\omega k} L_{mm} - L_{\omega m} L_{km}$$

At $D < 0$ the set (14) is hyperbolic, at $D > 0$ one is elliptic.

Now let us study the stability of periodic waves (11a, b), whose averaged Lagrangian has the form:

$$L(\omega, k, m) = (\omega^2 - k^2) \cdot f_1 + \alpha k^4 \cdot f_2 \quad (16)$$

where $\alpha = (2/\pi)^{2/3}$, functions f_1 and f_2 for RW and OW are respectively equal to:

$$\begin{cases} f_1 = f_1(m) = EK, \\ f_2 = f_2(m) = [(2 - m^2)E + (1 - m^2)K]K^3, \end{cases} \quad (17a)$$

$$\begin{cases} f_1 = f_1(m) = (E - m'^2 K)K, \\ f_2 = f_2(m) = [(2m^2 - 1)E + m'^2(1 - 3m^2)K]K^3. \end{cases} \quad (17b)$$

Here $E = E(m)$ is the complete elliptic integral of the second kind, $m'^2 = 1 - m^2$. Then using the Lagrangian (16) one can show, that the waves (11a,b) are stable under a condition:

$$A(m) - B(m)k^2 > 0, \quad (18)$$

where

$$A(m) = f_1^2 - 6(f_1)'f_1f_3/(f_3)' + 4(f_1)'f_2/(f_3)', \quad (19)$$

$$B(m) = 6\alpha(f_1f_2 + 2(f_1)'f_3(f_2 - 2f_1f_3)/(f_3)'),$$

$()' = (d/dm)$ and function f_3 is defined for each waves respectively:

$$f_3 = f_3(m) = \begin{cases} (2 - m^2)K^2, \\ (2m^2 - 1)K^2, \end{cases} \quad (20a)$$

$$(20b)$$

Using the condition (18) one can check the stability of periodic waves (11a,b) for each set of parameters ω, k, m . On Fig.2 the plot m versus k is presented. Curve 1 determine the boundary of region of waves existence, curve 2 is the boundary of stability region (section-lined area). As seen, under the given m for RW the shorter wave lengths are stable (Fig.2a), for OW the longer ones are stable (Fig.2b).

For the mBq soliton (11c) we obtain, that $D = 0$, i.e. the set (14) is parabolically degenerate. Thus the Whitham

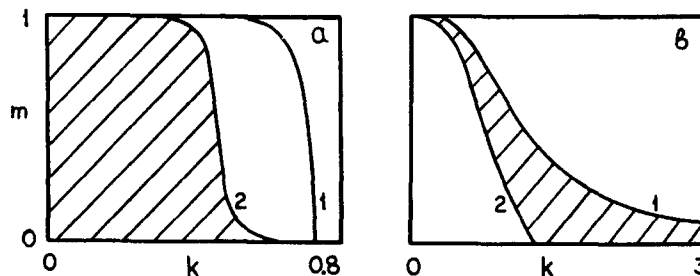


Figure 2. The existence and stable regions for a)RW and b)OW.

method does not give an information on the mBq soliton stability. However in [17] it has been investigated the stability condition for the solitary solutions of wide class of equations, whose special case is the equation (10). This condition has the form:

$$I(v^2) + 2v^2 \frac{d}{d(v^2)} I(v^2) < 0, \quad I(v^2) = \int_{-\infty}^{+\infty} (u_x)^2 dx. \quad (21)$$

Using this criterion we have found, that mBq soliton is stable at $v > (1/2)^{1/2}$. Thus the fast solitons are stable, that coincides with a result for Bq equation.

It is interesting to note the following peculiarity. One can see that both the RW, which is the sequence of kinks and the OW, which is the sequence of kink-antikink pairs, transform to the soliton (11c) at $m = 1$. For this the threshold wave velocity $v_{th} = \omega_{th}/k_{th} \rightarrow (1/2)^{1/2}$. But for RW the stability region is determined by the condition $v > v_{th}$ whereas for OW one is $v < v_{th}$. This fact can be apparently explained by the difference of a topological properties of solutions (11a,b).

In conclusion it is necessary note that at a simultaneous account of highest gradient terms and external magnetic fields the NLC dynamics can be reduced to other exactly integrated model, which is the combination of SG and mKdV equations [18].

REFERENCES

1. L. Lin, C. Q. Shu, G. Xu. J. Stat. Phys. 39:633(1985)
2. X. Y. Wang, Z. M. Sun. Nonlinear dynamical phenomena in liquid crystals// Int. Cent. Theor. Phys. (Prepr.). No. 305(1988).
3. "Solitons in Liquid Crystals", Eds. L. Lam, J. Prost. Springer-Verlag(1989).
4. G. Zhu. Phys. Rev. Lett. 49:1332(1982).
5. M. Lowe, J. R. Gollub. Phys. Rev. A. 31:3893(1985).
6. W. Helfrich. Phys. Rev. Lett. 1968. 21:1518(1968).
7. P. G. de Gennes. J. de Phys. (Fr). 32:789(1971).
8. F. Brochard. J. de Phys. (Fr). 33:607(1972).
9. L. Leger. Solid St. Comm. 11:1499(1972).
10. P. G. de Gennes. "The physics of liquid crystals", Clarendon Press, Oxford (1974).
11. V. I. Karpman, E. P. Maslov, V. V. Solov'yov. Zh. Eksp. Teor. Fiz. 84:288(1984).
12. O. H. Olsen, M. R. Samuelson. Phys. Rev. B. 28:210(1983).
13. B. A. Malomed. Physica D. 27:113(1987).
14. V. G. Kamensky, S. S. Rozhkov. Zh. Eksp. Teor. Fiz. 89:106(1985).
15. N. Flytzanis, St. Pnevmatikos, M. Remoissenet. Physica D. 18:4603(1985). Phys. Rev. B. 33:2308(1986).
16. J. G. Berryman. Phys. of Fluids. 19:771(1976).
17. G. E. Fal'kovich, M. D. Spektor, S. K. Turitsyn. Phys. Lett. A. 99:271(1983).
18. N. Flytzanis, St. Pnevmatikos, M. Remoissenet. Physica D, 26:311(1987).
19. G. B. Whitham, Linear and nonlinear wave, N.Y., 1974.
20. A. F. Givental. Teor. Math. Fiz. 82:28(1990).
21. F. Kh. Abdullaev, A. A. Abdumalikov, E. N. Tsoi. Phys. Lett. A 151:221(1990).

QUANTUM CAPTURE IN LB MONOLAYERS AND THE ROLE OF THERMAL FLUCTUATIONS

J.A. Tuszynski,* E.A. Bartnik† and K.J. Blinowska†

*Department of Physics, University of Alberta
Edmonton, Alberta, T6G 2J1, Canada

†Faculty of Physics, University of Warsaw
Hoza 69 Street, 00-681, Warsaw, Poland

ABSTRACT

A model of efficient energy transfer in Langmuir-Blodgett monolayers involving direct exciton capture on bound states of an acceptor molecule is studied numerically and analytically. It is shown that the capture mechanism survives thermal fluctuations affecting the coupling constant up to magnitudes corresponding to lattice melting and into the fluid state. A theoretical explanation is outlined.

1. INTRODUCTION

Nearly lossless transfer of energy over distances of up to 100 nm was experimentally discovered by Kuhn^{1,2} and Möbius³ in a type of Langmuir-Blodgett monolayers⁴ usually called J-aggregates. A J-aggregate is a monolayer, a micelle or a vesicle formed as a functional unit acting as an entity in a purposeful manner.¹ Structurally, it is a compact and regular arrangement of chromophores attached to hydrophobic carbon tails. The interstices between the carbon tails are filled with molecules (e.g. octadecane) which make the layer rigid and compact. Using LB techniques, Kuhn¹ has prepared J-aggregates in which as little as one in 10,000 molecules of chromophore was an acceptor, the rest being donors. In such structures, it was discovered¹ that, when irradiated with ultraviolet or visible light, donor fluorescence was strongly quenched. Simultaneously, an acceptor fluorescence line appeared, which was somewhat red shifted. It thus appears that the monolayer acts as a cooperative molecular array which, after absorbing a photon, channels the energy laterally over exceptionally long distances to a particular energy-accepting molecule. The effect has not been observed in aggregates where the molecular "filler" is absent and whose structure is less rigid and less ordered.

Thus, excited J-aggregates can be viewed as a large array of coupled quantum oscillators. A different (guest) molecule characterized by a resonance frequency slightly lower than the host molecule's would therefore act as an energy trap once it is incorporated into the lattice. In addition to energy trapping by the guest molecules in the J-aggregate there exists the possibility of electron transfer from the excited host molecule to a guest molecule resulting in a quenching of the J-aggregate's fluorescence.

Studies of energy transfer in photosynthetic and biological systems such as chlorophyll indicate⁵ that: (a) lattice models are usually closer to reality than random arrangements, (b) transport is best described as hopping, and (c) exciton trapping on a small fraction (typically 1%) of photochemical reaction centers is not diffusion limited.

There exists a vast body of literature concerned with the question of exciton transport and trapping in molecular crystals and biological molecular aggregates. Since these systems bear a relationship with J-aggregates, we first give a brief overview of the most important results known to date which will serve as guidelines for the development of our models.

The main dividing line in the study of excitons is whether they are localized (incoherent) or delocalized (coherent). It is believed⁶ that exciton migration in the absence of phonons occurs coherently at first with $\langle x^2 \rangle \propto t^2$, where x denotes position and t time. Later in time the process becomes incoherent and satisfies the relationship $\langle x^2 \rangle \sim t$ typical for diffusion. The two regimes leave their imprint on the absorption lines. Lorentzian character of the absorption lines is due to coherent behavior while Gaussian forms arise due to incoherent motion. The former is highly temperature dependent and occurs with weak exciton-phonon coupling, the latter takes place when exciton-phonon coupling is strong. In general, therefore, one should expect an intermediate regime where both localized and delocalized excitons participate in energy transfer.^{6,7,8} The problem is rather complex and the presence of traps makes it even more complicated. Our approach should explore the many possible modes of behavior that exist and discuss the physical manifestations of each of them.

In fact, a recent paper⁹ lists the following six pathways to energy relaxation in LB monolayers with dye molecules present: (i) monomer fluorescence, (ii) aggregate fluorescence, (iii) energy trapping, (iv) energy migration between donors, (v) excimer formation, and (vi) energy migration to lower energy sites and trapping there. The various processes are manifested by inhomogeneous broadening of phosphorescence spectra.

II. THE QUANTUM MODEL

The molecules that we are concerned with are chromophores, i.e. they have a delocalized electron which can be excited by light to a higher energy level above the ground state with Ω denoting the energy difference. Note that throughout this paper we have used units with $\hbar = 1$. We model this system by an oscillator with an appropriate energy spacing. In addition, the close packing of chromophores induces a strong electron-electron interaction (of dipole-dipole type) with resonant energy J . The parameters Ω and J are difficult to calculate *ab initio* from theory but, fortunately, we can estimate them from the monomer and dimer experimental spectra. We have then the following Hamiltonian typical for the molecular exciton model in a dimer⁶

$$H_2 = \Omega (A_1^\dagger A_1 + A_2^\dagger A_2) - J (A_1^\dagger A_2 + A_2^\dagger A_1) \quad , \quad (1)$$

where the operators A_α^\dagger , A_α ($\alpha = 1, 2$) refer to a creation and destruction of a quantum of excitonic energy at site α , respectively. Hence, the eigenvalues E are found as $E = \Omega \pm J$. Using the data for oxycyanine yields: $\Omega = 3.125$ eV for a monomer, $E = 3.261$ eV for a dimer, and, consequently, the coupling constant J is calculated as $J = 0.136$ eV. These data will be used for modeling of monolayer assemblies composed of both donor and acceptor molecules. Note that a typical transit time⁶ between two sites of a molecular dimer is on the order of 10^{-14} s, i.e. much too short to account for the observed migration and

transport effects in J-aggregates. To properly simulate exciton kinetics we require lattice models.

Since the bricklayer structure appears highly anisotropic with substantial elongation along the x-axis, it seems appropriate to study a one-dimensional approximation to the problem as a first step towards understanding cooperative behavior. The model Hamiltonian is composed of two parts:

$$H_o^{1D} = H_o^{1D} + H_{acc}^{1D} \quad (2)$$

where the donor molecules are accounted for through

$$H_o^{1D} = \sum_{n=-\infty}^{+\infty} \Omega A_n^+ A_n - J A_n^+ (A_{n-1} + A_{n+1}) \quad (3)$$

and the acceptor contribution is

$$H_{acc}^{1D} = -V A_o^+ A_o + (J_o - J) \{A_o^+ (A_1 + A_{-1}) + A_o (A_1^+ + A_{-1}^+)\} \quad (4)$$

Taking the eigenfunction in the form of a linear superposition of excitations

$$|\psi\rangle = \sum_{n=-\infty}^{+\infty} a_n A_n^+ |\Omega\rangle \quad (5)$$

yields a very important relation between the binding energy z and the decay rate of the wave function

$$(z - \Omega) = -J(\mu + 1/\mu) \quad (6)$$

where we have used: $a_n = \mu^n$. In order to have the wave function centered around the acceptor and extending over many sites it is required that μ be close to 1. Introducing dimensionless quantities: $w = V/J$ and $\gamma = J_o/J$, it can be shown that the eigenvalue problem yields

$$\mu_{1,2} = \frac{1}{2(1 - 2\gamma^2)} \left\{ w \pm (w^2 - 4 + 8\gamma^2)^{1/2} \right\} \quad (7)$$

It is easily seen that with γ small we need $w = 2$. Then, taking $w = 2$ an optimal case is found for $\gamma \ll 1$ as $\mu = 1 - \sqrt{2} \gamma$.

Numerical simulations of the time-dependent Schrödinger equation for the chain Hamiltonian of eq. (2) were recently performed which involved solving coupled differential equations.^{10,11} The numerical simulation was performed¹¹ for the chain of 1000 molecules. In these simulations the acceptor was placed in the middle of the string of molecules. The initial condition assumed the same probability of excitation for each particle. This situation corresponds to the irradiation of the molecular assembly by a short laser pulse. It can then be seen that the acceptor causes the probability distribution $a_n(t)$ to evolve in time, especially at locations in its immediate vicinity. In general, the probability amplitude at a given site tends to oscillate with the exception of the acceptor site itself where the excitation probability increases. In general, no case led to the observation of a large probability of excitation at the acceptor site (Fig. 1). However, for the optimal choice of parameters the situation changes dramatically (Fig. 2). The probability at the acceptor site attains very large values at the cost of the neighboring sites, whose excitation probabilities decrease. In other words, the acceptor absorbs the probability amplitude from the neighboring sites. Furthermore, the probability of excitation at the acceptor site increases to large values before the disturbance has propagated over a long distance, i.e. the process is very fast.

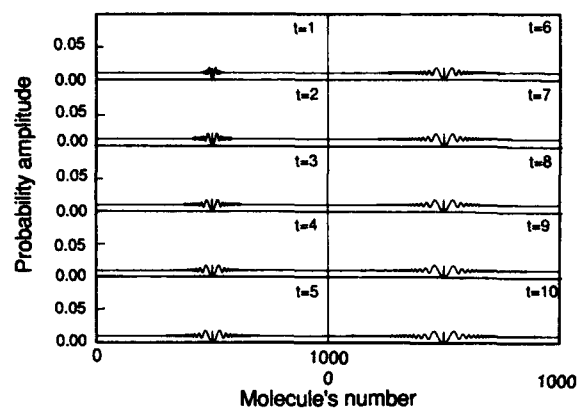


Fig. 1 Time evolution of the excitation probability for non-optimal parameters $w=5$, $\gamma=1$, shown in steps from $t=1$ to $t=10$. A string of 1000 molecules, with the acceptor located at molecule number 500, was used.

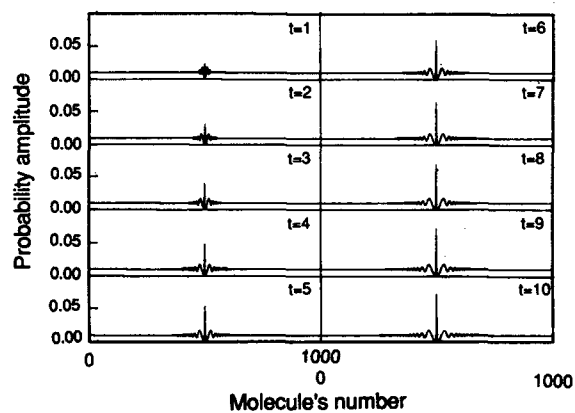


Fig. 2. Time evolution of the excitation probability for a near-optimal set of parameters: $w=2$, $\gamma=0.1$. The same setting as in Fig. 1 has been used.

III. THERMAL FLUCTUATIONS

A natural question that arises in this context is the stability of the phenomenon with respect to positional disorder. The fluctuations of the molecular site distances (denoted by d) can be readily related to the changes of coupling constant J , since $J \sim d^{-6}$ (due to dipole-dipole interactions of excited electrons). We can replace J by $J \pm \Delta J$ with ΔJ being a random probabilistic variable. The first calculation we carried out was to estimate the typical size of $\Delta d/d$ for the Debye model of acoustic phonons as applied to the assumed brick layer lattice¹² of a J-aggregate. In the harmonic approximation the Hamiltonian is given by

$$H \simeq \sum_{i=1}^m \int \frac{d^m k}{(2\pi)^m} \hbar \omega_i(k) \left[\frac{1}{2} + a_k^+ a_k \right], \quad (8)$$

where k labels normal modes, i denotes branches of acoustic phonons, m is the lattice dimensionality, the frequency is $\omega \simeq k(W/M)^{1/2}$ with M being the monomer's mass and W its stiffness constant. To calculate thermal averages we denote $d = u_{n+1} - u_n$ to represent the relative displacement and we find that in 2-D and in the high-temperature limit

$$\langle d^2 \rangle = (4\pi^2)^{-1} \sum_{i=1,2} \int d^2 k_i (M\omega_{k_i})^{-1} (1 - \cos k_i) \langle a_{k_i}^+ a_{k_i} + a_{k_i} a_{k_i}^+ \rangle \simeq (4\pi \hbar^2 / M k_B \theta_D) (T/\theta_D), \quad (9)$$

where θ_D denotes the Debye temperature.¹³ Assuming that the unit monomer (oxycyanine) contains 20 carbon atoms we find $M \simeq 4 \cdot 10^{-25}$ kg. Taking a low estimate of the Debye temperature as $\theta_D \simeq 300$ K, we obtain at a room temperature limit $\sqrt{\langle d^2 \rangle} \simeq 0.1$ Å as compared with the typical lattice separation of 16 Å. Note also that in the crystal phase the temperature dependence of the fluctuations in the coupling constant J will be: $\Delta J/J \propto T^{1/2}$, with a maximum value of the relative fluctuation at approximately 0.04.

At higher temperatures, but certainly below the room temperature range, the aggregate will experience a substantial softening of the lattice and eventually become a two-dimensional anisotropic fluid. This results from a weakening of the harmonic terms in the Hamiltonian and a simultaneous development of strong anharmonicities. To describe this cross-over region between a two-dimensional crystal and a liquid we adopt a semi-classical picture with a Landau-Ginzburg Hamiltonian of the type¹⁴

$$H_{LG} \equiv \int d^2 x [A_2 \rho^2 + A_4 \rho^4 + D (\nabla \rho)^2], \quad (10)$$

where ρ describes a local mass density and D is a Ginzburg inhomogeneity parameter. As we approach the melting temperature $T \rightarrow T_m$, $A_2 \rightarrow 0$ linearly with T . In order to properly describe this regime we adopt the following procedure: (i) Fourier transform ρ into k -space, (ii) rewrite H_{LG} accordingly, and (iii) approximate H_{LG} by including only paired-up modes in the interaction part (i.e. k and $-k$ components). Thus,

$$H_{LG} \equiv \sum_{k < \Lambda} \left[(A_2 + Dk^2) |\rho_k|^2 + \frac{6}{\Delta} A_4 |\rho_k|^4 \right], \quad (11)$$

where Δ is the cross-sectional area of the system and Λ is the cutoff such that $\Lambda = 2\pi/d$. Using a recently developed non-Gaussian method¹⁵ of treating fluctuations for strongly anharmonic systems we find that close to T_m

$$\langle |\rho_k|^2 \rangle \sim \exp \left[- \left(\frac{\Delta}{k_B T A_4} \right)^{1/2} D k^2 \right] . \quad (12)$$

Since at temperatures T close to the critical point T_m the long wavelengths dominate and the first mode to soften at T is: $k_c^2 = -\frac{A_2}{D}$, where $A_2 = a(T - T_m)$. Thus, using eq. (12) and the above we obtain

$$\langle |\rho_k|^2 \rangle \sim \exp \left[+ \left(\frac{\Delta}{k_B T A_4} \right)^{1/2} A_2 \right] . \quad (13)$$

This means that density fluctuations grow exponentially up to their maximum value as the density approaches ρ_c^0 at $T = T_m$. This is approximated according to

$$\sqrt{\frac{\langle |\rho_k|^2 \rangle}{\rho_c^0}} = \exp \left[\alpha \left(\frac{T - T_m}{\sqrt{T}} \right) \right] , \quad (14)$$

with $\alpha = \frac{1}{2} \sqrt{\frac{\Delta}{k_B A_4}}$ on approaching T_m from below.

Above the melting temperature we expect a typical behavior for liquids where fluctuations, over a broad range of temperatures below boiling are virtually independent of temperature. Based on the structure factor $S(q)$ for typical three-dimensional liquids¹⁶ it

can be surmised that*: $\frac{\sqrt{\langle (\Delta d)^2 \rangle}}{d} \sim \frac{0.5\text{\AA}}{30\text{\AA}}$. Hence, it translates into $\Delta J/J \sim 0.10$.

To summarize this theoretical part we expect 3 regimes to occur: (i) the crystal phase (low temperatures) with $\Delta J/J \sim \sqrt{T}$, (ii) the melting region (intermediate temperatures) with $\Delta J/J \sim \exp[\alpha(T - T_m)/\sqrt{T}]$, and (iii) the liquid phase where $\Delta J/J \equiv \text{const}$. We then proceed to perform numerical experiments intended to examine the influence of fluctuations in J on the quantum capture process by an acceptor. The numerical findings are quite remarkable and are illustrated in Fig. 3. What appears to occur is that the quantum capture mechanism persists up to the value of $\Delta J/J \sim 0.1$ which corresponds to a two-dimensional liquid regime as seen in Fig. 4. Moreover, as can be seen in Fig. 3, it is crucial that the random noise generated through fluctuations ΔJ does not destroy the main feature of the system, i.e. the existence of a shallow bound state on the acceptor.¹⁰ The failure to satisfy this requirement would either cause the level to be too deep and as a result the fine tuning required for capture disappears or the acceptor state becomes too shallow leading to scattering but no binding. However, we must emphasize the surprising property of resilience of the quantum capture mechanism against very large structural fluctuations (beyond their thermal value for a crystal lattice).

* Based on experimental surface pressure-area isotherms in Ref.1, we estimate the mean intermonomer distance to increase to approximately 30Å in the fluid like phase.

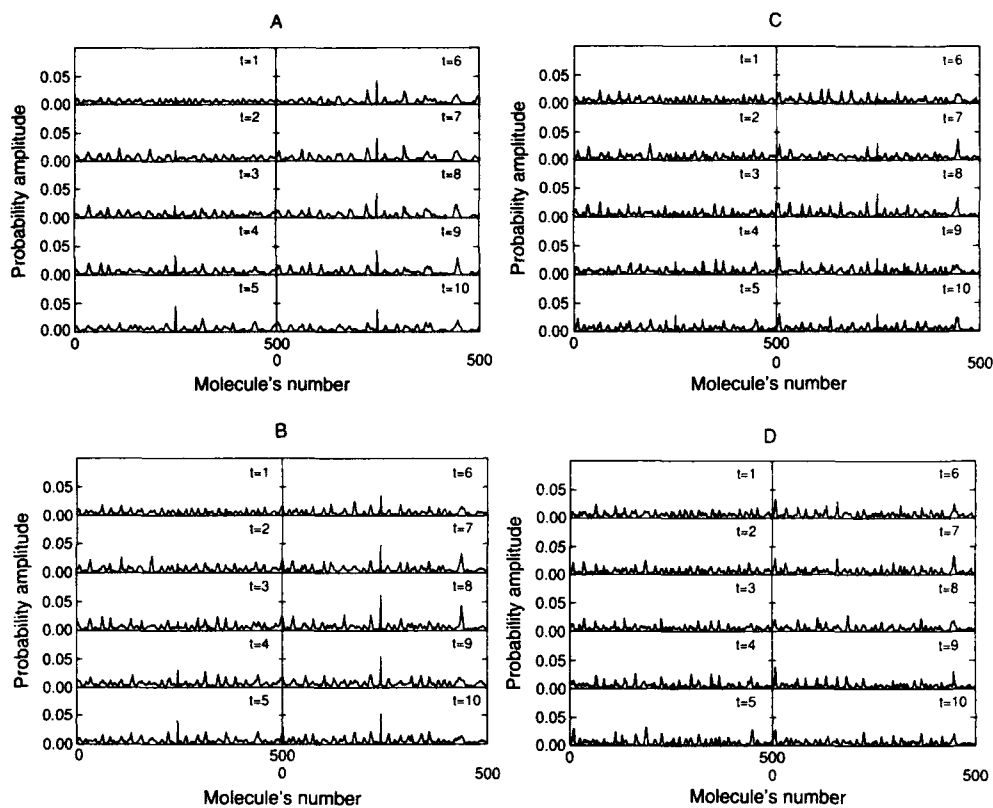


Fig. 3. Time evolution of the probability distribution when the fluctuations ΔJ of the coupling constant are added. Here, $\Delta J = \sigma_J R$, where R is a random number scaled into the unit interval (0,1) and $\sigma_J = 0.01$. R changes for each evolution. A string of 500 molecules, with the acceptor located at molecule number 250, was used. (A) $\sigma_J = 0.01$, (B) $\sigma_J = 0.0175$, (C) $\sigma_J = 0.0205$, (D) $\sigma_J = 0.0025$.

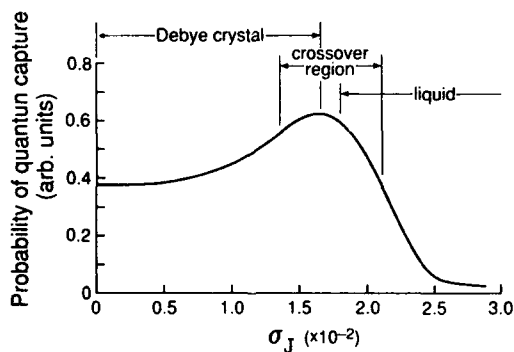


Fig. 4 Probability of quantum capture as a function of noise level σ_J .

In fact, a simple explanation of this behavior can be deduced from perturbation theory. Taking the fluctuations in eq. (2) as the perturbation

$$\Delta V = \sum_n \Delta J_n A_n^* (A_{n-1} + A_{n+1}) \quad (15)$$

where ΔJ_n represents the white noise with variance σ_J , the first order energy shift is

$$\Delta E = \langle \psi_0 | \Delta V | \psi_0 \rangle \quad (16)$$

This can be easily evaluated since the wave function is simply:¹¹ $\psi(n) = z^n$ where $0 < z < 1$. Outside the acceptor, and shallow bound states, z is very close to 1. Then,

$$\Delta E \cong (1 - z^2) \sum_n \Delta J_n z^{2n} \quad (17)$$

Hence,

$$\sqrt{\langle (\Delta E)^2 \rangle} = \sigma_J \sqrt{1 - z^2} = \frac{\sigma_J}{\sqrt{N}} \quad (18)$$

where $N \equiv (1 - z^2)^{-1}$ is the spatial extent of the wave function. We, therefore, come to the seemingly paradoxical conclusion that the shallower the bound state and the longer its extent, the smaller is the effect of fluctuations. Therefore, we have demonstrated both numerically and analytically that the quantum capture by a shallow bound state, as postulated in refs. 10-11, is remarkably stable against random disorder of liquid-type. This fact has obvious biological implications; for example in the understanding of cellular membranes.

IV. DISCUSSION

Capture of exciton energy by impurity molecules (traps) depends critically on whether the excitons are coherent or incoherent. In both of these cases the temperature dependence of the energy transfer is different. For deep trap levels the probability of coherent exciton capture is largely temperature independent up to high temperatures where it is proportional to $\exp(-\Delta E/kT)$ with ΔE denoting activation energy. For shallow energy traps (as is believed to be the case with J-aggregates), if the trap depth is much less than the Debye energy, then one acoustic phonon is sufficient to capture an exciton on an impurity.⁷ Otherwise, exciton capture is a multiphonon process. As a consequence one finds that at low temperatures (compared to trap depth energy) the capture cross-section is proportional to $T^{1/2}$, while at high temperatures it is proportional to $T^{5/2}$. Then the probability of capture shows a cross-over from a nearby constant value at low temperatures to that proportional to T^3 at high temperatures. This temperature dependence is not compatible with the one found experimentally,^{12,17} where the efficiency of energy transfer was estimated to be proportional to T between 20 and 300 K, which agrees better with the incoherent exciton mechanism. On the other hand, for shallow energy traps it was found¹⁸ that coherent excitons are more likely to be captured. The quenching rate of coherent excitons by isolated impurities is proportional to the cubic power of their concentration.⁸ In order to resolve this discrepancy Möbius and Kuhn^{12,17} proposed a finite-size domain of coherent excitations whose size increases with the coupling constant but decreases with T^{-1} due to thermal fluctuations. They found the lifetime of excitons to be proportional to $T^{-1/2}$ which is consistent with a coherent exciton model. This intermediate picture has been

recently simulated numerically¹⁹ and an empirical relationship was found that gives the size of the coherence domain as: $N_{\text{eff}} = 3000/T(\text{K})$. The inclusion of acoustic and optical phonons may reduce N_{eff} to 1 at room temperature.

The mechanism proposed by us is not inconsistent with the postulate about the domains of exciton coherence. The range of the possible capture distance is determined by the properties of the acceptor and donor molecules. In agreement with our finding it was observed⁷ that incoherent excitons with the inclusion of phonons, are characterized by an effective radius R_0 for capture by a trap, which typically exceeds 10 lattice periods. The quenching rate is proportional to the square of the concentration of impurities. The transfer probability for exciton migration depends inversely on the sixth power of the distance between sites and, at low temperatures is proportional to the absolute temperature i.e. is thermally activated. This is consistent with experimental observations²⁰ for molecular crystals such as naphthalene, where the efficiency of energy transfer is proportional to T for low concentrations of acceptor molecules (10^{-4} to 10^{-2}). A possible explanation of that is a combined kinetic and diffusion model-thermal fluctuations as well as phonons assist in hopping. It seems that the process of quantum energy capture in J-aggregates is a complex one and various mechanisms contribute differently at different temperature regimes. It is most likely that both coherent and incoherent excitons are at play over a broad temperature ranges and impurity concentration values. Further investigations are necessary to provide a complete theory of phenomenon.

ACKNOWLEDGMENTS

This research was supported by NSERC and NATO.

REFERENCES

1. H. Kuhn, Synthetic molecular organizates, *J. Photochem.* 10:111 (1979).
2. H. Bücher and H. Kuhn, Scheibe aggregate formalism of cyanine dyes in monolayers, *Chem. Phys. Lett.* 6:183 (1970).
3. D. Möbius, Designed monolayer assemblies, *Ber. Bunsenges Phys. Chem.* 82:848 (1978).
4. R.H. Tredgold, The physics of Langmuir-Blodgett films, *Rep. Prog. Phys.* 50:1609 (1987).
5. R.M. Pearlstein, Excitons in photosynthetic and other biological systems, in: "Excitons," E.I. Rashba and M.D. Sturge, eds., North-Holland, Amsterdam (1982).
6. M. Pope and C.E. Swenberg, "Electronic Processes in Organic Crystals," Clarendon Press, Oxford (1982).
7. V.M. Agranovich and M.D. Galanin, "Electronic Excitation Energy Transfer in Condensed Matter," North-Holland, Amsterdam (1982).
8. R.P. Hemenger, K. Lakatos-Lindenberg and R.M. Pearlstein, Impurity quenching of molecular excitons. III Partially coherent excitons in linear chains, *J. Chem. Phys.* 60:3271 (1974).
9. N. Tamai, T. Yamazaki and I. Yamazaki, Picosecond dynamics of excitation-energy relaxation of dye molecules in L-B monolayers, *Can. J. Phys.* 68: 1013 (1990).
10. E.A. Bartnik, K.J. Blinowska, Efficient energy transfer in L-B monolayers by optimized quantum capture, *Phys. Lett. A* 134:448 (1989).
11. B.A. Bartnik, K.J. Blinowska and J.A. Tuszynski, The possibility of an excitonic fast and nearly lossless energy transfer in biomolecular systems, *Phys. Lett. A* 159:67 (1991).
12. D. Möbius and H. Kuhn, Energy transfer in monolayers with cyanine dye Scheibe aggregates, *J. Appl. Phys.* 64:5138 (1988).
13. C. Kittel, "Quantum Theory of Solids," John Wiley & Sons, New York (1963).
14. J.A. Tuszynski, M.J. Clouter and H. Kieft, Non-gaussian models for critical fluctuations, *Phys. Rev. B* 33:3423 (1986).

15. J.A. Tuszynski and A. Wierzbicki, Non-gaussian approach to critical fluctuations in the Landau-Ginzburg model and finite-size scaling, *Phys. Rev. B* 43:8472 (1991).
16. N.H. March and M. Parrinello, "Collective Effects in Solids and Liquids," A. Hilger, Bristol (1982).
17. D. Möbius and H. Kuhn, Monolayer assemblies of dyes to study the role of thermal collisions in energy transfer, *Isr. J. Chem.* 18:375 (1979).
18. I.S. Osad'ko, Theory of light absorption and emission by organic impurity centers, p. 437, in: "Spectroscopy and Excitation Dynamics of Condensed Molecular Systems," V.M. Agranovich and R.M. Hochstrasser, eds., North-Holland, Amsterdam (1983).
19. F.C. Spano, J.R. Kuklinski and S. Mukamel, Temperature-dependent superradiant decay of excitons in small aggregates, *Phys. Rev. Lett.* 65:211 (1990).
20. R. Kopelman, Energy transport in mixed molecular crystals, p.139, in: "Spectroscopy and Excitation Dynamics of Condensed Molecular Systems," V.M. Agranovich and R.M. Hochstrasser, eds., North-Holland, Amsterdam (1983).

SOLITON MECHANISM OF OPTICAL ANISOTROPY PHOTOINDUCTION IN TWO-DIMENSIONAL MOLECULAR SYSTEMS

Yu. B. Gaididei

Bogolyubov Institute for Theoretical Physics
Ukrainian Academy of Sciences
252143 Kiev, Ukraine

INTRODUCTION

The change in the anisotropic optical properties of a crystal under light irradiation, i.e. photoinduced optical anisotropy (POA), has been the subject of investigations for a long period¹. Recently POA in Langmuir-Blodgett (LB) films after irradiation was recorded². In the layer plane (plane XOY) these films are optically isotropic. However, after the action produced by a linearly polarized light propagating along the OZ axis with a frequency within the absorption region of the substance, the films became biaxial.

This paper aims to clarify the nature of the POA of layered molecular systems. It is shown that changes in the energy of the orientation interaction between molecules in the excited state with respect to the ground state cause their rearrangement in the layer. Intermolecular orientational interaction provides a coherent and cooperative soliton character of rearrangement.

ORIENTATION ORDER IN THE LAYER

We assume that the centres of molecules form a square lattice. The energy of molecular orientational ordering per unit area has the form

$$F = I(\nabla\Phi)^2 - \frac{1}{2}A \cos 4\Phi(\vec{r}) \quad (1)$$

where $\varphi(\vec{r})$ is the angle formed by the large molecule axis and the X axis, I and A are positive energy constants. We will discuss the orientational distribution that characterized by fourth-order symmetry axis (optical isotropic distribution). Such a distribution may arise near orientational defects. For example, in LB films these defects may be created by the molecules whose aliphatic end is directed to the hydrophilic side. In this case a boundary condition

$$\vec{r} \nabla \Phi(\vec{r}) \Big|_{\vec{r} \rightarrow 0} = 0 \quad (2)$$

takes place ($\vec{r} = 0$ is the defect position). The simplest example of such a distribution is

$$\varphi = -\arctan \frac{\sinh \alpha y}{\sinh \alpha x}, \quad \alpha^2 = \frac{2A}{I}. \quad (3)$$

It is seen that this vortex-like structure may be regarded as an intersection of two mutually perpendicular $\frac{\pi}{2}$ -kinks situated on the lines $y = \pm x$.

The optical anisotropy is characterized by the quantity

$$q = \frac{\kappa_{xx} - \kappa_{yy}}{\kappa_{xx} + \kappa_{yy}} = \frac{1}{S} \int d\vec{r} \cos 2\varphi(\vec{r}) \quad (4)$$

where $\kappa_{xx}(\kappa_{yy})$ is the film absorption coefficient of the light polarized along the $X(Y)$ axis, S is the area of the incident beam. Inserting (3) into (4) we see that $q = 0$ in this case.

When a molecular laser is irradiated by polarized light $\vec{E}(\vec{r}, t) = \vec{E} \cos(\vec{Q}\vec{r} - \omega t)$ (ω is the electronic eigenfrequency of the laser) some molecules occur excited and in the orientational energy there are terms that depend on the number of excited molecules,

$$F_{\text{int}} = -\frac{1}{2} A_{\text{ex}} P(\vec{r}) \cos 2\varphi(\vec{r})$$

where $A_{\text{ex}} \sim (\mu_{\text{ex}} - \mu_{\text{gr}})^2$ (μ_{ex} (μ_{gr}) is the molecular dipole moment in the excited (ground) state), $P(\vec{r})$ is the probability for finding the r th molecule in the excited state. The order in the irradiated layer can be described by the equations³:

$$I \nabla^2 \varphi(\vec{r}) - (A - A_{\text{ex}} P(\vec{r})) \sin 4\varphi(\vec{r}) = 0 \quad (5)$$

$$P(\vec{r}) = P \cos^2(\varphi(\vec{r}) - \Psi) \quad (6)$$

where $P = \frac{(Ed)^2}{\Gamma(\gamma)}$ (d is the transition dipole moment, $\Gamma(\gamma)$ is the transversal (longitudinal) relaxation rate of the excited state). If in the absence of radiation, the orientation order is determined by the function (3) then as follows from Eqns (5) and (6), in the vicinity of the vortex centre we can write approximately

$$\varphi = -\theta - \frac{1}{32} w (\alpha\rho)^2 \ln(\alpha\rho) \sin 2(\theta - \Psi) \quad (\alpha\rho < 1) \quad (7)$$

where $x = \rho \cos \theta$, $y = \rho \sin \theta$, $w = \frac{A_{\text{ex}}}{A} p$. Far from the vortex centre

$$1 \ll (\text{sh}^2 \alpha x + \text{sh}^2 \alpha y) < R_c \quad (8)$$

where $\ln R_c = -\frac{2}{3}(6w)^{-\frac{2}{3}} \ln(6w)$ ($w \ll 1$), the orientation order is described by the function

$$\varphi = \varphi_0 - \frac{1}{4} (6w)^{\frac{1}{3}} [(\text{sh}^2 \alpha x + \text{sh}^2 \alpha y)^{(6w)^{\frac{2}{3}}} - 1] \sin 2\varphi_0 \cos 2\Psi \quad (9)$$

At $x, y \rightarrow \infty$ the steady state (3) is unstable and one can show³ that the walls $y = \pm x$ move with a linear velocity $v = -\frac{5w\sqrt{A\gamma}}{24\lambda} \cos 2\Psi$ (the parameter λ characterizes the dissipation process in the orientation system).

It is worth noting that the walls can move freely in the continuum approximation only. Taking into account the discreteness of the lattice, one can show that the solitons move in some periodic potential profile⁴. Consequently the molecular system rearranges under the action of the light if the condition

$$w > (\alpha a)^{-2} \exp[-\pi^2(\alpha a)^{-1}] \quad (10)$$

holds (a is the lattice constant). Here the right hand side is the dimensionless height of the potential barrier. We see from (10) that the walls with the width $\alpha^{-1} = (2/3) a$ can move in the LB film with $A_{ex} \sim A$ under the action of the light creating $N_{ex} = 10^{-6} N$ excitations in the layer (N is the total number of molecules in the layer).

Inserting (7) and (9) in (4) we obtain that the optical anisotropy coefficient of the irradiated film can be written as follows

$$q = \frac{\pi^2}{2} (6w)^{-\frac{1}{2}} \frac{\exp[(6w)^{\frac{2}{3}} \alpha R] - (6w)^{\frac{2}{3}} \alpha R - 1}{(\alpha R)^2}$$

where R ($R \ll R_c$) is the mean distance between defects in the film.

If $R \gg R_c$ there are parts of walls that move nearly freely. In this case the optical anisotropy coefficient increases in time with a velocity $\frac{dq}{dt} \sim \frac{v}{R} \tanh \alpha R$.

REFERENCES

1. T.S.Narasimhamurthy. "Photoelastic and Electrooptic Properties of Crystals" Plenum Press. New York (1981).
2. M.Barnik, V.M.Kozenkov. S.P.Palto, N.M.Shtykov and S.G.Yudin, J. Mol. Electron., 5:53 (1989).
3. Yu.Gaididei and A.S.Trofimov, J. Mol. Electron., 5:239 (1989).
4. Yu.B.Gaididei and A.A.Vakhnenko, Theor. Math. Phys., 69:350(1986) (in Russian)

OPTICAL SECOND HARMONIC GENERATION IN LANGMUIR-BLODGETT FILMS

Tommy Geisler

Danish Institute of Fundamental Metrology
Lundtoftevej 100, building 307
DK-2800 Lyngby, Denmark

INTRODUCTION

Materials displaying nonlinear optical (NLO) effects are attracting increasing interest because of their potential applications in devices for processing optical information in optical communication systems¹⁻². Many organic materials have been shown to possess very large nonlinearities which can be attributed to the highly polarisable π -electrons³. A large molecular hyperpolarizability, β , responsible for second-order effects can be achieved in the charge asymmetric donor-acceptor molecules. However, to achieve large bulk second-order effects it is necessary to arrange the individual molecules in a noncentrosymmetric structure in order to avoid cancellation of the individual molecular nonlinearities.

A technique suited to construct artificial super-molecular arrays without inversion symmetry is the Langmuir-Blodgett (LB) deposition technique⁴. This is a molecular assembly technique where successive close-packed ordered insoluble monolayers of amphiphilic molecules (i.e. they consist of a hydrophobic and a hydrophilic part) are transferred from a water-air interface onto a solid substrate by repeatedly move the substrate vertically down and up through the monolayer. By derivatising highly NLO molecules with long hydrocarbon chains they may be candidates for LB film formation. The high degree of orientational order in LB films makes them suitable for optical second-order nonlinear processes like second harmonic generation (SHG). Furthermore, because of their welldefined thickness they are well qualified as waveguides if scattering losses can be overcome⁵.

In the present paper we evaluate the NLO properties of two different types of LB films by use of SHG measurements. One type of film is made of N-docosyl-4-nitroaniline (DCpNA)⁶ where the nonlinear chromophore (4-nitroaniline, pNA) is an intramolecular donor-acceptor system. While another type represents a new approach where a layer of donor-molecules, {7-(N-octa-dodecylaminomethyl)-8-16-dioxadibenzo(f,g]perylene}, is alternated with a layer of acceptor-molecules, {2-octadecylthio-1,4-benzoquinone} such that a close contact between the donor- and acceptor moiety is obtained, and they thereby form an intermolecular donor-acceptor interface⁷.

OPTICAL SECOND HARMONIC GENERATION

The NLO properties of the films were probed by second harmonic generation (SHG) measurements. The experimental setup is shown in figure 1. The laser is a 1000 pps Q-switched Nd:YAG laser operating at 1064 nm with a pulse duration of 140 nsec and an energy of less than 1 mJ. After passing through several filters and polarizing optics the fundamental beam was weakly focused on the sample. The polarization could be rotated by a $\lambda/2$ -plate. After suitable filtering (a combination of an IR-filter and a monochromator) the beam from the SHG (at 532 nm) was detected in a transmission geometry by a photomultiplier in connection with a photoncounter.

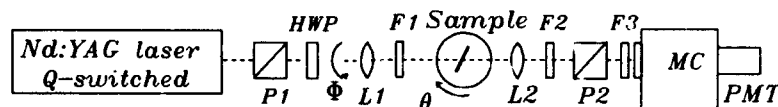


Figure 1: The experimental setup used for the SHG measurements on LB films. P1 and P2 are polarizers for 1064 nm and 532 nm, respectively. L1 and L2 are lenses, F2 and F3 are IR-blocking filters and F1 is a IR-pass filter. HWP is a halfwave plate.

In the following we consider the ultrathin LB film (with a few layers) as a 2-dimensional nonlinear polarization sheet on a linear substrate. The nonlinear polarization $\mathbf{P}(2\omega)$ responsible for the SHG is related to the incident electric field $\mathbf{E}(\omega)$ via a third rank susceptibility tensor $\chi^{(2)}$, as

$$P_i(2\omega) = \chi_{ijk}^{(2)} E_j(\omega) E_k(\omega), \quad (1)$$

where i, j, k denote vector components with respect to the x, y, z coordinate system with xy in the plane of the film and z parallel with the surface normal. The different nonvanishing tensor components of $\chi^{(2)}$ can be assessed by measuring the SHG for different combinations of polarizations and angle of incidence, θ . We consider a linearly polarized incoming laser beam polarized at an angle Φ with respect to the plane of incidence (the xz -plane). At normal incidence (i.e. $E_x(\omega) = 0$) the SHG polarized in the x -direction is given by

$$\begin{aligned} I_x^{2\omega}(\Phi) &= A \cdot |\chi_{xxx}^{(2)} E_x^\omega E_x^\omega + \chi_{xyx}^{(2)} E_y^\omega E_x^\omega + \chi_{xyy}^{(2)} E_y^\omega E_y^\omega|^2 \\ &= A \cdot |\chi_{xxx}^{(2)} \cos^2 \Phi + \chi_{xyx}^{(2)} \sin 2\Phi + \chi_{xyy}^{(2)} \sin^2 \Phi|^2 (E^\omega)^4, \end{aligned} \quad (2)$$

and there is made no assumptions regarding the symmetry of the film.

In figure 1 we have shown the SHG as a function of the incident polarization angle, Φ , from a bilayer sample of DCpNA oriented such that the dipping-axis is parallel with the x -axis. In the nonlinear chromophore of DCpNA the molecular hyperpolarizability β is dominated by a single component along the charge-transfer axis ($\hat{\zeta}$), i.e. that $\beta = \beta_{\zeta\zeta\zeta}$. The nonlinear susceptibility is then related to β through the following equation

$$\chi_{ijk}^{(2)} = N_s f_\omega^2 f_{2\omega} \langle (\hat{i}\hat{\zeta})(\hat{j}\hat{\zeta})(\hat{k}\hat{\zeta}) \rangle \beta, \quad (3)$$

where N_s is the surface density of molecules, f_ω and $f_{2\omega}$ are local field factors. The brackets denote an averaging over molecular orientations. From Eq. 3 the following relations are obtained

$$\begin{aligned}
\chi_{xxx}^{(2)} &= N_s f_\omega^2 f_{2\omega} \langle \sin^3 \psi \rangle \langle \cos^3 \phi \rangle \beta \\
\chi_{xyy}^{(2)} &= N_s f_\omega^2 f_{2\omega} \langle \sin^3 \psi \rangle \langle \cos \phi \sin^2 \phi \rangle \beta \\
\chi_{xyx}^{(2)} &= N_s f_\omega^2 f_{2\omega} \langle \sin^3 \psi \rangle \langle \cos^2 \phi \sin \phi \rangle \beta,
\end{aligned} \tag{4}$$

where ψ is the polar angle between the molecular axis \hat{z} and the surface normal, and ϕ is the azimuthal angle. A strong anisotropy with the nonlinear chromophores oriented in the dipping direction is responsible for the large $\chi_{xxx}^{(2)}$ -component. The almost negligible $\chi_{xyx}^{(2)}$ -component is due to a nearly symmetric arrangement with respect to the dipping-axis. However, films of DCpNA lose their ability to generate second harmonic which probably is due to reorientation of the chromophores into a centrosymmetric structure.

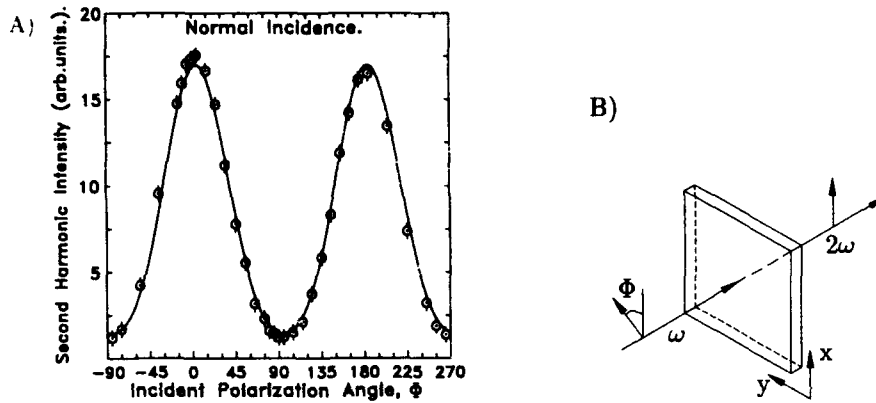


Figure 2: A) The second harmonic intensity $I_x^{2\omega}(\Phi)$. Symbols represent experimental points and the solid line shows the theoretical fit using Eq. 2, with the following ratios between tensor components $\chi_{xyy}^{(2)}/\chi_{xxx}^{(2)} = 0.307$ and $\chi_{xyx}^{(2)}/\chi_{xxx}^{(2)} = 0.056$. B) This shows the experimental configuration used.

The alternated donor acceptor films exhibit isotropy around the surface normal which reduces the $\chi^{(2)}$ to only two nonzero independent components, namely $\chi_{zzz}^{(2)}$ and $\chi_{zyy}^{(2)} = \chi_{zzx}^{(2)} = \chi_{zxx}^{(2)} = \chi_{zyx}^{(2)}$, where also Kleinman symmetry is assumed. The p-polarized SHG is given by

$$\begin{aligned}
I_p^{2\omega}(\Phi) &= |F_{zzz}\chi_{zzz}^{(2)}E_z^\omega E_z^\omega + F_{zyy}\chi_{zyy}^{(2)}E_y^\omega E_y^\omega + F_{zxx}\chi_{zxx}^{(2)}E_x^\omega E_x^\omega + 2F_{zzx}\chi_{zzx}^{(2)}E_z^\omega E_x^\omega|^2 \\
&= |[(F_{zxx} + 2F_{zzx}) \cdot \chi_{zzx}^{(2)} + F_{zzz} \cdot \chi_{zzz}^{(2)}] \cos^2 \Phi + F_{zyy} \cdot \chi_{zyy}^{(2)} \sin^2 \Phi|^2 (E^\omega)^4 \\
&= |a \cdot \cos^2 \Phi + b \cdot \sin^2 \Phi|^2 (E^\omega)^4,
\end{aligned} \tag{5}$$

where the factors F_{ijk} are geometry dependent and contains both the linear and non-linear Fresnel factors. From the ratio

$$\frac{a}{b} = \frac{F_{zxx} + 2F_{zzx}}{F_{zyy}} + \frac{F_{zzz} \chi_{zzz}^{(2)}}{F_{zyy} \chi_{zyy}^{(2)}} \tag{6}$$

we can calculate the ratio between the two tensor components.

In figure 3 we have shown the rotation pattern at an angle of incidence equal to 45°. The fit with Eq. 5 gives $a/b = -13.93$ from this we calculate $\chi_{zzz}^{(2)}/\chi_{zyy}^{(2)} = -74.41$.

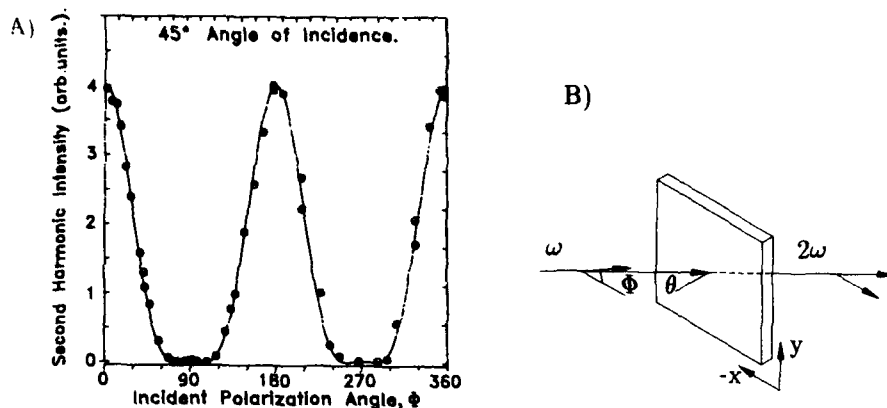


Figure 3: A) The second harmonic intensity $I_p^{2\omega}(\Phi)$. Symbols are experimental points and the solid line shows the theoretical fit using Eq. 5, with $a/b = -13.93$. B) This shows the experimental configuration used.

This shows that the major nonlinear component is perpendicular to the film plane as could be expected because of the intermolecular donor-acceptor interface.

CONCLUSION

SHG has been used to evaluate the nonlinear properties of two different types of LB films. An anisotropic structure was observed for the intramolecular donor-acceptor type film of DCpNA. Also a considerably nonlinearity was obtained in an intermolecular donor-acceptor type of film. This might open for new types of super-molecular arrays for nonlinear optical waveguides.

REFERENCES

- [1] D.S. Chemla and J. Zyss, Eds., "Nonlinear Optical Properties of Organic Molecules and Crystals", Vol. I,II, Academic Press, New York (1987).
- [2] S.R. Marder, J.E. Sohn and G.D. Stucky, Eds., "Materials for Nonlinear Optics: Chemical Perspectives", ACS Symposium Series 455, (1991).
- [3] D.J. Williams, Organic Polymeric and non-polymeric materials with large optical nonlinearities, *Angew. Chem. Int. Ed. Engl.* 23:690 (1984).
- [4] A. Ulman, "An Introduction to Ultrathin Organic Films, From Langmuir-Blodgett to Self-Assembly", Academic Press, Inc., New York (1991).
- [5] Ch. Bosshard, M. Flörsheimer, M. Küpfer and P. Günter, Cerenkov-type phase-matched second-harmonic generation in DCANP Langmuir-Blodgett film waveguides, *Optics Commun.* 85:247 (1991).
- [6] T. Geisler, S. Rosenkilde, P.S. Ramanujam, W.M.K.P. Wijekoon and P.N. Prasad, Second harmonic generation in anisotropic Langmuir-Blodgett films of N-docosyl-4-nitroaniline *Physica Scripta* 46:127 (1992).
- [7] T. Bjørnholm, T. Geisler, J. Larsen and M. Jørgensen, Nonlinear optical phenomena due to donor-acceptor interfaces created in Langmuir-Blodgett films, *J. Chem. Soc., Chem. Commun.* 1992:815 (1992).

NONLINEAR ENVELOPE WAVES IN INHOMOGENEOUS MEDIA

Boris A. Malomed

Department of Applied Mathematics
School of Mathematical Sciences
Tel Aviv University
Ramat Aviv 69978, Israel

In a number of physical problems, one deals with evolution of envelopes of high-frequency waves in inhomogeneous nonlinear media (see Ref. 1 and references therein). Of special interest is the situation when the wave is passing from a focussing domain into a defocussing one, or vice versa. For instance, the envelope solitons cannot exist in the defocussing medium, hence they must decay when entering it from the focussing domain. This effect has been recently analyzed in detail.¹ Here I will concentrate on the case when a continuous wave (cw) is traveling from the defocussing domain, where it is stable, into the focussing one, where it is subject to the modulational instability (MI). The analysis will be developed in terms of the well-known model of an inhomogeneous nonlinear optical fiber based on the following modified nonlinear Schrödinger (NS) equation:²

$$iu_z + \frac{1}{2}a(z)u_{tt} + |u|^2u + ibu_{ttt} = 0 \quad (1)$$

written in the standard notation, $a(z)$ being the spatially inhomogeneous dispersion coefficient. The last term with real b takes account of the higher dispersion, which is, generally speaking, necessary near the point where $a(z)$ vanishes. The exact cw solution to Eq. (1) is

$$u_0(t, z) = Q_0^{1/2} \exp(i \int k(z) dz - i \omega t), \quad (2)$$

where Q_0 is the power of the wave, and the local wave number is

$$k(z) = -\frac{1}{2}a(z)g^2 + Q_0 - bg^3. \quad (3)$$

To analyze the stability of this solution, the disturbed wave is taken in the form

$$u(t,z) = Q_0^{1/2}(1 + n(t,z)) \exp(i \int k(z)dz - igt + if(t,z)). \quad (4)$$

The amplitude and phase disturbances $n(t,z)$ and $f(t,z)$ are represented as follows:

$$n(t,z) = Q_0^{1/2}N(z) \exp(-iGt - igG \int a(z)dz - ibg^3z - 3ibg^2Gz), \quad (5a)$$

$$f(t,z) = F(z) \exp(-iGt - igG \int a(z)dz - ibg^3z - 3ibg^2Gz), \quad (5b)$$

to arrive at the following equations for $N(t,z)$ and $F(t,z)$:

$$\frac{dN}{dz} = \frac{1}{2}a(z)G^2F + 3bgG^2F, \quad (6a)$$

$$\frac{dF}{dz} = -\frac{1}{2}a(z)G^2N + 2Q_0N - 3bgG^2N. \quad (6b)$$

In what follows, the fundamental assumption will be adopted: a characteristic length at which the coefficient $a(z)$ varies is much larger than a characteristic scale of variation of the functions $N(z)$ and $F(z)$. In this case, a solution to Eqs. (6) can be looked for in the quasi-stationary approximation as follows:

$$N(z) = N_0(z) \exp(\int s(z)dz), \quad F(z) = F_0(z) \exp(\int s(z)dz), \quad (7)$$

$s(z)$, $N_0(z)$, and $F_0(z)$ being slowly varying functions. Insertion of Eqs. (7) into Eqs. (6) yields the instability gain $s(z)$ in the approximate form:

$$s(G, z) = G((\frac{1}{2}a(z) + 3bg)(2Q_0 - (\frac{1}{2}a(z) + 3bg)G^2)^{1/2}, \quad (8)$$

where G is assumed positive.

If the dispersion coefficient changes its sign at the point $z = 0$, it is natural to assume the linear dependence

$$a(z) = a'z. \quad (9)$$

The exponential amplification of the small disturbances is determined by the integral gain

$$S(G, z) = \int_{-\infty}^z \text{Re}(s(z')) dz'. \quad (10)$$

Inserting Eq. (9) into Eq. (8), one notes that the integrand is different from zero in the interval

$$0 < z' + 6bg/a' < 4Q_0/a'G^2. \quad (11)$$

When z exceeds the value $z_{\max}(G) = 4Q_0/a'G^2 - 6bg/a'$ (see Eq. (11)), $S(G, z)$ saturates as the function of z and attains the value

$$S(G) = \pi Q_0^2/a'G^2. \quad (12)$$

If one regards $S(G, z)$ as a function of G at fixed z , it takes the maximum value

$$S_{\max}(z) = S(G_{\max}(z)) = (\pi Q_0/2)(z + 6bg/a'), \quad (13)$$

$$G_{\max}^2 = 2b^{-1}Q_0/(z + 6bg/a'). \quad (14)$$

At $G \rightarrow 0$, S vanishes $\sim G$, and it is identically equal to zero at

$$G^2 > 4b^{-1}Q_0/(z + 6bga') = 2G_{\max}^2(z), \quad (15)$$

see Eqs. (11) and (14).

At the nonlinear stage of development of the MI, competition of the disturbances with different frequencies G takes place. In the optical fibers, the initial disturbances may be produced by quantum fluctuations.³ A relevant problem is to find a frequency selected by the nonlinear competition. Let us assume that the initial disturbances are Gaussian, i.e.,

their powers $P_0(G)$ do not depend on the frequency G . It is natural to define the winner of the nonlinear competition as the frequency for which the modulation depth attains first the full power of the underlying cw. With the logarithmic accuracy, the corresponding integral gain is $S = \frac{1}{2} \ln(Q_0/P_0)$ (recall P_0 is the initial power of the disturbance). Equating this expression to that (13), one finds the shortest length z at which the full depth of the modulation is attained:

$$z + 6bg/a' = (\pi Q_0)^{-1} \ln(Q_0/P_0) . \quad (16)$$

Then, making use of eq. (14), one finds the corresponding frequency:

$$G^2 = 2\pi(a')^{-1} Q_0^2 / \ln(Q_0/P_0) . \quad (17)$$

The analysis developed is valid provided that, as it was presumed above, the length given by Eq. (16) is much larger than the characteristic spatial scale of the MI, which is $\sim s^{-1} \sim G^{-1} Q_0^{-1/2} (a'z + 6bg)^{-1/2}$ according to Eq. (8). With regard to Eqs. (16) and (17), this condition takes the form

$$\ln^2(Q_0/P_0) \gg \pi^2/2 . \quad (18)$$

Thus, the cw power Q_0 must be sufficiently large as compared to the power P_0 of the initial disturbances, but the relation between the parameters Q_0 and b may be arbitrary.

Earlier,⁴ it was proposed to superimpose a specially generated disturbance with a given frequency G on the cw in order to control the development of the MI. The results set forth here suggest another way to achieve the same purpose: One can adjust the gradient a' of the dispersion coefficient to select the necessary value of G . In practice, one can produce the expedient gradient, employing the carrying frequency of the cw close to the zero-dispersion point and imposing, e.g., a temperature gradient or mechanical stress on the fiber.

Let us now give some estimates concerning the realizability of this mechanism in real nonlinear fibers. Taking the cw power 200 W and the typical value of the nonlinearity parameter (which did not appear in the notation adopted) $0.015 \text{ W}^{-1}/\text{m}$ for a silica fiber, one obtains the MI length $\sim 0.3 \text{ m}$. Thus, it is sufficient to have the inhomogeneous segment of the fiber few meters

long. The mechanism considered can also be realized in terms of stationary light beams in nonlinear planar light guides, and in a number of other inhomogeneous nonlinear systems.

In conclusion, it is relevant to note that a similar effect may take place in a bimodal optical fiber. In this case, the fiber can be itself pretty homogeneous, while the effective inhomogeneity is induced by the energy transfer between the two modes. It is assumed that the intermode coupling is generated by the stimulated Raman scattering, the pump wave belonging to the normal-dispersion spectral region, while the Stokes wave lying in the region of the anomalous dispersion. The bimodal MI sets in when the ratio of the powers of the two waves passes through a certain critical value. This problem can also be analyzed in the quasi-stationary approximation. The final result, to be presented in a detailed form elsewhere, is that the bimodal instability splits the original cw into a chain of solitons with the peak power $W \sim Q_0 A^{-3/2} (E \ln(Q_0/P_0))^{-1/2}$, where Q_0 and P_0 are, as above, the powers of the cw and initial disturbances, A is the ratio of the dispersion coefficients in the modes with the anomalous and normal dispersion, and E the coefficient of the energy exchange between the modes via the stimulated Raman scattering (to obtain this estimate, it was assumed that all the cw energy was transformed into solitons, and one soliton was generated per one period of the growing modulational disturbance). Thus, if the fiber is sufficiently long, and the coupling coefficient E is sufficiently small, we can produce very short solitons with a very high peak energy. As is well known, in many applications it is important to render the solitons as short as possible. For comparison, the usual MI in the homogeneous monomode fiber would produce the solitons with the peak power having the same order of magnitude as the initial cw power Q_0 .

REFERENCES

1. B.A. Malomed and V.I. Shrira, Soliton caustics, *Physica D* 53: 1 (1991).
2. P.K.A. Wai, C.R. Menyuk, H.H. Chen, and Y.C. Lee, Soliton at the zero-group-dispersion wavelength of single-mode fiber, *Optics Lett.* 12:627 (1987).
3. J.P. Gordon and H.A. Haus, Random walk of coherently amplified solitons in optical fibers, *Optics Lett.* 11:665 (1986).
4. A. Hasegawa, Generation of a train of soliton pulses by induced modulational instability in optical fibers, *Optics Lett.* 9:288 (1984).

LYAPUNOV STABILITY OF VECTOR SOLITONS IN OPTICAL FIBERS

Vladimir Mezentsev,¹ and Sergei Turitsyn^{1,2}

¹ Institut of Automatics and Electrometry
630090 Novosibirsk, Russia

²Institut für Theoretische Physik I, Heinrich-Heine-
Universität Düsseldorf, D-4000 Düsseldorf 1, Germany

INTRODUCTION

The nonlinear interaction of the two polarizations in optical fibers, which results from the tensor character of the susceptibility of nonlinear optical media, has recently attracted substantial attention. As was noted in¹ isotropic single-mode fibers are really bimodal because of the presence of a small intrinsic birefringence that can lead to the splitting of the pulses with the different polarizations. This effect can substantially limit the possibilities of using such fibers for the purpose of information transmission. However, as was shown by Menyuk¹, the Kerr effect can stabilize solitons against splitting due to birefringence. The either of the two polarization modes is able to capture the other one such that the two pulses can propagate together in spite of the group-velocity mismatch.

The copropagation of two high-intensity optical pulses in a nonlinear medium with the Kerr-type nonlinearity is governed by the incoherently coupled nonlinear Schrödinger equations. These equations describe both the evolution of two coupled waves with the same polarizations but different frequencies and the propagation of two waves with the same frequency but different polarizations. In this paper the main attention will be paid to optical pulse propagation in the anomalous dispersion regime of a birefringent fiber, but our result can be also applied to a wide array of different physical contexts which may be described by two nonlinear coupled Schrödinger equations.

BASIC EQUATIONS AND STATIONARY SOLUTIONS

By using the well-known variables expressed in soliton units¹, master equations, describing the evolution of the two polarization modes in a nonlinear optical fiber, may be written in dimensionless form :

$$i(U_z + \delta U_t) + \frac{1}{2}U_{tt} + (|U|^2 + \alpha|V|^2)U = 0 \quad (1)$$

$$i(V_z - \delta V_t) + \frac{1}{2}V_{tt} + (|V|^2 + \alpha|U|^2)V = 0. \quad (2)$$

In the case of silica or similar fibers, where the dominant contribution to the $\lambda^{(3)}$ is of electronic origin, the coefficient α is : for elliptical eigenmodes, $2/3 < \alpha < 2$; for linearly polarized modes, $\alpha = 2/3$, and for circular polarized modes, $\alpha = 2$.

Equations (1),(2) have been studied numerically¹ and by using variational approach². It was shown that for small amplitudes the two pulses separate due to the different group velocities. Above a certain amplitude threshold a fraction of the energy in one polarization is captured by the another one and solitons consisting of both polarizations are formed. The amplitude threshold increases with the strength of the birefringence parameter δ . The bound state with the mixed polarization results when the partial pulses in each polarization shift their phases in such a way that their group velocities become equal.

Contrary to the nonlinear Schrödinger equation, Eqs. (1, 2) can not be solved by using the inverse scattering transform (IST). Therefore, many important questions concerning the soliton dynamics in the framework of Eqs. (1, 2) are still opened. For example, determination of the parameters of the initial pulse with the arbitrary profile, which are necessary for establishing of vector solitons.

In the present paper we prove stability of the vector solitons for the case of equal amplitudes in each polarization and obtain sufficient integral conditions for the mutual trapping of fractional pulses.

Equations (1,2) have a Hamiltonian form:

$$iU_z = \delta H / \delta U^*, \quad iV_z = \delta H / \delta V^*, \quad (3)$$

with the Hamiltonian :

$$H = \frac{i}{2}\delta \int (UU_t^* - U^*U_t + V^*V_t - VV_t^*)dt + \frac{1}{2} \int (|U_t|^2 + |V_t|^2)dt - \frac{1}{2} \int (|U|^4 + |V|^4 + 2\alpha|U|^2|V|^2)dt. \quad (4)$$

We investigate stability of a stationary solution of Eqs. (1, 2) of the form,

$$U_0(z, t) = \frac{1}{\sqrt{(1+\alpha)}} \exp \left[\frac{i}{2}(1+\delta^2)z - i\delta t \right] \text{sech}(t), \quad (5)$$

$$V_0(z, t) = \frac{1}{\sqrt{(1+\alpha)}} \exp \left[\frac{i}{2}(1+\delta^2)z + i\delta t \right] \text{sech}(t), \quad (6)$$

Hamiltonian H takes the following value on the soliton solutions:

$$H[U_0, V_0] = -\frac{\delta^2}{2}(N_1 + N_2) - \frac{(1+\alpha)^2}{24}(N_1^3 + N_2^3). \quad (7)$$

here $N_1 = \int |U|^2 dt$ and $N_2 = \int |V|^2 dt$ are integrals of motion.

The soliton solutions (5), (6) of Eqs. (1, 2) can be viewed as solutions of the Euler equation that corresponds to the following variational problem:

$$\delta S = \delta(H + \lambda^2 N) = 0. \quad (8)$$

Equation (8) means that all localized stationary solutions of Eqs. (1, 2) realize the stationary points of the Hamiltonian H while N is fixed.

SOLITON STABILITY

For proving soliton stability it is sufficient to present the Lyapunov function L which satisfies the following conditions:

1. $L[U_0, V_0] = 0$, a minimum of L is attained on the stationary solutions;
2. $L[U, V] \geq 0$, L is a non-negative functional for the perturbed states;
3. $\frac{\partial L}{\partial z} \leq 0$, L is a non-increasing function of z .

The present method of stability investigation is naturally formulated for Hamiltonian systems (see e.g. 3). If the Hamiltonian of the system H is bounded for the fixed N , one may use as the Lyapunov function the following combination, $L = H - \min(H)$.

Let us show now the boundedness of H for the fixed N . By using the Hölder inequality one may estimate the first term in the Hamiltonian:

$$\frac{i}{2} \delta \int (UU_t^* - U^*U_t + V^*V_t - VV_t^*) dt \leq \frac{\delta^2}{2} (N_1 + N_2) + \frac{1}{2} \int (|U_t|^2 + |V_t|^2) dt. \quad (9)$$

At the next step, we use the following inequality to estimate the nonlinear term:

$$\int f^4 dt \leq \frac{1}{\sqrt{3}} \left(\int f_t^2 dt \right)^{1/2} \left(\int f^2 dt \right)^{3/2}. \quad (10)$$

After substitution of these inequalities into the Hamiltonian (9) we obtain the resulting formula:

$$H \geq -\frac{\delta^2}{2} (N_1 + N_2) - \frac{(1 + \alpha)^2}{24} (N_1^3 + N_2^3). \quad (11)$$

The remarkable fact is that the minimum of the Hamiltonian H , which we have found is reached *exactly* on the soliton solutions (5), (6): $H[U_0, V_0] = \min H$. It means that the soliton solutions (5), (6) realize the minimum of the H for the fixed N and so the Lyapunov function L for the bound state in the form (5), (6) can be constructed.

SUFFICIENT CRITERION FOR MUTUAL TRAPPING OF PARTIAL

Because Eqs. (1), (2) are not integrable, there is no exact answer even on the following simply formulated question: Which kind of initial conditions for the Eqs. (1), (2) lead to appearance of the vector soliton (5), (6)? In order to find a working criterium of establishing of vector soliton from an arbitrary initial pulse in the framework of Eqs. (1), (2), let us consider the following equality:

$$\begin{aligned} \frac{d^2}{dz^2} \int t^2 (|U|^2 + |V|^2) dt &= 2H + 2\delta^2 N + \\ &+ \int (|U_t|^2 + |V_t|^2) dt + i\delta \int (UU_t^* - U^*U_t - VV_t^* + V^*V_t) dt. \end{aligned} \quad (12)$$

The last term in Eq. (12) can be estimated as above. Inserting the estimation (9) into (12), one obtains:

$$\frac{d^2}{dz^2} \int t^2 (|U|^2 + |V|^2) dt \geq 2H + \delta^2 N,$$

the sufficient conditions of spreading or splitting of the pulses for simple configurations. Termin "simple" means that in each polarization distribution with only one

maximum exists. For such configurations, under the condition $2H + \delta^2 N > 0$ the integral $\int t^2(|U|^2 + |V|^2)dt$ tends to infinity as $(H + \frac{1}{2}\delta^2 N)z^2$ that corresponds either dispersional spreading of initial distributions or splitting appart of the partial pulses in each of the two polarizations. In both situations a vector soliton does not appear. For the more complicated configurations one need another approach.

Therefore, we obtain now an exact condition for the mutual trapping of the pulses from different polarizations. It would be reasonable to define the following criterium of a cross capture in the framework of Eqs. (1,2). One may say about a capture then the cross-integral $\int |U|^2|V|^2dt$ is bounded from below by some positive constant.

In order to get needed criterium, we rewrite the expression for Hamiltonian:

$$\alpha \int |U|^2|V|^2dt = -H + \frac{i}{2}\delta \int (UU_t^* - U^*U_t + V^*V_t - VV_t^*)dt + \frac{1}{2} \int (|U_t|^2 + |V_t|^2)dt - \frac{1}{2} \int (|U|^4 + |V|^4)dt \quad (13)$$

Noting that the nonlinear term in the right-hand side of Eq. (13) can be estimated by using formula (10) we easily get ($I_1 = \int |U_t|^2dt, I_2 = \int |V_t|^2dt$),

$$\alpha \int |U|^2|V|^2dt \geq -H - \frac{\delta^2}{2}N + \frac{1}{2}(I_1 + I_2) - \frac{1}{2\sqrt{3}}I_1^{1/2}N_1^{3/2} - \frac{1}{2\sqrt{3}}I_2^{1/2}N_2^{3/2} \geq -H - \frac{\delta^2}{2}N - \frac{1}{24}(N_1^3 + N_2^3). \quad (14)$$

Thus, for the arbitrary initial distribution with:

$$H < -\frac{\delta^2}{2}N - \frac{1}{24}(N_1^3 + N_2^3)$$

the cross-integral $\int |U|^2|V|^2dt$ is bounded from below by some positive constant. It means that some part of energy in one polarization is captured by another during the propagation along the fiber.

We would like to point out that the criterium obtained can be used for an initial pulse with an arbitrary shape, not only for the sech-type pulses, which were considered in^{1,2}.

In conclusion, we have proved stability of vector solitons by constructing the Lyapunov function. We have found analitically the integral requeriments on the parameters of the injected pulses which are sufficient for mutual trapping of fractional pulses of different polarizations.

REFERENCES

1. C. R. Menyuk, Stability of solitons in birefringent optical fibers. II. Arbitrary amplitudes, *J. Opt. Soc. Am. B* 5:392 (1988).
2. Yu. S. Kivshar, Soliton stability in birefringent optical fibers. Analytical approach, *J. Opt. Soc. Am. B* 7:2204 (1990).
3. S. K. Turitsyn, Stability of multidimensional solitons, *Theoret. Math. Physics* 64:797 (1985).

CHAOS IN SEMICONDUCTOR LASERS WITH OPTICAL FEEDBACK

J. Mørk, B. Tromborg, J. Mark, and V. Velichansky*

TFL Telecommunications Research Laboratory
Lyngsø Allé 2, DK-2970 Hørsholm, Denmark

*P. N. Lebedev Physical Institute
Leninsky Pr. 53, Moscow, Russia

INTRODUCTION

In this paper we present experimental and theoretical results on the nonlinear dynamics of a semiconductor laser exposed to optical feedback (see Fig. 1). This relatively simple system displays a wealth of interesting phenomena, which only now are starting to be understood. The delayed feedback turns the system infinite-dimensional, which together with inherent nonlinearities in the light-matter interaction gives the rich dynamics. The well-known Ikeda ring cavity system¹ is in some senses the passive counterpart of this active system.

Technologically, intentional feedback has been used to reduce the linewidth of semiconductor lasers by several orders of magnitude (from tens of MHz to a few kHz, say). On the other hand, feedback due to reflections at various interfaces is very difficult to avoid. Feedback fractions as small as 10^{-8} (-80 dB) have thus been shown to affect laser operation and for feedback levels in the range of 10^{-4} to 10^0 the laser linewidth broadens to several tens of GHz, with detrimental effect for most applications^{2,3}. The phenomenon has been denoted "coherence collapse"² and is now believed to be a manifestation of ultrafast optical chaos.



Figure 1. Semiconductor laser with feedback from an external mirror. The distance to the mirror (~ 10 -100 cm) is much larger than the laser diode length ($\sim 300 \mu\text{m}$).

MODEL AND BASIC PROPERTIES

The laser dynamics is described by the Lang and Kobayashi equations⁴ for the

complex electric field E and the carrier density N

$$\frac{dE}{dt} = \frac{1}{2}(1 + j\alpha)(G(N) - \tau_p^{-1})E(t) + \gamma E(t - \tau) \quad (1)$$

$$\frac{dN}{dt} = J - \frac{N}{\tau_s} - G(N)|E|^2. \quad (2)$$

Here, G is the gain, which to a good approximation increases linearly with N , α introduces an important amplitude-phase coupling, J is the pumping current, and τ_p and τ_s are the photon and carrier lifetimes. Finally, $|\gamma|$ and $\arg(\gamma)$ reflect the level and the phase of the externally reflected field, and τ is the roundtrip time in the external cavity.

For $\gamma = 0$, (1) and (2) reduce to the usual equations for a (solitary) semiconductor laser oscillating in a single diode cavity mode. Upon inclusion of feedback, the stationary solutions of (1) and (2) show that the original mode is split into a group of modes with frequency spacing approximately equal to the mode spacing τ^{-1} of the external cavity. The number of modes increases with feedback level through usual saddle-node bifurcations, and in the presence of noise the laser may jump between the different modes. For not too strong feedback levels, it was shown⁵ that the modehopping dynamics can be quantitatively described by an analytical potential model derived from (1) and (2). The model gives excellent agreement with experimental results, and identifies the mode closest to the original diode cavity mode as the dominant mode. As the feedback is increased this mode becomes increasingly dominant. At a certain feedback level, however, the mode loses stability through a Hopf bifurcation and a stable limit cycle solution is created⁶. The frequency of this solution is approximately given by the relaxation oscillation frequency of the solitary laser, which is the characteristic resonance frequency for the exchange of energy between the photon and carrier populations.

QUASIPERIODIC ROUTE TO CHAOS

The evolution of the limit cycle for increasing feedback is illustrated in the calculated bifurcation diagram in Fig. 2, where we plot the carrier density N in an appropriately chosen Poincaré section. The limit cycle first bifurcates into a quasiperiodic solution (torus), where the second frequency is close to $1/\tau$, which is followed by a frequency locked solution of order four that period doubles. The period-eight solution then bifurcates into a quasiperiodic solution and finally becomes chaotic.^{6,7}

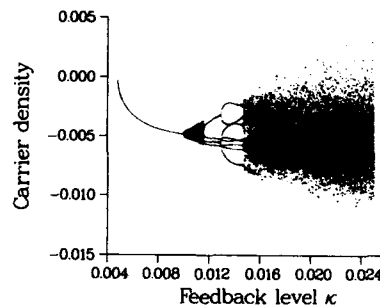


Figure 2. Theoretical bifurcation diagram.

Experimentally obtained phase diagrams for the transition to chaos are presented in Fig. 3. The figure essentially shows the laser intensity $I(t)$ versus $I(t - T)$, with T fixed. Since the dynamics occur on a very short time scale (the basic period is about 200 ps) the detected signal was first frequency down-converted.⁷ The results in Fig. 3 were supplemented with measurements of the intensity noise spectra.⁷ In conclusion, the experimental results strongly support the quasiperiodic route to chaos predicted in Fig. 2. In this feedback range we have also observed the existence of three-frequency tori in numerical simulations, and nearly degenerate Hopf bifurcations leading to competing attractors have been predicted theoretically and seen experimentally.^{6,7}

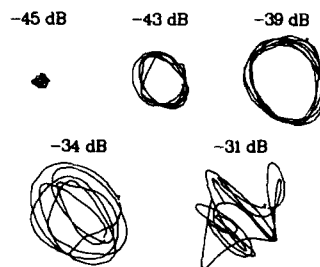


Figure 3. Experimental phase portraits for different levels of feedback.

LOW-FREQUENCY INTENSITY FLUCTUATIONS

The region of chaos extends to very high levels of feedback, but by anti-reflection coating the facet facing the external mirror it is possible to reach another region of stable narrow linewidth operation.³ Fig. 4 shows experimental time-series for a fixed high feedback level and increasing bias current, which is another way of entering the

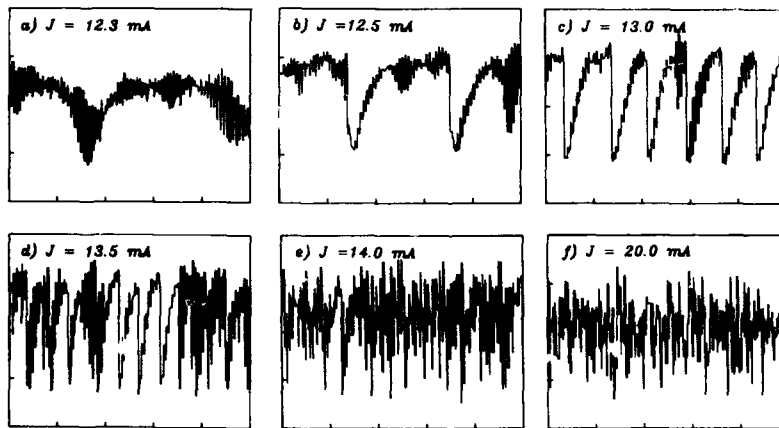


Figure 4. Measured time dependence of output power. Horizontal scale: 200 nsec/div.

region of chaos. For bias currents close to threshold the laser emission is stable, but for slightly larger currents the laser intensity undergoes sudden randomly occurring drop-outs, followed by intensity build-up occurring in steps of duration τ . The rate of dropouts increases with current. Based on similar experimental observations, an intermittency route to chaos was suggested.⁸ We have, however, previously shown that

these low-frequency intensity fluctuations (LFF) are explained by a simple iterative model in terms of dynamic bistability.⁹ During most of the build-up, the laser intensity is monostable, but from a certain point it becomes bistable, and a new drop-out occurs after a statistically distributed first passage time. The theory also led to predictions about the spectral distribution of the laser light in the different steps, which were largely confirmed by recent measurements, cf. Fig. 5. Just before the drop-out (step no. 0), laser emission occurs in the low-frequency region. It switches to the high-frequency side after the drop-out, and then slowly drifts back again during intensity build-up. There are still features of the spectra in Fig. 5 that are not well understood, but we believe the results demonstrate that the LFF are not chaotic in nature. Fig. 4, however, show that the LFF are interrupted by bursts of high-frequency oscillations, and the rate of these bursts increases with current. This resembles an intermittency route to chaos - but on the background of stochastic LFF. Furthermore, numerical simulations with high time resolution show that the LFF actually are deeply modulated by high-frequency oscillations. These results may indicate that chaos occurs on a short time scale, whereas the slow (average) LFF dynamic is governed by a simple bistability phenomenon.

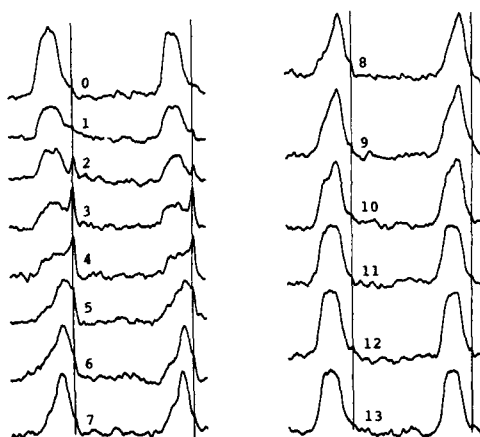


Figure 5. Experimental spectra taken at different (numbered) steps of the LFF, corresponding (approximately) to the time series in Fig. 4c. Two spectral orders (spaced by 190 GHz) are shown, and the frequency increases towards right.

REFERENCES

1. K. Ikeda, H. Daido, and O. Akimoto, *Phys. Rev. Lett.* **45**, 709 (1980).
2. D. Lenstra, B. H. Verbeek, and A. J. den Boef, *IEEE J. Quantum Electron.* **21**, 674 (1985).
3. R. W. Tkach, and A. R. Chraplyvy, *J. Lightwave Technol.* **LT-4**, 1655 (1986).
4. R. Lang, and K. Kobayashi, *IEEE J. Quantum Electron.* **QE-16**, 347 (1980).
5. J. Mørk, M. Semkow, and B. Tromborg, *Electron. Lett.* **26**, 609 (1990).
6. J. Mørk, B. Tromborg, and J. Mark, *IEEE J. Quantum Electron.* **28**, 93 (1992).
7. J. Mørk, J. Mark, and B. Tromborg, *Phys. Rev. Lett.* **65**, 1999 (1990).
8. J. Sacher, W. Elsässer, and E. O. Göbel, *Phys. Rev. Lett.* **63**, 2224 (1989).
9. J. Mørk, B. Tromborg, and P. L. Christiansen, *IEEE J. Quantum Electron.* **24**, 123 (1988).

PULSE COLLISIONS IN BIMODAL WAVEGUIDES

D.F.Parker and C.Sophocleous

Department of Mathematics and Statistics
University of Edinburgh
King's Buildings
Edinburgh EH9 3JZ, Scotland

PULSE SOLUTIONS OF THE COUPLED NLS EQUATIONS

In an ideal axisymmetric optical fibre the electric field is

$$\begin{aligned} \underline{E}(r, \theta, z, t) &\simeq [A^+ \underline{E}^+(r, \theta) e^{i\theta} + A^- \underline{E}^-(r, \theta) e^{-i\theta}] e^{i\psi} + c.c. \\ \underline{E}^\pm &= iE_1 \underline{e}_r \pm E_2 \underline{e}_\theta + E_3 \underline{e}_z, \quad \psi = kz - \omega t, \end{aligned} \quad (1)$$

with real $E_j = E_j(r)$. At 'monomode' frequencies ω , the *dispersion relation* defines a single positive value $k = k(\omega)$ with corresponding phase speed ω/k and group speed $c_g = [k'(\omega)]^{-1}$. Under Kerr-law nonlinearity, the amplitudes A^+ and A^- of left- and right-handed modes evolve according to the coupled Nonlinear Schrödinger (NLS) equations

$$iA_\tau^\pm = A_{xx}^\pm + (|A^\pm|^2 + h|A^\mp|^2)A^\pm, \quad (2)$$

where $x \equiv \epsilon(z - c_g t)$, $\tau \equiv -\frac{1}{2}c_g'(\omega)\epsilon^2 z$. The constant $h (\simeq 2$ in the weak-guiding approximation) is defined (Parker and Newbould, 1989) in terms of cross-sectional integrals involving \underline{E}^\pm .

Solutions with $A^- \equiv 0$ ($A^+ \equiv 0$) describe left-handed (right-handed) circularly polarized modes governed by a single NLS equation (for $A^+(\tau, x)$ or $A^-(\tau, x)$, respectively). Solutions $A^\pm = e^{\mp i\alpha} a(\tau, x)$ (i.e. $A^-/A^+ = e^{2i\alpha}$) give

$$\underline{E} \simeq a(\tau, x)[\underline{E}^+ e^{i(\theta-\alpha)} + \underline{E}^- e^{i(\alpha-\theta)}] e^{i\psi} + c.c.$$

which may be regarded as linearly polarized in the plane $\theta = \alpha$ with complex amplitude $2a(\tau, x)$ satisfying the NLS equation

$$ia_\tau = a_{xx} + (1+h)|a|^2 a. \quad (3)$$

Since a general pair (A^+, A^-) of complex amplitudes may be written as

$$A^\pm = (p \pm q)e^{i(\beta \mp \alpha)}; \quad p \equiv \frac{1}{2}(|A^+| + |A^-|), \quad q \equiv \frac{1}{2}(|A^+| - |A^-|),$$

it is seen that the fields (1) are a superposition of two linearly polarized modes having respective amplitudes $p, |q|$, polarization angles $\theta = \alpha, \alpha + \frac{1}{2}\pi$ and phases $\beta, \beta + \frac{1}{2}\pi \operatorname{sgn} q$. Thus, at any (τ, x) , the modal field locally is elliptically polarized with principal axis aligned along $\theta = \alpha = \frac{1}{2}(\arg A^- - \arg A^+)$. It has left- or right-handed orientation depending as $q > 0$ or $q < 0$ ($|A^+| > |A^-|$ or $|A^+| < |A^-|$).

This account concerns collisions between pulses

$$A^\pm = F_\pm(\sigma) \exp -i(\beta^\pm \tau + V\sigma + \delta^\pm), \quad \sigma \equiv x - \hat{x} - 2V\tau, \quad (4)$$

where $\beta^\pm, \delta^\pm, \hat{x}$ and the 'speed' $2V$ are constants and where $F_\pm(\sigma)$ are real symmetric, nondistorting pulse envelopes which may be parametrized as $F_\pm(\sigma) = \Gamma f_\pm(\Gamma\sigma; \rho)$, where

$$f_\pm''(\eta) + (f_\pm^2 + hf_\mp^2 - p_\pm^2)f_\pm = 0, \quad p_\pm^2 = (\beta^\pm - V^2)/\Gamma^2. \quad (5)$$

The conditions $f_+ = \cos\rho, f_- = \sin\rho, f'_\pm = 0$ at $\eta = 0$ with $f_\pm \rightarrow 0$ as $\eta \rightarrow \infty$ define an eigenvalue problem for $p_+(\rho)$ and $p_-(\rho)$.

Solutions may be written $f_+(\eta; \rho) = f(\eta; \rho), f_-(\eta; \rho) = f(\eta; \frac{1}{2}\pi - \rho), p_+(\rho) = p(\rho), p_-(\rho) = p(\frac{1}{2}\pi - \rho)$, where $f(\eta; \rho)$ and $p(\rho)$ are displayed in Fig. 1 for $h = 2$. The corresponding pulses

$$A^+ = \Gamma e^{-i\delta^+} e^{-i(V\sigma + \beta^+ \tau)} f(\Gamma\sigma; \rho), \quad A^- = \Gamma e^{-i\delta^-} e^{-i(V\sigma + \beta^- \tau)} f(\Gamma\sigma; \frac{1}{2}\pi - \rho)$$

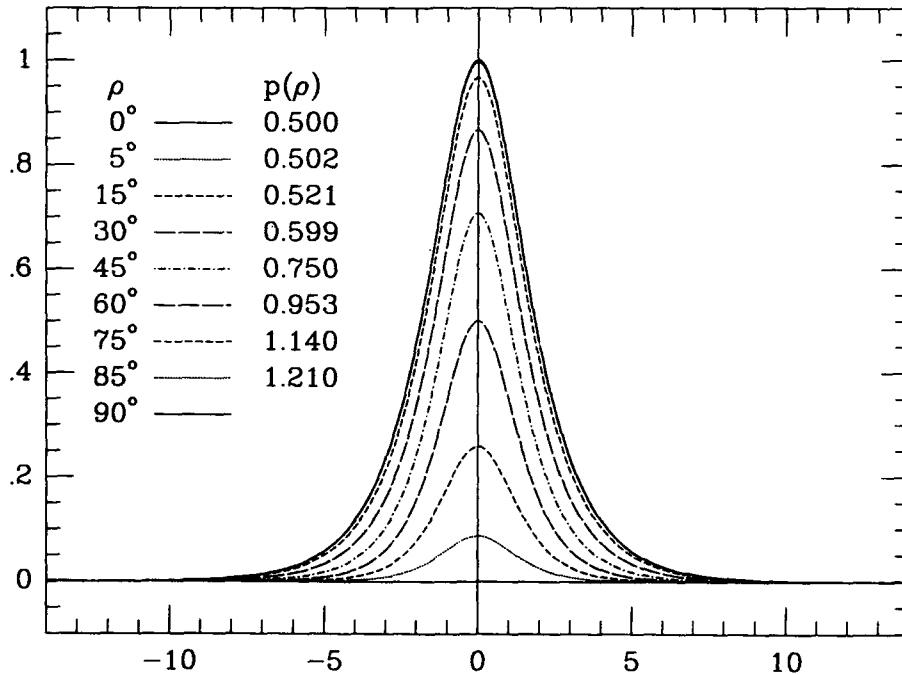


Figure 1. Pairs of pulse envelope profiles $f(\eta; \rho), f(\eta; \frac{1}{2}\pi - \rho)$, $h = 2$.

are elliptically polarized with polarization angle $\frac{1}{2}(\delta^+ - \delta^-) - \frac{1}{2}(\beta^+ - \beta^-)\tau$ which evolves with τ (just as elliptically polarized, but modulationally unstable, uniform wavetrains rotate as they travel).

The special cases: (1) $f(\eta; 0) = \text{sech}(\eta/\sqrt{2})$, $p(0) = 1/\sqrt{2}$ with $f_- \equiv 0$, and (2) $f(\eta; \frac{1}{4}\pi) = (1/\sqrt{2})\text{sech}(\frac{1}{2}\sqrt{1+h}\eta)$, $p(\frac{1}{4}\pi) = \frac{1}{2}\sqrt{1+h}$ with $A^- = e^{2i\alpha}A^+$ describe sech-envelope solutions of the appropriate uncoupled NLS equations.

NUMERICAL COLLISION EXPERIMENTS

For collision studies, the invariance of (2) to translations in x , τ , $\arg A^\pm$ and a Galilean invariance (shift in carrier frequency) allows the choice of incident pulses as

$$A^\pm = \gamma_1 \exp -i[V\sigma_1 + V^2\tau + \gamma_1^2 p_\pm^2(\rho_1)\tau] f_\pm(\gamma_1\sigma_1; \rho_1) + \gamma_2 \exp -i[-V\sigma_2 + V^2\tau + \gamma_2^2 p_\pm^2(\rho_2)\tau - \beta \pm \alpha] f_\pm(\gamma_2\sigma_2; \rho_2), \quad (6)$$

with respective amplitudes γ_1 , γ_2 and ellipticities ρ_1 , ρ_2 , where $\sigma_1 = x - \hat{x}_1 - 2V\tau$, $\sigma_2 = x - \hat{x}_2 + 2V\tau$. The right-travelling pulse (subscript 1) has polarization and phase at the pulse-peak $\sigma_1 = 0$ both chosen as zero at $\tau = 0$. The left-travelling pulse has polarization $\theta = \alpha$ and phase β at $\tau = 0$, $\sigma_2 = 0$.

Despite non-integrability of (2) (except for $h = 1$, Zakharov and Shul'man, 1982) earlier studies for $\rho_1 = \frac{1}{4}\pi$, $\rho_2 = \frac{1}{4}\pi$ or 0 (Newbould, 1989) show that, after collision, profiles of A^\pm separate into two new pulses (subscripts 3,4) having form

$$A^\pm \simeq \sum_{j=3,4} \gamma_j \exp -i[V_j\sigma_j + V_j^2\tau + \gamma_j^2 p_\pm^2(\rho_j)\tau - \beta_j \pm \alpha_j] f_\pm(\gamma_j\sigma_j; \rho_j) \quad (7)$$

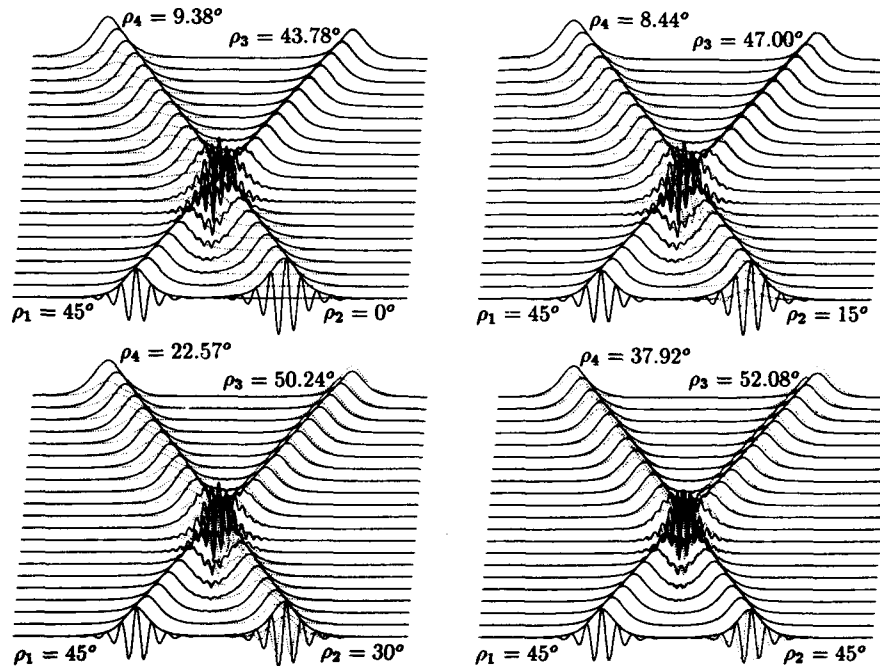


Figure 2. Evolution of $|A^+|$ — $|A^-|$ $\text{Re}|A^+|$, $\text{Re}|A^-|$ also shown at $\tau = 0$.

with $\sigma_j \equiv z - \hat{x}_j - 2V_j\tau$ and $V_3 \simeq V$, $V_4 \simeq -V$. Figure 2 shows $|A^+|$ and $|A^-|$ for a linearly polarized pulse $\rho_1 = \frac{1}{4}\pi$ colliding with pulses having various ellipticities ρ_2 , with $V = 4$, $\alpha = \frac{1}{4}\pi$, $\beta = 0$; $\gamma_1 = \gamma_2 = 1$, $\hat{x}_1 = 12.5$, $\hat{x}_2 = 27.5$. Two pulses emerge with little additional radiation, even though the pulse parameters are considerably modified. Tests show that ρ_3 , ρ_4 , γ_3 and γ_4 are insensitive to the relative phase β and that $V_3 \simeq 4$, $V_4 \simeq -4$ with $\gamma_3, \gamma_4 \simeq 1$.

For smaller relative 'speed' $4V$, separation into two pulses is less perfect, as seen in Figure 3. For $V = 0.4$, the linearly polarized pulse becomes virtually circular, while the elliptical pulse becomes almost linear. It is found that the right-travelling signal depends strongly on α ; for example, for $\alpha = 0^\circ$ it appears to broaden and decay without establishing a permanent form.

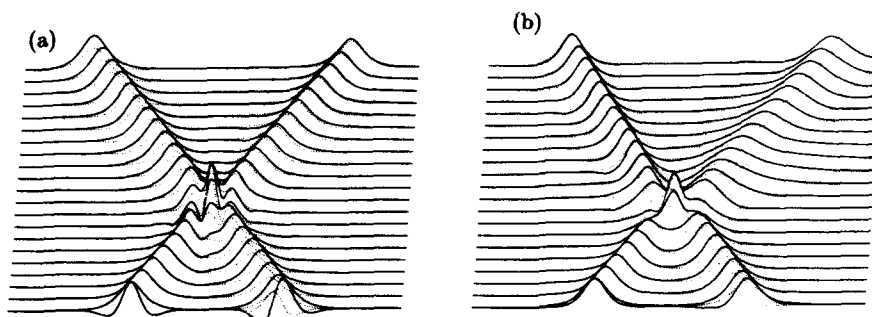


Figure 3. Collisions for $\rho_1 = 45^\circ$, $\rho_2 = 30^\circ$, $\alpha = 45^\circ$, $\beta = 0^\circ$; $\gamma_1 = \gamma_2 = 1$; (a) $V = 1.0$, (b) $V = 0.4$.

Finally, Figure 4 shows the collision of two elliptically polarized pulses $\rho_1 = \rho_2 = 30^\circ$, $\gamma_1 = \gamma_2 = 1$ for $V = 4$. For $\alpha = 45^\circ$, two substantially different pulses emerge, while for $\alpha = 0^\circ$ the pulses have $\rho_3 = \rho_4$.

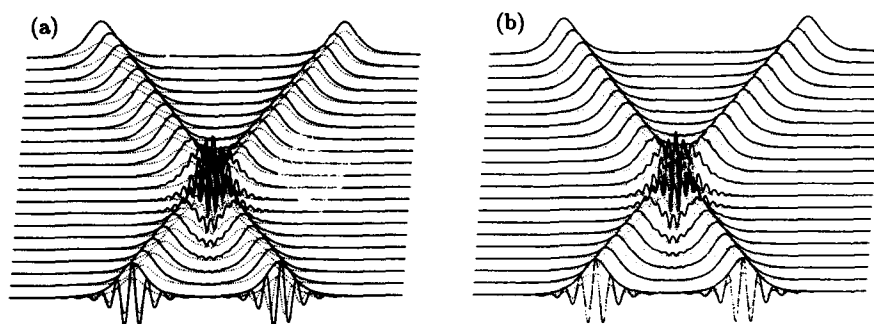


Figure 4. Collisions of elliptically polarized pulses for (a) $\alpha = 45^\circ$, (b) $\alpha = 0^\circ$.

REFERENCES

- Newbould, G.K., 1989, PhD Thesis, University of Nottingham.
- Parker, D.F., and Newbould, G.K., 1989, Coupled nonlinear Schrödinger equations arising in fibre optics, *J. de Physique* C3:137.
- Zakharov, V.E., and Shul'man, E.I., 1982, To the integrability of the system of two coupled nonlinear Schrödinger equations, *Physica* 4D:270.

DYNAMIC RESPONSE OF SEMICONDUCTOR NONLINEAR OPTICAL WAVEGUIDES

P.S.Spencer and K.A.Shore

University of Bath
School of Electronic and Electrical Engineering
Bath, BA2 7AY UK

ABSTRACT

Pump-probe excitation of passive nonlinear semiconductor optical waveguides is examined in the slowly varying envelope approximation. It is shown that the pump pulse may be used to control the chirp imposed on the probe pulse by self and induced phase modulation.

1 INTRODUCTION

An initial investigation of the dynamic response of multiple pulses in a nonlinear medium can be obtained using a pump-probe type experiment.

This technique uses an intense pump pulse to induce changes in the optical properties of the medium, which then subsequently perturbs the propagation of a much weaker probe pulse.

The electric field of the pulses will be taken as,

$$E(z, t) = 1/2\Re[\mathcal{A}(z, t) \exp i(\beta_0 z - \omega_0 t)] \quad (1)$$

where $\mathcal{A}(z, t)$ is the complex envelope function, β_0 is the propagation constant and ω_0 is the carrier frequency. In the subsequent sections the usual convention of dropping the \Re operator will be used.

2 TIME DOMAIN COUPLED PUMP-PROBE EQUATIONS

When a weak probe pulse enters a nonlinear medium which has just been subjected to an intense pump pulse, the changes induced in the medium by the pump alter the propagation of the probe pulse. An induced phase modulation, (IPM) is generated

as well as the usual self phase modulation, (SPM). The IPM induced by the pump dominates over the probe's SPM.

Similarly the pump will feel the presence of the probe through a very small IPM component. However the pump's SPM dominates over the IPM generated by the probe.

By making the slowly varying envelope approximation it is possible to obtain two coupled equations for the propagation of the pump and probe envelope functions, $A_p(z, t)$ and $A_s(z, t)$, [1],

$$i \left(\frac{\partial A_p}{\partial z} + \frac{1}{v_p} \frac{\partial A_p}{\partial t} \right) + \frac{\omega_p n_{2p}(\omega_p)}{c} [|A_p|^2 A_p + 2 |A_s|^2 A_p] + i \alpha_p A_p = 0 \quad (2)$$

$$i \left(\frac{\partial A_s}{\partial z} + \frac{1}{v_s} \frac{\partial A_s}{\partial t} \right) + \frac{\omega_s n_{2s}(\omega_s)}{c} [|A_s|^2 A_s + 2 |A_p|^2 A_s] + i \alpha_s A_s = 0 \quad (3)$$

Here β_i , ω_i , $n_{2i}(\omega_i)$ and α_i are the propagation constant, carrier frequency, nonlinear index and absorption respectively. The subscript 'i' takes the value of either 's' or 'p' to signify the signal or pump pulses. If the pulse widths are such that the nonlinearity occurs because of steady state Band-filling, [2] can be used to calculate $n_2(\omega)$.

In the pump-probe approximation $|A_s|^2 \ll |A_p|^2$ and hence Eqn(2) can be simplified by neglecting the IPM term, $2 |A_s|^2 A_p$. Similarly, the SPM term in eqn(3), $|A_s|^2 A_p$, can be ignored.

By writing the pulses in terms of their amplitude and phase,

$$A_p(z, t) = a(z, t) \exp[i\phi(z, t)] \quad (4)$$

$$A_s(z, t) = b(z, t) \exp[i\theta(z, t)] \quad (5)$$

and assuming the following initial conditions,

$$a(0, t) = a_0 F[(t - t_0)/\tau] \quad (6)$$

$$b(0, t) = b_0 G[t/\tau] \quad (7)$$

$$\phi(0, t) = \theta(0, t) = 0 \quad (8)$$

the subsequent solutions to eqn(2-3) are then,

$$a(z, t) = a_0 F[(t - t_0 - z/v_p)/\tau] \exp(-\alpha_p z/2) \quad (9)$$

$$b(z, t) = b_0 G[(t - z/v_s)/\tau] \exp(-\alpha_s z/2) \quad (10)$$

$$\phi(z, t) = \frac{\omega_p n_{2p}(\omega_p)}{c} \left(\frac{1 - \exp(-\alpha_p z)}{\alpha_p} \right) a_0^2 F^2[(t - t_0 - z/v_p)/\tau] \quad (11)$$

$$\theta(z, t) = \frac{2\omega_p n_{2p}(\omega_p) a_0^2}{c} \int_0^z \exp(-\alpha_p z') F^2[(t - t_0 - z'/v_s - z'(1/v_p - 1/v_s))/\tau] dz' \quad (12)$$

Here τ is the pulse width and $F[t, z]$ and $G[t, z]$ are, as yet unspecified, initial pulse profiles. The initial time displacement between the two pulses is denoted by t_0 .

3 PUMP-PROBE INTERACTION

The Eqns(9-12) describe the propagation of pump and probe pulses in the same waveguide and overlapping in time. The overlap between the two pulses alters the phase of the probe signal significantly. The probe experiences a phase variation across the pulse which is no longer proportional to its own intensity or centered about its peak value. The maximum phase change now occurs at a position that is dependent on both the initial time delay between the pulses and the difference in their group velocities. The changes induced in the pump by the probe are small and can be neglected.

These changes in the phase in turn alter the chirp, $\delta\omega$, induced across the pulse.

$$\delta\omega = -\frac{\partial\theta(z,t)}{\partial t} \quad (13)$$

The minus sign in eqn(13) occurs because the harmonic time variation of the pulse has been assumed to be of the form $\exp(-i\omega t)$.

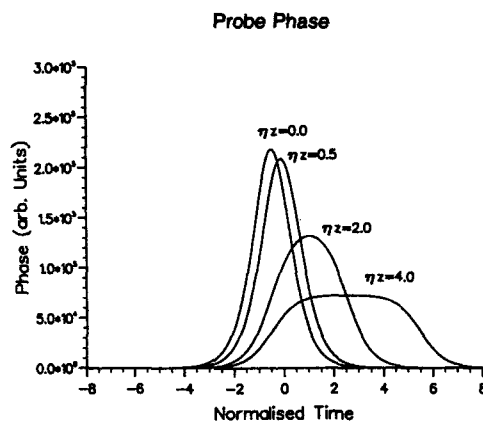


Figure (1). The Probe pulse phase for $\eta z = 0.0, 0.5, 2.0$ and 4.0 . The time delay was set at $T_0 = -0.5$.

4 RESULTS

Both the magnitude and position of the probe's phase and chirp can be controlled by the pump pulse, as can be seen in figures(1 & 2). The initial pulse profile was taken to be $\text{sech}^2(t/\tau)$. Two parameters can be used to describe the relationship between the pump and the probe's phase, $\eta = (1/v_p - 1/v_s)/\tau$ and $T_0 = t_0/\tau$. The value of ηz influences both the maximum magnitude and width of the phase variation across the probe. Higher values result in a lower and broader phase profile. ηz is a measure of the walk-off between the two pulses as they propagate down the guide. The normalised time delay, T_0 , shifts the phase profile around within the probe pulses, in units of the pulse width.

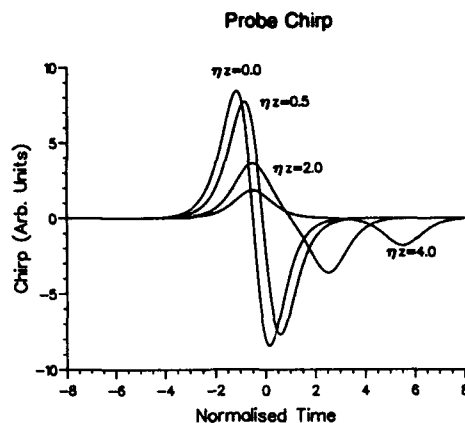


Figure (2). The Probe pulse chirp for $\eta z = 0.0, 0.5, 2.0$ and 4.0 . The time delay was set at $T_0 = -0.5$.

5 ACKNOWLEDGEMENT

This work was performed under a UK SERC CASE award with British Telecom Laboratories, Martlesham Heath, UK. The authors thank Dr M.J.Adams and Dr M.G.Burt for helpful discussions on the work and for comments on this paper.

6 REFERENCES

- [1] J.T.Mannassah, Optics Letters, 14, 386, (1989).
- [2] M.G.Burt, Semicond. Sci. Technol., 5, 1215, (1990).

DYNAMICS OF A FIBRE LASER COUPLED TO A NONLINEAR FIBRE CAVITY

M.P. Sørensen¹, T. Geisler², K.A. Shore,³
P.L. Christiansen¹, J. Mørk⁴, and J. Mark⁴

¹Laboratory of Applied Mathematical Physics
The Technical University of Denmark, DK-2800 Lyngby, Denmark

²Danish Institute of Fundamental Metrology
Bldg. 307, Lundtoftevej 100, DK-2800 Lyngby, Denmark

³Bath University, School of Electronic and Electrical Engineering
Bath, BA2 7AY, United Kingdom

⁴Telecommunications Research Laboratory
Lyngsø Alle 2, DK-2970 Hørsholm, Denmark

INTRODUCTION

Solid state lasers coupled to nonlinear auxiliary external fibre cavities have been demonstrated to exhibit optical pulse compression using the Additive Pulse Modelocking (APM) technique^{1,2}. In APM, pulse compression is obtained by the interferometric addition of a laser pulse and a chirped pulse which is produced via self-phase modulation in a nonlinear external cavity. In order to obtain pulse narrowing it is required that constructive interference occurs near the peak of the pulse and that destructive interference arises towards the wings of the pulse. APM has led to the generation of 100 fs pulses using mode-locked colour centre lasers.

Recent work³ has examined a number of alternative structures which may be utilised for APM. Here we direct our attention to modelling an APM configuration constructed from an erbium doped fibre laser coupled to a nonlinear external fibre cavity.

APM MODELLING

The basic fibre laser and nonlinear cavity arrangement is shown schematically in Fig. 1. The fibre laser is coupled to a passive nonlinear fibre through a mirror with reflectivity r . The lettering $a_{1,n}$ and $a_{2,n}$ denote the light pulses arriving at the mirror from the fibre laser and the passive fibre, respectively. $b_{1,n}$ and $b_{2,n}$ are superpositions

of the transmitted and reflected parts of the incoming pulses, i.e.

$$\begin{aligned} b_{1,n} &= r a_{1,n} + \sqrt{1-r^2} a_{2,n} \\ b_{2,n} &= \sqrt{1-r^2} a_{1,n} - r a_{2,n} \end{aligned} \quad (1)$$

n counts the number of cavity round trips made by the pulses in the APM configuration.

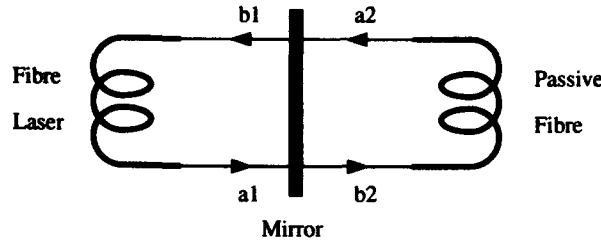


Figure 1. Schematic diagram of the all-fibre pulse mode locking configuration.

Following earlier work on optical soliton theory⁴⁻⁶ we describe the propagation of the optical pulse in both the laser and external cavity fibre by means of an extended non-linear Schrödinger (NLS) equation which includes gain, loss, and terms due to the self-frequency shift

$$\begin{aligned} \frac{\partial A}{\partial z} + \beta_1 \frac{\partial A}{\partial t} + \frac{i}{2} \beta_2 \frac{\partial^2 A}{\partial t^2} - i\gamma |A|^2 A + \\ \frac{\alpha}{2} A - \frac{1}{6} \beta_3 \frac{\partial^3 A}{\partial t^3} + \kappa_1 \frac{\partial}{\partial t} (|A|^2 A) + \kappa_2 A \frac{\partial}{\partial t} |A|^2 \\ = \frac{G_0}{1 + \frac{P}{P_{sat}}} \left(A + \frac{1}{\omega_b^2} \frac{\partial^2 A}{\partial t^2} \right) \end{aligned} \quad (2)$$

$A = A(z, t)$ is the electric field amplitude measured in units of \sqrt{W} (W =Watt) at the cross sectional position z and at time t in the fibre. β_1 is the inverse group velocity which equals n_g/c where n_g is the group refractive index and c is the velocity of light in vacuum. The parameter β_2 is related to the dispersion parameter D through $\beta_2 = -\lambda_0^2 D / (2\pi c)$ with λ_0 being the wavelength of the carrier wave. The parameter $\gamma = n_2 \omega_0 / (c A_{eff})$ measures the strength of the nonlinearity of the fibre where n_2 is the nonlinear index coefficient, A_{eff} the effective core area and ω_0 is the frequency of the carrier wave. α represents the linear loss in the fibre laser as well as in the passive fibre cavity. Third order dispersion is included in the β_3 -term and the nonlinear terms in κ_1 and κ_2 arise from the self-frequency shift with $\kappa_1 = 2\gamma/\omega_0$ and $\kappa_2 = i\gamma T_R$. T_R is related to the slope of the Raman gain and is assumed to vary linearly with frequency in the vicinity of the carrier frequency. The right hand side of Eq. (2) models a bandwidth limited gain including steady state saturation². The parameters G_0 and ω_b are the gain

and the bandwidth, respectively. In the passive fibre G_0 is zero. P is the total pulse power defined by

$$P = F_{rep} \int_{-\infty}^{\infty} |A(z, t)|^2 dt \quad (3)$$

F_{rep} is the repetition frequency of the pulse and P_{sat} is the saturation power of the fibre laser. The assumption here is that the saturation of the gain is in response to the average power in the pulse and that dynamical saturation effects are not significant.

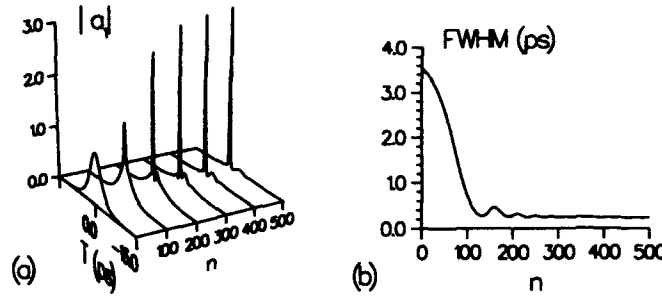


Figure 2. (a) Pulse amplitude $a_{1,n}(t)$ as function of n and time t . (b) Full Width Half Maximum (FWHM) as function of n . Parameter values: $G_0 = 0.43m^{-1}$, $\psi = -2.36$, $\lambda_0 = 1.55\mu m$, $n_g = 1.45$, $n_2 = 3.2 \cdot 10^{-20}m^2/W$, $\beta_1 = 4.83 \cdot 10^{-9}s/m$, $\beta_2 = -3.44ps^2/km$, $\beta_3 = 0.1ps^3/km$, $D = 2.7ps/(km \cdot nm)$, $\alpha = 0.39dB/km$, $A_{eff} = 39(\mu m)^2$, Fibre length=2.05 m, $F_{rep} = 1.0 \cdot 10^8 Hz$, $P_{sat} = 2mW$, $r=0.9$, $\eta = 0.8$, $T_R = 5fs$, and $\omega_b = 2.35 \cdot 10^{13} Hz$.

As a short hand notation we introduce an operator $\hat{O} = \hat{O}(A(z=0), G_0)$ which accounts for the propagation of the light pulse through the fibre section with gain G_0 . $G_0 = 0$ models the passive fibre. APM requires that the distances between the two fibres and the coupling mirror are balanced and thereby utilizing the effect of a small intensity dependent dynamic phase shift resulting in coherent addition only towards the peak of the pulse. In our model this is achieved by multiplying the outgoing pulse $a_{2,n}$ from the passive fibre with the factor $\exp(-i\psi)$, where ψ is the static phase shift or phase bias¹. Furthermore, there are coupling losses when the pulse enters and leaves a fibre. This coupling loss is denoted by η and it is assumed to have the same magnitude for both fibres. The model can now be completed by

$$\begin{aligned} a_{1,n} &= \eta \hat{O}(\eta b_{1,n-1}, G_0) \\ a_{2,n} &= \eta e^{-i\psi} \hat{O}(\eta b_{2,n-1}, 0) \end{aligned} \quad (4)$$

which is to be solved numerically together with with Eq. (1) describing the coupling at the mirror.

SIMULATIONS OF PULSE COMPRESSION

In a full numerical simulation of the APM configuration it is possible to obtain detailed information about the transient dynamical behaviour during pulse compression and to obtain the final steady state pulse. This is demonstrated in Fig. (2a) showing an initial pulse $a_{1,0}(t) = B_1 \text{sech}(B_2 t)$ launched toward the mirror with $a_{2,0}(t) = b_{1,0}(t) = b_{2,0}(t) = 0$ and using $G_0 = 0.43 \text{m}^{-1}$ and $\psi = -2.36$. Fig (2b) depicts the Full Width at Half Maximum (FWHM) as function of the number n of cavity round trips. It is seen that after about 300 round trips the FWHM has decreased from 3.53ps to 234 fs. Starting out with longer pulses results in the same final steady state indicating that substantial greater compression factors can be achieved.

Referring to previous results^{7,8} it is mentioned that the phase bias ψ plays an important role for the stability of the single pulse propagation. Only within a narrow interval of the phase bias values is it possible to obtain single pulse propagation. Outside this range the pulse either dies out or breaks up into multiple pulses.

A too small gain G_0 inhibits single pulse propagation, in this case the initial pulse dies out. Increasing the gain reduces the FWHM to a limiting value and for a sufficiently high gain the pulse breaks up into multiple propagating pulses. This break up phenomenon limits achievable pulse-shortening in this APM system.

ACKNOWLEDGEMENTS

This work has received financial support from the Danish Research Academy [Grant No. 5900103] and from the British Council. We acknowledge Prof. E.P. Ippen, MIT, for useful discussions.

REFERENCES

1. J. Mark, L.Y. Liu, K.L. Hall, H.A. Haus, and E.P. Ippen, *Opt. Lett.* **14**, 48:50 (1989).
2. E.P. Ippen, H.A. Haus, and L.Y. Liu, *J. Opt. Soc. Am. B6*, 1736:1745 (1989).
3. H.A. Haus, J.G. Fujimoto, and E.P. Ippen, *J. Opt. Soc. Am. B8*, 2068:2076 (1991).
4. F.M Mitschke and L.F. Mollenauer, *Opt. Lett.* **11**, 659:661 (1986).
5. J.P. Gordon, *Opt. Lett.* **11**, 662:664 (1986).
6. A. Hasagawa and F. Tabbert, *Appl. Phys. Lett.* **23**, 142:144 (1973).
7. M.P. Sørensen, K.A. Shore, T. Geisler, P.L. Christiansen, J. Mørk, and J. Mark, *Opt. Comm.* **90**, 65:69 (1992).
8. T. Geisler, K.A. Shore, M.P. Sørensen, P.L. Christiansen, J. Mørk, and J. Mark, *Submitted to J. Opt. Soc. Am. B*.

THE LIFETIME OF MOLECULAR (DAVYDOV'S) SOLITONS

A.S.Davydov*

Bogolyubov Institute for Theoretical Physics
Ukrainian Academy of Sciences
252143 Kiev, Ukraine

INTRODUCTION

There is a very important problem in the science of bioenergetics - how to store and transport biological energy in the protein structures. An answer to this problem was suggested in 1973 by Davydov¹⁻³ who proposed a model for the energy transport in quasi-one-dimensional biological systems. The basic idea for this model was that transport energy is done due to separated formations, so-called Davydov's solitons that almost freely travel through the system.

Theoretical investigations of the lifetime of Davydov's solitons in one-dimensional systems prove to be the most difficult problem in the theory of solitons. In the present paper we discuss some questions which are to be solved to estimate correctly the lifetime of solitons in molecular systems. The problem of calculating the lifetime of solitons has arisen in recent years with a view to clearing up whether the lifetime of the Davydov's soliton at nonzero temperature is long enough for it to be used in biology. I think that many of the previous estimates of Davydov's soliton stability at finite temperature should be revised.

Some authors revealed nonstationary states as states described by the part H_0 of a total Hamiltonian H . The remaining part $V = H - H_0$ was considered as the reason for transition to other states. But division of Hamiltonian into parts H_0 and V is arbitrary and nonsingle-valued. So the lifetime obtained by these calculations is also non-one-valued. Therefore, it is no wonder that they obtained not real lifetime τ . For example, in the paper by Bolterauer⁴ it was obtained $\tau = 10^{-14} - 10^{-12}$ s. Cottingham and Schweitzer⁵ obtained $\tau = 10^{-14} - 10^{-12}$ s. These authors do not astonish these values are smaller than the lifetime on one isolated intramolecular vibration (10^{-12} s) in condensed medium, so they devoid of a physical meaning.

On the other hand Bolterauer⁶ and other authors (see references in ⁷) found solitons to be stable at $T = 30$ K. Cruzeiro et al.⁷ derived a thermally averaged Hamiltonian and found stable solitons at 300 K. But in those papers, as in the paper by Davydov⁸, it was really considered not the lifetime of solitons but their properties at finite temperature after thermalization. And what is more, the calculation is fulfilled as in the paper⁷ under condition that $\int |\Psi|^2 = \text{const}$, which corresponds to the assumption about an infinite lifetime of soliton.

*deceased February 1993

THE PROPERTIES OF SOLITONS AT DIFFERENT TEMPERATURES

The exceptional stability of solitons is stipulated by the mutual influence of two phenomena: the dispersion and the nonlinearity. The dispersion induces diffusion of the localized excitation, organized from the monochromatic waves. In the linear system this diffusion does not compensate because of the independence of plane waves. In the nonlinear system there takes place the rearrangement of the energy between them. The energy is taken away from fast growing waves and passes to the waves lagging. As a result the excitation remains localized.

At present while investigating the thermal stability of a soliton nobody really considers the lifetime as a soliton creates at some moment, but considers its properties in a system which is in contact with the thermostat at different temperatures. When investigating the properties of solitons at different temperatures it is very important to take into account that there are two types of phonons in the theory of solitons: 1) the virtual phonons which describe the displacement of the equilibrium positions of molecules of a chain under creation of the soliton and 2) the real phonons which describe the vibrations of molecules round the new equilibrium positions. Only real phonons go into thermal equilibrium. The virtual phonons do not depend on the temperature. The method of separating real and virtual phonons was proposed by Davydov in ⁸ where the influence of temperature on the properties of solitons was investigated.

A. Davydov was the first to consider the quantum mechanical effect of the quasi-one-dimensional chain of N periodically repeated neutral molecules at sites na maintaining contact with a thermostat at temperature $T \neq 0$. Stationary states of one intramolecular vibration or one extra electron in this chain in the short range approximation are described by the Hamiltonian $H = H_o + H_{ph} + H_{int}$ where

$$H_o = -J \sum_{n=1}^N [2A_n^+ A_n - (A_n^+ A_{n+1} + h.c.)]$$

is the operator of energy counted off from the energy band bottom of a free quasi-particle (an electron, or intramolecular vibration) with effective mass $m = \hbar^2/2a^2J$.

For a quantum description, it is convenient to express the displacements, U_n at the n -th molecule from its equilibrium position, na , through the operator of creation, b_q^+ , and annihilation, b_q , of phonons by the formula

$$U_n = \sqrt{\frac{a\hbar}{2MV_oN}} \sum_q |\xi|^{-\frac{1}{2}} (b_q + b_q^+) \exp(in\xi), \quad \xi = aq,$$

where M is the mass of a molecule, a is the equilibrium distance between molecules, V_o is the velocity of a long-wave sound. The wave number, q , runs N discrete values. The energy operator of short-range deformational interaction of a quasi-particle with the displacement has, in the linear approximation, the form

$$H_{int} = N^{-\frac{1}{2}} \sum_{n,q=1} F(q) A_n^+ A_n (b_q + b_{-q}) \exp(in\xi),$$

$$F(q) = F^*(-q) = ia\lambda \sqrt{\frac{\varepsilon(q)}{2MV_o^2}} |\xi|^{-1} \sin(\xi).$$

Here $a\lambda$ is the energy of the deformational potential. The operator of the longitudinal deformation energy of the chain has the form

$$H_{ph} = \sum_q \varepsilon(q) b_q^+ b_q,$$

$$\varepsilon(q) = \hbar|q|V_0$$

is the energy of a phonon with a wave number q .

Stationary states of the chain are described by the average of the energy

$$\mathcal{H} = \langle \Psi | H | \Psi \rangle, \langle \Psi | \Psi \rangle = 1. \quad (1)$$

In this expression, the wave function $|\Psi\rangle$ is defined by

$$|\Psi\rangle = \sum_n \prod_q \varphi_n(t) S_{nq}(t) A_n^+ | \cdots \nu_q \cdots \rangle$$

where

$$S_{nq} \equiv \exp [\tilde{\beta}_{qn}(t) b_q - \tilde{\beta}_{qn}^*(t) b_q^+]$$

is the unitary displacement operator. The functions $\tilde{\beta}_{qn}(t)$ are modulated waves

$$\tilde{\beta}_{qn}(t) = \beta_{qn}(t) \exp(-in\xi). \quad (2)$$

The action of the unitary operator S_{nq} upon the operators b_q and b_q^+ leads to their displacement by complex numbers $\tilde{\beta}_{nq}$ and $\tilde{\beta}_{nq}^*$ because

$$b_q \equiv S_{nq}^+ \tilde{b}_n S_{nq} = \tilde{b}_q - \tilde{\beta}_{nq}.$$

These equations show that the interaction of a quasi-particle with the chain results in the vibration of the molecules about the new equilibrium positions $\tilde{\beta}_{nq}$. These vibrations are characterized by the new creation and annihilation operators (b_q^+, b_q) of real phonons. The real phonons describe the vibration of molecules around the new equilibrium positions. Only real phonons go into thermal equilibrium. The function (2), which describes the displacements of the equilibrium positions of molecules of a chain under creation of soliton, is temperature-independent. In quantum theory these displacements correspond to the virtual phonons. Take into account these properties of real and virtual phonons, very important in the theory of solitons which circumscribe thermodynamically equilibrium states.

In the chain in thermal equilibrium with the thermostat at temperature T , the statistical average of model Hamiltonian (1) is reduced to replacing the quantum number ν_q of real phonons by their averages

$$\langle \langle \nu_q \rangle \rangle = \left[\exp \left(\frac{\varepsilon(q)}{kT} \right) - 1 \right]^{-1}.$$

After calculation, the averaged value of (1) is transformed to the energy functional

$$\begin{aligned} \langle \langle H \rangle \rangle = & - \sum_{n, \nu_q} \{ J[2|\varphi_{qn}|^2 - \exp(W_n) (\varphi_{qn}^* \varphi_{qn} + c.c)] - \\ & N^{-\frac{1}{2}} F(q) |\varphi_{qn}|^2 (\beta_{qn} + \beta_{qn}^*) + \varepsilon(q) [\langle \langle \nu_q \rangle \rangle + |\varphi_{qn}|^2 |\beta_{qn}|^2] \}, \end{aligned}$$

where the Debye-Waller factor $\exp(W_n)$ is defined by

$$W_n = \frac{1}{2} \sum_q |\beta_{qn}^2 \xi^2 (1 + 2\langle \langle \nu_q \rangle \rangle)|. \quad (3)$$

The energy functional (3) describes both nonlocalized and autolocalized states. The autolocalized states are stationary states in which the distances or the orientations of

the molecules change in some finite region of the chain, i.e. there is a local violation of translational symmetry. This localization region may occupy any part of the chain. Consequently, general translational symmetry is preserved. Therefore, these autolocalized states are characterized by the energy and total momentum related to the movement of the localization region along the chain with a constant velocity that depends on the value of the wave number k .

The autolocalized states arising under the short-range interaction are described by nonlinear differential equations. They are usually called solitons to distinguish them from the autolocalized states first introduced in 1933 by Landau¹⁰ and elaborated by Pekar¹¹ when describing the electron motion in ionic crystals. The latter states were called polarons, because they are caused by the long-range (Coulomb) interactions of electrons with the field of electric polarization of a crystal which is described by the longitudinal optical phonons. The properties of polarons are defined by integro-differential equations.

Now we investigate the case when the autolocalized quasi-particle occurs in finite region of a long aN ($N \gg 1$) molecular chain³. Assume that the state of quasi-particle in such a chain is described by the function

$$\Phi_n(t) = \Phi(n) \exp[i(kan - \omega t)]$$

with a fixed wave number k , and the real nonzero amplitude $\Phi(n)$ only in some finite (not too small) region of a chain.

Near the region in which quasi-particles are mainly distributed, the energy functional (3) takes the form

$$\langle\langle H \rangle\rangle = \sum_n \{ J(2|\Phi|^2 - [\Phi_n^* - \Phi_{n+1} + c.c.] \exp(-W_n) + \sum_q \epsilon(q)[\langle \nu_q \rangle + |\beta_{nq}|^2] - \quad (4)$$

$$-N^{-\frac{1}{2}} \sum_q F(q)|\Phi|^2(\beta_{qn} + \beta_{qn}^*) \}, \quad \epsilon(q) = \hbar \Omega_q. \quad (5)$$

In states in which the quasi-particle location region exceeds much the distance between the molecules $|\Phi_n|^2 \ll 1$, at low temperatures ($\theta < \theta_D$), from (5) we can obtain

$$i\hbar \frac{\partial \Psi_n}{\partial t} = J[2\Phi_n - (\Phi_{n+1} + \Phi_{n-1})] \exp(-W_n) + G(n)|\Phi_n|^2 \Phi_n \quad (6)$$

where a nonlinear parameter $G(n)$ is

$$G(n) \approx G = \frac{D}{1-s^2}, \quad D^2 \equiv a^2 \chi^2 / MV_o^2, \quad s^2 \ll 1 \quad (7)$$

and Debye-Waller factor $\exp(-W_n)$ is defined by

$$W_n = B_n [1 + 2 \exp\left(\frac{\pi \epsilon_o}{\theta}\right) \exp(-W_n)]. \quad (8)$$

Here

$$B_n \approx 7.3 \cdot 10^{-5} D^4 / \epsilon_o J^2 \ll 1.$$

In the continuum approximation (6) takes the form

$$\{i\hbar \frac{\partial}{\partial t} - 2J[(1 - \exp(-W))] + \frac{\hbar^2 e^{-W}}{2m} \frac{\partial^2}{\partial x^2} + G|\Phi|^2\} \Phi = 0. \quad (9)$$

Its solutions on the infinite chain can be written in the form

$$\Phi(x, t) = \Phi(z) \exp[i(kz - \omega t)], \quad (10)$$

where $\Phi(z)$ is a smooth real function in the system of coordinates z , moving with constant velocity V , thus,

$$z \equiv x - x_0 - Vt, \quad V = \hbar k/m \ll V_0.$$

It obeys the equation

$$\left[\Lambda + \frac{\hbar^2}{2\tilde{m}} \frac{d^2}{dz^2} + G \right] \Phi(z) = 0, \quad \tilde{m} = m \exp(W). \quad (11)$$

The localized solutions of (11), normalized on the infinite chain, is defined by the function

$$\Phi(z) = \sqrt{a\theta/2} \operatorname{sech}(z\theta) \quad (12)$$

with parameters

$$Q \equiv Ge^W/4aJ, \quad \Lambda \equiv -a^2\chi^2 e^W/16J.$$

The energy of the chain deformation in the region of the n 'th molecule is

$$E_{def} = \frac{D}{2a} \int \Phi^2(z) dz = D^2 e^W / 24J. \quad (13)$$

The energy of the quasi-particle in the potential field of the deformation well that moves with velocity V , is defined by

$$\hbar\omega = 2J[1 - \exp(-W)] + a^2(k^2 - Q^2)J \exp(-W). \quad (14)$$

The first term in (14) indicates a decrease in resonance interaction caused by the fluctuations at intermolecular distances. The second term characterizes the energy gain by binding at the quasi-particle in the field of deformation.

To calculate the total energy $E(V)$, transferred by a moving soliton, we must add to (14) the energy of deformation. So we obtain

$$E(V) = 2J[1 - e^{-W}] - \frac{D^2}{48J} e^W + \frac{1}{2} m V^2 e^W. \quad (15)$$

At temperature θ that is smaller than maximum energy of phonons, ϵ_0 , and at small velocities, the soliton total energy (15) can be written as

$$E(V) = E(0) + \frac{1}{2} M_{sol} V^2, \quad \theta < \epsilon_0,$$

where

$$E(0) = 2J[1 - e^{-W}] - \frac{D^2}{48J} e^W$$

is the soliton energy at rest, and

$$M_{sol} = m e^W [1 + a^2 \chi^4 / 12 \hbar^2 M^2 V_0^2]$$

is its effective mass.

At zero temperature the function $W = 0$. With rising temperature, the energy gain when the rest quasi-particles are bound with deformation, is defined by

$$\Delta E = \frac{D^2}{48J} + W(2J^2 - D^2)/48J.$$

If the inequality $2J^2 > D^2$ is fulfilled, the increasing temperature (under $\theta < \epsilon_0$) causes increase in W and stabilizes the soliton. Its binding energy and effective mass increases, but in agreement with (12) the effective size decreases.

THE TOPOLOGICAL STABILITY OF SOLITONS

When investigating the lifetime of solitons we need to know the initial time when it was created. The time evolution of soliton state will depend essentially on the time when the thermodynamic equilibrium with a thermostat is established. The soliton can pass a long distance before its parameters (W and others) will be thermalized. As we know while studying the lifetime of solitons due to thermal motion nobody has taken into account these very important circumstances. The main disadvantage of current theoretical research of excitons is also the neglect of topological stability of solitons.

The soliton is organized as quasi-particle coupled with the local deformation on the chain. The space distribution of a quasi-particle (an exciton for a vibrational excitation or an electron of the conduction band) in a system $\xi = x - Vt$ moving with velocity V is defined by the bell-shaped function

$$\Phi^2(\xi) = (2Q)^{-1} \text{sech}^2(Q\xi). \quad (16)$$

The decrease in the intermolecular distances in the region of a bisoliton is described by the function $\rho(\xi) \sim \Phi^2(\xi)$. This decrease is caused by displacements of equilibrium positions of molecules and is described by the function

$$U(\xi) = 4[1 - \tanh Q\xi] = \begin{cases} 0 & , \text{at } \xi > 0 \\ 2A & , \text{at } \xi < 0 \end{cases} \quad (17)$$

So, when a soliton moves with velocity V all equilibrium positions of molecules behind it are displaced by the values $2A$, but in front of it, the positions of molecules are not changed. For the soliton to disappear, one needs to waste an energy to transfer a quasi-particle into a free non-local state (exciton or electron in the conduction band) and returns all molecules which were displaced to their initial states. This circumstance prevents the destruction of a soliton and guarantees its topological stability.

On account of topological stability solitons can be created and disappear only at the ends of molecular chain. This very important property was not taken into account in works devoted to the calculations of the lifetime of a soliton. Therefore, the estimate of the lifetime of solitons made previously require a total revision. We remind once more that usually one considers not the lifetime, that is the time of the existence of a soliton from the moment of its appearance, but only the properties of an existing soliton at different temperatures.

THERMALIZATION OF SOLITONS

In nonlinear system with dispersion, that is the medium, where the phase velocity at monochromatic values is the function of wave length and its amplitude, the perfect way of the energy transport is realized by the nonlinear solitary waves. These waves transfer energy without loss and preserve their form. These unusual properties of bell-shaped moving local excitation enabled Zabusky and Kruskal¹¹ to call them solitons. In contrast to the monochromatic waves, which describe periodic repetition in space the elevation and deeping on the surface of a water, on contraction and rare-action of a density, or deviation from average values of the other physical properties, solitons are characterized by single excitations, spread as unit with constant velocity without damping.

For the first time solitary waves were observed by John Scott Russel more than 150 years ago. Many times he observed the movements of the barges along the channel Edinburgh-Glasgow. He published in 1844 these observations in paper "Report on

Waves"¹². He discovered, that under a sharp stop of a barge from it a part of the waves is repeated and with a big velocity rolled, receiving the form of a single elevation, continuing its way along the channel without any noticeable change in its shape and does not decrease its velocity. This wave was called the wave of translation or solitary wave.

Only after one hundred years, the interest in the solitary wave renewed. Particular interest induced the paper which was published in 1955 by collaborators of the Los Alamos Scientific Laboratory Fermi, Pasta and Ulam¹³. In this paper the condition of thermalizing energy in nonlinear vibrational systems was investigated. Using the new computer they attempted to clear up the conditions of the thermalization of the vibrations in a chain of periodically situated particles which linear and quadratic forces operate. It was well known that in a condensed medium the vibrations of atoms can be represented in the form of a superposition of monochromatic vibrations. In a linear medium these vibrations are independent. Under weak nonlinearity between monochromatic vibrations interactions arise which reduce to the thermalization. The precise calculations by Fermi, Pasta and Ulam showed that in a system with quadratic nonlinearity the thermalization does not occur. This result appear to be paradoxical for a long time. It was resolved by Zabusky and Kruskal¹¹ only ten years after. They showed that long-wave excitations in a discrete chain are described by nonlinear equations. Their solutions were stable bell-shaped excitations. It was found that the nonlinear interaction does not cause the exchange of energy between them. This was the reason for the absence of thermalization in the nonlinear system which was investigated.

In the papers by Fermi, Pasta and Ulam and Zabusky and Kruskal, the process of thermalization in mechanical nonlinear vibration systems was investigated. In 1979 Eilbeck (in collaboration with A.C.Scott) investigated the propagation of Davydov solitons along peptide chain of the biological systems. They made a computer film¹⁴ which demonstrated the propagation of soliton in form of a local bell-like-excitation along the peptide chain after it being created at the end of the chain moving to the other end of the chain. Simultaneously with the soliton acoustic wave packet was excited. The acoustic wave packet was moving with velocity bigger than that of a soliton, leaving it unchanged. Thus, the Eilbeck film visually demonstrated the stability of Davydov's soliton relative to their interaction with the packet of acoustic waves. This interaction is a reason of thermalization. Therefore, the soliton can be displaced on a long distance transposing the energy excitation before the thermalization being arisen.

The exceptional stability of solitons is stipulated by the mutual influence of two phenomena: the dispersion and the nonlinearity. The dispersion induces diffusion of the localized excitation, organized from the monochromatic waves. In the linear system the diffusion does not compensate because of the independence of plane waves. In the nonlinear system there takes place the rearrangement of the energy between them. The energy is taken away from fast going waves and passes to the wave lagging. As a result, the excitation remains localized.

SOLITON GENERATION AND DISINTEGRATION IN MOLECULAR CHAIN

According to what has been said previously, because of the topological stability solitons can be created and disintegrated at the end of molecular chain only. The possible mechanism of soliton creation may be the following. An electron beam, light quanta, local hydroless molecule ATP etc. excited the impurity molecule at the end of the chain principal molecule. The excitation transfer into the neighbouring molecule of the chain with which the impurity molecule is connected.

The process has been studied by Brizhik and others¹⁵. It is characterized by two

parameters: parameter Γ which defines a nonresonance excitation transfer from exciting impurity molecule onto a neighbouring one of the basic chain and J is the resonance excitation transfer constant between the basic molecules of a chain. If the condition $\Gamma \gg J$ is satisfied, the excitation of impurity molecule will be localized at the molecule of a chain nearest to the impurity at the moment t_0 satisfying the inequality $\hbar/\Gamma \ll t_0 \ll \hbar/J$. In this case the inverse transfer along the chain by resonance mechanism.

There is a low and fast process of disintegration of solitons. At slow process the complete annihilation of soliton takes place, that is, the transfer of a soliton into a nonlocalized state (excitation) and removal of a local deformation in the chain. At fast processes the transfer of soliton from quasi-localized state into nonlocalized takes place so fast that a local deformation has no time to disappear.

As is known, at the moment of light absorption by molecular systems, the coordinates of heavy particles are unable to displace (the Frank-Condon principle). Since the formation of a soliton is connected with the displacement of equilibrium positions of heavy particles (the peptide groups in the muscle molecules, for example). So under the influence of electromagnetic radiation, solitons disintegrate into rapidly relaxing excitons and local deformation of the chain. This process will be called fast annihilation of the soliton. The process of fast annihilation can occur at any place of the chain. At fast annihilation, the energy expenditure is required, which equals the binding energy of a quasi-particle with local deformation of a chain. For rest of the solitons an energy deformation of chain is equal to $U/2$. So, for slow process one needs to spend the energy equal to $2U/3$.

Using the idea of solitons Davydov proposed in 1973 a new hypothesis of the mechanism of the shortening of sarcomere length that evolved contraction of striated muscle^{2,16}. According to this hypothesis under a nerve impulse the calcium ions reach the first series of myosin molecule heads at the ends of thick filament initiate the hydrolysis of the ATP molecules attached to them. The energy released generates solitons in a long helical section of myosin molecules which make up the thin filament of the muscle fibers. They move from ends to the center and the displacement of the surrounding action proteins.

* Spending their kinetic energy for the works necessary to contract the muscle fiber, the solitons are slowed down and, stopping near the centers of the thick filaments, are annihilated, giving up the rest of their energy to thermal motion. This is the reason for the heating of the muscle during their work. Thus, only the kinetic energy of solitons is used in the contraction of the muscle fibers of the living organisms.

Thus, the disintegration (and so lifetime) of solitons are always stipulated by external action of soliton.

REFERENCES

1. A.S.Davydov, J.Theor.Biol. 38:559(1979), Phys.Scr. 20:387(1982), Usp.Fiz. Nauk 138:603(1980).
2. A.S.Davydov. "Biology and Quantum Mechanics", Pergamon, New York (1982).
3. A.S.Davydov. "Solitons in Molecular Systems" D.Reidel Publish. Co., Dordrecht (1985); Second Ed. (1991).
4. H.Bolterauer, Quantum effect on Davydov soliton, In: Davydov's Soliton Revisited, P.L.Christiansen and A.C.Scott Eds.(1991), NATO ASI Series, Physics 243:99.

5. J.P.Cottingham, J.W.Schweitzer, Perturbation estimate of the lifetime of Davydov soliton at 300K. *Rev.Lett.* 62:1752 (1985).
6. H.Bolterauer, "Structure, Coherence and Chaos" P.L.Christiansen and R.D. Parmentier Eds., Manchester University Press, p.619-624 (1987).
7. L.Cruzeiro, J.Halding, P.L.Christiansen, O.Skovgaard and A.C.Scott, Temperature effect on Davydov soliton, *Phys.Rev.Lett.* 62, 1752 (1989).
8. A.S.Davydov, Quantum theory of motion of quasi-particle in molecular chain with thermal vibration taken into account, *Phys.Stat.Sol.(b)* 138:559 (1986).
9. L.Landau, Über die Bewegung der Electronen in Crystallgitter, *Phys.Z.Sov* 8:664(1933).
10. C.I.Pekar, Autolocalization of an electron in crystals, *Zh.Eksp. and Fiz.* 16:335(1976).
N.I.Zabusky and M.D.Kruskal, *Phys.Rev.Lett.* 15:240(1965).
12. J.Scott-Russel, "Report on Waves", *Proc.Roy.Soc., Edinburgh*, 319(1844).
13. E.Fermi, J.Pasta, S.Ulam, Studies of nonlinear problems, Los Alamos, Report LA, p.1940(1955).
14. J.C.Eilbeck. "Davydov solitons a 16 mm mute film", (1979).
15. L.S.Brizhik, Yu.B.Gaididei, V.A.Vakhnenko, Soliton generation semi-infinite molecular chains, *Phys.Stat.Sol.(b)* 146:605(1988).
16. A.S.Davydov, Solitons, Bioenergetics and mechanism of muscle contraction, *Int.J.Quantum Chemistry.* 26:5(1979).

ENERGY TRANSDUCTION AND DETERMINISTIC PROTEIN MOTIONS

R. J. Dwayne Miller, J. Deak, S. Palese, M. Pereira,
L. Richard, and L. Schilling

Department of Chemistry and Institute of Optics
University of Rochester
Rochester, N. Y. 14627

The activity of numerous biological molecules is controlled by the binding of a receptor which produce changes in structure. These structural changes, in turn, modify the barriers to various catalytic and transport functions. The molecular response function to the stimulus for motion involves specific structural changes that require the correlated displacement of thousands of atoms. Given the enormous number of degrees of freedom involved in these functionally relevant motions, it is clear that the energy of interaction with the receptor is being transferred in a highly directed fashion into the key atomic displacements. To understand the biomechanics, it is necessary to determine how energy is exchanged amongst these different degrees of freedom and the length scale of the forces displacing the atoms. In this regard, heme proteins provide ideal model systems. Large amounts of energy can be optically deposited in the center of the protein and the spatial dispersion or redistribution of this energy can be monitored using optical probes sensitive to vibrational or translational energy. It is also possible to optically trigger the functionally important structural changes involved in the allosteric regulation of oxygen transport in heme proteins. Thus, both energy exchange processes and functionally important motions can be studied in a single system.

EXPERIMENTAL STUDIES

Vibrational Energy Relaxation in Proteins

The first experimental studies of vibrational energy redistribution in proteins took advantage of the high sensitivity of thermal phase grating spectroscopy to follow the vibrational to translational energy transfer into the heme protein's solvation shell.¹ This energy transfer process is the final step in the overall energy redistribution. This study exploited the ability to optically excite the heme and create a non-equilibrium condition in which the absorbed photon energy is converted into vibrational energy of the

central heme moiety on a picosecond time scale. The excess vibrational energy transfers to other vibrational modes of the surrounding protein, spatially propagates to the protein's exterior, and ultimately exchanges energy with the water through collisional interactions. The thermal grating studies found that this exchange process had an effective time constant less than 22 picoseconds. This work has been further validated by infrared studies of the water heating.² In addition, time resolved anti-Stokes Raman studies, using resonant enhancement to follow the decay of the excess vibrational energy of the heme, have found that the transient vibrational energy transfers from the heme to the surrounding protein within 2-5 picoseconds.³ The thermal grating studies in conjunction with the Raman and infrared studies demonstrate that vibrational energy flow in these large molecular systems is occurring within the statistical limit for intramolecular vibrational energy redistribution.⁴

The main conclusion to be drawn from this work is that biological molecules are extremely efficient at redistributing vibrational energy. The entire relaxation process, from the decay of the initially excited modes to collisional exchange with the water, is occurring on a picosecond time scale. Thus, it is very unlikely that energy can be specifically channelled into atomic displacements through strongly coupled vibrational modes as the lifetimes of any given mode is extremely short. The efficient energy redistribution is going to make any mode strongly damped by the huge network of anharmonic interactions between atomic sites. This dissipation process needs to be considered in any model for functionally relevant structural changes of biomolecules.

Picosecond Phase Grating Studies of Global Protein Motion

More recently, the phase grating method has been applied to the study of tertiary structural changes in heme proteins. These changes are central to the allosteric regulation of hemoglobins and form the basis for theories of molecular cooperativity. In these studies, the tertiary structural change is optically initiated by the photodissociation of CO. This ligand exhibits unit quantum efficiency for photodissociation in less than 100 femtoseconds with recombination occurring much slower than the ensuing protein relaxation. This work discovered that the protein motion to the deoxy structure launches coherent acoustic waves which match the grating wave vector.⁵

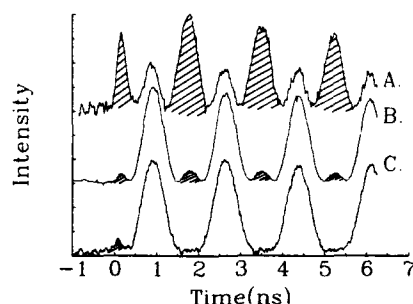


Figure 1. Grating dependence on protein (excitation energy=2 mJ/cm²; excitation wavelength=532 nm, probe wavelength=1.064 μ m). The marked areas depict the maxima of the protein wave, while other maxima are the positions of the thermally driven acoustics. A. Carboxymyoglobin. B. Carboxyhemoglobin. C. Carboxyheme Octapeptide.

The generated acoustics are non-thermal and satisfy $t=0$ strain boundary conditions. Representative results are shown in figure 1. These results clearly demonstrate that the signal depends on the protein structure surrounding the heme. In the case of hemoglobin, the quaternary structure mechanically constrains the tertiary displacements of the individual subunits. Consistent with this concept, the amplitude of the carboxyhemoglobin (HbCO) acoustics are found to be smaller relative to carboxymyoglobin (MbCO) which exists as a single heme protein without quaternary constraints. In the study of carboxyheme octapeptide, there is a small signal at $t=0$, but no acoustics are observed other than the thermal mechanism. Carboxyheme octapeptide is basically the isolated heme without the protein matrix. In the absence of the surrounding globin, the acoustics associated with the tertiary structural changes (the protein wave) are not observed. Thus, the carboxyheme octapeptide study demonstrates that the rapid density changes observed for MbCO and HbCO originate from changes in the surrounding protein holding the heme in place.

In these studies, the protein motion triggered by the CO dissociation leads to material displacement which is holographically recorded as density induced changes in the index of refraction. In order for this motion to couple to the fluid hydrodynamics, as observed, requires a global change in protein structure (volume change caused by a net displacement of the exterior atoms relative to the interior). Thus, the phase grating gives a real time method of monitoring global protein motion. The grating formation dynamics provide a direct determination of the time evolution of the protein strain ($\Delta V/V$). This is one of the key parameters needed to understand the mechanics.

A four pulse grating geometry has been used to study the short time changes in protein strain for carboxymyoglobin (MbCO). These studies serve as a model for tertiary structural changes of the individual heme protein monomers of hemoglobin. The laser system used for these studies consists of a hybridly modelocked dye laser synchronously amplified by a Nd^{+3} :YLF regenerative amplifier. The grating excitation pulses were 1-2 ps in duration at 585 nm. The nonresonant probe pulse was provided by the 50 ps pulses from the regenerative amplifier at 1.053 μm which were upconverted with a residual dye pulse in the signal detection to conserve the time resolution. Previous studies of the grating formation dynamics were limited by an optical Kerr effect (OKE) which obscured the native protein response function.⁶

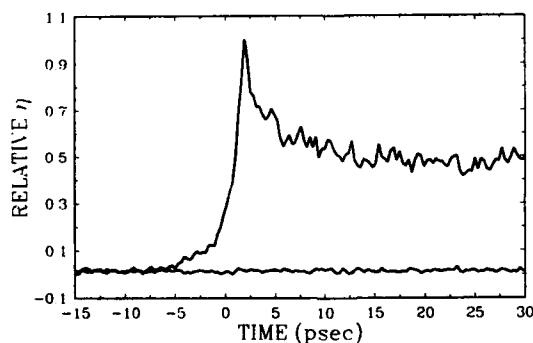


Figure 2. Picosecond phase grating studies of MbCO. The upper curve is the data collected for MbCO, while the lower curve shows the background signal for the buffer alone.

This problem was reduced by using a polarization analyzer and choosing probe polarizations that minimized the OKE signal. The results from this study are shown in figure 2. In the MbCO studies, a pulse width limited rise and decay is observed. This signal component accounts for approximately 50 % of the grating amplitude and may be due to transitions from the short lived (≤ 3.2 ps) deoxyMb state accessed during the CO photodissociation.⁷ The exact origin of this signal component (electronic or protein structural changes) can be determined through a wavelength dependence with shorter pulses. Regardless of this complication, it is clear that the protein motion which couples to the acoustics has a rise time of less than 5 picoseconds. There is no evidence for significant, slower, relaxation processes indicative of conformational substates along the relaxation coordinate at 298 K. At temperatures near the zero thermal expansion point, however, nanosecond relaxation components are discernable in the absence of the thermal acoustic interference. The amplitude of these relaxation components is less than 10 % of the protein driven component. Therefore, the fast initial change in protein strain appears to be the dominant relaxation step.

The grating studies probe the global protein motion. These changes in protein volume require a net displacement of the exterior atomic positions relative to the interior. On the other hand, time resolved Raman studies of the proximal histidine provide a measure of the local protein motion (changes in protein structure at a specific site). The proximal histidine is the closest contact point of the globin to the heme and is considered the focal point for the forces that drive the atomic displacements. Time resolved Raman studies have found that the proximal histidine motion is complete on a ten picosecond time scale or less.⁸ The close correspondence in dynamics over these two length scales of motion provides evidence that the initial structural changes are propagated by collective modes. To be specific, in order for the dynamics of the acoustic strain of the protein to be correlated to the proximal histidine motion, the exterior atomic displacements would have to be synchronized with the interior displacements at the heme which would produce a segmental motion. This type of displacement is by definition a collective mode. The correlation of dynamics for two different length scales of motion is the most stringent test for the involvement of collective modes. However, it would be desirable to have better time resolution in the Raman studies to determine the exact degree of correlation between the protein strain and proximal motion.

It should also be noted that the observed rise time for the changes in protein strain alone argues for the involvement of collective modes. An analysis of the normal modes of deoxyMb and MbO₂ by Seno and Gō has determined that greater than 60 % of the structural changes can be accounted for by the displacement of five spatially extended modes of the protein with frequencies ranging between 5 and 12 cm⁻¹.⁹ The vibrational periods of these modes correspond closely to the observed grating dynamics. Based on the vibrational energy relaxation studies discussed above, these modes would be overdamped. Thus, the observed grating dynamics also indicate that the initial protein response to ligand dissociation is the coupling of the heme to collective modes of the surrounding globin structure. This finding is important as this is the most efficient mechanism possible for the correlated displacement of atomic coordinates. Furthermore, this rapid initial phase of the structural relaxation would minimize the total conformational phase space the protein would have to sample to arrive at the global energy minimum corresponding to the new structure.

Femtosecond Transient Birefringence Studies

The grating studies provide information on the protein's structural relaxation processes that lead to changes in volume or strain. There is also the possibility that there

are structural changes in protein shape rather than volume. These dynamics would lead to changes in the symmetry of the protein and would modify the material birefringence. Femtosecond studies of these changes which follow CO photodissociation from MbCO were conducted with a synchronously amplified CPM operating at 627 nm, which is on the tail of the Q band of MbCO. The excitation and probe pulses were 50 fs in duration with the probe polarization 45° relative to the excitation. The probe intensity was monitored through an analyzer which was adjusted to be orthogonal (homodyne detection) or rotated from the orthogonal position (heterodyne detection) relative to the input probe polarization. Homodyne has the advantage of detection against a zero background, however the observed signal goes as the square of the polarization rotation. Heterodyne detection can be used to produce a linear response. The nonresonant optical Kerr effect (OKE) for water serves as a control for the system without the protein present. In the case of water the OKE signal consists mainly of terms pertaining to the nuclear motion of the solvent. The electronic contribution was conveniently smaller than the observed nuclear terms and the calculated n_2 is approximately 20 times higher than those based on measurements which yield primarily electronic results.¹⁰ The data was fit according to the models developed by D. McMorro et al.¹¹ which assumes that the OKE response can be fit to a differential equation equivalent to a driven damped harmonic oscillator. The data is deconvolved with the laser autocorrelation function in order to account for the spectral bandwidth of the laser excitation. Figure 3A shows the observed OKE signal for water and 3B its Fourier transform.

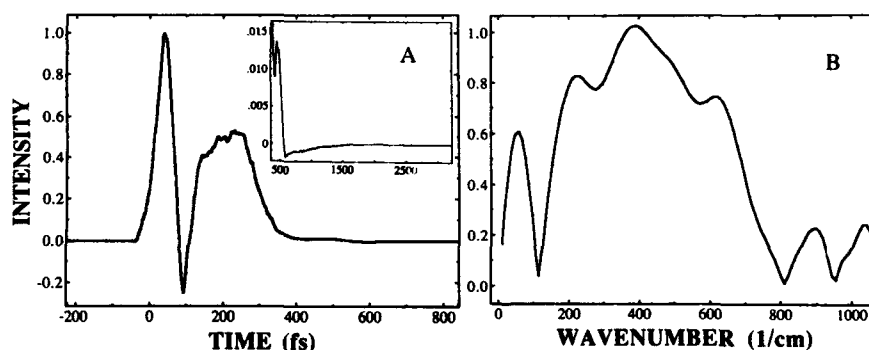


Figure 3. Transient birefringence signal for neat water utilizing heterodyne detection (pulse width= 50 fs, wavelength= 627 nm, excitation level 500 nJ/pulse). A) The signal consists of two different heterodyne levels which have been correspondingly scaled, 45° for $t < 350$ fs and 2.5° for $t > 350$ fs. B) The Fourier transform of the heterodyne signal that has been deconvolved with the laser autocorrelation.

The deconvolved OKE data can be fit to four distinct librational components. These consist of three broad peaks centered at 224 cm^{-1} ($A=.80$), 388 cm^{-1} ($A=1.0$), and 617 cm^{-1} ($A=.73$), where the highest peak has been normalized to unity. The linewidth (damping parameter) was assumed to be the same for these components and had a best fit of 180 cm^{-1} (58 fs). In addition, there exists a peak centered at 56 cm^{-1} ($A=.59$) which has a linewidth (damping parameter) of 78 cm^{-1} (134 fs). In order to verify the results of the OKE experiment the Fourier transform of the data should be similar to

spectra found utilizing depolarized light scattering (DLS) techniques. Indeed the 56 cm^{-1} , 224 cm^{-1} , and 388 cm^{-1} modes correspond to those observed in DLS spectra.¹² In addition to the librational modes, there are three diffusional relaxation components. The slowest component of $7.4 \pm .4\text{ ps}$ can be assigned to diffusional rotational relaxation and closely agrees with the theoretical value of 8 ps .¹³ A $1.6 \pm .3\text{ ps}$ relaxation which most likely corresponds to the transverse dielectric relaxation of water. The $322 \pm 33\text{ fs}$ relaxation can be assigned to the longitudinal dielectric relaxation and again closely agrees with the theoretical value of 300 fs .¹³ In the present context, the most important feature of these results is that the nonresonant water contribution to the signal is negligible for $t > 300\text{ fsec}$. This experimental approach is capable of accessing the low frequency modes of protein structures ($< 100\text{ cm}^{-1}$) with minimal interference from the surrounding water. In cases, where the high frequency components of the protein are needed, this well characterized water response can be subtracted.

In the protein studies, the pulse width could not be maintained due to the absorption peak at 580 nm . Any dispersion which occurs in the overlap region between the pump and probe is not compensable, and the pulse width broadened to roughly 100 fs FWHM. The MbCO response is dominated at short times by the electronic contribution. In addition, there exist two components of 195 fs ($A=.41$) and $2.4 \pm .2\text{ ps}$ ($A=.59$) respectively. The 195 fs component can be assigned to the 56 cm^{-1} librational mode of water based on the relative amplitude expected from the pure water sample at these

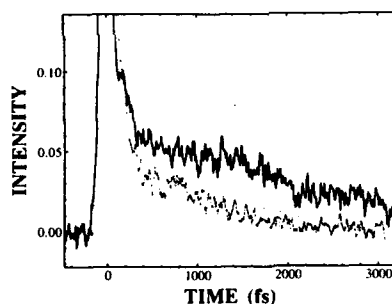


Figure 4. Transient birefringence studies. MbCO is the solid line and deoxyMb is the dashed data using heterodyne detection (input pulse width = 50 fs , wavelength = 627 nm , excitation level 200 nJ/pulse).

excitation levels. The possibility that the 2.4 ps relaxation corresponds to structural relaxation induced by the CO dissociation can be checked by comparing deoxyMb under the same conditions. The deoxyMb serves as a control in which the protein does not undergo any structural changes. The OKE signals for MbCO and deoxyMb are shown in figure 4. In this figure, the data is normalized relative to the 56 cm^{-1} component of water which serves as an internal reference.

As seen in figure 4, deoxyMb also exhibits a similar 195 fs ($A=.60$) and $2.2 \pm .4\text{ ps}$ ($A=.40$) relaxation components. However, the amplitudes and exact temporal dependence is not the same as that observed for MbCO.

The physical origin of the induced birefringence in the proteins can arise from two

different processes at this excitation wavelength. The first is that the excited deoxyMb electronic state, produced in both cases, produces an anisotropy in the sample either through imaginary contributions to n_2 or by thermalization of this short lived state and asymmetric expansion of the protein. The second possibility corresponds to the direct laser excitation of the low frequency Raman active modes of the protein. Within this interpretation, the frequency response is qualitatively in agreement with the normal mode analysis of myoglobin⁹ and the dominant mode observed would correspond to protein relaxation times comparable in time scale to that indicated in the grating studies. Given that the amplitudes of the two responses are not the same for MbCO and deoxyMb suggests the later explanation is the correct one. The dissociation of the CO ligand and subsequent heme doming would be expected to further displace the protein modes than that induced by the laser field alone. The contributions from excited state effects would be expected to give the opposite trend, i.e., the changes in optical density and thermal heating of MbCO are less than that for deoxyMb. Based on the observed differences between MbCO and deoxyMb, these studies provide supporting evidence for the low frequency protein modes implicated in the grating studies. However, a definitive assignment of the transient birefringence awaits a comparison of these results to nonresonant excitation studies in which excited state and CO dissociation processes can be singled out.

Thermal Phase Grating Studies of Structural Relaxation

The grating studies give information on structural relaxation components that lead to volume changes. These structural changes are analogous to collective acoustic modes in solid state systems. The observed dynamics are consistent with an initially rapid phase for the structural relaxation in which the doming of the heme, upon ligand dissociation, couples to spatially extended modes of the surrounding protein on a picosecond time scale. Other studies have given evidence for multiexponential processes occurring on much longer time scales which are indicative of conformational substates along the reaction coordinate.¹⁴ The energetics associated with each phase of the structural relaxation can be used to determine the relative importance of each phase of the protein relaxation. In addition, the energetics determine the amplitudes of the driving forces and the time scale under which the protein accesses the stored energy in its structure.

The energetics for the protein relaxation have been determined using thermal phase grating methods. The experimental setup is identical to the phase grating studies discussed previously⁵ with the exception that the medium was changed to 75% glycerol/water in which the thermal acoustics dominate. The thermal acoustics can be readily distinguished from the protein driven acoustics by the phase of the observed acoustic modulation. In the thermal case, the first maximum in the thermal signal appears at one half an acoustic period from $t=0$ which is determined by the speed of sound for thermal expansion over the grating fringe spacing.⁴ The important feature of this experiment is that the amplitude and dynamics of the thermal grating are related to the energy relaxation process.

These experimental studies are shown in figure 5. The decay of the acoustic modulation is due to acoustic attenuation in viscous medium. In this study, the deoxyheme protein analogue serves as the signal reference for 100% energy deposition of the absorbed photon energy within the impulsive limit, relative to the current grating acoustic period. In making a direct comparison of the MbCO and HbCO to their deoxy analogue under identical conditions it is clear that less energy is dissipated in the myoglobin case. The difference in energetics is related to the Fe-CO bond energy and any energy stored in the protein structure which is released during the structural relaxation. The

results to date show that MbCO is endothermic by 21 ± 2 kcal/mole in which the energy relaxation is complete in less than 200 ps.

This energy is close to the expected Fe-CO bond enthalpy¹⁵ and represents the fraction of the photon energy that remains stored in the system. There does not appear to be a substantial amount of energy stored in the protein for the oxy (ligated) to deoxy structure transition. Myoglobin appears to act essentially as an elastic basket for the iron ligand. In contrast, carboxyhemoglobin is endothermic by 11 ± 3 kcal/mole, i.e., ~ 10 kcal/mole of excess energy is released. This energy difference between monomeric myoglobin and tetrameric hemoglobin is related to structural differences in the two proteins. This is an intriguing finding as it may be related to quaternary structure effects. If so, the difference in energetics would reflect the energy stored at the subunit interface, which is the distinguishing quaternary feature, and would be related to the energy of molecular cooperativity. The origin of the structural dependence needs to be studied further with hemoglobin subunits to rule out effects due to the tertiary structural difference between Mb and Hb.

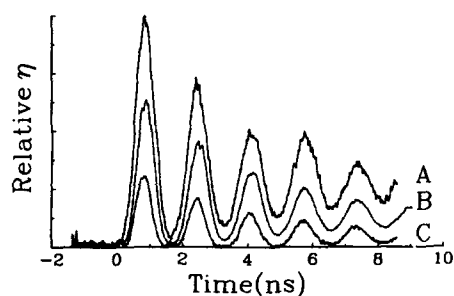


Figure 5. Phase grating studies of the protein energetics in 75% glycerol/25% water using 532 nm excitation and a $1.064 \mu\text{m}$ probe. A. Deoxy-heme protein B. HbCO. C. MbCO.

It is interesting to note that for both MbCO and HbCO the observed energetics are very similar to thermodynamic measurements of the heme protein/CO reaction. The thermodynamic values represent the steady state limit for complete conversion from the ligated to deoxy equilibrium structures. This value for the observed energetics is attained in less than the 200 picosecond resolution of the thermal grating in its present configuration. This observation and the lack of any significant slow relaxation components (between 200 ps and 10 ns) suggest that the protein relaxation is energetically complete on a picosecond time scale. The protein accesses any stored potential energy in its structure on an exceedingly fast time scale.

CONCLUSIONS

Both the time scale for the observed global relaxation and energetics from the grating studies are consistent with a collective mode mechanism for the initial tertiary structural changes. Slower relaxation components have been observed which are in-

dicative of the involvement of conformational intermediates in the complete relaxation process. However, from the study of the energetics and the amplitude of the protein strain associated with a collective mode response, it appears the initial picosecond relaxation step is the dominant phase of the structural relaxation. The acting forces displacing the atoms appear to be extensively distributed throughout the protein. Given the rapid energy redistribution mechanisms present in these large molecules, this rapid phase of the structural changes would be important in propagating the system as far as possible towards the global energy minimum corresponding to the final equilibrium structure. This may be a general feature of protein response functions.

Most important, the fast changes in protein volume or strain provide a simple framework to understand the mechanics of the communication pathway between the subunits in hemoglobin. Each subunit would act to alter the $\alpha\beta$ interface force balance with the ensuing strain changes at the tertiary level. At some point the cumulative effect of ligand dissociation is to displace the force balance to favor the R to T quaternary structure change. This cooperative molecular response is occurring within linear limits of the atomic displacements, at the tertiary level. However, it is the modulation of the barrier height (an exponential dependence) at the quaternary level which imparts the nonlinearity essential for a molecular amplifier. The enhanced sensitivity of hemoglobin to oxygen concentrations through this cumulative strain effect is essential for the efficient transport of oxygen.

ACKNOWLEDGEMENTS

The authors would like to thank Prof. George McLendon for his assistance in the preparation of the protein samples and Dr. Bill Lotshaw for valuable advice in the optical Kerr effect experiments. This research was supported by the NIH (1 RO1 GM41909-01A1).

REFERENCES

1. L. Genberg, F. Heisel, G. McLendon, and R. J. D. Miller, Vibrational Energy Relaxation Processes in Heme Proteins: Model Systems of Vibrational Energy Dispersion in Disordered Systems, *J. Phys. Chem.* 91:5521 (1987).
2. P. A. Anfinsen, C. Han, and R. M. Hochstrasser, Direct Observation of Ligand Dynamics in Hemoglobin by Subpicosecond Infrared Spectroscopy, *Proc. Natl. Acad. Sci. USA* 86:8387 (1989).
3. R. Lingle, X. B. Lu, H. P. Zhu, S. C. Yu, J. B. Hopkins, and K. D. Straub, Direct Observation of Hot Vibrations in Photoexcited Deoxyhemoglobin using Picosecond Raman Spectroscopy, *J. Am. Chem. Soc.* 113:3992 (1991).
4. R. J. D. Miller, Vibrational Energy Relaxation and Structural Dynamics of Heme Proteins, *Annu. Rev. Phys. Chem.* 42:581 (1991).
5. L. Genberg, L. Richard, G. McLendon, and R. J. D. Miller, Direct Observation of Global Protein Motion in Hemoglobin and Myoglobin on Picosecond Time Scales, *Science*. 251:1051 (1991).
6. R. J. D. Miller, J. Deak, S. Palese, M. Pereira, L. Richard, and L. Schilling, Energetics and Dynamics of Global Protein Motion, in "Ultrafast Phenomena VIII", Martin and Migus, eds., Springer-Verlag, Berlin (1992).
7. J. W. Petrich, and J. L. Martin, Ultrafast Absorption and Raman Spectroscopy of Hemeproteins, *Chem. Phys.* 131:31 (1989).
8. E. Findsen, T. W. Scott, M. Chance, and J. M. Friedman, Picosecond Time-Resolved Raman Studies of Photodissociated Carboxymyoglobin, *J. Am. Chem. Soc.* 107:3355 (1985).
9. Y. Seno, and N. Gö, Deoxymyoglobin Studied by the Conformational Normal Mode

- Analysis II. The Conformational Change upon Oxygenation, *J. Mol. Biol.*, 216:111 (1990).
10. J. F. Reinjtos, Nonlinear optical processes, in: "Encyclopedia of Lasers and Optical Technology," R. Meyers, ed., Academic Press Harcourt Bruce Janovich, San Diego 369 (1991).
 11. D. McMorow, W. Lotshaw, and G. Kenny- Wallace, Femtosecond Optical Kerr Studies on the Origin of the Nonlinear Responses in Simple Liquids, *IEEE Quantum Electron.* 24:433 (1988).
 12. G. Walrafen, M. Fischer, M. Hokmabadi, and W. Yang, Temperature Dependence of the Low Frequency Raman Scattering from Water, *J. Chem. Phys.* 85:6970 (1986).
G. Walrafen, M. S. Hokmabadi, and W. H. Yang, Reply to Comment on: a New Method of Determining Stokes Base Line Shapes from 20-4600 cm^{-1} and its Relation to Collision Induced Raman Scattering from Liquid Water, *J. Chem. Phys.* 87:4555 (1988).
 13. M. Maroncelli, and G. Fleming, Computer Simulation of the Dynamics of Aqueous Solvation, *J. Chem. Phys.* 89:5044 (1988).
 14. X. Xie, and J. Simon, Protein Conformational Relaxation following Photodissociation of CO from Carbonmonoxymyoglobin: Picosecond Circular Dichroism and Absorption Studies, *Biochemistry.* 30:3682 (1991).
 15. F.C. Mills, G.K. Ackers, H.T. Gaud, and S.J. Gill, Thermodynamic Studies on Ligand Binding and Subunit Association of Human Hemoglobins, *J. Bio. Chem.* 254:2875 (1976).

SOLITON STATES IN A CHAIN WITH TWO ATOMS IN A UNIT CELL

Larisa S. Brizhik

Bogolyubov Institute for Theoretical Physics
Ukrainian Academy of Sciences
252143 Kiev, Ukraine

The soliton mechanism of the energy transport, suggested by Davydov and Kislukha¹, was further developed and applied to the wide variety of phenomena in physics and biology^{2,3}. The mechanism is based on the model of 1D chain with an extra quasiparticle (exciton, electron or hole), interacting with longitudinal displacements of atoms. Real systems differ from this model first of all by a complicated structure, and in their spectra there are various branches of vibrations. Naturally the following questions arise: i) why the Davydov model takes into account the interaction with acoustical phonons only, and to what extent this model is applicable to real systems, and ii) is the Davydov soliton stable under the interaction with other vibrational modes.

To answer this questions qualitatively, one can consider two-atom chain with atom masses M_1, M_2 ; energy levels E_1, E_2 ; the electron-phonon interaction constants χ_1, χ_2 ; and exchange interaction parameters $J_{2n,2n+1} = -J_{2n-1,2n} = J$ in the case of opposite atom symmetries (this model describes, for instance, the copper-oxygen chains in metal-oxide compounds⁴), respectively. The spectrum of this chain consists of two electron bands with the dispersion laws

$$\varepsilon_{\alpha,\beta}(k) = \frac{1}{2}[E_1 + E_2 \mp \sqrt{\Delta^2 + 16J^2 \sin^2(ka)}], \quad \Delta = E_1 - E_2 > 0, \quad (1)$$

and two phonon branches with dispersion laws

$$\Omega_{op,ac}(k) = \kappa \left[\frac{1}{\mu} \pm \sqrt{\frac{1}{\mu^2} - \frac{4 \sin^2(ka)}{\mu M}} \right] \quad (2)$$

where $M = M_1 + M_2$, $\mu = M_1 M_2 / M$.

The Hamiltonian of the system can be written in the form⁵

$$H = \sum_{k=-\pi/a}^{\pi/a} \sum_{\mu=\alpha,\beta} \varepsilon_{\mu}(k) A_{\mu,k}^+ A_{\mu,k} + \sum_{q=-\pi/a}^{\pi/a} \sum_{s=op,ac} \hbar \Omega_s(k) (b_{q,s}^+ b_{q,s} + 1/2) + H_{int}, \quad (3)$$

where $A_{\mu,k}^+, A_{\mu,k}$ are creation and annihilation operators of an electron with wave vector k in the lower $\mu = \alpha$ or upper $\mu = \beta$ band, $b_{q,s}^+, b_{q,s}$ are creation and annihilation operators of phonons with wave vector q of optical or acoustical mode.

In the general case in this representation the hybridization of the interaction of electrons from the lower and upper bands with both branches of vibrations takes place, which leads to the interaction Hamiltonian in (3) being given in the form

$$H_{\text{int}} = \frac{1}{\sqrt{N}} \sum_{k,q,\mu,\mu',s} \chi_{\mu,\mu'}^*(k,q) A_{\mu,k}^+ A_{\mu',k-q} (b_{q,s} + b_{-q,s}^\dagger). \quad (4)$$

If the ground state of the chain corresponds to one electron per atom, then the conductivity of the chain is stipulated by donor or acceptor impurities which supply the system with electrons in the valence band, or with holes in the conductive band. These states of the chain can be described by wave functions $|\Psi_e\rangle = A_{\beta,k}^+ |\Phi_v\rangle$ and $|\Psi_h\rangle = A_{\alpha,k} |\Phi_v\rangle$ with $|\Phi_v\rangle = (\prod_{k,\sigma} A_{\alpha,k,\sigma}^\dagger |0\rangle)$ being the wave function of the ground state. In the long-wave approximation the nondiagonal coefficients of the electron-phonon interaction matrix equal zero $\chi_{\alpha,\beta}^*(k,q) \simeq 0$ for $\alpha \neq \beta$ and the rest are of the form

$$\chi_{\alpha}^{\text{op}} = 2i\chi_2 \sqrt{\frac{\hbar M_2}{2M M_1 \Omega_0}} qa, \quad \chi_{\alpha}^{\text{ac}} = 2i\chi_2 \sqrt{\frac{\hbar}{2M V_0}} \frac{qa}{\sqrt{|q|}}, \quad (5)$$

$$\chi_{\beta}^{\text{op}} = -2i\chi_1 \sqrt{\frac{\hbar M_1}{2M M_2 \Omega_0}} qa, \quad \chi_{\beta}^{\text{ac}} = 2i\chi_1 \sqrt{\frac{\hbar}{2M V_0}} \frac{qa}{\sqrt{|q|}}. \quad (6)$$

Therefore, the ratios of constants for each electron band are

$$\frac{|\chi_{\alpha}^{\text{op}}|^2}{|\chi_{\alpha}^{\text{ac}}|^2} \propto \frac{M_2}{M_1} \sqrt{\frac{\mu}{M}}, \quad \frac{|\chi_{\beta}^{\text{op}}|^2}{|\chi_{\beta}^{\text{ac}}|^2} \propto \frac{M_1}{M_2} \sqrt{\frac{\mu}{M}}. \quad (7)$$

As it follows from (7), in the case of big difference of neighboring atom masses the interaction of charge carriers in each band prevails with one phonon mode only. I.e. if the inequality $M_1 \ll M_2$ holds, then the electron in conductive band interacts more intensively with acoustical phonons $|\chi_{\beta}^{\text{ac}}|^2 \gg |\chi_{\beta}^{\text{op}}|^2$, while the hole in the valence band interacts more intensively with the optical phonons $|\chi_{\alpha}^{\text{op}}|^2 \gg |\chi_{\alpha}^{\text{ac}}|^2$.

With all these taken into account, the Hamiltonian (2) - (3) allows for the localized state of the electron, interacting with acoustical phonons, which is described by Davydov soliton function with the localization parameter

$$g = \frac{4m\chi_1^2 a^2}{\hbar^2 \kappa (1 - s^2)} \quad (8)$$

and energy

$$E_s = \frac{1}{2}\Delta - \frac{2m\chi_1^4 a^2}{3\hbar^2 \kappa^2} + \frac{1}{2}m_s(V)V^2, \quad (9)$$

which at $V = 0$ is less than the energy of the conductive band bottom.

In the meantime, the hole in the valence band interacts mainly with optical phonons, and can be also in the autolocalized state, the function of which satisfies the equation

$$\pm \lambda x = \sqrt{1 - 2\Psi^2 G} - \ln \left| \frac{1 + \sqrt{1 - 2\Psi^2 G}}{\Psi} \right| + c \quad (10)$$

where

$$G = \frac{8a^3 m \chi_2^2 M_2^2}{\hbar^2 \kappa M^2}, \quad \lambda^2 = m \frac{(\Delta - 2\varepsilon)}{\hbar^2}, \quad (11)$$

and c being the constant of integration. But this state is energetically unadvantageous, because its energy equals the value

$$E_h = \frac{1}{2}\Delta + \frac{\hbar^2\lambda}{2mG}[1 - 2\lambda G - (1 - 3\lambda G)^{1/3}] \quad (12)$$

which is bigger than the energy of the delocalized state of the hole in the valence band $\Delta/2$.

If the opposite inequality $M_1 \gg M_2$ takes place, under the same definition $E_1 > E_2$, then a hole in the valence band corresponds to the Davydov soliton with parameters (8) - (9), while an extra electron in the conductive band is in the delocalized state.

As the next step we shall take into account the influence of optical phonons on the Davydov soliton, which is formed by the electron or hole, interacting with acoustical phonons. As it was shown above, in the case of big difference of atom masses the soliton interaction with optical phonons can be considered within the perturbation method. This system can be described in the continuum approximation by the system of three equations⁶

$$i\hbar \frac{\partial \Psi}{\partial t} + \frac{\hbar^2}{2m} \frac{\partial^2 \Psi}{\partial x^2} + \chi_1 \rho \Psi = \epsilon \chi_2 u \Psi, \quad (13)$$

$$\left(\frac{\partial^2}{\partial t^2} - V_{ac}^2 \frac{\partial^2}{\partial x^2} \right) \rho + \frac{\chi_1 a^2}{M} \frac{\partial^2}{\partial x^2} |\Psi|^2 = 0, \quad (14)$$

$$\left(\frac{\partial^2}{\partial t^2} - V_{op}^2 \frac{\partial^2}{\partial x^2} + \Omega_0^2 \right) u + \frac{\epsilon \chi_2}{\mu} |\Psi|^2 = 0, \quad (15)$$

where in view of the above investigations ϵ is considered to be a small parameter, ρ describes the deformation of the chain, and u is the deviation of interatomic distance from the equilibrium value, caused by the optical mode. The weak interaction of the soliton with optical phonons results in the dependence of soliton parameters on time, which can be calculated by the Van-der-Pool method in the way similar to⁷. This leads to the conclusion that soliton wave vector k and phase θ become the oscillating functions of time

$$k(t) = k_0 - \epsilon \alpha \sin(\omega t), \quad \theta(t) = \hbar \theta_0 / 2m + \epsilon \beta (\cos(\omega t) - 1) \quad (16)$$

with small amplitudes of oscillations

$$\alpha = \frac{a^2 q^2 \chi_2 A \pi}{2 \hbar \omega g d (1 + D)}, \quad \beta = \frac{a q \pi A \chi_2}{\hbar g^2 \omega d}, \quad (17)$$

and frequency ω , determined by optical phonons

$$\omega = \hbar k_0 q / m - \Omega_{op}(q), \quad \Omega_{op}^2(q) = \Omega_0^2 - V_{op}^2 q^2 \quad (18)$$

while the amplitude and the width of the soliton are not changed⁸. Here k_0 and θ_0 are the nonperturbed values of soliton wave vector and phase

$$k = mV/\hbar, \quad \theta_0 = \hbar(k^2 + g^2)t/2m, \quad (19)$$

the nonlinearity parameter g is determined in Eq.(8), q and A are the momentum and amplitude of optical phonons, and

$$d = \sinh \left(\frac{qa\pi}{2g} \right), \quad D = \frac{4\chi_1^2 g}{3mV_{ac}^2 \kappa (1 - s^2)}, \quad (20)$$

The weak interaction of the soliton with optical phonons leads also to the small change of soliton envelope and the appearance of the tail of small amplitude, oscillating in time with characteristic frequency ω , and its overtones $\omega_{1,2} = \omega \pm \hbar g^2/2m$, $\omega_{3,4} = \omega \pm \hbar g^2/4m$. The effective mass and energy of the soliton, interacting with optical phonons, were calculated in Ref.⁶.

In the case, when the interaction of the Davydov soliton with optical phonons is strong enough, the soliton changes the form and its velocity decreases linearly with time⁶.

ACKNOWLEDGEMENTS

I am most grateful to V. Enolskii and A. Eremko for the fruitful collaboration, and to P. Christiansen and A. Scott for the warm hospitality and the help in getting financial support in Denmark.

REFERENCES

1. A.S. Davydov, and N.I. Kislukha, Solitary excitons in one-dimensional chains, Phys. stat. sol.(b) 59:465(1973).
2. A.S. Davydov. "Solitons in Molecular Systems," D. Reidel Pub. Co., Dordrecht, Boston, Lancaster (1987).
3. A.C. Scott, Davydov's soliton, Phys. Rep. *:*(1992).
4. J.C. Bednorz, and K.A. Müller, Possible high- T_c superconductivity in the Ba-La-Cu-O system, Z. Phys. B64:189(1986).
5. L.S. Brizhik, and A.A. Eremko, Soliton states in a chain with two atoms per unit cell, Phys. stat. sol.(b) 164:525(1991).
6. L.S. Brizhik, and V.Z. Enolskii, The calculation of electrosoliton effective mass in one-dimensional molecular chain, Dokl. Ak. Nauk UkrSSR 6:59(1982).
7. A.S. Davydov, and A.A. Eremko, The deceleration of a soliton in one-dimensional molecular chain, Teor. Math. Fiz. 43:367(1980).
8. L.S. Brizhik, and V.Z. Enolskii, The interaction of an extra electron with optical and acoustical phonons in 1D chain, Ukr. Fiz. Zh. 29:340(1984).

PROTON TRANSPORT IN HYDROGEN-BONDED CHAINS : A TWO-COMPONENT SOLITON MODEL INCLUDING DIPOLE INTERACTIONS

I. Chochliouros and J. Pouget

Laboratoire de Modélisation en Mécanique (associé au CNRS)
Université Pierre et Marie Curie, 4 place Jussieu
75252 Paris Cédex 05, France

Abstract : We study the dynamics of protons in hydrogen-bonded quasi 1-D networks, in terms of a diatomic lattice model with a doubly periodic on-site potential. In our model we can describe simultaneously the formation and the propagation of the ionic and Bjerrum defects using well-known soliton properties. We extend the model by considering the interaction between the two sublattices and by introducing the dipole interactions due to the proton motions. We consider a sinusoidal form for the dipole moment and we study the equations of motions for both protons and heavy ions. The existence of a double sine-Gordon equation for the proton motion in the continuum limit, makes the study more appealing. We discuss the results and probable extensions of the work.

INTRODUCTION AND PRESENTATION OF THE MODEL

Electrical conductivity in H-bonded crystals is an old problem that recently has been revived with the introduction of new techniques and ideas from nonlinear physics. Hydrogen bonding is not important only in living matter but it also provides the dominant mechanism in a variety of chemical substances. The most important point is that an understanding of the electrical properties of systems with H-bonds will provide information for a wealth of physical and biological [1] systems and processes, ranging from relatively "simple" systems such as ice [1], to the more complicated processes of proton transport across cellular membranes.

In previous scientific works [2,3] it has been attempted to explain the protonic conductivity by using different models based on either the ionic [2] or the bonding [3] defect formation and propagation. Although these models can describe energy transport, dielectric polarization and proton storage, they are not able to justify a permanent flow of protonic mass and charge, necessary to explain the non-transient protonic conductivity. For this reason we have to consider a model [4,5] that can describe simultaneously both types of defects.

We consider a system with the diatomic structure of Fig.1. We focus our attention only on longitudinal vibrations of both ions of the chain neglecting any interaction with the rest of the 3-D lattice. We assume that our chain can be described by a linear chain with bond lengths equal to the projections of the bond lengths of the original zig-zag chain onto an axis. In our model we do not consider the electronic degrees of freedom

and we do not take into account quantum effects. We also define a doubly periodic substrate potential with two potential barriers, an intra-bond and an inter-bond with heights h_1, h_0 in order to explain the formation of the ionic and the Bjerrum defects correspondently. The potential is shown in Fig.1.

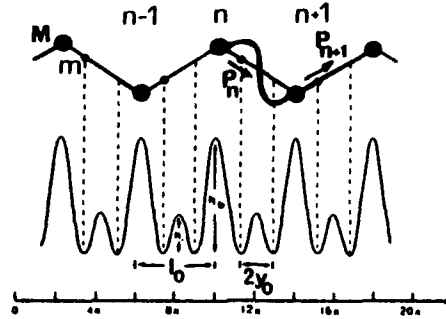


Figure 1 : The zig-zag geometry of the H-bonded network. We plot the substrate potential $V_p(y; \alpha)$, ($0 < \alpha < 1$), and the sinusoidal variation of the dipole moment P .

The Hamiltonian of the system consists of the sum of four parts. The proton part is given as

$$H_p = \sum_n \left[(1/2)m(dy_n/dt)^2 + (1/2)K_1(y_{n+1} - y_n)^2 + S_p V_p(4\pi y_n/l_0) \right] . \quad (1)$$

Where the first term is the kinetic energy of the proton masses, the second stands for the interaction between first proton neighbours, while the last term represents the dynamical support of the protonic sublattice created by the more rigid heavy ions, the long range interactions and the 3-D atomic environment of the network. The displacement y_n of the n -th proton is measured from the middle of the distance of the bond that links the ions and l_0 is the equilibrium distance between neighbour unit cells. The heavy ion part of the Hamiltonian is given as

$$H_o = \sum_n \left[(1/2)M(dY_n/dt)^2 + (1/2)K_2(Y_{n+1} - Y_n)^2 + S_o V_o(Y_n/l_0) \right] . \quad (2)$$

For the heavy ions of mass M the first two terms have the same physical meaning as the corresponding terms of the r.h.s. of Eq.(1). The third term is due to the on-site potential V_o which guarantees the rigidity of the heavy ion frame and represents the coupling of the ion chain to the rest of the 3-D system. K_1, K_2 are lattice force constants, S_p, S_o are potential barriers, and Y_n is the displacement of the n -th ion measured from its equilibrium position.

$$H_{int} = \sum_n (Y_n - Y_{n-1}) \Phi(4\pi y_n/l_0) . \quad (3)$$

The large proton mobility and the large mass M compared to m , permit the separation of the dynamics of the system into two interacting sublattices.

H_{int} can be considered as a special but satisfactory approximation of more generalized expressions [6]. The coupling constant χ depends on the system and its sign plays an important role in the physics of the problem. The Hamiltonian H_{dd} is introduced as a result of the dipole interactions due to the proton motion. We consider the dipoles placed on the protons and we examine their mutual interaction. We consider a sinusoidal form for the dipole moment (given in Eq.(4), where λ is a constant), which fulfils certain physical prerequisites [7].

$$H_{dd} = \beta_1 \sum_n P_n P_{n+1} , \quad P_n = \lambda \sin(2\pi y_n / l_0) . \quad (4)$$

EQUATIONS OF MOTIONS

If we consider that the longitudinal displacements of the heavy ions are very small compared to the proton displacements, we can assume that the geometry of the zig zag model remains statistically stable and we can approximate the H_{dd} by Eq.(4), where β_1 is a constant which may account for the environment of the chain. One convenient way for further work is to introduce the dimensionless quantities $u_n = 4\pi y_n / l_0$ and $w_n = Y_n / l_0$. With these definitions the substrate potentials in Eqs.(1),(2) can be written as

$$V_p(u_n; \alpha) = [2/(1-\alpha^2)] [\cos(u_n/2) - \alpha]^2 , \quad V_0(w_n) = (1/2)w_n^2 . \quad (5)$$

The on-site potential V_p for the proton sublattice depends on the parameter α which controls the relative widths of both barriers as well as the distance between the two proton minima in each lattice cell. The on-site harmonic potential V_0 is taken to be parabolic. According to the definitions of V_p we consider the interaction function $\Phi(u_n) = \cos(u_n/2) - \cos(u_0/2)$ with $u_0 = 2\arccos(\alpha)$ and $\pm u_0$ are the two proton minima. We measure everything in the units ϵ_0 for energy, $t_0 = (M/K_2)^{1/2}$ for time, l_0 for length. In this way we obtain a dimensionless discrete set of equations of motion which cannot be solved for the general case. If we consider the continuum limit, the N coupled difference differential equations reduce to the following two partial differential equations

$$u_{\tau\tau} - c_0^2 u_{xx} + \Omega_1^2 (dV_p/du) + \chi_1 w_x (d\Phi/du) + 2D \sin u = 0 . \quad (6a)$$

$$w_{\tau\tau} - v_0^2 w_{xx} + \Omega_2^2 (dV_0/dw) - \chi_2 (d\Phi/dx) = 0 . \quad (6b)$$

Where $\tau = t/t_0$, $c_0 = t_0 (K_1/m)^{1/2}$, $v_0 = t_0 (K_2/M)^{1/2}$, $\chi_2 = t_0^2 \chi / M l_0$, and also $\Omega_1 = (4\pi t_0 / l_0) (S_p/m)^{1/2}$, $\Omega_2 = (t_0 / l_0) (S_0/M)^{1/2}$, $B = \beta_1 \lambda^2$, while it is $\chi_1 = (4\pi)^2 t_0^2 \chi / m l_0$ and $D = (4\pi)^2 t_0^2 B / l_0^2 4m$. This coupled set can be solved analytically in few cases. For $\Omega_2 = 0$ we can obtain a double sine-Gordon equation for the proton motion, and one easily integrable form for Eq.(6b). If we are looking for localized solutions, moving at a characteristic velocity v , we can introduce the new variable $\xi = x - v\tau$, and by considering zero integration constant for Eq.(7b), we can write

$$u_{\xi\xi} + \frac{\epsilon}{(v^2 - c_0^2)} \left[-\sin u + \frac{(\epsilon + 2D)}{\epsilon} 2\alpha \sin(u/2) \right] = 0 . \quad (7a)$$

$$w_{\xi} = \chi_2 [\cos(u/2) - \alpha] / (v^2 - c_0^2) . \quad (7b)$$

Where we call $\epsilon = [\Omega_1^2 / (1 - \alpha^2)] - 2D + \chi_1 \chi_2 / 4 (v^2 - v_0^2)$ the new effective barrier height. Analogous expressions we can obtain if we consider the oxygens as frozen or if we examine the particular case $v = v_0$ which is the velocity of sound in the ionic sublattice.

RESULTS AND CONCLUSIONS

The DSG equation has been extensively studied [8]. If we follow certain methods [8] we can obtain two types of kink solutions for Eq.(7a): a small kink I, corresponding to the transition from $-u_0$ to $+u_0 \text{ mod}(4\pi)$, and a large kink II, corresponding to the transition from $+u_0$ to the minimum at $(4\pi - u_0) \text{ mod}(4\pi)$. Transitions in the opposite sense correspond to anti-kinks. Introducing these solutions into Eq.(7b) and after integration we obtain for w again two kinks.

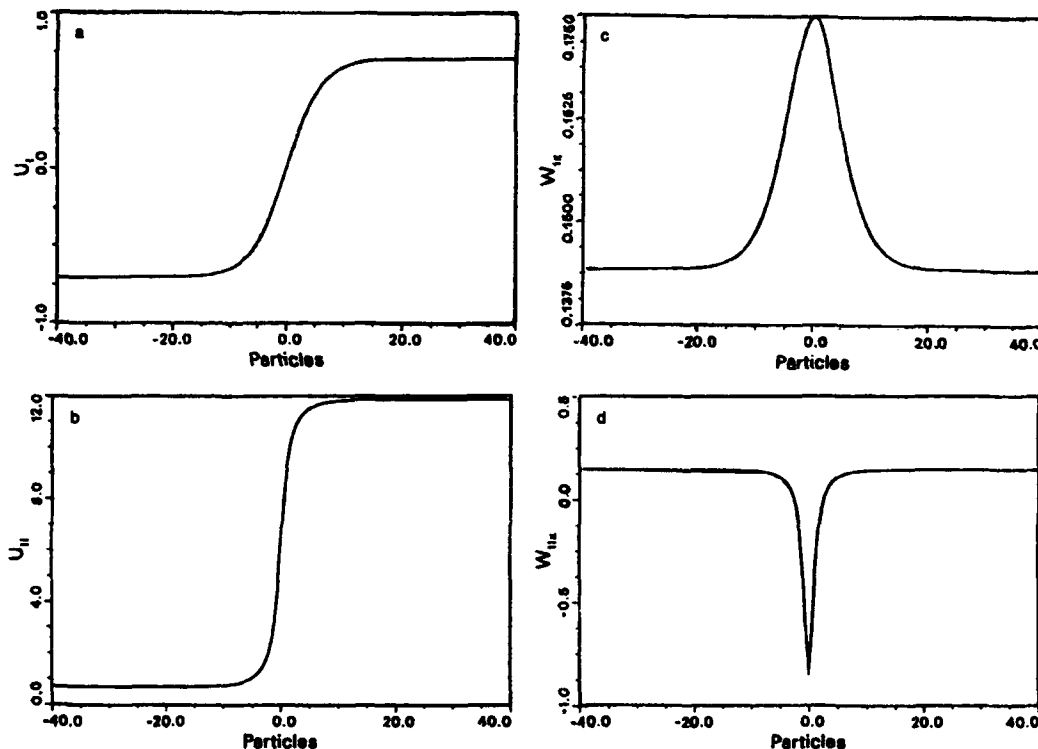


Figure 2 : A representation of the proton displacement $u(\xi)$, in which we distinguish two types of kinks. We also plot the derivative w_ξ , given by Eq.(7b). The solution w_ξ -pulse I (b) corresponds to the small kink I (a), while the solution w_ξ -pulse II (d) corresponds to the large kink II (c).

We note that the kink(antikink) I corresponds to $I^- (I^+)$ ionic defect, while the kink(antikink) II corresponds to the $L(D)$ Bjerrum defect. A schematic representation is given in Fig.2. The protonic kinks (Fig.2(a) and 2(c)) are accompanied by compressions (Fig.2(b)) or rarefactions (Fig.2(d)) of the heavy sublattice around the ionic defect.

In further works we can study the model by considering a more generalized two-parameter [6] potential $V_p(u; \alpha, \beta)$ where β can regulate the relative heights of the intra- and inter-bond activation barriers. If $\alpha = \beta = 0$ the study reduces to a generalized sine-Gordon case for the protons. An impor-

tant characteristic of the model is the correct response of the four defects to an externally applied dc electric field. The extension of analytical and numerical calculations should be very interesting in the presence of damping, dc electric field and temperature, but this will be the aim of future studies.

REFERENCES

- [1] A. S. DAVYDOV, *Solitons in Molecular Systems* (Reidel, Boston, 1985); *Physics and Chemistry of Ice*, eds by E. Whalley, S. J. Jones and L. W. Gold (Royal Society of Canada, Ottawa, 1973).
- [2] V. Ya. ANTONCHENKO, A. S. DAVYDOV, and A. V. ZOLOTARYUK, *Phys. Stat. Sol. B* 115, 631 (1983); M. PFYLLIDIS, St. PNEVMATIKOS, and N. FLYTZANIS, *Phys. Rev. A* 36, 903 (1987).
- [3] A. I. SERGIENKO, *Phys. Stat. Sol. B* 144, 471 (1987); E. S. KRYATCHKO, *Chem. Phys. Lett.* 141, 346 (1987).
- [4] A. V. ZOLOTARYUK in : *Biophysical Aspects of Cancer*, eds by J. Fiala and J. Pokorny (Charles Univ. Press, Prague, 1987) p.179.
- [5] St. PNEVMATIKOS, *Phys. Rev. Lett.* 60, 1534 (1988); G. P. TSIRONIS and St. PNEVMATIKOS, *Phys. Rev. B* 39, 7161 (1989).
- [6] St. PNEVMATIKOS, G. P. TSIRONIS and A. V. ZOLOTARYUK, *Journal of Mol. Liq.* 41, 85 (1989).
- [7] E. WHALLEY, *Journal of Glaciology*, Vol. 21, 13 (1978).
- [8] R. M. DeLEONARDIS and S. E. TRULLINGER, *Phys. Rev. B* 27, 1867 (1983).

THE ULTRASONIC CHARGE-DENSITY-WAVES AND INTEGRABLE MANY PARTICLE HÉNON-HEILES SYSTEM

P.L. Christiansen

Laboratory of Applied Mathematical Physics
Danish Technical University
2800 Lyngby, Denmark

Yu.B. Gaididei

Institute of Theoretical Physics
Ukrainian Academy of Sciences
252130 Kiev, Ukraine

V.Z. Enol'skii, D.V. Leykin

Institute of Metal Physics
Ukrainian Academy of Sciences
252142 Kiev, Ukraine

INTRODUCTION

The problem of the self consistent behavior of conductivity electrons interacting with phonons of the quasi one dimensional crystal (the Pierls-Fröhlich problem) was recently analyzed for the case of acoustic phonons ^{1,2}. It was shown, that charge density waves (CDW) propagating with velocities being less than the sound velocity can be described in terms of one-gap potentials, in mentioned works. When velocity is close to sound velocity, the approach developed in refs ^{1,2} fails. In present paper we show, that including anharmonism of acoustic phonons into consideration allows to describe both subsonic and ultrasonic CDW. It is also shown, that the problem in question is connected with the many particle system, which can be considered as a many particle generalization of the Hénon-Heiles system, which originally appeared in astrophysics. Under certain conditions on the parameters, the ultrasonic CDW problem appears to be completely integrable in terms of hyperelliptic theta functions. As the particular case the elliptic one-gap potential is considered.

THE HAMILTONIAN AND EQUATIONS OF SELFCONSISTENCY

Let us consider $2N$ electrons interacting with acoustic phonons of crystal. Let us assume Hamiltonian of the system in the form

$$H = -J \sum_{n,\sigma} a_{n,\sigma}^\dagger (a_{n+1,\sigma} + a_{n-1,\sigma} - 2a_{n\sigma}) + \chi \sum_{n,\sigma} a_{n,\sigma}^\dagger a_{n\sigma} (\hat{u}_{n+1} - \hat{u}_{n-1}) + \sum_q \Omega_q b_q^\dagger b_q + F_{anharmonic}, \quad (1)$$

$$\sum_{n,\sigma} a_{n,\sigma}^\dagger a_{n\sigma} = 2N.$$

Here $a_{n,\sigma}^\dagger (a_{n,\sigma})$ is the creation (annihilation) electron operator on the site n with the spin projection σ ($\sigma = \uparrow, \downarrow$), J is the matrix element of the transition operator of an electron, $b_q^\dagger (b_q)$ is the creation (annihilation) acoustic phonon operator with the wave vector q and frequency $\Omega_q = 2\sqrt{\frac{w}{M}} \left| \sin \frac{qa}{2} \right|$ (a - lattice constant, w - elasticity constant, M - atom mass),

$$\hat{u}_n = \frac{1}{\sqrt{L}} \sum_q \sqrt{\frac{\hbar a}{2M\Omega_q}} \exp\{iqna\} (b_q + b_{-q}^\dagger) \quad (2)$$

is the operator of the displacement of the n -th atom, χ is the constant of the electron-phonon interaction. The last term in (1) is the operator of anharmonic phonon interaction. We shall investigate the effects of anharmonism of third order, and we assume, that $H_{anharmonic}$ has the following form

$$H_{anharmonic} = \frac{\alpha w}{3} \sum_n (\hat{u}_n - \hat{u}_{n+1})^3. \quad (3)$$

The total momentum of the system,

$$P = \hbar \sum_q q (b_q^\dagger b_q + \sum_\sigma a_{q\sigma}^\dagger a_{q\sigma}) \quad (4)$$

appears to be the integral of motion and therefore states of the system can be classified by the value of (4).

We investigate states of the system which are characterized by the value of the total momentum with the help of the variation method, looking for the extremum of the functional

$$F = \langle \Psi | H - vP | \Psi \rangle, \quad (5)$$

where v is the Lagrange multiplier, which has the sense of the velocity of the excitation propagation along the crystal, and $|\Psi\rangle$ is the trial wave function, which we take in the form

$$|\Psi\rangle = \prod_{\nu,\sigma} \sum_n \Psi_{\nu,n}^* a_{\nu\sigma}^\dagger \exp\left\{\sum_q (Z_q b_q^\dagger - Z_q^* b_q)\right\}, \quad (6)$$

where $\Psi_{\nu,n}$ and Z_q are the variation parameters, and $\Psi_{\nu,n}$ are orthonormalized

$$\sum_n \Psi_{\nu,n}^* \Psi_{\nu',n} = \delta_{\nu\nu'} \quad (7)$$

We find by substituting (6) into (5) and varying over $\Psi_{\nu,n}$ and Z_q that the extremum of the functional (5) is realized on the states (6), with the parameters satisfying the system of equations

$$\begin{aligned} & -J(\Psi_{\nu,n+1} + \Psi_{\nu,n-1} - 2\Psi_{\nu,n}) - i\hbar v \frac{\partial}{\partial x} \Psi_{\nu,x} |_{x=n} \\ & + \chi(u_{n+1} - u_{n-1})\Psi_{\nu,n} = E_\nu \Psi_{\nu,n}, \end{aligned} \quad (8)$$

$$\begin{aligned} & -w(u_{n+1} + u_{n-1} - 2u_n) + Mv^2 \frac{\partial^2}{\partial x^2} u_x |_{x=n} + 2\chi \sum_\nu \{ |\Psi_{\nu,n+1}|^2 - |\Psi_{\nu,n-1}|^2 \} \\ & + \alpha[(u_n - u_{n+1})^2 - (u_n - u_{n-1})^2] = 0, \end{aligned} \quad (9)$$

where $u_n = \langle \Psi | \hat{u}_n | \Psi \rangle$ is the average of the displacement of the cite n .

The eqs.(8,9) yield in the continuum approximation ($\Psi_{\nu,n} \equiv \Psi_\nu(na) = \Psi_\nu(x)$, $\Psi_{\nu,n+1} = \Psi_\nu(x) + a \frac{d\Psi_\nu(x)}{dx} + \dots$) the system of the equations

$$\varphi_\nu'' - 2R\varphi_\nu + \mathcal{E}_\nu \varphi_\nu = 0, \quad (10)$$

$$R'' + BR - \epsilon R^2 + 2 \sum_\nu |\varphi_\nu|^2 = 0, \quad (11)$$

written with respect to the quantities

$$R(x) = \frac{\chi}{J} \frac{\partial u(x)}{\partial x}, \quad \varphi_\nu(x) = \sqrt{\frac{24\chi^2}{Jw}} \Psi_\nu(x) \exp(-i \frac{\hbar v}{2J} x), \quad (12)$$

where the notations $J\mathcal{E}_\nu = E_\nu - \frac{\hbar^2 v^2}{4J}$, $B = 12(1 - v^2/v_0^2)$, $\epsilon = 6 \frac{a^2 \chi}{J}$ are used ($v_0 = a\sqrt{w/M}$ is the sound velocity). We remark, that the sum over ν in (11) includes N lower eigenvalues of (10). If we use the real and imaginary parts of the functions $\varphi_\nu(x)$, $\varphi_\nu(x) = f_\nu(x) + ig_\nu(x)$, we obtain from (10, 11)

$$f_\nu'' - 2Rf_\nu + \mathcal{E}_\nu f_\nu = 0, \quad g_\nu'' - 2Rg_\nu + \mathcal{E}_\nu g_\nu = 0, \quad (13)$$

$$R'' + BR - \epsilon R^2 + 2 \sum_\nu (f_\nu^2 + g_\nu^2) = 0, \quad (14)$$

where the summation in (14) is taken over N first states of eqs.(13). The system (13,14) is a generalization of the system considered recently in ³. It also can be considered as a particular case of the Many Particle Hénon-Heiles system (MPHHS). The description of the standard Hénon-Heiles system (HHS) see e.g. in ⁴⁻⁶.

INTEGRABLE MANY PARTICLE HÉNON-HEILES SYSTEM

Consider the system

$$\ddot{q}_i - 2q_{n+1}q_i + A_i q_i = 0, \quad i = 1, \dots, n, \quad (15)$$

$$\ddot{q}_{n+1} + 4A_{n+1}q_{n+1} - \sum_{i=1}^n q_i^2 - \epsilon q_{n+1}^2 = 0 \quad (16)$$

with the Hamiltonian

$$H = \frac{1}{2} \left(\sum_{i=1}^{n+1} \dot{q}_i^2 + \sum_{i=1}^n A_i q_i^2 + 4A_{n+1}q_{n+1}^2 \right) - q_{n+1} \sum_{i=1}^n q_i^2 - \frac{\epsilon}{3} q_{n+1}^3. \quad (17)$$

We call system (15,16) MPHHS because at $n = 1$ it becomes the standard HHS ⁴. The HHS is completely integrable at the following three cases (see, e.g. ^{5,6} i) $\epsilon = 1$, $A_1 = 4A_2$; ii) $\epsilon = 6$, A_1, A_2 - arbitrary; iii) $\epsilon = 16$, $4A_1 = A_2$.)

The system (15,16) possesses two remarkable reductions.

a) at $q_{n+1} = \text{const}$ it reduces to the Neumann system ⁷ which describes the motion of a particle over a sphere in the field of second order potential.

b) at $q_{n+1} = \sum_{i=1}^n q_i^2$ it reduces to the anisotropic oscillator in the fourth order potential ⁷,

$$\ddot{q}_i - 2 \sum_{k=1}^n q_k^2 q_i + A_i q_i = 0, \quad i = 1, \dots, n. \quad (18)$$

Painlevé analysis of the system leads to the conclusion, that it is integrable when $\epsilon = 6$, $A_i, i = 1, \dots, n+1$ - arbitrary. Lax representation, $L_t = [L, M]$ of the system is written explicitly in the form of 2×2 -matrices

$$L = \begin{pmatrix} V(z) & U(z) \\ W(z) & -V(z) \end{pmatrix}, \quad M = \begin{pmatrix} 0 & 1 \\ 2q_{n+1} + z & 0 \end{pmatrix}$$

depending on the spectral parameter z . For the matrix elements we have

$$U(z) = 4(z + A_{n+1} - q_{n+1}) - \sum_{i=1}^n \frac{q_i^2}{z + A_i}, \quad (19)$$

$$V(z) = -\frac{\dot{U}(z)}{2} = 2p_{n+1} + \sum_{i=1}^n \frac{q_i p_i}{z + A_i}, \quad (20)$$

$$\begin{aligned} W(z) &= -\frac{\ddot{U}(z)}{2} + (z + 2q_{n+1})U(z) \\ &= -4z^2 - 4A_{n+1}z - 4q_{n+1}^2 + \sum_{k=1}^n q_k^2 - 4zq_{n+1} + \sum_{i=1}^n \frac{p_i^2}{z + A_i}. \end{aligned} \quad (21)$$

The particular cases of the above Lax representation were given in ^{5,6}. The algebraic curve $C_{n+1} = (w, z)$ of genus $n+1$ is defined in terms of (19-21) as

$$w^2 = V(z)^2 + U(z)W(z) \quad (22)$$

and therefore has following form

$$w^2 = -16z^3 - 32A_{n+1}z^2 - 16A_{n+1}^2z + 8H + \sum_{k=1}^n \frac{F_k}{z + A_k}, \quad (23)$$

where H is (17) at $\epsilon = 6$ and $F_j, j = 1, \dots, n$ are the additional integrals of motion

$$\begin{aligned} F_m &= 4(A_{n+1} - A_m - q_{n+1})(p_m^2 - (2q_{n+1} - A_m)q_m^2) + \\ &+ (8A_{n+1}q_{n+1} - 12q_{n+1}^2 - \sum_{i=1}^n q_i^2)q_m^2 + 4q_m p_m p_{n+1} \\ &+ \sum_{1 \leq k < m \leq n} \frac{(q_m p_k - q_k p_m)^2}{A_m - A_k}. \end{aligned} \quad (24)$$

The integrals (17,24) are independent and are in involution with respect to standard Poisson brackets. Let us construct the separated variables following the usual scheme

(see, e.g. ⁸) which defines them in terms of zeros $\mu_j, j = 1, \dots, n+1$ of polynomial $U(z)$. The set of these zeros defines the parabolic coordinates ^{9,10} in terms of which the system becomes

$$\sum_{i=1}^{n+1} \frac{\mu_i^k d\mu_i}{y_i} = 0, k = 0, \dots, n, \sum_{i=1}^{n+1} \frac{\mu_i^n d\mu_i}{y_i} = i dt, \quad (25)$$

where y is given by the formula

$$y^2 = w^2 \prod_{m=1}^n (z + A_m) \equiv \prod_{j=1}^{2n+3} (z - z(Q_j)), z(Q_{2n+4}) = \infty, Q_i \neq Q_j. \quad (26)$$

We introduce the canonical homology basis $(a_1, \dots, a_{n+1}; b_1, \dots, b_{n+1})$, the conjugated holomorphic differentials $v = (v_1, \dots, v_{n+1})$ normalized in such a way that the Riemann matrix has the form

$$\left(\oint_{a_1} v, \dots, \oint_{a_{n+1}} v; \oint_{b_1} v, \dots, \oint_{b_{n+1}} v \right) = (1_{n+1}; \tau). \quad (27)$$

We also introduce the standard theta function

$$\theta(z; \tau) = \sum \exp i\pi \{ (m, \tau m) + 2(z, m) \}, \quad (28)$$

where (\cdot, \cdot) denotes the Euclidean scalar product and the summation runs over all set of integers $m \in \mathbb{Z}^{n+1}$. Using the known hyperelliptic theta formulae ¹¹,

$$\prod_{j=1}^{n+1} (\mu_j + A_k) = h_k \frac{\theta(\int_{Q_0}^{Q_k} v + (\int_{Q_0}^{\mu_1} + \dots + \int_{Q_0}^{\mu_{n+1}})v + K; \tau)}{\theta(\int_{Q_0}^{Q_{2g+2}} v + (\int_{Q_0}^{\mu_1} + \dots + \int_{Q_0}^{\mu_{n+1}})v + K; \tau)}, k = 1, \dots, n \quad (29)$$

with the constants h_k we obtain

$$q_k^2(t) = q_k^2(0) \frac{\theta^2(U_0 + K; \tau) \theta^2(Ut + U_0 + \int_{\infty}^{A_k} v + K; \tau)}{\theta^2(U_0 + \int_{\infty}^{A_k} v + K; \tau) \theta^2(Ut + U_0 + K; \tau)}, k = 1, \dots, n$$

$$q_{n+1}(t) = -\frac{\partial^2}{\partial t^2} \ln \theta(Ut + U_0 + K; \tau) + \sum_{i=1}^n A_i + 4A_{n+1} + \sum_{j=1}^{n+1} \oint_{a_j} z v_j(z), \quad (30)$$

where K is the vector of Riemann constants, U_0 arbitrary vector of the Jacobian of the curve, the vector U comes from the decomposition $v(z) = U d\zeta + \dots, z = 1/\zeta^2 = \infty$. The solution (30) is the quasiperiodic function of time and includes periodic ones as particular case.

To return to the initial problem we have to set $n = 2N$ and tend in pairs $A_{2j-1} \rightarrow A_{2j} = \mathcal{E}_j, j = 1, \dots, n/2$. The curve becomes singular and theta functions in (30) reduce to lower genera.

ONE-GAP POTENTIAL

Let us consider the important from the physical point of view case of one-gap potential, i.e. the potential generating one gap in the spectrum of elementary excitation. In this case the atom displacement is described by the formula

$$R(x) = R_0 + \wp(x + \omega'), \quad (31)$$

where p is the Weierstrass elliptic function ¹² and the value of the constant R_0 will be given below. One can check, that this case corresponds to the curve C_3 with two singular points. Two branches of elementary excitation correspond to (31):

1) $\mathcal{E}_\nu = 2R_0 - p(is + \omega)$, where $-\omega' \leq is \leq \omega'$ and the quantity $\nu = i(\zeta(is + \omega) - (is + \omega)\frac{\eta}{\omega})$, $|\nu| \leq \frac{\pi}{2\omega}$ has the sense of wave vector and

$$|\varphi_\nu(x)|^2 = \frac{24\chi^2 p(\omega + is) - p(x + \omega')}{LJ\omega p(\omega + is) + \frac{\eta}{\omega}}. \quad (32)$$

2) $\mathcal{E}_\nu = 2R_0 - p(is)$, where $-\omega' \leq is \leq \omega'$ and the quantity $\nu = i(\zeta(is) - is\frac{\eta}{\omega})$, $|\nu| \geq \frac{\pi}{2\omega}$ and

$$|\varphi_\nu(x)|^2 = \frac{24\chi^2 p(is) - p(x + \omega')}{LJ\omega p(is) + \frac{\eta}{\omega}}. \quad (33)$$

The above relations show, that there exists a gap in the spectrum, $\mathcal{E}|_{\nu \rightarrow \pi/2\omega - 0} - \mathcal{E}|_{\nu \rightarrow \pi/2\omega + 0} = p(\omega') - p(\omega + \omega') = e_3 - e_2$ and the value

$$N(x) = 2 \sum_\nu |\varphi_\nu|^2 = \frac{2}{\pi} (\nu_F - \frac{\eta}{\omega} s_F - s_F p(x + \omega')), \quad (34)$$

where $\nu_F = \pi\sigma/2$ (σ is linear density of electrons in crystal), and the value s_F is defined by $\nu_F = i[\zeta(is_F + \omega) - (is_F + \omega)\eta/\omega]$ for $\nu < \pi/2\omega$ and $\nu_F = i[\zeta(is_F) - (is_F)\eta/\omega]$ for $\nu > \pi/2\omega$ describes periodic distribution of electrons in crystal (CDW). The parameter of the distribution can be found from the selfconsistency equations

$$1 - \frac{v^2}{v_0^2} - \frac{4\chi^2}{\pi J\omega} s_F = R_0, \quad 1 - \frac{v^2}{v_0^2} - \left(\frac{4\chi^2}{\pi J\omega}\right)^2 s_F^2 + \frac{8\chi^2}{\pi J\omega} \left(\nu_F - \frac{s_F\eta}{\omega}\right) = \frac{g_2}{12}, \quad (35)$$

which analysis combined with the ground state minimization over periods, will be given elsewhere.

REFERENCES

1. E.D. Belokolos, Theory of Fröhlich conductivity, *Preprint ITP-91-6P*, Kiev (1991)
2. A.A. Eremko, Selfconsistent state of electrons in a deformed lattice, *Phys. Rev B* (1992)
3. P.L. Christiansen, J.C. Eilbeck, V.Z. Enol'skii and Ju.B. Gaididei, Ultrasonic Davydov solitons and Hénon-Heiles system, *Phys. Lett.*, 166A:129 (1992).
4. M. Hénon and C. Heiles, The applicability of the third integral of motion: some numerical experiments, *Astrophys.*, 63:73 (1964).
5. A.C. Newell, M. Tabor and Y.B. Zeng, A unified approach to Painlevé expansions, *Physica D*, 29:1 (1987).
6. A.P. Fordy, The Hénon-Heiles system revisited, *Physica D*, 52:204 (1991).
7. A.M. Pelelomonov Integrable systems of classical mechanics and Lie algebras, Basel-Boston-Berlin, Birkhäuser (1990)
8. E.K. Sklyanin, Separation variables in the Gaudin model, *J. Sov. Math.*, 47:2478 (1989)
9. E.G. Kalnis and W. Jr. Miller, Separation of variables on n -dimensional Riemann manifold.
1. The n -sphere S_n and Euclidean n -space R_n , *J. Math. Phys.*, 27:1721 (1986)
10. V.B. Kuznetsov, Quadrics on real Riemannian spaces of constant curvature. Separation of variables and connection with Gaudin magnet, *J. Math. Phys.*, 33:3240 (1992).
11. J. Fay, Theta functions on Riemann surfaces, *Lect. Notes Math*, 352, Springer, Heidelberg (1973)
12. H. Bateman, A. Erdélyi, Higher Transcendental Functions, v.3, McGraw-Hill Book Co., New York, 1955.

THE FRÖHLICH CHARGE-DENSITY-WAVE AS A LATTICE OF DAVYDOV'S SOLITONS

A.A. Eremko

Bogolyubov Institute for Theoretical Physics
Ukrainian Academy of Sciences
252143 Kiev, Ukraine

A self-consistent state of the conduction electrons and lattice deformation in one-dimensional metal was considered by Fröhlich in 1954¹. This state was then called the charge density wave (CDW) and today it is widely studied both theoretically and experimentally²⁻⁴. The Fröhlich assumption that only one phonon mode with the wave number $q = 2k_F$ (k_F is the Fermi wave number) is occupied macroscopically and interacts intensively with electrons, is often used for the explanation of certain properties of the CDW.

Here, investigating the Fröhlich problem, the exact solution to a system of nonlinear equations for the electron wavefunctions is obtained. It is shown that the CDW represents a set of periodically distributed bisolitons considered by Davydov and Brizhik⁵. The analysis of the exact solution evidently shows the presence of harmonics $\nu_n = \nu n$ in addition to the fundamental frequency ν , in current oscillations spectrum, called narrow band noise³.

In continuum approximation without account of Coulomb interaction between electrons, a system of N_e electrons interacting with the lattice vibrations is described by Fröhlich Hamiltonian¹

$$H = \sum_{j=1}^{N_e} \left[-\frac{\hbar^2}{2m} \frac{\partial^2}{\partial x_j^2} + \frac{1}{\sqrt{N}} \sum_q \chi(q) e^{iqx_j} (b_q + b_{-q}^\dagger) \right] + \sum_q \hbar V_a |q| b_q^\dagger b_q. \quad (1)$$

Here m is the effective electron mass in the conduction band, $V_a = a\sqrt{w/M}$ is the sound velocity in the chain with lattice constant a , atom masses M and the elasticity coefficient w ;

$$\chi(q) = 2i\chi \sqrt{\frac{\hbar}{2MV_a}} \frac{q}{\sqrt{|q|}} \quad (2)$$

where χ is the parameter of deformational short-range interaction of the electrons with atom displacements.

To find out the wavefunction of the system we make use of the variational method

and take into account that the total momentum operator

$$P = - \sum_{j=1}^{N_e} i\hbar \frac{\partial}{\partial x_j} + \sum_q \hbar q b_q^+ b_q \quad (3)$$

commutes with the Hamiltonian (1). If we take interest in the state of the system with certain value of the total momentum, the wavefunction should be found from the condition of functional extremum¹

$$F = \langle \Psi | H - VP - \epsilon N_e | \Psi \rangle \quad (4)$$

where ϵ and V are the Lagrange multipliers.

The wavefunction of the system is written as

$$\Psi(\{x_j, \sigma_j\}, \{b_q^+\}) = e^{i \frac{mV}{\hbar} \sum_{j=1}^{N_e} x_j} \Phi(\{x_j, \sigma_j\}) e^S |0\rangle \quad (5)$$

where

$$S = \frac{1}{\sqrt{N}} \sum_q (\beta_q b_q^+ - \beta_q^* b_q) \quad (6)$$

and

$$\Phi(\{x_j, \sigma_j\}) = \frac{1}{\sqrt{N_e!}} \det |\varphi_{\lambda, \alpha_i}(x_j, \sigma_j)|, \quad i, j = 1, 2, \dots, N_e. \quad (7)$$

Here $|0\rangle$ is the phonon vacuum state and $\varphi_{\lambda, \alpha}(x, \sigma) = \xi_\alpha(\sigma) \psi_\lambda(x)$ are the orthonormalized one-electron wavefunctions involving both the space $\psi_\lambda(x)$ and spin $\xi_\alpha(\sigma)$ ($\sigma = +1, -1$; $\alpha = +1, -1$) functions.

Using the independent variations of the functional (4) with respect to β_q and the electron wavefunctions, we get a system of equations

$$\beta_q = - \frac{\chi^*(q) f(q)}{\sqrt{N} \hbar (V_a |q|)} \quad (8)$$

$$\left[-\frac{\hbar^2}{2m} \frac{d^2}{dx^2} + U(x) \right] \psi_\lambda(x) = \epsilon_\lambda \psi_\lambda(x) \quad (9)$$

where

$$f(q) = \sum_{j=1}^{N_e} \int \Phi^* e^{-iqx_j} \Phi dv = \int_{-L/2}^{L/2} e^{-iqx} \rho_1(x) dx \quad (10)$$

and

$$U(x) = \frac{1}{\sqrt{N}} \sum_q \chi(q) (\beta_q + \beta_{-q}^*) e^{iqx} \quad (11)$$

The function

$$\rho_1(x) = \sum_\lambda n_\lambda |\psi_\lambda(x)|^2 \quad (12)$$

describes the electron density distribution along the chain (n_λ is the number indicating how many times (generally 1 or 2) the coordinate function ψ_λ is included in the determinant (7)).

If we substitute (8) into (11) we get the following expression for the self-consistent potential

$$U(x) = - \frac{4\chi^2 a}{w(1-s^2)} \rho_1(x) \quad (13)$$

where $s = V/V_a$ is the ratio of the velocity V and the sound velocity V_a .

The exact self-consistent solution of the equations (8)-(9) is⁶

$$U(x) = \frac{\hbar^2}{m} [\mathcal{P}(x + \omega') + \frac{\eta'}{\omega'}] \quad (14)$$

$$\psi_\lambda(x) = e^{ikx} u_\lambda(x), \quad u_\lambda(x) = A_\lambda \frac{\sigma(x + \omega' + \lambda)}{\sigma(x + \omega')} e^{-\frac{\pi}{2} \lambda x} \quad (15)$$

where $\eta = \zeta(\omega)$, $\eta' = \zeta(\omega')$ and $\mathcal{P}(z)$, $\sigma(z)$, $\zeta(z)$ are \mathcal{P} -, σ -, and ζ -Weierstrass functions⁷. The elliptic Weierstrass function $\mathcal{P}(z)$ is doubly-periodic function with periods denoted as 2ω and $2\omega'$. For the self-consistent solution these parameters equal to⁶

$$\omega = \frac{\pi}{2k_F}, \quad \omega' = \frac{i\pi}{2\kappa} \quad (16)$$

where $k_F = \pi n_e/2a$ is the Fermi wave number of free electrons, $n_e = N_e/N$ is electron concentration in the chain, and $\kappa = \kappa_0/(1-s^2)$, $\kappa_0 = 4m\chi^2 a/\hbar^2 \omega$.

Functions (15) are the eigenfunctions of the Schrödinger equation (9) with a single-gap periodic Lamé potential (14) with A_λ being normalization constants. The electron state spectrum is given in parametric form by the relations

$$k = i[\zeta(\lambda) - \frac{\eta}{\omega}\lambda], \quad \mathcal{E} = \frac{\hbar^2}{2m} [2\frac{\eta'}{\omega'} - \mathcal{P}(\lambda)] \quad (17)$$

via the parameter λ . In the electron spectrum there are two bands: the lower completely occupied band for $\lambda = i\alpha + \omega$ with energy $E_1 \leq \mathcal{E}_1(\alpha) \leq E_2$ and upper empty one for $\lambda = i\alpha$ with energy $\mathcal{E}_0(\alpha) \geq E_3$. The parameter λ is a double quantum number, $\lambda = i\alpha + \mu\omega$, that determines the number of the allowed bands ($\mu = 1, 0$) and the states inside the band - either α or k in view of their one-to-one correspondence. The energy band boundaries are $E_i = \frac{\hbar^2}{2m} [2\frac{\eta'}{\omega'} - \mathcal{P}(\omega_i)]$, $i = 1, 2, 3$; $\omega_1 = \omega$, $\omega_2 = \omega + \omega'$, $\omega_3 = \omega'$ and $E_1 < E_2 < E_3$.

Thus, in one-dimensional system of N_e electrons at zero temperature the electron-phonon interaction results in a self-consistent Peierls periodic chain deformation with the period determined by the first relation (16). Deforming the chain, the electrons create for themselves a single-gap periodic potential (14) in which the second parameter (imaginary period of the function $\mathcal{P}(z)$) is given by the second relation in (16). The energy gap, a single one in the electron spectrum, separates the occupied states from the free sublevels. The ground state energy then gets decreased extremely. The total momentum and total energy of the system will be equal to

$$\langle P \rangle = \langle \Psi | P | \Psi \rangle = (m + m_1) V N_e, \quad (18)$$

$$E = \langle \Psi | H | \Psi \rangle = [\frac{\hbar^2 k_F}{\pi m} (\eta - \kappa) + \frac{1}{2} (m + 2m_1) V^2] N_e \quad (19)$$

where

$$m_1 = \frac{2\hbar^2 k_F}{\pi m \kappa V_a^2 (1-s^2)} [\kappa^2 - \eta^2 + \frac{\pi^2}{48 k_F^2} g_2(\omega, \omega')] \quad (20)$$

characterized the increase of CDW effective mass per electron due to the deformation (g_2 is the invariant of Weierstrass function⁷).

In moving reference frame the CDW state represents the Peierls dielectric. In the laboratory reference frame, the transition to which is given by the unitary transformation $T(P) = \exp(-iVPt/\hbar)$, the wavefunction (5) describes the Fröhlich "sliding-mode" conductivity with total current $I = eN_e V$ generated by the motion of the CDW

as the entity along the chain with velocity V . Using the formulae of the elliptic functions theory⁷, the electron density distribution along the chain can be written as

$$\rho_1 = \frac{1}{\kappa} \left[-\frac{\eta'}{\omega'} - \mathcal{P}(x - Vt + \omega') \right] = \sum_{n=-\infty}^{\infty} \frac{\kappa}{\cosh^2[\kappa(x - Vt - \pi n/k_F)]} = \quad (21)$$

$$= \frac{n_e}{a} \left[1 + \frac{4\pi k_F}{\kappa} \sum_{n=1}^{\infty} \frac{nq^n}{1 - q^{2n}} \cos 2k_F n(x - Vt) \right] \quad (22)$$

where $q = \exp(-\pi k_F/\kappa)$. The integration ρ_1 over one period 2ω reveals that there are two electrons per each CDW period. According to (21) the CDW represents a lattice of periodically distributed Davydov's solitons (more exactly bisolitons). If inequality $\frac{k_F}{\kappa} > 1$ is satisfied the bisolitons are strongly overlapped. In this case parameter q is small, and the first term of expansion of expression (22) with respect to q corresponds to the Fröhlich approximation. When there holds the inequality $\frac{k_F}{\kappa} < 1$, the distance between bisolitons in CDW will be larger than its size. In this case the momentum (18) and the energy (19) of CDW will equal respectively to the sums of momenta and energies of $N_e/2$ noninteracting bisolitons⁶ considered in Ref.5.

The current, flowing through the chain cross-section $x = x_0$, can be written in the form:

$$j_{CDW} = eV\rho_1(x_0, t). \quad (23)$$

The expression (22) represents the Fourier cosine series and can be used for harmonic analysis of the current, resulting from the CDW motion. As it follows, the current consists of the constant term $\langle j_{CDW} \rangle = en_e V/a$ and oscillating one, which is characterized by the fundamental frequency $\nu = \langle j_{CDW} \rangle / (2e)$ and its harmonics $\nu_n = \nu n$ with amplitudes

$$C_n = \langle j_{CDW} \rangle \frac{4\pi k_F n}{\kappa \sinh(\pi k_F n / \kappa)}. \quad (24)$$

Such current oscillations (narrow band noise) were observed in CDW compounds as $NbSe_3$, TaS_3 etc. (see for example Grüner's review³).

REFERENCES

1. H. Fröhlich, Proc. R. Soc. London, A223:296(1954).
2. D. Jerome, H. J. Shultz, Adv. Phys., 31:299(1982).
3. G. Grüner, Progr. Low Temp. Phys., 12:195(1989).
4. E. D. Belokolos, Teor. Mat. Fiz., 45:286(1980).
5. L. S. Brizhik, A. S. Davydov, Fiz. Nizkikh Temp., 10:748(1984).
6. A. A. Eremko, Phys. Rev. B, 46:(1992)(to be published).
7. H. Bateman, A. Erdélyi, Higher Transcendental Functions, v.3, McGraw-Hill Book Co., New York, 1955.

INELASTIC NEUTRON SCATTERING STUDY OF THE QUANTUM SINE-GORDON BREATHER IN 4-METHYL-PYRIDINE

François Fillaux,¹ Colin J. Carlile,² and Gordon J. Kearley³

¹ Laboratoire de Spectrochimie Infrarouge et Raman
Centre National de la Recherche Scientifique
2 rue Henry-Dunant, 94320 Thiais, France

² ISIS Pulsed Neutron Facility
Rutherford Appleton Laboratory
Chilton, Didcot, Oxon OX11 0QX, U.K.

³ Institut Laue-Langevin
156X, 38042 Grenoble Cedex, France

INTRODUCTION

The rotational dynamics of the methyl groups in 4-methyl-pyridine (4MP or γ -picoline) have been thoroughly investigated using many techniques. The first Inelastic Neutron Scattering (INS) experiments on 4MP showed a band near $520 \mu\text{eV} / 4.19 \text{ cm}^{-1}$ which was assigned to the methyl tunneling transition.¹ This is one of the highest frequency ever observed for this kind of transition and a sixfold potential with a low barrier was proposed. With a better resolution ($\sim 15 \mu\text{eV}$), this band appeared to be split into several components.² As well as the main band at $510 \mu\text{eV} / 4.11 \text{ cm}^{-1}$, weaker bands at $468 \mu\text{eV} / 3.77 \text{ cm}^{-1}$ and $535 \mu\text{eV} / 4.31 \text{ cm}^{-1}$ were partially resolved. This splitting was interpreted as being due to coupled pairs of methyl groups, as in lithium acetate ($\text{CH}_3\text{COOLi} \cdot 2\text{H}_2\text{O}$ or LiAc).³ However, further studies on isotopic mixtures of fully-hydrogenated and fully-deuterated molecules have shown spectacular frequency shifts depending on concentration and temperature which cannot be explained by coupled pairs.⁴ The sine-Gordon theory, however, when applied to an infinite chain of coupled methyl groups gives a remarkably good agreement with the experimental observations. The main band at $510 \mu\text{eV}$ was re-interpreted as being due to the transition to the first-excited traveling state of the massive quantum particle referred to as a sine-Gordon breather. The weaker side-bands correspond to in-phase ($535 \mu\text{eV}$) and out-of-phase ($468 \mu\text{eV}$) tunneling transitions for the chain.⁴

It is widely accepted that partial deuteration of the methyl group lowers the symmetry of the effective potential. The tunneling is removed. However, the traveling states of the sine-Gordon breather are not expected to be destroyed. The frequency should be af-

fects mainly by the change of the particle mass. Therefore, partial deuteration is very useful to distinguish between the single particle and the collective rotations of the methyl groups. In the present paper we present INS spectra of pure 4MP- ch_2d at various temperatures. The observed frequency-shifts are consistent with the sine-Gordon theory.

INS SPECTRA

The INS spectra (fig. 1) reveal two components in the $450 \mu\text{eV} / 3.60 \text{ cm}^{-1}$ region. At 2 K they are well resolved. At higher temperature the band at $388 \mu\text{eV} / 3.13 \text{ cm}^{-1}$ merges progressively into the band at $436 \mu\text{eV} / 3.51 \text{ cm}^{-1}$. The frequency of this latter band is almost unaffected between 2 K and 5 K. In addition, there is a weak band at $74 \mu\text{eV} / 0.59 \text{ cm}^{-1}$. Its intensity increases with temperature.

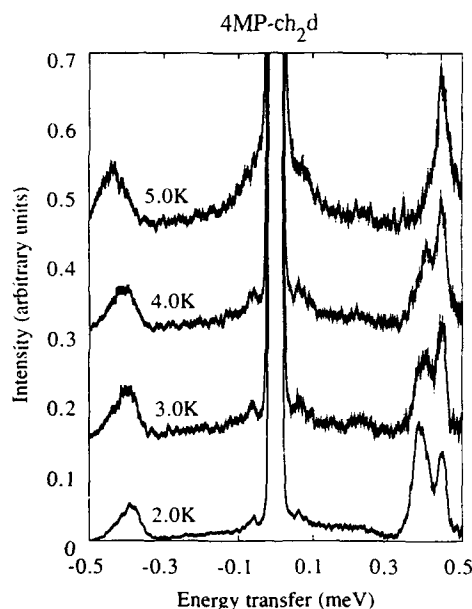


FIG. 1. Inelastic neutron scattering spectra of partially deuterated 4-methyl-pyridine ch_2d at various temperatures.

THE SINE-GORDON MODEL

The dynamics of the methyl groups in 4MP is that of an infinite chain of coupled rotors.⁴ The Hamiltonian is :

$$H_c = \sum_j \left\{ -\frac{\hbar^2}{2I} \frac{\partial^2}{\partial \theta_j^2} + \frac{V_0}{2} [1 - \cos 3\theta_j] + \frac{V_c}{2} [1 - \cos 3(\theta_{j+1} - \theta_j)] \right\} \quad (1)$$

where θ_j is the angular coordinate of the j th rotor in the one-dimensional chain with parameter L . V_0 is the on-site potential which does not depend on the lattice position and

V_c is the coupling ("strain" energy) between neighboring rotors. When $\theta_{j+1} - \theta_j$ is sufficiently small, Eq. (1) is equivalent to the sine-Gordon equation :

$$H_c = \sum_j \left\{ -\frac{\hbar^2}{2I} \frac{\partial^2}{\partial \theta_j^2} + \frac{V_0}{2} [1 - \cos 3\theta_j] + \frac{9V_c}{4} [\theta_{j+1} - \theta_j]^2 \right\} \quad (2)$$

The dynamics of this system are quite different and much richer than those of the single particle or coupled pair. The rotational motions of the single particle, i.e., small oscillations around the equilibrium position, become a continuum of roton states in the infinite chain. Tunneling for the single particle gives an analogous collective tunneling for the whole chain. However, in contrast to rotons, there is no continuum of states. Only in-phase and out-of-phase permutations of the protons are allowed by the translational symmetry of the chain.

In addition to these collective excitations, spatially localized excitations may occur in the chain. Analytical formulas are known for the kink, or soliton, and for the breather mode, or doublet, in the sine-Gordon equation.⁴ In the ideal case, these excitations have infinite lifetimes and behave like massive pseudoparticles traveling along the chain. Solitons carry the mean position of the methyl groups from one minimum of the local potential (say $\theta = 0$) to another minimum (say $\theta = 2\pi/3$) and vice versa for antisolitons. These pseudoparticles disappear at low temperature. The breather mode, on the other hand, is a soliton-antisoliton bound pair (or doublet). At very low temperature, only breather modes survive while the density of solitons and antisolitons vanishes.

Quantization of the sine-Gordon equation gives mass renormalization for the particles. In addition, the continuum of mass (or rest energy) states for the classical breather turns into a discrete spectrum $E_B(l)$ characterized by the quantum number l . The number of states depends on the potential periodicity : in the threefold case there is only one mass state ($l = 1$) which is the ground state.

The breather mode behaves like a free quantum-particle in a periodic medium. Because of the translational symmetry of the chain, steady propagation can occur only for discrete values of the energy :⁴

$$E_n = \left[E_B^2(l) + n^2 \hbar^2 \omega_c^2 \right]^{1/2}, \quad n = 0, \pm 1, \pm 2, \dots \quad (3)$$

For low potential barriers the harmonic frequency $\hbar\omega_c$ is not relevant. The effective value $\hbar\omega'_c$ depends on the mean-square amplitude for the internal oscillation of the breather mode.^{4,5} The spectra reveal that the effective potential for partially deuterated and fully hydrogenated methyl groups are very close to each other, both being amenable to interpretation as sine-Gordon systems.⁵

The in-phase and out-of-phase tunneling transitions are calculated at 341 μeV / 2.75 cm^{-1} and 262 μeV / 2.11 cm^{-1} , respectively. Therefore, the simple sine-Gordon Hamiltonian [Eq. (2)] does not account for the existence of an additional band at very low temperature in the breather mode region (at 436 μeV , fig. 1).

The splitting of the breather band is due to the removal of the threefold symmetry in partially deuterated methyl groups. The Hamiltonian for an infinite chain of such particles is :

$$H'_c = H_c + \sum_j \left\{ \frac{V'_0}{2} [1 - \cos \theta_j] + \frac{V'_c}{2} \left[1 - \cos \left(\theta_{j+1} - \theta_j + p \frac{2\pi}{3} \right) \right] \right\}, \quad p = 0, \pm 1. \quad (4)$$

V'_0 destroys the on-site potential symmetry. This term probably has two distinct

physical origins : the mean crystal field including long-range atom-atom interactions and the local coupling with librations of the whole molecule.

V'_c is due to different potential energies for the non-bonded pairs (H-H, H-D and D-D). In the sine-Gordon system this term may induce order for the methyl-group conformations along the chain which can be either in-phase ($\theta_{j+1} - \theta_j = 0$) or out-of-phase ($\theta_{j+1} - \theta_j = \pm 2\pi/3$) with regard to the local angular coordinate.

$V'_c = 0.25 \text{ cm}^{-1}$ gives a breather mode splitting of $0.38 \text{ cm}^{-1} / 47 \text{ } \mu\text{eV}$ in agreement with the observation. The chains can thus be described as a series of two different types of ordered domains at very low temperature (fig. 2) ; one of the two bands corresponds to a dephasing of $\pm 2\pi/3$ for the methyl groups, while the domains where all the methyl groups are in phase with respect to the local coordinates correspond to the other band. Since these two bands are well resolved, breathers are presumably trapped in each domain and cannot readily cross the border between two adjacent domains.

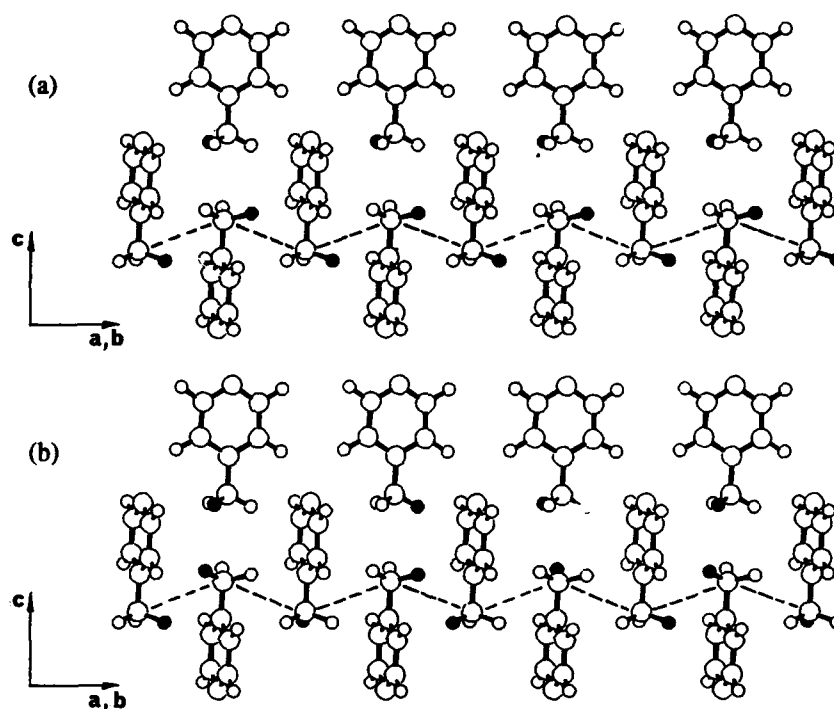


FIG. 2. Schematic view of chains of methyl groups in 4-methyl-pyridine ch_2d . Solid circles represent deuterium atoms. (a) In-phase conformation. (b) Out-of-phase conformation.

REFERENCES

1. B.Alefeld, A.Kollmar and B.A.Dasannacharya, J.Chem.Phys. 63:4415 (1975).
2. C.J.Carlike, S.Clough, A.J.Horsewill and A.Smith, Chem.Phys. 134:437 (1989).
3. A.Heidemann, H.Friedrich, E.Gunther and W.Hausler, Z.Phys. B, 76:335 (1989).
4. F.Fillaux and C.J.Carlike, Phys.Rev. B, 42:5990 (1990).
5. F.Fillaux, C.J.Carlike and G.J.Kearley, Phys.Rev. B, 44:12280 (1991).

MODELLING DNA DENATURATION

Virginia Muto, Fernando Vadillo and Mikel Lezaun

Departamento de Matematica Aplicada y
Estadística e Investigación Operativa
Facultad de Ciencias, Apartado 644
Universidad del País Vasco
E - 48080 Bilbao, Spain

INTRODUCTION

In the recent years much attention has been devoted to find a mechanism for energy transfer and localization in the DNA molecule, in particular in the context of the DNA denaturation problem^{1,2,3}. A first attempt to incorporate thermal effects in anharmonic models has been presented by Muto *et al.*^{4,3} who investigated the possibility of packets of energy (solitons) being generated thermally at physiological temperature and the lifetime of *open states*, that are the precursors of full denaturation. The models presented in these works were always dealing with a homogeneous DNA molecule. In reality DNA is a double helix built from two antiparallel linear polymers and the base in one side is complementary to the base in the other side. Guanine is associated to cytosine, adenine is associated to thymine, and they alternate in a random fashion. First studies of energy transfer in an inhomogeneous DNA molecule have been presented by Techera *et al.*⁵ and Muto⁶. In the present work, we are dealing with the local denaturation of an inhomogeneous DNA molecule.

THE PHYSICAL MODEL

The DNA molecule is described by two chains transversally coupled, where each chain simulate one of the two polynucleotide strands of the molecule³. Each of the two chains is a spring and mass system. Each one of the N masses of the model represents a single base of the base pair. The longitudinal springs, connecting masses of the same strand, represent the van der Waals potential between adjacent base pairs. The transverse springs, connecting corresponding masses of the two strands, represent the hydrogen bonds that connect the two bases in a pair. Since it is assumed to deal with an inhomogeneous DNA molecule, each particle in the mass and spring system has mass M_n , and the springs are assumed to be massless. For each base pair the model includes four degrees of freedom, u_n , x_n , and v_n , y_n , for the two strands, respectively. The $u_n = u_n(t)$ and $v_n = v_n(t)$, $n = 1, 2, \dots, N$, denote the

Research supported by project UPV 100.310-E096/91, Universidad del País Vasco.

transverse displacements (displacement along the direction of the hydrogen bonds). The $x_n = x_n(t)$ and $y_n = y_n(t)$, $n = 1, 2, \dots, N$, denote the *longitudinal displacements* (displacement along the direction of the backbone).

The anharmonic van der Waals potentials are described by the Toda potential. Denoting by I the first strand, the anharmonic potential is given by

$$V_{T,I}(l'_n - l_L) = \frac{a}{b_n} \exp[-b_n (l'_n - l_L)] + a (l'_n - l_L) \quad (1)$$

A similar expression holds for the potential of the second strand denoted by II . In the above expressions, $l_L = 3.4 \text{ \AA}$ is the distance along the helix axis between adjacent base pairs; $l'_n = \sqrt{(l_L + x_{n+1} - x_n)^2 + (u_{n+1} - u_n)^2}$ denotes the distance between two bases in the strand I ; a similar expression holds for l''_n which denotes the distance between two bases in the strand II .

The two bases in a pair are connected through hydrogen bonds which are modelled by a Lennard-Jones potential:

$$V_{LJ}(t'_n - l_T + l_H) = 4 \varepsilon_n \left[\left(\frac{\sigma}{t'_n - l_T + l_H} \right)^{12} - \left(\frac{\sigma}{t'_n - l_T + l_H} \right)^6 \right] \quad (2)$$

The length of the hydrogen bond between the two bases in a pair is given by $t'_n - l_T + l_H$. Here t'_n denotes the distance between two bases of the two strands and its expression is given by $t'_n = \sqrt{(l_T + v_n - u_n)^2 + (y_n - x_n)^2}$. Moreover, $l_T = 20 \text{ \AA}$ is the equilibrium distance between adjacent bases in a pair (the diameter of the helix), $l_H = 2^{1/6} \sigma$ is the equilibrium length of the hydrogen bond, and ε_n is the Lennard-Jones parameter, which gives the strength of the hydrogen bonds between its paired bases.

By fitting the Toda potential to a 6-12 van der Waals potential and considering experimentally measured properties of DNA, the following averaged values (the values for the homogeneous chain³) for the parameters are obtained: $M = \langle M_n \rangle = 6.41 \times 10^{-25} \text{ kg}$, $b = \langle b_n \rangle = 6.176 \times 10^{10} \text{ m}^{-1}$, $a = 2.5635 \times 10^{-10} \text{ N}$, $\varepsilon_{LJ} = 0.22 \text{ eV} = 0.35244 \times 10^{-19} \text{ N m}$, $\tilde{\varepsilon} = \langle \varepsilon_n \rangle = \varepsilon_{LJ}/10$, and $\sigma = 4.01 \times 10^{-10} \text{ m}$.

The equations of motion for the system are obtained from the Hamiltonian

$$H = \sum_{n=1}^N [T_n + V_{T,I}(l'_n - l_L) + V_{T,II}(l''_n - l_L) + V_{LJ}(t'_n - l_T + l_H)] \quad (3)$$

The kinetic energy T_n is given by $T_n = \frac{1}{2} M_n (\dot{x}_n^2 + \dot{u}_n^2) + \frac{1}{2} M_n (\dot{y}_n^2 + \dot{v}_n^2)$, and the anharmonic potentials $V_{T,I}(l'_n - l_L)$, $V_{T,II}(l''_n - l_L)$ and $V_{LJ}(t'_n - l_T + l_H)$ are given above. If we denote by $d_n^{(i)}$, $i = 1, 2, 3, 4$, the displacement variables, namely $d_n^{(1)} = x_n$, $d_n^{(2)} = u_n$, $d_n^{(3)} = y_n$, $d_n^{(4)} = v_n$, the equations of motion derived from the Hamiltonian (3) can be briefly written (for $i = 1, 2, 3, 4$, and $n = 1, 2, \dots, N$) as

$$M \ddot{d}_n^{(i)} = - \frac{\partial H}{\partial d_n^{(i)}} \quad (4)$$

In order to describe the interaction of the system with a thermal reservoir at a finite temperature T , a damping force and a noise force are added to the equations of motion (4) for the molecular displacement, namely

$$F_n^{(i)} = -M_n \Gamma \dot{d}_n^{(i)} + \eta_n^{(i)}(t) \quad (5)$$

Here Γ is the damping coefficient and $\eta_n^{(i)}(t)$ are the random forces acting on the bases, with zero mean and correlation functions $\langle \eta_n^{(i)}(t) \eta_{n'}^{(j)}(t') \rangle = 2 M_n \Gamma k_B T \delta_{nn'} \delta_{ij} \delta(t-t')$. Then the equations of motion for the system of particles are given by the perturbed version of system (4), namely

$$M_n \ddot{d}_n^{(i)} = - \frac{\partial H}{\partial d_n^{(i)}} - M_n \Gamma \dot{d}_n^{(i)} + \eta_n^{(i)}(t) . \quad (6)$$

NUMERICAL RESULTS AND DISCUSSION

DNA is a double helix built from two antiparallel linear polymers and the base in one side is complementary to the base in the other side. Guanine (G) is associated to cytosine (C); they are linked by three hydrogen bonds. Adenine (A) is associated to thymine (T); they are linked by two hydrogen bonds. We will consider (C) and (G) as "strong" bases (S), and (A) and (T) as "weak" ones (W).

From a biochemical point of view, the denaturation happens when the two strands of the DNA helix readily come apart, because the hydrogen bonds between its paired bases are disrupted. This can be accomplished by heating a solution of DNA or by adding acid or alkali to ionize its bases. The denaturation temperature depends markedly on its base composition.

Here, we are mainly interested in the dynamics of an inhomogeneous closed strand of DNA, with particular attention to the local denaturation. DNA sequences of the following type have been considered

$$XXXX \dots XX WS WS \dots WS WS XX \dots XXXX ,$$

where X stands for W , S or H type (H corresponds to the averaged values of a homogeneous chain).

The perturbed equations of motion (6) have been used to perform numerical studies. Concerning the values of the linear spring constant $\kappa = a/b$ and the Lennard-Jones parameter ϵ , used in the numerical simulations, the following values have been considered: $\kappa_{W-S} = 0.1 N$, $\kappa_{S-S} = \kappa_{W-W} = 29.9 N/m$, and $\kappa_{H-H} = 15.832 N$, $\epsilon_W = 0.8 \tilde{\epsilon}$, $\epsilon_S = 1.2 \tilde{\epsilon}$, and $\epsilon_H = \tilde{\epsilon}$, where κ_{W-S} , κ_{S-S} , κ_{H-H} and κ_{W-W} denote the linear spring constant κ for $W-S$, $S-S$, $H-H$ and $W-W$ couplings, respectively; and ϵ_W , ϵ_S and ϵ_H denote the Lennard-Jones parameter ϵ for W , S and H base pairs with $\tilde{\epsilon}$ previously given.

In the present work we considered the dynamics of three inhomogeneous DNA molecules, and we computed the corresponding hydrogen bond stretching in order to compare with the case of a homogeneous chain.

The results are shown in figure 1. Here we have considered a chain with $N = 64$ base pairs. The inhomogeneous piece of the DNA strand was considered to be 23 bases long with alternating bases of W and S type, $WS WS \dots WS WS$. The homogeneous parts on the left and right sides of the inhomogeneous one, were 21 and 20 bases long, respectively, of S , M and W type.

The open states are divided into three bins. The first bin contains open states with a life time shorter than 5 ps, which are not considered in the statistics. The second bin contains open states with lifetime between 5 and 20 ps. The averaged values of this group are plotted in figure 1 as open symbols. Finally, the third bin contains the open states with a lifetime longer than 20 ps. These averaged values are plotted in figure 1 as full symbols.

Thus, it results that at physiological temperature, the thermal fluctuations of the surrounding media cause the hydrogen bonds breaking, with a significant lifetime.

However, this does not imply that all bonds are permanently broken. Such a state of full denaturation requires higher temperatures than the ones investigated here.

What is more interesting to note is that the presence of inhomogeneities enhances the hydrogen bond breaking, namely in the three cases of inhomogeneous DNA there is a much higher number of open states: almost three times more for life times between 5 and 20 ps., and twice in the case of life times longer than 20 ps.

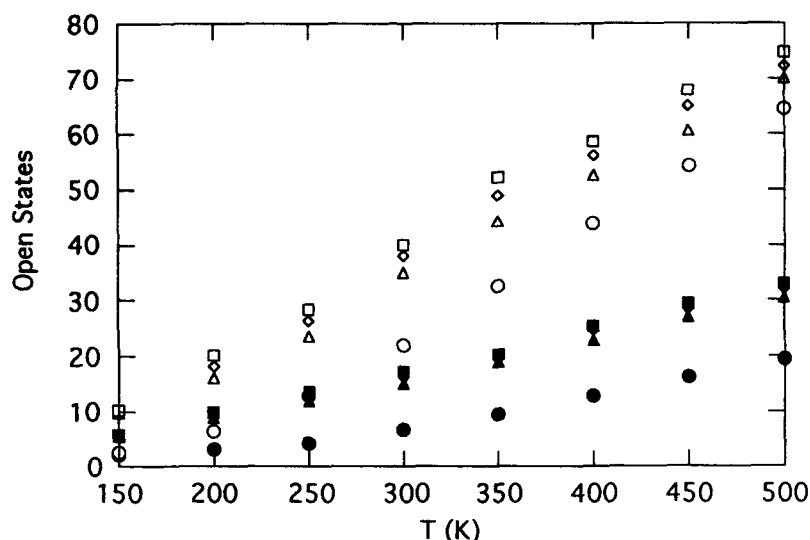


Figure 1. Number of open states as function of temperature: with life-time between 5 and 20 ps. (open symbols), with a life-time greater than 20 ps. (full symbols). Circles correspond to homogeneous chains; triangle to inhomogeneous chains with prevalence of bases of Strong type; diamond are for inhomogeneous chains with bases of Homogeneous type; and squares for inhomogeneous chains with bases of Weak type.

REFERENCES

1. M. Peyrard, A.R. Bishop, Statistical mechanics of a nonlinear model for DNA denaturation, *Phys. Rev. Lett.* **62** 2755:2758 (1989).
2. M. Techera, L.L. Daemen, E.W. Prohofsky, Nonlinear model of the DNA molecule, *Phys. Rev. A* **40** 6636:6642 (1989); Analysis of the breakdown of continuum and semidiscrete approximation of a nonlinear model for the DNA double helix, *Phys. Rev. A* **41** 4543:4546 (1990).
3. V. Muto, P.S. Lomdahl, P.L. Christiansen, Two-dimensional discrete model for DNA dynamics: longitudinal wave propagation and denaturation, *Phys. Rev. A* **42** 7452:7458 (1990).
4. V. Muto, A.C. Scott, P.L. Christiansen, A Toda lattice model for DNA: thermally generated solitons, *Physica D* **44** 75:91 (1990).
5. M. Techera, L.L. Daemen, E.W. Prohofsky, Analysis of a nonlinear model for the DNA double helix: energy transfer in an inhomogeneous chain, *Phys. Rev. A* **42** 1008:1011 (1990).
6. V. Muto, Anharmonic models for DNA dynamics, *Nanobiology* **1** (1992), in publication.

A PROTON PATHWAY WITH LARGE PROTON POLARIZABILITY IN BACTERIORHODOPSIN

Jerzy Olejnik¹, Bogumil Brzezinski¹ and Georg Zundel²

¹Faculty of Chemistry, A. Mickiewicz University, 60-780 Poznań Poland

²Institute of Physical Chemistry, University of Munich, Theresienstr. 41,
D-8000 München 2 (Germany)

With homoconjugated $B^+H \cdots B \rightleftharpoons B \cdots H^+B$ hydrogen bonds the proton fluctuates in a double minimum potential with a frequency larger than 10^{13} sec^{-1} . With heteroconjugated $AH \cdots B \rightleftharpoons A^- \cdots H^+B$ hydrogen bonds with double minimum the fluctuation frequency is slightly smaller but still very large. Calculations have shown that the polarizability caused by shifts of the proton within the hydrogen bonds due to electrical fields is about two orders of magnitude larger than polarizabilities arising due to deformation of electron systems. The same is true with hydrogen-bonded chains with multiminima potentials. The presence of such hydrogen bonds is indicated by continua in the infrared spectra. They arise since these hydrogen bonds strongly interact with their environments caused by their large proton polarizability. Such bonds or hydrogen-bonded chains with large proton polarizability are indicated by such continua^{1,2} (Fig 1).

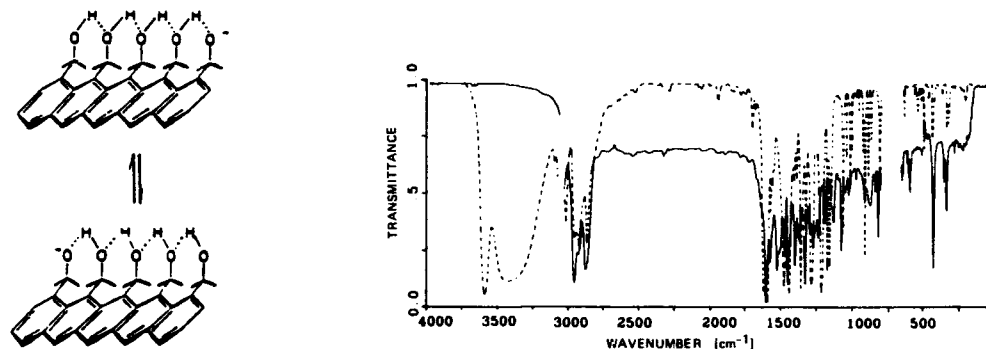


Fig. 1 FTIR spectra of (---) 1,11,12,13,14-pentahydroxymethylpentacene, and (—) of its tetrabutylammonium salt. (Taken from Ref. 3)

The equilibrium in the $AH \cdots B \rightleftharpoons A^- \cdots H^+ B$ hydrogen bonds is influenced very sensitively by local electrical fields and by specific interactions due to their large proton polarizability. Thus, such hydrogen bonds can be used as molecular switches, for instance in biology. Furthermore, such hydrogen-bonded chains with large proton polarizability are very fast and effective proton pathways.

The bacteriorhodopsin molecule is present in the purple membrane of halobacteria. If a trans-cis isomerization of the retinal residue R is induced by light absorption, protons are pumped from the inside of the purple membrane due to a photocycle. The intermediates of this photocycle can be stabilized [see for instance (4) and further references there].

PROTON PUMPING AND CONDUCTION

We have taken Fourier transform difference infrared (FTIR) spectra from the bacteriorhodopsin (BR) intermediates as well as from a modified bacteriorhodopsin BR_a intermediates⁵ with which the photocycle (Fig 2) is interrupted before the intermediate L550 is built up.

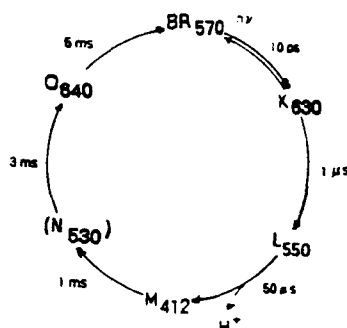


Fig. 2 Photocycle of Bacteriorhodopsin

Fig. 3a shows the FTIR difference spectrum of BR570 minus K630. The spectral changes observed with the K intermediate (negative bands) are mainly caused by the trans-cis isomerization of the retinal. But in the K intermediate already a weak very broad band is observed in the region $2800 - 2100 \text{ cm}^{-1}$ indicating the presence of a proton which is not well localized.

Fig. 3b shows the FTIR difference spectrum of BR570 (positive) and L550 (negative). In the spectrum of the intermediate L550 a pronounced continuum is found beginning at about 2800 cm^{-1} and extending toward smaller wave numbers. It demonstrates the presence of a proton pathway with large proton polarizability in the L550 intermediate.

Fig. 3c shows the respective difference spectra of the modified bacteriorhodopsin BR_a. No continuum is observed demonstrating that no proton pathway with proton polarizability is built up. This result is in good agreement with the observation that the photocycle is interrupted with the modified compound before L550 is formed.

Fig. 3d shows the FTIR difference spectrum BR570 minus M412. In the M412 intermediate the proton has already left the membrane at the outside. With M412 (negative bands) a continuum is found no longer. Instead of them a strong asymmetrical band is found in the region $2700 - 2300 \text{ cm}^{-1}$ and a weaker band in the region $2000 - 1700 \text{ cm}^{-1}$. They indicate that with M412 strong asymmetrical hydrogen bonds are formed in the active center of the BR intermediate M412.

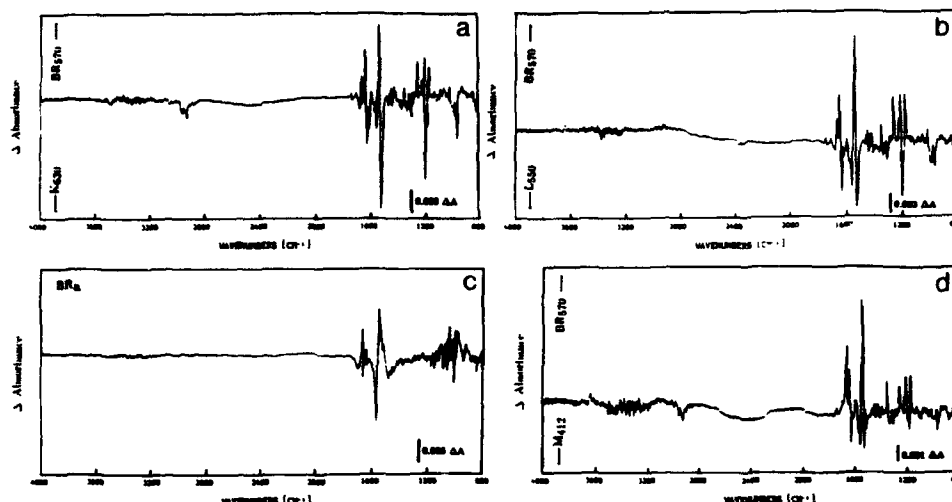


Fig. 3. FTIR difference spectra of the photo intermediates. a) BR570 minus K630, b) BR570 minus L550, c) BR570 minus the BR_a intermediate under the same conditions as in the case of BR in Fig.b, d) BR570 minus the intermediate M₄₁₂. (taken from ref. 5)

On the basis of these results, CPK model building, and literature data⁵⁻¹¹ the following picture of the proton pumping and conducting mechanism can be developed. The structural formula (Fig 4) shows two proton limiting structures of the structure which is probably built up in the L550 intermediate. The hydrogen-bonded pathway with large proton polarizability starts at Arg 82 and extends via tyrosins and probably structural water to the outside of the membrane. The proton potential between the Arg and the first Tyr residue is, however, still relatively asymmetrical. Thus, the excess proton cannot be removed at the outside of the pathway and transfer into the water phase.

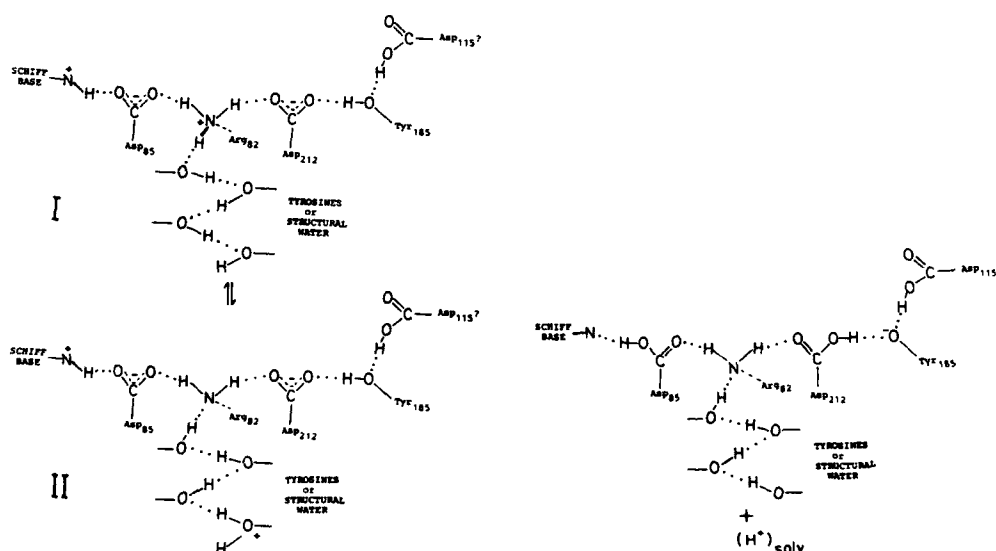


Fig. 4 Left hand side, two proton limiting structures of the proton pathway of the L550 intermediate of Bacteriorhodopsin. Right hand side, structure of the intermediate M₄₁₂.

From work of Siebert⁷ and Gerwaert and Heß⁸ it is, however, known that in the L to M step a proton transfers from the Schiff base to Asp 212. Furthermore, it is known from works of Rothschild's group⁹ that in the same step a proton transfers from Tyr 185 to Asp 85. We know, according to our investigations with model systems that these both hydrogen bonds may show large proton polarizability^{10,11}. Thus, the protons can easily be shifted within both hydrogen bonds by changes of local fields or specific interactions.

As described above in the step L to M two negative charges in the neighborhood of Arg 82 are neutralized. Thus, the protons in the hydrogen-bonded pathway are shifted to the outside and the last proton can transfer to the water phase. With M₄₁₂ the continuum is no longer observed since the hydrogen bonds in the chain are now asymmetrical and hence they show no longer proton polarizability (Fig 4). One observes, however, the bands of the very strong asymmetrical hydrogen bonds now present in the active centre.

REFERENCES

1. G. Zundel and M. Eckert, IR Continua of Hydrogen bonds and Hydrogen-bonded Systems, Calculated Proton Polarizabilities and Line Spectra, *J. Mol. Struct. (Theochem.)* 200:73 (1989).
2. G. Zundel and B. Brzezinski, Proton Polarizability of Hydrogen-bonded Systems due to Collective Proton Motion - With a Remark to Bacteriorhodopsin in: Proton Transfer in Hydrogen-bonded Systems, Proceedings of the Nato ARW, May 21-25, ed. T. Bountis ed. Plenum Publ. Co., London (1992).
3. B. Brzezinski and G. Zundel, An Intramolecular Chain of Four Hydrogen Bonds in 1,11,12,13,14-Pentahydroxymethylpentacene Tetrabutylammonium Salt. *Chem. Phys. Letters* 178:138 (1991).
4. K. J. Rothschild, Infrared Studies of Bacteriorhodopsin. *Photochem. Photobiol.* 47:883 (1988).
5. J. Olejnik, B. Brzezinski and G. Zundel, A Proton Path Way With Large Proton Polarizability and the Proton Pumping Mechanism in Bacteriorhodopsin - Fourier Transform Difference Spectra of Photoproducts of Bacteriorhodopsin and its Pentademethyl Analogue, *J. Mol. Struct.* (1992).
6. R. Henderson, J. M. Baldwin, T. A. Ceska, F. Zemlin, E. Beckmann and K.H. Downing, Model for the Structure of Bacteriorhodopsin Based on High-resolution Electron Cryomicroscopy, *J. Mol. Biol.* 213:899 (1990).
7. M. Engelhard, K. Gerwert, B. Hess, W. Kreutz and F. Siebert, Light-Driven Protonation Changes of Internal Aspartic Acids of Bacteriorhodopsin: An Investigation by Static and Time-Resolved Infrared Difference Spectroscopy Using [4-¹³C]Aspartic Acid Labeled Purple Membrane, *Biochem.* 24:400 (1985).
8. K. Gerwert, G. Souvignier and B. Hess, Simultaneous Monitoring of light-induced Changes in Protein Side-group Protonation, Chromophore Isomerization, and Backbone Motion of Bacteriorhodopsin by Time-resolved Fourier-transform Infrared Spectroscopy, *Proc. Natl. Acad. Sci. USA*, 87:9774 (1990).
9. M. Dunach, T. Marti, H. G. Khorana and K. J. Rothschild, UV-visible Spectroscopy of Bacteriorhodopsin Mutants: Substitution of Arg-82, Asp-85, Tyr-185, and Asp-212 Results in Abnormal Light-dark Adaptation, *Proc. Natl. Acad. Sci. USA*, 87:9873 (1990).
10. H. Merz and G. Zundel, Thermodynamics of Proton Transfer in Carboxylic Acid-Retinal Schiff Base Hydrogen Bonds with Large Proton Polarizability, *Biochem. Biophys. Res. Comm.* 138:819 (1986).
11. H. Merz, U. Tangermann and G. Zundel, Thermodynamics of Proton Transfer in Phenol-Acetate Hydrogen Bonds with Large Proton Polarizability and the Conversion of Light Energy into Chemical Energy in Bacteriorhodopsin, *J. Phys. Chem.* 90:6535 (1986).

EVALUATION OF THE STRENGTH OF COUPLING BETWEEN A VIBRATIONAL EXCITON AND A SPECIFIC LOW FREQUENCY MODE

P. Pumilia, R. Tubino¹, D. R. Ferro, G. Baldini², S. Abbate³

Istituto di Chimica delle Macromolecole, C.N.R.
via E. Bassini 15, I-20133 Milano (Italy)

¹Istituto di Matematica e Fisica, Università di Sassari
via Vienna 2, Sassari (Italy)

²Dipartimento di Fisica, Università di Milano
via Celoria 16, Milano (Italy)

³Dipartimento di Chimica-Fisica, Università di Palermo

THEORETICAL INTRODUCTION

In Davydov's theory, one dimensional sub-systems within molecular crystals may exhibit self-trapping of some high frequency phonons as these travel by dipole resonance interaction, due to coupling to some specific soft oscillation mode¹

This phenomenon should be particularly evident in hydrogen bond chains and therefore has been proposed as a possible mechanism in order to explain energy storage and transport processes in biological systems^{2,3}. In fact, due to the large deformability of the hydrogen bonds, a high frequency excitation, such as amide I, could be able to induce a distortion within its environment, allowing for the excitation to propagate, dressed by phonons, without dispersion.

Interpreting the vibrational exciton-phonon coupling χ parameter as related to the extent of lattice deformation involved when the high frequency excitation at a given lattice site occurs, a coarse grained evaluation can be gained using semi-empirical force fields to model interatomic forces. Adopting this point of view, we decided to perform some tentative calculations using acetanilide (ACN) molecular crystal as a model, for which infra-red absorption spectrum is well known.

Since ACN is structured in its solid phase by hydrogen bonds connections, linking the peptidic groups through the crystal body, it is a suitable compound to check if trapping process is supported.

Moreover, it can be regarded as a structural model for the spines of hydrogen bond chains stabilizing the α helical structure of proteins and according to A.C.Scott and G.Careri, Davydov-like solitons due to peptidic C=O vibrational excitation, can form and propagate over a threshold energy value.

Thus our work consisted in devising a numerical procedure for inspecting ACN

crystal modes, or combination thereof, possibly involved in Davydov-type self trapping, as C=O atomic group is brought to its first vibrational excitation level.

Setting up our computational device for simulations, based on the extensively employed Molecular Mechanics approach, we adopted MM3 force field, described later, being successfully employed in matching geometrical features and related energy differences, for crystal structures. Then an additional experimental parameter was added to the parameters deck, by introducing C=O transition dipole moment as due to a change in point charges and charge separation within the amidic group.

We consider an equally spaced chain of mass units representing the center of mass of the ACN molecules, connected through a force constant w , each unit being provided by an electric dipole moment μ_n associated to the C=O group, and describe the classical dynamics of the system through displacements vectors $u_n(t)$ from the equilibrium sites, by defining the conformational coordinate r_n :

$$r_n(t) = u_{n+1}(t) - u_n(t) \quad \text{yyt} \quad (1)$$

Following Davydov's theory, when a single C=O vibrational excitation is introduced into the chain, interacting by dipolar resonance J with its nearest neighbors, the hamiltonian describing the one dimensional system can be written:

$$H = H_{ex} + H_{vib} + H_{int} \quad (2)$$

$$H_{ex} = \sum_n (e_0 - D_n) B_n^\dagger B_n - J \sum_n (B_{n+1}^\dagger B_n + B_n^\dagger B_{n+1})$$

$$H_{vib} = (1/2M) \sum_n (p_n - p_{n+1})^2 + (1/2)w \sum_n r_n^2$$

$$H_{int} = \chi \sum_n r_n (B_n^\dagger B_n)$$

in which H_{vib} represents the low energy deformations in the conformational coordinates r_n and canonical conjugated momenta p_n ; H_{ex} describes the high frequency excitation via the creation and annihilation operators B_n^\dagger , B_n of the C=O excited state at site n , e_0 being the energy of excitation in the isolated unit and D_n standing for corrections to be applied to e_0 to account for the environment; H_{int} controls the mutual influence of the two above degrees of freedom via the constant χ .

Solving the Schrödinger equation with the continuum limit approximation, soliton solutions can be obtained, besides the ordinary exciton ones. The energy difference between the two kinds of excitations is shown to be a function of their respective velocities and the maximum is reached when they are at rest:

$$\Delta E = E_{sol}(V=0) - E_{ex}(V=0) = \chi^4 / 3w^2 |J| \quad (3)$$

Scott and Careri⁴ proposed to evaluate the soliton stabilization energy ΔE considering the discrete solution for the hamiltonian (2) and assuming that soliton solutions and low frequency modes are both strictly localized on a single site, thus obtaining:

$$\Delta E = \chi^2 / 2w \quad (4)$$

Equations (3) or (4) indicate that, in a one dimensional lattice, solitons can form only for sufficiently high values of the non linear coupling parameter χ and for low values of the intermolecular force constant w . Both these ingredients are usually found in chains of hydrogen bonded molecules, which can be therefore considered as systems apt to support the spatial propagation of solitons.

To compute the above parameters Careri⁴ follows an experimental approach,

evaluating χ through the equation:

$$\chi = d(h\nu)/dr \quad (5)$$

in which $h\nu$ is the C=O high frequency energy and r , the low mode conformational coordinate, has been chosen to represent the hydrogen bond length. Then the experimental value of the coupling parameter χ for ACN crystal can be determined by examining the change in C=O stretching frequency ($\nu_{C=O}$) as a function of the hydrogen bond length ($r_{N::O}$) in a series of related molecules. This yields

$$\chi = h \cdot d(\nu_{C=O})/dr_{N::O} = .62 \times 10^{-10} \text{ N}. \quad (6)$$

Finally, assigning the splitting ΔE observed in the low temperature infrared absorption spectrum of ACN to the existence of both excitonic and solitonic excitations, the elastic constant of the low frequency motion involved can be computed from (4) as $w = 4.8 \text{ N/m}$, which indeed appears to be a reasonable value for hydrogen bond bending constant⁶

We point out that, in the approximation of sharp localization described above, both high and low frequency coupled modes are localized at the same site, while the original version of Davydov's theory implied a self-trapping dynamics as involving a lattice deformation spread over several sites.

In order to check if the same order of magnitude for the splitting ΔE can be obtained when effectively considering the center of mass positions as conformational coordinates and allowing the deformation to involve a larger extension of the chain, we set up a computational device for simulating the occurrence of a vibrational excitation in a crystal structure.

NUMERICAL MODEL FOR ACN

The energy function used in our calculation is in the form $E = E_{\text{bond}} + E_{\text{nonb}}$, in which E_{bond} evaluates the energy contributions due to the covalent structure distortions from a given ground state configuration and E_{nonb} accounts for non-bonded interactions such as electrostatic, Van der Waals and hydrogen bonds forces.

The general form is

$$E_{\text{nonb}} = (1/2) \sum [q_i q_j / \epsilon_r r_{ij} + B_{ij} \exp(-\beta r_{ij}) - A_{ij} r_{ij}^{-6}] \quad (7)$$

$$E_{\text{bond}} = (1/2) \sum [K_l (l - l_o)^2 + K_\theta (\theta - \theta_o)^2 + \\ + V_1 (1 + \cos(\gamma)) + V_2 (1 - \cos(2\gamma)) + V_3 (1 + \cos(3\gamma))]$$

in which l, θ, γ are bond length, bond angles, dihedral angles respectively, and subscript o indicates the conformation to which zero energy has been assigned; r_{ij} is the distance between the i -th and j -th particle, q_i, q_j are the atomic charges and ϵ_r is the effective dielectric constant.

The energy function above described was parametrized by using MM3 force field⁷⁻¹², which has been successfully tested on molecular crystals and amides^{8,9}.

Starting from crystallographic data¹³ a 1-dimensional chain of 13 units was set up; the 5 inner units was then relaxed with no lattice symmetry constraint, using energy optimization routines¹⁴.

Inside this free hydrogen bonded segment of 5 units the central was considered (fig.1).

First the elastic constant due to the total energy $E(r)$ of the system was obtained using the relation

$$w = 2(E(r) - E(r_0)) / \Delta r^2 \quad (8)$$

assuming that Δr is the change in the center of mass position of the central unit for a rigid translation of a molecule along the chain (Y) axis.

Vibrational excitation of the C=O unit following the absorption of an infrared quantum was simulated using the dipole transition moment $d\mu = 0.034e\text{\AA}$ taken from experimental infrared intensities data. Writing $d\mu$ as

$$d\mu(q, r_{C=O}) = qdr_{C=O} + r_{C=O}dq \quad (9)$$

in which $r_{C=O}$ is the C=O bond length, the simulation of the excited state can be obtained by a suitable rearrangement of charge distribution q and separation in the amidic group.

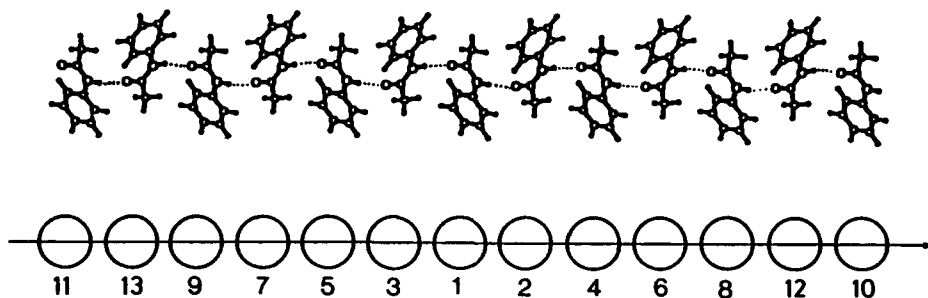


Figure 1. One dimensional arrangement of acetanilide molecules connected by hydrogen bonds between peptide units, used in our computations. C=O excitation has been located at site 1.

The stretching of the C=O bond, $dr_{C=O}$, due to excitation, was evaluated by considering the separation between the position of the maxima of the probability density function in the ground state and first excited state for an harmonic oscillator, yielding

$$dr_{C=O} = \pm 0.055 \text{ \AA}, \quad (10)$$

representing the elongation of the C=O bond during the fundamental vibration.

Finally a change in the charge distribution followed, according to the experimental value $d\mu^{15}$.

The simulation of C=O excitation was applied to the central unit (N.1 in fig. 1) and the crystal with such modifications, was again minimized in energy with respect to all atomic coordinates [See Table 1].

Table 1. Lattice distortion, due to C=O excitation at unit 1, evidenced through the change in hydrogen bond angle $d\theta$ and length dl along the chain direction.

		$\epsilon=1$	$\epsilon=3$	$\epsilon=4$	$\epsilon=10$
HN::O ₁ -2	$d\theta(\text{deg.})$ $dl (\text{\AA})$	0.6 -0.001	9.2 3.051	-5.9 .010	1.5 -0.012
HN::O ₃ -1	$d\theta(\text{deg.})$ $dl (\text{\AA})$	-1.0 .003	3.6 .013	-5.9 .018	0.7 -0.008
HN::O ₄ -2	$d\theta(\text{deg.})$ $dl (\text{\AA})$	0.8 .002	1.0 -0.001	2.2 -0.006	-4.5 .013
HN::O ₃ -5	$d\theta(\text{deg.})$ $dl (\text{\AA})$	0.1 .000	0.0 .003	-1.3 .004	-2.3 .002
HN::O ₅ -7	$d\theta(\text{deg.})$ $dl (\text{\AA})$	0.2 -0.003	2.9 -0.007	1.0 -0.009	-0.9 -0.010
HN::O ₆ -4	$d\theta(\text{deg.})$ $dl (\text{\AA})$	0.5 -0.002	4.1 -0.009	4.7 -0.014	-0.5 -0.005

Since the interaction between the high frequency C=O stretching motion and the low frequency hydrogen bond motion is considered in hamiltonian (2) only to the first order, the effect of this coupling results in a shift of the parabolic potential energy function along the deformation coordinate, without changing its curvature. Therefore the coupling parameter can be written as

$$\chi = w \cdot (r^* - r) \quad (11)$$

in which $(r^* - r)$ is the shift of the centers of mass due to the relaxation of the excited system.

From the knowledge of χ and w , we were able to derive, within the framework of Davydov's theory, the stabilization energy of the soliton by equation (3), which could be possibly detected through spectroscopical observations:

$$\Delta E = \chi^4 / 3w^2|J| \quad (12)$$

in which J is the dipolar resonance interaction between unit 1 and 3. It is given by

$$J = (1/R)[(d_1 \cdot d_2)R^2 - 3(d_1 \cdot R)(d_2 \cdot R)] \quad (13)$$

Where d_1, d_2 are the electric transition dipole moments. In our case¹⁶:

$$|d_1| = |d_2| = 0.24 \text{ Debye} = 8.0 \times 10^{-31} \text{ Cm} \quad (14)$$

By orienting the dipoles along the C=O bond directions in units 1 and 4 and by taking R as the vector connecting these bonds, we found $J = -8.16 \times 10^{-23} \text{ Joule} = -4.12 \text{ cm}^{-1}$.

RESULTS

In order to bypass non-stationary points in the potential energy function, several chain models was considered, by optimizing different starting configurations, using

different minimization algorithms^{12,14} and analysing different environments by changing the value of the dielectric constant.

In Table 2 we summarize the relevant parameters involved in the formation of the solitonic excitation, indicating for every value of the dielectric constant the result of several simulations.

Table 2. Relevant parameters in order to evaluate vibrational self-trapping conditions in different models.

models	1	2	3	4
ϵ	1	3	4	10
w	180 N/m	126 N/m	118 N/m	125 N/m
Δr	.002 Å	.012 Å	.032 Å	.035 Å
χ	$.36 \times 10^{-10} \text{N}$	$1.51 \times 10^{-10} \text{N}$	$3.76 \times 10^{-10} \text{N}$	$4.37 \times 10^{-10} \text{N}$

The obtained values for χ , using $\epsilon=1$, appears to be consistent with the experimental value as fitted by Careri for C=O vibrational excitation coupling to hydrogen bond lengths, obtained collecting crystallographic and infra-red absorption data of several hydrogen bonded chains in molecular crystals⁴.

Due to the high sensibility of the numerical evaluation of Δr and w from the ground state assumed in the molecular mechanics model, a better refined parameters deck should be used in order to get quantitative predictions about deformation induced within a given structure.

Despite the match with experimental data, results are not at variance with previous computations¹⁷, performed with a different force field, indicating that a simple rigid translation of molecular units along the chain axis could not be able to give rise to self-trapping of C=O vibrational excitation, as suggested in the original form Davydov's theory, since stabilization of the soliton solution with respect to the exciton one is vanishing, being evaluated as $\Delta E = .04 \text{ cm}^{-1}$ according to the relation (3) or $\Delta E = .35 \text{ cm}^{-1}$ when the approximation of sharp localization (equation (4)) is made.

In these conditions the soliton solution spreads over the whole chain, loosing its localization feature and coincides with exciton.

In Davydov's theory, the only degree of freedom we can consider is the rigid translation. Yet, in a real chain, as one can see from fig.2, the change in length between centers of mass is not the only effect induced by the excitation since rotations of the ACN units can also occur. A softer force constant could be associated to this latter kind of motion or to a flip-flop motion of the proton of the hydrogen bond, between two equilibrium positions, as suggested by A.C.Scott, making energetically advantageous the soliton formation.

It should be also possible that a several modes combine together to give rise to self-trapping, but evaluation of parameters related to these latter modes could be carried out only within a model including inter-chain interactions.

Moreover we notice that the induced displacements appear to be different in extent in forward and backward directions suggesting that two different coupling parameters χ_+ and χ_- should be considered in the hamiltonian (2)¹⁸

It has been proposed¹⁹ that a Davydov-like self-trapped propagation can take place along the spines of hydrogen bonded peptide groups which stabilize the quasi-periodic α helical structure in proteins.

According to Scott²⁰⁻²², in the α helical structure of proteins, threshold value for coupling should be $\chi_{th} = .45 \times 10^{-10} \text{N}$. Although the estimated value is close to the latter, the rigid rearrangement of peptidic units seems unable to follow the C=O excitation along the hydrogen bonded spines.

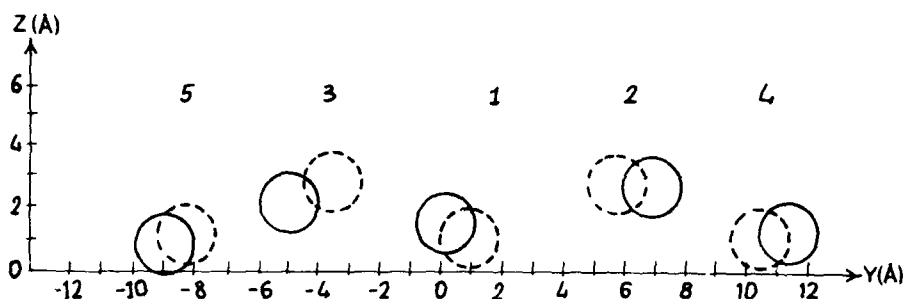


Figure 2. Schematic response of the one dimensional lattice to the introduction of a C=O vibrational excitation localized at site 1. Shifts in centers of mass occur mainly in the YZ plane; their value has been scaled by a factor 10^3

References

1. A.S.Davydov,,Excitons and solitons in quasi-one-dimensional molecular structures,*Ann. der Physik*,43:93,(1986)
2. M.V.Volkenstein,"Molecular Biophysics",Academic Press,(1977)
3. A.S.Davydov,A theory of the motion of an extra electron in quasi-one dimensional strucures,*Phys.Stat.Sol.,B*,102:275,(1980)
4. G.Careri,U.Buontempo,F.Galluzzi,E.Gratton, A.C.Scott, E.Shyamsunder, Spectroscopic evidence for Davydov-like soliton in acetanilide, *Phys.Rev.B*,30:4689,(1984)
5. J.C.Eilbeck,P.S.Lomdahl,A.C.Scott,Soliton structure in crystalline acetanilide, *Phys.Rev.B*,30:4703,(1984)
6. K.Itoh,T.Shimanouchi,Vibrational spectra of crystalline formamide, *J.Mol.Spectroscopy*,42:86,(1972)
7. J.H.Lii, N.L.Allinger,The MM3 force field for amides, polypeptides and proteins, *J.Comp.Chem.*,12:186,(1991)
8. N.L.Allinger,J.H.Lii,Benzene,aromatic rings, Van der Waals molecules and crystals of aromatic molecules in molecular mechanics (MM3), *J.Comp.Chem.*,8:1146,(1987)
9. N.L.Allinger, Y.H.Yuh, J.H.Lii,Molecular mechanics. The MM3 force field for hydrocarbons, *J.Am.Chem.Soc.*,111:8551,(1989)
10. N.L.Allinger, R,A.Kok, M.R.Imam,Hydrogen bonding in MM2, *J.Comp.Chem.*,9:591,(1988)
11. L.R.Schmits, N.L.Allinger,Molecular mechanics calculations (MM3) on aliphatic amines, *J.Am.Chem.Soc.*,112:8307,(1990)
12. D.R.Ferro,J.Hermans,Semiempirical energy calculations on model compounds of polypeptides. Crystal structures of DL-acetyl-leucine N-methylamide and DL-acetyl-amino-n-butyric acid N-methylamide, *Biopolymers*,11:105,(1972)
13. J J.Wasserman,R.R.Ryan,S.P.Layne, Structure of acetanilide (C_8H_9NO) at $113^\circ K$,*Acta Cryst.*,C41:783,(1985)
14. R.A.Donnelly,J.W.Rogers,*Int.J.Q.Chem.,Q.Chem.Symp.*,22,507,(1988)
15. Y.N.Chirgadze,N.A.Nevskaya,*Biopolymers*,15:607,(1976)
16. S.Krimm,in "Vibrational Spectra and Structure",vol 16, J.R.Durig ed.,Elsevier Press,Amsterdam,(1987) and T.C.Cheam,S.Krimm, Transition dipole interaction in polypeptides: ab initio calculation of transition dipole parameteres,*Chem.Phys.Lett.*,107:613

17. P. Pumilia, S. Abbate, G. Baldini, D. R. Ferro, R. Tubino, Nonlinear vibrational excitations in molecular crystals; molecular mechanics calculations, *Solid State Comm.*, 81:909, (1992)
18. A. F. Lawrence, J. C. McDaniel, D. B. Chang, B. M. Pierce, R. R. Birge, Dynamics of a Davydov model in α -helical proteins: effects of the coupling parameter and temperature, *Phys. Rev. A*, 33:1188, (1986)
20. A. C. Scott, Dynamics of Davydov solitons, *Phys. Rev. A*, 26:578, (1982)
21. L. MacNeil, A. C. Scott, Launching a Davydov soliton: I soliton analysis, *Physica Scripta*, 29:279, (1984)
22. L. MacNeil, A. C. Scott, Launching a Davydov soliton: II numerical studies, *Physica Scripta*, 29:284, (1984)

HIERARCHY OF NONLINEAR DYNAMIC MODELS OF DNA

Ludmila V. Yakushevich

Institute of Cell Biophysics
Russian Academy of Sciences
Pushchino, 142292 Russia

INTRODUCTION

DNA is a biological polymer which plays an important role in the conservation and transportation of genetic information. The number of theoretical models describing nonlinear properties of DNA is rather large. So, whenever we want to describe the nonlinear dynamics of some biological process involving DNA, a problem of correct choice of appropriate nonlinear model appears. It can be solved if we conceive the principle of internal logic connection (or hierarchy) between the models. In this work we propose a simple model of the hierarchy.

When constructing the dynamic hierarchy, we shall take into account that the nonlinear dynamics is only a part of the general dynamics, and the latter is strongly correlated with the structure. In other words, there is a correlation between the hierarchies of the structural, dynamic and nonlinear dynamic models of DNA. Therefore, it is convenient to begin with the constructing of the structural hierarchy and then pass to the dynamic one.

HIERARCHY OF STRUCTURAL MODELS

The first level. The simplest structural model of DNA is prompted by microphotos of the molecule where it looks like a thin elastic filament. So, in the first approximation it can be suggested that the uniform elastic rod with a circular section is the simplest structural model of DNA¹.

The second level. A more complex structural model takes into account that the DNA molecule consists of two polynucleotide chains interacting with one another by hydrogen bonds. Each of the chains can be modeled by an elastic uniform rod with a circular section. So, the complete model consists of two elastic rods weakly interacting with one another and being wound around each other to produce the double helix².

The third level. The next level model takes into account that each polynucleotide chain of the DNA molecule consists of three types mutually rigidly bound atomic subgroups (the bases, the sugar rings and the phosphate-carbon backbone pieces) with relatively weak and flexible bonds connecting them with each other³.

The fourth level. The fourth level of the hierarchy can be formed by the so called lattice models where a finite group of atoms (named nucleotide) forms a "unit cell" periodically repeating along the DNA molecule.⁴

The fifth level . The fifth (or the highest) level of the hierarchy is apparently formed by the most accurate structural model taking into account position of each atom of the DNA molecule.

HIERARCHY OF DYNAMIC MODELS

To construct the hierarchy of the dynamic models let us assume that the models described above are not static but

dynamic ones, that is the structural elements of the models are movable. To describe their motions a system of corresponding differential equations can be used. So, instead of a set of structural models described above, we obtain a set of systems of differential equations, and these systems form the dynamic hierarchy.

To illustrate this statement let us present here two examples. The first is the system of differential equations corresponding to the first level of the dynamic hierarchy and describing longitudinal, torsional and bending motions in the rod-like model of DNA. In the general case this system has the following form

$$\rho u_{tt} = Y u_{zz} + \text{nonlinear terms}^5 + \text{coupling terms}, \quad (1)$$

$$i \varphi_{tt} = C \varphi_{zz} + \text{nonlinear terms} + \text{coupling terms}, \quad (2)$$

$$S \rho y_{tt} = -B y_{zzzz} + \text{nonlinear terms}^6 + \text{coupling terms}, \quad (3)$$

where u , φ and y are the longitudinal, rotational and transverse displacements of the unit element of the rod placed near the point z at the moment t ; ρ , i and S are the density, the moment of inertia per unit length and the cross-sectional area of the rod; Y , C and B are the Young's modulus, the torsional and bending rigidities.

The second example is the system of differential equations corresponding to the next (second) level of the dynamic hierarchy and describing the longitudinal, torsional and transverse motions in both DNA strands. It consists of six differential equations. For simplicity, only two of them are presented here in the explicit form. They describe the torsional internal motions in the double rod-like model of DNA²

$$M u_{1tt} = \dots, \quad (4)$$

$$M u_{2tt} = \dots, \quad (5)$$

$$I \varphi_{1tt} = k a^2 \varphi_{1zz} + \alpha [2 \sin \varphi_1 - \sin(\varphi_1 + \varphi_2)] + \text{coupling terms}, \quad (6)$$

$$I\varphi_{2_{tt}} = ka^2\varphi_{2_{zz}} + \alpha[2\sin\varphi_2 - \sin(\varphi_1 + \varphi_2)] + \text{coupling terms}, \quad (7)$$

$$My_{1_{tt}} = \dots\dots\dots, \quad (8)$$

$$My_{2_{tt}} = \dots\dots\dots. \quad (9)$$

A set of the systems of nonlinear dynamic equations could be continued by the same method and higher (the third, the fourth and the fifth) levels of the hierarchy could be constructed.

REFERENCES

1. M.D.Barkley and B.H.Zimm, Theory of twisting and bending chain macromolecules, analysis of the fluorescence depolarization of DNA, *J.Chem.Phys.*, 70:2991 (1979).
2. L.V.Yakushevich, Nonlinear DNA dynamics: a new model, *Phys.Lett.*, A-136:413 (1989).
3. V.K.Saxena, L.L. Van Zandt and W.K. Schroll, Atomic motions and high frequency cutoff in biological macromolecules, *Chem.Phys.Lett.*, 164:82 (1989).
4. K.C.Girirajan, L. Young and E.W. Prohofsky, Vibrational free energy, entropy and temperature factors of DNA calculated by helix lattice approach, *Biopolymers*, 28:1841 (1989).
5. V.Muto, A.C.Scott and P.L.Christiansen, Microwave and thermal generation of solitons in DNA, *J.Physique*, 50:C3-217 (1989).
6. Y.H.Ichikawa, K.Konno and M.Wadati, Nonlinear transverse oscillations of elastic beam under tension, *J.Phys. Soc.Jap.*, 50:1799 (1981).

EVOLUTION AND CO-EVOLUTION IN A RUGGED FITNESS LANDSCAPE

Per Bak¹, Henrik Flyvbjerg², and Benny Lautrup²

¹Department of Physics
Brookhaven National Laboratory
Upton NY 11973, USA

²CONNECT, The Niels Bohr Institute
Blegdamsvej 17, DK-2100 Copenhagen Ø, Denmark

INTRODUCTION

We consider a variant of a simple, proto-typical model for biological evolution suggested by S. Kauffman [1, 2, 3, 4]: the co-evolution of abstract haploid organisms with a single copy of chromosomes. Evolution in this model is driven by random mutations of individual genes. Each species evolves in a fitness landscape which represents those aspects of its environment that remain unchanged on the time-scale of evolution. The fitness of any species depends on its position in its fitness landscape and on the state of other species. Species are, so to speak, part of each others *effective* landscapes. These may therefore change with time as species evolve.

It has been suggested [3] that this so-called *NKC*-model self-organizes dynamically to criticality [5] and thereby provides a simple model for the intermittency of extinction events observed in biological evolution by Raup [6]. The purpose of our investigation of this model is to demonstrate its capacity for self-organization to criticality, if it is there in the model. This article reports on some progress towards this end, in-as-much as we show that the first prerequisite, critical behaviour, is there in the model. We may hope then that a more realistic version of the model, suggested by our results, may self-organize to criticality. Whether this is the case, is not addressed here.

The letters *N*, *K*, and *C* in the model's name denote parameters for, respectively, the number of genes in the evolving organisms, the roughness of their fitness landscapes, and the strength of their mutual dependence. We study the model with maximally rugged fitness landscapes, obtained for $K = N - 1$, so *K* does not occur as

an independent parameter in the present article. We demonstrate analytically that it possesses two phases, one phase with dynamics governed by attractive fixed points, and another phase with chaotic dynamics. The phases are separated by a critical line in the (N, C) -plane at $C \simeq N/\log N$. We have obtained closed expressions for the asymptotic dynamical activity of the system. This quantity turns out to be a natural order parameter for the system. We have also obtained closed expressions, valid anywhere in the two phases, for the system's relaxation time towards its asymptotic behaviour.

Some of the analytical results we discuss below for species evolving in isolation have been seen in numerical studies [7, 8], and derived in [9]. They represent a natural first insight, and are included to make the presentation self-contained. Different but related results have been obtained for the NK -model with general $K \gg 1$ in [10].

In the present article, results are derived in a heuristic manner. In this way we, hopefully, give the reader a qualitative understanding of the dynamics of the NKC -model. Stringent derivations and technical matters were given in [11] and [12], which we shall refer to as article I and article II.

THE SYSTEM

We consider an ensemble of mutually dependent and evolving species, an *ecosystem*. At any time, the state of any species is given by the state of its genome. This genome contains N genes. We shall assume the genes are binary variables, i. e. there are only two alleles, $A = 2$. We do not expect our results to change in any significant way if the number of alleles is changed, as long as it is small compared with N in results based on expansion in $1/N$. We do not distinguish between phenotypes and genotypes, and also neglect variations in type within a species. In real life, variation is responsible for the very existence of evolution. In the NKC -model, however, only this consequence of variation is modelled: evolution takes place, and is driven by a constant rate of mutations of individual, randomly chosen genes. If a mutation increases the fitness of a species, it is accepted, and the entire species is changed. If a mutation does not increase the fitness, it is rejected, and the species remains unchanged. Tie situations, with two genetic configurations having the same fitness, do not occur (have measure zero), due to the way we assign fitness to genetic configurations: If the time-scale that selection works on is much faster than the time-scale for mutations, this lends some justification to our "all or nothing" dynamics neglecting variations [13]. Proliferation and extinction of species are both neglected in the present article, though the model could be adapted to accommodate their description.

The fitness f of any of the evolving species is a random function of its N genes and of C other genes belonging to other species¹. These C other genes are chosen at random among the genes of other species. For a given sample of the kind of ecosystem described here, the particular choice for these C genes and the random fitness function define the sample, and remain fixed during evolution — the randomness is *quenched*.

The particular probability distribution $p(f)$ used to define the fitness function does not matter; we shall not even bother to introduce it in our considerations below,

¹At this point we differ slightly from Kauffman's own definition of the NKC -model. He defines the fitness function of a species as the sum of N random functions, one for each gene, depending on the gene and on K other genes in the species plus on C genes in other species. For $K = N - 1$, a species' fitness function is therefore an entirely random function of the N genes in the species, but a rather correlated function of the foreign genes it depends on. There is no good reason that the fitness function should be this way; it is just an accidental consequence of its parametrization. So for convenience we have simply assumed that the fitness function is a random function of *all* its variables.

because it turns out that it disappears again by a transformation of variables to $F = \int_{-\infty}^f df' p(f')$. In the case where p is uniform on the interval $0 \leq f \leq 1$, we have $f = F$. So for convenience we shall refer to F as the fitness, although F in the general case really denotes the probability for fitness less than f . The elimination of $p(f)$ in equations expresses that the value f of the fitness is irrelevant; only the probability F of being less fit matters.

We have two reasons to consider random fitness landscapes; the first reason is a conjecture, the second is proven correct in articles I and II:

1. Evolution in any fitness landscape having an effectively finite correlation length, will, when viewed at sufficiently coarse-grained scales of time and space (configuration space, i.e.) look like evolution in a random fitness landscape. So evolution in a random fitness landscape describes the large-scale behaviour of evolution in a large class of landscapes. Consequently, with this choice of landscape we are avoiding the particular, while treating a quite general case.
2. It is technically convenient: the absence of correlations allows us to derive a number of analytical results.

Notice that from a mathematical point of view, N might as well be the number of positions in the primary sequence of a protein, with $A = 20$ denoting the 20 amino acids that potentially could occur at each position. Or $A = 4$ could denote the 4 nucleotides possible at each site in a DNA sequence of length N .

Alternatively, we may think of the N genes and their A alleles as N Potts spins and their A possible values in an A -state Potts model. With $V = -f$ denoting the *energy* of a spin-configuration, we recognize in each species a sample of Derrida's random energy model [14, 15], and these samples are asymmetrically coupled to each other for $C \neq 0$. In this language, the dynamics of mutations described above is the random-site Metropolis algorithm at zero temperature.

ESTIMATING THE LENGTH OF WALKS

Evolution traces out a path in configuration space. At each time step, the path is either extended one step from its current end point to a nearest neighbor — when a mutation leading to higher fitness is offered to and accepted by evolution — or the path is *not* extended — because a mutation leading to lower fitness is offered and rejected. This path is often referred to as an *adaptive walk*.

In this section, we are not concerned with the temporal aspects of evolution, but only with the length ℓ of adaptive walks. This limitation simplifies the description a good deal. In subsequent sections, temporal aspects are treated.

Before we get involved with mathematics, let us estimate the average length of adaptive walks, and the average fitness they lead to. The qualitative picture thus obtained is confirmed by rigorous calculations in article I.

We assume N is large. The dimension of configuration space is N . We assume the length of adaptive walks is much smaller than \sqrt{N} , and find this assumption consistent with the results it leads to. Since the walk proceeds by random mutations, it proceeds in random directions in configuration space. There are many more directions than there are steps in the walk, by assumption. So each step in the walk has a different direction. In each step of the adaptive walk, the fitness F is increased. The value it increases to, is uncorrelated — to leading order in $1/N$; see article I — with its previous value, except it is larger, of course. Consequently, in each step $1 - F$ is halved,

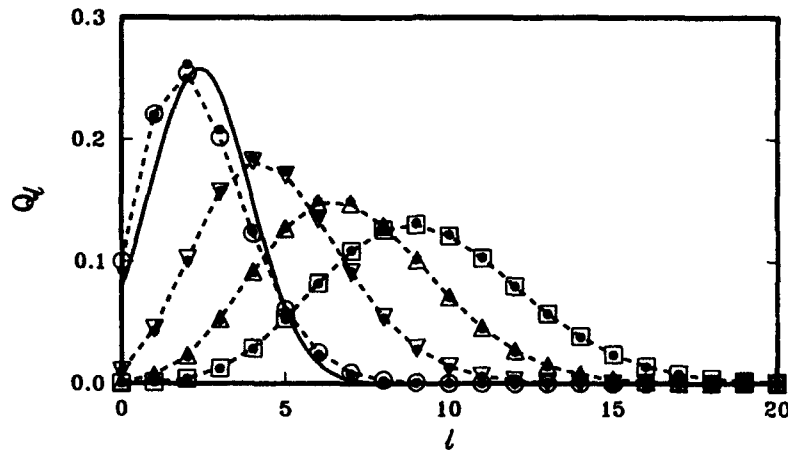


Figure 1: Q_ℓ versus ℓ for $N = 10$ (\circ), 100 (∇), 1000 (\triangle), and $10,000$ (\square). The connecting dashed lines are only meant to guide the eye. Poisson distributions with the same mean values are shown with the symbol \bullet . In the case of $N = 10$, the Gaussian distribution with same mean and variance as Q_ℓ is shown as a solid line.

on the average. Thus, starting the walk with $F = 0$, after ℓ steps the average fitness is $1 - 2^{-\ell}$. An adaptive walk stops when all neighbor positions have lower fitness than the current position. Since fitnesses are random and uncorrelated, this happens when N independent random numbers happen to be smaller than F . On the average, this occurs when $1 - F \sim 1/N$. This is our estimate for the average final fitness, and, setting $1 - F \sim 2^{-\ell}$, we have an estimate for the average length of an adaptive walk:

$$\bar{\ell} \simeq \log N / \log 2 \quad (1)$$

In the derivation of this result, we neglected correlations between fluctuations around the averages that we worked with. They do not change the logarithmic dependence on N in Eq. (1), but do change the coefficient of $\log N$; see article I.

In addition to a more precise result for the average length of adaptive walks, we want to know the probability distribution Q_ℓ for ℓ . In [8], "long upper tails containing little probability" were seen in numerical results for Q_ℓ . So one may wonder whether Q_ℓ decreases as a power of ℓ at large ℓ , or faster. In article I, it is shown that $(Q_\ell)_{\ell=0,1,2,\dots}$ is a Poisson distribution to leading order in $1/\log N$; see figure 1.

ESTIMATING THE DURATION OF WALKS

Since we let the adaptive walk start out with fitness $F = 0$, the probability Q_0 that it is at a local fitness maximum at time $t = 0$ after the first step is

$$Q_0 = 1/N \quad (2)$$

This is a rigorous result.

On the average, and to leading order in $1/N$, each step taken, including the first, reduces $1 - F$ by a factor 2. Each step thereby doubles the probability that the ensuing step will be the last, while it halves the probability per unit of time that the next step is taken. Consequently, the probability per unit of time for the walk to terminate is

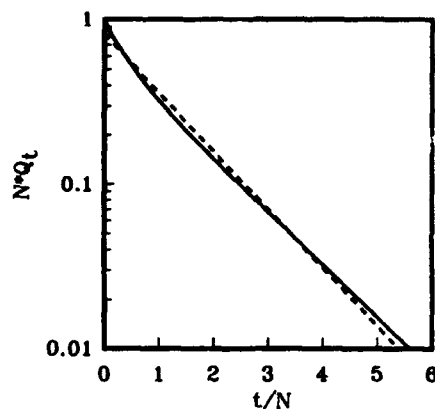


Figure 2: NQ_t versus t/N for $N = \infty$. Fully drawn curve: exact result from article I. Dashed curve: estimate from Eq. (3) with exact value for \bar{t} taken from article I.

constant during the walk. This means

$$Q_t = \frac{1}{\bar{t}} \exp(-t/\bar{t}) \quad (3)$$

Using the exact result in Eq. (2), we have the estimates

$$\bar{t} = N \quad (4)$$

and

$$Q_t = \frac{1}{N} \exp(-t/N) \quad (5)$$

This last equation shows that NQ_t remains a finite function of t/N in the limit $N \rightarrow \infty$, and its k 'th moment is proportional to N^k . In particular we see that the standard deviation

$$\sigma(t) = N \quad (6)$$

scales like the average \bar{t} . This is in contrast to the scaling laws found for the average length of walks and its standard deviation; see article I.

In article I it is shown how this section's estimates are modified when one accounts properly for fluctuations and their correlations. The result for NQ_t is shown in figure 2.

MASTER EQUATION

Because each species evolves by mutation of randomly chosen genes in a random fitness landscape, its path of evolution through configuration space can be replaced by a random walk, to leading order in N [11]. This result causes vast simplifications in the description of the system's dynamics, which, on the other hand, is exact then only to leading order in N . But that is a small price to pay, as we imagine N is large anyway.

We include two additional simplifications in the description: instead of keeping fixed the C randomly chosen foreign genes that any species depends on, we re-choose them at random any time we need them, i. e. we exchange "quenched" randomness for "annealed". If the total number of species in the ecosystem is effectively infinite

and this assumption is the second simplification we add to the description — then there is no difference between results based on quenched and annealed randomness. This is because the set of species that any species depends on, directly or via other species, forms a C-branched tree with each node of the tree representing a species and each oriented branch a dependency [16, 17]. So while our exchange of quenched for annealed randomness amounts to a mean-field approximation, we nevertheless expect the mean-field theory to be exact, because the system effectively is infinite dimensional through its random connections.

The second assumption, an effectively infinite number of species in the ecosystem, makes a description in terms of density functions possible: let $\rho_M(F; t)$ denote the relative number of species which have fitness F and M less fit one-mutant neighbors at time t . A change in a random gene will then lead to higher fitness — and therefore be accepted — with probability

$$A(t) = \sum_{M=0}^N (1 - M/N) \int_0^1 dF \rho_M(F; t) \quad (7)$$

because $1 - M/N$ is the probability that the change of one random gene leads to higher fitness in a species which has M less fit one-mutant neighbors. We note that $A(t)$ also is the rate at which mutations are accepted by the ecology from the constant rate of mutations offered. So $A(t)$ is a measure of the evolutionary activity in the ecology. We shall find it a useful quantity below, and refer to it as the *activity*.

The probability that such a mutation is accepted *and* results in fitness F for the changed species, is

$$\Phi(F; t) = \int_0^F dF' \phi(F'; t), \quad (8)$$

where

$$\phi(F'; t) = \frac{1}{1 - F'} \sum_{M=0}^N (1 - M/N) \rho_M(F'; t) \quad (9)$$

is the contribution to this probability from species with fitness F' . This contribution does not depend on F as long as $F \geq F'$. This is so because we have assumed the fitness landscape is uncorrelated. The factor $1/(1 - F')$ in this expression is the normalization factor for the constant distribution for F with $F \geq F'$.

With this notation we can write down the master equation for $\rho_M(F; t)$:

$$\begin{aligned} \frac{\partial}{\partial t} \rho_M(F; t) = & -(1 - \frac{M}{N}) \rho_M(F; t) + B_{M,N}(F) \Phi(F; t) \\ & - \frac{C}{N} A(t) \rho_M(F; t) + \frac{C}{N} A(t) B_{M,N}(F) \end{aligned} \quad (10)$$

This non-linear integro-differential equation expresses that the relative number of species with fitness F , and M less fit 1-mutant neighbors, changes for four different reasons, corresponding to the four terms on the right-hand-side of Eq. (10). The time-scale in Eq. (10) has been chosen such that in one unit of time one mutation is offered per species — to be accepted or rejected.

The first term on the right-hand-side of Eq. (10) is the rate at which species with fitness F , and M less fit neighbors, mutate to higher fitness.

The second term on the right-hand-side is a rate of change of less fit species into species with fitness F and number of less fit neighbors M . The function $B_{M,N}(F)$ is the binomial distribution with mean F :

$$B_{M,N}(F) = \frac{N!}{M! (N - M)!} F^M (1 - F)^{N-M} \quad (11)$$

It represents the probability that M out of N one-mutant neighbors to a genome with fitness F are less fit than F . This probability is binomially distributed because the fitness landscape is random, with fitness F equidistributed in the interval $[0, 1]$ ².

The third term is a rate of loss of species with fitness F, M . This loss is not caused by a change in the genes of the species lost, but by a change in its fitness due to genetic changes in other species. Since the C genes in other species that any species depends on, are randomly chosen, this change is the product of the probability $A(t)$ that a mutation in a random species is accepted and the probability $C/N\rho_M(F; t)$ that the gene it occurs in is a gene on which a species with fitness F, M depends.

The fourth term on the right-hand-side of Eq. (10) is, like the second term, a rate of change of species into species with fitness F, M . It complements the third term: species that change fitness due to genetic changes in other species, can change their fitness to F with equidistributed F . When they have done that, they have M less fit neighbors with probability $B_{M,N}(F)$.

We note that Eq. (10) conserves the total probability, as it should:

$$\frac{\partial}{\partial t} \int_0^1 dF \sum_{M=0}^N \rho_M(F; t) = 0. \quad (12)$$

ESTIMATING THE PHASE STRUCTURE

Clearly, a static solution to Eq. (10) is provided by

$$\rho_M(F; t) = \delta_{M,N} \rho(F), \quad (13)$$

for any distribution $\rho(F)$. This solution corresponds to all species being at local fitness maxima. In the language of [1, 2, 3], borrowed from economics, the system is at a Nash equilibrium. Whether this fixed point for the dynamics is attractive or repulsive with respect to perturbations of $\rho_M(F)$, depends on the value of C . For $C = 0$ it is attractive, since in this case each species evolves in a fixed landscape, and consequently arrives at a local maximum. At the other extreme, $C/N \gg 1$,

$$\rho_M(F; t) = B_{M,N}(F) \quad (14)$$

is a static solution to leading order in N/C . It corresponds to totally random fitness F , and maximum activity $A = 1/2$.

At intermediate values of C , we can easily imagine the existence of a static solution with a finite activity A corresponding to a certain fraction of all species being in states that evolve. The activity is maintained by a balance between the rate at which species evolve towards fitness maxima, and the rate at which species are set back in evolution by their dependence on other species. We expect the activity A to increase with C .

On the other hand, we can also imagine that C can be too small to sustain a finite activity. In article we show that isolated species on the average change

$$\mu_1 = \log N + 0.09913... + \mathcal{O}(N^{-1}) \quad (15)$$

²Strictly speaking, this probability for M less fit neighbors is $B_{M',N'}(F)$, with $N' < N$ and $M' = M - (N - N')$, because we already know that one or more 1-mutant neighbor configurations are less fit. But we can neglect this difference in calculations to leading order in $1/N$ for reasons similar to those given in appendix A in article I.

genes in their evolution to a local maximum. So do species in the NKC -model studied here, if they are not set back in evolution by their dependence on other species. Thus μ_1 is the minimal number of genetic changes per species by which the NKC -model can evolve to the fixed point Eq. (13). If, in doing so, each species on the average sets back less (or more) than one other species in evolution, the fixed point Eq. (13) will (or will not) be attractive.

We can make the argument more precise by making it perturbative: suppose for a given value of C the system has been arranged to be at the fixed point solution Eq. (13), and we change the fitness of one species to a random value. Since the other species do not evolve, the one singled out evolves as an isolated species, and arrives at a fitness maximum after having changed typically μ_1 of its genes. But the fitness of other species depend on the state of genes in the species that evolved; typically C other species will each depend on one gene. If any of these C genes were among the μ_1 genes that changed, the species depending on them were set back in evolution, and are now evolving, possibly setting back yet other species in their evolution. The question then is, if the chain reaction set off this way is sub- or super-critical. Will it die out or run away? The value for C which separates these two situations we call critical, and write it C_{crit} . It is the value for which, on the average, one out of C randomly chosen genes is among the μ_1 changed genes. Thus $1 = C_{\text{crit}}\mu_1/N$, or

$$C_{\text{crit}} = N/\mu_1 \quad (16)$$

We conclude that the species collectively evolve each to their own local fitness maximum and remain there with vanishing activity A for $C < C_{\text{crit}}$, while they evolve to a state with finite activity $A < 1/2$ for $C > C_{\text{crit}}$. The asymptotic value of the activity A for $t \rightarrow \infty$ can consequently be used as an order parameter distinguishing the two phases.

The arguments used in this section were based on average values. While we would not expect fluctuations to change the qualitative picture, they might change the coefficient in a scaling law like Eq. (16). Actually they do not. The perturbative result is exact, as shown in article II, where we also find the activity as a function of $c = C/N$. This function is shown in figure 3 for $N = 10$, $N = 100$, and N infinite. Also in article II, the systems relaxation time to the steady state is calculated for both phases, and found to diverge with mean field exponent -1 at C_{crit} .

CONCLUSIONS

For species evolving in isolation, we have obtained rigorous results to leading order in $1/N$ for the length and duration of adaptive walks in a special case of Kauffman's NK -model. We found that the average length scales as $\log N$, and so does the variance of the distribution of lengths. We have also obtained analytical expressions for the prefactors in these scaling laws, and found that to leading order in $1/\log N$, lengths are Poisson distributed.

For the duration of adaptive walk, we found qualitatively different results. While the average duration is proportional to N with a constant of proportionality we have found analytically, the variance of the duration is proportional to N^2 , again with analytically known coefficient. So while typical *lengths* of adaptive walks are relatively close to their average, typical *durations* vary over a range with magnitude equal to their average. We extended this result by showing analytically that in the limit $N \rightarrow \infty$, t/N has a finite distribution. Numerically, we found this distribution falls off exponentially for $t/N \geq 1$.

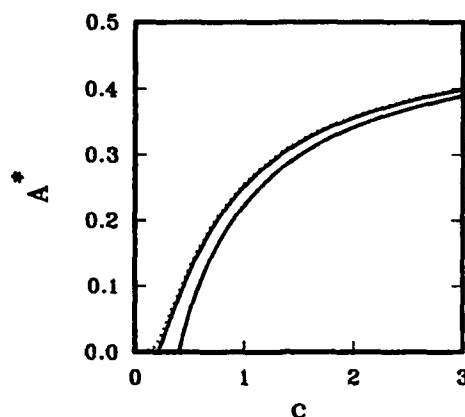


Figure 3: The asymptotic activity A^* versus the connectivity c for $N = 10$ and $N = 100$ (full curves) and for N infinite (dotted curve).

For co-evolving species, we have shown analytically that a variant of Kauffman's *NKC*-model has two phases; a *frozen* phase in which all species eventually stop evolving, because they all reach local fitness maxima, and a *chaotic* phase characterized by a balance between the number of species at local fitness maxima, and the number evolving towards such maxima, and changing the fitness landscape of other species in the process. As order parameter we used the asymptotic *activity*, the fraction of species changing genetically per unit of time. We gave a closed expression determining the asymptotic activity as an implicit function of the connectivity between species. We also gave expressions for the system's relaxation time to the asymptotic activity. On the line separating the two phases in the system's parameter space, the relaxation time diverges with mean field exponent -1.

We obtained these results in a mean field description of the model, keeping only leading terms in an expansion in $1/N$, N being the number of genes per species. Since N typically is very large, however, our leading-order approximation in N is very good. We do not expect any qualitative differences between our leading order $1/N$ -expansion results and exact results as concerns the existence of the two phases, the location of the phase boundary, and the relaxation time. As for the exponent -1 for the divergence of the relaxation time, we have argued that it is an exact result. These results all depend on the number of species S being effectively infinite, and certainly much larger than both the number of genes N and the connectivity C .

It may well be possible to obtain other analytical results for the *NKC*-model, using the methods of the present paper. For example one may try to find the Lyapunov exponents of the chaotic phase.

As for the purpose of our investigation — the demonstration of self-organized criticality in the *NKC*-model — we see no way that the maximally rugged variant studied here can be driven with perturbations from its frozen phase into a “poised”, critical state, as was done in [18] with Conway's *Game of Life*. The maximally rugged variant cannot be “pumped up” to a “poised” state — at least not in the mean field description — because after the model has responded to a perturbation it is back in the same state as it was before the perturbation was applied. This is not necessarily a short-coming of the mean field description. It willingly describes for example the build-up of the self-organized critical state of conservative sand pile models [19]. Rather, it is due to the maximal ruggedness of the fitness landscape. Its total absence of correlations

makes any perturbation of a species wipe out all memory of the fitness the species had acquired before the perturbation was applied. There is, so to speak, no such thing as a perturbation of *fitness* in the maximally rugged case. Genetic configurations may be perturbed by having just one or a few genes changed. But that typically results in a finite change of fitness in a maximally rugged landscape.

On the other hand, maximal ruggedness of the model's fitness landscape is crucial for our ability to derive analytical results, and these results are important in view of the difficulty of a numerical simulation of the model. So we are reluctant to abandon it. That leaves us with another, biologically appealing possibility: we can make the model more realistic (and computationally even more difficult) by treating N and C as dynamical parameters of the individual species, add criteria for their evolutionary change, and ask if evolution drives their averages onto the critical line found in the present paper. That study has yet to be done. Methods and results that appear to make such an undertaking feasible, were presented in articles I and II, and discussed above.

Acknowledgements

We thank Bernard Derrida and Thordur Jonsson for discussions. PB's research was supported by the Division of Materials Science, US DOE, under contract DE-AC02-76CH00016. HF and BL were supported by the Danish Natural Science Research Council and the Danish Technical Research Council under contracts 11-9450-1 and 5.26-1818, respectively.

References

- [1] S. A. Kauffman and S. Levin, *J. theor. Biol.* 128 (1987) 11
- [2] S. A. Kauffman, *Origins of Order: Self-Organization and Selection in Evolution* (Oxford Univ. Press, Oxford, 1990)
- [3] S. A. Kauffman and S. Johnsen, *J. theor. Biol.* 149 (1991) 467
- [4] S. A. Kauffman, *Scientific American* 264 (1991) 78
- [5] P. Bak, C. Tang and K. Wiesenfeld, *Phys. Rev. A* 38 (1987) 364
- [6] D. M. Raup, *Science* 231 (1986) 1528
- [7] E. Weinberger, *J. theor. Biol.* 134 (1988) 125
- [8] C. A. Macken and A. S. Perelson, *Proc. Natl. Acad. Sci. USA* 86 (1989) 6191
- [9] C. A. Macken, P.S. Hagan, and A. S. Perelson, *SIAM J. Appl. Math.* 51 (1991) 799
- [10] E. D. Weinberger, *Phys. Rev. A* 44 (1991) 6399
- [11] H. Flyvbjerg and B. Lautrup, *Evolution in a Rugged Fitness Landscape*, NBI-CS-92-32; submitted to *Phys. Rev. A*.
- [12] P. Bak, H. Flyvbjerg and B. Lautrup, *Co-evolution in a Rugged Fitness Landscape*, NBI-CS-92-33; submitted to *Phys. Rev. A*.
- [13] J. Gillespie, *Evolution* 38, (1984) 1116
- [14] B. Derrida, *Phys. Rev. B* 24 (1981) 2613
- [15] E. Gardner and B. Derrida, *J. Phys. A: Math. Gen.* 22 (1989) 1975
- [16] B. Derrida and G. Weisbuch, *J. Physique* 47 (1987) 1297
- [17] B. Derrida, E. Gardner and A. Zippelius, *Europhys. Lett.* 4 (1987) 167
- [18] P. Bak, K. Chen, and M. Creutz, *Nature* 342 (1989) 780
- [19] P. Bak and H. Flyvbjerg, unpublished

CHAOS IN A MODEL OF HIV INFECTION OF THE IMMUNE SYSTEM

Ole Lund¹, Erik Mosekilde,¹ and Jan Hansen²

¹System Dynamics Group
Physics Laboratory III
The Technical University of Denmark
DK - 2800 Lyngby, Denmark

²Department of Infectious Diseases
Hvidovre Municipal Hospital
DK - 2650 Hvidovre, Denmark

ABSTRACT

The paper discusses how chaotic dynamics can develop in a recently proposed model of the interaction between human immunodeficiency virus (HIV) and the human immune system. The model describes the state and number of T_4 lymphocytes as they interact with HIV and with another infectious agent. An analysis shows that when the probability of infection of lymphocytes through contact with HIV exceeds a certain threshold, oscillations in the concentration of free virus can arise through a Hopf bifurcation. Oscillations may occur even in the absence of a secondary infectious agent. If the infection probability is further increased, chaotic oscillations develop through a cascade of period-doubling bifurcations. The degree of chaos is quantified in terms of the two largest Lyapunov exponents. The spectrum of singularities $f(\alpha)$ and the generalized dimensions D_q are both obtained for a typical chaotic solution.

INTRODUCTION

During recent years, our knowledge of the human immune system has grown as a result of the intensive AIDS research. This has caused the models used to describe the immune system to become increasingly complicated, and attention may have been drawn away from the possibility that a few simple processes could be responsible for the observed complex behavior. Anderson and May (1989) proposed a simple model consisting of five differential equations which can, in part, explain experimental data. With their model they observed oscillations which were "often of an erratic and apparently unpredictable nature".

The analysis reported in this paper was performed to ascertain that this behavior is chaotic, to determine the route to chaos, and to quantify the chaotic behavior. A preliminary account of our results was published by Mosekilde et al. (1991).

In vitro experiments have shown that damped oscillations can occur in the number of activated T cells after stimulation of the T cells with antigens (Zöller et al. (1985)). It is therefore plausible that *in vivo*, too, the immune system can respond in an oscillatory fashion to an antigen. Epidemiological models normally assume that the infectiousness in an individual remains constant from the time he has acquired an infection until he is removed from the pool of infected persons, either by recovery or by death (Stanley (1989)). HIV infected individuals go through a long latent-carrier state before AIDS develops. During this latent state, research indicates that the concentration of HIV in the blood varies with time (Hansen (1991), Anderson and May (1988)). Such fluctuations can give rise to difficulties in predicting the spread of the disease (Stanley (1989)). The oscillations might also explain why the T_4 cell count (which is the best available single indicator of the prognosis (Hofmann (1990))), correlates so poorly with the development of the disease in individuals. The transmission probability also depends on the presence of genital ulcers (Stanley (1989)).

In the Anderson and May model, the population of T_4 lymphocytes is divided into three subpopulations: Non-activated and non-infected cells; activated but non-infected cells; and infected cells. Non-infected cells can be activated via contact with HIV. The activated cells can subsequently be infected with HIV. In the present paper a more detailed analysis of the dynamics of the model is performed.

A bifurcation analysis is presented in which the behavior of the model is investigated as a function of a parameter which describes the probability of the activated lymphocytes being infected via contact with HIV. It is shown how deterministic chaos develops through a cascade of period-doubling bifurcations, and the spectrum of singularities $f(\alpha)$ and the generalized dimensions D_q are calculated for a typical chaotic solution.

Recent research indicates that mutations in the virus population may play a role in the bursts of HIV which are seen during the symptomfree period. This offers an alternative explanation to the chaotic bursts described in our model. A more realistic description of the interaction between HIV and the immune system must, therefore, include the effects of such mutations. In its present stage the model represents a first, tentative step towards modeling the interaction between HIV and the immune system. It shows how complicated dynamics can arise in a simple model of a biological system.

GENERAL BACKGROUND

The purpose of the immune system is to eliminate foreign invaders. The word immunology originates from the Latin word *immunis* which means free of burden. Persons who do not succumb to a disease when infected are therefore said to be immune. Immunity is due to a memory mechanism which ensures that when the immune system has encountered an infection it will, if it later encounters the same infection, react faster and more strongly.

The white blood cells, which are responsible for the immune response, are produced in the bone marrow, and some are thereafter matured in the thymus. These cells are called T lymphocytes. A subpopulation is called T_4 cells. The subscript 4 delineates that these T cells have a protein called CD4 inserted into the cell membrane. They are therefore also referred to as $CD4^+$ T cells. These cells play a central role in a normal immune response since they send out chemical signals (called interleukins and interferons) which are essential to the functioning of other cells in the immune system. Lymphocytes are divided into a large number (appr. 10^9) of clones, each of which responds to

only one or a few antigens. The response mediated by lymphocytes is therefore referred to as the specific response. A normal immune response is initiated when an antigen presenting cell phagocytoses (engulfs) and digests a microbial pathogen. These cells are called antigen presenting cells since they have the ability to break down the invader into short amino chains and display the antigens on the cell surface. When a T cell, specific for one of these antigens, encounters such a cell it will become activated, i.e., it will start to proliferate (to divide), and send out chemical signals that activate other cells. Among these cells are the so-called B cells which will start to produce specialized proteins, called antibodies, that neutralize the antigen.

AIDS (Acquired Immuno-Deficiency Syndrome) was defined as a new disease in USA in 1981 after a number of unexpected deaths among young homosexual men caused by Kaposi Sarcoma, opportunistic infections, or both. In 1983, the virus HIV (Human Immuno-Deficiency Virus), which causes the disease, was identified. HIV is capable of infecting the immune system, leading to a gradual break down of the immune defense. The average survival time for people infected with AIDS is 7-11 years.

One of the most striking characteristics of the course of the disease is the selective depletion of the CD4+ subset of the helper/inducer T cells (Rosenberg and Fauci (1990)). *In vitro* HIV can directly infect and kill CD4+ T cells, and it is therefore likely that *in vivo*, too, the CD4+ cells can be killed by the direct cytopathic effect of HIV.

DESCRIPTION OF THE MODEL

The Anderson and May model considers five populations:

- Non-infected and non-activated T_4 lymphocytes P .
- Non-infected but activated T_4 lymphocytes X .
- Infected T_4 lymphocytes Y .
- Free HIV V .
- An opportunistic infection I .

The model assumes that the number of non-infected and non-activated T_4 cells is increased through a constant production Λ of these cells in the thymus and decreased through normal deaths at a constant per capita death rate μ . In addition, the number of immature cells may be reduced by removal from the pool through activation. The lymphocytes are activated by contact with a cell that presents HIV antigens. The action of the antigen presenting cells is not explicitly included in the model, so implicitly it is assumed that the number of cells presenting HIV antigens is proportional to the population of free HIV.

The population of activated but non-infected T cells grows through cell division. The rate of cell division is increased via the presence of the opportunistic infection. The population of activated lymphocytes is decreased when the activated cells become infected. The model crudely assumes that only activated cells can be infected. Recent research has shown that non-activated cells can also become infected, but in this case the infection remains latent until the cells are stimulated (Rosenberg and Fauci (1990)). The population of activated cells may also be reduced through the action of so-called suppressor cells which ensure that the number of activated cells does not continue to

grow after an infection has been eliminated. This contributes a term proportional to X^2 .

The population of infected cells decreases at a constant (high) per capita death rate α . According to the model, proliferation of infected cells is negligible.

The population of free HIV, i.e., HIV outside cells, increases as the infected cells die. New HIV viruses bud from the surface of infected T_4 cells. The HIV population decreases at a constant per capita death rate b . This population is also reduced through absorption by infected cells and by elimination through the immune response. The elimination is assumed to be proportional to the number of T_4 cells.

The population of the opportunistic infection (which can be viral, bacterial or protozoan) is increased by proliferation with a rate constant c . It is decreased due to the effect of the immune response.

The above assumptions lead to the following five nonlinear, coupled differential equations (Anderson and May (1989)).

$$\frac{dP}{dt} = \Lambda - \mu P - \gamma PV \quad (1a)$$

$$\frac{dX}{dt} = \gamma PV + rX + kIX - \beta XV - dX^2 \quad (1b)$$

$$\frac{dY}{dt} = \beta XV - \alpha Y \quad (1c)$$

$$\frac{dV}{dt} = \lambda \alpha Y - bV - \delta(X + Y)V - \sigma XV \quad (1d)$$

$$\frac{dI}{dt} = cI - hIX \quad (1e)$$

In these equations βXV is the rate of infection of activated cells, where β is the probability of infection through contact.

DISCUSSION OF THE MODEL

Some of the assumptions on which the model is based are questionable. For example, the model includes only one population of T_4 lymphocytes, and the same lymphocytes which are activated by HIV are assumed to be stimulated by the opportunistic infection. It is not likely that the same clone of T_4 lymphocytes can be activated both by HIV and by the opportunistic infection via antigen presenting cells.

In reality, not only activated T_4 lymphocytes can be infected by HIV. Non-activated lymphocytes can also be infected, but in that case the infection will stay latent until the cells reach some level of activation. Moreover, HIV does not infect only T_4 lymphocytes: it can infect other cells as well. Among these are the bone marrow stem cells, and infection of these cells can lead to a lower production of lymphocytes. HIV can also infect macrophages. These can serve as a hiding place for HIV and secure their survival.

Finally, the model fails to recognize that the secondary infectious agent may actually be present all the time and that the outburst of this infection could be caused by the gradual weakening of the immune response as the HIV infection proceeds.

In spite of these shortcomings, the Anderson and May model represents a interesting attempt seriously to model the progress of an HIV infection. Other simple models have been proposed to explain the interaction between HIV and the immune system. Thus, McLean and Kirkwood (1990) proposed a model very similar to the one above but with a more detailed description of the activation and proliferation of the T_4 cells. Reibnegger

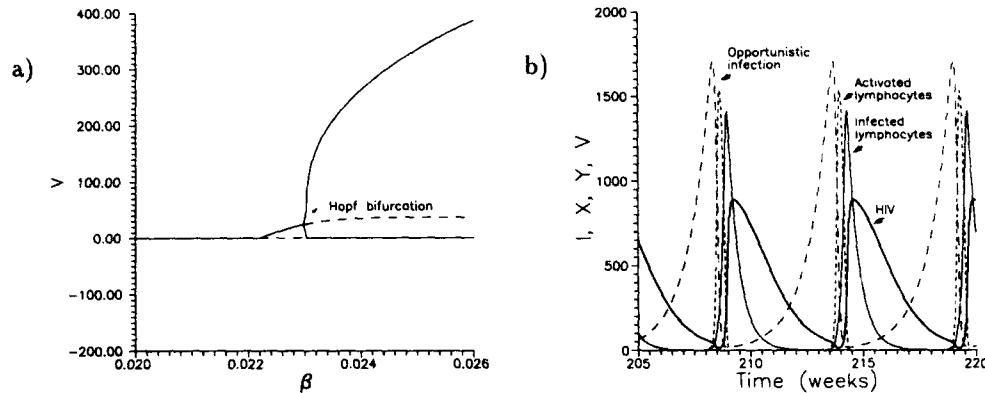


Figure 1: a) Bifurcation diagram showing the variation in the steady state HIV population as a function of the infection probability β . The steady state solution corresponding to $V = 0$ is stable until $\beta = 0.0222$ where it exchanges stability with another steady state solution. This is stable until $\beta = 0.0229$ where a Hopf bifurcation occurs, and the steady state is replaced by a stable limit cycle. The two branches are drawn through the maximum and minimum values of V in this cycle. Note that although small V is not identical zero. b) Temporal variation of the main state variables. Standard parameter values were used. In the series of peaks, the opportunistic infection I leads, followed by the activated lymphocytes X , the infected lymphocytes Y and the free HIV V .

et al. (1987) showed how the action of the immune system might exacerbate the disease. Nowak et al. (1991) proposed a model where the effects of new HIV strains, as a result of mutations in the HIV population, are taken into account.

STEADY STATE

Using the program PATH (Kaas-Petersen (1987)), the steady state solutions have been followed under variation of the probability of infection of T_4 cells through contact with HIV. Other parameter values correspond to 'standard parameters' (see below). The results are illustrated in figure 1a.

When β is smaller than 0.0222 week^{-1} , the solution with $P = \Lambda/\mu$, $X = r/d$ and $Y = V = I = 0$ is stable. This corresponds to a situation where both infections are eliminated.

When β becomes greater than 0.0222 week^{-1} , this solution becomes unstable and is replaced by an steady state solution with a non-vanishing population of HIV i.e. $V \neq 0$. When β becomes greater than 0.0229 week^{-1} , a Hopf bifurcation occurs, and the stable equilibrium point is replaced by a limit cycle. This Hopf bifurcation is of the supercritical type, which implies that in addition to the stable limit cycle an unstable equilibrium point is born out of the stable equilibrium point (see e.g. Guckenheimer and Holmes (1983)).

SIMULATION RESULTS

In the numerical experiments we have used the parameter values used by Anderson and May (1989) as standard values, i.e.

$$\Lambda = 1.0, \mu = 0.1, \gamma = 0.01, r = 1.0, d = 0.001, k = 0.01, \lambda\alpha = 10.0, b = 1.0, \delta = 0.01, \\ \sigma = 0.1, c = 1.0, h = 0.01, \alpha = 2.0 \text{ and } \beta = 0.1.$$

All rate constants are in units of week^{-1} . The integration is performed with a 3./4. order Runge-Kutta pair routine with variable time step and error control (Enright et al. (1986)).

With the above parameter values, the model exhibits self-sustained oscillations in the absence of an opportunistic infection, i.e., when equation 1e is not included. Large amplitude oscillation is triggered by the (random) arrival of an opportunistic infection. As previously noted, a more realistic assumption would be that this infection is present from the very beginning but that it is not until the functioning of the immune system is strongly impaired that it can blow up within the host. It is actually difficult to find biological processes operating on long enough time scales (years) to explain the gradual breakdown of the immune system. Nowak et al. (1991) suggested the existence of an antigenic diversity threshold, i.e., a maximum number of different strains of HIV that the immune system can handle at a time. When this threshold is exceeded, the immune system can no longer suppress the HIV strains, and a stage of fast T cell depletion is reached.

The model is characterized by the occurrence of time constants of very different size. Most of the time, the state variables change very slowly. In these periods the changes are primarily due to the death-/birth rates of the various populations. However, such periods are interrupted by short periods characterized by fast changes of the variables. Figure 1b shows the temporal variation of the various populations in more detail. In the beginning the opportunistic infection I grows. This causes growth of the population of activated lymphocytes. When the population of activated lymphocytes grows, the population of the opportunistic infection decreases due to the action of the lymphocytes. When the opportunistic infection has been defeated, the rapid growth of activated lymphocytes stops, and soon the population of activated lymphocytes decreases as the cells are infected by HIV. This in turn leads to an increase in the population of infected lymphocytes. Finally, the population of free HIV V starts to grow as infected lymphocytes lyse. Thereafter a new period of slower change starts.

PERIOD-DOUBLING ROUTE TO CHAOS IN THE ANDERSON AND MAY MODEL

When people are infected with HIV, outbreaks of HIV antigenemia are often observed throughout the long and variable incubation period. To investigate which oscillatory patterns the model can exhibit we have performed a bifurcation analysis where the mode of behavior has been determined for different values of β (hereafter referred to as the bifurcation parameter). Other parameters remain equal to the 'standard parameters' described above.

The bifurcation diagram figure 2a shows the value of V at the intersection points between the trajectory and the Poincaré surface $I = 40V$ for β varying between 0.1 and 1.0.

The system follows a period-doubling route to chaos. When β is between 0.1 and appr. 0.16 a period-1 attractor exists. When β becomes greater than 0.16, this attractor becomes unstable and is replaced by a period-2 attractor. This attractor is stable until β is increased to appr. 0.47, at which point another bifurcation occurs and the period-2 attractor is replaced by a period-4 attractor. With further increase of β , a cascade of period-doubling bifurcations occurs, and, finally, when β becomes greater than appr.

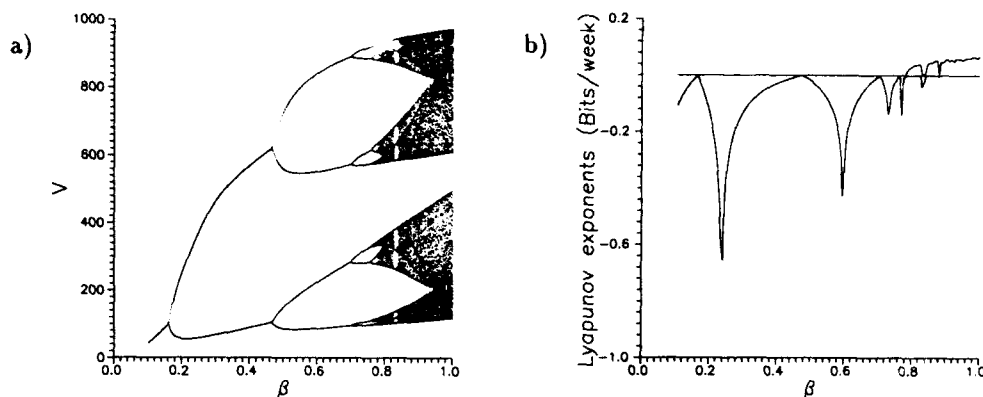


Figure 2: Bifurcation diagram and Lyapunov exponents. a) Bifurcation diagram showing the intersections of the post-transient solutions with the Poincaré plane $V = 40I$ for different values of β . b) The two largest Lyapunov exponents as functions of β . Standard parameters have been used, except that the bifurcation parameter β is varied between 0.1 and 1.0.

0.77, the attractor becomes chaotic. The bifurcation diagram figure 2a also indicates that there are windows in the chaotic range in which the dynamics is periodic. For β near 0.83, for instance, a period 12-attractor seems to exist. When β is decreased, this periodic attractor disappears via an intermittency route to chaos.

Another way to characterize the dynamics of a system is by means of its Lyapunov exponents. In practice, the Lyapunov exponents can most easily be calculated by the method described by Wolf et al. (1985). In the periodic realm, the largest Lyapunov exponent is zero, and the second largest is negative. The vanishing exponent indicates that close to the attractor points on the same trajectory will neither diverge nor converge exponentially in time. The negative exponent indicates that points close to the periodic solution will be attracted to it.

Figure 2a - 2b shows that both of the largest Lyapunov exponents become zero at the period-doubling bifurcation points. A positive Lyapunov exponent can be taken as definition of chaos. If the largest Lyapunov exponent is positive, adjacent trajectories will separate exponentially in time. The largest exponent thus determines for how long time predictions can be made for the system (Wolf et al. (1985)). The unit for the Lyapunov exponents is bits per week. If the initial conditions are specified with a precision of N bits, i.e., as one out of 2^N equally possible states, then the maximal time in which predictions can be made for the system is $T_{max} = N/\Sigma$, where Σ is the sum of the positive Lyapunov exponents. The largest Lyapunov exponent of the system is appr. 0.1 bits/week for $\beta = 1$. If the initial state of the system is known with a precision of, say, one per thousand, which in binary representation corresponds to appr. 10 bits ($2^{10} = 1024$) then the maximal theoretical time for which predictions can be made for the system is $10 \text{ bits}/(0.1 \text{ bits/week}) = 100 \text{ weeks}$.

Figure 3a shows a set of return maps for different values of β . All maps are characterized by a steep upward slope for small values of V_n . The curves then pass through a maximum and bend downwards for higher values of V_n . This represents the nonlinear folding of the system by which a high abundance of HIV in one cycle gives rise to very low values in the next cycle. The return maps also show that there is an underlying structure behind the chaotic behavior since each intersection point of the trajectories with the Poincaré surface is a relatively smooth function of the last intersection point.

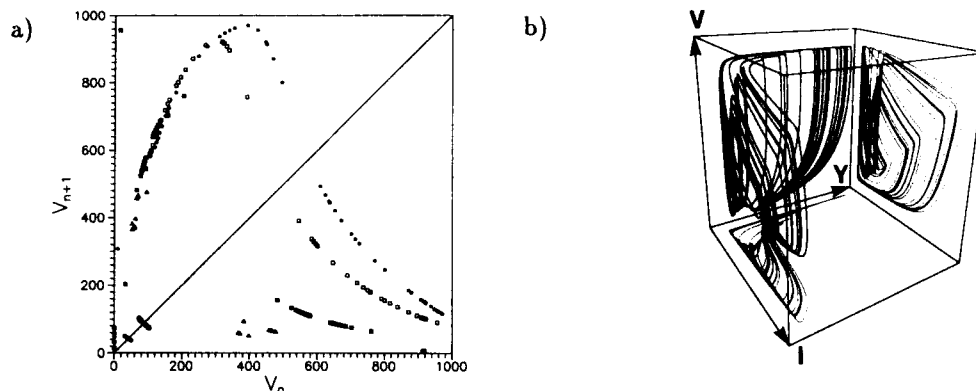


Figure 3: a) Sequence of return maps for different values of β : $\beta = 0.1$ (closed circles), $\beta = 0.15$ (open circles), $\beta = 0.25$ (closed triangles), $\beta = 0.3$ (open triangles), $\beta = 0.45$ (closed squares), $\beta = 78$ (open squares), and $\beta = 1.0$ (stars). The return maps move upwards with increasing β while at the same time the slope at the point where a map crosses the diagonal increases. Other parameters are as standard parameters. b) Phase plot in three-dimensions showing the opportunistic infection I , the population of free HIV V and the infected lymphocytes Y . $\beta = 1.0$. Other parameters are as standard parameters.

For $\beta = 1.0$ the oscillations shift between high and low peaks in an apparently random way. Figure 3b shows a phase plot of the attractor for $\beta = 1.0$. For this attractor the generalized dimensions D_q and the spectrum of singularities $f(\alpha)$ were calculated using the method described by Jensen et al. (1985). In short, D_q , α and $f(\alpha)$ can be obtained from the distribution of points in a Poincaré section of the chaotic attractor using

$$D_q = (q-1)^{-1} \tau(q), \quad (2a)$$

$$\alpha(q) = \frac{d\tau(q)}{dq}, \text{ and} \quad (2b)$$

$$f(\alpha) = q \frac{d\tau(q)}{dq} - \tau(q) \quad (2c)$$

$\tau(q)$ is determined as the best linear fit in a plot of $\log \langle p_i(l)^{q-1} \rangle$ vs. $\log l$. Here, $p_i(l)$ is the probability that other points in the Poincaré section fall within the distance l of the i 'th point in the set and $\langle \rangle$ denotes the average for all points. The Y and I coordinates of 50,000 intersections between a trajectory and the above defined Poincaré plane were used. Figure 4a shows that the calculated D_q curve depends on the range of l values used for the fit. In all cases, 20 different values of l have been used, but for the solid curve $-3 < \log_{10} l < -1$, for the dashed curve $-2.5 < \log_{10} l < -0.5$, and for the dotted curve $-3.5 < \log_{10} l < -1.5$. The $f(\alpha)$ curve corresponding to the solid curve in figure 4a is shown in figure 4b. The algorithm produced negative values of $f(\alpha)$ for large values of $|q|$ (not shown in the plot), indicating that 50,000 points are insufficient to establish appropriate dimension measures, especially for the sparsely visited regions of this attractor.

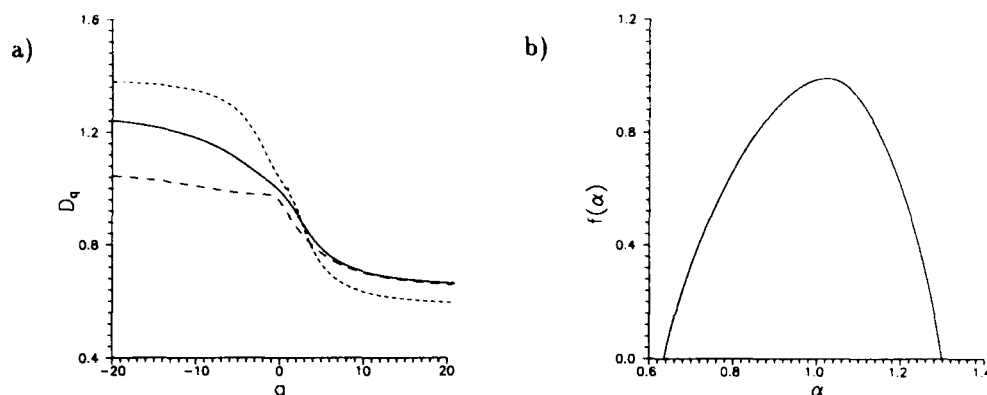


Figure 4: a) The generalized dimension D_q as a function of q . The solid curve was obtained for $-3 < \log_{10} l < -1$, the dashed curve for $-2.5 < \log_{10} l < -0.5$, and the dotted curve for $-3.5 < \log_{10} l < -1.5$. b) The spectrum of singularities $f(\alpha)$ for l values corresponding to the solid curve in figure 4a. $\beta = 1.0$. Other parameters attain standard values.

CONCLUSION

We have shown that oscillations can occur in the model both in the number of T_4 lymphocytes and in the number of free HIV. Such oscillations can severely complicate attempts to predict the spread of the disease because models of this spread normally assume a constant level of infectiousness from a time after the infection to the time where the person is removed from the infected population. Such oscillations might also explain why the number of T_4 cells correlates so poorly with the clinical prognosis.

From our investigations, we can conclude that the model exhibits chaotic behavior for some parameter values. This may be a part of the explanation why the disease develops so differently in individuals.

It must be stressed, however, that the very complicated processes involved in the regulation of the immune system and in the replication of the HIV virus are represented in a very simplified manner and that some of the assumptions on which the model is based are doubtful. There are indications that the clinically observed oscillations are due to mutations of the HIV such that each new HIV strain initiates a new immune response. Nevertheless, the model illustrates how very complicated dynamics can arise in a relatively simple nonlinear system. In other words: when a biological system exhibits 'fuzzy' dynamics it does not necessarily imply that the system is very complicated or that it is influenced by random noise. Even very simple nonlinear dynamical systems can exhibit a wide variety of behavior, and we believe that many multi-species systems are likely to exhibit chaotic dynamics for realistic parameter ranges.

ACKNOWLEDGMENTS

We are grateful to Jesper Skovhus Thomsen for his assistance in calculating the D_q and $f(\alpha)$ curves. M. Hewitt is acknowledged for his comments on the manuscript.

REFERENCES

- Anderson, R.M., and R.M. May, 1988, Epidemiological Parameters of HIV Transmission, *Nature* 333: 514 - 519.
- Anderson, R.M., and May R.M., 1989, Complex dynamical behavior in the interaction between HIV and the immune system, in *Cell to Cell Signalling, From Experiments to Theoretical Models*, ed. A. Goldbeter, 335 - 349, New York: Academic Press.
- Enright, H. W., Jackson, K. R., Nørsett, S. P., and Thomsen, P. G., 1986, Interpolants for Runge-Kutta formulas, *ACM Trans. Math. Soft.* 12: 193 - 218.
- Guckenheimer J., and Holmes, P., 1983, *Nonlinear Oscillations, Dynamical Systems, and Bifurcations of Vector Fields*, New York: Springer-Verlag.
- Hansen, J. E. S., Department of Infectious Diseases, Hvidovre Municipal Hospital, 1991, Pers. comm.
- Hofmann, B, 1990, *AIDS Immunology, HIV Induced Cellular Immune Deficiency*, Copenhagen: Lægeforeningens Forlag.
- Jensen, M. H., Kadanoff, L. P., Libchaber, A., Procaccia, I., and Stavans, J., 1985, Global universality at the onset of chaos: Results of a forced Rayleigh-Benard experiment, *Phys. Rev. Lett.* 55 (25): 2798 - 2801.
- Kaas-Petersen, C, 1987, *PATH User's Guide*, Leeds, U.K.: Center for Non-Linear Studies, University of Leeds.
- McLean, A. R., and Kirkwood, T. B. L., 1990, A model of human immunodeficiency virus infection in T helper cell clones, *J. Theor. Bio.* 147: 177 - 203.
- Mosekilde, E., Lund, O., and Mosekilde, Li., 1991, Structure, complexity and chaos in living systems, in *Complexity, Chaos and Biological Evolution*, ed. E. Mosekilde and Li. Mosekilde, 2 - 30, New York :Plenum Press.
- Nowak, M. A., Anderson, R. M., McLean, A. R., Wolfs, T. F. W., Goudsmit, J., and May, R. M., 1991, Antigenic diversity threshold and the development of AIDS, *Science*: 963 - 969.
- Reibnegger, G., Fuchs, D., Hausen, A., Werner, E. R., Dierich, M. P., and Wachter, H., 1987, Theoretical implications of cellular immune reactions against helper lymphocytes infected by an immune system retrovirus, *Proc. Natl. Acad. Sci.* 84: 7270 - 7274.
- Rosenberg, Z. F., and Fauci, A. S., 1990, Immunopathogenic mechanisms of HIV infection: cytokine induction of HIV expression, *Immunol. Today* 11: 176 - 181.
- Stanley, E. A, 1989, Mathematical models of the AIDS epidemic: A historical perspective, in *Lectures in The Sciences of Complexity*, ed. D. Stein, 827 - 840: Addison-Wesley Longman.
- Wolf, A., Swift, J.B., Swinney, H. L., and Vastano, J.A., 1985, Determining Lyapunov exponents from a time series, *Physica* 16D: 285 - 317.
- Zöller, M., Lopatta, D., Benato, B., and Andrighetto, G., 1985, Oscillation of antibody production and regulatory T cells in response to antigenic stimulation, *Eur. J. Immunol.* 15: 1198 - 1203.

PHASE LOCKING OF THE BONHOEFFER - VAN DER POL MODEL

M. Friedman², S. Goshen², A. Rabinovitch¹ and R. Thieberger^{1,2}

1. Physics Dept., Ben-Gurion University, Beer Sheva, Israel

2. Physics Dept., NRCN, P.O.Box 9001, Beer Sheva, Israel

In the last decade there has been a great deal of interest in theoretical and experimental studies of periodically forced non linear systems. The neural information propagated along an axon belongs to this category (see e.g. papers in Degn et al.,1987). Stimulated responses of action potentials in squid giant axons can be understood in terms of a dissipative structure that behaves as a nonlinear neural oscillator. In this work we will consider the Bonhoeffer van der Pol (BVP) model (FitzHugh,1969)

$$\begin{aligned} \dot{x} &= x - x^3/3 - y + I(t) \\ \dot{y} &= c(x + a - by) \end{aligned} \quad (1)$$

for this problem; here x is the membrane potential, y is a variable representing the time constant of recovery of the membrane from stimulation (called the refractivity), $I(t)$ is the membrane current (an input function), and a, b, c are positive constants representing the membrane radius, the specific resistivity of the fluid inside the membrane and the temperature factor, respectively. These constants satisfy the inequalities $b < 1$ and $3a+2b \geq 3$.

Recently, two studies of these equations, have been conducted (Rajasekar and Lakshmanan,1988a,1988b; Wang,1989) and in accord with them we adopt the values :

$$a = 0.7, \quad b = 0.8, \quad c = 0.1, \quad I(t) = A_0 + A_1 \cos(\omega_1 t) \quad (2)$$

where A_0, A_1 and ω_1 are parameters of the input function. An experimental paper by K.Aihara and G.Matsumoto in Degn et al.(1987) p.121, considers such an $I(t)$ and shows the existence of mode locking and of intermittency.

The main emphasis in the above mentioned theoretical papers was on the bifurcation scheme for $A_0 = 0$. In one of the papers (Rajasekar and Lakshmanan, 1988b) a brief discussion concerning the devil's staircase (requiring $A_0 \neq 0$) only for the case $\omega_1 = 1$ and for arbitrarily chosen values of A_1 , was presented. The ensuing winding number was plotted as function of A_0 , and was thus restricted to only a part of the range of possible values. A careful discussion of some problems concerning this issue is given elsewhere (Yasin et al., 1992).

In two recent experimental papers on normal squid axons (Matsumoto et al., 1987; Takahashi et al., 1990) forced by a train of pulses (contrary to the cosine force discussed here) a global bifurcation diagram was obtained. One of the interesting features was that the values of locked modes were restricted to specific winding numbers, w_r , and did not extend over the complete Farey tree. We wanted to check if we could get a qualitatively similar behaviour in our periodically forced BVP equations, for cases closer to the experimental case, which could indicate a similar underlying pattern.

In contrast to the previous study (Rajasekar and Lakshmanan, 1988b) where $A_0 > 0.3$ was used in order to have an autonomous limit cycle, we use $A_0 = 0.15$. This value is within a range of a stable focal point attractor, in agreement with the experimentally studied squid axon case where only nonoscillatory neurons were treated. The above mentioned experiments (Takahashi et al., 1990) used trains of pulses of constant height and of varying time intervals, as the forcing term. Therefore we chose our cosine term, $J(t)$, as the first two terms in a Fourier approximation to a pulse train. If we denote by S the area below a single pulse, by d half the pulse's width and by T the time interval between consecutive pulses we obtain:

$$J(t) \equiv f_0 + f_1 \cos(2\pi t/T), \quad f_0 = A_0 + S/T, \quad f_1 = 2S \sin(2\pi d/T)/(2\pi d) \quad (3)$$

As a demonstration we calculated one specific case: $A_0 = 0.15$, $S = 3.7$, $d = 0.15$ the results are shown in fig. 1. Except for very few irregular regions between $w_r = 1/2$ and $2/3$ and between $w_r = 2/5$ and $3/7$ we obtained only locked modes behaving as $n/(n+1)$ above $w_r = 1/2$ and as $n/(2n+1)$ below $w_r = 1/2$. This is qualitatively in agreement with the experimental result (Takahashi et al., 1990). For the pulse train case the values $n/(n+1)$ correspond to an output train $'1^n 0'$ while $n/(2n+1)$ corresponds to an output train $'(10)^n(100)'$.

We did not attempt to push this agreement farther or to check the respective widths of the locked regions, since we do not expect those to agree with our crude picture. We would like to mention that while studying this equation we noticed that the above mentioned modes prevail for a wide range of values of S and A_0 . The main difference being in the width of the different locked mode regions.

We see that although our $J(t)$ is a cosine and only a first approximation to a pulse and our equations (BVP) are only an approximation to the axon behaviour, a part of the mathematical structure of the equations seems to be already fairly similar in the two cases.

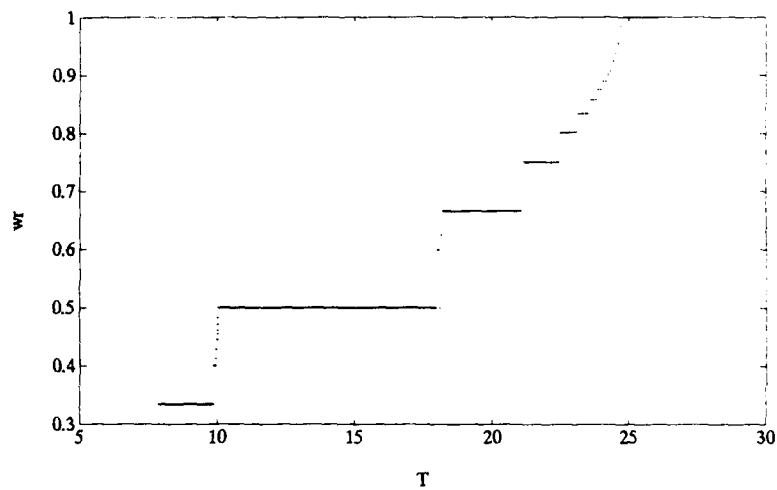


Fig. 1 : Mode locking for BVP oscillator under cosine type forcing. $A_0=0.15$, $S=3.7$, $d=0.15$
 A_0 is the basic time independent forcing term, S is the area below the pulse, d half the pulse width, wr is the winding number, T the time interval between consecutive pulses.

References

- Degn H., Holden A.V. and Olsen L.F., 1987, Editors, *Chaos in Biological Systems*, Plenum Press, New-York.
- FitzHugh R. (1969) in *Biological Engineering*, edited by Schwan H.P., Mc Graw-Hill, New-York.
- Matsumoto G., K. Aihara K., Hanyu Y., Takahashi N., Yoshizawa S. and Nagumo J-i, 1987, *Phys. Lett.*, **A123**, 162.
- Rajasekar S. and Lakshmanan M., 1988a, *J. Theor. Biol.* **133**, 473.
- Rajasekar S. and Lakshmanan M., 1988b, *Physica*, **D32**, 146.
- Takahashi N., Hanyu Y., Musha T., Kubo R. and Matsumoto G., 1990 *Physica*, **D34**, 318.
- Yasin S., Friedman M., Goshen S., Rabinovitch A. and Thieberger R., 1992, unpublished.
- Wang W., 1989, *J. Phys.* **A22**, L627.

CONTINUOUS OR DISCRETE STATE DYNAMICAL SYSTEMS AS MODELS FOR COMPUTATION IN NEURAL SYSTEMS

Arun V. Holden

Department of Physiology and
Centre for Nonlinear Studies
University of Leeds
Leeds LS2 9JT UK

INTRODUCTION

Two major advances in the mathematics of nonlinear systems have been the description of chaos in nonlinear ordinary differential systems and of solitons in nonlinear partial differential equations. The importance of these phenomena in laboratory and even planetary physics has reinforced the belief that nature is best described by smooth functions defined in continuous time on continuous space. However, all computational studies on nonlinear systems are in fact realised in discrete time on a discrete space grid. Biological systems are inherently discrete - populations are composed of individuals, tissues are composed of cells, and cells composed of molecules: a discrete description may be more appropriate than a continuous description. Further, discrete systems can exhibit richer behaviours than continuous systems they are related to (e.g. chaos in the quadratic interval map); a discrete system is not simply an approximation to a continuous system. Improvements in the availability of computer power, and advances in VLSI technology, have led to a resurgence in interest in simple discrete systems - cellular automata and coupled map lattices - as a class of models that offers new insights into spatially extensive nonlinear systems.

My particular interest is in pattern generation by nervous systems and models of nervous systems. Sherrington described the pattern of activity in the waking brain as *"the head-mass becomes an enchanted loom where millions of flashing shuttles weave a dissolving pattern, always a meaningful pattern though never an abiding one; a shifting harmony of subpatterns"*. This idea underlies most of current neurophysiological thinking, but mathematical modelling based on nonlinear interacting systems of neurone like elements has added little to this description as a crucial feature of the patterned activity in neural systems is its meaning.

Here I review some recent work that approaches models of the behaviour of neural systems (an example of the behaviours of nonlinear complex systems) within the framework of the *theory of synchronous concurrent algorithms* - this approach allows us to consider the models as computing systems, rather than as dynamical systems whose behaviour can be explored using computing systems. This approach is obviously relevant in studying information handling systems such as neural networks, but it also provides an approach to complexity in general e.g. the models of computation for

algebras that form rings and fields developed for dynamical systems in Blum, Shub and Smale are special cases of the models of computation that we use below^{3,4}.

EXCITATION EQUATIONS AND MAPS

One of the major successes of modern biology is the description of an action potential (in the giant axon of the squid) by four coupled nonlinear ordinary differential equations (ODEs) - the Hodgkin Huxley membrane equations^{5,6}. When these are combined with Kelvin's 1855 cable equation the resultant parabolic nonlinear partial differential system provides a quantitatively accurate and mechanistically precise description of propagating nerve impulses, which forms a necessary but not sufficient basis for perception.

For networks of interconnected neurones, where the neurones themselves can have complicated oscillatory and even chaotic behaviours, we need simple models that retain the rich behaviour, and methods of further simplifying these models. Our approach is to start with a simple model 3 variable ODE that was derived from experimentally obtained current-voltage relations, and that describes the periodic patterned and bursting activity of neurones, reduce it to a map^{8,10}. The return map obtained via Poincaré section provides a set of different one-dimensional maps for different sets of parameter values. The bifurcation diagrams for such maps adequately reproduces the qualitative features of the bifurcation diagram obtained from numerical integration of the ODE. These maps are then incorporated in small networks of coupled maps, and in large, locally or globally coupled map lattices; and to develop general approaches to the behaviour of networks of coupled maps.

COUPLED MAP LATTICES

A coupled map lattice is characterised by its lattice architecture, states at each lattice state, its local dynamics at each site and its behaviour; and its global dynamics.

Lattice architecture Let X be a set of lattice points. For each $x \in X$, let

$$Nhd(x) = \{x, y_1, \dots, y_{k(x)-1}\}$$

be a given set of neighbourhood points.

Lattice state Let A be a set of data used to describe the state of the lattice at a point $x \in X$. The global state of the lattice is represented by a map

$$\sigma : X \rightarrow A$$

where $\sigma(x)$ is the local state at $x \in X$. Let $[X \rightarrow A]$ be the set of all possible states at the lattice.

Local dynamics The local dynamics at lattice point $x \in X$ is constructed from the following:

i) An *isolated local process* at x governed by a law. This can be represented by the *local map*

$$f_x : A \rightarrow M$$

where M is a set of all possible auxiliary or derived values for the states of points, and $f_x(a)$ is the value generated at x when in state a .

ii) A *process of interaction* that combines the isolated processes located in a neighbourhood of x . This can be represented by the map

$$g_x : M^{k(x)} \rightarrow A$$

which couples the values generated by the states of the points in the neighbourhood

$$\text{Nhd}(x) = \{x, y_1, \dots, y_{k(x)-1}\}.$$

Global dynamics The global dynamics of the CML is given by the family $\langle V_x : x \in X \rangle$ of local state functions of the form

$$V_x : T \times [X \rightarrow A] \rightarrow A$$

defined by

$$V_x(0, \sigma) = \sigma(x)$$

$$V_x(t+1, \sigma) = g_x(f_x(V_x(t, \sigma)), f_{y_1}(V_{y_1}(t, \sigma)), \dots, f_{y_{k(x)-1}}(V_{y_{k(x)-1}}(t, \sigma)))$$

This family is naturally combined into the *global state function*

$$V : T \times [X \rightarrow A] \rightarrow [X \rightarrow A]$$

defined by

$$V(t, \sigma)(x) = V_x(t, \sigma).$$

SYNCHRONOUS CONCURRENT ALGORITHMS

A *synchronous concurrent algorithm* (SCA) is an algorithm based on a network of processing elements called *modules*, connected together by *channels*, that compute and communicate data in parallel and are synchronised by a global clock $T = \{0, 1, 2, \dots\}$. The SCA processes a clocked sequence $a(0), a(1), a(2), \dots$ of data taken from a set A : this sequence is a function $a : T \rightarrow A$. Each module m is a computational device with n input channels and one output channel that implements function $f_m : A^n \rightarrow A$.

Communication between modules occurs along channels that can transmit only a single datum $a \in A$ in any time cycle; channels can branch but not merge. A *source* is a module that reads data into the network: it has no input channels, and a single output. A network with n sources will process n streams a_1, a_2, \dots, a_n that form the vector-valued stream $a : T \rightarrow A^n$. A

sink is a module from which data is read out of the network; it has a single input channel and no output channel. Two modules are *neighbours* if the output channel of one is an input channel of the other. The *architecture* is the structure of a finite network of modules connected by channels.

Mathematically, an SCA consists of some sets of data, time cycles and data streams, and some basic functions on these sets, which are combined using the network architecture to form a system of equations whose solution is the system of functions that give the state and output of the SCA. In order to understand the formalisation (e.g. to establish the existence and uniqueness of solutions) we must examine these components more carefully.

The data set A , clock T and stream $[T \rightarrow A]$ are combined with the component functions of the k modules

$$f_1 : A^{n(1)} \rightarrow A, \dots, f_k : A^{n(k)} \rightarrow A$$

and the constants and operations on time

$$0 \text{ and } t+1$$

and read function

$$\text{eval} : T \times [T \rightarrow A] \rightarrow A$$

$$\text{eval}(t, a) = a(t)$$

to form an algebra \bar{A}

$$(A, T, [T \rightarrow A] \mid f_1, \dots, f_k, 0, t+1, \text{eval}).$$

The equations are derived from the topology of the network and the unit delay hypothesis; the equations have the form of a *system of primitive recursion equations* over the operations of \bar{A} . Thus we have a method that allows us to specify the state and output from a network of any architecture if we know the architecture, functionalities of the modules and initial inputs. The general CML model of computation is a special case of an SCA.

COMPUTATIONAL POWER OF SCA AND CML

Most models of computation are designed to compute functions

$$f: \mathbb{N}^n \rightarrow \mathbb{N}$$

on the set \mathbb{N} of natural numbers.

Recently, models of computation have been developed to compute functions

$$f: A^n \rightarrow A$$

on any data set A . They start from the set A and a family of basic functions $\sigma_1, \dots, \sigma_k$ on A which taken together form an algebra

$$(A, \sigma_1, \dots, \sigma_k).$$

Many of these models are natural generalisations of models of computations invented for \mathbb{N} . We have analysed computation by SCAs using any model of computation that satisfies certain axioms and shown for CMLs:

If the local and coupling maps are computable in the classical models of real number computation then so are the state maps. Furthermore, all the standard examples of local and coupling maps considered are computable and so therefore are their corresponding state maps.

The key point is that for a large class of mathematical theories about the computation of functions, including the standard theories of describing the computable functions on real numbers, we have shown that a CML model for computation does not yield processes, behaviours, or input-output functions that are new.

To approach the question: *Can physical and biological systems perform computations that cannot be performed by digital computation?* We have addressed the question: *Can systems faithfully modelled by CMLs perform computations that cannot be performed by digital computation?* and given one precise sense in which the answer is likely to be 'No'.

ACKNOWLEDGEMENT

This work was supported by UK MRC SPG 9017859.

REFERENCES

1. C.S.Sherrington, "Man and His Nature" Cambridge University Press (1940)
2. L.Blum, M.Shub, S.Smole, On a theory of computation and complexity over the real number: NP-completeness, recursive function and universal machine, *Bull. Amer. Math. Soc. (N.S.)* 21 1-46 (1989).
3. A.V.Holden, J.V.Tucker, H.Zhang, M.J.Poole, Coupled map lattices as computational systems. *Chaos 2* in press
4. J.V.Tucker and J.I.Zucker, Examples of semicomputable sets of real and complex numbers, In J.P.Meyers Jr. & M.J.O'Donnell, editors, Constructivity in Computer Science, Lecture Notes in Computer Science 613 Springer Verlag (1992)
5. A.L.Hodgkin, A.F.Huxley A quantitative description of membrane current and its application to conduction and propagation in nerve. *J.Physiol* 117 500-544 (1952)
6. A.V.Holden, The mathematics of excitation. In "Biomathematics in 1980" ed. L.M.Ricciardi, A.C.Scott. North Holland 15-48 (1982)
7. A.C.Scott Neurophysics Wiley Interscience New York (1977)
8. A.V.Holden and Y-S Fan, From simple to complex oscillatory behaviour via intermittent chaos in the Rose - Hindmarsh model. *Chaos, Solitons & Fractals*. In press.
9. A.V.Holden and Y-S Fan, From simple to simple bursting oscillatory behaviour via chaos in the Rose - Hindmarsh model for neuronal activity *Chaos, Solitons & Fractals*. In press
- 10 A.V.Holden and Y-S Fan, Crisis induced chaos in the Rose - Hindmarsh model for neuronal activity. *Chaos, Solitons & Fractals*. submitted
- 11 K.Kaneko (ed) "Coupled Map Lattices - Theory and Applications". John Wiley (1992).

TURING STRUCTURES IN *DROSOPHILA* MORPHOGENESIS

Axel Hunding

Chemistry Department C116
H. C. Ørsted Institute
University of Copenhagen
Universitetsparken 5
DK 2100 Copenhagen Ø, Denmark

INTRODUCTION

The spontaneous formation of complex patterns and form in biological systems is largely unexplained. Turing(1952) demonstrated however that autocatalytic biochemical reactions coupled to internal diffusion, but without external control, could break up from the original homogeneous state and form stable well defined inhomogeneous concentration gradients and patterns. General reaction-diffusion systems may be described by

$$\partial \mathbf{c} / \partial t = \mathbf{F}(\mathbf{c}) + \mathbf{D} \Delta \mathbf{c} \quad (1)$$

where \mathbf{c} is the concentration vector, \mathbf{F} is the chemical kinetics rate vector and the last term describe Fickian diffusion. If the Jacobian $\mathbf{J} = \partial \mathbf{F} / \partial \mathbf{c}$, evaluated at the homogeneous steady state, is of one of the forms (a) or (b):

$$\mathbf{J} = \begin{pmatrix} + & - \\ + & - \end{pmatrix} \quad (a) \qquad \mathbf{J} = \begin{pmatrix} - & - \\ + & + \end{pmatrix} \quad (b) \quad (2)$$

spontaneous pattern formation may occur if the rates and diffusion constants satisfy certain inequalities. In the case (a) one speaks of an activation- inhibition system, as c_1 activates both its own formation and that of c_2 , and c_2 inhibits both rates. The second class (b) were introduced by Sel'kov (1967) and studied by the so-called brussels group, the leader of which, I. Prigogine, got the Nobel price in 1977. Their work demonstrate that Turing structures are fully compatible with the second law of thermodynamics as living systems are open systems and they showed (1974) with bifurcation theory that the patterns found in computer simulations are genuine solutions to the nonlinear partial differential equations above. References to early work on such *spontaneous symmetry breaking* in biochemical systems is found in (Nicolis and Prigogine, 1977).

A particular Sel'kov type system may be written as

$$\frac{\partial c_1}{\partial t} = \nu - \frac{k_1 c_1 c_2^\gamma}{1 + K c_2^\gamma} + D_1 \Delta c_1 \quad (3)$$

$$\frac{\partial c_2}{\partial t} = \frac{k_1 c_1 c_2^\gamma}{1 + K c_2^\gamma} - k_2 c_2 + D_2 \Delta c_2 \quad (4)$$

Here component one is fed homogeneously from a source with rate ν and converted to component two with a rate displaying product activation with Hill constant γ greater than one. Component two is in turn consumed by first order kinetics. Thus the system is thermodynamically open and a flow of free energy through the system keeps it far from equilibrium. Both components satisfy a no flux condition $\partial c_i / \partial n = 0$ where $\partial / \partial n$ denotes the gradient along the outward normal at the surface. The emerging patterns are to a first approximation proportional to eigenfunctions ϕ_{nml} to the Laplacian satisfying

$$\Delta \phi_{nml} = -k_{nml}^2 \phi_{nml} \quad (5)$$

For one dimensional model systems of length L , these functions are simple cosine functions $\cos(n\pi x/L)$. The general 3 dimensional case is studied here as this makes comparisons to actual biological experiments feasible.

BIFURCATION THEORY

Analytical solutions to Eq(1) may be found by expanding c from the homogeneous stationary solution c_0 , i. e. $z = c - c_0$. Inserted in Eq(1) we get a linear and a nonlinear part

$$L(z) + N(z) = 0 \quad (6)$$

where

$$L(z) = Jz + D\Delta z \quad (7)$$

and by construction $Lz = 0$ for $z = 0$ (the homogeneous case). Nontrivial inhomogeneous solutions to $Lz = 0$ may be found by substituting $\delta_{nml} \phi_{nml}$ for z which yields

$$|J - k_{nml}^2 D| = 0 \quad (8)$$

This equation for the determinand specifies where bifurcation may occur to inhomogeneous solutions of geometry ϕ_{nml} . We then expand in a small parameter ϵ and collect terms to the same order in ϵ . A hierarchy of linear problems then arise which may be solved. The solution to the arising algebraic bifurcation equations shows that *nonlinear selection rules* apply and transitions to patterns with certain geometries are forbidden. The geometry of the bifurcating solutions is common to large classes of models with different chemistry details. Similar results have recently been obtained also in the case of Turing systems of the second kind

$$\partial c / \partial t = F(k(r), c) + \nabla \cdot D(r) \nabla c \quad (9)$$

in which one Turing system forces rate constants to be position dependent in a second system (Hunding & Brøns, 1990). It is thus meaningful to study pattern formation in a particular model system numerically as the patterns and pattern sequences recorded are common to a broad class of chemical networks. This makes comparisons to biological experiments reasonable.

NUMERICAL STUDY OF PREPATTERN FORMATION

Bifurcations to Eqs(1 & 9) have been investigated by numerical solution. The method of lines was used and thus the system of nonlinear partial differential equations was converted to a large system of ordinary differential equations by discretization of the Laplacian in three curvilinear coordinates. The resulting system is stiff and solved accordingly (modified Gear code). The Jacobian used in the corrector step is a sparse banded matrix which may be rearranged (chessboard numbering of meshpoints) to yield large blocks within which the solution vector elements may be iterated in parallel (RBSOR method). Implementation on vector computers results in a huge speed up: A factor of 500 speed up is achieved with the stiff code. The parallel code runs efficiently and close to the top speed of machines like the CRAY X-MP (160 MFLOPS) and the Fujitsu VP1100 (210 MFLOPS) rather than some 8 MFLOPS in scalar mode. A total speed up of a factor 12000 is thus achieved. This makes the numerical study of three dimensional pattern formation possible and thus direct comparison to biological experiments feasible.

TURING STRUCTURES IN MORPHOGENESIS

Originally Turing structures were suggested as prepatterns in morphogenesis. When two dimensional computer simulations appeared in the 1970's it became clear that patterns with wavelength much shorter than the dimensions of the embryo were hard to obtain reproducibly. This problem of stabilising certain short wave length patterns over other coexisting patterns may be solved by using Turing systems of the second kind Eq(9). The simplest such system is one in which rate constants (enzyme activation) vary with position along a gradient. This was shown to stabilise stripes perpendicular to the gradient. The problem of size regulation has been solved as well (Hunding and Sørensen, 1988). These recent developments make Turing patterns ideal candidates for spatial governors during early embryogenesis in the fruit fly *Drosophila*. Regions of activity of specific genes and their proteins are now available. The maternal genes *bicoid* and *nanos* provide gradients from the anterior and posterior ends of the egg respectively which in turn are used for activation of the gap genes. In the next level of the hierarchy the primary pair-rule genes appear. These genes are each expressed in a series of 7 stripes. The mechanism for the formation of these 'zebra' stripes is unknown. Activation by a combination of maternal and gap genes seems to be involved in the expression of particular stripes. Theoreticians have pointed out that the 'zebra' stripes alternatively may be generated by Turings mechanism, that is, by an autocatalytic reaction-diffusion system. The particular pair-rule stripes could then be activated by a combination of maternal, gap and Turing pattern interactions. Recent reviews have appeared by Ingham (1988), Hülskamp & Tautz (1991) and Pankratz & Jäckle (1990). References to Turing type models may be found in Hunding, Kauffman & Goodwin (1990).

Simulation of the pair-rule level is based on the following model. The maternal and gap genes are assumed to affect rate constants so that a Turing system of the second kind arises. This Turing system activates the pair-rule genes. Interactions among the pair-rule gene *eve* and other genes were build in mainly based on the study of *eve* patterns in gap and pair-rule mutants given by Carroll & Vavra (1988). Rate laws for the pair-rule genes following this model may be illustrated by *eve*:

$$\frac{d(eve)}{dt} = \frac{k_1}{1 + K_1(bcd)^n} \times \frac{(A)^n}{1 + K_2(A)^n} \times \frac{1}{1 + K_3(runt)^m} \times f(gap) \quad (10)$$



Figure 1: Computer simulated patterns of zebra stripes in *Drosophila*. Gene *eve* in wild type, *hb-* and *gt-* respectively. The deletions and enhancements of stripes as seen experimentally are captured by the computer model.

The substance A is one of the components of the stripe defining Turing system, which is activating *eve* expression. Both A, *bcd* and *runt* repression are here taken to be cooperative with Hill constants n and m greater than two. The last term $f(\text{gap})$ may be included to define activation or repression by cues defined by combinations of gap (or maternal) genes. The stabilization of the Turing zebra stripes is mainly due to the gradients from the *bcd*, *nos* system. Slight addition of influence from the gap genes has the role of enhancing the amplitude of the stripes in the central region. This model is robust towards gap gene mutants as the zebra stripe pattern is basically undistorted.

What emerges is then a robust zebra stripe prepattern which is then converted to actual activated genes quite possibly by specific combinations of gap genes acting as crude activators in their common regions. That is the system of such cues is not the stripe *generator* but essential for activating pair rule genes in specific regions over the Turing pattern.

Thus the model proposed on the basis of the present numerical study may be said to combine the two current rivaling models, as it indicates that cues are necessary to explain the experimentally observed result on zebra stripes caused by gap mutants, but Turing stripes are necessary to provide a stable underlying stripe generator.

Computed patterns for the most successful model so far is given in Figure 1. Stable zebra stripes are obtained and the results of some mutant calculations are given as well. Although the exact effect is not the same as what is seen experimentally in such mutants, several of the qualitative aspects are captured by the present computer model.

References

- [1] Carroll S. B. and Vavra S. H. The zygotic control of *Drosophila* pair-rule gene expression II. Spatial repression by gap and pair-rule gene products. *Development* 107, 673-683, 1989.
- [2] Hunding A. and Brøns M. Bifurcation in a spherical reaction-diffusion system with imposed gradient. *Physica D* 44, 285-302, 1990.
- [3] Hunding A, Kauffman S. A. & Goodwin B. *Drosophila* segmentation: Supercomputer simulation of prepattern hierarchy. *J. theor. Biol.* 145, 369-384, 1990.
- [4] Hunding A. and Sørensen, P. G. Size adaptation of Turing prepatterns, *J. Math. Biol.* 26, 27-39 (1988).
- [5] Hülkamp M. and Tautz D. Gap genes and gradients - the logic behind the gaps. *BioEssays* 13, 261-268, 1991.
- [6] Ingham P. W. The molecular genetics of embryonic pattern formation in *Drosophila* *Nature* 335, 25-34, 1988.
- [7] Pankratz M. J. and Jäckle H. Making stripes in the *Drosophila* embryo. *Trends in genetics* 6, 287-292, 1990.
- [8] Turing A.M. The chemical basis for morphogenesis. *Phil. Trans. R. Soc. London* B237, 37-72, 1952.

NONLINEAR FORECASTING OF RR-INTERVALS OF HUMAN ELECTROCARDIOGRAMS

Bodil L. Jørgensen^{1,2}, Anders Junker³, Hans Mickley³, Mogens Møller³,
Edmund Christiansen¹ and Lars F. Olsen²

¹ Institute of Mathematics and Computer Science

² Institute of Biochemistry

Odense University, Campusvej 55, DK-5230 Odense M, Denmark

³ Department of Cardiology, Odense University Hospital
DK-5000 Odense C, Denmark

INTRODUCTION

The heart is a typical nonlinear oscillator. In mammals the heartbeat is controlled by the heart's own pacemaker, called the *sinoatrial node* (SAN), which emits electrical pulses, that trigger the contraction of the heart muscle. The isolated SAN is a periodic oscillator¹, but in the intact heart the node is controlled by the autonomic nervous system. Parasympathetic nerves reduce the rate and sympathetic nerves increase the rate at which the SAN 'fires' its electrical pulses. The two types of nerves are therefore in a constant 'fight' to control the electrical activity of the SAN resulting in substantial fluctuations in the time intervals (RR-intervals) between successive heartbeats in healthy subjects. Recent studies of these fluctuations in RR-intervals as well as of whole electrocardiograms using nonlinear methods have indicated that the dynamics of the heart is chaotic²⁻⁴. On the other hand it has been known for more than a decade that certain heart dysfunctions and severe diabetes can be associated with a loss in the variability of the RR-intervals^{5,6}, suggesting that during these illnesses the heartbeat becomes more regular and hence 'less' chaotic. In this study we employ nonlinear forecasting to analyze the RR-intervals of electro-cardiograms from 120 patients who have experienced their first myocardial infarction, and 35 normal subjects. The purpose of this study was to evaluate if nonlinear forecasting could be used to characterize the dynamics of the heart and in particular if this method would reveal any differences between the normal subjects and the patients.

METHODS

Patient population. The patients were men of age 30 to 70 years, hospitalized at Odense University Hospital with a first acute myocardial infarction. Patients with insulin-dependent diabetes mellitus, permanent cardiac pacemaker and other chronic disabling

diseases were not included in the study. Also patients with conduction and rhythm disturbances on the 12 lead electrocardiogram at rest were excluded from analysis. At the same time other clinical data have been collected. These include exercise-ekg, ecco-cardiography and ST-segment analysis on Holter tapes. Consequently, the patient group is extremely well described. The normal subjects were men of the same age group as the patients who had volunteered for the study.

Follow up. All patients were followed up at regular intervals in the outpatient clinic including ambulatory monitoring. Primary endpoints were occurrence of arrhythmic or ischemic events. For patients who died, mode of death was determined.

Long-term electrocardiographic monitoring and analysis. Twenty-four hour ambulatory monitoring was initiated at discharge (median 11 days after infarction) with a 2-channel tape recorder (Tracker Reynolds). At the time of discharge the patients were fully mobilized with 6-8 hours of sleep and were encouraged to engage in normal daily activities. Tapes were analyzed for the presence of arrhythmias and fluctuations in RR-intervals on a commercially available device for tape-analysis (Pathfinder III ST, Reynolds). The tapes were analyzed visually to ensure that normal and extrasystolic beats were triggering the equipment correctly. The tapes were then digitized and transferred to a Personal Computer. Each beat was tagged as normal or not-normal according to its recognition by an algorithm used during tape analysis. Only normal-to-normal RR-intervals were used in the study.

Nonlinear forecasting Chaotic systems possess a property called 'sensitive dependence on initial conditions', and this property precludes long-term predictions. Nevertheless, attempts to predict the future in a chaotic time series can provide useful information about the system producing the time series, and may eventually be used as an alternative procedure for identifying chaotic dynamics. Special routines, called nonlinear forecasting programs, have been developed for such predictions^{8,9}. Basically these programs find states in the neighbourhood of a point, $X(t)$, whose future is to be predicted. The neighbouring points are chosen from previous records of states. To make a prediction we first fit a local chart that maps points of the neighbourhood into their future values and then evaluate the chart to $X(t)$. The procedure used here is similar to the zero-order local approximation described by Farmer and Sidorowich⁸. The method was applied to 15-20,000 RR-intervals recorded while the person was asleep. The RR-intervals were embedded in two dimensions as (RR_n, RR_{n+1}) using the reconstruction scheme proposed by Takens¹⁰. The first one third of the data was used to generate a library of patterns which then was used to make predictions of each of the remaining two thirds of data with prediction periods ranging from one to ten RR-intervals. For each prediction interval the correlation coefficient between predicted and observed RR-intervals was calculated.

RESULTS AND DISCUSSION

Fig. 1 shows the correlation coefficient versus the prediction period (T_p , measured as number of RR-intervals) for two normal subjects and two patients of age 55-58 years. We note that for all persons the predictability declines with increasing prediction period. This type of predictability profile is typical of chaotic dynamics, although it cannot be taken as unambiguous evidence for such dynamics⁹. We also note that in the patients the decline in predictability is slower compared to the normal subjects. As opposed to the pattern shown in Fig. 1 a completely random fluctuation would always give correlation coefficients close to zero independent of the length of the prediction interval, whereas dynamics corresponding to a periodic cycle would yield correlation coefficients close to one, also independent of the prediction period. It should be mentioned, however, that autocorrelated noise may show a similar predictability profile to those of Fig. 1⁹.

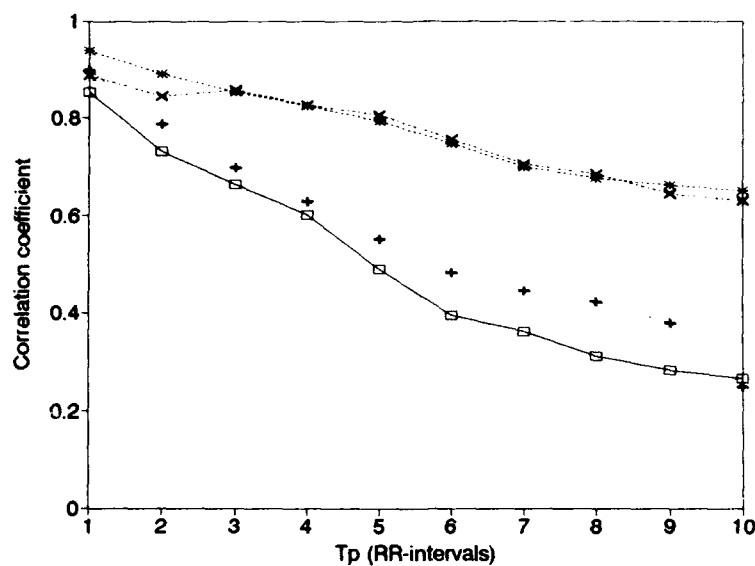


Figure 1. Correlation coefficient versus prediction time (T_p) for two normal subjects (—□— and —+—) and two patients (—x— and —*—).

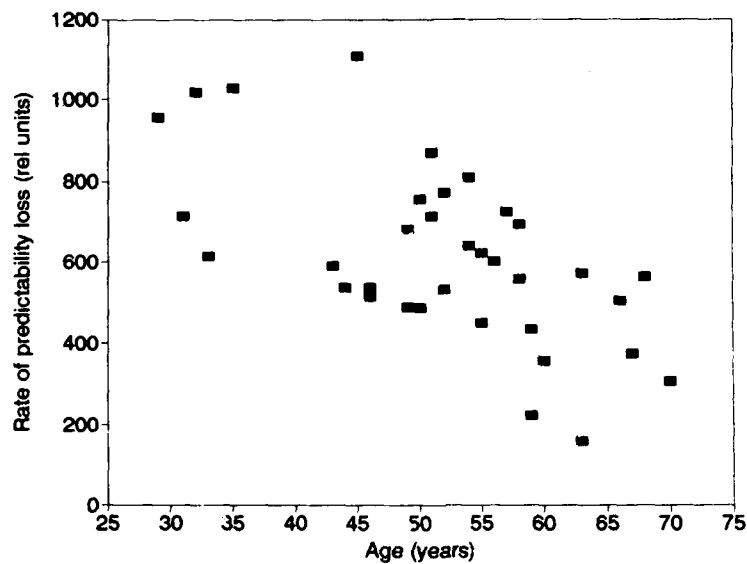


Figure 2. Rate of loss of predictability versus age for the 35 normal subjects. The rate is obtained as the slope calculated over the first 5 intervals of the curves corresponding to Fig. 1.

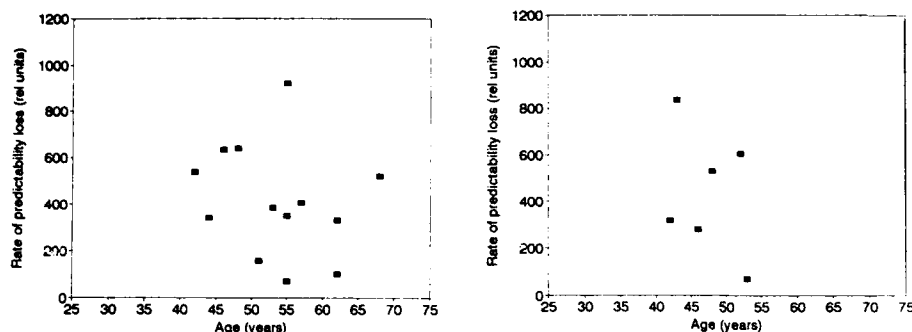


Figure 3. Rate of loss of predictability versus the age for 13 patients who experienced a second myocardial infarction during the follow up period (left) and 6 patients where sudden cardiac death or ventricular fibrillation occurred (right).

Fig. 2 shows a plot of the rate of loss of predictability versus age for the normal subjects. We note that the rate declines with increasing age, suggesting that the complexity of heart dynamics declines with age. Interestingly, computing the correlation dimensions of electrocardiograms, Kaplan et al¹¹ found a similar decline in complexity of the dynamics of electrocardiograms with age.

Fig. 3 shows similar plots to that of Fig. 2 for 13 patients who experienced a second myocardial infarction (MI) and 6 patients where sudden cardiac death (SCD) or ventricular fibrillation (VT) occurred. We note that 9 of the MI-patients and 3 of the SCD- and VT-patients have predictabilities which are substantially higher than the corresponding predictabilities of normal subjects of the same age. Thus, there seems to be a tendency that those heart patients, that experience major post infarction complications have more predictable electrocardiograms than the normal subjects.

REFERENCES

1. A. Noma, Mechanisms underlying cessation of rabbit sinoatrial node pacemaker activity in high potassium solutions, *Jap. J. Physiol.* 26:619 (1976).
2. A. Babloyantz and A. Destexhe, Is the normal heart a periodic oscillator, *Biol. Cybern.* 58:203 (1988).
3. M. Courtemanche, L. Glass, J. Belair, D. Scagliotti and D. Gordon, A circle map in the human heart, *Physica* 40D:299 (1989).
4. F. Ravelli and R. Antolini, Complex dynamics underlying the human electrocardiogram, *Biol. Cybern.* 67:57 (1992).
5. R.E. Kleiger, J.P. Miller, J.T. Bigger, A.J. Moss and the Multicenter Post-Infarction Research Group, Decreased heart rate variability and its association with increased mortality after acute myocardial infarction, *Am. J. Cardiol.* 59:256 (1987).
6. D.J. Ewing, J.M.M. Neilson, C.M. Shapiro, J.A. Stewart and W. Reid, Twenty four hour heart rate variability: effects of posture, sleep, and time of day in healthy controls and comparison with bedside tests of autonomic function in diabetic patients, *Br. Heart J.* 65:239 (1991).
7. D. Ruelle, Sensitive dependence on initial conditions and turbulent behavior in dynamical systems, *Ann. N.Y. Acad. Sci.* 316:408 (1979).
8. J.D. Farmer and J.J. Sidorowich, Predicting chaotic time series, *Phys. Rev. Lett.* 59:845 (1987).
9. G. Sugihara and R.M. May, Nonlinear forecasting as a way of distinguishing chaos from measurement error in time series, *Nature* 344:734 (1990).
10. F. Takens, Detecting strange attractors in turbulence, *Lect. Notes Math.* 898:366 (1981).
11. D.T. Kaplan, M.I. Furman, S.M. Pincus, S.M. Ryan, L.A. Lipsitz and A.L. Goldberger, Aging and the complexity of cardiovascular dynamics, *Biophys. J.* 59:945 (1991).

**THE ULTRADIAN CLOCK INTERACTS WITH
THE MITOTIC OSCILLATOR TO GIVE
DISPERSED AND QUANTIZED CELL CYCLE
TIMES. NOISY OR CHAOTIC TRAJECTORIES ?**

David Lloyd,¹ Alun L. Lloyd,² Lars Folke Olsen,³ Maksim N. Stolyarov⁴
and Evgenii I. Volkov⁴

¹Microbiology Group (PABIO), Univ. Wales College of Cardiff, P.O. Box
915, Cardiff CF1 3TL, Wales, UK

²Trinity College, Cambridge CB2 1TQ, England

³Biokemisk Institut, Odense Universitet, Campusvej 55, DK 5230 Odense
M, Denmark

⁴Department of Theoretical Biophysics, P.N. Lebedev Institute, Leninskii 53
Moscow, Russia

INTRODUCTION

In biological systems the cell is the unit of structure and function. Proliferation depends on the growth of individual cells followed by their division. This process, the cell division cycle, is rigorously controlled (Lloyd *et al.*, 1982b), and the elucidation of the mechanisms involved is the most central and important task in biological research. As well as providing new insights into normal growth processes, an understanding of dynamical models will provide a basis for the prevention of the abnormal uncontrolled proliferation characteristic of cancer (Gilbert and MacKinnon, 1992).

A number of simple limit-cycle models have been proposed (Sel'kov, 1970; Gilbert, 1974; Klevecz, 1976; Chernavskii *et al.*, 1977) to account for the cycle of processes whereby cells grow and divide, and biochemically plausible paired state variables (x,y) are easily identifiable (protein thiols / disulphides, phosphorylated proteins etc). However, individual cells have widely differing cell cycle times; the coefficient of variation sometimes reaches 15-25% (Brooks, 1985); this variability is usually modelled by inclusion of a "noise term" to take account of stochastic events (Gilbert, 1981; Mustafin and Volkov, 1977; Lloyd and Volkov, 1990). A further source of variability in cell division times is observed as a quantization, whereby incremental increases correspond to the period of a temperature-compensated oscillator (the ultradian clock), Lloyd *et al.*, 1982a; Lloyd and Kippert, 1987. Both dispersion and quantization can be simulated by a system in which ultradian clock pulses interact with the mitotic relaxation oscillator (Lloyd and Volkov, 1990; 1991; Lloyd, 1992). Here we show, that for certain parameter values, it is not necessary to use a "noise term" as the interacting oscillators can show chaotic dynamics.

THE MODEL

The following system of equations (Chernavskii *et al.*, 1977; Lloyd and Volkov 1990; 1991) was employed in which the cell cycle oscillator has a slow variable (τ_L of the order of hours) and a fast variable (τ_R of the order of minutes):

$$\begin{aligned}\tau_L \frac{dL}{dt} &= \eta - 2LR - DL \\ \tau_R \frac{dR}{dt} &= H + LR - R^2 - \frac{\gamma R}{(R + \delta)}\end{aligned}\quad (1)$$

where L and R are concentration terms, τ_L and τ_R are the characteristic times, and η , D , H , γ and δ are velocity constants.

Modulation by an output of the ultradian clock, period T_{UR} is simulated by the introduction of a harmonic term as a forcing function into the slow equation, which then becomes:

$$\tau_L \frac{dL}{dt} = \eta - 2LR - DL + C \sin \Omega t \quad (2)$$

where

$$T_{UR} = 2\pi / \Omega \ll T_{\text{cell cycle}}$$

The auto-oscillating solution considers that cells divide when $L(t)$ reaches a threshold to initiate a rapid phase of the cycle.

COMPUTER SIMULATIONS

Dynamic structure of the equations was studied numerically.

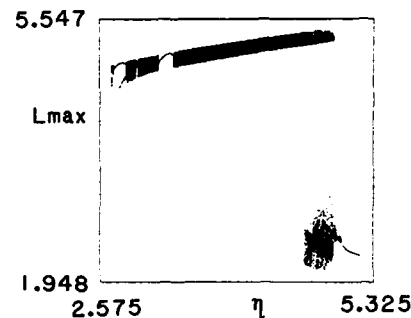


FIGURE 1. Bifurcation diagram for the model described in eqns. (1) and (2) as η varies between 2.5 and 5.2. For each value of η , 100 maxima of L are plotted following a transient of 100 time units. Other parameters were as follows : $D = 0.4$, $H = 0.15$, $\gamma = 1.5$, $\delta = 0.15$, $C = 0.45$, $\Omega = 5.0$, $\tau_L = 1$, and $\tau_R = 0.1$.

The bifurcation diagram (L_{\max} vs. η , Fig. 1) shows that a chaotic region begins at $\eta = 4.65$ and gives way to simple periodic oscillation at $\eta = 5.0$; the route to chaos is via a quasiperiodic regime. A time-one map (R vs. L at time intervals of T_{UR} , Fig. 2) has an intricate structure.

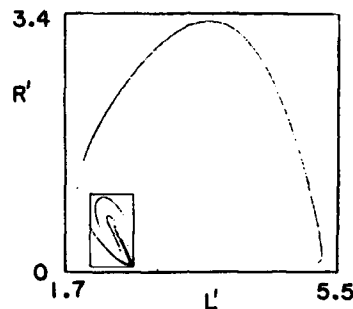


FIGURE 2. Time-one map of the simulation for $\eta = 4.95$. 50 000 corresponding values of R and L are plotted at intervals of $T_{UR} = 2\pi / \Omega$.

Calculation of the correlation dimension, D_2 (Grassberger and Procaccia, 1983) gave a value of 1.95, confirming the presence of a chaotic attractor. Lyapunov exponents (Wolf *et al.*, 1985), in bit per unit time, were $\lambda_1 = 0.21$, $\lambda_2 = 0$, $\lambda_3 = -6.32$ and the Lyapunov dimension $D_L = 2.03$. The positive value of λ_1 and non-integer D_L confirm chaotic dynamics. A relative frequency plot of cell cycle times for $\eta = 4.95$ shows a trimodal distribution with negatively - skewed dispersions (Fig. 3c): for comparison we also present (Fig. 3a,b) experimental data obtained by precise measurement of individual cell division times for the protozoan *Paramecium tetraurelia* (Lloyd and Kippert, 1987), and computer simulated results for a noisy relaxation oscillator (Lloyd and Volkov, 1990).

CONCLUSIONS

In the model presented here, dispersion and quantization of cell division times arises as a consequence of the interaction of two oscillators (the cell cycle oscillator and the ultradian clock) in the absence of external noise. Other models have invoked the presence of a chaotic attractor in cell cycle dynamics (Engleberg, 1968; Mackey, 1985; Mackey *et al.*, 1986; Grasman, 1990), but the present model is based on plausible biochemical processes (for the cell cycle oscillator) and an experimentally demonstrated intracellular timekeeper (the ultradian clock; Lloyd, 1992). It results in a frequency distribution of cell division times which closely resembles those observed for animal cells (Klevecz, 1976) and single-celled organisms (Lloyd and Kippert, 1987). It remains to be established that evolutionary selection of chaotic cell division dynamics may have certain advantages not seen for noisy dynamics, e.g. robust defence against perturbations, ease of synchronous coupling of dynamics between individuals of a population or in a multicellular tissue, construction of long period oscillations from high frequency ones (Klevecz, 1992).

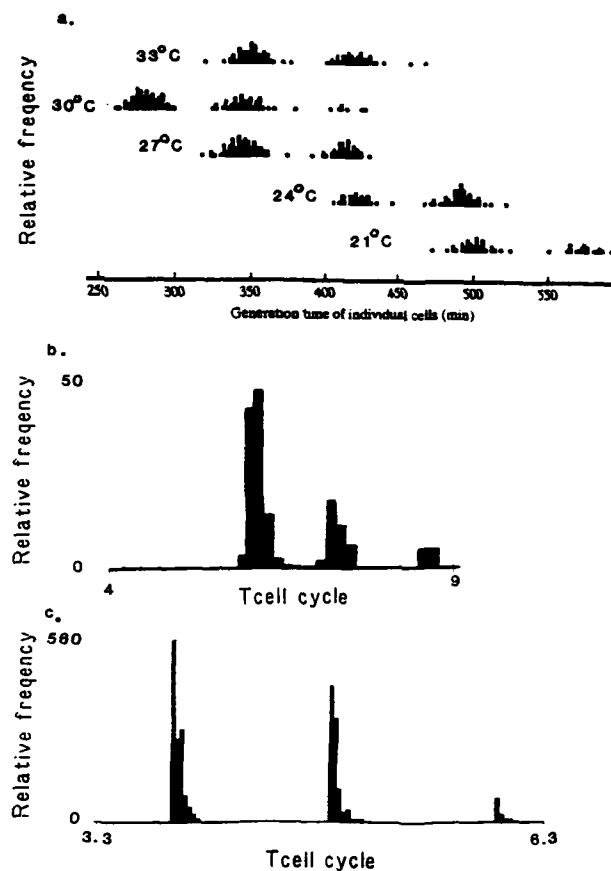


FIGURE 3. Quantized cell cycle times. (a) Experimentally observed distributions of times of individual *Paramecium tetraurelia* cells at various steady-state growth temperatures. Each square represents timing of division of an isolated organism. (Reproduced with permission from Lloyd and Kippert, 1987). (b) Generation time distributions from the model system incorporating noise (Lloyd and Volkov, 1990, Eq. 3) when $D = 0.4$, $H = 0.15$, $\gamma = 1.5$, $\delta = 0.15$, $C = 0.45$, $T_{UR} = 1.25$, $\eta = 5.55$, $\Delta\eta = 0.3$, $\zeta = \text{random numbers, } \in [0, 1]$, $\tau_L = 1$, and $\tau_R = 0.1$. (c) Frequency distribution of cell cycle times ($T_{\text{cell cycle}}$) for parameter values as follows: $\eta = 4.95$, $D = 0.4$, $H = 0.15$, $\gamma = 1.5$, $\delta = 0.15$, $C = 0.45$, $\Omega = 5.0$, $\tau_L = 1$, and $\tau_R = 0.1$.

ACKNOWLEDGMENTS

Supported by the Royal Society, the Danish Natural Science Council and the Eddington Fund, Trinity College.

REFERENCES

- Brooks, R. F., 1985, The transition probability model: successes, limitations and deficiencies, in "Temporal Order", L. Rensing and N. I. Jaeger, eds., Springer-Verlag, Berlin.
- Chernavskii, D. S., Palamarchuk, E. K., Polezhaev, A. A., Solyanik, G. I., and Burlakova, E. B., 1977, Mathematical model of periodic processes in membranes with application to cell cycle regulation, *BioSystems* 9 : 187.
- Engleberg, J., 1968, On deterministic origins of mitotic variability, *J. Theoret. Biol.* 20 : 249.
- Gilbert, D. A., 1974, The nature of the cell cycle and the control of cell proliferation, *BioSystems* 5 : 197.
- Gilbert, D. A., and MacKinnon, H., 1992, Oscillations and cancer, in "Ultradian Rhythms in Life Processes", D. Lloyd and E. L. Rossi, eds., Springer-Verlag, London.
- Grasman, J., 1990, A deterministic model of the cell cycle, *Bull. Math. Biol.* 52 : 535.
- Grassberger, P., and Procaccia, I., 1983, Measuring the strangeness of strange attractors, *Physica 9D* : 189.
- Klevecz, R.R., 1976, Quantized generation times in mammalian cells as an expression of the cellular clock, *Proc. Natl. Acad. Sci. U.S.A.* 73 : 4012.
- Klevecz, R.R., 1992, A precise circadian clock from chaotic cell cycle oscillations, in "Ultradian Rhythms in Life Processes", D. Lloyd and E. L. Rossi, eds., Springer-Verlag, London.
- Lloyd, D., 1992, Intracellular time keeping: epigenetic oscillations reveal the functions of an ultradian clock, in "Ultradian Rhythms in Life Processes", D. Lloyd and E. L. Rossi, eds., Springer-Verlag, London.
- Lloyd, D., and Kippert, F., 1987, A temperature-compensated ultradian clock explains temperature-dependent quantal cell cycle times, in "Temperature and Animal Cells", K. Bowler and B. J. Fuller, eds., Cambridge University Press.
- Lloyd, D., and Volkov, E. I., 1990, Quantized cell cycle times: interaction between a relaxation oscillator and ultradian clock pulses, *BioSystems* 23 : 305.
- Lloyd, D., and Volkov, E. I., 1991, The ultradian clock: timekeeping for intracellular dynamics, in "Complexity, Chaos and Biological Evolution", E. Mosekilde and L. Mosekilde, eds., Plenum Press, New York.
- Lloyd, D., Edwards, S. W., and Fry, J. C., 1982a, Temperature-compensated oscillations in respiration and cellular protein content in synchronous cultures of *Acanthamoeba castellanii*, *Proc. Natl. Acad. Sci. U.S.A.* 79 : 3785.
- Lloyd, D., Poole, R. K., and Edwards, S. W., 1982b, The Cell Division Cycle: Temporal Organization and Control of Cellular Growth and Reproduction, Academic Press, London.
- Mackey, M. C., 1985, A deterministic cell cycle model with transition probability-like behaviour, in "Temporal Order", L. Rensing and N. I. Jaeger, eds., Springer-Verlag, Berlin.
- Mackey, M. C., Santavy, M., and Seleпова, P., 1986, A mitotic oscillator with a strange attractor and distributions of cell cycle times, in "Nonlinear Oscillations in Biology and Chemistry", H. Othmer, ed., Springer-Verlag, Berlin.
- Mustafin, A. T., and Volkov, E. I., 1977, On the distribution of cell generation times, *BioSystems* 15 : 111.
- Sel'kov, E. E., 1970, Two alternative self-oscillating stationary states in thiol metabolism - two alternative types of cell division normal and malignant ones, *Biophysika* 15 : 1065.
- Wolf, A., Swift, J. B., Swinney, H. L., and Vastano, J. A., 1985, Determining Lyapunov exponents from a time series, *Physica 16D* : 285.

A SOLITONIC MODEL FOR THE "INFORMATION STRINGS"

M.V. Sataric⁽¹⁾, J.A. Tuszyński⁽²⁾ and R.B. Žakula⁽³⁾

⁽¹⁾ Faculty of Technical Sciences, 21000 Novi Sad
F.R. Yugoslavia

⁽²⁾ Department of Physics, University of Alberta
Edmonton, Canada, T6G 2J1

⁽³⁾ Institute of Nuclear Sciences "Boris Kidrič"
Belgrade, F.R. Yugoslavia

Abstract An attempt is made to provide physical picture of transfer of informations in cell microtubules. The quantitative model adopted for this purpose is classical u^4 -model in the presence of a constant intrinsic electric field. It is demonstrated that soliton formation in the form of kinks may be energetically favorable under realistic conditions of physical parameter values.

INTRODUCTION

Of the various filamentary structures which comprise the cytoskeleton, microtubules (MT's) are the most prominent ones. Their structure and function is best characterized and they appear to be very suited for dynamic information processing^[1].

MT's represent hollow cylinders formed by protofilaments aligned along their axes (see Fig.1) and whose lengths may span macroscopic dimensions.

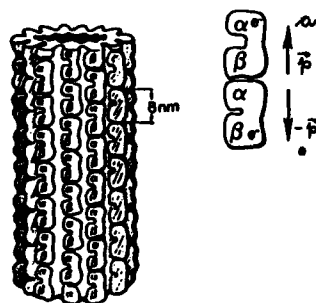


Figure 1. Left: MT structure from x-ray diffraction crystallography. Right top: MT-tubulin dimer subunits composed of α - and β -monomers.

In vivo, the cylindrical walls of MT's are assemblies of 13 longitudinal protofilaments each of which is a series of subunit proteins known as tubulin dimers. Each tubulin subunit is a polar, 8-nm dimer. It consists of two, slightly different 4-nm monomers with molecular weight of 55 kilodaltons. Each dimer may be viewed as an electric dipole \vec{p} which arises from the fact that 18 calcium ions (Ca^{++}) are bound within each dimer. Thus, MT's can be identified as "electrets" or oriented assemblies of dipoles. Barnett^[2] proposed that filamentary cytoskeletal structures may operate much like information strings analogous to semiconductor word processors. He conjectured that MT's are processing channels along which strings of bits of information can move.

THE PHYSICAL MODEL

In the theoretical model that is put forward here the basic assumption is that the dipoles within protofilaments form a system of oscillators with only one degree of freedom (DF) collinear with axys of MT. This DF is the longitudinal displacement of center of mass of dimers at the position n denoted by u_n so that we have model Hamiltonian as follows

$$H = \sum_{n=1}^N \left[\frac{1}{2} M \left(\frac{\partial u_n}{\partial t} \right)^2 + \frac{1}{4} k (u_{n+1} - u_n)^2 - \frac{A}{2} u_n^2 + \frac{B}{4} u_n^4 - c u_n \right] \quad (1)$$

The first term on the right hand side (1) represents the kinetic energy of the longitudinal displacement of one dimer with effective mass M . If the stiffness parameter k is sufficiently large long wavelength excitations of the displacement field will be formed. The parameters A and B involved in double-well potential have the following meanings; A is usually assumed to be a linear function of temperature and B is a positive, temperature-independent crystalline-field quartic coefficient.

The last term in eq.(1) arises from the experimental fact that the cylinder of a MT taken as a whole represents one giant dipole. Together with the polarized water surrounding it, MT generates a nearly uniform intrinsic electric field (IEF) with the magnitude E parallel to its axis. So it is legitimate that the additional potential energy of a dipole due to the electric field is

$$V_{el} = -c u_n ; \quad c = q_{eff} E , \quad (2)$$

where q_{eff} denotes the effective charge of a single dimer. If we finally consider the viscosity of the solvent taking into account the viscous force acting on the dimer's motion

$$F = -\gamma \frac{\partial u_n}{\partial t} , \quad (3)$$

where γ represents the damping coefficient (DC), the equation of motion for system (1) in the continuum approximation becomes

$$M \frac{\partial^2 u}{\partial t^2} - k R_0^2 \frac{\partial^2 u}{\partial x^2} - A u + B u^3 + \gamma \frac{\partial u}{\partial t} - q_{eff} E = 0 \quad (4)$$

where R_0 represents the equilibrium separation between centers of adjacent dimers, and x-axis is aligned along the MT's axis. The equation (4) has a unique bounded kink-like excitation (KLE)

$$u(\xi) = \left(\frac{|A|}{B}\right)^{1/2} \left\{ 1 - \frac{\sigma}{2} - 2[1 + \exp(\sqrt{2}\xi)]^{-1} \right\} \quad (5)$$

where we use the set of denotations

$$\left. \begin{aligned} \xi &= \left(\frac{|A|}{M(v_0^2 - v^2)}\right)^{1/2} (x - vt) \quad ; \quad v_0 = R_0 \left(\frac{k}{M}\right)^{1/2} \\ \sigma &= q_{eff} B^{1/2} (|A|)^{-3/2} \cdot E \end{aligned} \right\} \quad (6)$$

The main point is that the above bounded solution (5) propagates along the protofilament with a fixed terminal velocity v which depends on the IEF. We now assess the magnitude E of IEF at least semi-quantitative. We take into account that MT's length L is much greater than the diameter of its cylinder which is physically quite reasonable. Hence, for the positions along the MT which are far enough from its ends, we simply have

$$E = \frac{Q_{eff}}{4\pi\epsilon_0 r^2} \quad (7)$$

where Q_{eff} represents the effective charge on the MT ends while r denotes the distance from one end to the relevant point along MT. If we suppose that one MT is moderately long $L = 10^{-6}m$, the effective charge consists then of 2×13 protofilament ends each of which has a charge of $18 \times 2e$ ($e = 1,6 \cdot 10^{-19}C$). Consequently $Q_{eff} \simeq 10^3 e$ so that we estimate $E \sim 10^6 \frac{V}{m}$.

In the other hand, at present we do not have the exact values of the crystalline-field coefficients A and B for MT but we will do a rough assess taking $A \sim 500 Jm^{-2}$ for $T = 300^\circ K$ and $B \sim 10^{24} Jm^{-1}$.

Using these estimations the dimensionless parameter σ from eq.(6) has the following order of magnitude

$$\sigma \simeq 5 \cdot 10^{-10} \cdot E \quad (8)$$

It is therefore clear that even for strong fields the inequality $\sigma \ll 1$ holds.

It implies that the travelling terminal velocity of KLE is small in comparison with the sound velocity ($v \ll v_0$). This brings about the simple relation between terminal velocity and IEF as follows

$$v = \frac{3v_0}{\gamma|A|} \left(\frac{MB}{2}\right)^{1/2} q_{eff} \cdot E \quad (9)$$

In other words, we have obtained a linear response relationship. Then, the corresponding KLE mobility μ may be introduced as follows

$$\mu = \frac{3v_0}{\gamma|A|} \left(\frac{MB}{2}\right)^{1/2} q_{eff} \quad (10)$$

In order to estimate KLE mobility it is necessary to assess the DC (γ) using simple considerations from fluid mechanics. First of all, each dimer could be approximated by a sphere with mass M . The drag force exerted by the fluid on the sphere is thus

$$F_v = -6\pi R\eta \frac{\partial u}{\partial t} = -\gamma \frac{\partial u}{\partial t} \quad (11)$$

The absolute viscosity of water for physiological temperature ($300^\circ K$) has the following value $\eta = 7 \cdot 10^{-4} \text{ kgm}^{-1} \text{ s}^{-1}$. Inserting $R = 4 \cdot 10^{-9} \text{ m}$ into eq.(11) one obtains $\gamma = 5,6 \cdot 10^{-11} \text{ kg s}^{-1}$.

The final quantity to estimate is the sound velocity v_0 . Hakim et al's [3] experimental measurements of the sound velocity in DNA give the value $v_0 = 1,7 \cdot 10^3 \text{ ms}^{-1}$. Finally then, putting $M = 55 \cdot 10^3 \times 2 \cdot 10^{-27} \text{ kg} \simeq 1,1 \cdot 10^{-22} \text{ kg}$ and $q_{eff} = 18 \times 2 \times 1,6 \cdot 10^{-19} \text{ C}$, formula (10) gives approximately

$$\mu \simeq 3 \cdot 10^{-6} \text{ m}^2 \text{ V}^{-1} \text{ s}^{-1} \quad (12)$$

If the intrinsic field has the value $E = 10^5 \text{ Vm}^{-1}$ the KLE velocity is on the order of $v \simeq 0,3 \text{ ms}^{-1}$. The time of propagation of one KLE through one MT ($L \sim 10^{-6} \text{ m}$) is thus $\tau = Lv^{-1} \sim 3 \cdot 10^{-6} \text{ s}$. It is obvious then that increasing MT's length the time of information propagation as carried by KLE increases due to the following two reasons. First, the magnitude of the IEF decreases which results in decreasing the KLE velocity. Second, the length of the path increases. A very important physical parameter characterizing the MT's system is the polarization switching time τ_s . A crude estimate gives $\tau_s \sim (n_0 v)^{-1}$, where n_0 represents the number of KLE's per unit length. For typical ferroelectrics n_0 is on the order of 10^{-5} m and its value is almost temperature independent. Under these circumstances the switching time is in a $\mu \text{ sec}$ rang.

CONCLUSION

In this paper biophysical picture regarding the structure and function of MT's has been presented in order to motivate the proposed physical model of their nonlinear dipolar excitations. Model parameters have been estimated with the use of available experimental data. It was found that a unique bound solution exists which possesses a unique velocity of propagation proportional to the magnitude of the electric field. In addition to the intrinsic constant electric field one may also consider an additional externally applied electric field which could be seen as a significant control mechanism in KLE dynamics. For example, applying an external electric field to a microtubule may halt the KLE's motion and "freeze" the information carried by it.

REFERENCES

- [1] Dustin, P. (1984) Microtubules. Springer, Berlin;
- Hameroff, S.R. (1987) Ultimate Computing, North-Holland, Amsterdam;

- Rasmussen, S. Karamporsala, H. Vaidyanath, R. Jensen, K. and Hameroff, S. (1990) Physica D, 42, 428-449.
- [2] Barnett, M.P. (1987) Molecular systems to process analog and digital data associatively in Proceedings of the Thirs Molecular Electronic Device Conference (F. Carter. Ed.) Research Laboratory, Washington, D.C.
- [3] Hakim, M.B., Lindsay, S.M. and Powell, J. (1984) Biopolymers 23, 1185.

**ROTATING VORTICES INITIATION IN CARDIAC MUSCLE:
PULSE CHEMISTRY CONTROL**

C.F.Starmer¹, V.I.Krinsky², D.N.Romashko², R.R.Aliev²

¹Duke Univer. Medical Center, Durham,
USA, North Carolina, 27710

²Inst. Theor. & Exper. Biophysics, Pushchino,
Russia, 142292

Excitation wave in cardiac muscle is a strongly nonlinear wave, whose amplitude and form do not change during propagation. In this respect, it resembles a soliton, although the mechanisms of their propagation are quite different: the soliton spreads without decay only in one-dimensional media, while the electrochemical wave in the heart do not decay even in two and three dimensions.

The wave in the heart, as well as any wave, can diffract. However, in some respects it behaves similar to particles: two colliding waves annihilate. And again it differs from solitons, which can penetrate one through another. Wave in the heart belongs to the general class of autowaves.¹⁻³ They are governed by the reaction-diffusion equation: $dU/dt = D\Delta U + f(U)$, where $D\Delta U$ is the diffusion term, $f(U)$ - a nonlinear function.

The behavior of cardiac muscle can be modified by drugs. Many drugs can bind to only one of ionic channel states. This provides the basis for "pulse chemistry"⁴ where binding is possible during channel residence in one state while unbinding is permitted during channel residence in other states. Pulse chemistry thus provides a dynamic way to modify vortex formation and maintenance.⁴ If a drug binds to inactivated channels, then

$$db/dt = kd(1-b)(1-h) - lb \quad (1)$$

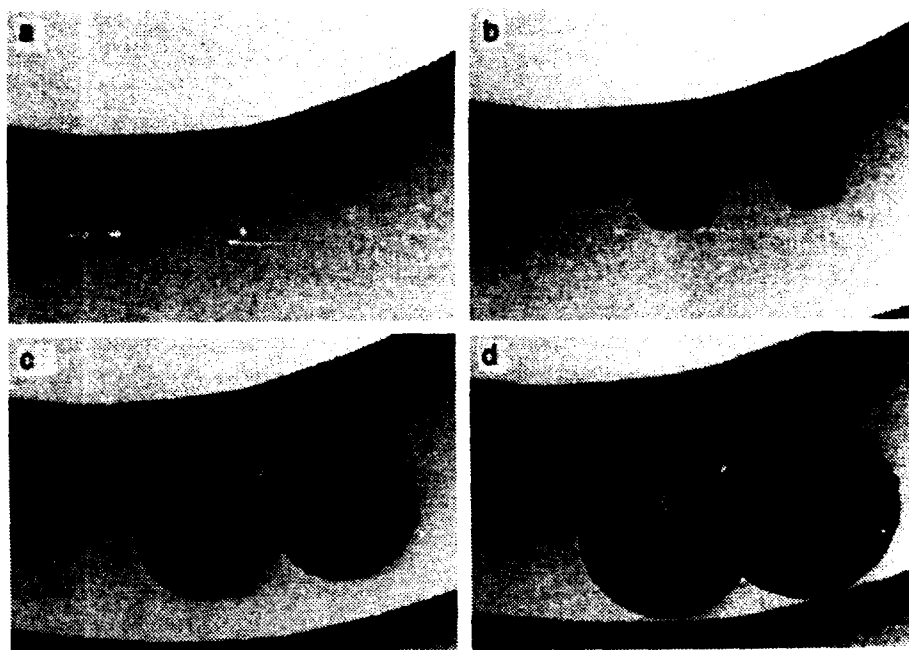


Figure 1. Experiments on 2D vulnerability (in BZ reaction).
Time: (a)- 0 s, (b)- 30 s, (c)- 85 s, (d)- 121 s.
Composition: Sodium Bromate, Malonic Acid and Sulfuric Acid:
0.25 M; Ferroin: 6.25 mM.

where b is the fraction of blocked channels, $(1-b)$ is the fraction of inactivated channels, d - drug concentration, k and l are constants of drug binding and unbinding. We studied vortex formation in the FHN equations expanded by eq. (1):

$$\begin{cases} C\partial E/\partial t = g_{Na}(1-b)(E-E_r^3/3-v_r) - g_K(v-v_r) + D\Delta E, \\ \partial v/\partial t = (V(E)-v)/\tau_v, \\ \partial b/\partial t = (B(E)-b)/\tau_b, \end{cases} \quad (2)$$

where E - membrane voltage, $g_K(v-v_r)$ - potassium current, g_{Na} - sodium conductance, $V(E)$ and $B(E)$ - steady state values of variables v and b ; and C , v_r , τ_v , τ_b - parameters.

In numerical and chemical experiments, vortices were initiated by two stimuli separated by time interval T .⁴ Range of T when stimuli led to vortices initiation (vulnerable window, VW) was determined. Evolution of three perturbations (seen as

dark points in (a)) is shown in Fig.1. The perturbations were imposed at different distances from the front. Only the perturbation in the center results in spiral wave formation (this corresponds to vulnerability).

Investigations of parameters influence on VW unexpectedly showed that widely used antiarrhythmic drugs - Na channel blockers - should increase VW and thus promote vortex initiation. We found that, at the contrary, K blockers should decrease VW and suppress vortex formation (Fig.2). This means that new effective antiarrhythmic drugs may be found among K blockers.

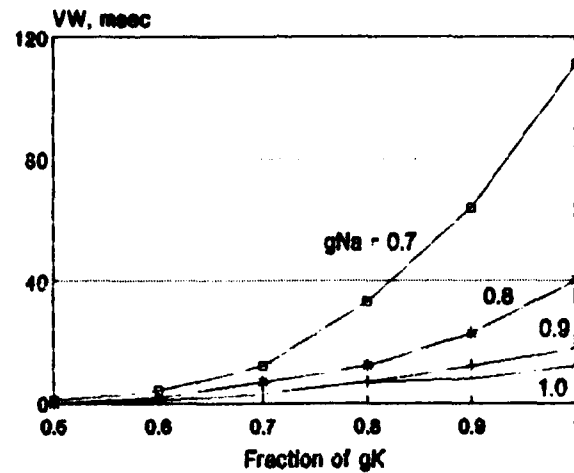


Figure 2. The dependencies of vulnerable window (VW) on g_K for different g_{Na} . Note that VW is always decreased as g_K falls.

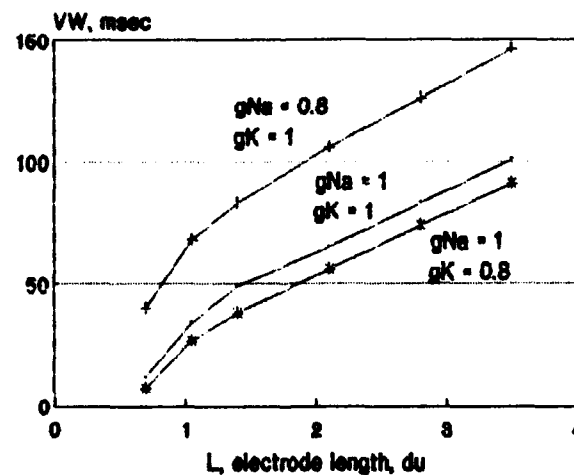


Figure 3. VW vs stimulating electrode length L . VW increases with electrode length. For large L ($L > 2$), function $VW(L)$ is linear.

The developed simple analytical theory, which is based on singular perturbation method, shows that VW is proportional to stimulating electrode length L (Fig.3): $VW = L_{\text{eff}}/V$, where V - wave velocity, $L_{\text{eff}} \approx L$.

The approach is based on the phase plane analysis of the media state at the points of stimulation. Vortex formation (vulnerability) is observed when excited region shrinks at one end of the stimulating electrode and expands at the other. It occurs when a point of the medium corresponding to zero-velocity propagation of the excitation front, is covered by the stimulating electrode. The appropriate time interval is L/V . The matter of the next-order approximations is the estimation of the difference ($L_{\text{eff}} - L$) and the deviation from linearity at small electrode size L .

Similar approaches can be used in analysis of vortices formation in three dimensional media.^{2,5}

References

1. A.C.Scott, "Active and Nonlinear Propagation in Electronics", Wiley-Interscience, N.Y. (1970).
2. "Self-Organization: Autowaves and Structures Far from Equilibrium", Ed.V.Krinsky, Springer-Verlag, Berlin (1984).
3. K.I.Agladze, V.I.Krinsky and A.M.Pertsov, Chaos in the non stirred B-Z reaction is induced by interaction of waves and stationary dissipative structures, *Nature*, 308:834 (1984).
4. C.F.Starmer, A.A.Lastra, V.V.Nesterenko, and A.O.Grant, Proarrhythmic response to sodium channel blockade, *Circ.* 84:1364 (1991).
5. A.M.Pertsov, R.R.Aliev and V.I.Krinsky, Three-dimensional twisted vortices in an excitable chemical medium, *Nature*, 345:419 (1990).

PARTICIPANTS

F. Kh. Abdullaev, Thermophysics Department, Uzbek Academy of Sciences,
700135 Tashkent - 135, Chilanzar, Uzbekistan,

Mariana Amato, Dipartimento di Produzione Vegetale, Università della
Basilicata, I-85100 Potenza, Italy

Serge Aubry, Laboratoire Léon Brillouin, CEN Saclay, F-91191 Gif-sur-Yvette Cedex
France

Philip Bagger, Røglevangen 3, Svogerslev, DK-4000 Roskilde, Denmark

Ole Bang, Laboratory of Applied Mathematical Physics, Technical University of
Denmark, DK-2800 Lyngby, Denmark

Paola Barbara, Dipartimento di Fisica, Università di Salerno,
I-84081 Baronissi SA, Italy

Mariette Barthes, Groupe Dynamique Phases Condensés, Université Montpellier II,
F-34095 Montpellier Cedex 05, France

Michele Bartuccelli, Department of Mathematical & Computing Sciences, University of
Surrey, Guildford, Surrey, GU2 5XH, UK

David N. Beratan, Department of Chemistry, University of Pittsburgh~
Pittsburgh, PA 15260, USA

Lisa Bernstein, 3234 Urey Hall, University of California San Diego,
La Jolla, CA 92093, USA

Alan Bishop, Theoretical Division & CNLS, Los Alamos National Laboratory,
Los Alamos, NM 87545, USA

Hannes Bolterauer, Institut für theoretische Physik der Universität Giessen,
D-6300 Giessen, Germany

Tassos Bountis, Department of Mathematics, University of Patras, 26110 Patras
Greece

Larisa S. Brizhik, Institute for Theoretical Physics Academy of Sciences of Ukraine,
Kiev, Ukraine

David W. Brown, Institute for Nonlinear Sciences, University of California, San Diego,
La Jolla, CA 92093-0402, USA

Robin K. Bullough, Department of Mathematics UMIST,
Manchester M60 1QD, UK

David Campbell, Department of Physics, University of Illinois,
Urbana, IL 61801, USA

Giorgio Careri, Dipartimento di Fisica, Università degli studi di Roma,
I-00185 Roma, Italy

Ioannis Chochliouros, Laboratoire de Modélisation en Mécanique Université Pierre et
Marie Curie, F-75252 Paris Cedex 05, France

Erik Adler Christensen, Laboratory of Applied Mathematical Physics
Technical University of Denmark, DK-2800 Lyngby, Denmark

Peter Leth Christiansen, Laboratory of Applied Mathematical Physics,
Technical University of Denmark, DK-2800 Lyngby, Denmark

Matteo Cirillo, Dipartimento di Fisica, Università di Roma "Tor Vergata",
I-00173 Roma, Italy

Christophe Claude, Institut für Theoretische Physik I, Heinrich-Heine Universität
Düsseldorf, D-4000 Düsseldorf, Germany

Giovanni Costabile, Dipartimento di Fisica, Università di Salerno,
I-84081 Baronissi SA, Italy

Leonor Cruzeiro-Hansson, Crystallography Department, Birkbeck College,
London WC1E 7HX, UK

Predrag Cvitanovic, Niels Bohr Institute,
DK-2100 Copenhagen, Denmark

Alfonso D'Anna, Physics Department, Technical University of Denmark,
DK-2800 Lyngby, Denmark

Sergei Darmanyan, Thermal Physics Department, Uzbek Academy of Sciences,
700135 - 135, Chiranzar, Uzbekistan

Alexander S. Davydov, Institute of Theoretical Physics, Academy of Sciences of Ukraine,
252143 Kiev, Ukraine

Silvana De Lillo, Dipartimento di Fisica, Università degli Studi di Perugia,
I-06100 Perugia, Italy

Palle Dinesen, Fensmarkgade 36, 3th.,
DK-2200 Copenhagen N, Denmark

E.N. Economou, Foundation for Research and Technology, Institute of Electronic
Structure & Lasers, Heraklion 71110, Greece

Thomas Eickermann, Institut für Theoretische Physik, University Düsseldorf,
D-4000 Düsseldorf, Germany

J. C. Eilbeck, Department of Mathematics, Heriot-Watt University Riccarton,
Edinburgh EH15 4AS, UK

Mark Eligh, Physics and Materials Science Department, Elsevier,
NL-1000 AC Amsterdam, Holland

Victor Z. Enol'skii, Department of Theoretical Physics, Institute for Metal Physics,
Kiev 42, 252680, Ukraine

Alexander Eremko, Institute for Theoretical Physics, Academy of Sciences of Ukraine,
252130 Kiev, Ukraine

Henrik Feddersen, Department of Mathematics, Heriot-Watt University Riccarton,
Edinburgh EH14 4AS, Scotland, UK

Giovanni Filatella, Department of Physics, Università di Salerno,
I-84081 Baronissi SA, Italy

F. Fillaux, LASIR, C.N.R.S., ~F-94320 Thiais,
France

Jan Finjord, Høgskolesenteret i Rogaland,
N-4004 Stavanger, Norway

Gerd Michael Fischer, Physics Department, Technical University of Denmark,
DK-2800 Lyngby, Denmark

N. Flytzanis, Physics Department, University of Crete,
Heraklion, Greece

Henrik Flyvbjerg, Niels Bohr Institute "Connect",
DK-2100 Copenhagen Ø, Denmark

A.P. Fordy, School of Mathematics, University of Leeds,
Leeds LS2 9JT, UK

Yu. B. Gaididei, Institute for Theoretical Physics Academy of Sciences of Ukraine,
Kiev 252130, Ukraine

Tommy Geisler, Danish Institute of Fundamental Metrology,
Technical University of Denmark, Bldg. 307, DK-2800 Lyngby, Denmark

Paola Giannattasio, Istituto di Fisica, Università di Salerno,
I-84081 Baronissi SA, Italy

Henriette Gilhøj, Laboratory of Applied Mathematical Physics, Technical University of
Denmark, DK-2800 Lyngby, Denmark

Celso Grebogi, Laboratory for Plasma Research, University of Maryland,
College Park, MD 20742, USA

Niels Grønbech-Jensen, Department of Applied Physics, Stanford University,
Stanford, California 94305, USA

Hichem Hadouaj, Laboratoire de Modélisation en Mécanique
Université Pierre et Marie Curie, F-75252 Paris Cedex 05, France

P.A. Hansson, Department of Medical Electronics, St. Bartholomew's Hospital~
West Smithfield, London EC1A 7BE, UK

Jarmo Hietarinta, Department of Physics, University of Turku,
SF-20500 Turku, Finland

Ryogo Hirota, Department of Information & Computer Sciences
Science & Engineering, Waseda University, Tokyo 169, Japan

Jesper Holm, Department of Physics, Technical University of Denmark,
DK-2800 Lyngby, Denmark

Axel Hunding, Kemisk Laboratorium 3, H.C. Ørsted Institute,
DK-2100 Copenhagen Ø, Denmark

Flemming If, Laboratory of Applied Mathematical Physics
Technical University of Denmark, DK-2800 Lyngby, Denmark

C. Schelde Jacobsen, Department of Physics, Technical University of Denmark,~
DK-2800 Lyngby, Denmark

Marek Jaworski, Institute of Physics Polish Academy of Sciences,
02 668 Warszawa, Poland

Michael Jørgensen, Laboratory of Applied Mathematical Physics,
Technical University of Denmark, DK-2800 Lyngby, Denmark

**Tomasz Kapitaniak, Institute of Applied Mechanics, Technical University of Lodz,
90-924 Lodz, Poland**

D.J. Kaup, Physics Department, Clarkson University, Potsdam, NY 13699, USA

**V.M. Kenkre, Department of Physics and Astronomy, University of New Mexico,
Albuquerque, NM 87131-1156, USA**

**Yuri S. Kivshar, Institut für Theoretische Physik I,
Heinrich-Heine-Universität Düsseldorf, D-4000 Düsseldorf, Germany**

**Carsten Knudsen, Department of Physics, Technical University of Denmark,
DK-2800 Lyngby, Denmark**

**Valentin Krinsky, Institute of Theoretical & Experimental Biophysics,
Pushchino Moscow Region, 142 292, Russia**

J. Krumhansl, 515 Station Road, Amherst, MA, USA

**Martin Kruskal, Department of Mathematics Hill Center, Rutgers University,
New Brunswick, NJ 08903, USA**

**Christoph Kuhn, Physikalische Chemie, ETH,
CH-8092 Zürich-Zentrum, Switzerland**

**Victor A. Kuprievich, Institute for Theoretical Physics
Academy of Sciences of Ukraine, 252130 Kiev, Ukraine**

**Tom Kuusela, Department of Applied Physics, University of Turku,
SF-20500 Turku, Finland**

**Anders Kühle, Department of Physics
Technical University of Denmark, DK-2800 Lyngby, Denmark**

**Britt Larsen, Department of Physics, Technical University of Denmark,
DK-2800 Lyngby, Denmark**

**Nikos Lazarides, Laboratory of Applied Mathematical Physics,
Technical University of Denmark, DK-2800 Lyngby, Denmark**

**Alun Lloyd, University of Wales,
Cardiff CF1 3TL, UK**

**David Lloyd, School of Pure and Applied Biology, University of Wales,
Cardiff CF1 3TL, UK**

Peter Lomdahl, Theoretical Division, T-11, Los Alamos National Laboratory,
Los Alamos, NM 87545, USA

Ole Lund, Department of Physics, Technical University of Denmark,
DK-2800 Lyngby, Denmark

Vagn Lundsgaard Hansen, Mathematical Institute, Technical University of Denmark
DK-2800 Lyngby, Denmark

Alan Luther, NORDITA,
DK-2100 Copenhagen Ø, Denmark

Jens Peter Lynov, Optics and Fluid Dynamics Department, Risø National Laboratory,
DK-4000 Roskilde, Denmark

Vladimir Makhankov, Joint Institute for Nuclear Research, LCTA,
Moscow 101000, Russia

Boris Malomed, Department of Applied Mathematics, Tel Aviv University,
Ramat Aviv 69978, Israel

Coraci P. Malta, Forschungszentrum, Jülich, Bochum,
Germany

Riccardo Mannella, Dipartimento di Fisica, Università di Pisa,
I-56100 Pisa, Italy

David W. McLaughlin, Department of Mathematics, Princeton University,
Princeton, NJ 08544 - 1000, USA

Peter Miller, Program in Applied Mathematics, University of Arizona,
Tucson, AZ 85721, USA

R.J. Dwayne Miller, Department of Chemistry, University of Rochester,
Rochester, New York 14627, USA

Linn F. Mollenauer, AT & T Bell Labs,
Holmdel NJ 07733, USA

Jerry Moloney, Department of Mathematics & Optical Sciences, University of Arizona,
Tucson, Arizona 85721, USA

Roberto Monaco, Istituto di Cibernetica del C.N.R.
Napoli, I-Arco Felice, NA, Italy

Erik Mosekilde, Department of Physics, Technical University of Denmark,
DK-2800 Lyngby, Denmark

Ole Mouritsen, Department of Physical Chemistry, Technical University of Denmark,
DK-2800 Lyngby, Denmark

Virginia Muto,,Departamento de Matematica Aplicada, Universidad del Pais Vasco,
E-48080 Bilbao, Spain

Jesper Mygind, Department of Physics, Technical University of Denmark,
DK-2800 Lyngby, Denmark

Jesper Mørk, TFL, Telecommunications Research Laboratory,
Lyngsø Alle 2, DK-2970 Hørsholm, Denmark

Alan Newell, Department of Mathematics, University of Arizona,
Tucson, Arizona 85721, USA

Phuong Nguyen, Kampsax 4402,
Kollegiebakken 9, DK-2800 Lyngby, Denmark

Lars Folke Olsen, Biokemisk Institut, Odense Universitet,
DK-5230 Odense M, Denmark

Ole Hvilsted Olsen, Biostructure Department, Novo Nordisk,
DK-2880 Bagsværd, Denmark

A.R. Osborne, Program in Nonlinear Physics, Università degli Studi di Torino,
I-10125 Torino, Italy

L.A. Ostrovsky, Institute of Applied Physics, Academy of Sciences,
603 600 Nizhij Novgorod, Russia

Ed Overman, Department of Mathematics, Ohio State University,
Columbus, Ohio 43210, USA

Sergio Pagano, Istituto di Cibernetica del CNR,
Napoli, I-80042 Arco Felice, NA, Italy,

Paul Papatzacos, Høgskolesenteret i Rogaland,
N-4001 Stavanger, Norway

David F. Parker, Department of Mathematics & Statistics, University of Edinburgh,
Edinburgh EH9 3JZ, UK

Bob Parmentier, Dipartimento di Fisica, University of Salerno,
I-84081 Baronissi SA, Italy

Theodore Pavlopoulos, Asklipiou 79, 10680 Athens, Greece

Niels Falsig Pedersen, Department of Physics, Technical University of Denmark,
DK-2800 Lyngby, Denmark

Poul Chr. Pedersen, NOVO-Nordisk, Scientific Computation,
DK-2880 Bagsværd, Denmark

Michel Peyrard, Laboratoire de Physique, Ecole Normale Supérieure de Lyon,
F-69364 Lyon Cedex 07, France

Brian M. Pierce, Hughes Aircraft Company,
Long Beach, CA 90810-0399, USA

Louis J. Piscitelle, Department of Army, US Army Natick Research,
Development and Engineering Center, Natick, MA 01760-5017, USA

K. Porsezian, Nonlinear Dynamics, Department of Physics,
Bharathidasan University, Tamil Nadu, India

Joël Pouget, Laboratory de Modélisation en Mécanique,
Université Pierre et Marie Curie, F-75252 Paris Cedex 05, France

Christian Poulsen, Electromagnetics Institute,
Technical University of Denmark, DK-2800 Lyngby, Denmark

Thomas H. Povlsen, Henrikshave 46,
DK-2150 Vedbæk, Denmark

B.N. Prasanna, 33 Second Main Road, Vyalikaval,
Bangalore - 560 003, India

Paolo M. Pumilia, Istituto di Chimica delle Macromolecole,
Consiglio Nazionale delle Ricerche, I-20133 Milano, Italy

Mikhail Rabinovich, Institute of Applied Physics, Academy of Sciences,
Nizhni Novgorod 603 600, Russia

A. Rabinovitch, Physics Department, Ben Gurion University,
Beer Sheva, 84105, Israel

P.S. Ramanujam, Optics and Fluid Dynamics Department, Risø National Laboratory,
DK-4000 Roskilde, Denmark

Henrik Rasmussen, Department of Applied Mathematical & Theoretical Physics,
University of Cambridge, Cambridge CB3 9EW, UK

Jens Juul Rasmussen, Optics and Fluid Dynamics Department,
Risø National Laboratory, DK-4000 Roskilde, Denmark

Steen Rasmussen, CNLS & Theoretical Division, Los Alamos National Laboratory,
Los Alamos, NM 87545, USA

Michel Remoissenet, Faculté des Sciences et Techniques,
Université de Bourgogne, F-21000 Dijon, France

Gerald Ristow, Kranichsteiner Strasse 15,
D-6000 Frankfurt/Main 70, Germany

Claudia Rohner, Kranichsteiner Strasse 15,
D-6000 Frankfurt/Main 70, Germany

Michael Rose, Laboratory of Applied Mathematical Physics,
Technical University of Denmark, DK-2800 Lyngby, Denmark

Giacomo Rotoli, Department of Physics, Università di Salerno,
I-84081 Baronissi SA, Italy

Valery I. Rupasov, Institute of Spectroscopy, Russian Academy of Sciences,
142092 Troitsk, Moscow Region, Russia

Mario Salerno, Dipartimento di Fisica Teorica, Università di Salerno,
I-84081 Baronissi SA, Italy

Alexander Samsonov, Ioffe Physical Technical Institute, Russian Academy of Sciences,
St. Petersburg 194021, Russia

Alwyn Scott, Laboratory of Applied Mathematical Physics/Depart of Mathematics,
Technical University of Denmark/University of Arizona, DK-2800 Lyngby/Tucson AZ
85721, Denmark/USA

Milan Sejka, Statsholdervej 13, DK-2400 Copenhagen NV, Denmark,

Alan Shore, Bath University, School Electronic and Electronic Engineering,
Bath, BA2 7AY, UK

Ya. G. Sinai, Landau Institute, Moscow V-334, Russia

Takis Skiniotis, Department of Mathematics, University of Patras,
261 10 Patras, Greece

Peter Skovgård, Kampsax 4404, Kollegiebakken 9, DK-2800 Lyngby, Denmark

Jesper Skovhus Thomsen, Department of Physics, ~
Technical University of Denmark, DK-2800 Lyngby, Denmark

Eva Slivsgaard, Laboratory of Applied Mathematical Physics,
Technical University of Denmark, DK-2800 Lyngby, Denmark

G. Stépán, Department Applied Mechanics, Technical University of Budapest,
H-1521 Budapest, Hungary

Mads Peter Sørensen, Laboratory of Applied Mathematical Physics,
Technical University of Denmark, DK-2800 Lyngby, Denmark

Shozo Takeno, Laboratory of Physics, Kyoto Institute of Technology,
Kyoto 606, Japan

A Tamasevicius, Semiconductor Physics Institute,
2600 Vilnius, Lithuania

Jussi Timonen, University of Jyväskylä, Department of Physics,
SF-40351 Jyväskylä, Finland

Morikazu Toda, Tokyo University of Education,
Shibuya-ku, Tokyo 151, Japan

Jens Trandum, Wesselsvej 92, DK-4700 Næstved, Denmark

Hans True, Laboratory of Applied Mathematical Physics,
Technical University of Denmark, DK-2800 Lyngby, Denmark

George Tsironis, Physics Department, University of North Texas,
Denton, TX 76203, USA

Sergei Turitsyn, Institut für Theoretische Physik I, Universität Düsseldorf,
D-400 Düsseldorf 1, Germany

J.A. Tuszynski, Department of Physics, University of Alberta,
Edmonton, AB T6G 2J1, Canada

Alexey Ustinov, Department of Physics, Technical University of Denmark,
DK-2800 Lyngby, Denmark

Poul Varming, Tagensvej 15,
DK-2200 Copenhagen N, Denmark

Luis Vazquez, Departamento de Fisica Teorica I,
Universidad Complutense de Madrid, E-28040 Madrid, Spain

Giuseppe Vitiello, Dipartimento di Fisica, Università di Salerno,
I-84081 Baronissi SA, Italy

Miki Wadati, Department of Physics, University of Tokyo,
Bunkyo-ku, Tokyo 113, Japan

Xidi Wang, Department of Chemistry 0340, University of California, San Diego,
La Jolla, California 92093, USA

Shinsuke Watanabe, Department of Energy Engineering,
Yokohama National University, Hodogaga, Yokohama 240, Japan

Ludmila V. Yakushevich, Institute of Cell Biophysics, Academy of Sciences,
Pushchino 142292, Russia

Norman J. Zabusky, Department of Mechanical & Aerospace Engineering,
Rutgers University, Piscataway, NJ 08855-0909, USA

J. Zagrodzinski, Institute of Physics, Polish Academy of Sciences,
02 668 Warsaw, Poland

V.E. Zakharov, Department of Mathematics, University of Arizona,
Tucson, Arizona 85721, USA

Wojciech J. Zakrzewski, Department of Mathematical Sciences, University of Durham,
Durham, DH1 3LE, UK

Fei Zhang, Departamento de Fisica Teorica I,
Universidad Complutense de Madrid, E-28040 Madrid, Spain

Alexander Zolotaryuk, Institute for Theoretical Physics,
Academy of Sciences of Ukraine, 252 130 Kiev, Ukraine

Georg Zundel, Physikalisch-Chemisches Institut, Universität München,
D-8000 München 2, Germany



Index

- Abel equation 126
- Ablowitz-Ladik equation 86, 217, 224, 227, 257
- Acetanilide 477
- Acoustic waves 121
- Adriatic sea 33
- Aerodynamic decelerator 161
- AIDS 499
- Anderson localization 85
- Anderson-May model 502
- Bäcklund transform 1, 8, 11
- Balance equation analysis 56
- Bénard-Marangoni convection 142
- Benjamin-Feir instability 197
- Bilinear equation 7, 203
- Bjerrum defects 449
- Boussinesq equation 376
- Breather 86, 299, 372, 465
- Brillouin flow 19, 22
- Casorati determinant 9
- Charge density wave 455, 461
- Chaos
 - control 129, 157
 - fluid flow 45
 - Hamiltonian systems 129
 - heart dynamics 129
 - HIV model 499
 - NLS equation 109
 - railway vehicle dynamics 165
 - semiconductor lasers 409
 - spatial 139
 - ultradian clock 527
- Chazy's equation 3, 4
- Cold-fluid plasma 19
- Collective coordinates 268
- Cooper pair 302, 333, 355
- Coriolis parameter 59
- Coupled map lattices 514
- Courant-Isaacson-Rees algorithm 82
- Crossed-field devices 17
- Cyclones 60
- Cytoskeleton 533
- D-operators 203
- Diatomic lattice 64, 449
- Dimer 239
- Direct scattering transform 30
- Discrete systems 7, 37, 63, 185, 195, 203, 223, 227, 231, 249, 257
- DNA molecule 263, 469, 485
- Driven cavity problem 45
- Duffing equation 125
- Eckhaus equation 105
- Ehrenfest theorem 107
- Elastic surface wave 55
- Electrocardiograms 523
- Elliptic functions 38, 273, 298
- Elliptic integrals 38, 297
- Evolution 489
- Faraday ripples 142
- Feigenbaum scaling 109
- Fermionic polaron model 227
- Ferroelastic-martinsite transformation 255
- Fiske steps 353
- FitzHugh-Nagumo model 127
- Floquet discriminant 32
- Flutter 161
- Fluxon 267, 312, 339, 347, 351
- Fourier-Chebyshev expansion 52
- FPU lattice 192, 223
- Frenkel-Kontorova model 195
- Frobenius expansion 1
- Frölich Hamiltonian 461
- Fuchs indices 2
- Galerkin approximation 45
- Gauge equivalence 244
- Gaussian stream-function 60
- Ginzburg-Landau equation 48, 254, 385
 - complex 97
- Globular protein 436
- Hasegawa-Mima equation 59
- Hartree approximation 232
- Hartree voltage 21
- Heisenberg spin chain 243
- Helicoidal waves 297
- Hénon-Heiles system 455
- High T_c superconductivity 265, 343, 350, 359, 363, 367
- HIV infection model 499

- Hopf algebra 177
- Hopf bifurcation 45, 109, 166, 171, 410, 499
- Hubbard model 227, 265
- Hyperelliptic function 33
- Ikeda ring cavity 409
- Inverse spectral transform (IST) 1, 118, 376
 - numerical 27
 - periodic 29
- J-aggregates 381
- Jacobi formula 7, 10
- Jordan-Wigner map 177
- Josephson junction 117, 267, 293, 333, 343, 351, 355
 - array 86, 326, 339, 347, 363, 367
- Jost function 244
- Kadomtsev-Petviashvili (KP) equation 7, 253
 - discrete space-time 9
- KAM surface 130
- Karhunen-Loève expansion 110
- Kawahara equation 193
- KdV-Burgers equation 126
- Kerr effect 405, 437
- Kink 65, 69, 278, 295, 452, 535
 - see also* Soliton
- Klein-Gordon equation 67, 293
 - discrete 63, 223
 - nonlinear 77, 120
- Kobayashi equation 409
- Kolmogorov length scale 98
- Kolmogorov-Sinai entropy 148
- Korteweg-de Vries (KdV) equation 8, 27, 117
 - time-like 28
- Kuramoto-Sivashinsky equation 128
- Lamb dipole 52
- Lamé equations 273
- Lang equation 409
- Langmuir-Blodgett film 231, 381, 391, 394
- Lattice models *see* Discrete systems
- Lax pair 8, 244, 458
- Liquid crystals 371
- Lotka-Volterra equations 14
- LR factorization method 12
- Lyapunov dimension 97
- Lyapunov exponent 141, 158, 499
- Lyapunov stability 405
- Magnetron 18
- Marchenko equation 80
- Master equation 494
- McCumber branch 267, 304, 365
- Microtubules 533
- Mitotic oscillator 527
- Modified KdV equation 8
- Monodromy matrix 29, 103
- Morphogenesis 519
- Morse potential 208
- Mössbauer effect 261
- Naimark-Sacker bifurcation 47
- Navier-Stokes equations 45, 51, 98
- Neumann system 458
- Neural systems 513
- Newel-Whitehead-Sigel equation 143
- NKC model 489
- Nonlinear filtering 34
- Nonlinear Fourier analysis 27
- Nonlinear optics 85, 394, 399, 405, 409
- Nonlinear Schrödinger (NLS) equation 17, 57, 85, 105, 117, 123, 197, 243, 399, 405, 422
 - 2D model 196
 - and chaos 108
 - coupled 413
 - discrete 224, 227, 241, 257
 - modulational instability 22
 - unstable version 101
- Number state method 227
- Optical anisotropy photoproduction 391
- Optical fibre 399, 405, 413, 421
- Painlevé analysis 1, 127
- Partition function 40
- Peierls-Nabarro potential 224
- Period-doubling 47, 504
- Phase locking 509
- Phase transitions 249
- Plana's expansion 43
- Plücker relation 7, 10
- Predator-prey equations 14
- Poincaré section 110, 273, 506
- Poisson bracket 102, 458
- Poisson equation 19, 47, 52
- Polaron 85, 213, 231, 265
- Proton pumping 474
- Pulson 200
- Pump-probe equations 418
- Q-boson 217
- Quantum groups 177, 219
- Quantum inverse scattering 218, 227
- Quasicrystals 144
- R-matrix 103
- Rayleigh component 55
- Rayleigh surface wave 56
- Reaction-diffusion systems 517
- Reynold's number 45, 53
- Riccati equation 128
- Riemann theta function 352, 455
- Rossby wave 59
- Rotating wave approximation 64, 204
- Schrödinger equation, nonlinear *see* Nonlinear Schrödinger equation
- Self-focussing 85, 121, 231
- Semiconductor optical waveguide 417
- Serret-Frenet equations 244
- Shimmying wheels 169

- Sine-Gordon 2D model 196, 308
- Sine-Gordon equation 8, 64, 86, 110, 113, 117, 268, 283, 289, 333, 347
 - discrete 258, 364
 - double 449
 - mechanical analog 284
 - quantum 465
- Skryme model 73
- Soliton 34, 37, 78, 85, 143, 174, 186, 231, 236
 - 2D structure 73
 - chaotic 173
 - collective coordinates 115
 - Davydov soliton 231, 241, 425, 445, 464, 477
 - formation 23
 - gap soliton 63
 - in liquid crystals 375
 - optical 403, 405
 - in polyacetylene 67
 - quantum soliton 227
 - soliton band 227
 - soliton-impurity interaction 113, 117
 - soliton-soliton collision 57
 - solutions 7, 10, 39, 109
 - subsonic 57
 - transsonic 57
- Squeezed states 177
- Squid axon 509
- Stationary solution 65
- Stochastic resonance 153
- Su-Schrieffer-Heeger model 67
- Swift-Hohenberg equation 146
- Taylor-Proudman theorem 53
- Thermal fluctuations 385, 425
- Toda equation 37, 190, 261
 - discrete-time 7
 - driven, damped 235
 - 2D equation 10
- Toda potential 470
- Transport properties 85
- Turbulence 46
- Turing structure 517
- Two-wave interaction 7, 13
- Ultradian clock 527
- Ursell number 34
- Van der Pol model 509
- Verlet algorithm 68
- Vibron 86, 204
- Vlasov-Poisson Model 18
- Vortex
 - breakdown 46
 - in cardiac muscle 539
 - dipole 51, 61
 - sheet 53
 - structure 59
- Weierstrass function 125, 463
- Weyl-Heisenberg algebra 179, 219
- Whitham method 377
- Wronskian 8, 29
- XY model 367
- Yangs' equation 221
- Zakharov-Shabat scattering problem 111
- Zakharov system 56
- Zero field step (ZFS) 267, 341